

**7th Int. Symp. on High Performance  
Capillary Electrophoresis  
Würzburg, 29 January–2 February 1995**

JOURNAL OF

# CHROMATOGRAPHY A

INCLUDING ELECTROPHORESIS AND OTHER SEPARATION METHODS

## EDITORS

U.A.Th. Brinkman (Amsterdam)  
R.W. Giese (Boston, MA)  
J.K. Haken (Kensington, N.S.W.)  
C.F. Poole (London)  
L.R. Snyder (Orinda, CA)  
S. Terabe (Hyogo)

EDITORS, SYMPOSIUM VOLUMES,  
E. Heftmann (Orinda, CA), Z. Deyl (Prague)

## EDITORIAL BOARD

D.W. Armstrong (Rolla, MO)  
W.A. Aue (Halifax)  
P. Boček (Brno)  
P.W. Carr (Minneapolis, MN)  
J. Crommen (Liège)  
V.A. Davankov (Moscow)  
G.J. de Jong (Groningen)  
Z. Deyl (Prague)  
S. Dilli (Kensington, N.S.W.)  
Z. El Rassi (Stillwater, OK)  
H. Engelhardt (Saarbrücken)  
M.B. Evans (Hatfield)  
S. Fanali (Rome)  
G.A. Guiochon (Knoxville, TN)  
P.R. Haddad (Hobart, Tasmania)  
I.M. Hais (Hradec Králové)  
W.S. Hancock (Palo Alto, CA)  
S. Hjertén (Uppsala)  
S. Honda (Higashi-Osaka)  
Cs. Horváth (New Haven, CT)  
J.F.K. Huber (Vienna)  
J. Janák (Brno)  
P. Jandera (Pardubice)  
B.L. Karger (Boston, MA)  
J.J. Kirkland (Newport, DE)  
E. sz. Kováts (Lausanne)  
C.S. Lee (Ames, IA)  
K. Macek (Prague)  
A.J.P. Martin (Cambridge)  
E.D. Morgan (Keele)  
H. Poppe (Amsterdam)  
P.G. Righetti (Milan)  
P. Schoenmakers (Amsterdam)  
R. Schwarzenbach (Dübendorf)  
R.E. Shoup (West Lafayette, IN)  
R.P. Singhal (Wichita, KS)  
A.M. Siouffi (Marseille)  
D.J. Strydom (Boston, MA)  
T. Takagi (Osaka)  
N. Tanaka (Kyoto)  
K.K. Unger (Mainz)  
P. van Zoonen (Bilthoven)  
R. Verpoorte (Leiden)  
Gy. Vigh (College Station, TX)  
J.T. Watson (East Lansing, MI)  
B.D. Westerlund (Uppsala)

## EDITORS, BIBLIOGRAPHY SECTION

Z. Deyl (Prague), J. Janák (Brno), V. Schwarz (Prague)

# JOURNAL OF CHROMATOGRAPHY A

INCLUDING ELECTROPHORESIS AND OTHER SEPARATION METHODS

**Scope.** The *Journal of Chromatography* publishes papers on all aspects of **chromatography, electrophoresis** and other separation methods. Contributions consist mainly of research papers dealing with chromatographic theory, instrumental developments and their applications. Section *A* covers all areas except biomedical applications of separation science which are published in section *B*: *Biomedical Applications*.

**Submission of Papers.** The preferred medium of submission is on disk with accompanying manuscript. Manuscripts (in English; four copies are required) should be submitted to: Editorial Office of *Journal of Chromatography A*, P.O. Box 681, 1000 AR Amsterdam, Netherlands, Telefax (+31-20) 485 2304. Review articles are invited or proposed in writing to the Editors who welcome suggestions for subjects. An outline of the proposed review should first be forwarded to the Editors for preliminary discussion prior to preparation. Submission of an article is understood to imply that the article is original and unpublished and is not being considered for publication elsewhere. For copyright regulations, see below.

**Subscription information.** For 1996 Vols. 715–748 of *Journal of Chromatography A* (ISSN 0021-9673) are scheduled for publication. Subscription prices for *Journal of Chromatography A + B* (combined), or for section *A* or *B* are available upon request from the publisher. Subscriptions are accepted on a prepaid basis only and are entered on a calendar year basis. Issues are sent by surface mail except to the following countries where air delivery via SAL is ensured: Argentina, Australia, Brazil, Canada, China, Hong Kong, India, Israel, Japan, Malaysia, Mexico, New Zealand, Pakistan, Singapore, South Africa, South Korea, Taiwan, Thailand, USA. For all other countries airmail rates are available upon request. Claims for missing issues must be made within six months of our publication (mailing) date. Please address all your requests regarding orders and subscription queries to: Elsevier Science B.V., Journal Department, P.O. Box 211, 1000 AE Amsterdam, Netherlands. Tel.: (+31-20) 485 3642; Fax: (+31-20) 485 3598. Customers in the USA and Canada wishing information on this and other Elsevier journals, please contact Journal Information Center, Elsevier Science Inc., 655 Avenue of the Americas, New York, NY 10010, USA, Tel. (+1-212) 633 3750, Telefax (+1-212) 633 3764.

**Abstracts/Contents Lists** published in Analytical Abstracts, Biochemical Abstracts, Biological Abstracts, Chemical Abstracts, Chemical Titles, Chromatography Abstracts, Current Awareness in Biological Sciences (CABS), Current Contents/Life Sciences, Current Contents/Physical, Chemical & Earth Sciences, Deep-Sea Research/Part B: Oceanographic Literature Review, Excerpta Medica, Index Medicus, Mass Spectrometry Bulletin, PASCAL-CNRS, Referativnyi Zhurnal, Research Alert and Science Citation Index.

**US Mailing Notice.** *Journal of Chromatography A* (ISSN 0021-9673) is published weekly (total 52 issues) by Elsevier Science B.V., (Sara Burgerhartstraat 25, P.O. Box 211, 1000 AE Amsterdam, Netherlands). Annual subscription price in the USA US\$ 6863.00 (US\$ price valid in North, Central and South America only) including air speed delivery. Second class postage paid at Jamaica, NY 11431. **USA POSTMASTERS:** Send address changes to *Journal of Chromatography A*, Publications Expediting, Inc., 200 Meacham Avenue, Elmont, NY 11003. Airfreight and mailing in the USA by Publications Expediting.

**Advertisements.** The Editors of the journal accept no responsibility for the contents of the advertisements. Advertisement rates are available on request. Advertising orders and enquiries may be sent to *International:* Elsevier Science, Advertising Department, The Boulevard, Langford Lane, Kidlington, Oxford, OX5 1GB, UK; Tel: (+44) (0) 1865 843565; Fax: (+44) (0) 1865 843952. *USA and Canada:* Weston Media Associates, Dan Lipner, P.O. Box 1110, Greens Farms, CT 06436-1110, USA; Tel: (203) 261 2500; Fax: (203) 261 0101. *Japan:* Elsevier Science Japan, Ms Noriko Kodama, 20-12 Yushima, 3 chome, Bunkyo-Ku, Tokyo 113, Japan; Tel: (+81) 3 3836 0810; Fax: (+81) 3 3839 4344.

**See inside back cover** for Publication Schedule and Information for Authors.

© 1995 ELSEVIER SCIENCE B.V. All rights reserved.

0021-9673/95/\$09.50

No part of this publication may be reproduced, stored in a retrieval system or transmitted in any form or by any means, electronic, mechanical, photocopying, recording or otherwise, without the prior written permission of the publisher, Elsevier Science B.V., Copyright and Permissions Department, P.O. Box 521, 1000 AM Amsterdam, Netherlands.

Upon acceptance of an article by the journal, the author(s) will be asked to transfer copyright of the article to the publisher. The transfer will ensure the widest possible dissemination of information.

*Special regulations for readers in the USA* – This journal has been registered with the Copyright Clearance Center, Inc. Consent is given for copying of articles for personal or internal use, or for the personal use of specific clients. This consent is given on the condition that the copier pays through the Center the per-copy fee stated in the code on the first page of each article for copying beyond that permitted by Sections 107 or 108 of the US Copyright Law. The appropriate fee should be forwarded with a copy of the first page of the article to the Copyright Clearance Center, Inc., 222 Rosewood Drive, Danvers, MA 01923, USA. If no code appears in an article, the author has not given broad consent to copy and permission to copy must be obtained directly from the author. The fee indicated on the first page of an article in this issue will apply retroactively to all articles published in the journal, regardless of the year of publication. This consent does not extend to other kinds of copying, such as for general distribution, resale, advertising and promotion purposes, or for creating new collective works. Special written permission must be obtained from the publisher for such copying.

No responsibility is assumed by the Publisher for any injury and/or damage to persons or property as a matter of products liability, negligence or otherwise, or from any use or operation of any methods, products, instructions or ideas contained in the materials herein. Because of rapid advances in the medical sciences, the Publisher recommends that independent verification of diagnoses and drug dosages should be made.

Although all advertising material is expected to conform to ethical (medical) standards, inclusion in this publication does not constitute a guarantee or endorsement of the quality or value of such product or of the claims made of it by its manufacturer.

Ⓢ The paper used in this publication meets the requirements of ANSI/NISO Z39.48-1992 (Permanence of Paper).

Printed in the Netherlands

For Contents see p. VII.

# ELSEVIER SCIENCE

World Class Publishing

*Advertising*

REACH

THE

CORE

NOT

THE

PERIPHERY



## PLEASE CONTACT

### INTERNATIONAL:

The Advertising Sales Manager  
Elsevier Science Ltd  
The Boulevard  
Langford Lane  
Kidlington  
Oxford OX5 1GB  
Tel (+44) (0)1865 843565  
Fax (+44) (0)1865 843952

### USA/CANADA:

Daniel S Lipner  
Weston Media Associates  
P O Box 1110  
Greens Farms  
CT 06436-1110  
USA  
Tel 203 261-2500  
Fax 203 261-0101

### JAPAN:

Ms Noriko Kodama  
ES - Tokyo Branch, 20-12 Yushima, 3 chome  
Bunkyo-Ku, Tokyo 113, Japan  
Tel (+81) 3 3836 0810  
Fax (+81) 3 3839 4344

# Separations as sharp as a razor with the ultrapure NUCLEOSIL®

## Separation of natural porphyrins

Column: ET 250/8/4 NUCLEOSIL® 120-5 C<sub>18</sub>

Eluent: A methanol, 12.5 mM tetrabutylammonium dihydrogen phosphate, pH 6.6  
B 40 mM NaH<sub>2</sub>PO<sub>4</sub>, pH 5.6 in water

Flow rate: 0.7 ml/min

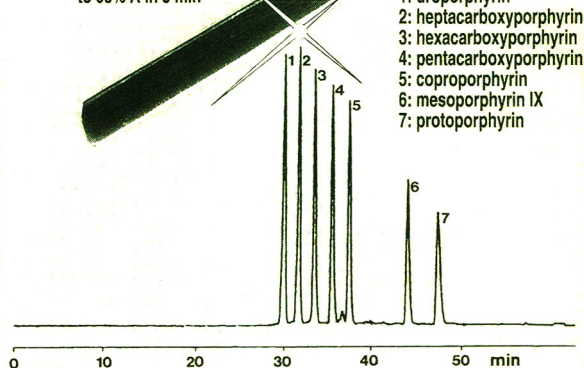
Detection: fluorescence 400 nm / 600 nm

Gradient: 45% A (10 min)

to 75% A in 5 min,

to 85% A in 5 min,

to 98% A in 5 min



Peaks:

- 1: uroporphyrin
- 2: heptacarboxyporphyrin
- 3: hexacarboxyporphyrin
- 4: pentacarboxyporphyrin
- 5: coproporphyrin
- 6: mesoporphyrin IX
- 7: protoporphyrin

Specialists in  
Chromatography

○ NUCLEOSIL®  
HPLC packings for  
analytical and preparative separations

○ spherical particles

○ pore sizes from 50 to 4000 Å

○ outstanding separation performance and  
very good reproducibility from lot to lot

○ high pressure stability even for wide pore materials

○ numerous chemically bonded phases

Please ask for further information!

**MACHERY-NAGEL**



MACHERY-NAGEL GmbH & Co. KG · P.O. Box 10 13 52  
D-52313 Düren · Germany · Tel. (02421) 969-0 · Fax (02421) 969 199  
Switzerland: MACHERY-NAGEL AG · P.O. Box 224 · CH-4702 Oensingen · Tel. (062) 76 20 66  
France: MACHERY-NAGEL S.a.r.l. · B.P. 135 · F-67722 Hoerd · Tel 88.51.76.89

AVAILABLE AT YOUR FINGERTIPS:

NOW AVAILABLE:

# THE ELSEVIER SCIENCE COMPLETE CATALOGUE ON INTERNET

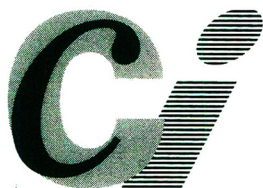
# THE ELSEVIER SCIENCE COMPLETE CATALOGUE 1995 ON CD-ROM

These catalogues feature all journals, books and major reference works from Elsevier Science. Furthermore they allow you to access information about the electronic and CD-ROM products now published by Elsevier Science. Demonstration examples of some of these products are included.

## Features include:

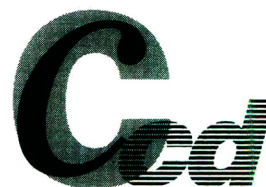
- All the journals, with complete information about journal editors and editorial boards
- Listings of special issues and volumes
- Listings of recently published papers for many journals
- Complete descriptions and contents lists of book titles
- Clippings of independent reviews of published books
- Book series, dictionaries, reference works
- Electronic and CD-ROM products
- Demonstration versions of electronic products
- Free text search facilities
- Ordering facilities
- Print options
- Hypertext features

ELSEVIER SCIENCE



Catalogue on **INTERNET**

ELSEVIER SCIENCE



Catalogue on **CD-ROM**

## Extra features with the Catalogue on Internet

- Alerting facility for new & forthcoming publications
- Updated monthly

**ELSEVIER SCIENCE  
COMPLETE CATALOGUE  
INTERNET: TRY IT TODAY!**

gopher to: [gopher.elsevier.nl](mailto:gopher.elsevier.nl)  
WWW: <http://www.elsevier.nl/>

**CD-ROM** (published yearly, free of charge)  
Please contact:

Customer Service Department  
Tel.: +31 (20) 485 3757  
Fax: +31 (20) 485 3432  
e-mail: [nlinfo-f@elsevier.nl](mailto:nlinfo-f@elsevier.nl)



ELSEVIER



PERGAMON



NORTH  
HOLLAND



EXCERPTA  
MEDICA

JOURNAL OF CHROMATOGRAPHY A

VOL. 716 (1995)



# JOURNAL OF CHROMATOGRAPHY A

INCLUDING ELECTROPHORESIS AND OTHER SEPARATION METHODS

## EDITORS

U.A.Th. BRINKMAN (Amsterdam), R.W. GIESE (Boston, MA), J.K. HAKEN (Kensington, N.S.W.),  
C.F. POOLE (London), L.R. SNYDER (Orinda, CA), S. TERABE (Hyogo)

## EDITORS, SYMPOSIUM VOLUMES

E. HEFTMANN (Orinda, CA), Z. DEYL (Prague)

## EDITORIAL BOARD

D.W. Armstrong (Rolla, MO), W.A. Aue (Halifax), P. Boček (Brno), P.W. Carr (Minneapolis, MN), J. Crommen (Liège), V.A. Davankov (Moscow), G.J. de Jong (Weesp), Z. Deyl (Prague), S. Dilli (Kensington, N.S.W.), Z. El Rassi (Stillwater, OK), H. Engelhardt (Saarbrücken), M.B. Evans (Hatfield), S. Fanali (Rome), G.A. Guiochon (Knoxville, TN), P.R. Haddad (Hobart, Tasmania), I.M. Hais (Hradec Králové), W.S. Hancock (Palo Alto, CA), S. Hjertén (Uppsala), S. Honda (Higashi-Osaka), Cs. Horváth (New Haven, CT), J.F.K. Huber (Vienna), J. Janák (Brno), P. Jandera (Pardubice), B.L. Karger (Boston, MA), J.J. Kirkland (Newport, DE), E. sz. Kováts (Lausanne), C.S. Lee (Ames, IA), K. Macek (Prague), A.J.P. Martin (Cambridge), E.D. Morgan (Keele), H. Poppe (Amsterdam), P.G. Righetti (Milan), P. Schoenmakers (Amsterdam), R. Schwarzenbach (Dübendorf), R.E. Shoup (West Lafayette, IN), R.P. Singhal (Wichita, KS), A.M. Siouffi (Marseille), D.J. Strydom (Boston, MA), T. Takagi (Osaka), N. Tanaka (Kyoto), K.K. Unger (Mainz), P. van Zoonen (Bilthoven), R. Verpoorte (Leiden), Gy. Vigh (College Station, TX), J.T. Watson (East Lansing, MI), B.D. Westerlund (Uppsala)

## EDITORS, BIBLIOGRAPHY SECTION

Z. Deyl (Prague), J. Janák (Brno), V. Schwarz (Prague)



ELSEVIER

Amsterdam – Lausanne – New York – Oxford – Shannon – Tokyo

---

*J. Chromatogr. A*, Vol. 716 (1995)

© 1995 ELSEVIER SCIENCE B.V. All rights reserved.

0021-9673/95/\$09.50

No part of this publication may be reproduced, stored in a retrieval system or transmitted in any form or by any means, electronic, mechanical, photocopying, recording or otherwise, without the prior written permission of the publisher, Elsevier Science B.V., Copyright and Permissions Department, P.O. Box 521, 1000 AM Amsterdam, Netherlands.

Upon acceptance of an article by the journal, the author(s) will be asked to transfer copyright of the article to the publisher. The transfer will ensure the widest possible dissemination of information.

*Special regulations for readers in the USA* – This journal has been registered with the Copyright Clearance Center, Inc. Consent is given for copying of articles for personal or internal use, or for the personal use of specific clients. This consent is given on the condition that the copier pays through the Center the per-copy fee stated in the code on the first page of each article for copying beyond that permitted by Sections 107 or 108 of the US Copyright Law. The appropriate fee should be forwarded with a copy of the first page of the article to the Copyright Clearance Center, Inc., 222 Rosewood Drive, Danvers, MA 01923, USA. If no code appears in an article, the author has not given broad consent to copy and permission to copy must be obtained directly from the author. The fee indicated on the first page of an article in this issue will apply retroactively to all articles published in the journal, regardless of the year of publication. This consent does not extend to other kinds of copying, such as for general distribution, resale, advertising and promotion purposes, or for creating new collective works. Special written permission must be obtained from the publisher for such copying.

No responsibility is assumed by the Publisher for any injury and/or damage to persons or property as a matter of products liability, negligence or otherwise, or from any use or operation of any methods, products, instructions or ideas contained in the materials herein. Because of rapid advances in the medical sciences, the Publisher recommends that independent verification of diagnoses and drug dosages should be made.

Although all advertising material is expected to conform to ethical (medical) standards, inclusion in this publication does not constitute a guarantee or endorsement of the quality or value of such product or of the claims made of it by its manufacturer.

♻️ The paper used in this publication meets the requirements of ANSI/NISO 239.48-1992 (Permanence of Paper).

Printed in the Netherlands



SYMPOSIUM VOLUME



**SEVENTH INTERNATIONAL SYMPOSIUM ON  
HIGH PERFORMANCE CAPILLARY ELECTROPHORESIS**

*Würzburg (Germany), 29 January–2 February 1995*

*Guest Editor*

**H. ENGELHARDT**

(Saarbrücken, Germany)

The articles submitted for the Symposium Volumes on the *7th International Symposium on High Performance Capillary Electrophoresis* are published in two consecutive Volumes of the *Journal of*

*Chromatography A*, Vols. 716 and 717 (1995). The Foreword only appears in Vol. 716. A combined Author Index to both Vols. 716 and 717 only appears in Vol. 717.

## CONTENTS

(Abstracts/Contents Lists published in *Analytical Abstracts*, *Biochemical Abstracts*, *Biological Abstracts*, *Chemical Abstracts*, *Chemical Titles*, *Chromatography Abstracts*, *Current Awareness in Biological Sciences (CABS)*, *Current Contents/Life Sciences*, *Current Contents/Physical, Chemical & Earth Sciences*, *Deep-Sea Research/Part B: Oceanographic Literature Review*, *Excerpta Medica*, *Index Medicus*, *Mass Spectrometry Bulletin*, *PASCAL-CNRS*, *Referativnyi Zhurnal*, *Research Alert* and *Science Citation Index*)

7TH INTERNATIONAL SYMPOSIUM ON HIGH PERFORMANCE CAPILLARY ELECTROPHORESIS, WÜRZBURG, 29 JANUARY–2 FEBRUARY 1995, PART I

Foreword by H. Engelhardt (Saarbrücken, Germany) . . . . .	1
THEORY, PRACTICE AND NEW TECHNIQUES IN CZE	
Emersion peaks in capillary electrophoresis by C.L. Colyer and K.B. Oldham (Peterborough, Canada) . . . . .	3
Dynamic simulator for capillary electrophoresis with in situ calculation of electroosmosis by R.A. Mosher (Tucson, AZ, USA) and C.-X. Zhang, J. Caslavská and W. Thormann (Berne, Switzerland) . . . . .	17
Preparation and stability tests for polyacrylamide-coated capillaries for capillary electrophoresis by H. Engelhardt and M.A. Cuñat-Walter (Saarbrücken, Germany) . . . . .	27
Some practical aspects of utilizing the on-line combination of isotachopheresis and capillary zone electrophoresis by L. Křivánková, P. Gebauer and P. Boček (Brno, Czech Republic) . . . . .	35
Investigation and optimisation of the use of organic modifiers in micellar electrokinetic chromatography by A.E. Bretnall and G.S. Clarke (Moreton, UK) . . . . .	49
Polymer-supported pseudo-stationary phase for electrokinetic chromatography. Electrokinetic chromatography in a full range of methanol–water mixtures with alkylated starburst dendrimers by N. Tanaka, T. Fukutome, K. Hosoya, K. Kimata and T. Araki (Kyoto, Japan) . . . . .	57
Micellar electrokinetic chromatography–mass spectrometry using a high-molecular-mass surfactant. On-line coupling with an electrospray ionization interface by H. Ozaki, N. Itou and S. Terabe (Hyogo, Japan) and Y. Takada, M. Sakairi and H. Koizumi (Tokyo, Japan) . . . . .	69
Optimization of resolution in micellar electrokinetic chromatography via computer-aided simultaneous variation of concentrations of sodium dodecyl sulfate and urea as modifier by U. Pyell and U. Bütehorn (Marburg, Germany) . . . . .	81
Control of the electroosmotic flow by metal-salt-containing buffers by R. Brechtel, W. Hohmann, H. Rüdiger and H. Wätzig (Würzburg, Germany) . . . . .	97
Capillary electrochromatography of small molecules in polyacrylamide gels with electroosmotic flow by C. Fujimoto and J. Kino (Hamamatsu, Japan) and H. Sawada (Toyohashi, Japan) . . . . .	107
Capillary zone electrophoresis with indirect UV detection applying a UV-absorbing counter ion by J. Collet and P. Gareil (Paris, France) . . . . .	115
Post-column reaction system for fluorescence detection in capillary electrophoresis by R. Zhu and W.T. Kok (Amsterdam, Netherlands) . . . . .	123
Integrated optical detection cell based on Bragg reflecting waveguides by T. Delonge and H. Fouckhardt (Braunschweig, Germany) . . . . .	135
Optimum conditions for preparative operation of capillary zone electrophoresis by A. Cifuentes, X. Xu, W.T. Kok and H. Poppe (Amsterdam, Netherlands) . . . . .	141
Analysis of protein fractions by micropreparative capillary isoelectric focusing and matrix-assisted laser desorption time-of-flight mass spectrometry by F. Foret, O. Müller, J. Thorne, W. Götzinger and B.L. Karger (Boston, MA, USA) . . . . .	157
Capillary zone electrophoresis at subzero temperatures. I. Separation of the <i>cis</i> and <i>trans</i> conformers of small peptides by S. Ma, F. Kálmán, A. Kálmán, F. Thuncke and C. Horváth (New Haven, CT, USA) . . . . .	167

ห้องสมุดมหาวิทยาลัยศิลปากร

21 S.F. 2538

(Continued overleaf)

Use of negatively charged sulfobutyl ether- $\beta$ -cyclodextrin for enantiomeric separation by capillary electrophoresis by C. Desiderio and S. Fanali (Rome, Italy) . . . . .	183
Buffer effects in the desionoselective/ionoselective/duoselective separation selectivity model-assisted optimization of the capillary electrophoretic separation of enantiomers. I. Low-pH phosphate buffers by R.L. Williams and G. Vigh (College Station, TX, USA) . . . . .	197
Evaluation of the parameters determining the performance of electrochromatography in packed capillary columns by B. Behnke, E. Grom and E. Bayer (Tübingen, Germany) . . . . .	207

## CARBOHYDRATES

Analysis by capillary electrophoresis–laser-induced fluorescence detection of oligosaccharides produced from enzyme reactions by X. Le, C. Scaman, Y. Zhang, J. Zhang, N.J. Dovichi, O. Hindsgaul and M.M. Palcic (Edmonton, Canada) . . . . .	215
Nanomolar determination of aminated sugars by capillary electrophoresis by Y. Zhang, E. Arriaga, P. Diedrich, O. Hindsgaul and N.J. Dovichi (Edmonton, Canada) . . . . .	221
Sensitive determination of sugars by capillary zone electrophoresis with indirect UV detection under highly alkaline conditions by X. Xu, W.T. Kok and H. Poppe (Amsterdam, Netherlands) . . . . .	231
Separation of 8-aminonaphthalene-1,3,6-trisulfonic acid-labelled neutral and sialylated N-linked complex oligosaccharides by capillary electrophoresis by A. Klockow (Basle and Zürich, Switzerland), R. Amadò (Zürich, Switzerland) and H.M. Widmer and A. Paulus (Basle, Switzerland) . . . . .	241
High-resolution capillary electrophoresis and polyacrylamide gel electrophoresis of heparins by R. Malsch, J. Harenberg and D.L. Heene (Mannheim, Germany) . . . . .	259

## CARBOXYLIC ACIDS AND ORGANIC ANIONS

Capillary zone electrophoresis of organic acids in serum of critically ill children by V. Dolník and J. Dolníková (Brno, Czech Republic) . . . . .	269
Utilization of fluorescein sodium salt in laser-induced indirect fluorimetric detection. II. Application to organic anions by A.M. Desbène, C.J. Morin and N.L. Mofaddel (Evreux and Mont Saint Aignan, France) and R.S. Grout (Gagny, France) . . . . .	279
Capillary electrophoretic determination of organic acids with indirect detection by C.H. Wu, Y.S. Lo, Y.-H. Lee and T.-I. Lin (Taipei, Taiwan) . . . . .	291
Capillary zone electrophoresis in organic solvents: separation of anions in methanolic buffer solutions by M. Chiari (Milan, Italy) and E. Kenndler (Vienna, Austria) . . . . .	303
Determination of inorganic and small organic anions in pure boric acid using capillary zone electrophoresis by J. Boden, M. Darius and K. Bächmann (Darmstadt, Germany) . . . . .	311

## AMINO ACIDS, PEPTIDES, PROTEASES

Optical resolution of amino acid derivatives by micellar electrokinetic chromatography with sodium N-tetradecanoyl-L- glutamate by K. Otsuka, H. Kawakami and W. Tamaki (Osaka, Japan) and S. Terabe (Hyogo, Japan) . . . . .	319
Capillary electrophoretic methods for a clear identification of selenoamino acids in complex matrices such as human milk by B. Michalke (Neuherberg, Germany) . . . . .	323
Study of the racemization of L-serine by cyclodextrin-modified micellar electrokinetic chromatography and laser-induced fluorescence detection by G. Nouadje, M. Nertz and F. Courderc (Toulouse, France) . . . . .	331
Capillary electrophoretic determination of amino acids. Improvement by cyclodextrin additives by Y.-H. Lee and T.-I. Lin (Taipei, Taiwan) . . . . .	335

Determination of thiols by capillary electrophoresis with electrochemical detection using a palladium field-decoupler and chemically modified electrodes by X. Huang and W.T. Kok (Amsterdam, Netherlands) . . . . .	347
Inhibition of dipeptidyl peptidase IV (DP IV) by anti-DP IV antibodies and non-substrate X-X-Pro- oligopeptides ascertained by capillary electrophoresis by T. Hoffmann, D. Reinhold and T. Kähne (Magdeburg, Germany), J. Faust and K. Neubert (Halle, Germany), R. Frank (Heidelberg, Germany) and S. Ansorge (Magdeburg, Germany) . . . . .	355
Studies of complexes between proteases, substrates and the protease inhibitor $\alpha_2$ -macroglobulin using capillary electrophoresis with laser-induced fluorescence detection by O.-W. Reif and R. Freitag (Hannover, Germany) . . . . .	363
Evaluation of an optically active crown ether for the chiral separation of di- and tripeptides by R. Kuhn, D. Riestler, B. Fleckenstein and K.-H. Wiesmüller (Reutlingen, Germany) . . . . .	371
Determination of $\alpha$ -difluoromethylornithine in blood by microdialysis sampling and capillary electrophoresis with UV detection by T. Hu, H. Zuo, C.M. Riley, J.F. Stobaugh and S.M. Lunte (Lawrence, KS, USA) . . . . .	381
Derivatization of dipeptides with 4-fluoro-7-nitro-2,1,3-benzoxadiazole for laser-induced fluorescence and separation by micellar electrokinetic chromatography by I. Beijersten and D. Westerlund (Uppsala, Sweden) . . . . .	389
Capillary zone electrophoretic resolution of recombinant human bone morphogenetic protein 2 glycoforms. An investigation into the separation mechanisms for an exquisite separation by K. Yim, J. Abrams and A. Hsu (Andover, MA, USA) . . . . .	401



















ELSEVIER

Journal of Chromatography A, 716 (1995) 1

---

---

JOURNAL OF  
CHROMATOGRAPHY A

---

---

## Foreword

---

The 7th International Symposium on High Performance Capillary Electrophoresis, HPCE'95, took place in Würzburg, Germany, from 29 January to 2 February 1995. In contrast to the meetings held so far in the southern parts of the USA where the weather conditions were always good, a meeting in Germany during early winter can afford some meteorological "excitement". This time there were heavy rains, causing the river Main adjacent to the meeting place to rise to unexpected heights. The main concern of the chairman before opening the meeting was whether the meeting would have to be cancelled. Undeterred by extensive TV coverage of the floods, their enthusiasm for capillary electrophoresis lured our participants to Würzburg and to HPCE'95.

The number of participants approached that of HPCE'94 in San Diego (700), and almost 400 papers covering a wide range of applications were presented. The large number of participating students showed clearly that CE is a young and attractive separation technique in university research. In the exhibition 16 companies demonstrated their newest developments in instrumentation and supplies for CE.

HPCE'95 proved CE to be a mature technique with sufficient reproducibility for qualitative and quantitative analysis. Several papers described how the quantitative analytical capabilities of HPLC can be achieved with HPCE, but in a

fraction of the time. Numerous industrial applications showed that CE has become a widely accepted separation technique. Miniaturization of CE systems continued to be a major focus for future developments in single molecule detection and in the use of chip technologies.

The success of the meeting is the result of the contributions of many individuals. Special thanks are due to Tom Gilbert for the key role he played in the technical part of running the symposium, and his patience with all the problems arising from the necessary transatlantic communications, and to Shirley Schlessinger who again demonstrated her expertise and skill in meeting administration. To my co-workers I owe thanks for their enthusiastic commitment in helping to run the meeting smoothly. The scientific programme was carefully put together with the advice and help of my co-members of the Advisory Scientific Committee. Last but not least I wish to express my thanks to Dr. Zdenek Deyl for the editorship of this special issue.

Finally, it is my great pleasure to invite you to HPCE'96, to be held in Orlando, FL, 21–25 January 1996, under the chairmanship of Professor Barry L. Karger, Barnett Institute, Northeastern University, Boston, MA.

Saarbrücken, Germany

H. Engelhardt



## Emersion peaks in capillary electrophoresis

Christa L. Colyer, Keith B. Oldham\*

*Department of Chemistry, Trent University, Peterborough, Ontario K9J 7B8, Canada*

### Abstract

An anomalous phenomenon in capillary electrophoresis (CE), referred to as the 'emersion peak,' has been observed. The emersion peak is generated at the inlet end of the capillary whenever this end is temporarily removed from the solution prior to application of the electrophoretic field. This phenomenon, which is believed to have physical origins at the capillary inlet, is transported along the capillary at the rate of electroosmotic flow and is detected by on-column UV absorbance. Emersion peaks have been observed in a CE system with a uniform sodium benzoate electrolyte without sample injection or deliberately-formed concentration boundaries, and are attributed to the adsorption of benzoate at the air–solution interface formed upon emersion of the capillary inlet. Emersion peak size has been found to depend on the number of emersions, the duration of each emersion, the height to which the inlet is raised above the supply electrolyte reservoir during an emersion, the delay between completion of the emersion and application of the electric field, and the cut of the capillary forming the inlet end.

### 1. Introduction

The ability to inject and manipulate extremely small samples in capillary electrophoresis (CE) is, in part, responsible for the widespread use and application of this technique. For example, newly-developed methods of sample injection, such as the slide-type Nano-injector [1] and the Microdrop injector [2] permit reproducible small-volume injections in CE systems. Furthermore, it is now possible to use CE to analyze single biological cells [3–5], or to perform CE on a microchip [6–8]. When dealing with such small samples, the quantitative ability of CE may be compromised. Compensation for sampling biases, in order to improve quantitative precision in CE, has been addressed [9]. However, unintentional sample injection, by way of spontaneous [11] (also referred to as ubiquitous [12])

injection, may still interfere with small samples. Spontaneous injection is facilitated by simply bringing the capillary inlet into contact with (and subsequently withdrawing it from) the sample solution. Grushka and McCormick [12] were the first to investigate this phenomenon, which Dose and Guiochon [10,13] later attributed to diffusion into or out of the capillary inlet. Most recently, Fishman and co-workers [11] more fully characterized spontaneous injection. They proposed that an interfacial pressure difference, formed at the inlet of the capillary upon removal from the sample solution, was responsible for the unintentional injection of sample by way of spontaneous fluid displacement. The intentional use of spontaneous fluid displacement as a method of microcolumn sample injection has also been discussed [14].

However, before the capillary inlet is inserted into and subsequently removed from the sample solution, it is necessary for it to be removed from

\* Corresponding author.

the running electrolyte supply reservoir. We have found that absorbance signals, representing localized enhancements of the running electrolyte concentration and herein referred to as 'emersion peaks,' are generated at the inlet end of the capillary when this end is temporarily removed from the running electrolyte supply reservoir prior to application of the electric field necessary for electrophoresis. When the field is subsequently applied, the emersion peak, which represents a concentration excursion, is swept along the column and past the detector by way of electroosmosis alone in a two-ion electrolyte system. Both electrokinetic and hydrodynamic injections necessitate removal of the capillary inlet from its running electrolyte reservoir, and thus, involve emersion. As such, it is possible that an emersion peak is generated every time a sample is injected, and that this peak may introduce errors if the sample contains a neutral species, because the neutral signal and emersion signal will coincide.

The present work focuses on emersion peaks and does not involve the injection, intentional or otherwise, of a sample. Studies were conducted in a simple CE system with on-column UV absorbance detection and, in most instances, a sodium benzoate solution as the running electrolyte. The size of the emersion peak was found to be dependent on several factors, including: the cut of the capillary inlet, the height, duration and number of emersions, and the delay time between emersion and application of the electric field. During an emersion, an air-solution interface is created at the capillary inlet. We believe that the electrolyte may be positively adsorbed at this interface, and that this enriched interface may enter the capillary by spontaneous fluid displacement [15], thereby generating an emersion peak.

## 2. Experimental

### 2.1. Instrumentation

An Isco Model 3850 capillary electropherograph (Lincoln, NE, USA) with on-column UV

absorbance detection was employed for all experiments described herein. The high-voltage power supply of this instrument was operated in constant voltage (15–30 kV) mode. Emersion peaks were generated as a result of removing either the capillary end from the running electrolyte reservoir housing the high-voltage electrode (prior to positive polarity experiments), or the capillary end from the electrolyte reservoir housing the grounded electrode (prior to negative polarity experiments). No intentional sample injection was conducted. The humidity and temperature inside the capillary compartment were not closely controlled. However, a fan inside the compartment maintained good ambient circulation, and several small, water-filled beakers in the compartment maintained an atmosphere saturated enough with water vapour to prevent significant evaporation from the running electrolyte reservoirs during any given day of experimentation. The analogue current, voltage and absorbance outputs of the instrument were monitored by a Hewlett-Packard Model HP-3497A Data Acquisition Unit which, in turn, was interfaced to a Hewlett-Packard Model HP-9000 (Series 200) computer. Partial control of the CE system, along with data collection, analysis, and storage, was enabled by HP Basic 3.0 computer programs written in-house.

### 2.2. Capillary columns

Fused-silica capillaries with an external polyimide coating were employed in these studies (Polymicro Technologies, Phoenix, AZ, USA). Nominal capillary dimensions were 50  $\mu\text{m}$  inside diameter, 156.5  $\mu\text{m}$  wall thickness, 16  $\mu\text{m}$  coating thickness, while measured dimensions ranged from 75.60 cm to 89.25 cm total length, and 28.70 cm to 59.25 cm working length (that is, length between inlet end and detector). Capillary columns were cut to length using a blunt, Isco ceramic capillary cutter. Optical and scanning electron microscopies were used to examine the cuts. Every effort was made to obtain 'clean' cuts (at 90° to the capillary axis, with no silica debris and no polyimide stripping), although each was inevitably unique and could therefore-lead to



different air–solution interfaces when removed from the electrolyte reservoir.

New capillaries were subjected to a conditioning procedure in order to develop reproducible electroosmotic flow. Conditioning consisted of filling the capillary with 1.0 *M* NaOH (BDH, Toronto, Canada) for one hour, followed by leaving it filled with 0.10 *M* NaOH overnight. The capillary was then flushed sequentially with distilled, deionized water, 0.10 *M* HCl (Baxter/Canlab, Toronto, Canada), and again with water. Despite this initial treatment, reproducible electroosmotic flow was not achieved until the capillary had undergone several weeks of regular use. The most effective method of maintaining the electroosmotic flow-rate at a stable value appeared to be filling the capillary with water for extended periods of time (at least two days) when not in use. After initial capillary conditioning, we therefore adopted a simple treatment which consisted of filling the capillary with water whenever it was idle, followed by refilling the column with fresh water for one hour prior to daily experimentation. With the exception of intentional emersions, care was taken to keep the capillary ends wet at all times, by immersion in running electrolyte during experimentation or in water during storage.

### 2.3. Solutions

The vast majority of emersion peak experiments were conducted with a 20.0 *mM* sodium benzoate (NaBz) solution as the running electrolyte, prepared by dissolving reagent grade NaBz (Caledon, Georgetown, Canada) in deionized and distilled water. The measured pH of this solution was 6.98 at 23°C. However, emersion peak experiments were also conducted with several other running electrolytes, all prepared from analytical grade reagents, including 20.0 *mM* potassium benzoate (KBz) (Aldrich, Milwaukee, WI, USA), 20.0 *mM* sodium salicylate (NaSal) (BDH), and 15.0 *mM* trisodium citrate (Na<sub>3</sub>Cit) (BDH). The measured pH values of these solutions were 7.01 at 20°C, 5.85 at 24°C, and 8.22 at 25°C, respectively. Although the results are not presented here, the emersion of

the capillary inlet from these other electrolytes also resulted in emersion peak formation. Prior to use, all solutions were degassed under vacuum by a water aspirator for approx. one hour after having been filtered through a cellulose acetate syringe filter (pore size 0.45 μm; Nalge Company, Rochester, NY, USA, and Lida, Kenosha, WI, USA).

### 2.4. Procedure

A ‘typical’ emersion experiment involved lifting the inlet end of the capillary above the running electrolyte solution in the supply reservoir for a certain period of time before returning it to its original position. The number, height and duration of emersions were sometimes varied. Upon completion of an emersion, two to five seconds passed (the ‘standard delay’) before application of the electric field. In some instances, this delay time was varied to determine its effect on the size of the emersion peak. Absorbance and current data were recorded while the run was in progress (that is, while the electric field was applied). Following an experiment, two to five minutes (the ‘standard interlude’) routinely elapsed with no field applied before commencement of the next experiment.

Since these experiments do not involve sample injection, it should be noted that the capillary ‘inlet’ does not necessarily refer to that end of the capillary physically located near the injection port. ‘Inlet’ simply refers to the end through which electroosmotic flow carries solution into the capillary. In all cases, emersion peaks resulted from emersion of the capillary inlet, but in some cases (specifically, positive polarity experiments) this involved emersion of the capillary end nearest to the high-voltage electrode and in other cases (specifically, negative polarity experiments) this involved the capillary end nearest to the grounded electrode. The solution reservoir in which the inlet end of the capillary is submerged is called the ‘supply reservoir,’ while the outlet end is submerged in the ‘receiving reservoir.’ Care was taken to equalize the solution levels in the two reservoirs, except when hydrodynamic flow was intentionally induced.

### 3. Results

The initial discovery of an emersion peak occurred by accident following a trimming of the inlet end of an installed capillary column in order to remove a suspected blockage. When the trimmed end was returned to its original position in the 20.0 mM NaBz supply electrolyte reservoir, and the electric field necessary for electrophoresis was applied, a prominent absorbance signal appeared in the capillary electropherogram after a time corresponding with that of a marker of electroosmotic flow. The field was then disabled and several minutes were allowed to pass before the field was reapplied. The inlet end of the capillary was not removed from solution in this second instance, and no absorbance signal was observed in the corresponding electropherogram. Thus, it appeared as if the removal of the column end from the supply reservoir, necessitated by the trimming procedure, was somehow responsible for the absorbance signal in the first run. To test the validity of this hypothesis, we conducted experiments employing intentional emersion manoeuvres, including variations of the number of emersions, the duration of the emersion, the 'delay time' (that is, the time elapsed between completion of an emersion and application of the high voltage), the height to which the capillary inlet was lifted during an emersion, the position of the capillary outlet relative to the elevated inlet, the capillary cut, and the concentration of the running electrolyte. Results from each variation of emersion experiment are presented here, and the possible causes of the emersion peak, as inferred from these results, are considered in the Discussion section of this paper.

#### 3.1. Number of emersions

The size of the emersion peak was found to increase with the number of emersions of the capillary inlet. Multiple emersions were conducted by removing the capillary inlet from the supply electrolyte reservoir to some specified height for some specified duration, and then returning the capillary inlet to its original posi-

tion. Then, within less than two seconds, the inlet was removed again to the same height for the same length of time. This procedure was repeated until the desired number of emersions had been conducted. Typical electropherograms generated after three and five emersions of the inlet end of the capillary are shown in Fig. 1. During each emersion, the capillary inlet was raised 17 mm above the level of solution in the supply reservoir for no more than two seconds. The amounts of NaBz representative of these emersion peaks, along with emersion peaks generated after two and ten emersions of a given capillary inlet, are shown in Fig. 2. For five or fewer emersions, the size of the emersion peak appears to depend linearly on the number of emersions. Peak size levels off, however, after ten emersions, perhaps indicating that some sort of saturation process occurs.

#### 3.2. Duration of emersion

The time spent out of the supply reservoir by an elevated capillary inlet was varied in order to determine its effect on the size of the resulting emersion peak. Increasing the duration of the emersion from two seconds or less to two minutes resulted in a linear increase in emersion peak size, as shown in Fig. 3. These were single

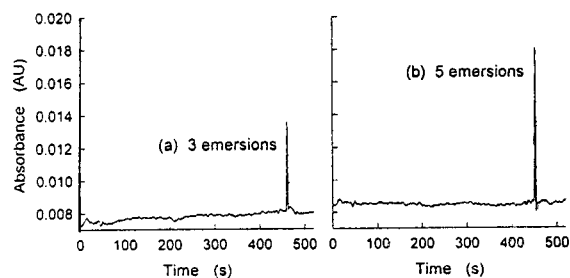


Fig. 1. Capillary electropherograms showing typical emersion peaks resulting from (a) 3 emersions and (b) 5 emersions of the capillary inlet, each to a height of 17 mm above the level of solution in the supply reservoir for  $\leq 2$  s. Following the emersions, a 2–5 s (standard) delay occurred prior to application of a constant voltage of 24.97 kV across the 89.25 cm long capillary (inlet-to-detector length: 59.25 cm). The original running electrolyte was 20.0 mM NaBz and detection was at 225 nm.

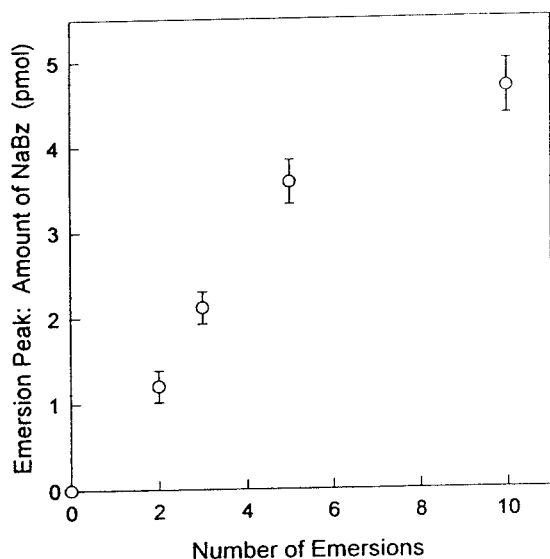


Fig. 2. The amount of NaBz representative of an emersion peak as a function of the number of emersions of the capillary inlet. Error bars are based on propagated error in the calculated amounts of NaBz. Experimental conditions as described in Fig. 1.

emersion experiments, with the capillary inlet raised 17 mm above the level of solution in the supply reservoir. Furthermore, these emersion peak experiments were conducted by emerging the end of the capillary located in the electrolyte reservoir housing the grounded electrode and subsequently applying a negative voltage. Thus, the capillary end located at the grounded side of the apparatus served as the 'inlet' for these experiments. Similar results were obtained when the high-voltage end served as inlet, indicating that the phenomenon of the emersion peak is in no way dependent on some feature of the high-voltage end of the apparatus.

### 3.3. Delay time

Under normal experimental conditions, a two to five second delay (referred to as the 'standard delay') occurred between the time the capillary inlet was replaced in the electrolyte reservoir following an emersion and the subsequent application of high voltage. Since there is no electric field applied along the column during this delay,

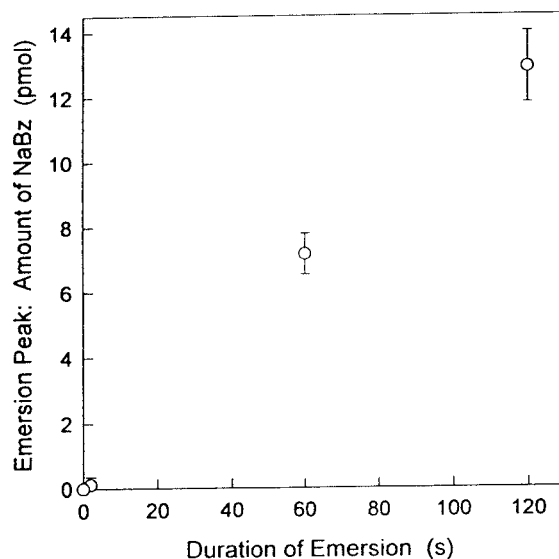


Fig. 3. The amount of NaBz representative of an emersion peak as a function of the period of time during which the capillary inlet was removed from solution during an emersion. Error bars are based on propagated error in the calculated amounts of NaBz. Results are for single emersions to a height of 17 mm, with 20.0 mM NaBz running electrolyte, an applied voltage of  $-25.04$  kV, inlet-to-detector and total capillary lengths of 28.70 cm and 82.35 cm, respectively, and detection at 225 nm. Standard delay time was employed in all cases.

there will be no migration or electroosmosis taking place. However, transport of NaBz into or out of the column can occur by diffusion during the delay if a concentration gradient exists at the interface between the solution in the capillary and that in the bulk reservoir [10]. Furthermore, replacing the capillary inlet in the electrolyte reservoir may initiate convective mixing at the interface between the solution in the capillary and that in the bulk reservoir. A study was undertaken to determine the effect of delay time on the size of the emersion peak resulting from 10- and 60-s single emersions. Different capillary inlets were used for the 10- and 60-s emersion experiments. In all cases, the inlet was raised to a height of 17 mm above the level of solution in the supply reservoir during emersion. The amounts of NaBz representative of the resulting emersion peaks are shown as a function of the delay time in Fig. 4. The amount of NaBz

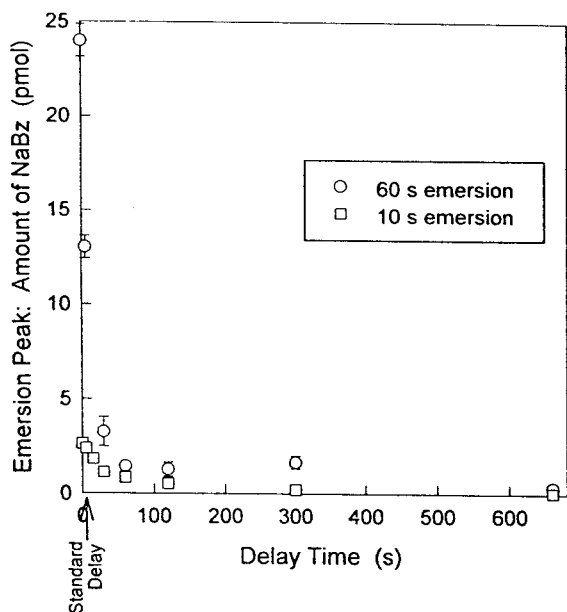


Fig. 4. Emersion peak, represented as an amount of NaBz, as a function of the delay time (that is, the time between replacing the capillary inlet in the electrolyte reservoir following an emersion and the subsequent application of high voltage).  $\circ$  = Results from single, 60 s emersions to a height of 17 mm; with 20.02 mM NaBz running electrolyte, 15.00 kV applied voltage, capillary length 87.30 cm, inlet-to-detector length 50.20 cm, and detection at 225 nm.  $\square$  = Results from single, 10 s emersions to a height of 17 mm; with 20.00 mM NaBz, 15.00 kV applied voltage, capillary length 85.50 cm, inlet-to-detector length 48.75 cm and detection at 225 nm. Standard deviation of the mean associated with each data point is less than the size of the data symbol or is shown as an error bar.

in the 10- and 60-s emersion peaks appears to decrease exponentially at short delay times. Regardless of delay time, emersion peaks generated by 60-s emersions are always larger than those generated by emersions of shorter duration (10 s).

### 3.4. Height of emersion

The capillary positioner of the electropherograph allows the capillary inlet to be lifted to a maximum height of 17 mm above the level of solution in the supply electrolyte reservoir. Thus, in a 'normal' emersion experiment, the inlet is raised 17 mm above the solution for some period

of time, as discussed previously. It is possible, however, to emerge the capillary inlet to shorter heights, and it was found that the size of the emersion peak was dependent upon the height of the emersion. For 10- and 60-s single emersions with standard delay times, the effect of emersion height on the amount of NaBz in the emersion peak is shown in Fig. 5. As expected, the emersion peaks resulting from 60-s emersions are larger at every emersion height than those resulting from 10-s emersions. Both durations of emersion, however, gave rise to increasingly large emersion peaks as the height of the emersion increased. For emersion heights below 10 mm, the amount of NaBz in the emersion peak appears to increase linearly with height. Above 10 mm, however, the amount of NaBz in the emersion peak apparently begins to level off. This would indicate that some sort of saturation

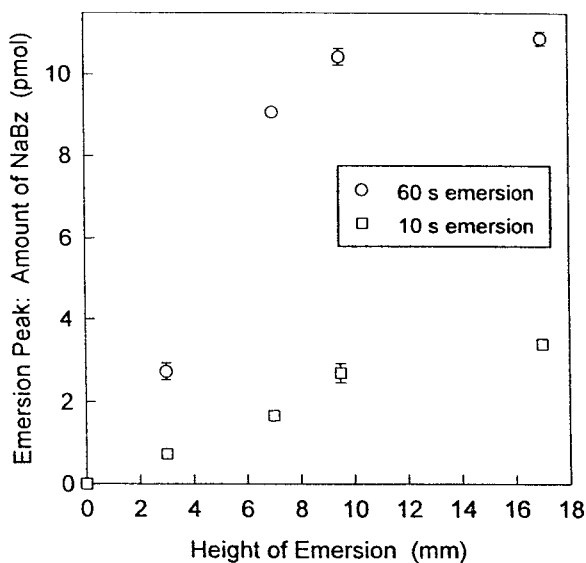


Fig. 5. Emersion peak, represented as an amount of NaBz, as a function of the height to which the capillary inlet was raised above the level of solution in the supply reservoir during single 10 s ( $\square$ ) and 60 s ( $\circ$ ) emersions. Experimental conditions: 20.01 mM NaBz running electrolyte, 15.00 kV applied voltage, inlet-to-detector and total capillary lengths of 48.75 cm and 75.60 cm, respectively, and detection at 225 nm. Standard delay time was employed in all experiments. Standard deviation of the mean associated with each data point is less than the size of the data symbol or is shown as an error bar.

point or upper limit to the size of an emersion peak was being approached.

### 3.5. Position of capillary outlet relative to emersed inlet

By emerging the capillary inlet, a gravitational head is created, thereby generating a hydrodynamic flow of solution in the capillary toward the outlet end. The extent of this flow is limited by the surface tension of the solution in the capillary, which prevents solution from receding into the column and leaving behind a gap or slug of air. The size of the gravitational head can be altered not only by altering the height of the emersion, but also by changing the elevation of the capillary outlet, together with the receiving reservoir, during an emersion. Such outlet elevation can 'compensate' for some or all of the inlet elevation, thus reducing the effective height of the emersion. The difference between the elevation of the capillary inlet and the capillary outlet/receiving reservoir is referred to as the 'inlet head'. When the outlet is raised above the inlet, the inlet head is negative. The effect of inlet head on emersion peak size was determined by conducting a set of experiments in which the capillary outlet, together with the receiving reservoir, was raised to varying heights just before the inlet was emersed for 60 s to its maximum height (17 mm) above the level of solution in the supply reservoir. At the end of each emersion, the capillary inlet and outlet were respectively returned to their original positions, and the high voltage applied after the standard delay time had elapsed. The results of these experiments are shown in Fig. 6. For positive inlet heads, the amount of NaBz representative of the emersion peak increases with increasing head, just as it did with increasing emersion height in Fig. 5. The size of an emersion peak for any given positive inlet head in Fig. 6, however, differs from that in Fig. 5 for a comparable emersion height. This apparent discrepancy may be attributed to the fact that the two sets of experiments were conducted one month apart and so some property of the capillary inlet may well have changed due to conditioning, wear, etc. (see section

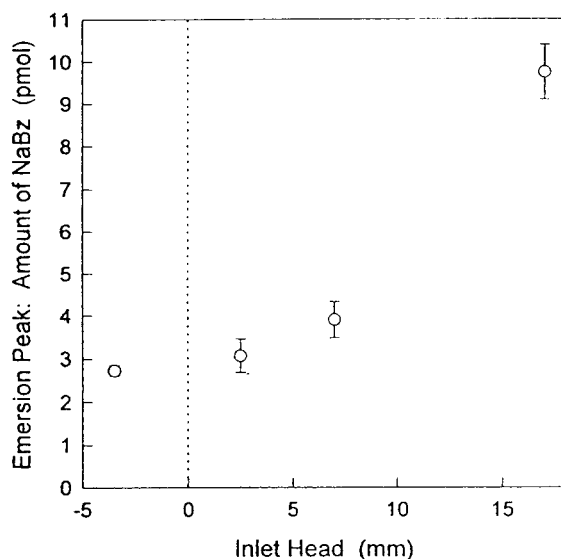


Fig. 6. The amount of NaBz representative of an emersion peak as a function of the inlet head (that is, the difference between the elevation of the capillary inlet and outlet). Error bars are based on the standard deviation of the mean associated with each point. Results are for single, 60 s emersions with inlet height equal to 17 mm in all cases. Capillary length: 85.50 cm and inlet-to-detector length: 48.75 cm. Other experimental conditions are as described in Fig. 5.

entitled Capillary cut). The emersion peak does not disappear when the inlet head is negative; it is simply diminished in size relative to peaks generated from positive inlet heads during emersion. This is in agreement with the findings of Fishman et al. [11] and Grushka and McCormick [12] who found that spontaneous sample injection could occur even when hydrostatic flow is towards the inlet end of the capillary.

### 3.6. Capillary cut

As mentioned above, the cut of the capillary forming the inlet end can have a significant effect on the size of emersion peaks generated at that end. Optical and scanning electron microscopies were used to determine that the cuts appeared clean, although there was no way to ensure that the wall thickness at all points along the capillary was equal, or that the angle of the cut relative to the capillary axis was exactly right. Hence, each

Table 1  
The effect of capillary cut on the amount of NaBz in emersion peaks

Capillary cut <sup>a</sup>	Capillary length (cm)	Inlet-to-detector length (cm)	Emersion peak: amount of NaBz <sup>b</sup> (pmol)
a	87.30	50.20	13.2 ± 0.6 ( <i>n</i> = 13)
b	86.45	49.70	2.2 ± 0.3 ( <i>n</i> = 8)
c	85.50	48.75	9.7 ± 0.5 ( <i>n</i> = 10)

<sup>a</sup> Electrophoresis experiments conducted with cuts a to c of this capillary involved a single emersion of the inlet to a height of 17 mm for 60 s with an applied voltage of 15.00 kV. In all cases, the running electrolyte was 20.0 mM NaBz, the standard delay time was employed, and detection was at 225 nm.

<sup>b</sup> Amounts of NaBz represent averages of the number *n* of replicate experiments indicated in parentheses, expressed ± standard deviation of the mean.

cut exposed a new and different annulus of the capillary to the solution. These different cuts or annuli resulted in different sizes of emersion peaks, as documented for one particular capillary in Table 1. For this capillary, the average amount of NaBz in the peak generated by one, 60 s emersion to a height of 17 mm, ranged from 2.2 (± 0.3) pmol to 13.2 (± 0.6) pmol, depending upon the cut. Even though the height of emersion, the number of emersions, and the duration of emersion were not varied, the size of the resulting emersion peaks in these experiments differed significantly, therefore indicating the importance of the capillary cut.

### 3.7. Running electrolyte concentration

Although the vast majority of our experiments were conducted using 20.0 mM NaBz as the

running electrolyte, some involved other electrolyte concentrations. Table 2 shows the effect of running electrolyte concentration on emersion peak size for single emersions of capillary cut 'c' to a height of 17 mm above the level of solution in the supply reservoir. The enhancement, equal to the amount of NaBz calculated from emersion peak size, is an absolute quantity. That is, it is not calculated relative to the running electrolyte concentration, but rather, it represents an absolute increase in the amount of NaBz present. No trend towards increasing or decreasing peak size with increasing electrolyte concentration is evident from the results in Table 2. In fact, within the ranges of uncertainty given by the standard deviations associated with each amount of NaBz, the enhancement represented by the emersion peaks appears to be constant, regardless of running electrolyte concentration.

Table 2  
The effect of running electrolyte concentration on the amount of NaBz in emersion peaks resulting from single emersions (10 and 60 s) of capillary cut c to a height of 17 mm

NaBz concentration (mM)	Amount of NaBz representative of emersion peaks <sup>a</sup> (pmol)	
	10 s Emersion peak	60 s Emersion peak
10.00	1.9 ± 0.2	7.3 ± 0.2
20.00	2.4 ± 0.2	9.7 ± 0.5
29.99	1.9 ± 0.4	8.6 ± 0.1

Other experimental conditions: 15.00 kV applied voltage, 85.50 cm capillary length, 48.75 cm inlet-to-detector length, standard delay time, and detection at 225 nm.

<sup>a</sup> Amounts of NaBz represent averages of 2 to 10 replicate runs, and are expressed with average deviations or standard deviations of the mean.

#### 4. Discussion

It is evident from these results that a narrow zone of enriched electrolyte is somehow being formed at the capillary inlet during emersion, and that this zone is then swept along the column and past the detector by electroosmosis. The result is the appearance of an emersion peak: a small but well-defined peak in the electropherogram corresponding to the time of electroosmotic flow, appearing even in the absence of any intentionally (or unintentionally) loaded sample. Based on our experimental results, the most feasible explanation for the emersion peak phenomenon is the adsorption of benzoate ions at the air–solution interface created at the elevated capillary inlet during emersion. It may be thermodynamically favourable [16] for benzoate ions (or other organic anions) to align themselves at the air–solution interface, with sodium counterions (or other cations) close by in the solution, thereby creating a region of ‘enriched’ sodium benzoate solution. This region would then be ‘loaded’ into the column by way of spontaneous fluid displacement [15], forming a concentration excursion which would later be swept past the detector by electroosmotic flow, and which would appear as an emersion peak.

It is useful to compare the amount of NaBz representative of a ‘typical’ emersion peak to the amount which could be adsorbed at a ‘typical’ air–solution interface in order to determine the feasibility of this mechanism of peak formation. If we assume that a monolayer of benzoate is adsorbed at the air–solution interface, and that each benzoate ion occupies  $60 \text{ \AA}^2$  [17], then the surface concentration of benzoate would be about  $3 \cdot 10^{-6} \text{ mol m}^{-2}$ . If the interface formed is hemispherical (concave inside the capillary), the amount of adsorbed benzoate would be only 0.01 pmol, whereas at a pendant hemispherical interface (extending to the outer capillary wall), the amount of adsorbed benzoate would be 0.6 pmol. Often, the droplet remaining on the capillary inlet as a result of emersion extends beyond the annulus of the capillary [18]. At such a pendant ‘extended’ hemispherical interface (extending from the annulus along the capillary wall

to a distance equal to the previous immersion), the amount of adsorbed benzoate would be 19 pmol. The last two of these proposed geometries for the air–solution interface would allow for sufficient adsorption of benzoate to produce an enhancement ‘typical’ of an emersion peak, and so adsorption may be a possible explanation for this phenomenon. Furthermore, the last two geometries would require the subsequent action of spontaneous fluid displacement to transport the enhanced electrolyte region inside the capillary inlet. Without spontaneous fluid displacement, the enriched region of solution in the pendant droplet would simply be ‘washed away’ upon reimmersion of the inlet in the supply electrolyte reservoir, and so no emersion peak would be observed.

According to this proposed mechanism of emersion peak formation, there are three main factors which could affect peak size: the size/shape of the initial air–solution interface; the time during which adsorption can occur at the interface; and the extent to which the enriched interface is transported into the capillary. These three factors could, in turn, be affected by variation of the number, duration, and height of emersions, as well as by variation of the capillary cut and running electrolyte concentration.

Increasing the number of emersions, or increasing the duration of any given emersion would provide a greater opportunity for the adsorption of benzoate at the air–solution interface, and for the subsequent transport of the enriched interface into the capillary column by way of spontaneous fluid displacement. With repeated emersions, new air–solution interfaces are being generated, and benzoate adsorption may occur at each new interface. Consequently, one would expect the size of the resulting emersion peak to increase with the number of emersions, as illustrated in Fig. 2. However, when more than one emersion is conducted, the duration of each is often brief ( $< 2 \text{ s}$ ). This brief emersion duration does not provide much time for the adsorbance-enriched electrolyte region to be transported into the capillary by spontaneous fluid displacement. Increasing the duration of any given emersion should provide additional

time for adsorption and/or spontaneous fluid displacement, thus producing a larger emersion peak. Such results were, indeed, observed (see Fig. 3) lending support to the interfacial adsorption hypothesis for emersion peak formation.

Regardless of the duration of emersion, increasing the emersion height would provide a greater driving force for fluid displacement by way of hydrodynamic flow. Such an increased opportunity for fluid displacement would allow more of the adsorption-enriched solution to enter the capillary inlet, and hence, the resulting emersion peak would be larger. Fig. 5 illustrates such an increase in emersion peak size with increasing emersion height.

It has been postulated [11] that increasing the emersion height may also increase evaporation from the capillary inlet, due to removal of the inlet from the humidified region directly above the supply electrolyte reservoir. If, indeed, evaporation from the capillary inlet was occurring, this may be construed as a possible contributor to the emersion peak. At first glance, the evaporation of solvent (water) from the running electrolyte on or just inside the elevated capillary inlet may be thought to leave behind a locally more concentrated region of electrolyte which would be seen as an emersion peak. However, Fishman et al. [11] found that evaporation from the capillary inlet did not simply concentrate the solution present at the inlet, but rather, resulted in solution loss from the inlet. In the present work, such solution loss would be expected to reduce the size of the emersion peak, since the adsorbance-enriched solution surface would be lost to evaporation. Emersion peaks, however, were seen to increase in size as the inlet was removed to greater heights (and supposedly less humid atmospheres) and thus, evaporation does not appear to significantly affect our results.

Furthermore, our study of the position of the capillary outlet relative to the emersed inlet does not indicate any significant variation in the humidity in the capillary compartment (which housed both the capillary inlet and outlet). During these experiments, the capillary inlet was

always lifted to the same position (17 mm) above the supply electrolyte reservoir, thereby minimizing any possible variation in humidity. The capillary outlet, however, together with the receiving electrolyte reservoir, was lifted to various heights. This resulted in a change in the 'inlet head,' that is, the difference between the elevation of the capillary inlet and the capillary outlet. Such a change in the inlet head would be expected to change the driving force for hydrodynamic flow and, thus, the extent of transport of the adsorption-enriched interface into the capillary inlet. If evaporation was solely responsible for the formation of the emersion peak, we would expect to see no variation in peak size during these experiments. However, the emersion peak size increased with increasing inlet head (see Fig. 6), suggesting that the transport of the enriched air-solution interfacial region into the capillary inlet is critical to the formation of an emersion peak. Perhaps surprisingly, the emersion peak existed even for negative inlet heads (that is, when hydrodynamic flow would be towards the capillary inlet). Others [11,12] have similarly found that spontaneous sample injection occurs even when there is solution flow towards the capillary inlet. It is reasonable to expect that adsorption of benzoate at the air-solution interface would occur regardless of the direction of solution flow, although the adsorption-enriched region would not be transported into the capillary as readily when solution flow is towards the inlet. The fact that emersion peak size is greatly reduced for negative inlet heads (see Fig. 6) indicates that less of the adsorption-enriched region is finding its way into the capillary. Perhaps some diffusive process or convective mixing is ensuring that some small amount of the enriched solution makes its way into the capillary even without the assistance of hydrodynamic flow or spontaneous fluid displacement.

To further investigate the effects of capillary compartment humidity on emersion peak formation, we intentionally generated a 'dry' atmosphere inside the capillary compartment. This was achieved by replacing the small water-filled beakers normally present in the compartment with dishes of Drierite (BDH): a hygroscopic



CaSO<sub>4</sub> compound coated with CoCl<sub>2</sub> indicator. The average amount of NaBz representative of emersion peaks was 11.5 ( $\pm$  2.1) pmol for the 'dry' capillary compartment under the following conditions: single, 60 s emersions to 17 mm above supply electrolyte reservoir; capillary length: 87.30 cm; inlet-to-detector length: 50.20 cm; applied voltage: 15.00 kV. When the Drierite was removed and the small water-filled beakers replaced in the capillary compartment, the average amount of NaBz representative of the subsequently generated emersion peaks was 13.3 ( $\pm$  1.1) pmol. Although the 'dry' atmosphere resulted in nominally smaller emersion peaks, there is no significant difference between the effects of 'dry' and 'wet' atmospheres on emersion peaks when the standard deviations of the means are considered.

To intentionally cause evaporation from the capillary inlet during some experiments, a stream of dry argon gas (Praxair, Mississauga, Canada) was directed at the capillary just above the inlet during emersion. All other conditions were the same as for the emersion experiments described above with water-filled beakers in the capillary compartment. The average size of emersion peaks generated with Ar flowing (two experiments) was only 7.4 ( $\pm$  0.2) pmol, compared to 13.3 ( $\pm$  1.1) pmol without Ar. This significant difference appears to support the idea of solution loss (as opposed to solution concentration) due to evaporation, thereby resulting in the diminution of emersion peak size. Of course, typical variations in humidity that may occur in our capillary compartment would never be as extreme as the effect of a direct stream of dry Ar gas, and so we may consider the effects of 'normal' evaporation on our emersion peaks to be minimal.

Another factor that appears to affect emersion peak size is the actual inlet itself (its shape, size, surface properties, etc.). This effect is confirmed by Cohen and Grushka [19], who have discussed the influence of capillary cut on separation efficiency and peak shape. Table 1 shows that similar emersion experiments conducted with different capillary inlets result in different emersion peaks. Factors such as surface morphology,

wettability, outside diameter, and angle of cut can modify the air–solution interface at the capillary inlet [11]. If adsorption of benzoate at the air–solution interface is indeed responsible for the formation of the emersion peak, then it is reasonable to expect to see variation in emersion peak size with variation, however subtle, of the capillary inlet. Optical and scanning electron microscopies have confirmed that each cut of the capillary is unique and may consequently lead to unique air–solution interfaces upon emersion.

Finally, our study of the effect of running electrolyte concentration on emersion peak size provides further support for interfacial adsorption as the mechanism of emersion peak formation. Virtually identical emersion peaks were obtained for emersion experiments conducted with sodium benzoate solutions ranging from 10.0 to 30.0 mM (see Table 2). Under moderate conditions, the size and shape of the air–solution interface formed at the capillary inlet should be almost independent of running electrolyte concentration. Thus, the amount of benzoate which can be adsorbed at that interface should be independent of running electrolyte concentration: different electrolyte concentrations simply represent different 'pools' from which the same maximum amount of surface-adsorbed benzoate is supplied. If the extent of surface adsorption is the same, then the resulting emersion peaks will be the same despite different running electrolyte concentrations, as was observed experimentally. These results support the idea of surface adsorption as a possible mechanism of emersion peak formation.

## 5. Conclusions

The existence of absorbance signals, representing localized enhancements of the running electrolyte concentration and referred to as 'emersion peaks,' has been documented. Emersion peaks are generated at the capillary inlet provided the inlet is removed from solution for some brief period of time before commencing the electrophoretic run. Emersion peaks repre-

sent concentration excursions which travel electroosmotically from the inlet and past the detector. The mechanism of emersion peak formation is believed to be the adsorption of the electrolyte anion (benzoate in these experiments) at the air–solution interface generated at the capillary inlet during emersion. Prior to application of the electric field for electrophoresis, the surface-enriched region of solution is transported into the capillary by way of spontaneous fluid displacement or hydrodynamic flow. Factors which affect the properties of the air–solution interface were shown to affect the emersion peak. These include the number of emersions, the duration of each emersion, the height to which the capillary inlet is lifted above the supply electrolyte reservoir during an emersion, and the capillary cut. In addition, emersion peak size was found to depend on the delay time between replacement of the capillary inlet in the supply electrolyte reservoir following an emersion and the subsequent application of the electric field. Evaporation which may occur under typical ambient conditions did not significantly affect emersion peak size.

Since it is necessary to emerge the capillary inlet prior to any sort of sample injection, an emersion peak would be generated in addition to any sample peaks in routine capillary electrophoresis. The emersion peak would coincide with the absorbance signal of any neutral sample component. Even in the absence of any neutrals, the emersion peak would appear at a time corresponding to electroosmotic flow and thus, could be mistaken as a bona fide neutral component of the sample. Thus, care must be taken to minimize the size of the emersion peak so that it will not lead to quantitative errors in capillary electrophoresis. Emersion peaks could be eliminated by designing strategies for sample injection that do not require emersion, or could be diminished by reducing the amount of electrolyte adsorbed at the air–solution interface or by limiting the transport of the adsorbance-enriched solution into the capillary inlet. Reducing the amount of adsorbed electrolyte could be achieved by minimizing either the duration or number of emersions, or by minimizing the size

of the air–solution interface (for example, by using capillaries with smaller outside diameters). Limiting the transport of the adsorbance-enriched solution into the capillary could be achieved by minimizing either the duration of the emersion or the height of the emersion (to minimize the contribution of forward hydrodynamic flow to the transport of the enriched solution). Also, countering spontaneous fluid displacement with hydrodynamic flow in the opposite direction (by creating, for example, a negative inlet head) would limit transport of the enriched solution into the capillary. At the very least, care should be taken to ensure that emersion of the capillary inlet is reproducible (same height, duration, etc.), that the inlet itself remains unchanged, and that the same delay time exists between emersion and initiation of an electrophoretic separation. In this way, it should be possible to minimize variability in the emersion peak size and, therefore, minimize the impact of emersion peaks on capillary electrophoresis experiments.

### Acknowledgements

We thank Dr. Artjom Sokirko of the Trent University Chemistry Department for many helpful discussions regarding this work. Also, we would like to acknowledge the generous financial support of the I.O.D.E., the Trent-Queen's Graduate Program in Chemistry, and the Natural Sciences and Engineering Research Council of Canada (NSERC).

### References

- [1] T. Hanai and J. Tsuruta, *Instrum. Sci. Technol.*, 22 (1994) 151.
- [2] D. Ziele, O. Brüggemann, M. Döring, R. Freitag and K. Schügerl, *J. Chromatogr. A*, 669 (1994) 254.
- [3] T.M. Olefirowicz and A.G. Ewing, *Chimia*, 45 (1991) 106.
- [4] A.G. Ewing, *J. Neurosci. Meth.*, 48 (1993) 215.
- [5] H.K. Kristensen, Y.Y. Lau and A.G. Ewing, *J. Neurosci. Meth.*, 51 (1994) 183.

- [6] D.J. Harrison, K. Fluri, K. Seiler, Z. Fan, C.S. Effenhauser and A. Manz, *Science*, 261 (1993) 895.
- [7] K. Seller, Z.H. Fan, K. Fluri and D.J. Harrison, *Anal. Chem.*, 66 (1994) 3485.
- [8] A. Manz, E. Verpoorte, C.S. Effenhauser, N. Burggraf, D.E. Raymond and H.M. Widmer, *Fresenius J. Anal. Chem.*, 348 (1994) 567.
- [9] T.T. Lee and E.S. Yeung, *Anal. Chem.*, 64 (1992) 1226.
- [10] E.V. Dose and G. Guiochon, *Anal. Chem.*, 64 (1992) 123.
- [11] H.A. Fishman, N.M. Amudi, T.T. Lee, R.H. Scheller and R.N. Zare, *Anal. Chem.*, 66 (1994) 2318.
- [12] E. Grushka and R.M. McCormick, *J. Chromatogr.*, 471 (1989) 421.
- [13] E.V. Dose and G.A. Guiochon, *Anal. Chem.*, 63 (1991) 1063.
- [14] H.A. Fishman, R.H. Scheller and R.N. Zare, *J. Chromatogr. A*, 680 (1994) 99.
- [15] A. Marmur, in M.E. Schrader and G.I. Loeb (Editors), *Modern Approaches to Wettability: Theory and Applications*, Plenum Press, New York, 1992, Ch. 12.
- [16] N.K. Adam, *The Physics and Chemistry of Surfaces*, Oxford University Press, London, 3rd ed., 1941, Ch. III.
- [17] E.G. Lewars, Optimized geometry calculation by Spartan SGI Version 3.1.3GL.
- [18] H.A. Fishman, personal communication, Dec. 1994.
- [19] N. Cohen and E. Grushka, *J. Chromatogr. A*, 684 (1994) 323.



## Dynamic simulator for capillary electrophoresis with in situ calculation of electroosmosis

Richard A. Mosher<sup>a</sup>, Chao-Xuan Zhang<sup>b</sup>, Jitka Caslavská<sup>b</sup>, Wolfgang Thormann<sup>b,\*</sup>

<sup>a</sup>Center for Separation Science, University of Arizona, Tucson, AZ 85721, USA

<sup>b</sup>Department of Clinical Pharmacology, University of Berne, Murtenstrasse 35, CH-3010 Berne, Switzerland

### Abstract

A dynamic computer model for the simulation of open-tubular capillary electrophoresis which includes in situ calculation of electroosmosis along the capillary column is described. For each column segment, electroosmosis is calculated with the use of a wall mobility, the voltage gradient and the dissociation of the wall represented by the dissociation of a weak monovalent acid. Then, the bulk capillary flow is taken to be the average of all of the segment flows and considered to represent a plug flow. This simple approach permits the combined simulation of the temporal behavior of electroosmosis and electrophoresis. Comparison of simulation data obtained with a wall  $pK$  of about 6 and a mobility between  $5 \cdot 10^{-8}$  and  $7 \cdot 10^{-8}$   $m^2/V \cdot s$  with data produced in untreated fused-silica capillaries shows that the model provides a good estimate of the magnitude and distribution of electroosmosis when having buffers of  $pH > 5.5$ . For lower  $pH$ , a  $pK$  lower than 6 has to be used, this representing a rough approximation only. The model also provides the whole dynamics of all components, the electrical column properties, and emulated detector responses for direct and indirect optical, conductivity,  $pH$  and electrochemical detection at specified capillary locations.

### 1. Introduction

Computer simulation of electrophoresis has demonstrated considerable value as a research tool. Many examples of qualitative and even quantitative agreement between predictions and experimental results have confirmed the utility of simulations for the prediction of separability, separation dynamics, zone characteristics and boundary structure, and also for the reproduction and explanation of some experimentally observed phenomena. Although most of the simulation work performed so far was limited to quiescent solution [1–4], models which include

imposed plug flow have been created, particularly to simulate the buffer and sample dynamics in open-tubular capillary electrophoresis [5–7] and in isotachopheresis with a counterflow [8].

In capillary electrophoresis, electrokinetic separations are carried out in capillaries or narrow-bore tubes having radii  $< 0.5$  mm. Instrumentation with open-tubular, fused-silica capillaries of very small I.D. (25–75  $\mu m$ ) is now available, in which electroosmotic and electrophoretic mass transport occur concomitantly. Electroosmosis thus plays a pivotal role in this process. It is dependent on surface charge ( $pH$ ), the electric field determined by current density and conductivity (composition of the solutions present in the capillary) and viscosity. These

\* Corresponding author.

three parameters are typically constant in capillary zone electrophoresis in which the sample is the only discontinuous element present, but may vary in configurations consisting of discontinuous buffer systems, such as capillary isotachopheresis and capillary isoelectric focusing.

The dynamic computer model developed at the University of Arizona [1–3] was adapted for use on a PC [4] and has also been modified to allow more specific treatments of capillary electrophoresis, including the addition of imposed plug flow along the separation axis and emulation of solute monitoring along specified locations along the capillary [7]. With this approach, the temporal behavior of electroosmosis cannot be predicted based on the calculated dynamics of the column properties, and thus simulated sample and buffer dynamics are dependent on the flow parameters initially imposed. These shortcomings prompted an extension of the model to include in situ calculation of electroosmosis. In this paper, a simple model for computer simulation of electroosmosis in capillary electrophoresis which is based on the dissociation of the silanol surface groups of the capillary wall is described. It predicts (i) the temporal behavior of electroosmosis and (ii) the electroosmotic pumping activity of each fluid element (segment) along the capillary column at specified time points after power application and provides the whole dynamics of all components, pH, conductivity, voltage gradient, current density and column resistance.

## 2. Theoretical

The dynamic computer model has been described in detail previously [1–4,7]. In the interest of clarity, the major points are outlined here. The model is one dimensional and based on the principles of electroneutrality and conservation of mass and charge. Isothermal conditions are assumed and relationships between the concentrations of the various species of a component are described by equilibrium constants. The model is capable of treating biprotic ampholytes, weak and strong monovalent acids and bases and

proteins. Component fluxes are computed on the basis of electromigration and diffusion in quiescent solution [1–4] or in presence of an imposed constant or time-dependent plug flow along the separation axis [7]. Initial conditions which must be specified for a simulation include the distribution of all components, the diffusion coefficient and net charge–pH relationships of the proteins, the p*K* and mobility values of the buffer constituents, the current density or applied constant voltage, the flow constants, the duration of the current flow, the column length and its segmentation and the permeabilities of the ends of the separation space. The program outputs concentration, pH and conductivity profiles as functions of time and allows the presentation of these data either as profiles along the column at specified time intervals or as data which would be produced by a detector at a specified column location, i.e., segment number.

The model for capillary electrophoresis with superimposed plug flow [7] has now been extended with the option of the in situ calculation of electroosmosis along the capillary column. For each column segment *i*, electroosmosis is calculated with the use of a wall or absolute electroosmotic mobility,  $\mu_0$ , the voltage gradient,  $E_i$ , and the degree of ionization of the wall,  $\alpha_i$ :

$$v_{EO,i} = \mu_0 E_i \alpha_i \quad (1)$$

In the present approach, the dissociation of the silanol groups of the capillary surface was assumed to be the only contribution to surface charge. The wall dissociation is therefore that of a weak monovalent acid for which the degree of ionization is given by

$$\alpha_i = 10^{(pH_i - pK)} / [1 + 10^{(pH_i - pK)}] \quad (2)$$

where p*K* is the p*K*<sub>a</sub> value of silanol (p*K* of the wall) and pH<sub>*i*</sub> is the pH of the solution in the capillary segment. The degree of ionization varies from 0 to 1.

In analogy with Darcy's equation, which is valid for pressure-driven flow, the bulk capillary flow is taken to be the average of all of the segment flows, i.e. the electroosmotic velocity in

open tubular fused-silica capillaries is computed by

$$v_{EO} = \frac{1}{n} \sum_{i=1}^n v_{EO_i} \\ = \mu_0 \cdot \frac{1}{n} \sum_{i=1}^n E_i \cdot 10^{(pH_i - pK)} / [1 + 10^{(pH_i - pK)}] \quad (3)$$

where  $n$  is the number of segments. The electroosmotic flow calculated according to Eq. 3 is assumed to be a plug flow and treated in the same way as the imposed flow in the previous version of the model [7]. The time dependence is given by the variability of the voltage gradient and pH. Thus, this simple approach requires  $\mu_0$  and the  $pK$  value of the wall as “specific” inputs and permits the combined simulation of the temporal behavior of electroosmosis and electrophoresis in both uniform and discontinuous buffer systems.

### 3. Experimental

#### 3.1. Chemicals

The chemicals used were of analytical-reagent or research grade.

#### 3.2. Computer simulations

The program was executed on an Excel AT 486 computer (Walz Computer, Berne, Switzerland) or a notebook 486 computer (Data 2000, Berne, Switzerland) running at 50 and 33 MHz,

Table 1  
Electrochemical parameters used in simulation

Compound	$pK_1$	$pK_2$	Mobility coefficient ( $10^{-8} \text{ m}^2/\text{V} \cdot \text{s}$ )
Tryptophan	2.38	9.40	2.54
Tryptamine	9.30		2.54
ACES	6.84		3.13
$\text{Na}^+$			5.19
$\text{H}^+$			36.27
$\text{OH}^-$			19.87

respectively. The component's input data for simulation are summarized in Table 1. All simulations were performed with a 5 cm separation space divided into 600 segments of equal length. For making plots, the data were imported into SigmaPlot Scientific Graphing Software version 4.01 (Jandel Scientific, Corte Madera, CA, USA) or into a software of our own design, termed 3DPLOT, which permits simple three-dimensional data presentation [7]. All plots were printed on an HP Laserprinter IIP (Hewlett-Packard, Widen, Switzerland).

#### 3.3. Instrumentation and experimental procedure

Electrokinetic measurements were made with two instruments featuring 50 or 75  $\mu\text{m}$  I.D. fused-silica capillaries which were purchased from Polymicro Technologies (Phoenix, AZ, USA) (products TSP/075/375 and TSP/050/375, respectively), a laboratory-made set-up described previously [7,9] and the Prince apparatus (Lauerlabs, Emmen, Netherlands). Prior to use, capillaries were etched with 1  $M$  sodium hydroxide solution for about 20 min. If not stated otherwise, the capillaries were conditioned for each experiment by rinsing with running buffer for at least 10 min.

### 4. Results and discussion

To simulate electroosmosis in fused-silica capillaries, two specific inputs are required, a wall or absolute electroosmotic mobility (serving for the calculation of electroosmotic transport) and a wall  $pK$  describing the dissociation of silanol groups on the capillary surface (representing surface charge as a function of pH). Selection of these values is crucial and depends on the physical configuration employed. Using fused-silica capillaries and uniform buffers, the net electroosmotic mobility is known to be dependent not only on pH and wall  $pK$  according to

$$\mu_{EO} = \mu_0 \cdot 10^{(pH - pK)} / [1 + 10^{(pH - pK)}] \quad (4)$$

but also on capillary conditioning [10]. Thus, in order to be able to characterize the capillaries employed, a titration curve was measured. The data presented in Fig. 1A were obtained using a 50  $\mu\text{m}$  I.D. capillary of 55 cm total and 45 cm effective length, 40 mM phosphate buffers in order of decreasing pH values and the Prince instrument. The temperature was kept at 35°C, a constant voltage of 20 kV was applied and the current was in the range 26–72  $\mu\text{A}$ . Phosphate buffers were prepared from stock solutions of  $\text{H}_3\text{PO}_4$ ,  $\text{NaH}_2\text{PO}_4$  and  $\text{Na}_2\text{HPO}_4$  (0.2 M each) and methanol was used as a marker substance for electroosmosis. Before each run, the capillary was flushed with running buffer for 5 min

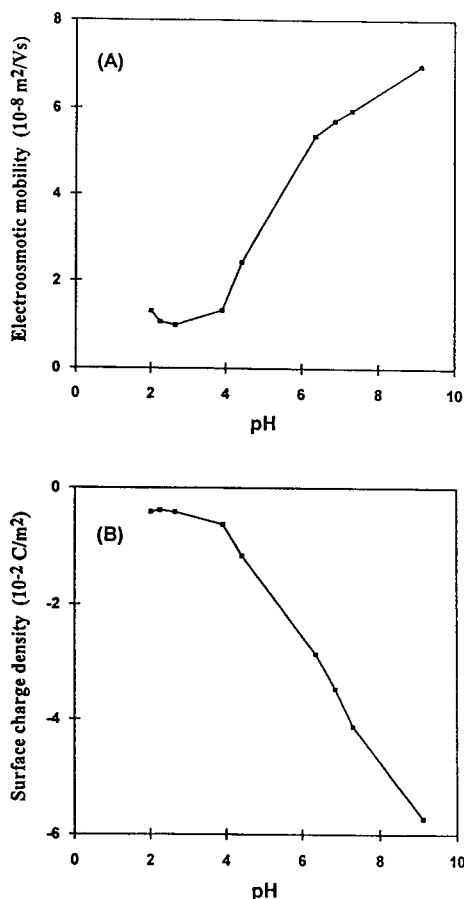


Fig. 1. Capillary titration data with (A) experimentally determined net electroosmotic mobility as a function of pH and (B) calculated surface charge density.

through application of a positive pressure of 3000 mbar. Sample application [water–methanol, (60:40)] was effected by a 20 mbar pressure for 6 s.

The pH dependence of the net electroosmotic mobility shown in Fig. 1A is comparable to that reported for a monitoring sequence in the order of decreasing buffer pH values [10]. Not surprisingly, the titration curve is characterized by a steep change in the pH 5–7 interval, this representing the dissociation of the silanol groups. Further, at low pH, the data do not reflect those expected from the vanishing dissociation of monovalent silanol [11], the residual mobility being ascribed to contributions made by anion adsorption. At high pH, a net electroosmotic mobility of larger than  $6 \cdot 10^{-8} \text{ m}^2/\text{V}\cdot\text{s}$  is observed, in agreement with reported values [10].

The small mobility increase observed at  $\text{pH} < 3$  can be ascribed to the decrease in ionic strength encountered when keeping the phosphate buffers at a constant 40 mM. Neglect of the  $\text{OH}^-$  concentration and assuming electroneutrality, the ionic strength of a phosphate buffer consisting of monovalent cations (e.g.  $\text{Na}^+$  and  $\text{K}^+$ ) is given by

$$\mu = \frac{K_1[\text{H}^+]^2 + 3K_1K_2[\text{H}^+] + 6K_1K_2K_3}{[\text{H}^+]^3 + K_1[\text{H}^+]^2 + K_1K_2[\text{H}^+] + K_1K_2K_3} \cdot C_p \quad (5)$$

where  $C_p$  is the total phosphate concentration (M) and  $K_{1,2,3}$  are the dissociation constants of phosphoric acid. The electroosmotic mobility is given by [12]

$$\mu_{\text{EO}} = -\frac{\epsilon_0 \epsilon_r \zeta}{\eta} = -\frac{\sigma}{\kappa \eta} \quad (6)$$

where  $\epsilon_0$  is the permittivity of vacuum ( $8.854 \cdot 10^{-12} \text{ C}^2/\text{N}\cdot\text{m}^2$ ),  $\epsilon_r$  the dielectric constant of the running buffer (75 for water at 35°C),  $\eta$  the viscosity of the solution ( $0.000719 \text{ N}\cdot\text{s}/\text{m}^2$  for water at 35°C),  $\zeta$  the zeta potential at the capillary wall,  $\sigma$  the surface charge density of the capillary wall ( $\text{C}/\text{m}^2$ ) and  $\kappa$  the Debye–Hückel parameter given by



$$\kappa^2 = \frac{2000F^2}{\epsilon_0 \epsilon_r RT} \cdot u$$

where  $F$  is the Faraday constant (96495 C/mol) and  $R$  the universal gas constant (8.31 J/K·mol). Substitution of the ionic strength expressed by Eq. 5 in Eq. 6, rearrangement and insertion of the measured mobility values permit the calculation of the surface charge density of the capillary wall (Fig. 1B), a property which provides direct insight into the degree of ionization of the silanol groups. Again, surface charge is shown not to become zero at low pH, this being another indication of anion adsorption on the capillary wall at pH < 4. Thus, selection of a wall pK of 6, which corresponds to the pK<sub>a</sub> value of the silanol groups [11], is unlikely to provide meaningful predictions for capillary electrophoresis in low pH buffers. For pH > 5.5, however, this could be different and was therefore investigated.

The capillary zone electrophoretic separation of tryptophan (Trp) and tryptamine (Tra) in a buffer composed of 100 mM of the weak acid N-[2-acetamido]-2-aminoethanesulfonic acid (ACES) and 90 mM NaOH was studied. Using the input parameters listed in Table 1, the pH and conductivity values of that buffer were

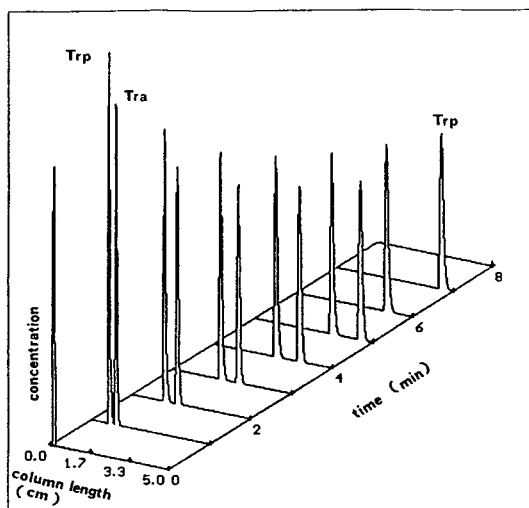


Fig. 2. Computer-predicted concentration profiles of Trp and Tra at 1-min intervals.

calculated to be 7.79 and 0.723 S/m, respectively. The simulation data depicted in Fig. 2 were obtained with an initial sample pulse at the anodic capillary end comprising Trp and Tra (0.5 mM each) and tenfold diluted running buffer. To simplify matters, the dynamic behavior was studied in a column of length 5 cm and with a constant applied voltage of 77.5 V (15.5 V/cm; initial current density 1000 A/m<sup>2</sup>). For the calculation of electroosmosis, a wall pK of 6 and a mobility of  $7 \cdot 10^{-8}$  m<sup>2</sup>/V·s were employed. For that configuration, a constant electroosmotic displacement towards the cathode of 106.8 μm/s was predicted. The data presented in Fig. 2 represent the predicted dynamics of the concentration profiles of the two solutes at 1-min intervals. In this system, Tra has a positive charge with electrophoretic and electroosmotic displacements being in the same direction. Tra is predicted to reach the cathodic end of the column after about 5.2 min of power application. Trp is partially negatively charged and thus electromigrates in the opposite direction to the cathodic electroosmotic flow. The latter displacement, however, is much stronger and Trp is predicted to leave the capillary column at its cathodic end after about 7.2 min. Separation is predicted to be fairly fast with full resolution being obtained in about 1 min.

The data presented in Fig. 3 depict the detector responses predicted for UV absorbance at 220 nm. Responses for detectors placed between 20 and 80% of the column length (10% interval) are shown, the signals representing the summation of the concentrations of Trp and Tra supplemented by 0.4% of the ACES concentration, this corresponding to equal absorption of the two solutes and the much smaller absorption of ACES at a wavelength of 220 nm. The decrease in the predicted detector response originates from the buffer difference between running buffer and applied sample, a change which is monitored only at low wavelengths (Fig. 4). The three-dimensional data shown in Fig. 4 were obtained with the laboratory-made instrument equipped with a 75 μm I.D. capillary of 70 cm total and 50 cm effective length. Sampling occurred for 5 s. The applied constant voltage

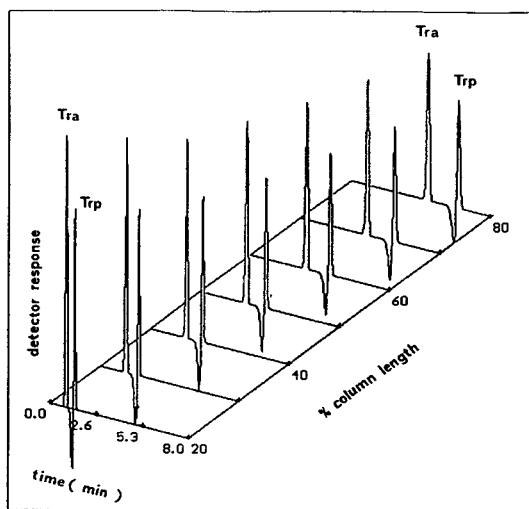


Fig. 3. Computer-predicted detector responses for detectors located between 20 and 80% of the column length (10% interval). The responses represent UV absorption at 220 nm.

was 15 kV and the sample components were dissolved in tenfold diluted running buffer. As predicted, Tra was detected first at 4.60 min after power application, whereas Trp (7.29 min) was monitored shortly after the detection of the capillary void volume at 6.93 min (marked with V). For close comparison of the simulation and experimental data, the following has to be considered. In the experiment, a voltage gradient of 214.3 V/cm was applied, this being 13.8 times larger than that employed for the simulation. On the other hand, the column length used for computer prediction was fourteen times shorter than that used experimentally. Hence the time

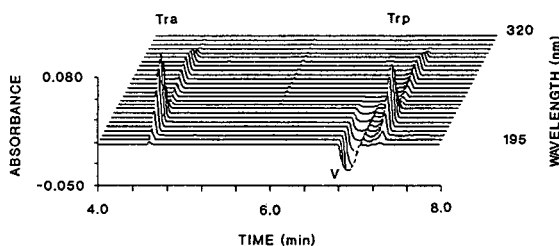


Fig. 4. Three-dimensional electropherogram depicting the separation of Trp and Tra, and the travelling buffer discontinuity (V), for absorption wavelengths between 195 and 320 nm (5-nm interval).

scales of prediction and experimental validation should be comparable. As is shown by the data presented in Fig. 5, this was essentially true. Evaluation of the experimental data revealed an electroosmotic net mobility of  $5.61 \cdot 10^{-8} \text{ m}^2/\text{V} \cdot \text{s}$ , this being about 80% compared with that employed for the simulation. Hence the experimentally determined detection time intervals are about 7.00/5.61 (the ratio of the two mobilities) longer than those predicted. For the detector profile depicted as the dashed line in Fig. 5, this difference was taken into account, and qualitative agreement between experiment and simulation was obtained. Further, the transport velocities of Tra and Trp in the simulation were significantly smaller than those in the experiment (see below). Therefore, the experimental peaks observed were sharper than those predicted (Fig. 5).

The dependence of electroosmosis on ionic

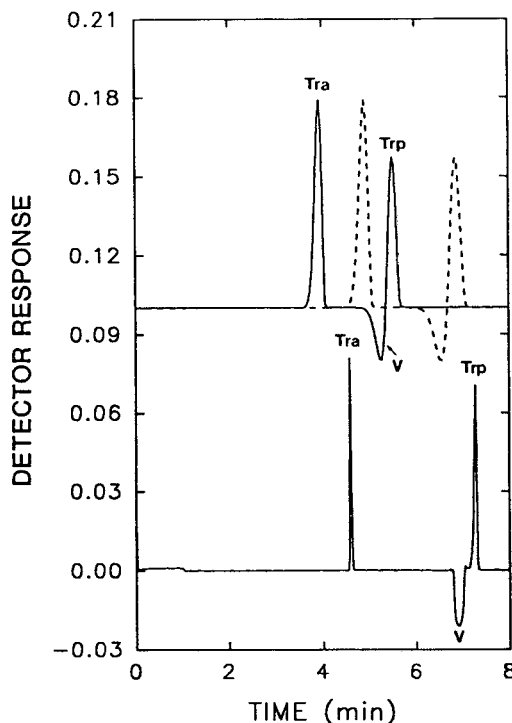


Fig. 5. Computer-predicted (top) and experimentally determined (bottom) absorption signals for a detector placed at 71.3% of the column length. For further explanation, see text.

strength is not taken into account with the present model. Electroosmosis is known to decrease as the ionic strength increases (Eq. 6 and Ref. [13]). For a buffer composed of 100 mM ACES and 90 mM NaOH (pH 7.79), the ionic strength is 89.96 mM. This is about 10% lower than the ionic strength of 103.5 mM calculated for 40 mM phosphate buffer (Fig. 1) at pH 7.79. Therefore, from this point of view, the electroosmotic mobility expected for the ACES buffer system should be higher than that with phosphate buffer. As discussed above, however, the opposite was found experimentally. Another aspect to be discussed is the impact of temperature. It is important to note that the experimental data presented in Figs. 4 and 5 were measured at ambient temperature (about 25°C), whereas the data presented in Fig. 1 were obtained at 35°C. According to Eq. 6, the surface charge is proportional to

$$\mu_{EO}\eta\sqrt{\frac{u}{T}} \quad (7)$$

where  $\eta$  and  $u$  are strongly and weakly, respectively, temperature dependent. Values for Eq. 7 were calculated by taking the viscosity of water at 25 and 35°C (0.8904 and 0.7194 cP, respectively), the experimentally determined mobilities for the two buffers ( $5.61 \cdot 10^{-8}$  and  $6.2 \cdot 10^{-8}$  m<sup>2</sup>/V·s (Fig. 1) for ACES and phosphate at pH 7.79, respectively), and neglecting the temperature dependence of  $u$ . The value for the ACES buffer obtained was found to be about 6% larger than that for the phosphate buffer. This similarity reveals that the surface charge mainly originates from the dissociation of the silanol groups and unlikely to be dependent on buffer composition when pH > 6. Further, temperature has a much stronger impact on electroosmosis than ionic strength. Also, the conclusion can be reached that the column conditioning for the two experimental set-ups was comparable.

For the system described, the model predicts a constant electroosmotic flow (Fig. 6). At constant voltage, the current density and column resistance, however, were determined to change as a function of time (Fig. 6). This was not only calculated by the model, but also observed

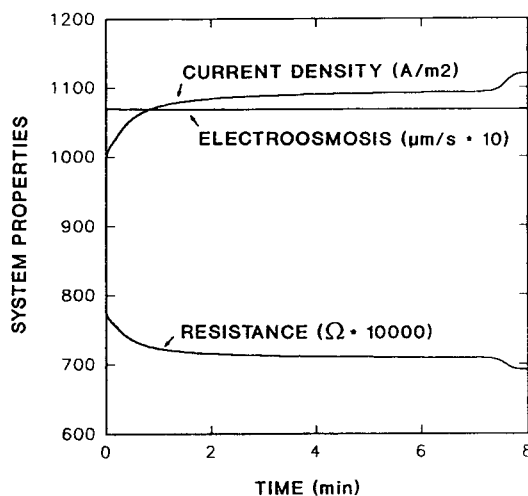


Fig. 6. Computer-predicted temporal variation of current density, resistance and electroosmosis.

experimentally, the current first increasing rapidly from 60 to 70 μA followed by a slow further increase to 75 μA. The change in these parameters is mainly attributed to the strong buffer discontinuity of the initial sampling pulse travelling through the column. Fig. 7A depicts the computer-predicted buffer change and the solute concentrations 2.5 min after power application. For the same time point, the distributions of pH, conductivity and electroosmosis are presented in Fig. 7B. The buffer discontinuity is predicted to leave the column shortly after 7 min (Fig. 3), this also being seen with the current density (resistance) increase (decrease) depicted in Fig. 6. Across the buffer change, the pH is predicted to remain almost constant, whereas the local conductivity and electroosmosis strongly change (Fig. 7B). These computer-simulated data are shown to further reveal interesting insight into the dynamics of the system's parameters which are difficult to monitor with customary absorption and fluorescence detection.

Simulation of the same zone electrophoretic separation but with the sample being applied in plain (undiluted) buffer, a configuration in which the two sample compounds are the only discontinuous elements in the column, was also investigated. With application of the same con-

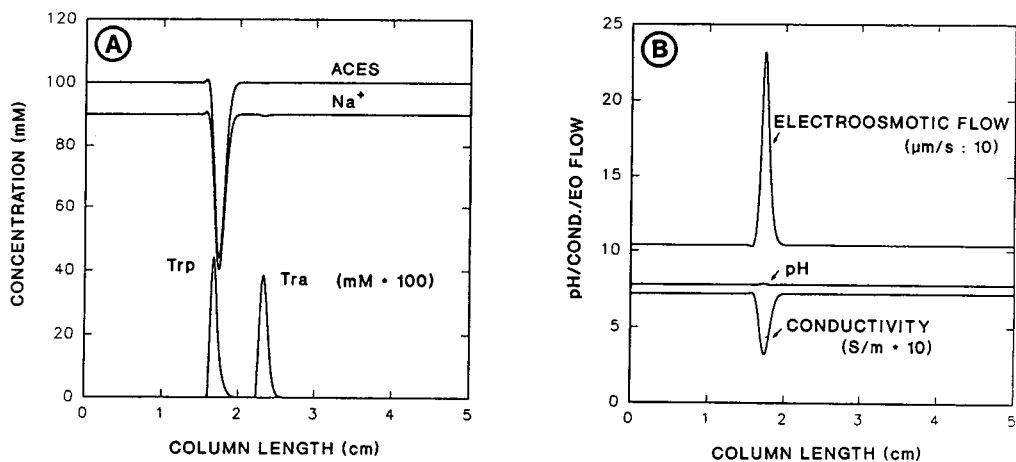


Fig. 7. Computer-predicted distributions of (A) concentrations of all components at 2.5 min of current flow and (B) pH, conductivity and electroosmosis for the same time point. For presentation, the concentrations of Trp and Tra in (A) were multiplied by 100.

stant voltage of 77.5 V, electroosmosis, current density and column resistance were calculated to be invariant, the values being  $106.8 \mu\text{m/s}$ ,  $1120 \text{ A/m}^2$  and  $0.0692 \Omega$ , respectively. For the two approaches, the electroosmotic flow is predicted to be the same. This, however, does not apply to the electrical properties of the two columns. Compared with the data presented in Figs. 2–7, the configuration with plain buffer in the sample is not associated with the initial sharpening of sample components (Fig. 8) or with a buffer discontinuity travelling with the velocity of electroosmosis. Not surprisingly, and in agreement with prediction by the model, the absorbance decrease associated with this buffer change (marked V in Figs. 4 and 5) was not detected when Trp and Tra were sampled together with undiluted buffer (data not shown).

With the same model, emulated detector signals for other detection properties, including conductivity, pH and indirect optical detection, can also be obtained. In fact, a detector response specificity to any component passing the detector can be assigned, permitting one to simulate any specific detector responses, including those obtained with electrochemical detection. The data presented in Fig. 9 are those for a detector placed at 71.3% of the column length, the upper

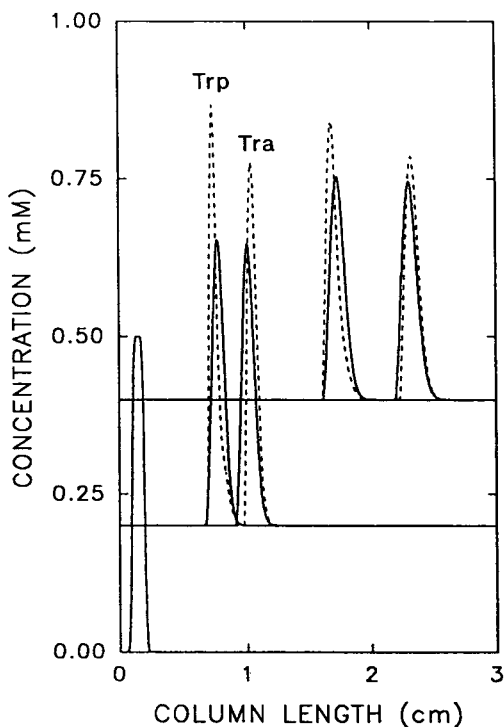


Fig. 8. Computer-simulated concentration profiles of Trp and Tra after 0, 1 and 2.5 min of current flow (from bottom to top with an offset of  $0.2 \text{ mM}$  between time points) and for the sample applied in plain buffer (solid lines) and in tenfold diluted buffer (broken lines).

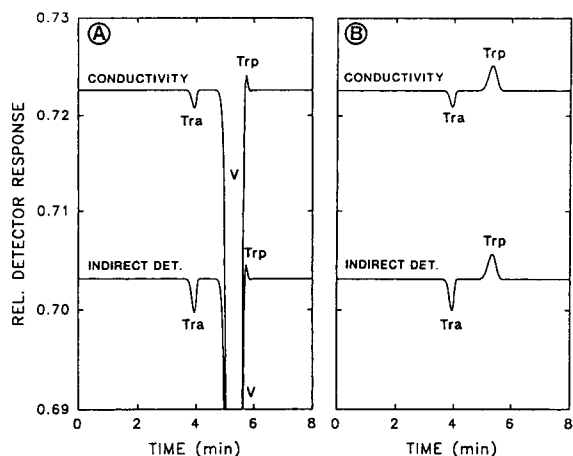


Fig. 9. Computer-predicted detector responses for conductivity (top) and indirect detection based on concentration changes of the buffer cation ( $\text{Na}^+$ , bottom) for sample applied (A) in tenfold diluted and (B) in plain buffer. The detector was placed at 71.5% of the column length. For conductivity and indirect detection, the ordinate scale represents  $\text{S/m}$  and  $\text{mM} \cdot 0.00781$ , respectively.

and lower graphs representing predicted responses for conductivity monitoring and indirect optical detection based on changes in the buffer cation ( $\text{Na}^+$ ), respectively. Data produced by ACES changes were determined to be similar to those of  $\text{Na}^+$  and are therefore not shown. Overall there is great similarity between the predicted responses of the two detectors. With tenfold diluted buffer in the initial sample zone (Fig. 9A), a very strong signal deviation across the travelling discontinuity (marked V) is predicted, a response which interferes considerably with the detection of Trp. Hence the use of conductivity and indirect absorbance detection cannot be recommended for compounds present within the buffer gradients originating from the initial sample buffer discontinuity. The monitoring of Tra, however, is not affected and could therefore be accessible with both detector systems. Having undiluted buffer in the sample (Fig. 9B) Tra and Trp are predicted to be detected by a signal decrease and increase, respectively.

## 5. Conclusions

The new model provides a realistic prediction of electroosmosis in fused-silica capillary electrophoresis. It is also capable of visualizing the whole dynamics of all components and column properties, including current density, voltage gradient and resistance. Emulated detector responses (at specified column locations) for absorbance, fluorescence, indirect optical, electrochemical, conductivity and pH detection are also obtained. It is important to realize that electroosmosis is considered to represent plug flow. Hence the predicted boundary dispersion is based solely on diffusion and electromigration. To compute electroosmosis in buffers with  $\text{pH} > 5.5$ , a wall  $\text{p}K$  of 6 and a wall mobility between  $5 \cdot 10^{-8}$  and  $7 \cdot 10^{-8} \text{ m}^2/\text{V}\cdot\text{s}$  are required to provide simulation data which are in good qualitative agreement with experimental data. This parameter selection is in agreement with titration curves, i.e., electroosmotic mobility vs. pH relationships, determined in fused-silica capillaries. For an environment with  $\text{pH} < 5.5$ , however, the same model can only be employed by specifying a wall  $\text{p}K$  lower than 6, which produces data of lower accuracy. More work is required to incorporate the impact of anions adsorbed on the capillary wall on electroosmosis. The use of the model to simulate electroosmosis in discontinuous buffers is in progress.

## Acknowledgement

This work was sponsored by the Swiss National Science Foundation.

## References

- [1] M. Bier, O.A. Palusinski, R.A. Mosher and D.A. Saville, *Science*, 219 (1983) 1281.
- [2] R.A. Mosher, D. Dewey, W. Thormann, D.A. Saville and M. Bier, *Anal. Chem.*, 61 (1989) 362.
- [3] R.A. Mosher, D.A. Saville and W. Thormann, *The Dynamics of Electrophoresis*, VCH, Weinheim, 1992.
- [4] R.A. Mosher, P. Gebauer, J. Caslavská and W. Thormann, *Anal. Chem.*, 64 (1992) 2991.

- [5] E.V. Dose and G.A. Guiochon, *Anal. Chem.*, 63 (1991) 1063.
- [6] S.V. Ermakov and P.G. Righetti, *J. Chromatogr. A*, 667 (1994) 257.
- [7] W. Thormann, S. Molteni, E. Stoffel, R.A. Mosher and J. Chmelík, *Anal. Methods Instrum.*, 1 (1993) 177.
- [8] R. Deshmukh and M. Bier, *Electrophoresis*, 14 (1993) 205.
- [9] J. Caslavská, S. Lienhard and W. Thormann, *J. Chromatogr.*, 638 (1993) 335.
- [10] W.J. Lambert and D.L. Middleton, *Anal. Chem.*, 62 (1990) 1585.
- [11] J.C. Jacquier, C. Rony and P.L. Desbene, *J. Chromatogr. A*, 652 (1993) 337.
- [12] P.D. Grossman, in P.D. Grossman and J.C. Colburn (Editors), *Capillary Electrophoresis: Theory and Practice*, Academic Press, San Diego, 1992, pp. 3–45.
- [13] F. Foret, L. Křivánková and P. Boček, *Capillary Zone Electrophoresis*, VCH, Weinheim, 1993, p. 45.

# Preparation and stability tests for polyacrylamide-coated capillaries for capillary electrophoresis

H. Engelhardt\*, M.A. Cuñat-Walter

*Instrumentelle Analytik, Umweltanalytik, Universität des Saarlandes, 66123 Saarbrücken, Germany*

---

## Abstract

The stability of polyacrylamide coatings at high pH values has been tested. It could be shown that overall stability is not limited by the coating of the fused-silica surface with organo silanes or Grignard reagents. The instability of polyacrylamide capillaries could be traced back to the hydrolysis of the amide bond at pH 10. The Si–O–Si surface bonds are not affected at this pH by hydrolysis.

The application of the sol–gel process to the preparation of stable homogeneous sublayers and a high density of olefinic groups within the capillary is described. The advantage of this method is the simple coating reaction and its independence of fused-silica surface properties.

---

## 1. Introduction

In the separation of biopolymers many efforts have been made to diminish the solute–capillary wall interactions. One approach was to use capillaries with a chemically modified surface. Usually two steps are applied to achieve the bonding [1–6]. In the first step olefinic groups are introduced on the surface of the fused-silica capillary and in the second step the final coating, in most cases acrylamide, is copolymerized with the olefinic sublayer. In capillary electrophoresis extreme pH values are desired, especially in the separation of proteins by capillary zone electrophoresis or isoelectric focussing. The stability of the surface coatings at high pH values is limited. This has been attributed to the instability of the bonds between the sublayer and the silica surface [2].

The methods described in the literature for the preparation of surface coatings differ mainly in the way the olefinic sublayer is bonded to the silica surface. Hjertén [1] condensed  $\gamma$ -methacryloxypropyltrimethoxysilane (MEMO) to the surface in an aqueous solution (pH 3.5 with acetic acid) at room temperature. This method (MEMO technique) has been widely applied for the preparation of olefinic sublayers. Because of the quoted instability, other approaches already known from the preparation of reversed-phase stationary phases for HPLC have been transferred to capillary surface modification [2–5]. Cobb et al. [2] treated the silica surface with thionylchloride and the silicic acid chloride prepared this way reacted further with vinyl magnesium bromide. Others used a long-chain alkoxysilane with a terminal olefinic group [3] or active silane transfer agents like acetylacetone vinyltrimethylsilylenolate [4] for the preparation of the olefinic sublayer prior to acrylamide polymerization. Olefinic polysiloxanes have also

---

\* Corresponding author.

been reacted with the capillary surface [6] to minimize the protein–capillary wall interactions.

For the second step – the polymerization of acrylamide – similar procedures have been used in all cases. Hjertén [1] applied ammonium persulfate as starter and TEMED (N,N,N',N'-tetramethylethylenediamine) as catalyst in aqueous solutions for the polymerization. Then the formed gel was flushed out of the capillary, with the surface coating remaining. In organic solvents AIBN (azodiisobutyronitrile) has been used as starter [3].

Characterization of the coatings is extremely difficult due to the very small surface area [7]. The most convenient way is to measure the dependence of the electroosmotic flow (EOF) on the pH of the buffer. The EOF is correlated with the silanol concentration on the surface. For uncoated surfaces the silanol concentration has been calculated from the EOF, and a good correlation with surface silanol concentrations discussed in literature has been found [7]. The reduction of the EOF achieved by the coating procedure, and its constancy during capillary use are the only means to describe the efficacy and stability of the bonding procedure. In this paper the stability of different coatings at high pH has been tested. Special attention has been paid to the stability of the different coating steps, because some indications have been found in literature that coating instability may also be traced back to acrylamide hydrolysis [8]. A new coating procedure using the sol–gel process for the preparation of stable olefinic sublayers will also be described.

## 2. Experimental

### 2.1. Reagent and materials

Fused-silica capillaries were purchased from Polymicro Technologies (German distributor: Laser 2000, Munich). Reagents for surface modification were purchased from different suppliers:  $\gamma$ -methacryloxypropyltrimethoxysilane (ABCR, Karlsruhe, Germany), acrylamide (BioRad, Munich, Germany), N,N-dimethylacrylamide,

AIBN and acrylic acid (Fluka, Neu-Ulm, Germany), ammonium persulfate and N,N,N',N'-tetramethylethylenediamine (Electran, UK) and vinyl magnesium bromide (Aldrich, Steinheim, Germany). The proteins were obtained from different suppliers such as cytochrome c (Sigma, Deisenhofen, Germany), chymotrypsinogen (Serva, Heidelberg, Germany) and lysozyme and ribonuclease A (Fluka, Neu-Ulm, Germany). Vinyltrichlorosilane, thionylchloride as well as all buffer substances were obtained from Fluka.

### 2.2. Coating procedures

Capillary pretreatment and modification with trichlorovinylsilane were performed according to a procedure described previously [5]. For MEMO modifications the capillary was filled with a solution of silane–methanol (50:50, v/v) and left for reaction over night at room temperature. Vinyl magnesium bromide was bonded as described in Ref. [2]. The procedure of Hjertén was used for linear polyacrylamide as well as for poly-N,N-dimethylacrylamide coatings [1]. In the same way capillaries were modified with polyacrylic acid.

### 2.3. Sol–gel procedure

The starting sol was obtained by adding 0.1 M hydrochloric acid in molar ratio to MEMO (MEMO–H<sub>2</sub>O, 1:1.5 or 1:3) and stirring at room temperature for 2 h. Then, the capillary was dynamically coated with this solution and heated to 130°C for 1 h in a GC oven under a slight nitrogen stream. After washing with dichloromethane, methanol and water the capillary was ready for use.

### 2.4. Apparatus

For all measurements a Beckman P/ACE System 2050 was used. Data acquisition was accomplished with Beckman Gold Software (V 7.12) and an IBM PS/2 personal computer. For coating procedures at higher temperatures the oven of a Carlo Erba GC 6000 Vega Series was used.



EOF/pH measurements always started at pH 3 (hysteresis). Between the individual runs the capillary was rinsed for several minutes with methanol, water and the corresponding running buffer. For stability measurements an aqueous solution of benzyl alcohol was injected and an electrical field was applied for 2 h at pH 10. Between the different runs the capillary was rinsed with fresh buffer. When after 2 h no peak appeared, an EOF of  $6 \cdot 10^{-6}$  cm<sup>2</sup>/Vs was assumed which corresponds to that migration time.

### 3. Results and discussion

#### 3.1. Characterization and stability of the olefinic sublayer

The EOF is the most important parameter in CZE separations. Its stability is important for the reproducibility of migration times. Absence of EOF is required for isoelectric focussing and capillary gel electrophoresis. The dependence of the EOF on pH shows a typical sigmoidal curve, caused by the dissociation of the surface silanol groups. In Fig. 1 the EOF measured for different preparation techniques of the olefinic sublayer is compared to the EOF obtained with the uncoated capillary of the same batch and identical surface pretreatment. It is important that the capillaries are taken from the same batch,

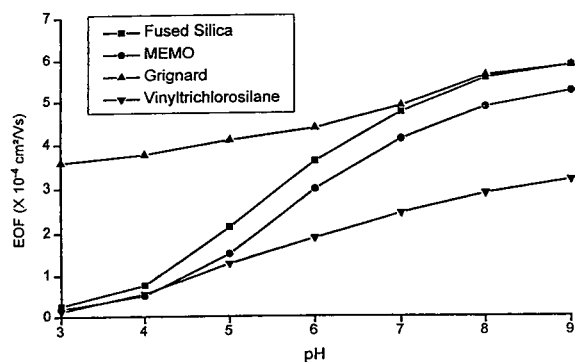


Fig. 1. EOF vs. pH curves for different vinyl-modified capillaries. Conditions:  $l = 30/37$  cm; buffer, 10 mM phosphate; neutral marker, benzyl alcohol; field, 432 V/cm.

because the EOF characteristics are also a function of the storage age of the capillary. A capillary stored for one year in the laboratory showed only half of the initial EOF measured immediately after delivery and opening.

As can be seen in Fig. 1, the capillary coated by the MEMO technique showed only a slight decrease of the EOF at high pH (approximately 10% reduction compared to that of the untreated one). When the surface concentration of dissociated silanols is the only cause for the EOF, one can assume that in this case only a small amount of these groups have been reacted by this treatment. The adsorption of the reagent onto the surface—a prerequisite for the condensation reaction [9]—is low in the polar reaction medium. Alkoxysilanes are also relatively stable at pH values between 3 and 5 in aqueous solution and the polycondensation reaction is slow [10]. On the other hand, chlorosilanes are very reactive with silanol groups. For capillaries treated with pure vinyltrichlorosilane (VTCS) and without catalyst the reduction of the EOF is about 50% of its initial value. Of course, in this case only part of the silanol groups are reacted and new ones are introduced by the trifunctional silanization reagent. When treating such a capillary with an active silanization reagent like bis-trimethylsilylacamide an additional EOF reduction of 20% has been observed. However, further studies showed that this procedure is not important for the preparation of good acrylamide-coated capillaries, and therefore it has been omitted.

The situation is different with regard to the capillaries prepared by the Grignard reaction. The treatment of fused-silica capillaries with thionyl chloride resulted in an increase of the EOF (after flushing the capillary with water). This can be attributed to an increase of the surface silanol concentration due to acid treatment by the formed hydrochloric acid [11]. After reaction with vinyl magnesium bromide the EOF is also at low pH values significantly higher than in the untreated capillary. At high pH values the EOF of the Grignard capillary is similar to that of the initial fused-silica capillary. The decrease of the EOF from the thionylchloride-treated

capillary to that reacted with vinyl magnesium bromide was around 10%.

Because of the small differences in EOF between the untreated capillary and those coated by the MEMO and Grignard technique, long-term stability measurements were not very reliable. However, it can be assumed that their behaviour is similar to that of the VTCS treated capillary, which is shown in Fig. 2. The capillary was continuously swept with the pH 10 buffer by the EOF. After every 2 h the buffer was changed and the EOF remeasured. Over a 80-h period of continuous treatment with buffer of pH 10 no increase in EOF could be noticed. This indicates that the sublayer is stable. One reason for this stability might be that the hydrophobic surface layer prevents the hydroxyl ions attacking the Si–O–Si bonds of the vinyl groups to the surface. The achievable surface coverage with VTCS is very high. With porous silica and identical reaction conditions surface concentrations around  $5 \mu\text{mol}/\text{m}^2$  have been achieved [12].

### 3.2. Characterization of the polyacrylamide layer

The same test procedure was applied to the different capillaries after the polymerization of acrylamide onto the surface. The results are summarized in Fig. 3. The importance of the

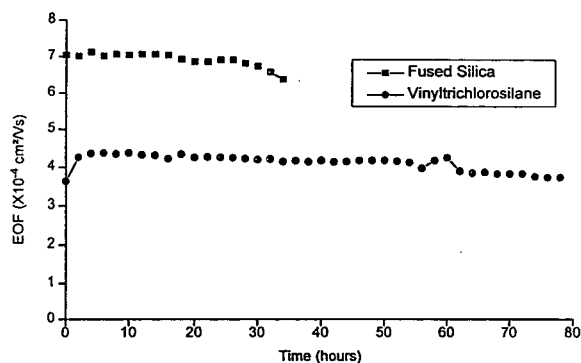


Fig. 2. Stability at pH 10 of a capillary modified with vinyltrichlorosilane. Conditions:  $l = 20/27$  cm; buffer, 10 mM phosphate pH 10; neutral marker, benzyl alcohol; field, 444 V/cm; measurement by procedure described in the text.

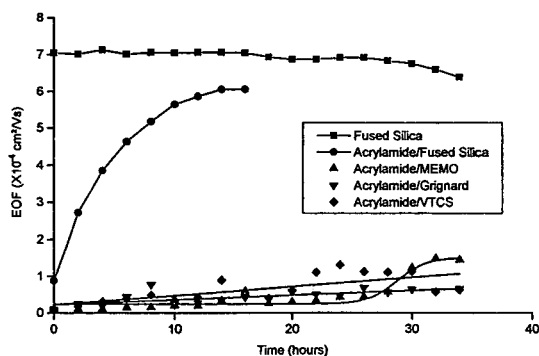


Fig. 3. Influence of the olefinic sublayer on the stability of polyacrylamide capillaries at pH 10. Conditions: see Fig. 2.

sublayer in the copolymerization of acrylamide with the olefinic groups bonded to the surface can be deduced from the behaviour of the capillary on which only acrylamide has been polymerized. In this capillary, where no covalent attachment of the polymer to the surface is possible, no constant EOF could be observed and after 10–15 h the EOF of the uncoated capillary was approached. Thus modification of a capillary surface only with physically adsorbed polyacrylamide does not give a stable coating.

The behaviour of the three other capillaries, where the subcoating was achieved by different methods, is very similar. The measurements at pH 10 exhibit a much lower EOF ( $<10^{-5} \text{ cm}^2/\text{Vs}$ ) than achieved with capillaries coated solely with the olefinic sublayer. The reason for this is the high viscosity of the polymeric acrylamide layer in the region of the electric double layer [1]. The identical behaviour of the three different capillaries supports the statement given above that the three different subcoatings are of identical stability, despite the different degrees of shielding of the surface silanols. An additional reason for this stability may be the extremely low diffusion coefficients of catalytic hydroxyl ions through the thick polymeric layer.

The increase of the EOF can only be attributed to the slow decomposition of the acrylamide groups. The instability of polyacrylamide is a well known fact from classical flat-bed gel electrophoresis [8,14]. The formed carboxylic groups are fully dissociated at this pH and contribute to

the EOF. Our results are partly in contradiction with those of others [13], where a different behaviour of the Grignard and MEMO sublayer was found. The experimental set-up differs, however, because only pH 8 has been used (here pH 10). At this pH hydrolysis of the amide group is less important. Moreover, the capillaries were stored in buffer, whereas in our more stringent experiments the buffer was continuously swept through the capillary by the EOF, and the electrical field was applied continuously. It has also been demonstrated with another coating than acrylamide that the MEMO sublayer is stable at pH 12 [15].

To prove the hypothesis that the obvious instability of polyacrylamide capillaries stems from the hydrolysis of the amide bond, acrylic acid itself has been polymerized either as pure acrylic acid or in a 1:1 mixture with acrylamide. As can be seen in Fig. 4, the EOF is lower than in the untreated capillary and remains constant over the whole test period. Surprisingly, the EOF of the polymeric layer obtained by copolymerization of acrylic acid and acrylamide also remains constant. One possible explanation for this stability might be the hindered attack of hydroxyl ions to the negatively charged polymeric layer. In the same figure the stability test of the acrylamide capillary from the previous figure is included for comparison. The behaviour of a capillary coated with *N,N*-dimethylacrylamide (DMA) is also shown. It has

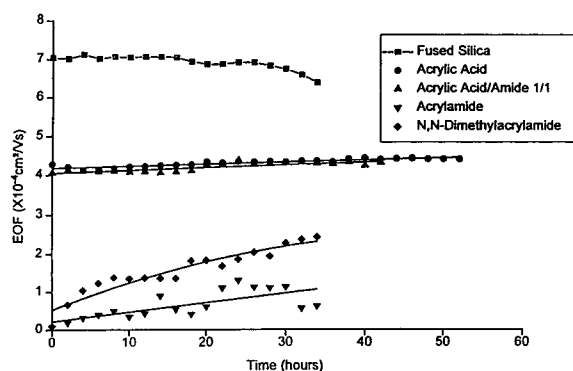


Fig. 4. Influence of the polymerized monomer on the stability at pH 10. Olefinic sublayer: vinyltrichlorosilane. Conditions: see Fig. 2.

been described [8] that disubstituted amides are substantially more resistant to alkaline hydrolysis than the unsubstituted species. Surprisingly, we found that the stability of the DMA-coated capillary seems to be lower than that of the plain acrylamide coating. One reason may be the higher hydrophobicity of the monomer which can result in a lower degree of polymerization (thin coating) due to a diminished incorporation of the monomer into the polymeric layer [8]. Polymerization at elevated temperatures should diminish these problems [8]. However, such an experiment has not been included in our studies.

To sum up, the instability of polyacrylamide-coated capillaries seems mainly to originate from hydrolysis of the amide group at the applied pH of 10. So far, no difference could be found between the different procedures for the preparation of the olefinic sublayer. The application of hydrolysis-stable monomers, however, is limited by their diminished accessibility to polymerization. Cross-linking with formaldehyde has also been mentioned to improve acrylamide stability [6]. Polymerization of other polar monomers with non-hydrolysable functional groups [14–17] might result in superior stable polar capillaries for the CZE of biopolymers.

Another way to characterize coatings is the analysis of proteins, where high plate numbers should be achieved. Fig. 5 shows the separation of basic standard proteins with a VTCS/polyacrylamide capillary at four different pHs. Even at pH 6 a highly efficient separation is achieved. As can be seen in Table 1, the plate numbers vary between 300 000 and 800 000.

### 3.3. Sublayers by the sol-gel process

Concerning the previously applied techniques, the efficiency and reproducibility of the sublayer preparation depends on the concentration and reactivity of the surface silanol groups on the fused-silica capillaries. As described and determined by EOF measurements [7], this concentration depends on the supplier and the history of the capillary. It is, on the other hand, desirable to have a constant homogenous and high-density surface concentration of polymerizable

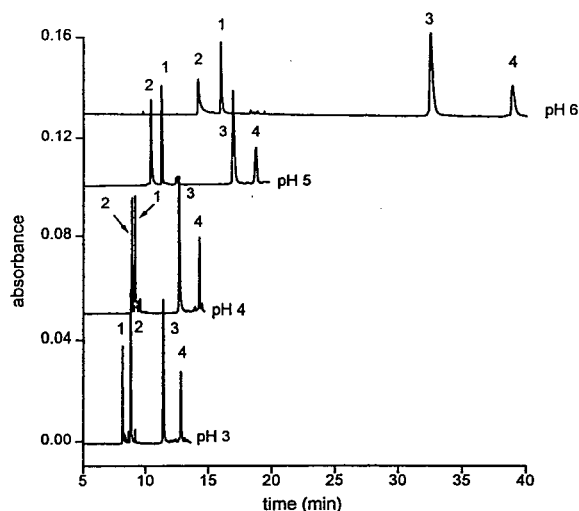


Fig. 5. Influence of pH on the separation of standard basic proteins with a polyacrylamide–vinyltrichlorosilane capillary. Peaks: 1 = cytochrome c, 2 = lysozyme, 3 = ribonuclease A, 4 = chymotrypsinogen. Conditions:  $l = 30/37$  cm; buffer, 50 mM phosphate; field, 270 V/cm; injection, pressure (0.5 p.s.i.), 1 s.

functional groups immobilized on the fused-silica surface. The only way to achieve this is by immobilizing a polysiloxane with easily polymerizable olefinic groups [6].

The sol–gel process [18,19] is a well-known chemical synthesis method for the preparation of glasses and ceramics. Starting from alkoxy-silanes, a growth process is initiated leading to oligomeric molecules or colloids, which form a three-dimensional network by condensation reactions. These intermediates can be stabilized in solution (sols), and can be used for coating techniques. In general, the alkoxy-silanes are reacted with a stoichiometric amount of water in

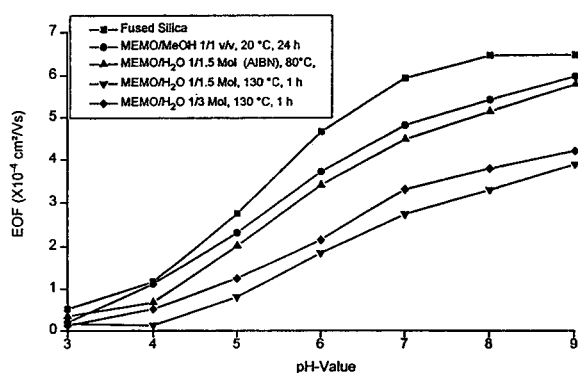


Fig. 6. EOF vs. pH curves for different MEMO modified capillaries using sol–gel process. Conditions: see Fig. 1.

the presence of a catalyst (acid or base). By applying organoalkoxysilanes with reactive functional groups, a mixed organic–inorganic network is generated under very smooth conditions at room temperature. By this process extremely stable layers with interesting mechanical properties can be obtained on different materials ranging from plastics to glass and metals.

Here, the sol–gel process has been used to prepare stable layers of MEMO within the capillary. The influence of the sol preparation and its bonding to the surface is demonstrated via EOF measurements in Fig. 6. For comparison the classical MEMO coating discussed in Fig. 1 has been included. As discussed, in this case the EOF was reduced only by about 10%. For the preparation of the sol, MEMO has been reacted at room temperature for 2 h with molar amounts of 0.1 M hydrochloric acid. Under these conditions mainly linear polycondensation products are formed, which still contain sufficient unreacted alkoxy groups (more than 5%

Table 1  
Number of theoretical plates per meter for standard basic proteins at different pH

	Cytochrome c	Lysozyme	Ribonuclease A	Chymotrypsinogen
pH 3	765 000	573 000	565 000	737 000
pH 4	615 000	754 000	427 000	746 000
pH 5	448 000	382 000	232 000	332 000
pH 6	851 000	230 000	506 000	358 000

Conditions: see Fig. 5.

after 14 days) [20]. The sol has then been dynamically coated onto the surface of the capillary and the condensation reaction with the surface has been achieved through heating to 130°C. As can be seen in Fig. 6, the EOF was decreased to about half its initial value. A similar reduction has been observed with the VTCS technique; however, with the sol-gel process the reproducibility was much higher. The ruggedness of the sol preparation and its immobilization has also been demonstrated. The amount of added aqueous acid (1.5 or 3.0 mol) had negligible influence on the EOF behaviour. Thus, a similar coating could be assumed.

In addition to the polycondensation process a cross-linking of the organic olefinic groups can be initiated in the sol-gel process by the addition of a radical starter such as AIBN (azodiisobutyronitrile). This procedure was also performed in a capillary with a precondensed MEMO. In this case the amount of sol immobilized on the surface is relatively small, as can be deduced from the still high EOF. The coating efficiency was similar to that of the initial MEMO procedure, at least a similar EOF/pH dependence has been achieved.

With these efficient coatings stability measurements have also been performed. It could be demonstrated again that the olefinic sublayer is stable over a long period of time with a constant low EOF at pH 10. It is no problem to react these fixed layers with monomers like acrylamide, which showed similar long term stability as the other polyacrylamide coatings. Only with the sol that had been additionally cross-linked in the organic part with AIBN no stable acrylamide layer could be formed due to the reduced concentration of remaining olefinic groups.

With these capillaries highly efficient protein separations have also been achieved. The advantage of the sol-gel process is the fact that, being independent on the initial surface properties of the fused-silica capillary, a homogenous sublayer with high reproducibility and high concentration

of olefinic groups can be achieved. Of course, this process is not limited to MEMO. This sol-gel process can be applied to a great variety of organosilica derivatives for the preparation of surface-coated capillaries for CE.

## References

- [1] S. Hjertén, *J. Chromatogr.*, 347 (1985) 191–198.
- [2] K.A. Cobb, V. Dolnik and M. Novotny, *Anal. Chem.*, 62 (1990) 2478–2483.
- [3] M. Huang, W.P. Vorkink and M.L. Lee, *J. Microcol. Sep.*, 4 (1992) 233–238.
- [4] M. Gilges, H. Husman, M.H. Kleemiß, S.R. Motsch and G. Schomburg, *J. High Resolut. Chromatogr.*, 15 (1992) 452–457.
- [5] J. Kohr and H. Engelhardt, *J. Microcol. Sep.*, 3 (1991) 491–495.
- [6] D. Schmalzing, C.A. Piggee, F. Foret, E. Carrilho and B.L. Karger, *J. Chromatogr. A*, 652 (1993) 149–159.
- [7] J. Kohr and H. Engelhardt, *J. Chromatogr. A*, 652 (1993) 309–316.
- [8] C. Gelfi, P. de Besi, A. Alloni and P.G. Righetti, *J. Chromatogr.*, 608 (1992) 333–341.
- [9] J. Rühle, *Nachr. Chem. Tech. Lab.*, 42 (1994) 1237–1246.
- [10] E.P. Plueddemann, *Silane Coupling Agents*, Plenum Press, New York, 1982.
- [11] K.K. Unger, *Porous Silica*, *J. Chromatogr. Lib. Vol. No. 16*, Elsevier, Amsterdam, 1979.
- [12] H. Engelhardt, H. Löw, W. Eberhardt and M. Mauß, *Chromatographia*, 27 (1989) 535.
- [13] M. Nakatani, A. Skibukawa and T. Nakagawa, *J. Chromatogr. A*, 661 (1994) 315–321.
- [14] M. Chiari, C. Micheletti, M. Nesi, M. Fazio and P.G. Righetti, *Electrophoresis*, 15 (1994) 177–186.
- [15] S. Hjertén and K. Kubo, *Electrophoresis*, 14 (1993) 390–395.
- [16] W. Götzinger, B.L. Karger, P. Shieh, N. Cooke, Poster P-637 presented at HPCE 95, Würzburg, Germany.
- [17] M.A. Cuñat-Walter, Ph.D. Thesis, Saarbrücken, 1995.
- [18] H. Schmidt, *J. Non-Crystalline Solids*, 100 (1988) 51–64.
- [19] H. Schmidt, *J. Sol-Gel Sci. Technol.*, 1 (1994) 217–231.
- [20] L. Delattre, C. Dupuy and F. Babonneau, First European Workshop on Hybride Organic-Inorganic Materials (Synthesis, properties and applications), Chateau de Bierville, France, 1993.





ELSEVIER

Journal of Chromatography A, 716 (1995) 35–48

JOURNAL OF  
CHROMATOGRAPHY A

# Some practical aspects of utilizing the on-line combination of isotachopheresis and capillary zone electrophoresis

Ludmila Křivánková, Petr Gebauer, Petr Boček\*

*Institute of Analytical Chemistry, Academy of Sciences of the Czech Republic, CZ-611 42 Brno, Czech Republic*

## Abstract

The on-line combination of isotachopheresis (ITP) and zone electrophoresis is a very effective tool for increasing the separation capability and sensitivity of capillary zone electrophoresis (CZE). Its most effective version is performed in column coupling instrumentation and is characterized by isotachopheresis in the first capillary serving as the efficient pre-separation and concentration stage followed by on-line transfer of the sample into the second capillary where analytical zone electrophoresis proceeds as the second stage. The on-line transfer of the sample from the first capillary into the second is always accompanied by the segments of some additional amounts of the leader and/or terminator from the ITP step. This results in transient survival of isotachopheretic migration during the second stage. Hence the separation process during the second stage can be characterized as the destacking of analytes followed by zone electrophoretic separation. In this paper, both a theoretical and an experimental study is presented showing that destacking of analytes is a selective process, which affects strongly the most important final analytical parameters of the detected zones, namely the detection time and zone variance, and thus it makes the simple use of detection data for qualitative analysis misleading. It was shown that both the detection time and variance of a zone of an analyte depend strongly on the amount of the accompanying segments of the leader/terminator transferred and on the actual type of electrolyte system selected from the generally possible types. These types are (i) L–S–L, where the leading electrolyte (L) from ITP stage serves as the background electrolyte (BGE) during CZE (S = sample), (ii) T–S–T, where the terminating electrolyte (T) from the ITP stage serves as the BGE during CZE, and (iii) BGE–S–BGE, where L, T and BGE are mutually different. Explicit equations were derived enabling one to predict migration time and zone variance for actual working conditions, and, for model systems, the theoretical data were calculated and verified experimentally. Further, it is shown that the systems T–S–T and L–S–L are user friendly and a simple standardization procedure was proposed, allowing correct qualitative evaluation of the analytical data in these systems. Finally, a theory is presented predicting the existence of anomalous variances of zones in the record of analysis in BGE–S–BGE systems and its experimental verification is given.

## 1. Introduction

It has been proved that the on-line combination of isotachopheresis (ITP) and zone electrophoresis is an effective tool for improving the

analytical expediency of capillary electrophoresis [1–22]. The concentration capability and reproducible sampling inherent in isotachopheresis are combined here with the high resolving power and high sensitivity of capillary zone electrophoresis (CZE). The concentration capability of ITP and the resolving power of CZE follow from

\* Corresponding author.

the principles of these methods and can be affected mainly by the composition of the electrolyte system used. The reproducibility of the sampling and the sensitivity of the methods are mainly influenced by the construction elements of the instrumentation and the type of detection used [23,24], although the selection of the electrolyte system also has a significant impact [25–28]. Owing to its capability to concentrate trace analytes from large sample volumes, it is always ITP which is used in the first stage of the analysis. Isotachophoretic migration during an electrophoretic analysis can be either arranged by directly implanting an ITP electrolyte system in the background electrolyte (BGE) chosen for CZE [3,6,7,10,13–15,17,19–21] or induced by the composition of the sample containing a major component playing for some time the role of the leading or terminating ion [11,19,27].

By far the most effective system described was that employing the capillary for the ITP separation coupled on-line with the second capillary destined for the CZE run [1,2,4–6,8–10,13,16,18]. Here, in addition to the concentrating effect, also the load capacity of the pre-separation ITP step can be increased by employing the first capillary of wider diameter compared with the second capillary [4,6,13,18]. The detectability can increase by more than  $10^3$ -fold [6,9,13,18] and a detection limit as low as  $10^{-9}$  mol/l has been reported [18]. Bulk to trace sample components in a concentration ratio up to  $10^5$ :1 can be determined simultaneously [1]. While the major component is detected in the ITP step and subsequently driven out of the system to the helping electrode, the minor components in the form of a short stack of sharp zones are driven by voltage into the second capillary where the zone electrophoretic migration occurs.

The timing of the transition of ITP into ZE migration depends on the electrolytes used both in the ITP and CZE step and on the amount of the ITP components transferred into the CZE mode. Here, attention must be paid to the fact that the stack of analytes is sandwiched between other zones migrating isotachophoretically, in-

cluding small parts of the leading and terminating zones as a residue of the ITP migration mode [4,22]. This influences strongly the results of the analysis, especially the detection times of analytes used for identification of the analytes in CZE separations [28]. From this point of view, three combinations of electrolyte systems can be distinguished having a distinct effect of the ITP transient stage on the resulting course of the separation. Either the leading (L) or the terminating (T) electrolyte from the ITP separation can be used as the BGE, or an electrolyte different from these can be applied. We then speak about T–S–T, L–S–L and BGE–S–BGE electrolyte systems (S = sample), and in each of them, the destacking proceeds differently, which affects the resulting image of the separation. The theory revealed that the sample components leave the transient ITP stack gradually in dependence on their mobilities and therefore each sample component starts its ZE migration at a different time and at a different position along the migration path [22]. Therefore, it is not possible to evaluate detection times from the CZE stage in combined ITP–CZE in the same simple way as is done in the single CZE separation mode. Many operational variables have to be taken into account; however, optimum conditions for the separation can be found and correct qualitative identification is also possible.

The temporal stacking effect influences also the zone dispersion. It was shown [29] for a single-capillary system that as long as a minor sample zone migrates in stack, it keeps its size (zone width, variance) almost constant and comparable to the size of the stacking (sharp) zone boundary. The normal dispersion process starts after the zone is destacked. Sample zones in ITP–CZE systems are thus usually sharper than those in comparable CZE systems because their dispersion is retarded during a part of their migration path.

This work was aimed at continuing the previous research [22] by investigating both theoretically and experimentally the major effects of temporal sample stacking in ITP–CZE systems on the final parameters of a sample zone. Atten-



tion is focussed especially on the qualitative identification of analytes and the efficiency of the separation.

## 2. Theory

### 2.1. General remarks

The same simple model as described previously [22] was used. The system is assumed to be closed (with zero electroosmotic flow) and diffusion to be the only dispersion effect present. The scheme of the column coupling part of the system is given in Fig. 1 for both T–S–T and L–S–L arrangements. Panels A show the moment when the current is just switched over across the system of both capillaries and the migration of the segment of ITP zones responsible for the transient stacking (i.e., L for the T–S–T system and T for the L–S–L system) into the analytical capillary starts. The original (ITP) zone stack still survives including the sample zone(s). Panels B show the moment when the migration of the stacking zone segment into the analytical capillary has just stopped. The time count begins ( $t = 0$ ) at the moment when only the BGE is present both in front of and behind the stacking and sample zones. This corresponds to the situation shown in panel A for the T–S–T system and in panel B for the L–S–L system.

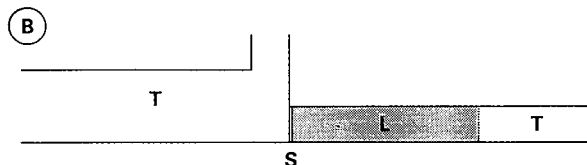
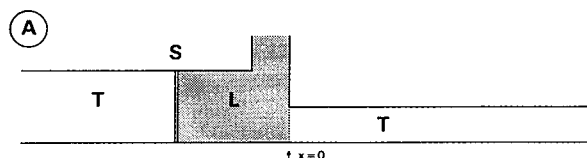
### 2.2. Effect of temporal stacking on detection time

In rigorous zone electrophoretic migration, the detection time  $t_x$  of an analyte X is the main directly available parameter for the qualitative evaluation of the analysis. It is indirectly proportional to the effective mobility:

$$t_{x,r} = \frac{x\kappa}{i\bar{u}_x} \quad (1)$$

where  $x$  is the migration path,  $\bar{u}_x$  is the effective mobility of analyte X,  $\kappa$  is the specific conductivity and  $i$  is the electric current density (assumed to be constant during the analysis). The

### T–S–T:



### L–S–L:

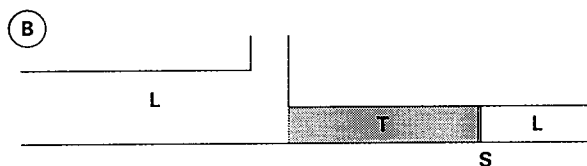
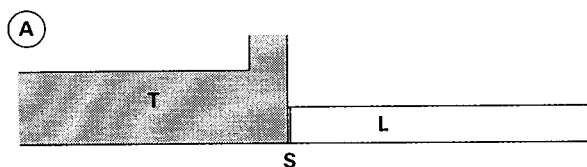


Fig. 1. Scheme of the interface in the column-coupling ITP–CZE arrangement for the T–S–T and L–S–L systems. The pre-separation (wide) capillary is located on the left and the analytical (narrow) capillary on the right. The leading, sample and terminating zones are marked as L, S and T, respectively. The arrow shows the origin of the longitudinal coordinate ( $x = 0$ , positive to the right) used in the calculations. For further explanation, see text.

simple relationship (1) is not valid, however, in processes where transient ITP migration takes place. The velocity of migration of an analyte differs in the ITP and ZE modes and, as a result, the detection time can be either increased or decreased when compared with the velocity of migration in the ZE mode only. It was shown [22] that the main factors bringing the differences are the magnitude of the segments of the leading zone introduced into the T–S–T system,

the magnitude of the segment of the terminating zone introduced into the L–S–L system and the magnitudes of both of them introduced into the BGE–S–BGE system.

The increase in the detection time of a zone stacked temporarily in a T–S–T system can be expressed by [22]

$$t_{x,r} = \frac{x_r \kappa_T}{i \bar{u}_x} + \frac{u_L - u_T}{u_L - \bar{u}_x} \cdot t_0 \quad (2)$$

where  $x_r$  is the distance of the detector from the inlet of the analytical capillary ( $x = 0$ ),  $\kappa_T$  is the specific conductivity of the background electrolyte (here formed by the terminator from the ITP step) in the analytical capillary,  $i$  is the electric current density in the analytical capillary and  $t_0$  is the time of the migration of the leading zone segment into the analytical capillary (i.e., into the ZE stage). This equation can be rewritten in the simple form

$$t_{x,r} = a_1 + b_1 t_0 \quad (3)$$

where  $a_1$  and  $b_1$  are constants, predicting a linear dependence of  $t_{x,r}$  on  $t_0$ ; Fig. 2 illustrates this, showing a calculated example for three model substances.

Eqs. 2 and 3 hold only for sample zones that had left the stack before they entered the detection cell, i.e. only such  $t_{x,r}$  values have physical meaning for which  $t_{x,r} > t_{z,r}$ , where  $t_{z,r}$  is the detection time of the stacking boundary given by [22]

$$t_{z,r} = \frac{\kappa_T}{i u_L} \left( \sqrt{x_r} + \sqrt{x_d} \cdot \frac{u_L - u_T}{u_T} \right)^2 \quad (4)$$

The coordinate  $x_d$  where the original ITP plateau disappears is given by [22,29]

$$x_d = t_0 \cdot \frac{i u_T^2}{\kappa_T (u_L - u_T)} \quad (5)$$

so that we can obtain  $t_{z,r}$  as a function of  $t_0$ :

$$t_{z,r} = \left( \sqrt{x_r \cdot \frac{\kappa_T}{i u_L}} + \sqrt{t_0 \cdot \frac{u_L - u_T}{u_L}} \right)^2 \quad (6)$$

The course of this function is shown in Fig. 2 by the dashed line. Only  $t_{x,r}$  values above this line are valid for the correct detection of zones. The

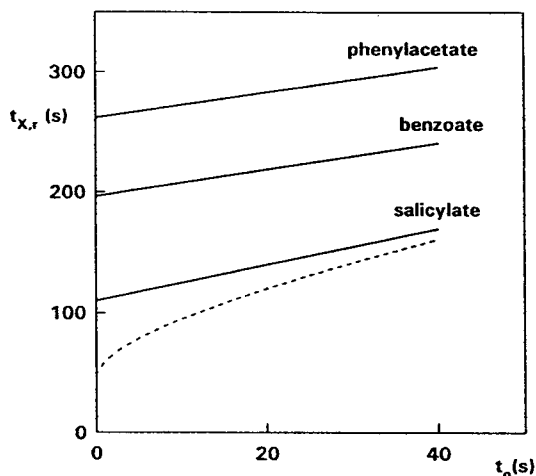


Fig. 2. Calculated dependence of detection time ( $t_{x,r}$ ) of salicylate, benzoate and phenylacetate on the time ( $t_0$ ) of migration of the leading zone into the analytical capillary in a T–S–T system composed of 0.01 M HCl– $\beta$ -alanine (pH 3.5) (leader) and 0.01 M acetic acid– $\beta$ -alanine (pH 4.3) (terminator, BGE). The effective mobilities of anions used in the calculation were  $(11.1, 33.3, 18.7 \text{ and } 14.0) \cdot 10^{-9} \text{ m}^2 \text{ V}^{-1} \text{ s}^{-1}$  for acetate, salicylate, benzoate and phenylacetate, respectively. The calculations were performed for an electric current of 50  $\mu\text{A}$  and a capillary of 300  $\mu\text{m}$  I.D. and 11.5 cm length. For explanation of the dashed curve, see text.

detection times below this dashed line represent the case when transient ITP survived on migrating up to the detection cell. As is seen, for the selected system and three analytes, the danger of being detected still in stack is small here and would require really large segments of the leader being introduced into the ZE stage. This is because the mobilities of all three analytes differ substantially from that of the leading ion.

For the L–S–L system, an equation analogous to Eq. 2 can be derived [22]:

$$t_{x,r} = \frac{x_r \kappa_L}{i \bar{u}_x} - \frac{u_L - u_T}{\bar{u}_x - u_T} \cdot t_0 = a_2 - b_2 t_0 \quad (7)$$

where  $t_0 = l_T \kappa_L / u_L i$  is the time of migration of the segment of the terminating zone into the analytical capillary and  $l_T$  is the final length of this zone. Again, a linear dependence of  $t_{x,r}$  on  $t_0$  is obtained, with the difference that the slope of the lines is negative, as is shown in Fig. 3 for an example of three model substances. Also here

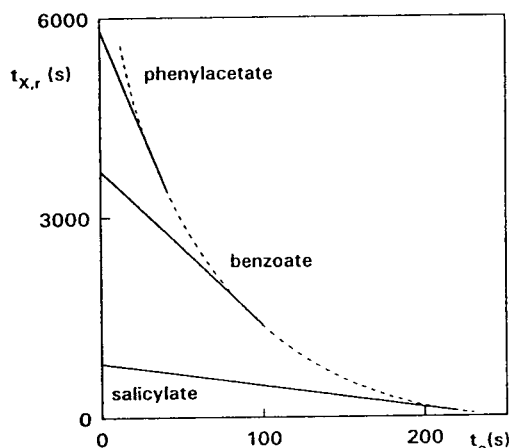


Fig. 3. Calculated dependence of detection time ( $t_{X,r}$ ) of salicylate, benzoate and phenylacetate on the time ( $t_0$ ) of migration of the terminating zone into the analytical capillary in an L–S–L system composed of 0.01 M HCl– $\beta$ -alanine (pH 3.5) (leader, BGE) and 0.01 M acetic acid– $\beta$ -alanine (pH 4.3) (terminator). The effective mobilities of anions used in the calculation were  $(25.3, 5.59$  and  $3.54) \cdot 10^{-9} \text{ m}^2 \text{ V}^{-1} \text{ s}^{-1}$  for salicylate, benzoate and phenylacetate, respectively. The calculations were performed for an electric current of  $50 \mu\text{A}$  and a capillary of I.D.  $300 \mu\text{m}$  I.D. and  $11.5 \text{ cm}$  length. For explanation of the dashed curve, see text.

the resulting linear dependence of  $t_{X,r}$  on  $t_0$  is limited by the condition that the analytes must be out of stack when passing the detector. This can be expressed by  $t_{X,r} > t_{z,r}$ , where  $t_{z,r}$  can be derived from Eq. 16 in Ref. [22]:

$$t_{z,r} = \frac{\kappa_L}{i u_T} \left( \sqrt{x_r} - \sqrt{x_d} \cdot \frac{u_L - u_T}{u_L} \right)^2 \quad (8)$$

By expressing  $x_d$  as

$$\begin{aligned} x_d &= t_d u_L \cdot \frac{i}{\kappa_T} = l_T \cdot \frac{u_L}{u_L - u_T} \\ &= t_0 \cdot \frac{i}{\kappa_L} \cdot \frac{u_L^2}{u_L - u_T} \end{aligned} \quad (9)$$

we can write Eq. 8 as a function

$$t_{z,r} = \left( \sqrt{x_r} \cdot \frac{\kappa_L}{i u_T} + \sqrt{t_0 \cdot \frac{u_L - u_T}{u_T}} \right)^2 \quad (10)$$

In Fig. 3, this function is represented by the dashed curve. The points where the straight lines

for actual analytes touch this dashed curve correspond to the limiting case when the analytes reach the detector just being destacked. Only points below the dashed curve have physical meaning and it can be seen that the impact of  $t_0$  on the analytical result is here obviously much more pronounced.

### 2.3. Effect of temporal stacking on efficiency

It has been shown [29] that the spatial variance in the detection cell,  $\sigma_{X,r}^2$ , of an electrophoretically migrating sample zone X that has undergone temporal stacking is given by

$$\sigma_{X,r}^2 = \sigma_{X,e}^2 + 2D_X(t_{X,r} - t_{X,e}) \quad (11)$$

where  $\sigma_{X,e}^2$  is the variance of this zone at time  $t_{X,e}$  when it leaves the temporal stack and  $D_X$  is the diffusion coefficient of the analyte X. When investigating this relationship for the T–S–T system, we can express  $t_{X,e}$  on the basis of equations given in Ref. [22] as

$$t_{X,e} = t_0 \cdot \frac{u_L(u_L - u_T)}{(u_L - \bar{u}_X)^2} \quad (12)$$

Using Eq. 12 and assuming that  $\sigma_{X,e}^2$  can be neglected, we obtain Eq. 11 in the form

$$\sigma_{X,r}^2 = 2D_X \left[ \frac{x_r \kappa_T}{i \bar{u}_X} - t_0 \cdot \frac{\bar{u}_X(u_L - u_T)}{(u_L - \bar{u}_X)^2} \right] \quad (13)$$

The time-based zone variance can be expressed as

$$\sigma_{X,t}^2 = \frac{\sigma_{X,r}^2}{v_{X,T}^2} \quad (14)$$

where  $v_{X,T} = \bar{u}_X \cdot i / \kappa_T$  is the zone electrophoretic migration velocity of X in the BGE (here BGE = T). Combining Eqs. 13 and 14, expressing  $D_X$  from the Nernst–Einstein equation as  $RTu_X/F$  and assuming the sample to be a strong electrolyte ( $u_X = \bar{u}_X$ ), we obtain

$$\begin{aligned} \sigma_{X,t}^2 &= \frac{2RT}{F} \left( \frac{\kappa_T}{i} \right)^3 \frac{x_r}{\bar{u}_X^2} - 2 \cdot \frac{RT}{F} \left( \frac{\kappa_T}{i} \right)^2 \\ &\times \frac{(u_L - u_T)t_0}{(u_L - \bar{u}_X)^2} = \frac{a_3}{\bar{u}_X^2} - \frac{b_3 t_0}{(u_L - \bar{u}_X)^2} \end{aligned} \quad (15)$$

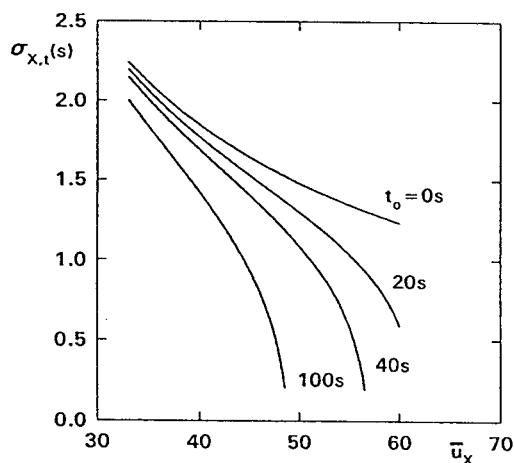


Fig. 4. Calculated dependence of zone width (expressed as time-based standard deviation,  $\sigma_{X,t}$ ) on the effective mobility ( $\bar{u}_X$ , in  $10^{-9} \text{ m}^2 \text{ V}^{-1} \text{ s}^{-1}$ ) of the analyte for various times ( $t_0$ ) of migration of the leading zone into the analytical capillary in a T-S-T system composed of 0.063 M HCl-histidine (pH 6.00) (leader) and 0.045 M aspartic acid-histidine (pH 6.15) (terminator, BGE). The calculations were performed for an electric current of 200  $\mu\text{A}$  and a capillary of 300  $\mu\text{m}$  I.D. and 13 cm length.

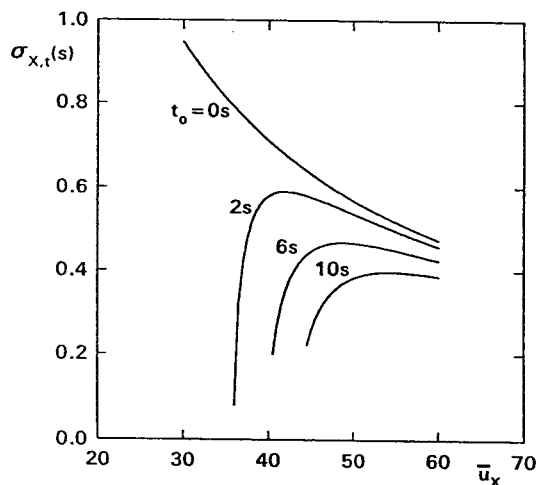


Fig. 5. Calculated dependence of zone width (expressed as time-based standard deviation,  $\sigma_{X,t}$ ) on the effective mobility ( $\bar{u}_X$ , in  $10^{-9} \text{ m}^2 \text{ V}^{-1} \text{ s}^{-1}$ ) of the analyte for various times ( $t_0$ ) of migration of the terminating zone into the analytical capillary in an L-S-L system composed of 0.01 M HCl-histidine (pH 6.00) (leader, BGE) and 0.0071 M aspartic acid-histidine (pH 6.15) (terminator). The calculations were performed for an electric current of 150  $\mu\text{A}$  and a capillary of 300  $\mu\text{m}$  I.D. and 13 cm length.

This equation shows the dependence of  $\sigma_{X,t}^2$  on  $\bar{u}_X$  and on  $t_0$ , as is illustrated in Fig. 4 for a given model example (T-S-T system, see captions). The curve for  $t_0 = 0$  represents rigorous zone electrophoresis. The larger is  $t_0$  (i.e., the longer the segment of L), the narrower is the mobility region of substances that can reach the detector already destacked (and more dispersed). For a given  $t_0$ , the zone dispersion decreases with increasing  $\bar{u}_X$  because the more mobile substances remain stacked for a longer time than the less mobile substances.

For the L-S-L system, Eq. 11 is also valid. For substitution of  $t_{X,r}$ , however, Eq. 7 must be used and for  $t_{X,e}$  it can be derived by using Eqs. 9, 11 and 18 in Ref. [22] (with  $t_0 = l_L/v_{T-L}$ ) that

$$t_{X,e} = t_0 \cdot \frac{u_T(u_L - u_T)}{(\bar{u}_X - u_T)^2} \quad (16)$$

Using a similar procedure as in the previous case, we obtain in analogy

$$\sigma_{X,r}^2 = 2D_X \left[ \frac{x_r \kappa_L}{i \bar{u}_X} - t_0 \cdot \frac{\bar{u}_X(u_L - u_T)}{(\bar{u}_X - u_T)^2} \right] \quad (17)$$

$$\sigma_{X,t}^2 = \frac{2RT}{F} \left( \frac{\kappa_L}{i} \right)^3 \frac{x_r}{\bar{u}_X^2} - 2 \cdot \frac{RT}{F} \left( \frac{\kappa_L}{i} \right)^2 \times \frac{(u_L - u_T)t_0}{(u_X - \bar{u}_T)^2} = \frac{a_4}{\bar{u}_X^2} - \frac{b_4 t_0}{(u_X - \bar{u}_T)^2} \quad (18)$$

Fig. 5 illustrates the dependence described by Eq. 18 for an L-S-L model example. The curve for  $t_0 = 0$  shows a similar course to that in Fig. 4, but for  $t_0 > 0$  the courses are different in principle. The differences are clearly seen for the other curves, which drop abruptly when approaching low  $\bar{u}_X$  values. This is explained by the fact that analytes with low mobilities (but not lower than  $u_T$ ) are stacked for a longer time than those with high mobilities. It should be stressed here that Fig. 5 predicts the existence of stacking-induced zone-variance inversion where the slowest zone is the narrowest and the fastest zone is the widest when passing the detector.

It is interesting to investigate now how the above-described rules for the zone variance demonstrate themselves in a more complicated system such as the BGE-S-BGE system. Here

the segments of the original leading and terminating zones are cut into the ZE stage. Depending on the mobility of the selected BGE, the analyte zones are stacked either by the leading or by the terminating segment and the whole train of transient ITP zones can be considered as consisting of two independent systems. The variance of an analyte zone is thus described either by Eq. 15 or by Eq. 18 modified as follows:

(i) for analytes with  $u_{\text{BGE}} < \bar{u}_X < u_L$ :

$$\sigma_{X,t}^2 = \frac{2RT}{F} \left( \frac{\kappa_{\text{BGE}}}{i} \right)^3 \frac{x_r}{\bar{u}_X^2} - 2 \cdot \frac{RT}{F} \times \left( \frac{\kappa_{\text{BGE}}}{i} \right)^2 \frac{(u_L - u_{\text{BGE}})}{(u_L - \bar{u}_X)^2} \cdot t_L \quad (19)$$

(ii) for analytes with  $u_T < \bar{u}_X < u_{\text{BGE}}$ :

$$\sigma_{X,t}^2 = \frac{2RT}{F} \left( \frac{\kappa_{\text{BGE}}}{i} \right)^3 \frac{x_r}{\bar{u}_X^2} - 2 \cdot \frac{RT}{F} \times \left( \frac{\kappa_{\text{BGE}}}{i} \right)^2 \frac{(u_{\text{BGE}} - u_T)}{(u_X - \bar{u}_T)^2} \cdot t_T \quad (20)$$

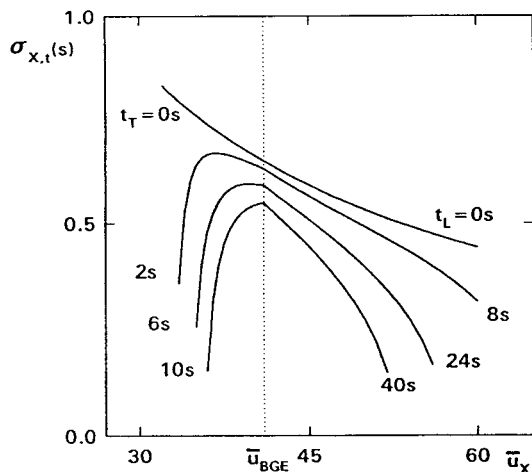


Fig. 6. Calculated dependence of zone width (expressed as time-based standard deviation,  $\sigma_{X,t}$ ) on the effective mobility ( $\bar{u}_X$ , in  $10^{-9} \text{ m}^2 \text{ V}^{-1} \text{ s}^{-1}$ ) of the analyte for various times ( $t_L$  and  $t_T$ ) of migration of the leading and terminating zone, respectively, into the analytical capillary in a BGE–S–BGE system composed of 0.01 M HCl–histidine (pH 6.00) (leader), 0.007 M aspartic acid–histidine (pH 6.15) (terminator) and 0.01 M acetic acid–histidine (pH 6.12) (BGE). The calculations were performed for an electric current of 100  $\mu\text{A}$  and a capillary of 300  $\mu\text{m}$  I.D. and 13 cm length.

where  $t_L$  and  $t_T$  represent the actual values of  $t_0$  corresponding to the amount of the introduced segments of the L and T zones, respectively. Note that both equations can be used simultaneously for the description of a system, although the starting points for the time count in the zone electrophoretic stage are not the same for cases (i) and (ii); this is because only the difference  $t_{X,r} - t_{X,e}$  appears in Eq. 11.

The practical impact of Eqs. 19 and 20 can be again best illustrated by a model example, as shown in Fig. 6. Here, the  $u_{\text{BGE}}$  value splits the plot into two areas which correspond to the two types of dependence shown in Figs. 4 and 5. In practice this predicts that the zones of analytes of intermediate mobilities (close to the  $u_{\text{BGE}}$  value) will be the broadest while zones of analytes of both high and low mobilities will be less broad owing to their longer stacking time.

### 3. Experimental

#### 3.1. Calculations

All calculations were performed for model systems of simplified behaviour. The input ionic mobilities and dissociation constants taken from literature [30] are listed in Table 1. All these values and the effective mobilities of weak acids and bases calculated for a given electrolyte

Table 1  
Constants used for the calculations

Substance	Ionic mobility ( $10^{-9} \text{ m}^2 \text{ V}^{-1} \text{ s}^{-1}$ )	$\text{p}K_a$
$\beta$ -Alanine	37.5	3.55
Acetate	42.4	4.75
Aspartate	31.6	3.9
Benzoate	33.6	4.2
Chloride	79.1	
$\text{H}^+$	362.5	
Histidine	29.6	6.04
Iodate	42	0.77
Maleate	41; 62.4	1.9; 6.22
Periodate	56.5	1.55
Phenylacetate	31.7	4.4
Salicylate	35.4	3.1

system were assumed to be constant during the analysis.

### 3.2. Instrumentation

A CS ZKI 01 isotachophoretic analyser (URVJT, Spišská Nová Ves, Czech Republic) equipped with a column-switching system was used. Both preseparation and analytical capillaries were made from PTFE and their I.D. was 0.3 mm. The preseparation capillary was equipped with a conductivity detector positioned 19 cm from the injection point and 5 cm from the bifurcation point. The analytical capillary was equipped with the UV and conductivity detectors placed at distances of 13 cm and 16 cm from the bifurcation point.

The pH of solutions was measured with a Model MS-20 ion activity meter (Laboratorní přístroje, Prague, Czech Republic) with a combined glass electrode.

### 3.3. Chemicals

Water deionized with a Miele Aqua Purificator G7749 was used for the preparation of both electrolyte systems and sample solutions. All the chemicals used were of analytical-reagent grade and purchased from Lachema (Brno, Czech Republic), except for aspartic acid and histidine, which were from Reanal (Budapest, Hungary).

### 3.4. Working procedures

The sample was introduced via a sampling valve of 24.5  $\mu$ l. The first (preseparation) capillary and the corresponding electrode vessels were filled with the isotachophoretic electrolyte system, i.e., with the leading and terminating electrolytes. The second (analytical) capillary and its electrode vessel were filled with the background electrolyte. In the first (ITP) stage, the current passed only through the first capillary between the corresponding electrode vessels containing the leading and terminating electrolyte, respectively. When the rear boundary of the leading zone in the first capillary approached the bifurcation point, the current was switched

over to pass through both the preseparation and analytical capillaries.

Suitable timing of this event must be found experimentally with the help of the tell-tale conductivity detector located near the end of the preseparation capillary. Since this detector is placed at a certain distance from the bifurcation block, the exact time when the L–T boundary appears at the bifurcation point must be found by using a suitable dye. This dye is injected as the only analyte into this system, migrates between the leading and terminating electrolyte and is both detected by the tell-tale detector and observed when it reaches the bifurcation point. The time necessary for the boundary to pass the distance between the detector and bifurcation point is constant for constant composition of the leading electrolyte and constant experimental conditions.

Hence the whole train of ionic species in question started to migrate into the analytical capillary. After the whole sample stack entered the analytical capillary, the current was switched off and the terminating electrolyte, now filling the whole preseparation capillary, was washed out and replaced with the BGE. After that the whole separation system was filled with BGE and the stack of sample zones was the only discontinuity in this electrolyte. When the terminator was used as the BGE, the washing step was omitted and the analysis could continue immediately after switching the current over.

The timing of the process is as follows. The time point at which the current is switched over across both capillaries defines the length of the segment of the leading zone entering the analytical capillary expressed in time units. The time of switching the current on after the flushing the terminator out of the preseparation capillary defines the length of the terminating electrolyte that has entered the analytical capillary together with the sample stack. The time counting for the CZE step begins at the moment when the sample being sandwiched by the segments of leading and terminating zones and the whole capillary system being filled with the BGE started to migrate. In the T–S–T system this means that the zone of the sample is still situated in the preseparation

capillary with a segment of leader in front of it, whereas in the L–S–L and BGE–S–BGE systems the sample is already in the analytical capillary followed by the terminator (L–S–L system) or sandwiched by the leader and terminator (BGE–S–BGE system) (see Fig. 1).

#### 4. Results and discussion

The effect of temporal stacking on the detection time is illustrated by Figs. 7 and 8. Fig. 7 is analogous to Fig. 2, showing experimental results in a commonly used ITP buffered electrolyte system (modelling here a T–S–T system) with  $\text{Cl}^-$  as the leading ion, histidine as the counter ion and aspartate playing here the role of the terminating ion. A  $10^{-6}$  M solution of anions of organic and inorganic acids was used as

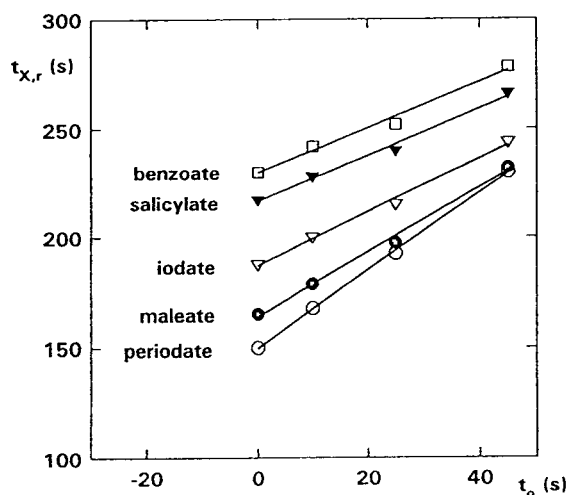


Fig. 7. Experimental verification of the dependence of the detection time ( $t_{x,r}$ ) on the length of the leading zone expressed as the time of its migration into the analytical capillary ( $t_0$ ) filled with terminator (T–S–T electrolyte system). Measurements were performed at a constant current of  $75 \mu\text{A}$  in both the ITP and CZE migration modes. Leading electrolyte, 10 mM HCl–histidine (pH 6.0); terminating electrolyte, 10 mM aspartic acid–histidine (pH 6.15). As the background electrolyte for CZE, the terminating electrolyte from the ITP step was used. Sample,  $25 \mu\text{l}$  of  $1 \cdot 10^{-6}$  M benzoate, salicylate, iodate, maleate and periodate.

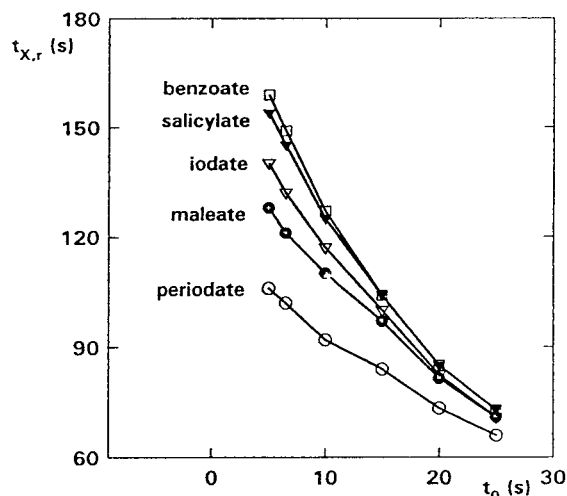


Fig. 8. Experimental verification of the dependence of the detection time ( $t_{x,r}$ ) on the length of the terminating zone expressed as the time of its migration into the analytical capillary ( $t_0$ ) filled with leading electrolyte (L–S–L electrolyte system). Measurements were performed at a constant current of  $75 \mu\text{A}$  in the ITP mode and  $150 \mu\text{A}$  in the CZE step. Leading electrolyte, 10 mM HCl–histidine (pH 6.0); terminating electrolyte, 10 mM aspartic acid. As the background electrolyte for CZE, the leading electrolyte from the ITP step was used. Sample,  $25 \mu\text{l}$  of  $1 \cdot 10^{-6}$  M benzoate, salicylate, iodate, maleate and periodate.

the model mixture. Fig. 7 confirms the linear character of the  $t_{x,r}$  vs.  $t_0$  dependence predicted by Eq. 3. It can be seen that the longer the segment of the leading zone that was cut into the analytical capillary, the greater is the prolongation of the detection time. When the segment of the leading zone is very long (i.e.,  $t_0$  is high), there is a risk that analytes with the largest mobility can still be migrating in stack when passing the detector (see maleate and periodate at  $t_0 = 40$  s).

Such effects (especially for low-mobility analytes) are more pronounced in Fig. 8, showing experimental results based on the same electrolytes as those in Fig. 7 but used in an L–S–L arrangement. The L–S–L system allows one to perform very fast analyses but there is a real danger that if the detector is not placed at a sufficient distance from the bifurcation point, some of the slower analytes can still migrate in

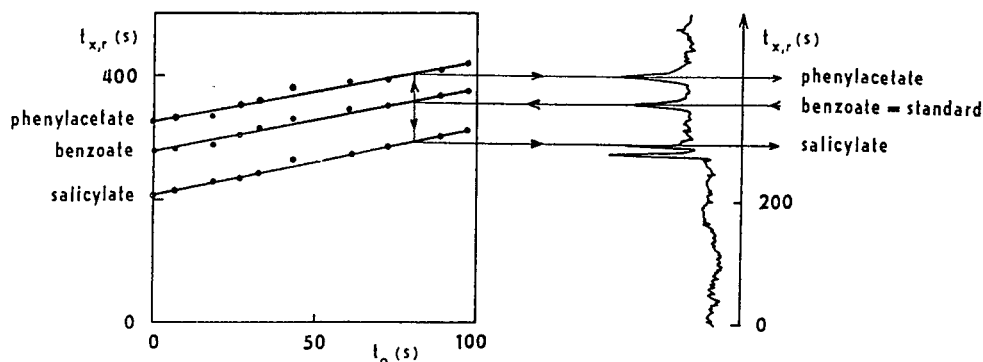


Fig. 9. Principle of the standardization method. To be able to identify analytes in the sample, the calibration graph for the dependence of the detection time of analytes and of an internal standard on the length of the leading electrolyte that had co-migrated with the sample into the CZE step in the case of the T-S-T system (or terminator in the case of the L-S-L system) has to be drawn and used as demonstrated here for the T-S-T system. Measurements were performed at a constant current of  $100 \mu\text{A}$  in the ITP mode and  $50 \mu\text{A}$  in the CZE step. Leading electrolyte,  $10 \text{ mM}$  HCl- $\beta$ -alanine (pH 3.5); terminating electrolyte,  $10 \text{ mM}$  acetic acid (pH 4.3). As the background electrolyte for CZE, the terminating electrolyte from the ITP step was used. Sample,  $25 \mu\text{l}$  of  $1 \cdot 10^{-7} \text{ M}$  salicylate, benzoate and phenylacetate mixture.

stack (see Fig. 8 at higher  $t_0$  values). Also here, the character of the curves fits well with the predictions (see Fig. 3).

Figs. 7 and 8 indicate that the methods (see Ref. [31] and citations therein) utilizing the migration times directly for qualitative evaluation of the analysis may be strongly misleading. Fig. 9 brings a possible solution to this problem, showing the principles of a simple standardization procedure. This procedure requires one to have the experimental dependences of  $t_{x,r}$  on  $t_0$  for all analytes of interest and for a selected standard substance. If this standard is added to the analysed sample and it is possible to recognise its peak in the electropherogram of this sample, we can determine the value of  $t_0$  corresponding to the sample and consequently identify the analyte peaks.

The effect of temporal stacking on the efficiency was investigated experimentally first in the most user-friendly T-S-T system. Fig. 10 shows the experimental dependence of time-based peak standard deviation on mobility for a series of weak acids analysed using a BGE composed of  $15 \text{ mM}$  aspartic acid-histidine (pH 6.15). The leader for the ITP step was  $10 \text{ mM}$  HCl- $20 \text{ mM}$  histidine (pH 6). Aspartic acid

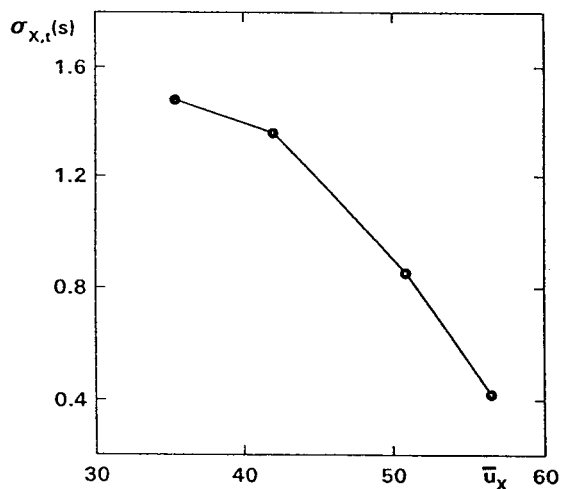


Fig. 10. Experimental verification of the time-based peak standard deviation ( $\sigma_{x,t}$ ) on the mobility of analytes ( $\bar{u}_x$ , in  $10^{-9} \text{ m}^2 \text{ V}^{-1} \text{ s}^{-1}$ ) in the T-S-T system. Measurements were performed at a constant current of  $150 \mu\text{A}$  in both the ITP and CZE modes. Leading electrolyte,  $10 \text{ mM}$  HCl-His (pH 6.0); terminating electrolyte,  $15 \text{ mM}$  aspartic acid-His (pH 6.15). As the background electrolyte for CZE, the terminating electrolyte from the ITP step was used. Length of the leading segment at the beginning of CZE separation,  $9 \text{ s}$ ; sample,  $25 \mu\text{l}$  mixture of  $1 \cdot 10^{-6} \text{ M}$  salicylate, iodate, maleate and periodate. The effective mobilities of the analytes at pH 6.00 were calculated from the data given in Table 1.



served as the terminator. Comparison of the results with Fig. 4 demonstrates good coincidence of the experiment with theory, i.e., zone variance in this system decreases with increasing effective mobility.

Fig. 11 presents this dependence for a BGE–S–BGE system composed of 10 mM HCl–histidine (pH 6.0) as the leading electrolyte, 10 mM aspartic acid as terminator and 10 mM acetic acid–histidine (pH 6.12) as BGE. Also here, the comparison with theory is satisfactory and one can see an anomalous course of the

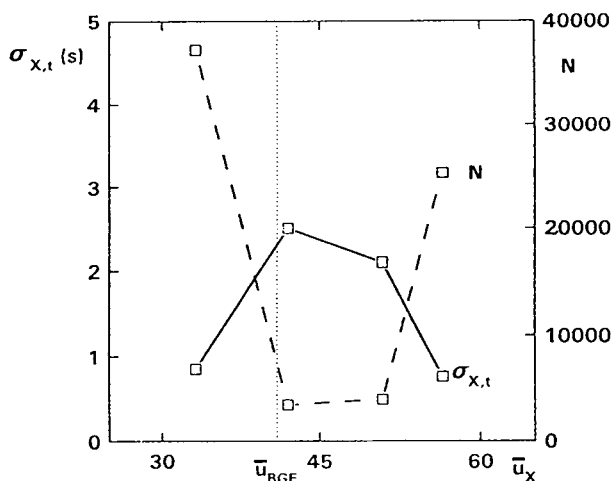


Fig. 11. Experimental verification of the combined effect of front and rear stack expressed as the dependence of the time-based zone width ( $\sigma_{x,t}$ ) and separation efficiency ( $N$ ) on the mobility of the analytes ( $\bar{u}_x$ , in  $10^{-9} \text{ m}^2 \text{ V}^{-1} \text{ s}^{-1}$ ). Measurements were performed at a constant current of 75  $\mu\text{A}$  in the ITP mode and 100  $\mu\text{A}$  in the CZE step. Leading electrolyte, 10 mM HCl–histidine (pH 6.0); terminating electrolyte, 10 mM aspartic acid; background electrolyte, 10 mM acetic acid–histidine (pH 6.12). The length of the leading segment co-migrating with the sample into the CZE mode was 15 s and the length of the terminating segment was 20 s. Sample, 25  $\mu\text{l}$  of a mixture of  $1 \cdot 10^{-6} \text{ M}$  benzoate, iodate, maleate and periodate. The effective mobilities of the analytes at pH 6.12 were calculated from the data given in Table 1. The dotted line corresponds to the splitting point given by the mobility of the BGE co-ion (acetate). Analytes with  $\bar{u}_x > \bar{u}_{BGE}$  are controlled by the leading ion as in the T–S–T system, whereas analytes with  $\bar{u}_x < \bar{u}_{BGE}$  are controlled by the terminating ion as in the T–S–T system.

dispersion of zones: the first and last zones are the sharpest with the highest separation efficiency and the zones of mobilities very close to the mobility of the co-ion are the most dispersed owing to their early destacking. Comparison with Fig. 6 confirms the predicted course of the curves, which can also be expressed in terms of efficiency (see left-hand scale in Fig. 11).

Fig. 12 shows a record of ITP–CZE separation performed in the BGE–S–BGE system where the anomalous zone width distribution is clearly seen, the first and last zones being the sharpest. The lengths of both the leading and terminating segments entering the analytical capillary influence the process of destacking and the migration times of analytes. The longer the segments, the closer the analytes are one to another and the sharper are their zones.

## 5. Conclusion

In the separation technique combining isotachopheresis and zone electrophoresis on-line, the presence of a segment of leading and/or terminating zones in the CZE stage can never be eliminated. This results in a temporal survival of ITP migration followed by a complicated process of sample destacking, which makes simple rules describing a CZE analysis misleading. The theory presented here describes the destacking process and shows the most important factors affecting this process.

Using a given instrument and electrolyte setup, the most important factor is the size of the ITP zones cut into the ZE stage. The effects of this factor on the detection time may be characterized in actual systems as follows. In T–S–T systems, the detection times of the analytes increase linearly with increasing amount of leader introduced. In L–S–L systems, the detection time decreases linearly with increasing amount of terminator introduced. These effects relate only to sample zones that are already destacked when passing the detector; to ensure this, the amount of the leader/terminator intro-

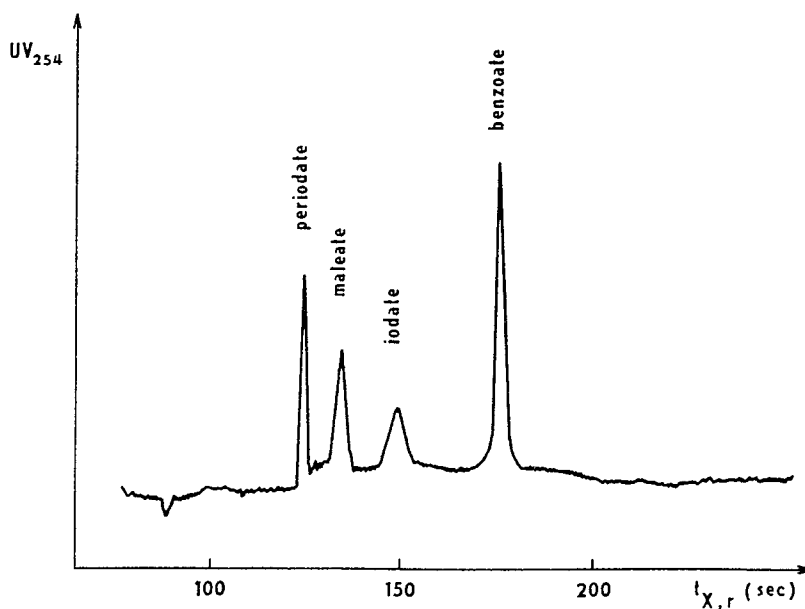


Fig. 12. Effects of destacking process in the BGE–S–BGE system. Experimental conditions as in Fig. 11 except for segment lengths. Leading segment = 15 s, terminator segment = 13 s.

duced must not exceed a certain value that differs from analyte to analyte. The qualitative identification of the analytes based on their variable detection times is possible using a standardization procedure requiring the sample to be run with one internal standard substance.

The temporal stacking also affects the final dispersion of the analyte zones at the point of detection, since the dispersion of zones is frozen as long as they are in stack. The longer the analyte zone remains stacked, the sharper is its peak when detected. The sharpest zones are therefore provided by high-mobility analytes in T–S–T systems and low-mobility analytes in L–S–L systems. BGE–S–BGE systems show an anomalous zone-dispersion distribution, with analytes of intermediate mobilities showing the most dispersed zones.

The theoretical and practical knowledge presented here enables one to formulate some rules for choosing a proper separation mode, electrolyte systems and parameters of the separation with respect to the nature of the sample. T–S–T and L–S–L modes of electrolyte combinations

offer simpler operation and evaluation than the BGE–S–BGE system. In the T–S–T system, the slow analytes are destacked first. They are more dispersed but, on the other hand, they are more distant from one another and the risk of stacked migration can be expected to be small. Hence, if the analytes of interest are slow, the T–S–T system may be recommended. If we are interested more in the fast components of the sample and the mobilities of these analytes are very close to the mobility of the leading ion, then it is more convenient to use the L–S–L system where these analytes leave the stack first and the risk of passing the detector still not destacked hardly exists. In both systems, qualitative identification of analytes employing one internal standard is possible on condition that the analytes migrate already fully destacked. The BGE–S–BGE system brings the most uncertainty into the separation and it cannot be recommended unless for a special case. Finally, one can conclude that the simplest to perform, evaluate and optimize seems to be the T–S–T system, in its version where the concentration of T serving as the BGE

is the same as the adjusted concentration of T in the ITP stage.

$\sigma_{X,e}^2$  variance of zone X when it leaves the stack  
 $\sigma_{X,r}^2$  detection variance of zone X

## Acknowledgements

This work was supported by grants from the Grant Agency of the Czech Republic, No. 203/94/0998, and the Grant Agency of the Academy of Sciences of the Czech Republic, No. 431404.

## Symbols

$D_X$  diffusion coefficient of analyte X  
 $i$  electric current density  
 $l_j$  length of the stacking zone  $j$  in the analytical capillary  
 $R$  gas constant  
 $T$  absolute temperature  
 $t_d$  time when the isotachophoretic plateau of the stacking zone in the analytical capillary disappears  
 $t_{X,e}$  time when substance X leaves the stack  
 $t_{X,r}$  time when zone X passes through the detector  
 $t_{z,r}$  time when the sharp boundary of the stacking zone passes through the detector  
 $t_0 (t_L, t_T)$  time of migration of the stacking zone into the analytical capillary  
 $u_X$  electrophoretic mobility of ion X  
 $\bar{u}_X$  effective mobility of substance X  
 $v_{T-L}$  isotachophoretic velocity in the analytical capillary  
 $v_z$  velocity of the sharp boundary of the L–T transition zone  
 $v_{Xj}$  migration velocity of analyte X in zone  $j$   
 $x_d$  coordinate at which the isotachophoretic plateau of the stacking zone in the analytical capillary disappears  
 $x_r$  position of the detector  
 $\kappa_j$  specific conductivity of zone  $j$

## References

- [1] D. Kaniansky and J. Marák, *J. Chromatogr.*, 498 (1990) 191.
- [2] F. Foret, V. Šustáček and P. Boček, *J. Microcol. Sep.*, 2 (1990) 229.
- [3] V. Dolník, K.A. Cobb and M. Novotny, *J. Microcol. Sep.*, 2 (1990) 127.
- [4] L. Křivánková, F. Foret and P. Boček, *J. Chromatogr.*, 545 (1991) 307.
- [5] D.S. Stegehuis, H. Irth, U.R. Tjaden and J. van der Greef, *J. Chromatogr.*, 538 (1991) 393.
- [6] F. Foret, E. Szoko and B.L. Karger, *J. Chromatogr.*, 608 (1992) 3.
- [7] Ch. Schwer and F. Lottspeich, *J. Chromatogr.*, 623 (1992) 345.
- [8] A.P. Tinke, N.J. Reinhoud, W.M.A. Niessen, U.R. Tjaden and J. van der Greef, *Rapid Commun. Mass Spectrom.*, 6 (1992) 560.
- [9] D.S. Stegehuis, U.R. Tjaden and J. van der Greef, *J. Chromatogr.*, 591 (1992) 341.
- [10] N.J. Reinhoud, A.P. Tinke, U.R. Tjaden, W.M.A. Niessen and J. van der Greef, *J. Chromatogr.*, 627 (1992) 263.
- [11] F. Foret, E. Szökő and B.L. Karger, *Electrophoresis*, 14 (1993) 417.
- [12] T.J. Thompson, F. Foret, P. Vouros and B.L. Karger, *Anal. Chem.*, 65 (1993) 900.
- [13] T. Hirokawa, A. Ohmori and Y. Kiso, *J. Chromatogr.*, 634 (1993) 101.
- [14] N.J. Reinhoud, U.R. Tjaden and J. van der Greef, *J. Chromatogr. A*, 653 (1993) 303.
- [15] N.J. Reinhoud, U.R. Tjaden and J. van der Greef, *J. Chromatogr.*, 641 (1993) 155.
- [16] D. Kaniansky, J. Marák, V. Madajová and E. Šimuničová, *J. Chromatogr.*, 638 (1993) 137.
- [17] L.M. Benson, A.J. Tomlinson, J.M. Reid, D.L. Walker, M.M. Ames, S. Naylor, *J. High Resolut. Chromatogr.* 16 (1993) 324.
- [18] D. Kaniansky, F. Iványi and F.I. Onuska, *Anal. Chem.*, 66 (1994) 1817.
- [19] M. Larsson and S. Någård, *J. Microcol. Sep.*, 6 (1994) 107.
- [20] M. Mazereeuw, U.R. Tjaden and J. van der Greef, *J. Chromatogr. A*, 677 (1994) 151.
- [21] S.J. Locke and P. Thibault, *Anal. Chem.*, 66 (1994) 3436.
- [22] L. Křivánková, P. Gebauer, W. Thormann, R.A. Mosher and P. Boček, *J. Chromatogr.*, 638 (1993) 119.

- [23] P. Boček, M. Deml, P. Gebauer and V. Dolník, *Analytical Isotachopheresis*, VCH, Weinheim, 1988.
- [24] F. Foret, L. Křivánková and P. Boček, *Capillary Zone Electrophoresis*, VCH, Weinheim, 1993.
- [25] L. Křivánková, F. Foret, P. Gebauer and P. Boček, *J. Chromatogr.*, 390 (1987) 3.
- [26] V. Šustáček, F. Foret and P. Boček, *J. Chromatogr.*, 545 (1991) 239.
- [27] P. Jandik and W.R. Jones, *J. Chromatogr.*, 546 (1991) 431.
- [28] H.W. Zhang, X.G. Chen and Z.D. Hu, *J. Chromatogr. A*, 677 (1994) 159.
- [29] P. Gebauer, W. Thormann and P. Boček, *J. Chromatogr.*, 608 (1992) 47.
- [30] J. Pospíchal, P. Gebauer and P. Boček, *Chem. Rev.*, 89 (1989) 419.
- [31] R. Vespalec, P. Gebauer and P. Boček, *Electrophoresis*, 13 (1992) 677.



ELSEVIER

Journal of Chromatography A, 716 (1995) 49–55

JOURNAL OF  
CHROMATOGRAPHY A

# Investigation and optimisation of the use of organic modifiers in micellar electrokinetic chromatography

Alison E. Bretnall\*, Graham S. Clarke

*Bristol-Myers Squibb Pharmaceutical Research Institute, Moreton, L46 1QW, UK*

## Abstract

The effect of organic modifiers (methanol, ethanol, propan-2-ol, butan-1-ol, butan-2-ol, acetone, methyl ethyl ketone and acetonitrile) on the micellar electrokinetic chromatographic (MEKC) resolution and migration time of seven model compounds has been investigated. The compounds used were all drugs reported to have cardiovascular antiarrhythmic activity. The organic modifiers have each been investigated at 5, 10 and 15% (v/v) of the electrophoretic buffer (100 mM borate buffer pH 8.1 containing 50 mM SDS as surfactant), to determine the optimum resolution and peak shape. The elution order under almost every condition corresponded to increasing molecular mass of the analyte drugs. Propan-2-ol at a concentration of 10% (v/v) gave optimum separation of the analytes. Replicate injections under these conditions gave excellent precision data for the migration time and corrected peak area. Other modifiers which gave baseline resolution of the analytes but less precise repeatability data were acetone and methyl ethyl ketone.

## 1. Introduction

Micellar electrokinetic chromatography (MEKC) is a high-resolution technique using surfactant micelles to provide a charged vehicle to perform an electrophoretic separation [1]. MEKC differs from capillary zone electrophoresis (CZE) in that both ionic [1,2] and neutral charged [3,4] analytes may be separated, whereas CZE only separates ionic analytes. Typically, anionic surfactants are included in the electrophoretic buffer at a concentration above its critical micelle concentration (CMC). The formation of micelles results in a pseudostationary phase created by the hydrophobic interior of the charged micellar structure which itself migrates towards the anode [5,6]. However, as the elec-

troosmotic flow (EOF) is faster than the anodic migration of the micelles, the net movement is in the direction of the EOF, i.e. towards the cathode. A mixture of analytes introduced into the EOF will therefore partition between the micelles and the electrophoretic buffer. The partitioning of each analyte will differ depending on its hydrophobic interaction with the micelle [7]. This is used to effect a separation of a mixture of analytes as the migration time of each component is a function of its partitioning with the micelle. The addition of small amounts of organic solvents to the MEKC buffer has several consequences [8], the most important being a change to the partitioning of the analyte between the micelle and the buffer [7,9–11], resulting in a different migration time for the analyte. The work reported here describes how different organic solvents modify the separation of a series

\* Corresponding author.

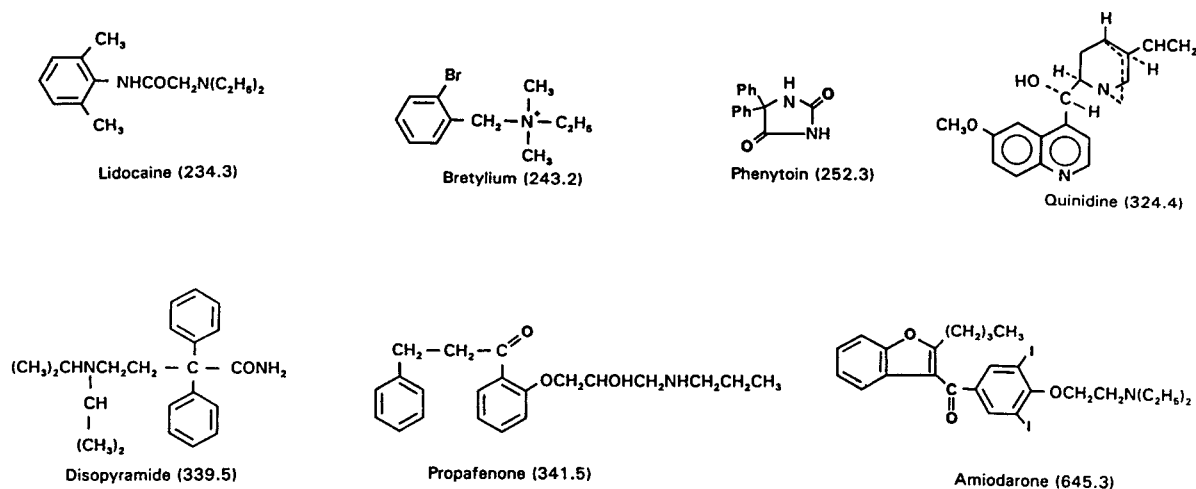


Fig. 1. Structures of drugs used in the electrophoretic optimisation (molecular masses in parentheses).

of seven model drug compounds (Fig. 1) which have cardiovascular antiarrhythmic activity.

## 2. Experimental

### 2.1. Reagents

The seven drugs studied were amiodarone hydrochloride, bretylium tosylate, disopyramide, lidocaine, phenytoin, propafenone and quinidine all obtained from Sigma (Poole, Dorset, UK). Purified water was provided by a Milli-Q Plus water purification system (Millipore, Watford, UK). Sodium dodecyl sulphate (SDS), sodium tetraborate, boric acid and sodium hydroxide, acetone, ethanol 96%, butan-1-ol, butan-2-ol, methyl ethyl ketone (Analar grade) and acetonitrile (Hipersolv grade) were obtained from BDH (Poole, Dorset, UK). Methanol and propan-2-ol (high purity grade) were purchased from Fisons Scientific Equipment (Loughborough, Leicestershire, UK)

### 2.2. Apparatus

A capillary electrophoresis P/ACE system 5510 (Beckman Instruments, High Wycombe, Bucks, UK) equipped with a diode array UV detector, an automatic injector, a fluid-cooled

cartridge and a System Gold data station was used in this study. All electrophoresis was carried out at 30°C, with an applied voltage of +25 kV and UV detection wavelength of 200 nm. Sample introduction was performed using the pressure option for 5 s. MEKC was performed in a 57 cm × 75 μm I.D. (50 cm to detector) fused-silica capillary tube (Beckman Instruments), and was rinsed with 0.1 M sodium hydroxide and the electrophoresis buffer before each electrophoretic separation. For all buffer systems used, individual solutions of each model analyte were injected to confirm the migration times.

## 3. Results and discussion

### 3.1. MEKC conditions

To investigate the effect of different organic solvents on the peak resolution and the migration time of the drug mixture, an electrophoretic buffer was identified to which organic solvents were added up to a level of 15% (v/v) in 5% increments. The electrophoretic buffer consisted of 50 mM SDS in 100 mM borate buffer, pH 8.1. There are several reported applications of the addition of methanol and acetonitrile to MEKC buffers [8,12,13] and part of this investigation

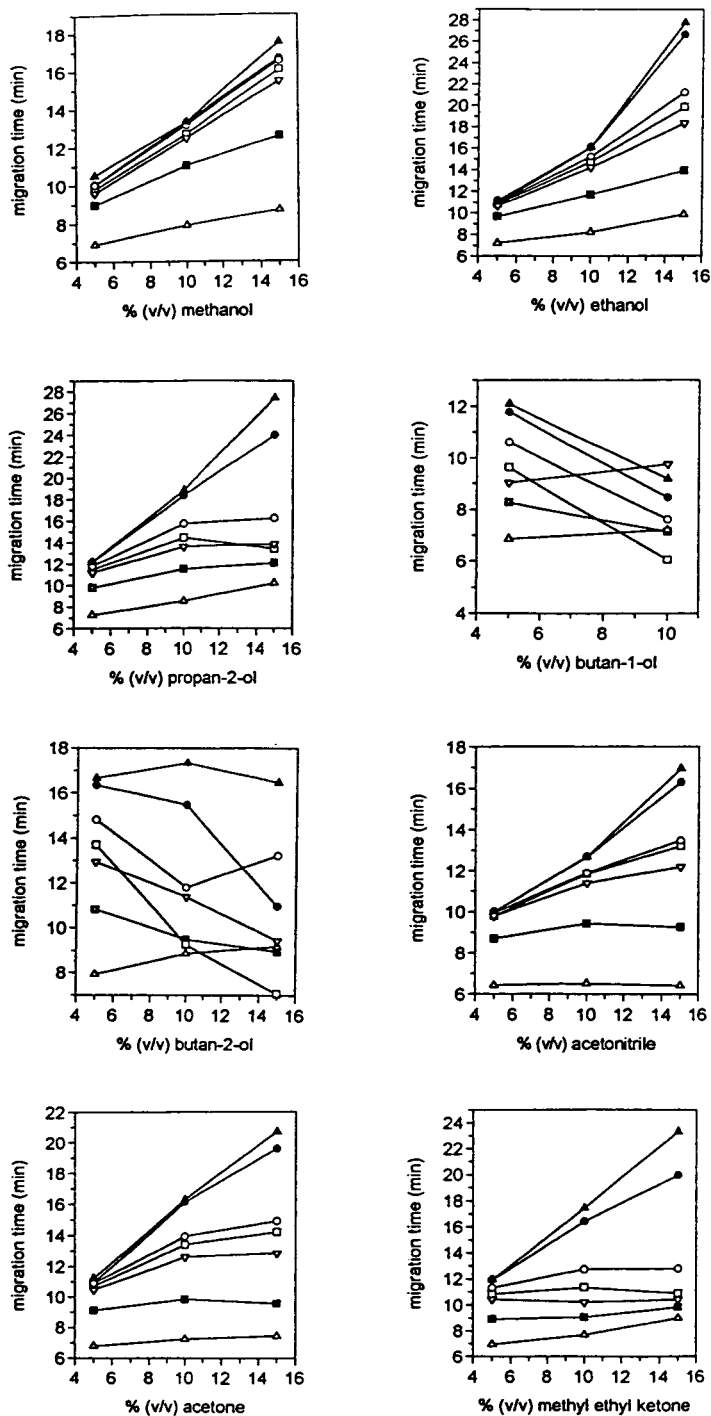


Fig. 2. Migration times of drug analytes in buffer solutions modified with organic solvents. ▲ = Amiodarone; ▽ = bretylium; □ = disopyramide; ■ = lidocaine; △ = phenytoin; ● = propafenone; ○ = quinidine.

focused on the use of other higher-molecular-mass alcohols. There are also reports of the use of acetone in MEKC buffers [12,14,15], and the effects of this solvent, together with another ketone (methyl ethyl ketone) has been investigated.

### 3.2. Analyte sample preparation

A mixture of the seven drugs was prepared in methanol at a concentration of 2 mg/ml (except amiodarone which was prepared at a concentration of 0.6 mg/ml for reasons of limited solubility). The solution was diluted to a concentration of 0.3 mg/ml (0.1 mg/ml of amiodarone) of each analyte in 50 mM SDS. Solutions of each individual analyte were also prepared at a concentration of 0.1 mg/ml in 50 mM SDS. These solutions were prepared in methanol at a concentration of 0.5 mg/ml and further diluted to 0.1 mg/ml in 50 mM SDS.

### 3.3. Optimisation of analyte separation

The criteria used for the optimisation of the separation of the seven drugs was the baseline resolution of each individual analyte, together with no peak splitting. The electropherograms generated with each buffer composition show a peak for each drug analyte and also a peak for

the tosylate counter-ion of bretylium. Five of the drugs in the mixture remained unresolved when MEKC was performed using electrophoretic buffer containing no organic solvent. The analyte mixture was separated using the electrophoretic buffer containing 5, 10 or 15% (v/v) of the organic solvent, except for the butan-1-ol which could not be used at concentrations greater than 10% (v/v) as it precipitated the buffer salts. The migration time of each analyte in the individual buffer systems generally correlated with an increase in molecular mass. The migration times for each analyte in relation to the organic solvents investigated are shown in Fig. 2. The migration order remained generally unchanged as the organic solvent content of the buffer increased. The analyte migration times also increased as the organic solvent content increased, with the exception of the butan-1-ol, where the migration times decreased with increasing organic content (5 to 10%) and butan-2-ol where little effect was observed as the concentration was changed. Table 1 shows the migration window (difference between the migration times of the first and last analyte) which increases with increasing organic solvent content. The migration window gives a measure of the total time taken to separate the analyte mixture in the electropherogram. It may be used for assessing whether the separation would be

Table 1  
Migration window for the MEKC separation using organic modifiers

Organic solvent	Migration window (min) for % organic solvent in electrolyte buffer					
	5% (v/v)		10% (v/v)		15% (v/v)	
Methanol	3.71	(7.95)	5.56	(10.47)	8.89	(13.10)
Ethanol	4.42	(8.72)	7.83	(12.21)	8.96	(18.84)
Propan-2-ol	5.40	(9.49)	10.32	(13.68)	17.25	(18.83)
Butan-1-ol	5.27	(9.46)	4.14	(7.69)	PPT <sup>a</sup>	–
Butan-2-ol	8.96	(12.17)	8.97	(12.85)	11.74	(11.44)
Acetonitrile	4.20	(7.81)	6.22	(9.58)	5.27	(11.69)
Acetone	5.10	(8.72)	9.05	(11.78)	13.28	(14.09)
Methyl ethyl ketone	5.73	(9.08)	10.07	(12.64)	14.32	(16.15)

Migration time corresponding to the centre of the migration window (i.e. the migration time of the first peak plus half the width of the migration window) is shown in parentheses. The migration window for unmodified electrolyte buffer is 2.85 min.

<sup>a</sup> PPT = organic solvent precipitated the buffer.



useful for determining additional analytes to those included in the described mixture. Also included in Table 1 (in parentheses) is the migration time corresponding to the centre of the migration window. This defines the position of the migration window in the electropherogram and indicates the time required for each separation.

Baseline resolution of all the analyte components without splitting of the peaks was only achieved with five organic solvent compositions, these being 10% (v/v) propan-2-ol and butan-2-ol and 15% (v/v) acetone, methyl ethyl ketone

and butan-2-ol (Table 2). Under all other conditions, at least two of the peaks were unresolved or one of the peaks was split. The butan-2-ol was not considered a suitable solvent to use as an organic modifier as the background UV absorption was very high at 200 nm which had the effect of making all analyte peaks very small. The 10% (v/v) propan-2-ol and the 15% (v/v) acetone and methyl ethyl ketone all show good resolution (Fig. 3) and the choice of organic solvent to be used as a modifier will depend on the desired width of the migration window. The propan-2-ol gave regularly spaced components in

Table 2  
Electrophoretic efficiency of the drug separation for different concentrations of organic modifier

Organic modifier	Concentration (% v/v)	Peaks unresolved	Split peaks
Methanol	5	Bretylium, disopyramide, quinidine, propafenone and amiodarone.	None
	10	Disopyramide and quinidine; propafenone and amiodarone.	None
	15	Quinidine and propafenone.	None
Ethanol	5	Bretylium, disopyramide, quinidine, propafenone and amiodarone.	None
	10	Propafenone and amiodarone.	None
	15	None	Lidocaine
Propan-2-ol	5	Propafenone and amiodarone.	None
	10	None	None
	15	Disopyramide and bretylium	None
Butan-1-ol	5	Phenytoin and tosylate ion	None
	10	Lidocaine and phenytoin	None
Butan-2-ol	5	Propafenone and amiodarone.	None
	10	None	None
	15	None	None
Acetone	5	Bretylium and disopyramide; propafenone and amiodarone	None
	10	Propafenone and amiodarone	None
	15	None	None
Methyl ethyl ketone	5	Propafenone and amiodarone.	None
	10	None	Disopyramide
	15	None	None
Acetonitrile	5	Bretylium, disopyramide, quinidine, propafenone and amiodarone.	None
	10	Disopyramide and quinidine.	None
	15	Disopyramide and quinidine.	None

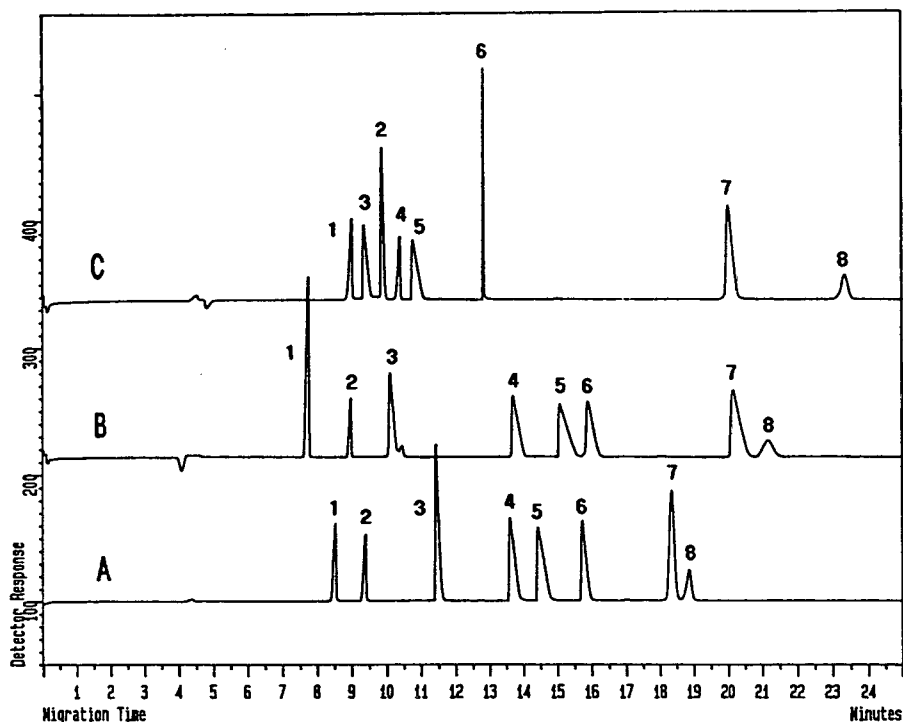


Fig. 3. Electropherograms of the drug analyte mixture using (A) 10% (v/v) propan-2-ol, (B) 15% (v/v) acetone and (C) 15% (v/v) methyl ethyl ketone as organic modifier in electrophoretic buffer. Peaks: 1 = phenytoin; 2 = tosylate ion; 3 = lidocaine; 4 = bretylium; 5 = disopyramide; 6 = quinidine; 7 = propafenone; 8 = amiodarone.

the electropherogram whereas with the ketone solvents, the spacing was irregular. If other analytes required separating from the drugs used in this analysis, the organic modifier could be selected to give optimum separation of the additional component from the existing drugs.

Use of organic modifiers is often avoided because of problems with evaporation of the organic solvent from the electrolyte buffer which

leads to poor precision between replicate injections [8,14]. The repeatability (R.S.D.) of both the migration time and the corrected peak area was determined over five replicate injections for the three buffer systems which gave the best separations. The data indicates that the repeatability of the migration time (Table 3) when these modifiers are incorporated into the electrophoretic buffer is excellent, especially propan-2-

Table 3

Repeatability data (% R.S.D.) for migration time for 10% (v/v) propan-2-ol, 15% (v/v) acetone and 15% (v/v) methyl ethyl ketone used as organic modifiers

Organic modifier (%, v/v)	Analyte drug						
	Phenytoin	Lidocaine	Bretylium	Disopyramide	Quinidine	Propafenone	Amiodarone
Propan-2-ol (10%)	0.19	0.13	0.22	0.23	0.20	0.47	0.50
Acetone (15%)	0.14	0.17	0.24	0.31	0.67	0.33	0.61
Methyl ethyl ketone (15%)	0.30	0.35	0.29	0.88	0.24	0.19	0.62

Table 4

Repeatability data (% R.S.D.) for corrected peak area for 10% (v/v) propan-2-ol, 15% (v/v) acetone and 15% (v/v) methyl ethyl ketone used as organic modifiers

Organic modifier (%, v/v)	Analyte drug						
	Phenytoin	Lidocaine	Bretylium	Disopyramide	Quinidine	Propafenone	Amiodarone
Propan-2-ol (10%)	2.53	1.22	0.37	0.32	0.29	0.37	0.33
Acetone (15%)	2.73	1.74	1.88	1.77	1.86	1.21	1.33
Methyl ethyl ketone (15%)	2.51	3.07	1.86	1.46	3.46	2.46	3.27

ol which has a %R.S.D. of 0.5 or less for all analytes in the mixture. The repeatability data for the corrected peak area (Table 4) indicates that propan-2-ol is superior to acetone and methyl ethyl ketone with excellent precision for all but one of the analytes in the mixture.

Other studies investigating the use of organic modifiers have typically used concentrations <10% (v/v) [12]. This investigation demonstrates that levels of organic solvent >10% are also able to effect a high-resolution separation of a mixture of seven analytes which are structurally dissimilar, with good precision for migration time and peak-area measurement.

#### 4. Conclusions

The addition of organic solvents as modifiers to the MEKC electrolyte buffer enhances the resolution of the seven drugs described. As has been previously demonstrated with beta-blockers, [12] the organic modifiers lengthen the migration time and widen the migration window. Although propan-2-ol gives the best resolution for all analytes in the mixture used here, excellent separation has also been demonstrated with low-molecular-mass ketones. Use of such modifiers gives further options in optimising the selectivity of the MEKC separation. No concerns were experienced with the repeatability of the peak migration time or the peak-area quantitation. The use of organic modifiers (including propan-2-ol and various ketones, as well as the

more commonly used methanol and acetonitrile) is therefore recommended where it has not been possible to achieve an analytical separation using unmodified MEKC buffers.

#### References

- [1] N.N. Charman, A.J. Humberstone and S.A. Charman, *Pharm. Res.*, 9 (1992) 1219.
- [2] B.R. Thomas and S. Ghodbane, *J. Liq. Chromatogr.*, 16 (1993) 1983
- [3] S. Terabe, K. Otsuka, K. Ichikawa, A. Tsuchiya and T. Ando, *Anal. Chem.*, 56 (1984) 834.
- [4] S. Terabe, K. Otasuka and T. Ando, *Anal. Chem.*, 57 (1985) 834
- [5] S.R. Rabel and J.F. Stobaugh, *Pharm. Res.*, 10 (1993) 171.
- [6] E.S. Ahuja, E.L. Little, K.R. Nielson and J.P. Foley, *Anal. Chem.*, 67 (1995) 26.
- [7] A.T. Balchunas and M.J. Sepaniak, *Anal. Chem.*, 59 (1987) 1470.
- [8] R. Weinberger and I.S. Lurie, *Anal. Chem.*, 63 (1991) 823.
- [9] J. Snopek, I. Jelinek and E. Smolkova-Keulemansova, *J. Chromatogr.*, 452 (1988) 571.
- [10] J. Gorse, A.T. Balchunas, D.F. Swaile and M.J. Sepaniak, *J. High Resolut. Chromatogr. Chromatogr. Commun.*, 11 (1988) 544.
- [11] A.T. Balchunas and M.J. Sepaniak, *Anal. Chem.*, 60 (1988) 617.
- [12] P. Lukkari, H. Vuorela and M.-L. Riekkola, *J. Chromatogr. A*, 655 (1993) 317.
- [13] S. Terabe, *J. Pharm. Biomed. Anal.*, 10 (1992) 705.
- [14] A.E. Bretnall and G.S. Clarke, *J. Chromatogr. A*, 700 (1995) 173.
- [15] K. Otsuka, M. Higashimori, R. Koike, K. Karuhaka, Y. Okada and S. Terabe, *Electrophoresis*, 15 (1994) 1280.





ELSEVIER

Journal of Chromatography A, 716 (1995) 57–67

JOURNAL OF  
CHROMATOGRAPHY A

# Polymer-supported pseudo-stationary phase for electrokinetic chromatography

## Electrokinetic chromatography in a full range of methanol–water mixtures with alkylated starburst dendrimers

Nobuo Tanaka\*, Takeshi Fukutome, Ken Hosoya, Kazuhiro Kimata, Takeo Araki  
*Department of Polymer Science and Engineering, Kyoto Institute of Technology, Matsugasaki, Sakyo-ku, Kyoto 606, Japan*

### Abstract

Alkylated polyamidoamine starburst dendrimers (PAMAM-SBDs) are used as high-performance carriers in electrokinetic chromatography (EKC) in a full range of water–methanol (up to 90%) mixtures. The sodium dodecyl sulfate–micellar EKC (SDS–MEKC) system showed a greater migration time window at 20% methanol, but its applicability is limited above 40% methanol. The SBDs modified with dodecyl groups provided high efficiency and much wider migration time windows than SDS micelle carriers at high methanol content, especially for hydrophobic compounds, based on their more hydrophobic properties and reduced electroosmotic mobility. Different selectivities were observed between octyl and dodecyl derivatives of SBDs, the latter showing some similarity with the SDS micelle carrier. The results, showing a nearly linear relation between  $\log k'$  and methanol content, indicate the possibility for the optimization of EKC separation with polymeric carriers by simply changing the organic solvent content to manipulate the solute retention as in reversed-phase liquid chromatography.

### 1. Introduction

Micellar electrokinetic chromatography (MEKC) utilizing micelles of ionic surfactants such as sodium dodecyl sulfate (SDS) as a pseudo-stationary phase, or a separation carrier, provides high performance separations and is applicable to a wide range of uncharged compounds [1–4]. This separation method makes use of the solute's partitioning between an aqueous phase, which undergoes electroosmosis, and a micelle phase, which undergoes electrophoretic migration. In principle, this technique is applic-

able for compounds with some water solubility. All the solutes are detected in a migration time window between the migration time of an unretained solute and that of a micelle.

Narrow migration time windows were observed in SDS–MEKC for hydrophobic compounds mostly partitioned in the micelle phase. Wider separation time windows can be obtained for these solutes by increasing their water solubility (partitioning into the aqueous phase) and by reducing the electroosmotic flow of the system. This can be effected by the addition of organic solvents [5–10], cyclodextrins [11–14], or urea [15] to the system.

The addition of organic solvents to the EKC

\* Corresponding author.

systems [5–10] seems to be the most straightforward approach for the separation of hydrophobic compounds, as is commonly practised in reversed-phase liquid chromatography (RPLC). The addition of organic solvents, however, is accompanied by some complexities in MEKC due to the simultaneous changes in osmotic velocity of the aqueous solution, in the partition coefficients of solutes between the micelle and aqueous phase, in micelle concentration due to the change in solubility of the surfactants, and in micelle composition due to the incorporation of an organic solvent into the micelle phase. The changes in these factors could result in complex selectivity changes, making improvement in separation unpredictable. In SDS–MEKC systems, acetonitrile, dimethylsulfoxide (DMSO), or acetone was added rather than methanol [5–10].

This approach, often studied with SDS–MEKC systems, would be more effective with polymeric carriers which are stable against organic solvents. Since we can avoid the problem of the variation in carrier concentration and composition, the changes in osmotic flow and the solute partition coefficients are the only factors to be taken into account. The variation in the separation profile is expected to be straightforward, and we can fully utilize the information from RPLC, where the solute retention can be manipulated by simply changing the concentration of an organic solvent. The use of polymeric carriers has been reported in EKC [16–18], and their possibilities should be fully examined.

Polyamidoamine-type SBDs (PAMAM-SBDs) [19,20] are used as a pseudo-stationary phase [21] and showed carbon skeleton selectivity for aromatic compounds [22]. The retentivity of SBDs, however, is relatively small due to their hydrophilic structures. The derivatization of PAMAM-SBDs is feasible, and this makes it possible to study the structural effect of a pseudo-stationary phase. The idea is similar to the modification of the silica surface with alkylsilyl groups to prepare a stationary phase for RPLC. We report here that alkylated half-generation SBDs showed increased retentivity for hydrophobic compounds, differentiating the alkyl as

well as functional groups based on their hydrophobic properties. The alkyl-SBDs, particularly the dodecyl derivative of PAMAM-SBDs at generation 3.5, provided high performance and permitted the separation of hydrophobic compounds in a full range, 0–90%, of methanol content in EKC.

## 2. Experimental

### 2.1. Equipment

#### *High-performance capillary electrophoresis (HPCE)*

A high-voltage power supply, HepLL-30P0.08 (Matsusada Precision Devices, Kusatsu, Japan), a variable-wavelength UV detector, UV-8 Model II (Tosoh, Tokyo, Japan), and a data processor, C-R6A (Shimadzu, Kyoto, Japan), were used. Detection was carried out at 210 nm for SDS–MEKC systems and at 254 nm for SBD systems due to the considerable UV absorption of SBDs at the lower wavelength. The scale bars attached to all the chromatograms indicate 0.005 AU. A fused-silica capillary of 50  $\mu\text{m}$  I.D. and 0.375 mm O.D. (Polymicro Technologies, Phoenix, AZ, USA) was used at ambient temperatures.

### 2.2. Materials

#### *Preparation of SBDs*

The SBDs were prepared starting from *p*-xylylenediamine (X) as a core, following the method reported by Tomalia et al. [23]. The size of the SBDs is described according to the original generation system [23]. One reaction cycle, Michael addition to methyl acrylate to form an ester terminal SBD of  $G = 0.5$  starting from the amine core, followed by the amide formation with ethylenediamine to regenerate an amine structure, provides a full generation SBD of  $G = 1.0$ . The reaction cycle was repeated to produce higher-generation SBDs. The SBDs used as carriers are described by the combination of the core (X) and the generation, that is the number of reaction cycles starting from the core. The SBD(X) of  $G = 3.5$ , supposedly possessing 32

terminal groups, was used as a support of alkyl groups in this study.

#### *Hydrolysis of half-generation SBDs*

Half-generation SBDs were used as carriers in EKC in a carboxylate form after hydrolyzing the terminal ester groups with equimolar sodium hydroxide in methanol [24].

#### *Alkylation of SBDs [22]*

SBD(X,  $G = 3.5$ ) (4.0 g) was dissolved in methanol (50 ml), to which octylamine (3.3 g, 1.2 mole equivalent to the ester groups) was added to prepare SBD(X)-C<sub>8</sub>. The solution was stirred for five days at room temperature. [SBD(X)-C<sub>12</sub> was prepared at 40°C.] After examining the extent of alkylation by NMR, sodium hydroxide (0.65 g, one mole equivalent to the remaining ester groups) was added. The resulting mixture was stirred for 9 h. After concentrating the solution to 20 ml by evaporation under reduced pressure, the solution was added to acetone to precipitate the partially alkylated SBD in a carboxylate form, SBD(X)-C<sub>8</sub>. SBD(X)-C<sub>12</sub> was prepared similarly.

#### *Characterization of SBDs*

<sup>1</sup>H NMR measurement was carried out on an XL-200 NMR instrument (Varian, Sunnyvale, CA, USA). The reaction cycle in SBD preparation and alkylation reaction was followed by NMR and elemental analysis.

#### *Size exclusion chromatography (SEC)*

Monodispersity of SBDs in molecular mass was examined by SEC by using TSK-G3000PW, 60 cm × 7.6 mm I.D. (Tosoh, Tokyo, Japan), in 50 mM phosphate buffer at pH 11. PAMAM-SBDs ( $G = 2.0, 4.0, \text{ and } 6.0$ ), commercially obtained (Polysciences, Warrington, PA, USA), were used as standards.

#### *Electrophoresis measurement*

The same instrument as described above was used in the absence of an EKC carrier. SBDs were injected as samples to the electrophoresis system to measure the electrophoretic mobility and monodispersity of alkyl SBDs. The capillary

was washed with 1 M sodium hydroxide solution prior to every injection.

#### *Electrokinetic chromatography (EKC)*

Methanol was added to 20 mM borate buffer solution containing a carrier to prepare a mixed separation solution. All separation solutions were filtered with a membrane filter (0.2 μm). Apparent pH values were measured by a pH meter. Injection was carried out by a siphoning method. The  $k'$  values were calculated by using the equation  $k' = (t_R - t_0)/t_0(1 - t_R/t_c)$  [2–4], where  $t_R$ ,  $t_0$ , and  $t_c$  are the elution times of the solute, the unretained solute, and the carrier, respectively. Methanol or formamide was used to measure  $t_0$  values, and Oil Yellow OB for  $t_{mc}$  in aqueous buffer for SDS–MEKC systems [25,26]. The  $t_{mc}$  in methanol–water mixtures at 40% or higher methanol content and  $t_{SBD}$  were calculated by the iterative method [27,28] assuming a linear relation between  $\log k'$  and carbon numbers of alkyl phenyl ketones and alkylbenzenes.

### **3. Results and discussion**

#### *3.1. Characterization of alkylated SBDs*

The PAMAM-SBDs prepared in this study showed better monodispersity in SEC than the standard SBDs obtained commercially that contained low-molecular-mass species. The alkylation of SBDs is expected to give a variety of products with a varying extent of alkylation. The NMR measurements indicated that SBD(X)-C<sub>8</sub> and SBD(X)-C<sub>12</sub> possess 6 and 14 alkyl groups per molecule on average, respectively, out of 32 terminal groups on the SBD(X,  $G = 3.5$ ). The difference in the extent of alkylation is presumably caused by the difference in reaction temperature, room temperature (ca. 25°C) for SBD(X)-C<sub>8</sub> and 40°C for SBD(X)-C<sub>12</sub>.

Table 1 lists the electrophoretic mobilities of the SBD carriers in buffer solution without SBDs as a component of the separation solution, and the electroosmotic mobilities under EKC conditions. The electroosmotic flow is suppressed by

Table 1  
Electrophoretic and electroosmotic mobilities of carriers

Methanol %	SDS		SBD(X)		SBD(X)-C <sub>8</sub>		SBD(X)-C <sub>12</sub>	
	$\mu_{eo}$	$\mu_{ep}$	$\mu_{eo}$	$\mu_{ep}$	$\mu_{eo}$	$\mu_{ep}$	$\mu_{eo}$	$\mu_{ep}$
0%	7.30	-4.37	5.12	-4.18	5.16	-3.79	6.11	-3.84
20%	4.14	-3.29	-	-2.42	3.34	-2.47	3.54	-2.38
40%	2.45	-2.31	2.43	-1.79	2.00	-1.81	2.62	-1.80
60%	1.47	-0.71	1.54	-1.71	1.46	-1.58	1.54	-1.47
80%	1.29	-0.22	1.77	-2.07	1.49	-2.21	1.00	-1.61

Electroosmotic mobilities were obtained from EKC experiments.

Electrophoretic mobilities of SBDs were measured in the absence SBDs in the separation solution.

Electrophoretic mobilities of SDS micelle were calculated from  $t_{mc}$  obtained by the iteration method from EKC experiments.

the presence of SBDs under EKC conditions, presumably due to the contribution of amino functionality of the SBDs [22]. The results agreed fairly well with those calculated from the  $t_{SBD}$  values by the iterative method. The mobilities of the SDS carriers were calculated from  $t_0$  and  $t_{mc}$  in EKC. SBDs migrated as a band under electrophoretic conditions in the presence of electroosmotic flow, as shown in Fig. 1. The electrophoresis under the reduced electroosmotic flow in the presence of organic solvents showed

broader peaks, presumably due to polydispersity in the alkylated SBDs which have different numbers of alkyl and terminal carboxylate groups.

An increase in the number of alkyl groups should lead to a decrease in the number of carboxylate groups, which in turn may lead to lower electrophoretic mobility. The contribution of this factor to EKC, however, can be counteracted, because the partition of a solute into such heavily alkylated SBDs would be greater

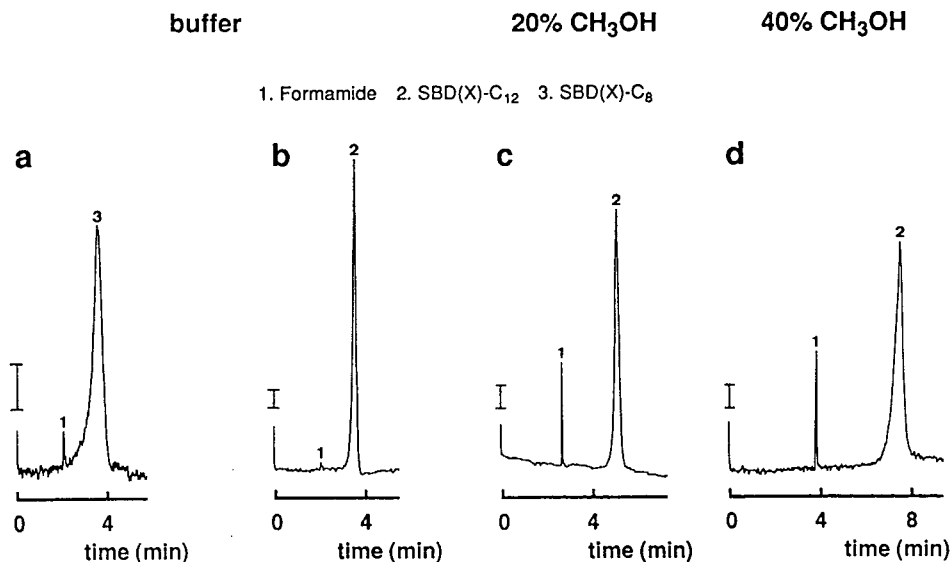


Fig. 1. Electrophoresis of SBD(X)-C<sub>8</sub> and SBD(X)-C<sub>12</sub> in 0–40% methanol–buffer. Buffer: 20 mM borate, pH 8.9.  $L = 48$  cm,  $l = 33$  cm. Detection: 210 nm. Sample: 1 = formamide, 2 = SBD(X)-C<sub>12</sub>, 3 = SBD(X)-C<sub>8</sub>. (a and b) Field strength 300 V/cm, in aqueous buffer, and (c and d) 400 V/cm, in 20 and 40% methanol.



than in less alkylated SBDs, which are supposed to show higher electrophoretic mobility. Therefore, the broad band seen with the SBD carriers will not directly mean greater broadening of a solute band under EKC conditions.

Although SDS–MEKC provided a wider separation time window at 20% methanol, the SBD carriers showed greater  $-\mu_{ep}/\mu_{eo}$  ratios, resulting in wider separation time windows than SDS–MEKC systems at higher methanol content. An infinite time window is expected when the ratio becomes unity. Some SBDs may have this property in the presence of 60–80% methanol.

### 3.2. SBD–EKC in aqueous solution

Although SDS–MEKC provided good separation for the relatively hydrophilic compounds, relatively narrow band spacing was observed between peaks 4 and 5, as shown in Fig. 2. This effect is generally seen with hydrophobic compounds that migrate near the elution time of the micelle, and is caused by the nearly complete partitioning of the hydrophobic solutes into the micelle phase [2–4]. SBD(X)-C<sub>8</sub> and SBD(X)-C<sub>12</sub> showed a large increase in retention and separation based on the size of the alkyl group of a solute compared with the parent SBD(X).

SBD(X)-C<sub>12</sub> showed a similar migration profile to SDS micelles, with good efficiency. The high efficiency of the SBD(X)-C<sub>12</sub> system is possibly provided by the narrow band of the carrier under electrophoretic conditions (Fig. 1).

Different selectivity was observed when the pseudo-stationary phase was composed with shorter alkyl groups. SBD(X)-C<sub>8</sub> showed a greater migration time window than SDS–MEKC, especially for alkyl phenyl ketones with C<sub>3</sub>–C<sub>5</sub>. The less hydrophobic structure of SBD(X)-C<sub>8</sub> than SDS micelles seems to contribute to the smaller partition coefficients for hydrophobic compounds. This effect and the greater  $t_{SBD}$  of this carrier make the separation profile similar to that in RPLC. SDS–MEKC and SBD(X)-C<sub>12</sub>–EKC gave a greater peak capacity for relatively hydrophilic solutes, and a smaller peak capacity for the hydrophobic solutes than SBD(X)-C<sub>8</sub> due to the more hydrophobic structure. In a sense, the SBD(X)-C<sub>12</sub> system showed some similarity with SDS–MEKC. The peak capacity for the hydrophobic compounds can be improved by additives, such as urea, cyclodextrins, or organic solvents, that should increase the solute partition into the aqueous phase.

Fig. 3 shows the separation of some benzene and naphthalene derivatives. SBD(X) without alkyl substituents separated the compounds with

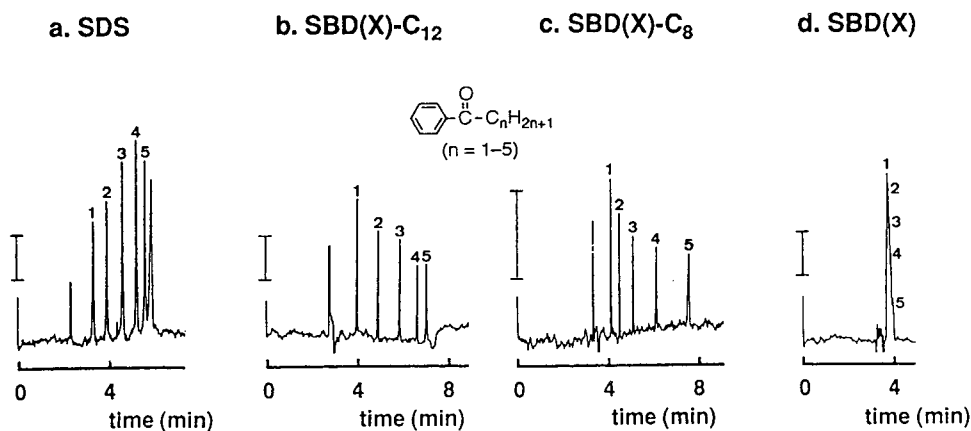


Fig. 2. Comparison of carriers for the separation of alkyl phenyl ketones. (a) SDS 30 mM, pH 9.4, (b) SBD(X)-C<sub>12</sub> 5 mM, pH 10.4, (c) SBD(X)-C<sub>8</sub> 5 mM, pH 10.1, and (d) SBD(X) 5 mM, pH 10.3. Buffer solution: 20 mM borate. Solute: alkyl phenyl ketones ( $C_6H_5-CO-C_nH_{2n+1}$ ,  $n = 1-5$ ). Numbers indicate the numbers of carbon atoms in the alkyl group. Field strength 300 V/cm. The last peak in (a) is Oil Yellow OB.

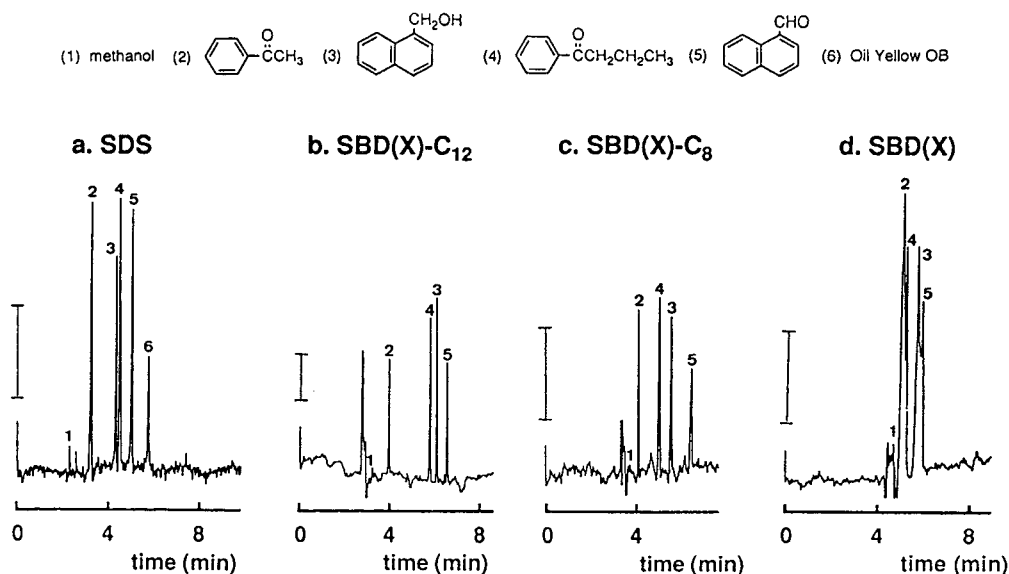


Fig. 3. Comparison of carriers for the separation of benzene and naphthalene derivatives. (a) SDS 30 mM, pH 8.9, (b) SBD(X)-C<sub>12</sub> 5 mM, pH 10.4, (c) SBD(X)-C<sub>8</sub> 5 mM, pH 10.1, and (d) SBD(X) 5 mM, pH 10.1. (a-c) Field strength 300 V/cm, (d) 250 V/cm. Solute: 1 = methanol, 2 = acetophenone, 3 = 1-naphthalenemethanol, 4 = phenyl propyl ketone, 5 = 1-naphthaldehyde, 6 = Oil Yellow OB. Other conditions as in Fig. 2.

different skeletons, benzene and naphthalene derivatives, but did not separate well the compounds with a difference in alkyl or functional groups on one skeleton. The hydrophobic recognition is very poor with this carrier [22]. This is in contrast to SDS-MEKC, where benzene derivatives with hydrophobic substituents are retained longer than naphthalene derivatives with hydrophilic substituents. The alkylated SBDs showed selectivities which lay in-between, with greater differentiation for the benzene and naphthalene derivatives than in SDS-MEKC, and greater differentiation for alkyl and polar substituents on one skeleton than the parent SBD(X). SBD(X)-C<sub>8</sub> showed selectivities somewhat similar to the parent SBD(X), and SBD(X)-C<sub>12</sub> to SDS micelle. The contribution of SBD skeleton to the solute binding seems to be more significant with SBD(X)-C<sub>8</sub>.

### 3.3. SBD-EKC in methanol-water mixtures

Fig. 4 shows the separation of alkyl phenyl ketones in 20-80% methanol with SBD(X)-C<sub>12</sub> and SDS micelle as a carrier. While SDS-MEKC

showed narrow band spacing for hydrophobic alkyl phenyl ketones in the absence of methanol, it showed much greater peak capacity in 20% methanol due to the increased partition of the solutes into the aqueous phase and the increased migration time window because of the reduced electroosmosis. The SDS system, however, showed an abnormal elution profile in 40% methanol, and very narrow migration time windows above 40% methanol. SBD(X)-C<sub>12</sub> showed consistent separation in the presence of 40-80% methanol. The comparison clearly shows the advantage of a polymer carrier in EKC that is stable against organic solvents.

Figs. 5 and 6 show the separation of aromatic hydrocarbons in 40-80% methanol. Good chromatograms were not obtained for aromatic hydrocarbons in 40% methanol with SDS carrier, as was the case with alkyl phenyl ketones. SDS-MEKC and SBD(X)-C<sub>8</sub> gave similar performance at 60% methanol for aromatic hydrocarbons. At 80%, however, the SDS carrier gave poorer resolution. SBD(X)-C<sub>12</sub> showed much better performance with a methanol content of 60% or greater for highly hydrophobic com-

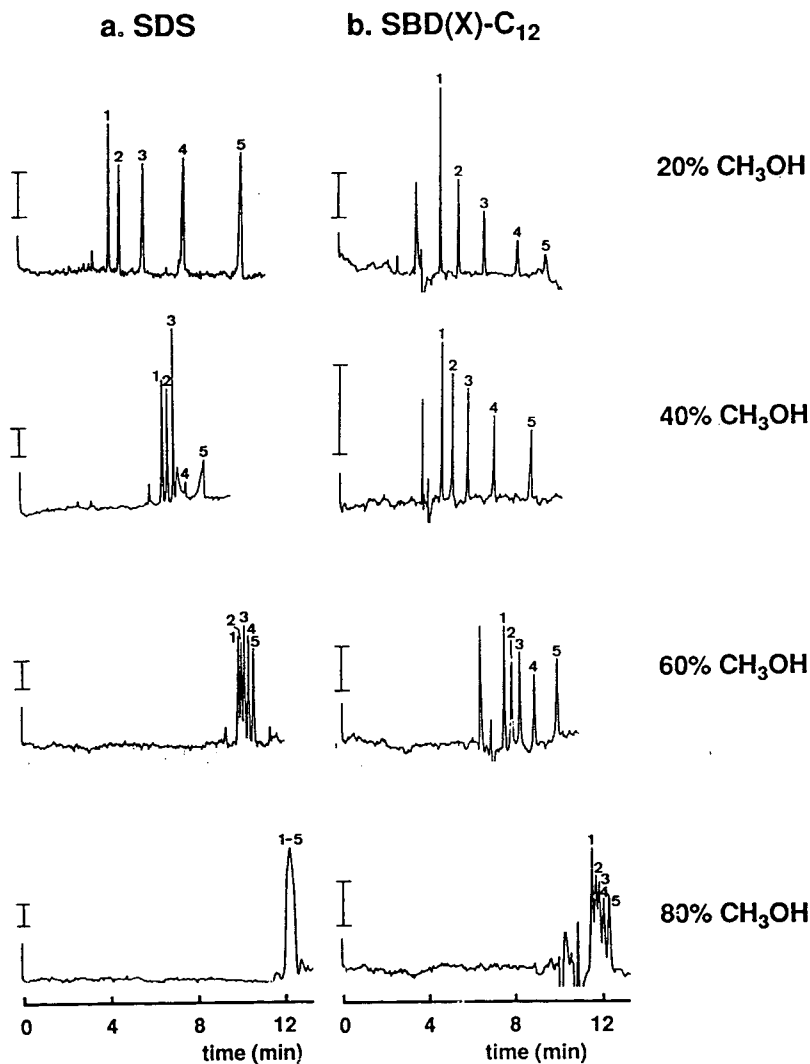


Fig. 4. Effect of methanol addition on the separation of alkyl phenyl ketones at 20–80% methanol. Solutes: alkyl phenyl ketones,  $C_6H_5-CO-C_nH_{2n+1}$  ( $n = 1-5$ ), as in Fig. 2. (a) 30 mM SDS, 20 mM borate, 400 V/cm, pH 9.3 in 20% methanol, pH 9.3 in 40% methanol, pH 9.0 in 60% methanol, and pH 9.5 in 80% methanol; (b) 5 mM SBD(X)- $C_{12}$ , 20 mM borate; pH 10.2, 400 V/cm in 20% methanol; pH 10.8, 500 V/cm in 40% methanol; pH 11.0, 500 V/cm in 60% methanol; and pH 11.2, 500 V/cm in 80% methanol.

pounds. The peak capacity for these solutes with this system is maximum at 60% methanol.

The improvement of separation with SBD(X)- $C_{12}$  was mainly due to the following two factors: (i) the increase in migration time of the solutes was provided by the increase in the migration time of the carrier at higher methanol content, and (ii) the optimum  $k'$  range was attained by

the decrease in  $k'$  values at higher methanol content. Relatively small  $k'$  values, 1–3, are required for optimum resolution [2–4].

It is interesting to note the elution-order change of the aromatic hydrocarbons with a difference in planarity with methanol content. The relative migration time of the bulky molecules, peaks No. 1 and 2 in Fig. 5, clearly shows

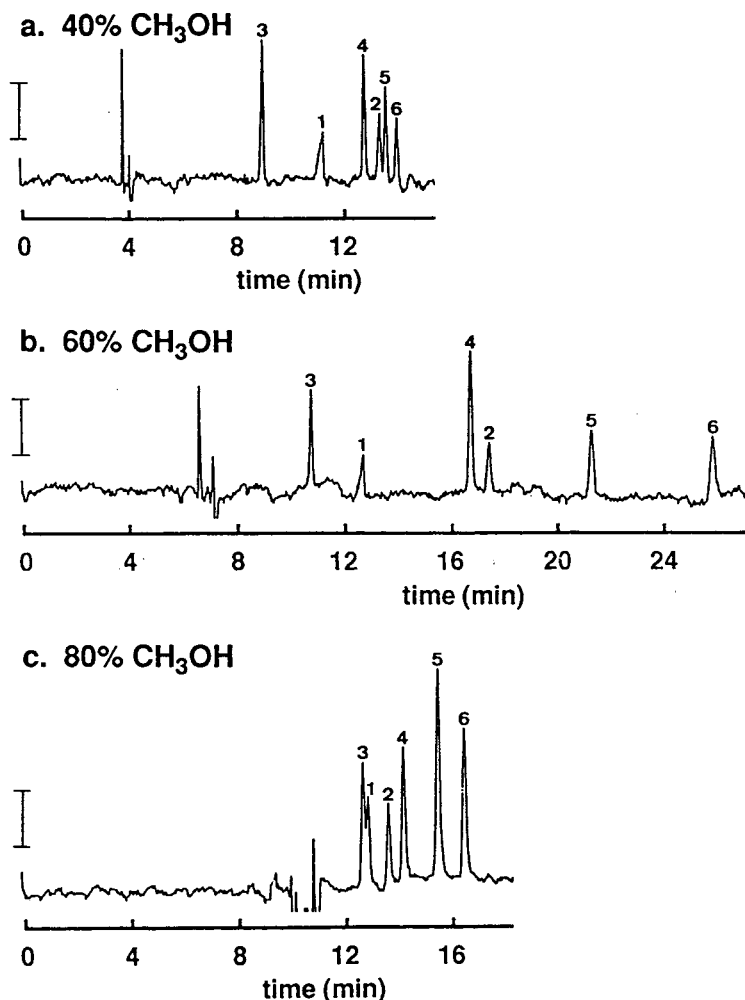


Fig. 5. Effect of methanol addition on the separation of aromatic hydrocarbons with SBD(X)-C<sub>12</sub>. SBD(X)-C<sub>12</sub> 5 mM, 20 mM borate, 500 V/cm. (a) pH 10.8 in 40% methanol, (b) pH 11.0 in 60% methanol, (c) pH 11.2 in 80% methanol. Solutes: 1 = diphenylmethane, 2 = *ortho*-terphenyl, 3 = naphthalene, 4 = anthracene, 5 = pyrene, 6 = triphenylene.

the tendency of preferential retention of planar polynuclear aromatic hydrocarbons relative to non-planar, bulky polyphenylalkanes with SBD(X)-C<sub>12</sub> at higher methanol content. The results with SBD(X)-C<sub>12</sub> in EKC are similar to those with C<sub>18</sub> stationary phases in RPLC, where planar compounds are preferentially retained at higher methanol contents [29]. The effect was not observed with short alkyl bonded phases, and seems to be related to the ordering of long alkyl chains at a higher methanol content

[29,30]. The effect of organic solvent content on the solute-carrier interaction will be an interesting subject to study.

The plots of  $t_R/t_0$  against methanol content in Fig. 7 indicate that the migration time window first increases by the addition of methanol to SDS-MEKC and SBD(X)-C<sub>12</sub> systems, as shown in Figs. 4 and 5. The separation with the SDS system, however, quickly diminishes upon further addition of methanol. The SDS system failed to provide separation even for the highly

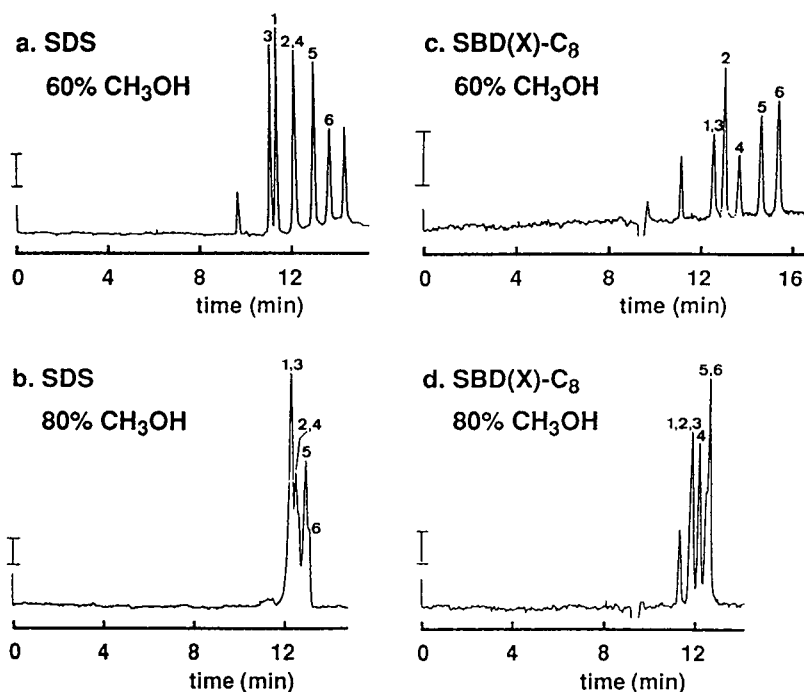


Fig. 6. Effect of methanol addition on the separation of aromatic hydrocarbons with SBD(X)-C<sub>8</sub> and SDS. (a, b) SDS: 30 mM, 20 mM borate, 400 V/cm. pH 9.4 in 60% and pH 11.4 in 80% methanol. (c, d) SBD(X)-C<sub>8</sub>: 5 mM, 20 mM borate, 400 V/cm. pH 9.9 in 60% and pH 11.4 in 80% methanol. Solutes as in Fig. 5.

hydrophobic compounds in 80% methanol. In contrast, SBD(X)-C<sub>12</sub> provided a much greater migration time window at higher methanol contents, with a maximum at 20% for the ketones and at 60% for the aromatic hydrocarbons.

It is generally seen that the migration times

and resolution of hydrophobic solutes which migrated near the carrier at low methanol concentration first increase with methanol content, followed by a decrease with further addition of methanol. The composition providing maximum migration time and peak capacity shifts toward the higher methanol content as the solutes become more hydrophobic. Once the maximum is reached, the migration time and peak capacity decrease with an increase in methanol content, as in RPLC.

The results suggest that the SBD(X)-C<sub>12</sub> keeps its hydrophobic property even at high methanol content, as the stationary phases for RPLC. This was not the case with the SDS micelle, which shows hydrophobic properties similar to or greater than that of SBD(X)-C<sub>12</sub> in an aqueous system, but much lower in the presence of methanol. The results suggest a change in the composition of the micelle with the surrounding solvent.

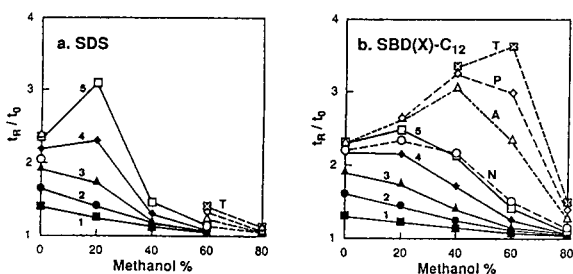


Fig. 7. Plots of  $t_R/t_0$  values for alkyl phenyl ketones and aromatic hydrocarbons against methanol content of the separation solution. Chromatograms are shown in Figs. 2 and 4-6. (a) SDS, (b) SBD(X)-C<sub>12</sub>. Solutes: alkyl phenyl ketones ( $n = 1-5$ ) as in Fig. 2, N = naphthalene, A = anthracene, P = pyrene, T = triphenylene.

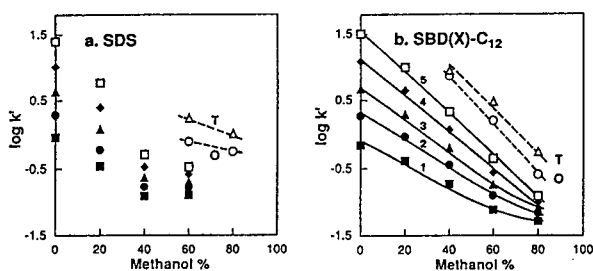


Fig. 8. Plots of  $\log k'$  values of alkyl phenyl ketones and aromatic hydrocarbons against methanol content. Chromatograms are shown in Figs. 2 and 4-6. Solutes as in Fig. 7.

Fig. 8 shows further similarity of SBD-EKC with SBD(X)-C<sub>12</sub> to the RPLC system. The nearly linear relation between  $\log k'$  and methanol content observed with this carrier, but not with SDS-MEKC, is very common in RPLC [31]. It is also noted that the selectivity in SBD-EKC can be altered by methanol content, as shown in Fig. 5. Such selectivity change with methanol content would appear as a cross-over in the plot. This suggests the possibility of optimization of separation conditions by changing the methanol content with these polymeric carriers, as in RPLC. Simulation of the migration profile from  $k'$  values requires electroosmotic and electrophoretic mobilities of the carrier.

Fig. 9 shows the separation of some aromatic hydrocarbons with SBD(X)-C<sub>12</sub> in 90% methanol. This carrier provided separation of hydrophobic compounds at high methanol content. The application of this type of carrier to the separation of more hydrophobic aromatic compounds would be of much interest in environmental analysis [11].

Further study is needed on the effect of the type of organic solvents and the structure of alkyl groups on SBDs on the selectivity in SBD-EKC. SBDs were employed as pseudo-stationary phase for EKC of neutral as well as ionic analytes [32,33]. The present results show that SBDs can be used as a support to construct a wide range of pseudo-stationary phases that may not be possible with a micellar carrier in terms of the density and chain length of the alkyl group. Various pseudo-stationary phases can also be developed by varying interacting groups as well

## SBD(X)-C<sub>12</sub> 90% CH<sub>3</sub>OH

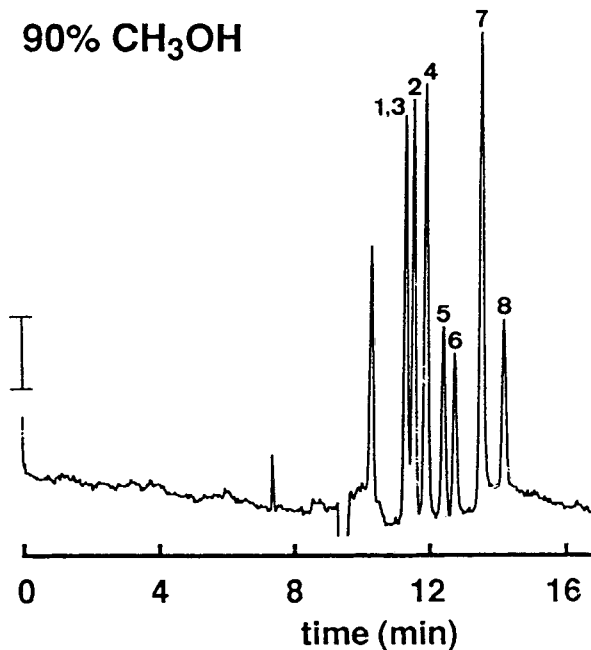


Fig. 9. Separation of aromatic hydrocarbons with SBD(X)-C<sub>12</sub> in 90% methanol-10% 20 mM borate buffer, 5 mM SBD(X)-C<sub>12</sub>. pH 10.1, 500 V/cm. Solutes: 1-6 = aromatic hydrocarbons as in Fig. 5, 7 = 3,4-benzopyrene, 8 = indeno[1,2,3-cd]pyrene.

as support structures. Suitable hydrophilic polymers that can be used as a support will further increase the usefulness of EKC. In the case of RPLC, stationary phase modification is mostly limited to silica surfaces.

## 4. Conclusion

SDS-MEKC showed excellent performance at low methanol content, but is not suitable for the separation of hydrophobic compounds at high methanol content. The alkylated SBDs showed increased retention and hydrophobic selectivity compared with the parent PAMAM-SBD(X). Selectivity can be altered with the chain length of the alkyl group. SBD(X)-C<sub>12</sub> can be used in 0-90% methanol and provided high efficiency as well as a much wider migration time window, especially for hydrophobic compounds, than

SDS–MEKC. A nearly linear relation was observed between  $\log k'$  values and methanol content. Optimum separation conditions can be attained for a wider range of solutes in SBD–EKC by adjusting the organic solvent content.

### Acknowledgements

The authors are grateful to Professor Shigeru Terabe and Dr. D.G. Patterson for their helpful suggestions. This work was supported in part by Grant No. 05640682 from the Ministry of Education.

### References

- [1] S. Terabe, K. Otsuka, K. Ichikawa, A. Tsuchiya and T. Ando, *Anal. Chem.*, 56 (1984) 111.
- [2] S. Terabe, K. Otsuka and T. Ando, *Anal. Chem.*, 57 (1985) 834.
- [3] S. Terabe, in N.A. Guzman (Editor), *Capillary Electrophoresis Technology*, Marcel Dekker, New York, 1993, Ch. 2.
- [4] S. Terabe, N. Chen and K. Otsuka, *Adv. Electrophoresis*, 7 (1995) in press.
- [5] K. Otsuka, S. Terabe and T. Ando, *Nippon Kagaku Kaishi*, (1986) 950.
- [6] A.T. Balchunas and M.J. Sepaniak, *Anal. Chem.*, 59 (1987) 1466; 60 (1988) 617.
- [7] J. Vindevogel and P. Sandra, *Anal. Chem.*, 63 (1991) 1530.
- [8] P. Lukkari, H. Vuorela and M.L. Riekkola, *J. Chromatogr. A*, 655 (1993) 317.
- [9] C. Stathakis, P.L. Warburton and R.M. Cassidy, *J. Chromatogr. A*, 659 (1994) 443.
- [10] K. Otsuka, M. Higashimori, R. Koike, K. Karuhaka, Y. Okada and S. Terabe, *Electrophoresis*, 15 (1994) 1280.
- [11] S. Terabe, Y. Miyashita, O. Shibata, E.R. Barnhart, L.R. Alexander, D.G. Patterson, B.L. Karger, K. Hosoya and N. Tanaka, *J. Chromatogr.*, 516 (1990) 23.
- [12] Y.F. Yik, C.P. Ong, S.B. Khoo, H.K. Lee and S.F.Y. Li, *J. Chromatogr.*, 589 (1992) 333.
- [13] S. Terabe, Y. Miyashita, Y. Ishihama and O. Shibata, *J. Chromatogr.*, 636 (1993) 47.
- [14] C.L. Copper and M.J. Sepaniak, *Anal. Chem.*, 66 (1994) 147.
- [15] S. Terabe, Y. Ishihama, H. Nishi, T. Fukuyama and K. Otsuka, *J. Chromatogr.*, 545 (1991) 359.
- [16] C.P. Palmer and H.M. McNair, *J. Microcol. Sep.*, 4 (1992) 509.
- [17] W. Schutzner, S. Fanali, A. Rizzi and E. Kenndler, *J. Chromatogr.*, 639 (1993) 375.
- [18] H. Ozaki, A. Ichihara and S. Terabe, *J. Chromatogr. A*, 680 (1994) 117.
- [19] D.A. Tomalia, H. Baker, J. Dewald, M. Hall, G. Kallos, S. Martin, J. Roeck, J. Ryder and P. Smith, *Polym. J. (Tokyo)*, 17 (1985) 117.
- [20] D.A. Tomalia, H. Baker, J. Dewald, M. Hall, G. Kallos, S. Martin, J. Roeck, J. Ryder and P. Smith, *Macromolecules*, 19 (1986) 2466.
- [21] N. Tanaka, T. Tanigawa, K. Hosoya, K. Kimata, T. Araki and S. Terabe, *Chem. Lett.*, (1992) 959.
- [22] N. Tanaka, T. Fukutome, T. Tanigawa, K. Hosoya, K. Kimata, T. Araki and K.K. Unger, *J. Chromatogr. A*, 699 (1995) 331.
- [23] D.A. Tomalia, M. Hall and D.M. Hedstrand, *J. Am. Chem. Soc.*, 109 (1987) 1601.
- [24] D.A. Tomalia, V. Berry, M. Hall and D.M. Hedstrand, *Macromolecules*, 20 (1987) 1164.
- [25] K. Otsuka, S. Terabe and T. Ando, *J. Chromatogr.*, 348 (1985) 39.
- [26] K. Otsuka, S. Terabe and T. Ando, *J. Chromatogr.*, 396 (1987) 350.
- [27] M.M. Bushy and J.W. Jorgenson, *J. Microcol. Sep.*, 1 (1989) 125.
- [28] M.M. Bushy and J.W. Jorgenson, *Anal. Chem.*, 61 (1989) 491.
- [29] N. Tanaka, K. Sakagami and M. Araki, *J. Chromatogr.*, 199 (1980) 327.
- [30] L.C. Sander, J.B. Callis and L.R. Field, *Anal. Chem.*, 55 (1983) 1068.
- [31] L.R. Snyder, in C. Horvath (Editor), *High-Performance Liquid Chromatography: Advances and Perspectives*, Vol. 1, Academic Press, New York, 1980, p. 207.
- [32] P.G.H.M. Muijselaar, H.A. Claessens, C.A. Cramers, J.F.G.A. Jansen, E.W. Meijer, E.M.M. de Brabander-van den Berg and S. van der Wal, *J. High Resolut. Chromatogr.*, 18 (1995) 121.
- [33] M. Castagnola, L. Cassiano, A. Lupi, I. Messina, M. Patamia, R. Rabino, D.V. Rossetti and B. Giardina, *J. Chromatogr. A*, 694 (1995) 463.







ELSEVIER

Journal of Chromatography A, 716 (1995) 69–79

JOURNAL OF  
CHROMATOGRAPHY A

# Micellar electrokinetic chromatography–mass spectrometry using a high-molecular-mass surfactant On-line coupling with an electrospray ionization interface

Hiroto Ozaki<sup>a,\*</sup>, Noritaka Itou<sup>a</sup>, Shigeru Terabe<sup>a</sup>, Yasuaki Takada<sup>b</sup>,  
Minoru Sakairi<sup>b</sup>, Hideaki Koizumi<sup>b</sup>

<sup>a</sup>*Faculty of Science, Himeji Institute of Technology, Kamigori, Hyogo 678-12, Japan*

<sup>b</sup>*Central Research Laboratory, Hitachi, Ltd., Kokubunji, Tokyo 185, Japan*

## Abstract

On-line coupling between micellar electrokinetic chromatography (MEKC) and mass spectrometry (MS) was studied with a high-molecular-mass surfactant and an electrospray ionization interface (ESI). A high-molecular-mass surfactant, butyl acrylate–butyl methacrylate–methacrylic acid copolymer sodium salt (BBMA), was employed as a pseudo-stationary phase for an on-line MEKC–MS system. BBMA and a minor component separated by size-exclusion chromatography were determined by ESI-MS. No major ion from the BBMA polymer was detected. The BBMA micelle functioned successfully as the pseudo-stationary phase in a 10 mM ammonium formate buffer containing 10% methanol. Five standard compounds, phenyltrimethylammonium chloride, 1-naphthylamine, quinine sulfate, tetraphenylphosphonium chloride and octaoxyethylenedodecanol, were separated by MEKC and detected by MS. The effects of the concentrations of BBMA on the separation and sensitivity in MEKC–MS were studied. MEKC–MS with BBMA was applied to the separation and detection of a standard mixture of sulfamides.

## 1. Introduction

Micellar electrokinetic chromatography (MEKC) is a mode of capillary electrophoresis (CE) in which ionic micelles are used as pseudo-stationary phases. Capillary zone electrophoresis (CZE) is a separation technique for ionic analytes only, whereas MEKC is capable of separating both ionic and non-ionic analytes. Almost all advantages of CZE apply to MEKC and many applications of MEKC separations have been

reported [1–5]. The most common detector for both CZE and MEKC is the UV absorbance detector. However, information on the analyte structure obtained from UV spectra is limited. Coupling of CZE or MEKC with general spectroscopic detection methods would therefore be useful. Mass spectrometry (MS) is compatible with CE with respect to the sample amount and is one of the most powerful detection methods for obtaining structural information on separated analytes.

On-line coupling techniques for CE–MS have been studied by several groups [6–18]. Electrospray ionization (ESI) interfaces for CE–MS have been developed by Smith and co-workers

\* Corresponding author. Present address: Kaneka Techno Research Co. Ltd., 1-2-80, Yoshida-cho, Hyogo-ku, Kobe 652, Japan.

[6–9]. Ionspray interfaces, a type of ESI using a high-velocity gas flow at the tip of the capillary, have been studied by Henion and co-workers [10,11] and Pleasance et al. [12]. A fast atom bombardment (FAB) ionization interface with a coaxial continuous flow was developed by Tomer and co-workers [13,14]. The latest work involved a coupling of CE with laser-desorption mass spectrometry, which was an off-line technique [15]. Several reviews on on-line CE–MS have been published [16–18]. Some other separation modes of CE such as capillary gel electrophoresis [10] and capillary isotachopheresis [19] have been studied for coupling with MS.

On the other hand, the direct coupling of MEKC with MS has not yet been developed, probably because of the presence of the surfactant in the running solution. On-line coupling of MEKC with ESI-MS was reported only with a coupled capillary set-up and on-line heart-cutting of the MEKC separation zones [20]. An off-line coupling of MEKC with MS was designed with a FAB interface [21], but it was difficult to obtain the signal for an analyte from a separated fraction owing to the existence of surfactant. Smith et al. [6] studied the ESI mass spectrum of sodium dodecyl sulfate (SDS), which is the surfactant most frequently employed as the pseudo-stationary phase in MEKC. They observed both positive and negative ESI spectra of SDS and suggested the possibility of MEKC–MS with SDS. In practice, however, MEKC–MS using SDS has not yet been reported, probably owing to the low ionization efficiency caused by a relatively high concentration of SDS. Varghese and Cole [22] used a cationic surfactant, cetyltrimethylammonium chloride, as an additive to the running solution to reverse the electroosmotic flow for CE–ESI-MS of cationic compounds. The separation mode described was not MEKC owing to the low concentration, below the critical micelle concentration (CMC) of the surfactant.

For on-line MEKC–MS, selection of an interface is important. ESI is one of the on-line interfacing methods which has been successfully used for CE–MS. The use of ESI for MEKC–

MS is expected to have the same advantages as in CE–MS. Operation and maintenance of the ESI interface are easy owing to the atmospheric pressure ionization inlet. Mass spectra obtained by ESI are simple because ESI is a soft ionization technique and yields only intact molecular ions without fragmentation. Spectra of biopolymers, peptides and proteins can be easily measured by CE–MS [16–18], because ESI yields stable multiple ions from high-molecular-mass analytes exceeding the hardware MS range. An analytical condition for peptide mapping was studied by CE–MS [23]. However, disadvantages of ESI are that it is not suitable for non-polar compounds because of the low ionization and information on molecular structure is limited to molecular mass only, hence a more advanced technique such a MS–MS is required for more information.

The choice of the surfactant added to the running solution in MEKC is also highly significant because surfactants are non-volatile and in many cases cause strong background ions in the mass spectra, as has been observed with SDS [6]. High-molecular-mass surfactants are oligomers of monomeric surfactants [24,25] or polymers which show surface-active properties as a whole [26,27], and they are expected to be useful as pseudo-stationary phases for MEKC–MS. Fig. 1 is a schematic illustration of an electrospray interface and the expected behaviour of micelles in the interface. In Fig. 1A, two main stages in the generation of gas-phase ions of analytes are shown: the first stage is the production of charged droplets (S with O), and the second the production of gas-phase ions from the charged droplets (S<sup>+</sup>). Fig. 1B shows that low-molecular-mass surfactant micelles produce abundant gas-phase surfactant ions. On the other hand, as shown in Fig. 1C, high-molecular-mass surfactant micelles will be stable in the ESI system because the micelle is a single covalently bonded molecule. Therefore, the high-molecular-mass surfactant micelle will not generate high levels of low-molecular-mass background ions.

A high-molecular-mass surfactant, which is an undecylenate oligomer synthesized by polymeriz-

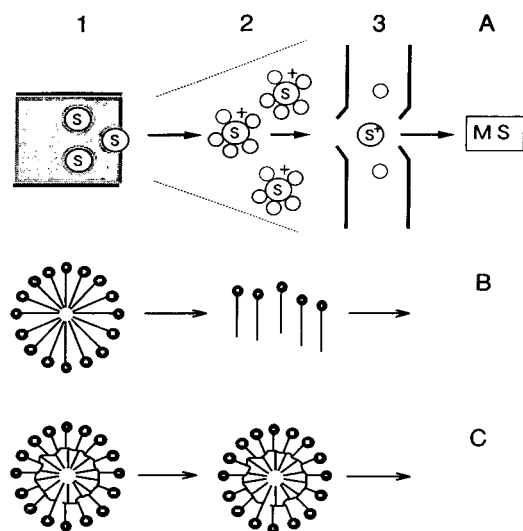


Fig. 1. (A) Schematic illustration of an electrospray interface and expected behaviour of (B) low-molecular-mass and (C) high-molecular-mass surfactant micelles. 1 = Capillary; 2 = electrospray; 3 = mass spectrometer; S = solute molecule; S<sup>+</sup> = solute molecular ion; O = solvent.

ing micellized sodium 10-undecylenate, was employed as a pseudo-stationary phase for MEKC by Palmer and co-workers [24,25]. We have reported MEKC with a high-molecular-mass surfactant, butyl acrylate-butyl methacrylate-methacrylic acid copolymer sodium salt (BBMA) [26,27]. The molecular mass of the BBMA was measured to be about 40 000 by size-exclusion chromatography (SEC) using standard polyoxyethylene glycols. BBMA showed high efficiency and significantly different selectivity in MEKC for naphthalene derivatives in comparison with SDS [26]. The CMC of BBMA was found to be effectively zero [26]. The CMC of BBMA was found to be effectively zero [26]. BBMA is therefore expected to be suitable for MEKC-MS because of the formation of the micelle at low surfactant concentrations, a higher molecular mass beyond the hardware mass range and high-efficiency separations.

In this paper, we describe an on-line MEKC-ESI-MS system with BBMA as the pseudo-stationary phase.

## 2. Experimental

### 2.1. Apparatus

A schematic diagram of the MEKC-ESI-MS system is presented in Fig. 2. The structure is almost the same as for a CE-ESI-MS system using a coaxial sheath liquid flow [6–9,23]. MEKC was performed with laboratory-built instruments which consisted of a Matsusada Precision Devices HCZE30PN0.25-LDSW high-voltage power supply (Kusatsu, Shiga, Japan) and a fused-silica capillary (50 cm × 50 μm I.D. × 150 μm O.D.) obtained from Tokyo Kasei (Tokyo, Japan). An ESI interface was laboratory-built and consisted of a stainless-steel tube of 190 μm I.D. and 350 μm O.D. (G 28), inside which the capillary was coaxially inserted, a polytetrafluoroethylene (PTFE) tee union, which held the stainless-steel tube, the capillary and a PTFE tube for the delivery of the sheath flow.

The MS system consisted of a modified Hitachi M-1000 LC-APCI-MS system (Tokyo, Japan), which was constructed from a quadrupole mass spectrometer and a differential pumping region.

MEKC using UV detection was performed on a Hewlett-Packard (Waldbronn, Germany) HP3DCE system and a Bio-Rad (Hercules, CA, USA) BioFocus 3000 system to establish the MEKC separation conditions.

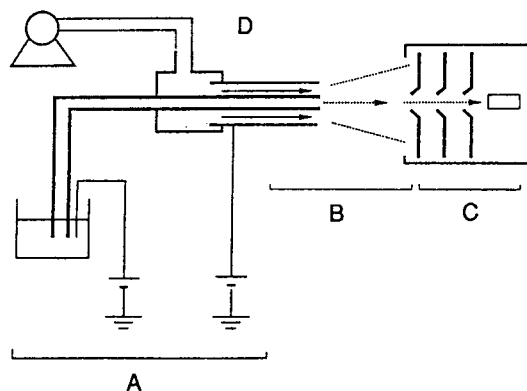


Fig. 2. Schematic illustration of experimental framework of the MEKC-ESI-MS system. A = MEKC; B = ESI; C = mass spectrometer; D = sheath liquid flow.

SEC of BBMA was performed with a Shimadzu (Kyoto, Japan) LC-9A liquid-delivery pump, a Shodex (Tokyo, Japan) RI SE-51 refractive index detector and Tosoh (Tokyo, Japan) TSK-gel G3000SW and G2000SW columns (both 60 cm × 8 mm I.D.) with a series connection.

## 2.2. Reagents

BBMA was provided as a 23% aqueous solution having a viscosity of 170 cP at 25°C by Dai-ichi Kogyo Seiyaku (Kyoto, Japan). As BBMA contains a minor amount of low-molecular-mass components, it was purified by the reprecipitation method with acetone [26,27]. Low-molecular-mass surfactants, SDS and cholic acid sodium salt, were purchased from Nacalai Tesque (Kyoto, Japan). Sodium laurate was obtained from Tokyo Kasei. 3-[(3-Cholamidopropyl)dimethylammonio]propanesulfonic acid (CHAPS) was supplied by Wako (Osaka, Japan). All other reagents were of analytical-reagent grade and water was purified with a Milli-Q system (Millipore). All sample compounds, phenyltrimethylammonium chloride, tetraphenylphosphonium chloride, quinine sulfate dihydrate, octaoxyethylenedodecanol and pentaoxyethylenedodecanol obtained from Wako, 1-naphthylamine from Merck (Darmstadt, Germany) and sulfamethazine, sulfisomidine, sulfadiazine and sulfisoxazole from Aldrich (St. Louis, MO, USA), were of analytical-reagent grade and used as received. Sample solutes were dissolved in about 50% aqueous methanol.

## 2.3. Procedure

On-line MEKC-ESI-MS work was performed with the system described above using BBMA solutions in 10 mM ammonium formate buffer (pH 7) containing 10% methanol. Samples were injected by the hydrostatic injection method (10–30 s at 15 cm). The MEKC applied voltage was 10 kV (13 kV at the capillary inlet and 3 kV at the end of the capillary located in the ESI interface).

The sheath liquid was water-methanol-formic acid (50:50:1, v/v/v) and was delivered by a Hitachi L6300 HPLC pump at ca. 5  $\mu$ l/min. Electrospray was performed using a 3 kV gradient between the capillary end and the first MS sampling orifice. The MS system was operated in the positive-ion mode. Almost all MS detection was obtained in the scanning mode, from  $m/z$  1 to 1000, at 4 s per scan. The drift voltage was 70 V, the focusing voltage 140–150 V and the resolution 50–55. The calibration of  $m/z$  for ESI-MS was effected with *p*-nitroaniline, 1-naphthylamine and 4,4'-diaminodiphenylmethane. Therefore, in the high-mass region, the  $m/z$  value was not exact because this calibration was effective in the lower mass region only. All work described was performed with the MEKC-ESI-MS system mentioned above at the Himeji Institute of Technology, except for the data in Fig. 10B, which were obtained with a fundamentally similar system at Hitachi Central Research Laboratory.

Off-line MS work was performed with another laboratory-built interface equipped with another fused-silica capillary using a sheath liquid flow. Sample solutions were introduced with a microsyringe. The other conditions were the same as in the on-line work.

MEKC using the UV detector was performed as described previously [26,27]. Fractionation of BBMA by SEC was performed with 50 mM ammonium carbonate (pH 8)-acetonitrile (20:80, v/v) at a mobile phase flow-rate of 0.8 ml/min. Each fraction was introduced into the mass spectrometer after adding 100  $\mu$ l of 20% formic acid to 2 ml of the fractionated solution.

## 3. Results and discussion

### 3.1. Optimization of the ESI interface

As the mass spectrometer employed in this study was operated in the positive-ion mode only, the ESI interface had to be optimized to produce positive ions efficiently. To generate positive ions by ESI, the liquid sprayed must be

acidic, generally of pH 3–5, as reported for CE–ESI–MS [9,16]. To meet this requirement, acidic buffers consisting of ammonium acetate or formate were employed in CE–ESI–MS or an acidic sheath flow was added to the running solution at the end of the separation capillary [9,16].

In this work, however, an acidic buffer was not used because BBMA is insoluble in water at low pH or it precipitates below pH 4 [26], and normal MEKC conditions in which the electroosmotic flow is strong were to be employed to take advantage of MEKC to separate non-ionic analytes. BBMA solutions in ammonium formate (pH 7) were employed and aqueous methanol (1:1) containing 1% formic acid was used as a sheath liquid to acidify the total liquid sprayed at the ESI interface. A similar procedure has also been employed for peptide mapping by CE–ESI–MS using a basic electrophoretic buffer and an acidic sheath liquid [23]. Optimization of positioning of the capillary tip in the ESI interface against the first MS sampling orifice is critical to the MS signal intensity of analytes because of the conical distribution of aerosol generated by the electrospray. It has been reported that the distributions of compositions were different among ions generated by ESI [28]. In this work, the capillary tip was positioned at a separation distance of 20 mm, offset 5 mm horizontally and 5 mm vertically from the centre of the orifice to maximize the signal intensity of ions generated from standard compounds. This fixed position may not have been optimum for all analytes, but repositioning of the capillary tip was not tried throughout this work.

The ESI interface system employed was evaluated under MEKC conditions using BBMA as a pseudo-stationary phase. Even the introduction of a 2% BBMA solution into the ESI–MS system generated a stable electrospray and did not impair the MS detection significantly. It was required to rinse the capillary with 1 M sodium hydroxide after each run to obtain reproducible migration times. Therefore, the effect of the introduction of the sodium hydroxide solution

into the ESI–MS system was investigated. When the sodium hydroxide solution was introduced, the electrospray became unstable and the signal intensity deteriorated. Thus, when the sodium hydroxide solution was introduced to rinse the capillary, the electrospray was interrupted.

### 3.2. Background ions from BBMA

Fig. 3 shows examples of the mass spectra of MEKC separation solutions: (A) ammonium formate buffer only, (B) buffer containing 2% BBMA and (C) buffer containing 50 mM SDS.

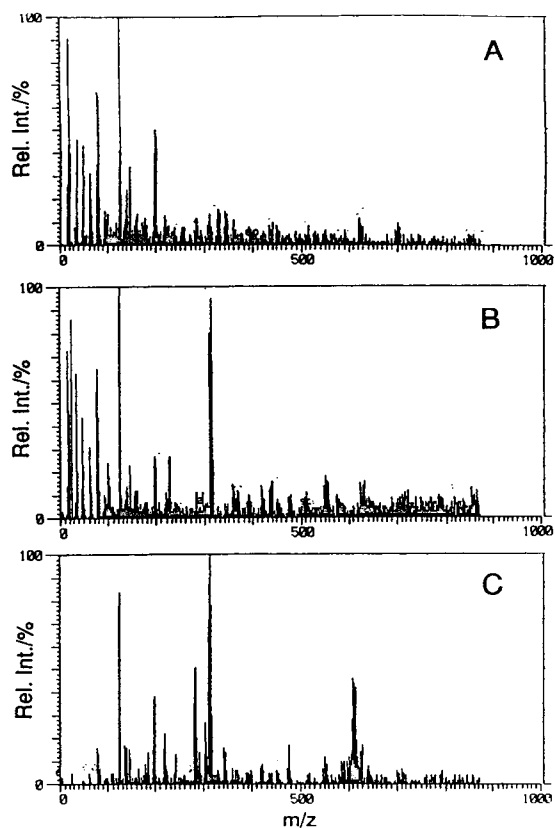


Fig. 3. ESI mass spectra of MEKC separation solutions: (A) 10 mM ammonium formate buffer (pH 7); (B) (A) + 2% BBMA; (C) (A) + 50 mM SDS. Conditions: electrospray voltage, 3 kV; MS scanning, from  $m/z$  1 to 1000 at 4 per scan; drift voltage, 70 V; focusing voltage, 140 V; resolution, 55; sheath liquid flow, water–methanol–formic acid (50:50:1, v/v/v) at ca. 5  $\mu$ l/min; sample solutions were introduced by syringe injection.

In the spectrum of 10 mM ammonium formate buffer (pH 7), many peaks below  $m/z$  200 were observed. The strongest peak was at ca.  $m/z$  120. It should have come from the buffer system, but could not be identified. In the spectrum with 2% BBMA added to the buffer, strong peaks were recorded at ca.  $m/z$  310, which was characteristic of the BBMA solution. In the spectrum of buffer containing 50 mM SDS, two very strong peaks were observed at ca.  $m/z$  310 and 610. The former was assigned to the molecular ion of SDS due to sodium attachment and the latter to the singly charged dimer. Both peaks showed a stronger intensity than those from the buffer system. Observation of the molecular ion of SDS due to sodium attachment in ESI-MS has

been reported by Smith et al. [6]. To identify the  $m/z$  310 ion generated from BBMA solution, BBMA was fractionated by SEC. Fig. 4 shows the SEC of BBMA and the ESI mass spectrum of each fraction. From fractions A and B, consisting of the polymer and oligomer of BBMA, no strong signals were observed. From fraction C, a strong  $m/z$  310 peak was recorded. It should be noted that signal intensities cannot be compared among different spectra, because the spectra show only signal intensities relative to the strongest peak. Using analytical SEC, it was clarified that an additive of BBMA appeared in this region, but no components of BBMA, butyl acrylate, butyl methacrylate or methacrylic acid sodium salt. Therefore, this ion was proba-

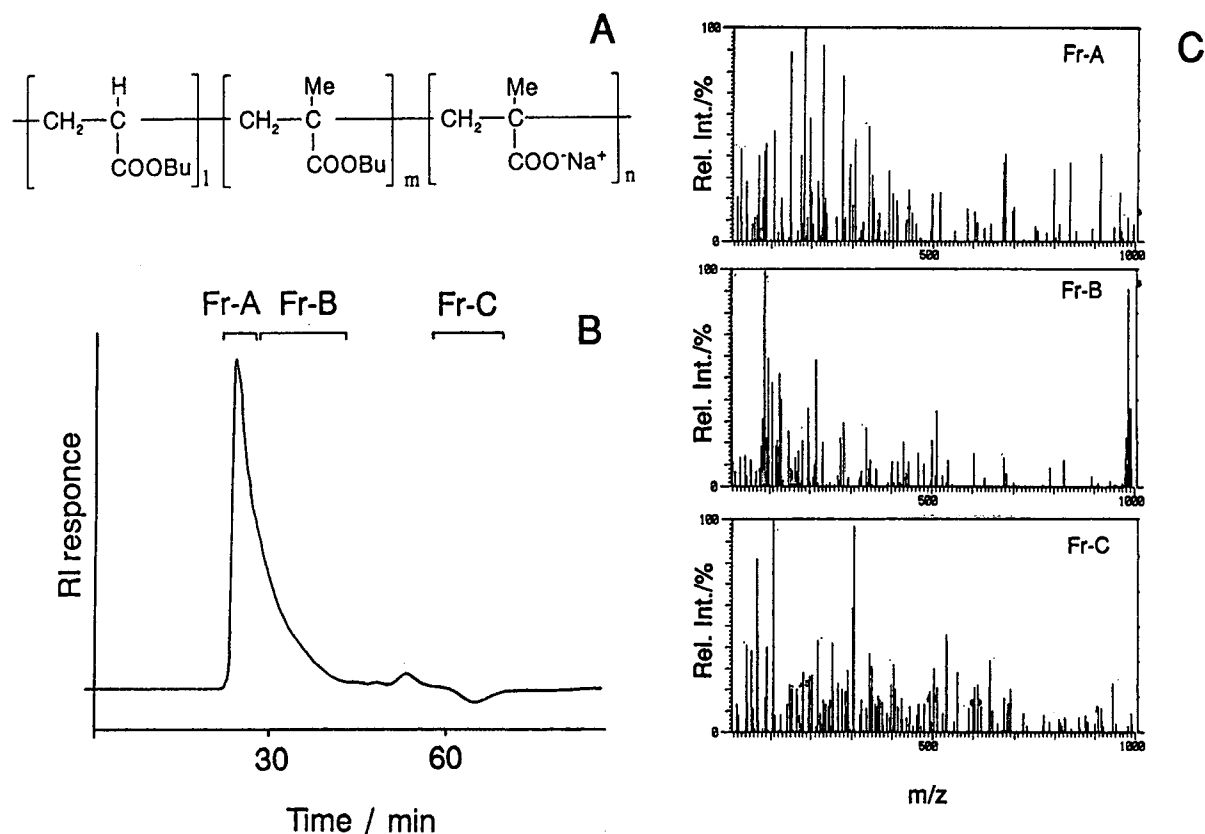


Fig. 4. (A) Molecular structure of BBMA; (B) SEC for fractionation of BBMA; (C) ESI mass spectra of fractions. SEC conditions (B): column, Tosoh TSK-gel G3000SW and G2000SW (both 60 cm  $\times$  8 mm I.D.) with a series connection; separation solution, 50 mM ammonium carbonate (pH 8)–acetonitrile (20:80, v/v) at 0.8 ml/min; detection, refractive index. MS conditions (C): sheath liquid flow, water–methanol (50:50, v/v) at ca. 5  $\mu$ l/min; drift voltage, 80 V; other MS conditions as in Fig. 3.

bly from the additive, the amount of which in BBMA was very small. The results shown in Figs. 3 and 4 strongly suggest that BBMA does not disturb the on-line measurement of the mass spectra of analytes separated by MEKC with BBMA as a pseudo-stationary phase.

Some ionic low-molecular-mass surfactants other than SDS were introduced into the ESI-MS system. Sodium cholate, sodium dodecane sulfonate and CHAPS produced strong signals of molecular ions due to cation attachment. Sodium laurate gave no strong ion.

### 3.3. ESI-MS of analytes

Fig. 5 shows an ESI mass spectrum of a standard mixture and the molecular structures of the analytes. The mixture was composed of a quaternary ammonium salt, an aromatic amine, an alkaloid, a quaternary phosphonium salt and a non-ionic surfactant having a polyoxyethylene group. Phenyltrimethylammonium chloride, 1-naphthylamine, quinine sulfate dihydrate and tetraphenylphosphonium chloride showed abun-

dant intact molecular ions. Octaoxyethylenedodecanol generated two intense molecular ions due to cation attachment. The more intense, higher mass ion was selected as the monitored ion of the single-ion chromatogram for the on-line MEKC-ESI-MS described below. On the other hand, no MS signals were observed from 1-naphthol and 1-naphthalenemethanol, which are usually used as MEKC standard compounds, or from phenanthrene and Sudan IV, which are used as micelle markers in MEKC. These compounds seemed not to be ionized by ESI-MS.

### 3.4. On-line MEKC-ESI-MS

Fig. 6 shows the single-ion chromatograms obtained by (A) MEKC-ESI-MS and (B) CE-ESI-MS. The solutes are the same as in Fig. 5. All the solutes were separated and detected successfully under the conditions of MEKC with 2% BBMA, as shown in Fig. 6A. The separation and sensitivity were practically reproducible in several successive runs. The migration times of all solutes in Fig. 6A were longer than the

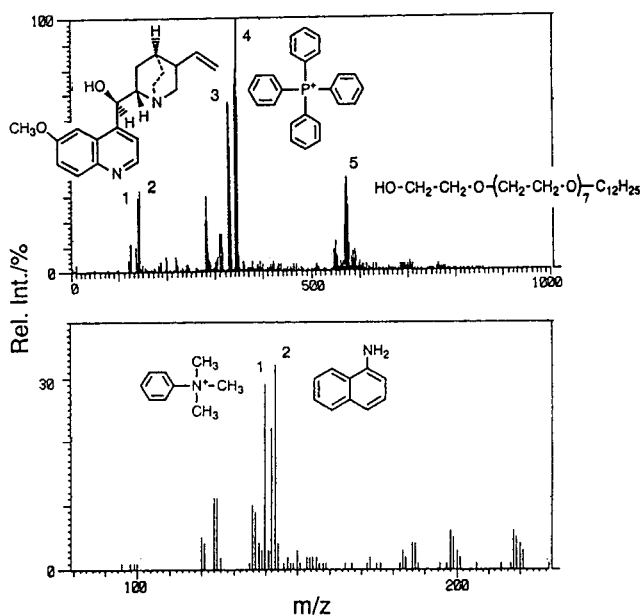


Fig. 5. Example of an ESI mass spectrum of standard mixture and molecular structures of the analytes. Peaks: 1 = phenyltrimethylammonium chloride; 2 = 1-naphthylamine; 3 = quinine sulfate; 4 = tetraphenylphosphonium chloride; 5 = octaoxyethylenedodecanol. Conditions as in Fig. 3.

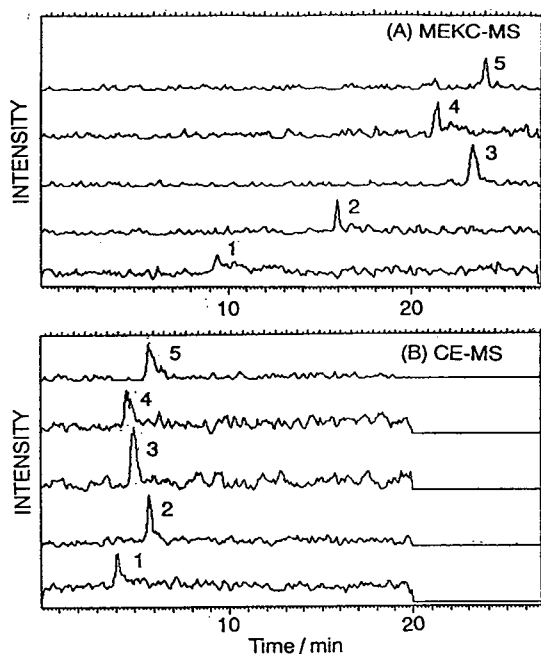


Fig. 6. Single-ion chromatograms obtained by (A) MEKC-ESI-MS and (B) CE-ESI-MS. Solutes as in Fig. 5. MEKC conditions: capillary, 50 cm  $\times$  50  $\mu$ m I.D.; separation solution, (A) 2% BBMA in 10% methanol and 10 mM ammonium formate buffer (pH 7) and (B) 10 mM ammonium formate buffer (pH 7); applied voltage, 13 kV. MS conditions as in Fig. 3.

corresponding times in Fig. 6B, where no micelle was used, and the solutes were separated more widely according to the MEKC mechanism; octaoxyethylenedodecanol migrated more slowly than 1-naphthylamine, although both are neutral and unresolved in Fig. 6B.

Fig. 7 shows mass spectra acquired from the peaks shown in Fig. 6A and B. Under the MEKC conditions with 2% BBMA, abundant intact molecular ions of quinine sulfate and tetraphenylphosphonium chloride and abundant intense octaoxyethylenedodecanol molecular ion due to cation attachment were observed, as shown in Fig. 7A, B and C. The signal at  $m/z$  310 in Fig. 7A, B and C was generated from the additive of BBMA as shown in Fig. 3B. Some peaks below  $m/z$  200 recorded in all spectra in Fig. 7 were from the buffer system as shown in Fig. 3A.

Fig. 8 shows the dependence of the migration

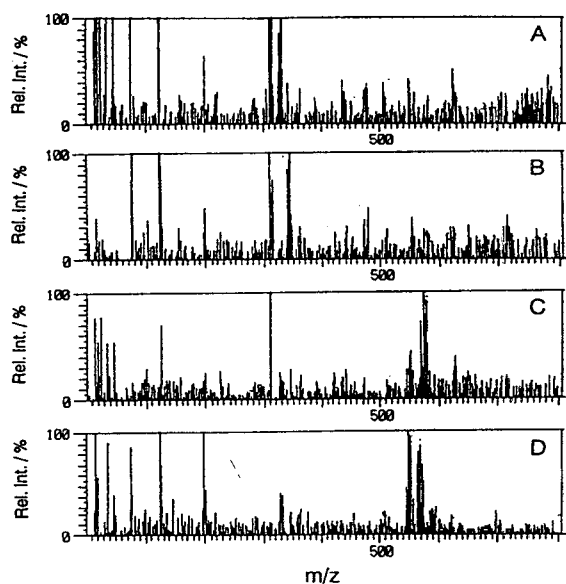


Fig. 7. Mass spectra acquired from (A) peak 3, (B) peak 4 and (C) peak 5 in MEKC-ESI-MS shown in Fig. 6A and (D) peak 5 in CE-ESI-MS shown in Fig. 6B. The MS intensity was normalized by the signal observed over  $m/z$  310.

time on the concentration of BBMA. The migration times of all solutes increased with increase in the concentration of BBMA. This result indicates that the separation is based on the differential partitioning of the solutes between

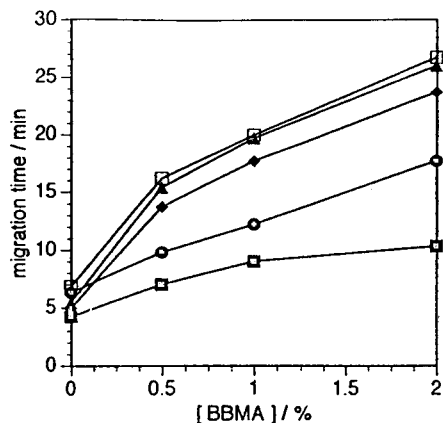


Fig. 8. Dependence of the migration time on the concentration of BBMA. Solute: □ = phenyltrimethylammonium chloride; ○ = 1-naphthylamine; ▲ = quinine sulfate; ◆ = tetraphenylphosphonium chloride; ◻ = octaoxyethylenedodecanol. Conditions as in Fig. 6.



the slower migrating BBMA micelle and the faster migrating surrounding aqueous phase. Octaoxyethylenedodecanol, a non-ionic surfactant, migrated last. In MEKC using octaoxyethylenedodecanol added to the BBMA solution, the capacity factors of solutes increase with increase in the concentration of octaoxyethylenedodecanol [27], which means that BBMA forms mixed micelles with octaoxyethylenedodecanol. Octaoxyethylenedodecanol was therefore more suitable as a tracer of the BBMA micelle than quinine sulfate, which is used as a tracer of the SDS micelle.

Fig. 9 shows the dependence of the MS intensities of phenyltrimethylammonium chloride and octaoxyethylenedodecanol on the concentration of BBMA. The signal intensity of phenyltrimethylammonium chloride decreased with increase in the concentration of BBMA. The intensity at 2% BBMA was ca. 20% of that in the absence of BBMA. The signal intensities of the other solutes except for octaoxyethylenedodecanol tended to decrease with increase in the concentration of BBMA. The signal intensity of octaoxyethylenedodecanol, however, was maximum at 1% BBMA. Further details of the mass spectrum of octaoxyethylenedodecanol were investigated at each concentration of BBMA. Fig. 7C and D indicate

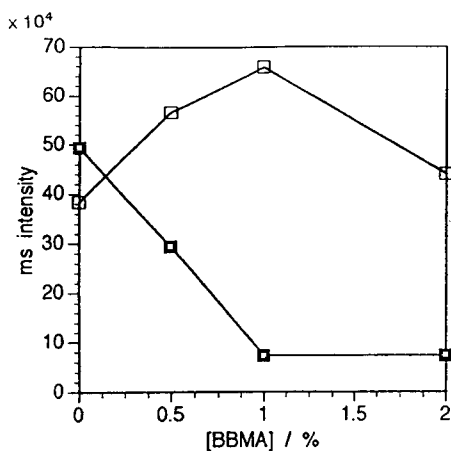


Fig. 9. Dependence of intensities on the concentration of BBMA. ■ = Phenyltrimethylammonium chloride; □ = octaoxyethylenedodecanol. Conditions as in Fig. 6.

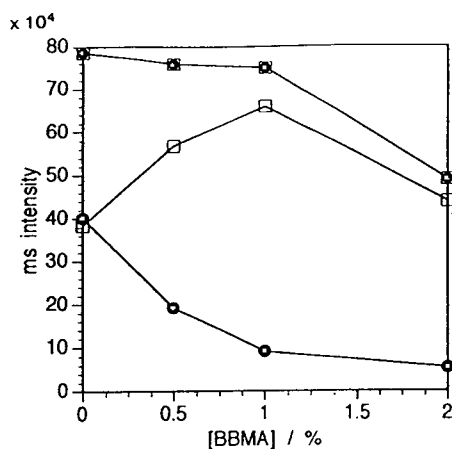


Fig. 10. Dependence of intensities on the concentration of BBMA. □ = Octaoxyethylenedodecanol high-mass peak,  $[M + NH_4]^+$ ; ● = octaoxyethylenedodecanol low-mass peak,  $[M + H]^+$ ; ■ = □ + ●. Conditions as in Fig. 6.

the difference in the mass spectra of octaoxyethylenedodecanol in the absence and presence of BBMA. Fig. 10 shows the dependence of the intensities of the two molecular ions of octaoxyethylenedodecanol, which are assigned due to proton attachment,  $[M + H]^+$ , and ammonium attachment,  $[M + NH_4]^+$ , on the concentration of BBMA. Fig. 9 shows the intensity of  $[M + NH_4]^+$ . However, the intensity of  $[M + H]^+$  decreased with increase in the concentration of BBMA, as shown in Fig. 10. A homologous non-ionic surfactant, pentaoxyethylenedodecanol, also showed the same tendency as octaoxyethylenedodecanol, producing the molecular ion due to ammonium attachment more than that due to proton attachment under MEKC-ESI-MS conditions with 2% BBMA. The sum of the intensities of  $[M + H]^+$  and  $[M + NH_4]^+$  for octaoxyethylenedodecanol decreased with increase in the concentration of BBMA, as shown in Fig. 10. It is generally noted that the MS intensity of the solute decreases with increase in the concentration of BBMA. This result is consistent with that observed as an effect on salt concentration on the ionization efficiency of ESI [29–31].

Fig. 11 shows (A) MEKC separation with a UV detector and (B) MEKC-ESI-MS of sulfamides. The single-ion chromatograms in Fig.

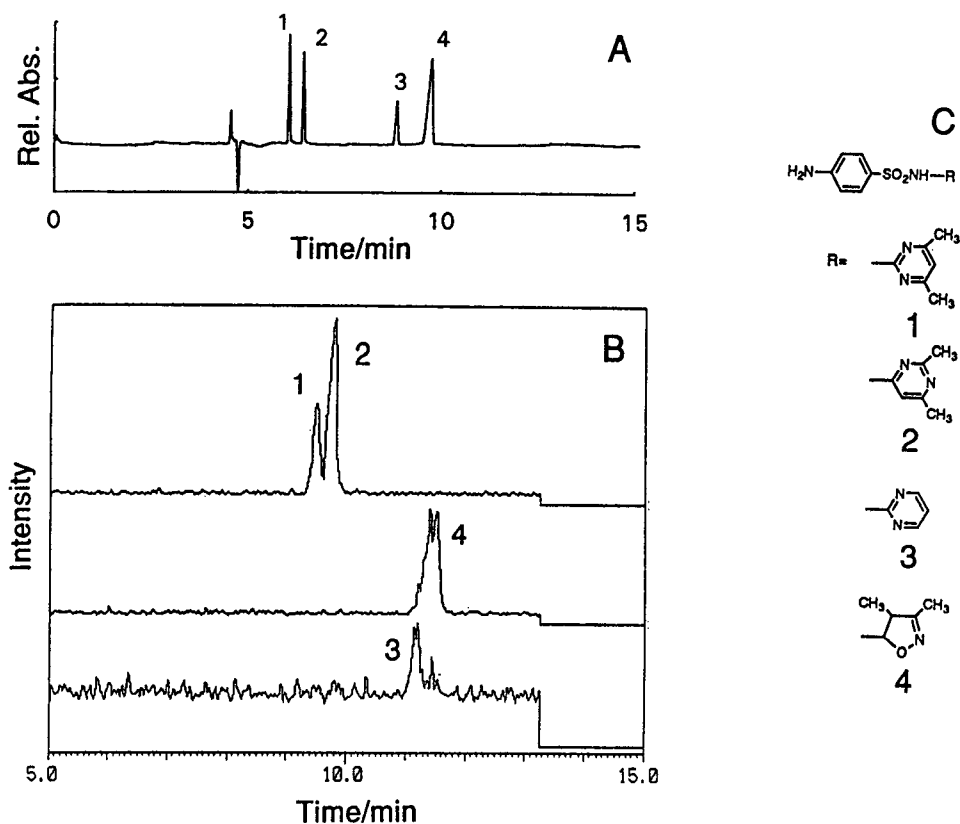


Fig. 11. (A) MEKC with a UV detector and (B) MEKC-ESI-MS of sulfamides and (C) their molecular structures. Solutes: 1 = sulfamethazine; 2 = sulfisomidine; 3 = sulfadiazine; 4 = sulfisoxazole. Conditions: (A) separation solution, 1% BBMA in 10% methanol and 100 mM borate–50 mM phosphate buffer (pH 7); capillary, 48 cm (40 cm to the detector)  $\times$  50  $\mu$ m I.D. fused silica; applied voltage, 20 kV; detection wavelength, 210 nm. (B) Other conditions as in Fig. 6 except for the interface; the MS instrument was operated in the SIM mode.

11B were recorded in the SIM mode without scanning. From Fig. 11B, all four sulfamides were separated and detected by MEKC-ESI-MS with 1% BBMA. All four sulfamides were easily separated by MEKC, as shown in Fig. 11A. The separation efficiency in MEKC-ESI-MS was far less than in conventional MEKC, as easily judged from the separation between peaks 1 and 2. The significant deterioration of separation efficiency was probably caused by the ESI interface. No optimization was tried to improve the efficiency in this study. To take advantage of the high-efficiency separation of MEKC, more work is needed to increase the separation efficiency in MEKC-ESI-MS.

#### 4. Conclusions

On-line MEKC-ESI-MS using BBMA, a high-molecular-mass surfactant, was achieved. This system was employed successfully under the conditions of MEKC with 2% BBMA. This concentration of BBMA is high enough for most purposes. Because the MS signal intensities of solutes decrease with increase in the concentration of BBMA, a separation solution containing a low concentration BBMA should be employed, especially for the detection of analytes for which the ionization efficiency is low. This work is preliminary and the performance of this system, in terms of both separation and

sensitivity, is not yet satisfactory. A more advanced ESI interface and optimization of MEKC, sheath flow and MS detection conditions will produce better performance in future work.

### Acknowledgements

The authors thank Mr. Akinobu Ichihara of Dai-ichi Kogyo Seiyaku for the supply of BBMA. S.T. is grateful to Sumitomo Chemical, Toray Research Centre and Kanegafuchi Chemical Industry for their financial support of this work. This work was supported in part by a Grant-in-Aid for Scientific Research (No. 06453070) from the Ministry of Education, Science and Culture, Japan.

### References

- [1] S. Terabe, K. Otsuka, K. Ichikawa, A. Tsuchiya and T. Ando, *Anal. Chem.*, 56 (1984) 111–113.
- [2] S. Terabe, K. Otsuka and T. Ando, *Anal. Chem.*, 57 (1985) 834–841.
- [3] J. Vindevogel and P. Sandra, *Introduction to Micellar Electrokinetic Chromatography*, Hüthig, Heidelberg, 1992.
- [4] S. Terabe, in N. Guzman (Editor), *Capillary Electrophoresis Technology*, Marcel Dekker, New York, 1993, pp. 65–87.
- [5] S. Terabe, N. Chen and K. Otsuka, *Adv. Electrophoresis*, 7 (1994) 87–153.
- [6] R.D. Smith, C.J. Barinaga and H.R. Udseth, *Anal. Chem.*, 60 (1988) 1948.
- [7] H.R. Udseth, J.A. Loo and R.D. Smith, *Anal. Chem.*, 61 (1989) 1989.
- [8] R.D. Smith, J.H. Wahl, D.R. Goodlett and S.A. Hofstadler, *Anal. Chem.*, 65 (1993) 574.
- [9] J.H. Wahl and R.D. Smith, *J. Capillary Electrophoresis*, 1 (1994) 62.
- [10] F. Garcia and J.D. Henion, *Anal. Chem.*, 64 (1992) 985–990.
- [11] I.M. Johansson, R. Pavelka and J.D. Henion, *J. Chromatogr.*, 559 (1991) 515–528.
- [12] S. Pleasance, P. Thibault and J. Kelly, *J. Chromatogr.*, 591 (1992) 325–339.
- [13] M.A. Moseley, L.J. Deterding, K.B. Tomer and J.W. Jorgenson, *Anal. Chem.*, 63 (1991) 109–114.
- [14] L.J. Deterding, C.E. Parker, J.R. Perkins, M.A. Moseley, J.W. Jorgenson and K.B. Tomer, *J. Chromatogr.*, 554 (1991) 329–338.
- [15] W. Weinmann, C.E. Parker, L.J. Deterding, D.I. Papac, J. Hoyes, M. Przybylski and K.B. Tomer, *J. Chromatogr.*, 680 (1994) 353–361.
- [16] R.D. Smith and H.R. Udseth, in N. Guzman (Editor), *Capillary Electrophoresis Technology*, Marcel Dekker, New York, 1993, pp. 525–567.
- [17] K.B. Tomer, in N. Guzman (Editor), *Capillary Electrophoresis Technology*, Marcel Dekker, New York, 1993, pp. 569–586.
- [18] W.M.A. Niessen, U.R. Tjaden and J. van der Greef, *J. Chromatogr.*, 636 (1993) 3–19.
- [19] R.D. Smith, J. A. Loo, C.G. Edmonds, C.J. Barinaga and H.R. Udseth, *Anal. Chem.*, 62 (1990) 882–899.
- [20] M.H. Lamoree, U.R. Tjaden and J. van der Greef, *J. Chromatogr.*, in press.
- [21] A.F. Lecoq, S.D. Biase and L. Montanarella, *J. Chromatogr.*, 638 (1993) 363–373.
- [22] J. Varghese and R.B. Cole, *J. Chromatogr. A*, 652 (1993) 369–376.
- [23] Y. Takada, K. Nakayama, M. Yoshida and M. Sakairi, *Anal. Sci.*, 10 (1994) 713–717.
- [24] C.P. Palmer, M.Y. Khaled and H.M. McNair, *J. High Resolut. Chromatogr.*, 15 (1992) 756–762.
- [25] C.P. Palmer and H.M. McNair, *J. Microcol. Sep.*, 4 (1992) 509–514.
- [26] H. Ozaki, A. Ichihara and S. Terabe, *J. Chromatogr. A*, 680 (1994) 117–123.
- [27] H. Ozaki, A. Ichihara and S. Terabe, *J. Chromatogr.*, in press.
- [28] K. Hiraoka, *Rapid Commun. Mass Spectrom.*, 6 (1992) 463.
- [29] L. Tang and P. Kerbarle, *Anal. Chem.*, 63 (1991) 2709–2715.
- [30] L. Tang and P. Kerbarle, *Anal. Chem.*, 65 (1993) 3654–3668.
- [31] L. Tang and P. Kerbarle, *Anal. Chem.*, 65 (1993) 972A–986A.





ELSEVIER

Journal of Chromatography A, 716 (1995) 81–95

JOURNAL OF  
CHROMATOGRAPHY A

# Optimization of resolution in micellar electrokinetic chromatography via computer-aided simultaneous variation of concentrations of sodium dodecyl sulfate and urea as modifier

Ute Pyell\*, Ulf Bütchorn

*Fachbereich Chemie der Philipps-Universität Marburg, Hans-Meerwein-Strasse, D-35032 Marburg, Germany*

## Abstract

A computer-aided method is presented that permits the simultaneous optimization of the concentration of an anionic surfactant (sodium dodecyl sulfate) and the modifier urea in the separation buffer in micellar electrokinetic chromatography (MEKC) after only three test runs. The underlying algorithm takes into account that resolution in MEKC is dependent on selectivity, retention factor and the ratio of the hold-up time to the migration time of the micelles ( $t_0/t_M$ ). All these factors are influenced by the buffer composition. The optimization method presented was applied to the separation of nitroaromatic compounds, urea pesticides and aliphatic amines derivatized with *p*-nitrobenzoic acid.

## 1. Introduction

Micellar electrokinetic chromatography (MEKC), first introduced by Terabe and co-workers [1,2], renders possible the separation of neutral and charged solutes by distributing them between an aqueous mobile phase and a retarded micellar phase (pseudo-stationary phase). Since its introduction in 1985, MEKC has already found various applications, especially in the analysis of nitroaromatic compounds [3,4] and in pharmaceutical analysis [5,8].

In spite of the growing importance of MEKC, there are only a few examples of computer-assisted systematic resolution optimization for this separation technique. Vindevogel and Sandra [9] used a Plackett–Burman statistical design to optimize the resolution of testos-

terone esters. The method required eight experiments for the optimization of five parameters. Yik and Li [10] used a three-dimensional overlapping resolution mapping scheme to optimize the resolution of dinitrophenyl-derivatized amino acids. The method required eleven preplanned experiments and predicted the optimum buffer pH, surfactant [sodium dodecyl sulfate (SDS)] concentration and modifier (tetrabutylammonium salt) concentration.

In the approach of Yik and Li [10], a theoretical model to describe the migration behaviour is not required. The same holds for the method of Vindevogel and Sandra [9]. Smith and Khaledi [11] tested another approach: they predicted the migration behavior of a homologous series of phenols over a two-dimensional pH–micelle concentration space. The model describes mobility in terms of the acid dissociation constant, the partition coefficient, the pH of the buffer and the

\* Corresponding author.

micelle concentration. Eighteen experiments were necessary to obtain the data set required for weighted non-linear regression in order to evaluate the physical and chemical constants of each solute. These constants form the data basis for subsequent predictions.

Quang et al. [12] predicted successfully the migration behavior of several acidic and basic solutes over a pH–micelle concentration factor space on the basis of only five experiments. The concentration of additives, however, is not taken into account in their optimization approach.

In a recent paper [13], we investigated whether at a given pH the buffer composition concerning the surfactant (SDS) concentration and the modifier (urea or glucose, respectively) concentration can be optimized rapidly by employing the basic equation for resolution ( $R_s$ ) developed by Terabe and co-workers [1,2]:

$$R_s = \frac{\sqrt{N}}{4} \cdot \frac{k}{k+1} \cdot \frac{\alpha-1}{\alpha} \cdot \frac{1-t_0/t_M}{1+t_0/t_M \cdot k} \quad (1)$$

where  $N$  = plate number,  $k$  = mean retention factor,  $\alpha$  = selectivity factor,  $t_0$  = migration time of the mobile phase and  $t_M$  = migration time of the micelles. We predicted the optimum surfactant or modifier concentration, keeping constant all other parameters, on the basis of only two test runs.

Terabe et al. [2] had already shown that the function  $f(k) = [k/(1+k)] \cdot (1-t_0/t_M)/[1+(k \cdot t_0/t_M)]$  passes through a maximum if  $t_0 \neq t_M$ . Foley [14] demonstrated that the basic equation for resolution in MEKC differentiated for  $k$  has a zero value if  $k = \sqrt{t_M/t_0}$ , provided that the other quantities in Eq. 1 are kept constant. He recommended tuning the phase ratio (volume of pseudo-stationary phase/volume of mobile phase) by varying the surfactant concentration in order to adjust the retention factors of the solutes to the derived optimum condition. In practice, however, with varying surfactant concentrations  $t_0/t_M$  is also strongly influenced [2,12,15]. This influence cannot be neglected in optimization algorithms.

Little and Foley [16] have shown in an experimental study that ignoring the influence of the surfactant concentration on  $t_0/t_M$  renders

incorrect predictions of the optimum buffer composition. They therefore suggested keeping the ratio  $t_0/t_M$  constant by adding a non-ionic surfactant to the separation buffer in order to simplify the optimization procedure. It must be stressed that this approach will only be successful if the solutes differ sufficiently in their retention factors. Generally, the ratio  $t_0/t_M$  should be minimized (while keeping  $t_0$  constant) as much as possible to enhance the resolution according to Eq. 1. In our approach [13], the surfactant concentration can be rapidly optimized, although  $t_0/t_M$  is largely dependent on the concentration of the surfactant examined (SDS).

Urea is reported [17] to be a versatile modifying additive to the mobile phase that improves the ratio  $t_0/t_M$  to a great extent without reducing strongly the electroosmotic velocity,  $v_{eo}$ . The addition of urea to the mobile phase also decreases the retention factors of the solutes, thus making it possible to adjust them to the optimum condition derived by Foley [14]. The urea and the surfactant concentrations are two important factors in controlling migration and resolution of neutral solutes. Owing to the interactive nature of these two factors, the simultaneous optimization of the urea and surfactant concentrations in the running buffer employed in MEKC is therefore desirable for many applications.

Alternatively, a reduction in the electroosmotic velocity, either by coating the inner wall of the capillary or by reducing the buffer pH, can be used to decrease the ratio  $t_0/t_M$  [15]. However, these methods increase the analysis time. Other organic modifiers have been used besides urea: acetonitrile [18], glucose [19], 2-propanol [20] and methanol [18]. These modifiers have the disadvantage that they reduce considerably the electroosmotic velocity resulting from their influence on viscosity and dielectric constant of the separation buffer [13,18–21]. Up to the present, only urea has been reported as a modifier that improves the elution range without substantially reducing the electroosmotic velocity [13,18].

Another possibility for improving the elution range without influencing the electroosmotic velocity is offered by reducing the chain length of the anionic buffer employed [15]. Modifying the chain length of the surfactant, however, can

have an undesirable effect on the critical micellar concentration (CMC) of the surfactant. With anionic surfactants, the CMC is reported to increase with shorter chain lengths [22]. SDS has been reported to have a low CMC under the conditions normally employed in MEKC [13]. The CMC of SDS is virtually unaltered by the addition of urea to the separation buffer.

If the separated solutes have an electrophoretic mobility, not only the apparent retention factors and  $t_0/t_M$  are influenced by the buffer composition but also the apparent selectivity factors,  $\alpha$ . The apparent selectivity factor for two solutes is the ratio of their apparent retention factors, ignoring electrophoretic effects.

In this paper, a computer-aided method based on a computer program called computer-assisted bivariate resolution optimization (CABRO) is presented that permits the prediction of the optimum buffer composition concerning the concentration of sodium dodecyl sulfate (SDS) and urea on the basis of only three test runs. Changes in the apparent selectivities, the retention factors and  $t_0/t_M$  are taken into consideration in the algorithm employed.

## 2. Experimental

### 2.1. Reagents

Chemicals used for separation studies were purchased from various suppliers. Sodium tetraborate, boric acid and urea (Merck, Darmstadt, Germany) and sodium dodecyl sulfate (Roth, Karlsruhe, Germany) used for the preparation of the separation buffers were of analytical-reagent grade. The urea pesticide standards were purchased from Riedel-de Haën (Seelze, Germany). Water was doubly distilled.

### 2.2. Derivatization of amines

The amines were dissolved in dry acetone. 4-nitrobenzoyl chloride was added in excess and the solution was kept at 50°C for 20 min. The solution was then made alkaline by adding an equal volume of aqueous disodium tetraborate (50 mmol/l). The solution was shaken and then

left for 20 min at 70°C in order to evaporate the acetone and to convert the excess of 4-nitrobenzoyl chloride into 4-nitrobenzoic acid.

### 2.3. Chromatographic measurements

All chromatographic measurements were carried out with a Beckman (Fullerton, CA, USA) P/ACE capillary electrophoresis system equipped with a UV absorbance detector. The temperature of the capillary was controlled by liquid cooling and was maintained at 25°C. Samples were injected by application of pressure for 1–2 s. Detection was performed at 254 nm. All separations were carried out at 25 kV. Data were recorded with Beckman System Gold software.

Fused-silica capillaries (75  $\mu\text{m}$  I.D., 375  $\mu\text{m}$  O.D.) were obtained from Polymicro Technologies (Phoenix, AZ, USA). The total length of the capillary was 56.5 cm and the length to the detector was 50 cm. The capillary rinsing procedures employed have already been presented in detail [23]. The elution time of the mobile phase,  $t_0$ , and the elution time of the micellar phase,  $t_M$ , were determined using formamide or thiourea and quinine hydrochloride, respectively, as markers. Peak identities were confirmed by spiking.

Studies with various concentrations of SDS and urea were performed either with a buffer containing 10 mmol/l  $\text{H}_3\text{BO}_3$  and 10 mmol/l  $\text{Na}_2\text{B}_4\text{O}_7$  or with a buffer containing 30 mmol/l  $\text{Na}_2\text{B}_4\text{O}_7$ .

### 2.4. Optimization software

All programs used for separation studies were written in Pascal employing Turbo Pascal 6.0.

## 3. Results and discussion

### 3.1. Correlation studies

In MEKC, the resolution of two closely adjacent peaks is dependent on the efficiency of the chromatographic system, the selectivity factor for the two solutes, the mean retention factor

and the ratio of the migration time of the mobile phase to that of the micelles according to Eq. 1. The retention factor of the first and the second solutes, contained in the original equation, was replaced by the mean retention factor.

In the following calculations, the efficiency of the chromatographic system is considered to be independent of the buffer composition. All other quantities,  $k$ ,  $t_0$  and  $t_M$ , are dependent on the buffer composition;  $\alpha$  is partially dependent on the surfactant and the modifier concentration [13].

In the first experimental step, the function  $y = f(c_{\text{SDS}}, c_{\text{urea}})$  was determined that best describes the dependence of  $k$ ,  $t_0$  and  $t_M$  on the surfactant concentration ( $c_{\text{SDS}}$ ) and the modifier concentration ( $c_{\text{urea}}$ ). Caffeine, *p*-nitrotoluene, 4-methyl-3-nitroaniline, 4-methyl-2-nitroaniline, 2-methyl-3-nitroaniline and naphthalene were used as test solutes. The surfactant concentration in the separation buffer was varied from 20 to 100 mmol/l in 20 mmol/l steps. The urea concentration was varied from 0.0 to 4.0 mol/l in 0.5 mol/l steps. The concentration of disodium tetraborate in the separation buffer was kept constant at 30 mmol/l in all measurements.

In Fig. 1a–e,  $t_0$ ,  $t_M$  and the retention factors of caffeine, *p*-nitrotoluene and naphthalene are plotted against  $c_{\text{SDS}}$  and  $c_{\text{urea}}$ . It can be seen that for  $t_0$  the resulting area can be approximated by a plane, described by the function

$$t_0 = f(c_{\text{SDS}}, c_{\text{urea}}) = a + bc_{\text{SDS}} + dc_{\text{urea}} \quad (2)$$

where  $a$ ,  $b$  and  $d$  are constants. The best fit was found for  $t_M$  with the function

$$\ln t_M = f(c_{\text{SDS}}, c_{\text{urea}}) = a' + b' \ln(c_{\text{SDS}}) + d'c_{\text{urea}} \quad (3)$$

where  $a'$ ,  $b'$  and  $d'$  are constants.

In Fig. 1f,  $\ln t_M$  is plotted against  $\ln c_{\text{SDS}}$  and  $c_{\text{urea}}$ . Whereas in Fig. 1b the resulting area is strongly vaulted, in Fig. 1f the area of the functional values can be approximated by a plane.

Terabe et al. [17] have reported that the logarithm of the retention factor for a solute

decreases linearly with increasing concentration of urea, if  $c_{\text{SDS}}$  is kept constant:

$$\ln k = \text{constant} + \text{constant}' \cdot c_{\text{urea}} \quad (4)$$

In early studies [2], it was shown that  $k$  is linearly dependent on  $c_{\text{SDS}}$  above the CMC. It was found that the CMC of SDS is between 1 and 4 mmol/l in the buffers usually employed in MEKC [13]. If the small  $y$ -intercept of the function  $k = f(c_{\text{SDS}})$  is neglected, the two functions  $k = f(c_{\text{SDS}})$  and  $k = f(c_{\text{urea}})$  can be combined by the following equation:

$$\ln k = f(c_{\text{SDS}}, c_{\text{urea}}) = a'' + b'' \ln c_{\text{SDS}} + d''c_{\text{urea}} \quad (5)$$

where  $a''$ ,  $b''$  and  $d''$  are constants. The area resulting from the function  $k = f(c_{\text{SDS}}, c_{\text{urea}})$  can also be approximated by a plane (Fig. 1c–e). The regression coefficients of regressions keeping one of the parameters ( $c_{\text{SDS}}$  or  $c_{\text{urea}}$ ) constant are significantly improved with Eq. 5 compared with the regression coefficients of regressions keeping one of the parameters ( $c_{\text{SDS}}$  or  $c_{\text{urea}}$ ) constant and approximating the function  $k = f(c_{\text{SDS}}, c_{\text{urea}})$  by Eq. 8.

The constants of Eqs. 2, 3 and 5 can be calculated from just three test runs with various surfactant and urea concentrations assuming a linear equation system.

### 3.2. Algorithm employed

The empirical equations (Eqs. 2, 3 and 5) were used to calculate the data base (a set of constants) for subsequent predictions of optimum conditions for separations in MEKC. Optimum is defined here as the condition that allows a separation to be performed in the shortest time, while the resolution of the worst separated peak pair exceeds a threshold value.

In the first step, the hold-up time, the migration time of the micelles and the retention times of the solutes of interest are entered for three different buffer compositions (various  $c_{\text{SDS}}$  and  $c_{\text{urea}}$ ). The selected values of  $c_{\text{SDS}}$  and  $c_{\text{urea}}$  should form a triangle, covering the area of interest. The user of the computer program also



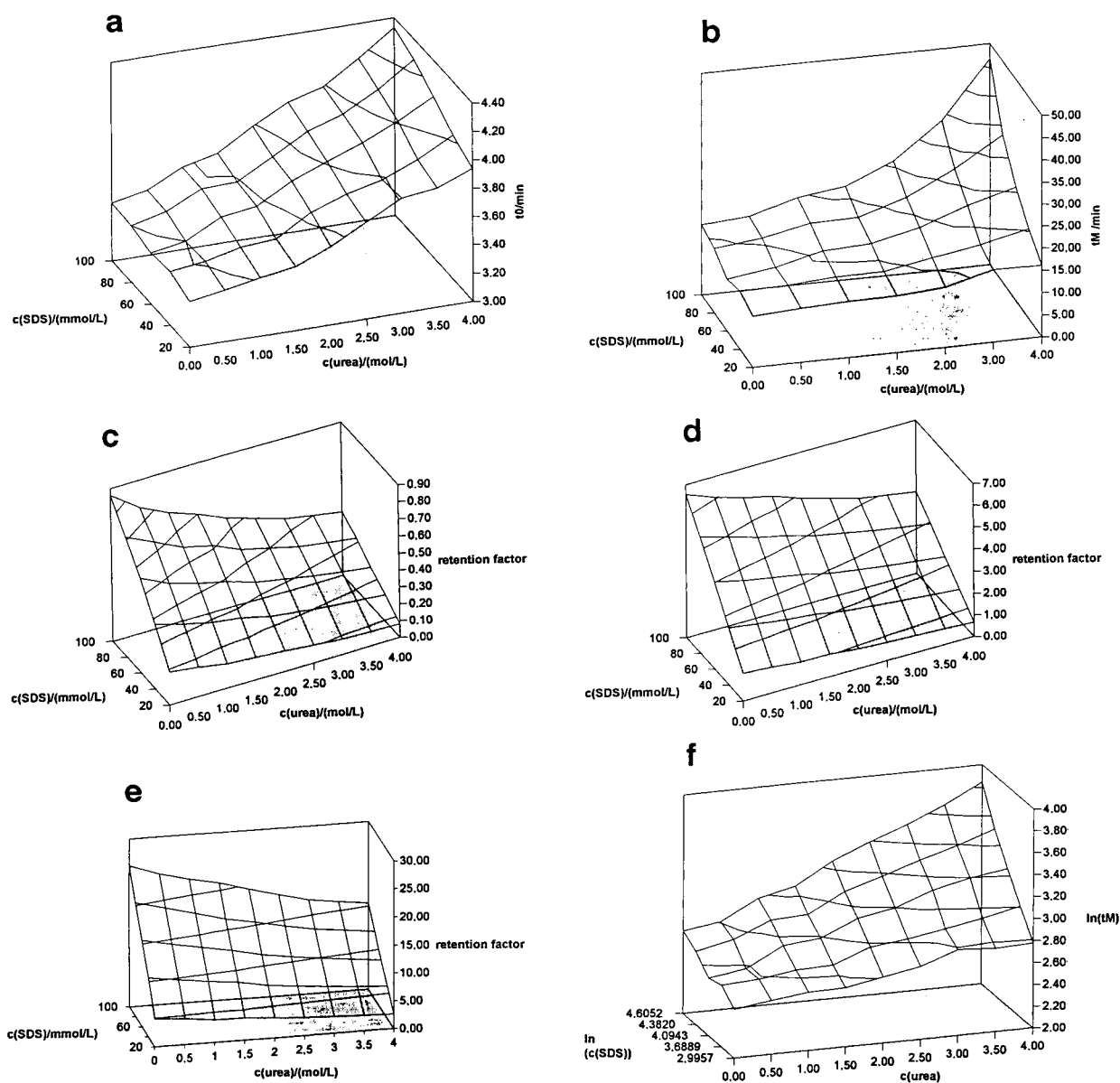


Fig. 1. Dependence of (a) the hold-up time (marker: formamide) on  $c_{\text{SDS}}$  and  $c_{\text{urea}}$ , (b) the migration time of the micelles (marker: quinine hydrochloride) on  $c_{\text{SDS}}$  and  $c_{\text{urea}}$ , (c–e) the retention factor of caffeine (c), *p*-nitrotoluene (d) and naphthalene (e) on  $c_{\text{SDS}}$  and  $c_{\text{urea}}$ , (f) the logarithm of the migration time of the micelles on  $\ln c_{\text{SDS}}$  and  $c_{\text{urea}}$ . Capillary, 565 (500) mm  $\times$  75  $\mu\text{m}$  I.D.; buffer,  $c(\text{Na}_2\text{B}_4\text{O}_7) = 30 \text{ mmol/l}$ ; voltage, 25 kV; temperature, 25  $^\circ\text{C}$ ; injection, pressure, 2.0 s; detection, photometric, 254 nm.

selects the minimum and the maximum values for  $c_{\text{SDS}}$  and  $c_{\text{urea}}$ , used for resolution optimization. Selected is also the minimum resolution that has to be reached for the worst resolved peak pair and the plate number that is approxi-

mated to be constant for all buffer compositions. The user can also fix the step width of the underlying algorithm ( $\Delta c_{\text{SDS}}$ ,  $\Delta c_{\text{urea}}$ ).

In a second step, the retention factors for three buffer compositions are calculated for all

solutes. Consecutively, the constants of Eqs. 2, 3 and 5 are calculated for  $t_0$ ,  $t_M$  and the retention factors of all solutes of interest. With these constants, the resolution for two adjacent peaks is accessible for any value of  $c_{\text{SDS}}$  and  $c_{\text{urea}}$  according to Eq. 1. The variable  $k$  is determined for each peak pair from the retention factors of solutes eluting in succession:

$$k = (k_1 + k_2)/2 \quad (6)$$

where  $k_1$  = retention factor of first solute and  $k_2$  = retention factor of second solute.

The selectivity factor is calculated for each peak pair and each buffer composition according to

$$\alpha = k_2/k_1 \quad (7)$$

For each buffer composition, the software generates a list of resolutions between adjacent peaks. If the elution order is dependent on the buffer composition, the resolutions for each possible peak pair have to be calculated.

In the third step, the resolutions obtained for various buffer compositions are compared with each other. The program suggests an optimum buffer composition, where the resolution of the worst separated peak pair exceeds a user-defined threshold value and the retention time of the last-eluted solute is minimum. The retention time of the last-eluting solute is approximately equivalent to the time of analysis. The program performs an adjustment of the buffer composition for a minimum time of analysis.

Optionally, the buffer composition can be calculated where the resolution of the worst separated peak pair is the highest in the selected range regardless of analysis time. If in the selected range the maximum resolution of the worst separated peak pair ( $R_{\text{max}}$ ) does not exceed the user-defined minimum, the buffer composition of  $R_{\text{max}}$  is suggested by the program as the optimum buffer composition.  $R_{\text{max}}$  corresponds to the best resolution of the worst-separated peak pair that can be obtained with SDS as surfactant and urea as modifier in the selected concentration range. If the predicted value is too low, the selectivity of the chromatographic system must be changed. This can be done by

selection of another surfactant, further additives or the derivatization of solutes prior to chromatographic separation.

In the final step, the program employed generates a list of retention times predicted for the optimized buffer composition and a simulated chromatogram.

Tentatively, a second algorithm was tested that is different from the one presented only concerning the equation that was used to describe the dependence of  $k$  on  $c_{\text{SDS}}$  and  $c_{\text{urea}}$ :

$$k = f(c_{\text{SDS}}, c_{\text{urea}}) = a^* + b^*c_{\text{SDS}} + d^*c_{\text{urea}} \quad (8)$$

where  $a^*$ ,  $b^*$  and  $d^*$  are constants. This equation describes in a simplified way the dependence of  $k$  on  $c_{\text{SDS}}$  and  $c_{\text{urea}}$ . The suggested buffer compositions calculated with algorithm 2, however, do not meet the requirements for a reliable optimization procedure. The results deviate strongly from those obtained with algorithm 1. The predicted buffer compositions did not allow an optimized separation concerning the test mixtures investigated. Therefore, all calculations were performed using Eq. (5) exclusively.

### 3.3. Urea and carbamate pesticides

The optimization software developed was applied to the separation of twelve urea and carbamate pesticides: carbofuran, phenmedipham, chlortoluron, diuron, fenuron, isoproturon, linuron, methabenzthiazuron, metobromuron, metoxuron, monolinuron and monuron. Urea and carbamate pesticides tend to decompose during gas chromatographic analysis. The main approach for their determination involves HPLC. Nine urea herbicides have already been successfully separated with MEKC and N-D-glucosyl-N-methylalkanamide surfactants as anionic borate complexes by Smith et al. [24].

Three test runs were performed with following separation buffers:  $c_{\text{SDS}} = 80$  mmol/l,  $c_{\text{urea}} = 3.0$  mol/l;  $c_{\text{SDS}} = 20$  mmol/l,  $c_{\text{urea}} = 3.0$  mol/l; and  $c_{\text{SDS}} = 20$  mmol/l,  $c_{\text{urea}} = 0.0$  mol/l. The concentrations of boric acid and disodium tetraborate were kept constant at 10 mmol/l.

As can be seen in Fig. 2a–c, co-elutions occur

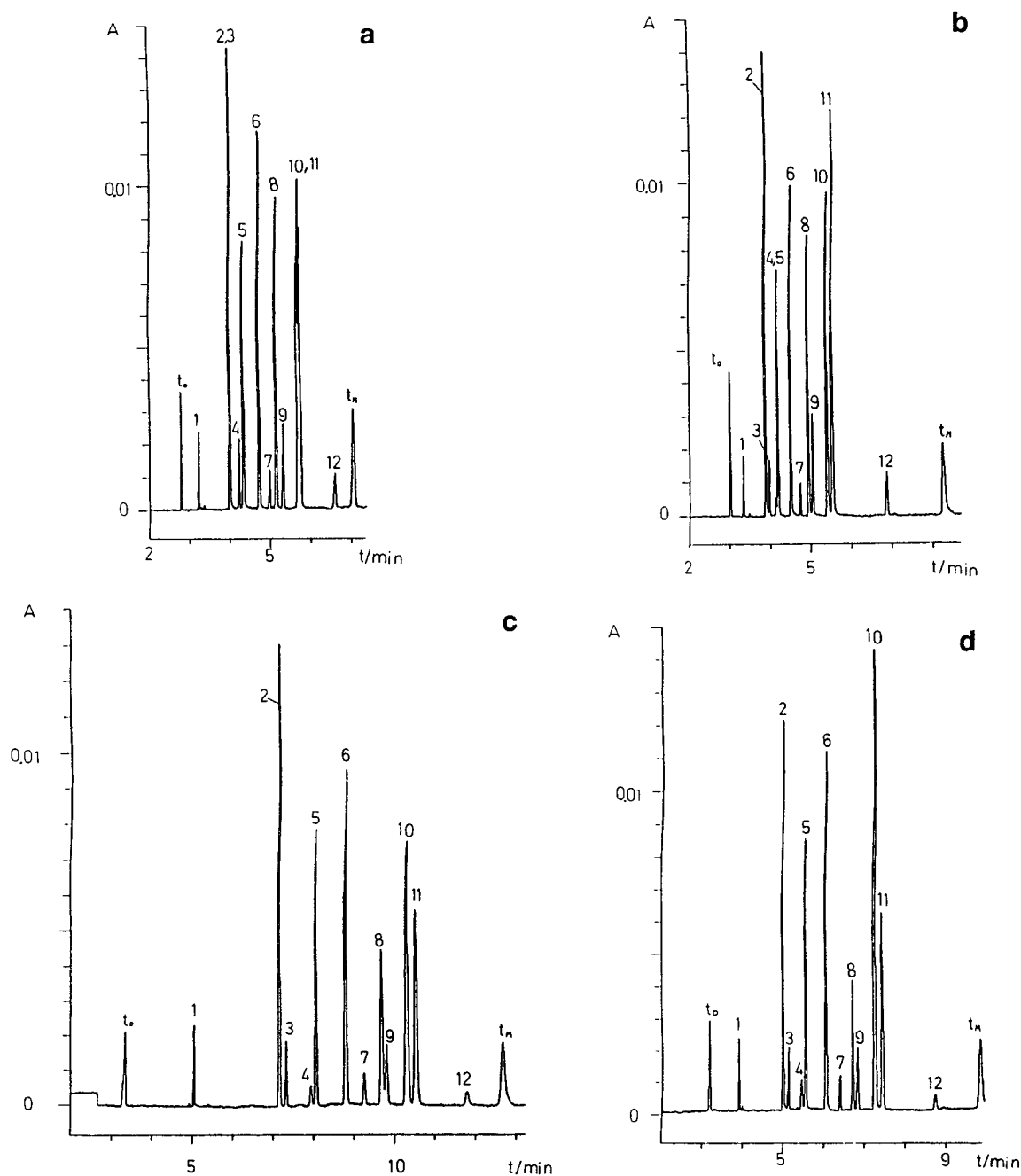


Fig. 2. Separation of twelve urea and carbamate pesticides by MEKC with various SDS and urea concentrations in the separation buffer. (a)  $c_{\text{SDS}} = 20 \text{ mmol/l}$ ,  $c_{\text{urea}} = 0.0 \text{ mol/l}$ ; (b)  $c_{\text{SDS}} = 20 \text{ mmol/l}$ ,  $c_{\text{urea}} = 3.0 \text{ mol/l}$ ; (c)  $c_{\text{SDS}} = 80 \text{ mmol/l}$ ,  $c_{\text{urea}} = 3.0 \text{ mol/l}$ ; (d)  $c_{\text{SDS}} = 35 \text{ mmol/l}$ ,  $c_{\text{urea}} = 3.25 \text{ mol/l}$ . Solutes: 1 = fenuron; 2 = monuron; 3 = metoxuron; 4 = monolinuron; 5 = carbofuran; 6 = metobromuron; 7 = chlortoluron; 8 = isoproturon; 9 = diuron; 10 = metabenzthiazuron; 11 = linuron; 12 = phenmedipham. Capillary, 565 (500) mm  $\times$  75  $\mu\text{m}$  I.D.; buffer,  $c(\text{Na}_2\text{B}_4\text{O}_7) = 10 \text{ mmol/l}$ ,  $c(\text{H}_3\text{BO}_3) = 10 \text{ mmol/l}$ ; voltage, 25 kV; temperature, 25°C; injection, pressure, 2.0 s; detection, photometric, 254 nm.

with all arbitrarily chosen buffer compositions. Opposite effects caused by an increase in the SDS concentration and by an increase in the urea concentration impede a rapid one-parameter optimization approach. It can be also seen that the elution window ( $t_0/t_M$ ) is strongly affected by the buffer composition while the hold-up time varies only marginally ( $t_0 = 2.78\text{--}3.35$  min).

The retention data for the three test runs were used for the prediction of the optimum buffer composition. The step width for  $\Delta c_{\text{SDS}}$  was fixed at 5 mmol/l and for  $\Delta c_{\text{urea}}$  at 250 mmol/l. The plate number was fixed at 100 000. The threshold value for the minimum resolution between each peak pair was fixed at 1.70, because the peak areas in the test solution are not equal. This threshold value was not exceeded. The maximum resolution obtainable for the worst separated peak pair is predicted to be 1.26 with a separation buffer containing 35 mmol/l SDS and 3.25 mol/l urea. In Fig. 2d, the chromatogram obtained with the optimized composition of the separation buffer is shown. In contrast to the test runs, nearly baseline resolution is achieved for all peaks.

In Table 1, the predicted retention times are compared with the retention times obtained with the suggested buffer composition. The comparison shows that the predicted retention times are overestimated with an approximately constant value of about 0.2 min. The differences between retention times of analytes eluting in succession are predicted with high accuracy. The optimization software developed generates a simulated chromatogram for the suggested buffer composition. The simulated chromatogram is depicted in Fig. 3. There is good agreement between the measured (Fig. 2d) and the simulated chromatograms.

The deviation of the predicted values from the experimentally determined retention times can be explained by the high standard deviation of the regression planes for  $t_0$  and  $t_M$  (Fig. 1a and b). During the use of a separation capillary, sorption and swelling processes alter the surface of the fused-silica capillary. These processes can be eliminated by rinsing procedures. The influence of various rinsing procedures on the

reproducibility in capillary electrophoresis has already been investigated extensively in the past [25,26]. In spite of these procedures, the surface of the capillary actually employed is altered irreversibly during its use and the capillary must be exchanged after a few months of use. The prediction of optimum conditions and of retention times in MEKC is therefore inherently hampered by the fact that the electroosmotic velocity cannot be kept completely constant. It is recommended to perform all test runs used for the prediction of optimum conditions on the same day.

### 3.4. Derivatized aliphatic amines

The determination of biogenic amines is of great interest in oenological studies owing to the potential toxicity of some of the aliphatic amines occurring in red and white wine [27]. At present, HPLC is the preferred method for the determination of biogenic amines in wine. We have studied the separation by MEKC of the amines methylamine, ethylamine, propylamine, isopropylamine, butylamine, 3-methylbutylamine, pentylamine, ethanolamine, morpholine, diethylamine, phenethylamine, tryptamine and 1,4-diaminobutane.

Prior to detection, a derivatization step is necessary to shift the absorption spectra of the analytes in order to permit photometric detection at longer wavelengths. Generally, *o*-phthalaldehyde (OPA) and dansyl chloride (Dns-Cl) are used as derivatizing agents [27]. Whereas OPA reacted only with primary amines, DNS-Cl turned out to form very non-polar derivatives that cannot be separated in MEKC with SDS- and urea-containing mobile phases owing to the high retention factors of these derivatives.

*P*-Nitrobenzoyl chloride forms stable amides with primary and secondary amines. The nitro group of the derivatizing agent provides sufficient polarity of the formed derivative, thus rendering possible subsequent separation by MEKC with SDS- and urea-containing mobile phases. Photometric detection can be performed at 254 nm.

Three test runs were performed with following

Table 1  
Predicted and measured retention times under optimized conditions

Component	Predicted retention time (min)	Measured retention time (min)	Predicted time difference between adjacent peaks (min)	Measured time difference between adjacent peaks (min)
Fenuron	3.76	3.91	1.01	1.08
Monuron	4.77	4.99	0.10	0.13
Metoxuron	4.87	5.12	0.35	0.33
Carbofuran	5.22	5.45	0.08	0.09
Monolinuron	5.30	5.54	0.49	0.50
Metobromuron	5.79	6.04	0.35	0.35
Chlortoluron	6.14	6.39	0.32	0.31
Isoproturon	6.46	6.70	0.11	0.12
Diuron	6.57	6.82	0.44	0.41
Methabenzthiazuron	7.01	7.23	0.21	0.19
Linuron	7.22	7.42	1.42	1.32
Phenmedipham	8.64	8.74	–	–
Ethanolamine	4.43	4.24	0.38	0.37
Methylamine	4.81	4.61	0.12	0.10
Morpholine	4.93	4.71	0.43	0.39
Ethylamine	5.36	5.10	0.53	0.46
Isopropylamine	5.89	5.56	0.24	0.20
By-product	6.13	5.76	0.36	0.32
Propylamine	6.49	6.08	1.24	1.04
Diethylamine	7.73	7.12	0.17	0.14
By-product	7.90	7.26	0.65	0.53
1-Butylamine	8.55	7.79	1.74	1.36
3-Methylbutylamine	10.29	9.15	0.44	0.35
Amylamine	10.73	9.50	0.25	0.19
Phenethylamine	10.98	9.69	0.66	0.54
By-product	11.64	10.23	0.47	0.45
Tryptamine	12.11	10.68	0.38	0.07
1,4-Diaminobutane	12.49	10.75	–	–
Trinitrotoluene	5.58	5.42	0.88	0.81
2,4-Dinitrotoluene	6.46	6.23	0.12	0.11
2,5-Dinitrotoluene	6.58	6.34	0.17	0.14
2,6-Dinitrotoluene	6.75	6.48	0.21	0.20
3,4-Dinitrotoluene	6.96	6.68	0.17	0.16
<i>o</i> -Nitrotoluene	7.13	6.84	0.10	0.11
2,3-Dinitrotoluene	7.23	6.95	0.11	0.09
<i>p</i> -Nitrotoluene	7.34	7.04	0.14	0.08
<i>m</i> -Nitrotoluene	7.48	7.12	–	–

separation buffers:  $c_{\text{SDS}} = 80 \text{ mmol/l}$ ,  $c_{\text{urea}} = 3.0 \text{ mol/l}$ ;  $c_{\text{SDS}} = 20 \text{ mmol/l}$ ,  $c_{\text{urea}} = 3.0 \text{ mol/l}$ ; and  $c_{\text{SDS}} = 20 \text{ mmol/l}$ ,  $c_{\text{urea}} = 0.0 \text{ mol/l}$ . The concentrations of boric acid and disodium tetraborate were kept constant at  $10 \text{ mmol/l}$ .

The chromatograms obtained are shown in Fig. 4a–c. With all arbitrarily chosen buffer

compositions, co-elutions occurred. *p*-Nitrobenzoic acid is one of the by-products of the derivatization procedure. The migration time of *p*-nitrobenzoic acid is virtually unaffected by the buffer composition, indicating that it does not interact with the micelles and it is retarded relative to the electroosmotic flow by its electro-

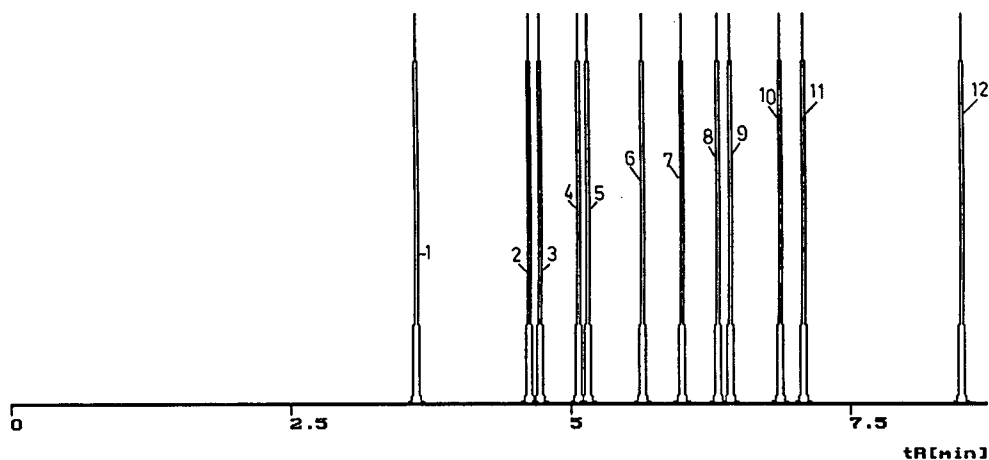


Fig. 3. Simulated chromatogram for the separation of twelve urea and carbamate pesticides under the conditions employed for the development of the chromatogram shown in Fig. 2d.

phoretic mobility. Because of its retention behavior, which differs completely from that of the solutes of interest, *p*-nitrobenzoic acid was excluded from the optimization process.

The retention data for the three test runs were used for the prediction of the optimum buffer composition. The step width for  $\Delta c_{\text{SDS}}$  was fixed at 5 mmol/l and for  $\Delta c_{\text{urea}}$  at 100 mmol/l. The plate number was fixed at 100 000. The maximum resolution obtainable for the worst separated peak pair is predicted to be 1.62 with a separation buffer containing 55 mmol/l SDS and 2.0 mol/l urea. In Fig. 4d the chromatogram obtained with the optimized composition of the separation buffer is shown. In contrast to the test runs, nearly baseline resolution is achieved for all peaks with the exception of *p*-nitrobenzoic acid, which was excluded from the optimization procedure. It co-elutes with one of the by-products of the derivatization reaction.

The two by-products can be easily separated from each other by variation of the urea concentration in the separation buffer. The resulting chromatogram is shown in Fig. 4e. It can be seen that, as predicted by the computer program, the resolution of other peak pairs is diminished on employing a separation buffer with lower urea concentration.

In Table 1, the predicted retention times for the separated amides are compared with the experimentally measured values. Whereas the predicted absolute migration times differ considerably from the measured migration times, there is good agreement for the time differences between adjacent peaks. The poor prediction of absolute migration times reflects the low day-to-day reproducibility of the electroosmotic velocity.

### 3.5. Nitrotoluenes

The determination of nitroaromatic compounds has become of increasing interest owing to the problem of explosives residues in soils near former ammunition plants. The concentrations of these residues are relatively high. The determination of nitroaromatic compounds in soil samples is possible by MEKC with photometric detection without preconcentration steps during sample preparation [4,28]. The large number of possible positional isomers makes their separation in reversed-phase HPLC difficult. The following congeners were successfully separated by MEKC following the procedure presented herein: 2,4,6-trinitrotoluene, 2,3-dinitrotoluene, 2,4-dinitrotoluene, 2,5-dinitrotol-

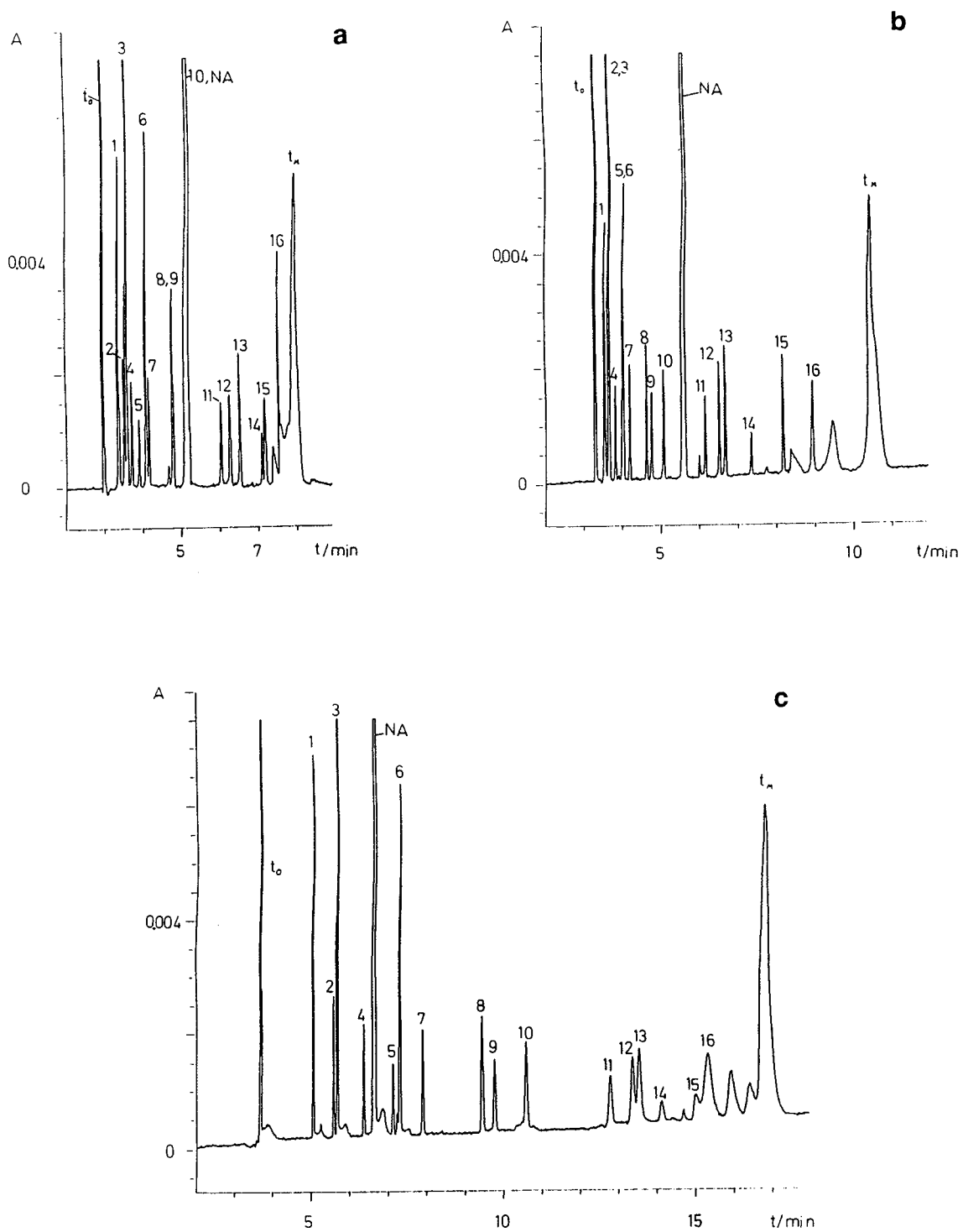


Fig. 4 (Continued on p. 92)

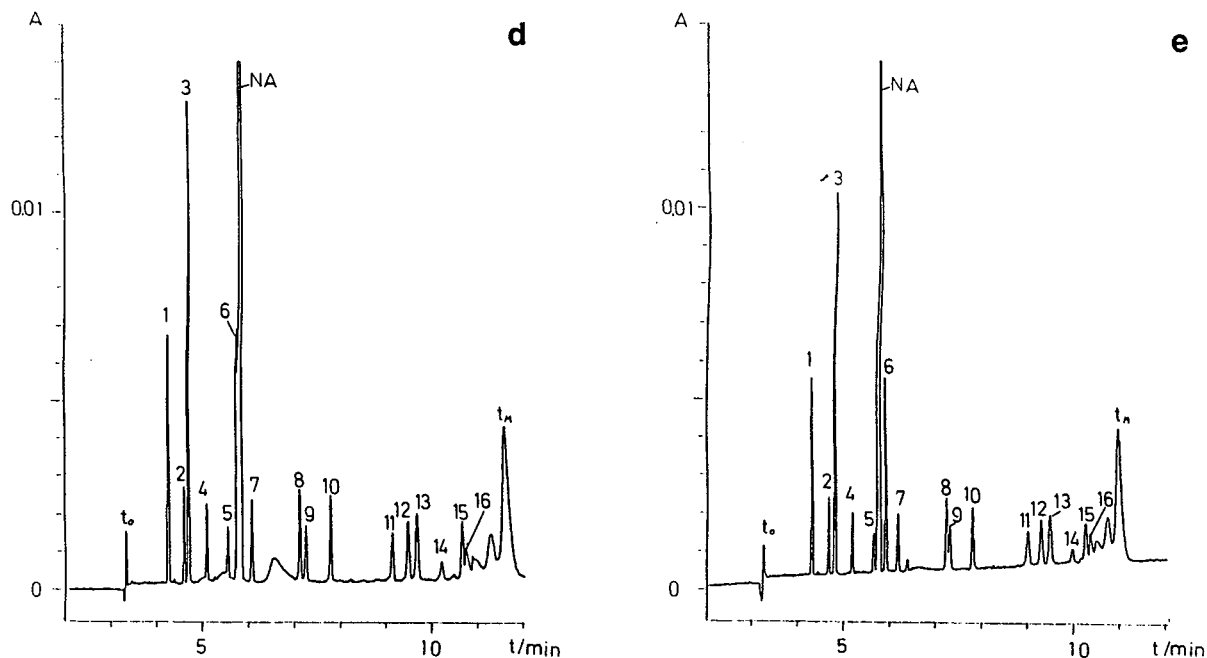


Fig. 4. Separation of thirteen aliphatic amines derivatized with *p*-nitrobenzoyl chloride by MEKC with various SDS and urea concentrations in the separation buffer. (a)  $c_{\text{SDS}} = 20$  mmol/l,  $c_{\text{urea}} = 0.0$  mol/l; (b)  $c_{\text{SDS}} = 20$  mmol/l,  $c_{\text{urea}} = 3.0$  mol/l; (c)  $c_{\text{SDS}} = 80$  mmol/l,  $c_{\text{urea}} = 3.0$  mol/l; (d)  $c_{\text{SDS}} = 55$  mmol/l,  $c_{\text{urea}} = 2.0$  mol/l; (e)  $c_{\text{SDS}} = 55$  mmol/l,  $c_{\text{urea}} = 1.25$  mol/l. Solutes: 1 = ethanolamine; 2 = methylamine; 3 = morpholine; 4 = ethylamine; 5 = isopropylamine, 6 = by-product; 7 = propylamine; 8 = diethylamine; 9 = by-product; 10 = 1-butylamine; 11 = 3-methylbutylamine; 12 = amylamine; 13 = phenethylamine; 14 = by-product; 15 = tryptamine; 16 = 1,4-diaminobutane. Capillary, 565 (500) mm  $\times$  75  $\mu$ m I.D.; buffer,  $c(\text{Na}_2\text{B}_4\text{O}_7) = 10$  mmol/l,  $c(\text{H}_3\text{BO}_3) = 10$  mmol/l; voltage, 25 kV; temperature, 25°C; injection, pressure, 1.5 s; detection, photometric, 254 nm.

uene, 2,6-dinitrotoluene, 3,4-dinitrotoluene, *o*-nitrotoluene, *m*-nitrotoluene and *p*-nitrotoluene.

Three test runs were performed with following separation buffers:  $c_{\text{SDS}} = 80$  mmol/l,  $c_{\text{urea}} = 3.0$  mol/l;  $c_{\text{SDS}} = 20$  mmol/l,  $c_{\text{urea}} = 3.0$  mol/l; and  $c_{\text{SDS}} = 20$  mmol/l,  $c_{\text{urea}} = 0.0$  mol/l. The concentrations of boric acid and disodium tetraborate were kept constant at 10 mmol/l.

The chromatograms obtained are shown in Fig. 5a–c. Co-elutions occur with all arbitrarily chosen buffer compositions. In one case the elution order is reversed by the addition of urea to the separation buffer, although an electrophoretic velocity of the solutes can be excluded. Possibly, the addition of urea to the separation buffer affects the retention mechanism of the polar nitroaromatic compounds by the micelles. Studies of the temperature dependence of the distribution coefficient between the micellar phase and the aqueous phase show that the

interaction of polar solutes with the micelles is substantially different from the interaction of non-polar solutes with the micellar phase [29]. In the case of polar solutes, the entropy change for the phase transfer of a solute from the aqueous phase into the micellar phase is negative, thus counteracting the transfer into the micellar phase. Terabe et al. [29] attributed the negative entropy change to the restricted motion of polar solutes on the surface of the micelles. This balance of forces might be influenced by urea in the counterlayer of the anionic micelles.

The retention data of the three test runs were used for a prediction of the optimum buffer composition. The step-width for  $\Delta c_{\text{SDS}}$  was fixed at 5 mmol/l and for  $\Delta c_{\text{urea}}$  at 100 mmol/l. The plate number was fixed at 100 000. The maximum resolution obtainable for the worst separated peak pair is predicted to be 1.41 with a separation buffer containing 55 mmol/l SDS and



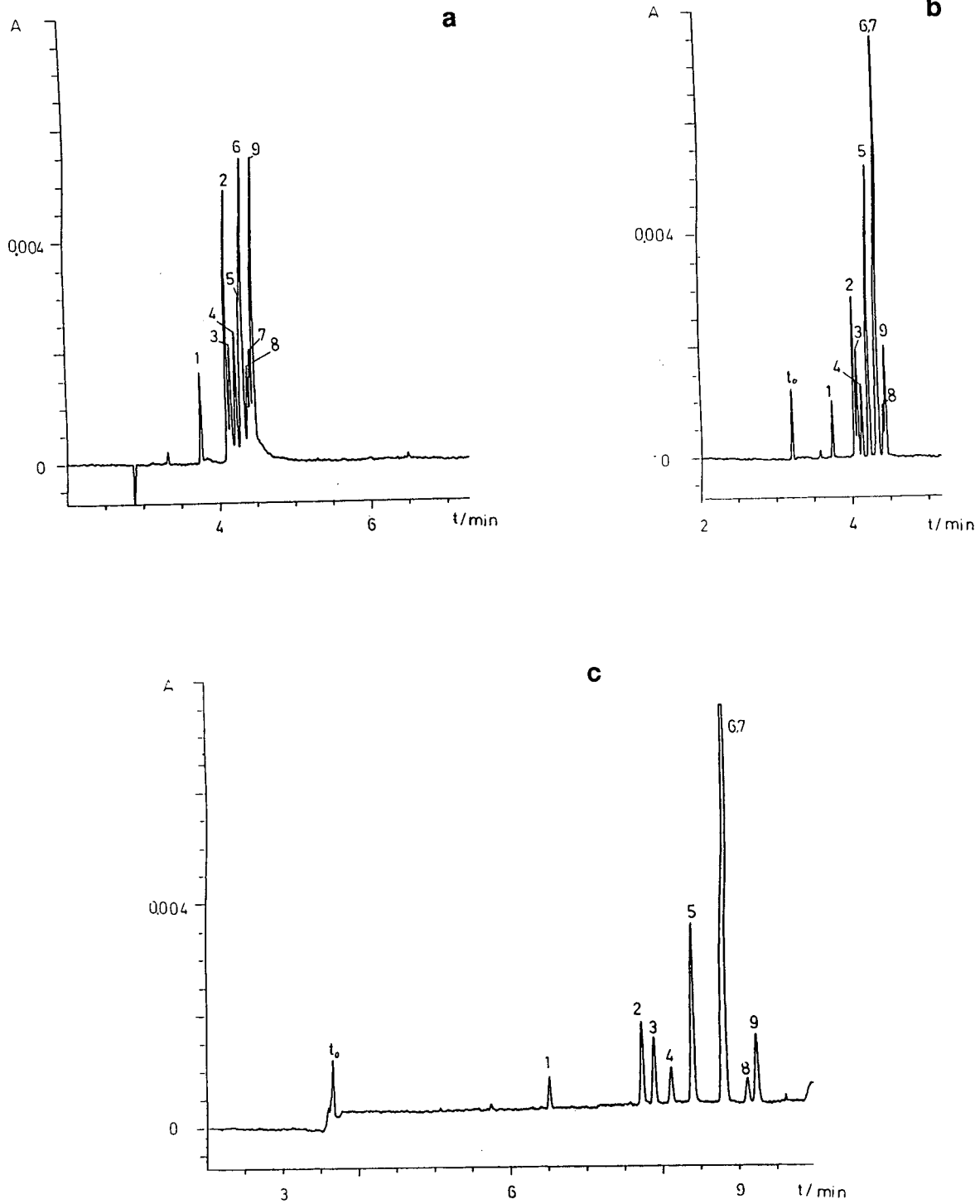


Fig. 5 (Continued on p. 94)

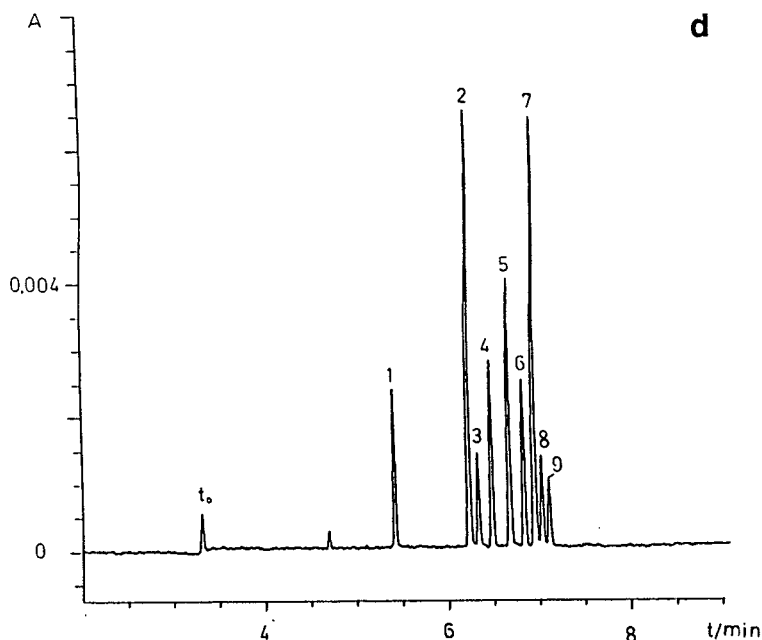


Fig. 5. Separation of nitrotoluenes by MEKC with various SDS and urea concentrations in the separation buffer. (a)  $c_{\text{SDS}} = 20$  mmol/l,  $c_{\text{urea}} = 0.0$  mol/l; (b)  $c_{\text{SDS}} = 20$  mmol/l,  $c_{\text{urea}} = 3.0$  mol/l; (c)  $c_{\text{SDS}} = 80$  mmol/l,  $c_{\text{urea}} = 3.0$  mol/l; (d)  $c_{\text{SDS}} = 55$  mmol/l,  $c_{\text{urea}} = 1.8$  mol/l. Solutes: 1 = 2,4,6-trinitrotoluene; 2 = 2,4-dinitrotoluene; 3 = 2,5-dinitrotoluene; 4 = 2,6-dinitrotoluene; 5 = 3,4-dinitrotoluene; 6 = *o*-nitrotoluene; 7 = 2,3-dinitrotoluene; 8 = *p*-nitrotoluene; 9 = *m*-nitrotoluene. Capillary, 565 (500) mm  $\times$  75  $\mu$ m I.D.; buffer,  $c(\text{Na}_2\text{B}_4\text{O}_7) = 10$  mmol/l,  $c(\text{H}_3\text{BO}_3) = 10$  mmol/l; voltage, 25 kV; temperature, 25°C; injection, pressure, 1.0 s; detection, photometric, 254 nm.

1.80 mol/l urea. In Fig. 5d, the chromatogram obtained with the optimized composition of the separation buffer is shown. In contrast to the test runs, nearly baseline resolution is achieved for all peaks. In Table 1 the predicted retention times for the optimized buffer composition are compared with the retention times obtained experimentally with this buffer composition. The comparison shows that the differences between retention times of analytes eluting in succession are predicted with high accuracy, although the predicted retention times are slightly overestimated.

The optimization of the separation of nitrotoluenes shows that the approach used herein for the optimization of the buffer composition can cope with a high dependence of the selectivity coefficients on the buffer composition and reversals of the elution order.

#### 4. Conclusions

It was shown that the composition of the separation buffer (with regard to the SDS and urea concentrations) can be rapidly optimized for a complex mixture of solutes by the developed computer-aided procedure. It is possible to predict the migration times of neutral solutes in MEKC on the basis of only three initial experiments. It was demonstrated that urea is an ideal modifier, because it extends the elution range without reducing substantially the electroosmotic velocity.

This study involved only two factors (SDS and urea concentrations). The concept, however, is entirely general and can be extended to other capillary electrophoretic systems such as MEKC with cationic micelles or cyclodextrin-modified capillary electrophoresis.

## Acknowledgement

The authors gratefully acknowledge financial support from the Deutsche Forschungsgemeinschaft.

## References

- [1] S. Terabe, K. Otsuka, K. Ichikawa, A. Tsuchiya and T. Ando, *Anal. Chem.*, 56 (1984) 111.
- [2] S. Terabe, K. Otsuka and T. Ando, *Anal. Chem.*, 57 (1985) 834.
- [3] D.M. Northrop, D.E. Matire and W.A. Crehan, *Anal. Chem.*, 63 (1991) 1038.
- [4] W. Kleiböhmer, K. Camman, J. Robert and E. Mussenbrock, *J. Chromatogr.*, 638 (1993) 349.
- [5] S. Fujiwara and S. Honda, *Anal. Chem.*, 59 (1987) 2773.
- [6] I.K. Sakodinskaya, C. Desidero, A. Nardi and S. Fanali, *J. Chromatogr.*, 596 (1992) 95.
- [7] W. Thormann, A. Minger, S. Molteni, J. Caslavská and P. Gebauer, *J. Chromatogr.*, 593 (1992) 275.
- [8] M. Amin, K. Harrington and R. von Wandruszka, *Anal. Chem.*, 65 (1993) 2346.
- [9] J. Vindevogel and P. Sandra, *Anal. Chem.*, 63 (1991) 1530.
- [10] Y.F. Yik and S.F.Y. Li, *Chromatographia*, 35 (1993) 560.
- [11] S.C. Smith and M.G. Khaledi, *J. Chromatogr.*, 632 (1993) 177.
- [12] C. Quang, J.K. Strasters and M.G. Khaledi, *Anal. Chem.* 66 (1994) 1646.
- [13] U. Pyell and U. Bütehorn, *Chromatographia*, 40 (1995) 175.
- [14] J.P. Foley, *Anal. Chem.*, 62 (1990) 1302.
- [15] J. Vindevogel and P. Sandra, *Introduction to Micellar Electrokinetic Chromatography*, Hüthig, Heidelberg, 1992, p. 144.
- [16] E.L. Little and J.P. Foley, *J. Microcol. Sep.*, 4 (1992) 145.
- [17] S. Terabe, Y. Ishihama, H. Nishi, T. Fukuyama and K. Otsuka, *J. Chromatogr.*, 545 (1991) 359.
- [18] J. Gorse, A.T. Balchunas, D.F. Swaile and M.J. Sepaniak, *J. High Resolut. Chromatogr.*, 11 (1988) 554.
- [19] T. Kaneta, S. Tanaka, M. Toya and H. Yoshida, *J. Chromatogr.*, 609 (1992) 369.
- [20] A.T. Balchunas and M.J. Sepaniak, *Anal. Chem.*, 60 (1988) 617.
- [21] C. Schwer and E. Kenndler, *Anal. Chem.*, 63 (1991) 1801.
- [22] E.A.G. Aniansson, S.N. Wall, M. Almgren, H. Hoffmann, I. Kielmann, W. Ulbricht, R. Zana, J. Lang and C. Tondre, *J. Phys. Chem.*, 80 (1976) 905.
- [23] U. Pyell and U. Bütehorn, *Chromatographia*, 40 (1995) 69.
- [24] J.T. Smith, W. Nashabeh and Z. El Rassi, *Anal. Chem.*, 66 (1994) 1119.
- [25] J. Kohr and H. Engelhardt, *J. Microcol. Sep.*, 3 (1991) 491.
- [26] S.C. Smith, J.K. Strasters and M.G. Khaledi, *J. Chromatogr.*, 559 (1991) 57.
- [27] O. Busto, Y. Valero, J. Guash and F. Borull, *Chromatographia*, 38 (1994) 571.
- [28] K. Camman, W. Kleiböhmer and E. Mussenbrock, *GIT Fachz. Lab.*, 38 (1994) 162.
- [29] S. Terabe, T. Katsura, Y. Okada, Y. Ishihama and K. Otsuka, *J. Microcol. Sep.*, 5 (1993) 23.





ELSEVIER

Journal of Chromatography A, 716 (1995) 97–105

JOURNAL OF  
CHROMATOGRAPHY A

# Control of the electroosmotic flow by metal-salt-containing buffers

R. Brechtel, W. Hohmann, H. Rüdiger, H. Wätzig\*

*Institute of Pharmacy and Food Chemistry, University of Würzburg, Am Hubland, D-97074 Würzburg, Germany*

## Abstract

New possibilities to suppress electroosmotic flow (EOF) were investigated. Buffers prepared from salts of zinc (up to 50 mmol/l), aluminium (up to 0.5 mmol/l) and barium (up to 250 mmol/l) lead to an effective reduction of EOF in Tris buffer, pH 7.4, 50 mmol/l. The dependence of EOF on different metal-salt concentrations is documented. The usefulness of barium-salt-containing buffers is demonstrated for pH values between 5 and 9.2. If the suppression is too strong, the EOF can be adjusted by mixtures of sodium and barium salts.

## 1. Introduction

The walls of fused-silica capillaries are negatively charged above pH 2.5, because the silanol groups are partly deprotonated. However, the net charge of a capillary is zero as there is an excess of cations in the buffer solution to compensate for the fixed negative charge at the wall. These cations are partly mobile. Normally, they are concentrated close to the capillary wall. If a voltage is applied, they migrate towards the cathode, along with the buffer solution due to hydrate binding and friction. The result is a flow of the bulk solution towards the cathode. This is called electroosmotic flow (EOF).

The electrokinetic behaviour of a charged surface depends on its  $\zeta$  (zeta) potential. The corresponding theoretical principles have been understood for a long time [1]. Two effects compensate for each other: electrostatic attraction and diffusion. The solution of the corre-

sponding differential equations leads to a Boltzmann distribution. The excess of cations decreases exponentially with distance from the capillary wall.

However, the details of this theory are still under discussion (reviewed in Ref. [2]). The contributions of specific adsorption, the consequences of competition of different ions for binding sites, and effects like secondary adsorption are not yet fully understood. Therefore, it is not simple to control the EOF via the zeta potential.

The EOF affects the resolution in capillary electrophoresis (CE). Usually a low EOF is desirable. There are many possibilities to achieve this: high buffer concentration, additional modifiers, low buffer pH and coated capillaries (reviewed in Refs. [3,4]). However, these methods often influence the selectivity as well. Especially when working with buffers of high pH, it is not easy to suppress the EOF effectively.

There are CE methods that use zinc [5–12] and barium salts [13] to improve the resolution.

\* Corresponding author.

In these cases the selectivity was not influenced, but the EOF decreased. This effect is studied systematically in this paper. According to earlier studies, salts of different metals should influence the zeta potential similarly [14]. Thus, the study of a few different salts should be sufficient to investigate the entire phenomenon.

## 2. Experimental

### 2.1. Effect of salt concentrations on EOF

The dependence of the EOF on different salt concentrations was investigated with a laboratory-built instrument [3], similar to the one described in Ref. [15]. The power supply HCN 35-35000 (FUG, Rosenheim, Germany) and UV detector Spectra 100 (ThermoSeparations, Darmstadt, Germany) were used. The detection wavelength was 214 nm. A recorder Linear 2030 000 (Gamma Analysen Technik, Bremerhaven, Germany) was employed at a chart speed of 1 cm/min.

Fused-silica capillaries from the same batch (Polymicro), 50  $\mu\text{m}$  internal diameter, 25 cm effective and 40 cm total length, were used. Fresh capillaries were pretreated by rinsing with 0.1 M NaOH for 5 min, applying 10 kV for 15 min, rinsing with buffer, and equilibrating for 30 min under the subsequent running conditions. Between experiments the capillary was rinsed with buffer for 5 min. If the species or the concentration of the additive was changed, the capillary was first rinsed with 0.1 M NaOH, followed by the new buffer, 5 min each. Then 15 kV was applied for 30 min ( $\text{Al}^{3+}$ : 60 min) to equilibrate the capillary.

If not stated otherwise, chemicals were of analytical grade, supplied by Merck (Darmstadt, Germany). All measurements were performed in Tris [tris(hydroxymethyl)aminomethane] buffer, pH 7.4, 50 mmol/l. This was prepared by dissolving 606 mg Tris (laboratory reagent grade; Boehringer-Mannheim, Germany) in 42.0 ml of 0.1 mmol/l HCl (volumetric solution), adding an appropriate amount of metal-salt stock solution and filling up to 100.0 ml with HPLC-grade

water (Millipore, Eschborn, Germany). Barium-containing buffers were prepared by dissolving the appropriate amount of  $\text{BaCl}_2 \cdot 2\text{H}_2\text{O}$  directly in Tris buffer. As stock solutions 2726 mg/200 ml (100 mmol/l)  $\text{ZnCl}_2$  and 120.7 mg/500 ml (1 mmol/l)  $\text{AlCl}_3 \cdot 6\text{H}_2\text{O}$  (laboratory reagent grade; Baker, Deventer, Netherlands) were used. All solutions were prepared fresh every day.

If possible, a separation voltage of 15 kV was used. The current was ca. 30  $\mu\text{A}$  at rather low concentrations of metal-salt buffer additives. If the additive concentration exceeded 10 mmol/l, a voltage lower than 15 kV was used. For most experiments the cathode was at the capillary outlet; for  $c_{\text{Zn}^{2+}} \geq 25$  mmol/l and  $c_{\text{Al}^{3+}} \geq 0.5$  mmol/l the anode was at the outlet. Normally, the EOF mobility was estimated by using acetanilide (330 mg/l, dissolved in Tris buffer) as neutral marker. If the EOF was very low ( $c_{\text{Zn}^{2+}} = 2\text{--}10$  mmol/l,  $c_{\text{Ba}^{2+}} \geq 100$  mmol/l), neostigmine bromide (516 mg/l, dissolved in Tris buffer, pharmacopoeia quality; Hoffmann-La Roche, Basle, Switzerland) was used as the cationic marker. Here the EOF was estimated indirectly from the known electrophoretic mobility of neostigmine.

The samples were injected electrokinetically (5 kV, 15 s). Mobility measurements were typically performed in triplicate.

### 2.2. Effect of addition of barium to buffers of various pH on EOF

The EOF obtained by addition of barium to buffers of various pH was investigated on a P/ACE 2100 (Beckman Instruments). Unless stated otherwise, the experimental conditions were as described above for barium salts. The thermostat was set to 30°C. Separation voltage was 20 kV. Capillary length was 30 cm effective, 37 cm total. A pressure difference of 34 hPa was applied for 4 s to inject the samples. Prior to each run, the capillary was rinsed for 2 min with separation buffer. Before the buffer system was changed, the capillary was rinsed for 30 min with 0.1 M NaOH, followed by a rinse of 5 min with

separation buffer and equilibration at 20 kV for another 30 min.

### 2.3. Preparation of borate buffers

The borate buffers, pH 9.2, 60 mmol/l (32.07 mmol/l  $\text{Me}^+$ ) were prepared by dissolving 371 mg of boric acid,  $\text{Ba}(\text{OH})_2 \cdot 8\text{H}_2\text{O}$  and 0.1 M NaOH with HPLC-grade water to 100.0 ml solution. The buffer with %Ba = 0 contained 0 mg of  $\text{Ba}(\text{OH})_2 \cdot 8\text{H}_2\text{O}$  (= Ba) and 32.07 ml 0.1 M NaOH (= Na); the others were prepared analogously: %Ba = 6.25: 31.5 mg Ba, 30.07 ml Na; %Ba = 12.5: 63 mg Ba, 28.06 ml Na; %Ba = 25: 126.5 mg Ba, 24.05 ml Na; %Ba = 50: 253 mg Ba, 16.03 ml Na; %Ba = 62.5: 316 mg Ba, 12.03 ml Na; %Ba = 100: 506 mg Ba; 0 ml Na.

The barium-free buffer was prepared by dissolving 233 mg of boric acid and 213 mg of sodium tetraborate decahydrate with HPLC-grade water to 100.0 ml solution. The barium-containing borate buffers, pH 8.5, 60 mmol/l (10.48 mmol  $\text{Me}^+$ ), were prepared by dissolving 371 mg of boric acid,  $\text{Ba}(\text{OH})_2 \cdot 8\text{H}_2\text{O}$  (= Ba) and 0.1 M NaOH (= Na) with HPLC-grade water to 100.0 ml solution. %Ba = 6.25: 11 mg Ba, 10.48 ml Na; %Ba = 12.5: 22 mg Ba, 9.78 ml Na; %Ba = 25: 44 mg Ba, 8.39 ml Na; %Ba = 50: 88 mg Ba, 5.59 ml Na; %Ba = 62.5: 110 mg Ba, 4.19 ml Na; %Ba = 100: 176 mg Ba.

The same recipes as for the 60 mmol/l buffers were used, but all weights and  $V_{\text{NaOH}}$  were multiplied by 2.862 ( $60 \times 2.862 = 171.7$ ).

### 2.4. Preparation of imidazole buffers

The buffers were prepared by dissolving 272 mg of imidazole, 20.0 ml of 0.1 M HCl,  $\text{BaCl}_2 \cdot 2\text{H}_2\text{O}$  and NaCl with HPLC-grade water to 100.0 ml solution.

The buffer with %Ba = 0 contained 0 mg of  $\text{BaCl}_2 \cdot 2\text{H}_2\text{O}$  (= Ba) and 187.5 mg of NaCl (= Na), corresponding to 32.07 mmol  $\text{Me}^+$ ; the others were analogously prepared: %Ba = 6.25: 24.5 mg Ba, 176 mg Na; %Ba = 12.5: 49 mg Ba, 164 mg Na; %Ba = 25: 98 mg Ba, 140 mg Na; %Ba = 50: 196 mg Ba, 94 mg Na; %Ba = 62.5: 249 mg Ba, 70 mg Na; %Ba = 100: 392 mg Ba.

### 2.5. Preparation of acetate buffers

The buffers were prepared by dissolving 1.60 ml of 1 M acetic acid (volumetric solution), sodium acetate trihydrate (= Na) and barium acetate (= Ba) with HPLC-grade water to 100.0 ml solution.

The buffer with %Ba = 0 contained 0 mg of Ba and 436 mg of Na, corresponding to 32 mmol/l  $\text{Me}^+$ ; the others were analogously prepared: %Ba = 6.25: 25.5 mg Ba, 409 mg Na; %Ba = 12.5: 51 mg Ba, 382 mg Na; %Ba = 25: 102 mg Ba, 327 mg Na; %Ba = 50: 205 mg Ba, 218 mg Na; %Ba = 62.5: 256 mg Ba, 163 mg Na; %Ba = 100: 410 mg Ba.

## 3. Results and discussion

### 3.1. Estimation of the mobility

The mobility,  $\mu$ , is defined as the ratio of velocity  $v$  and electrical field strength  $E$  (Eq. 1). The velocity is calculated by measuring the time  $t_M$  needed by the sample to pass the column length  $l$  to the detection window (Eq. 2);  $E$  is defined as the ratio of voltage  $U$  and overall column length  $L$  (Eq. 3).

If the EOF is high, its velocity  $v_{\text{EOF}}$  can simply be determined by Eq. 2, using the migration time of a neutral marker. However, if the EOF is low, it takes a very long time to measure it. In this case the EOF can be estimated indirectly. In preceding experiments the electrophoretic velocity  $v_e$  of a positively charged marker compound is determined from its total velocity  $v$  and the velocity of a neutral marker  $v_{\text{EOF}}$  (Eq. 4). Now  $v_{\text{EOF}}$  can be calculated from the total velocity of the cationic marker (Eq. 5), if this can be considered independent of the buffer composition.

$$\mu = \frac{v}{E} \quad (1)$$

$$v = \frac{l}{t_M} \quad (2)$$

$$E = \frac{U}{L} \quad (3)$$

$$v_e = v - v_{\text{EOF}} \quad (4)$$

$$v_{\text{EOF}} = v - v_e \quad (5)$$

However, in principle the electrophoretic mobility is dependent on ionic strength. Thus, the changes of  $v_e$  with buffer composition had to be investigated. The mean of  $v_e$  was  $(2.77 \pm 0.09) \cdot 10^{-8} \text{ V}^{-1} \text{ s}^{-1} \text{ m}^2$  for barium-salt concentrations between 0 and 10 mmol/l ( $n = 12$ ). The average of three measurements at 0 and 10 mmol/l barium was  $2.67 \cdot 10^{-8}$  and  $2.85 \cdot 10^{-8} \text{ V}^{-1} \text{ s}^{-1} \text{ m}^2$ , respectively. The mean of  $v_e$  was  $(2.56 \pm 0.16) \cdot 10^{-8} \text{ V}^{-1} \text{ s}^{-1} \text{ m}^2$  for zinc-salt concentrations between 0 and 1 mmol/l ( $n = 9$ ). The average of three measurements at 0 and 1 mmol/l zinc was  $2.63 \cdot 10^{-8}$  and  $2.60 \cdot 10^{-8} \text{ V}^{-1} \text{ s}^{-1} \text{ m}^2$ , respectively. No significant dependence was observed between electrophoretic mobility and ionic strength under these conditions.

### 3.2. Relationship between the concentration of different metal salts and EOF mobility

The dependence of the electrophoretic mobility on the salt concentration is demonstrated in Figs. 1–3. These results can be understood easily

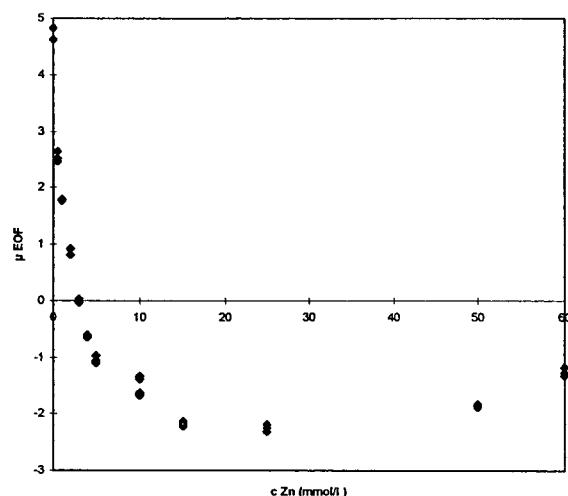


Fig. 1. Dependence of the EOF ( $\mu$  in  $10^{-8} \text{ V}^{-1} \text{ s}^{-1} \text{ m}^2$ ) on the zinc-salt concentration, measured in Tris buffer, pH 7.4, 50 mmol/l. Mobility measurements were performed in triplicate.

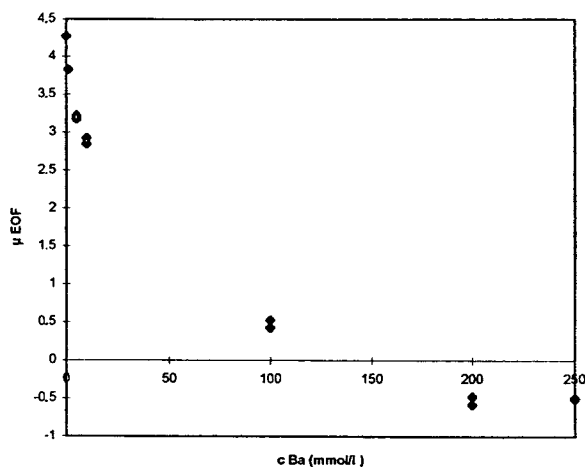


Fig. 2. Dependence of the EOF ( $\mu$  in  $10^{-8} \text{ V}^{-1} \text{ s}^{-1} \text{ m}^2$ ) on the barium-salt concentration, measured in Tris buffer, pH 7.4, 50 mmol/l. Mobility measurements were typically performed in triplicate (except  $c = 250$  mmol/l, which was measured twice).

(compare Fig. 4). The EOF towards the cathode is caused by the negatively charged silica glass surface (i). If cations are adsorbed to this surface, its charge and thus the EOF decrease (ii). At high cation concentrations the surface charge can even be inverted. The resulting excess of solvated anions leads to an EOF towards the

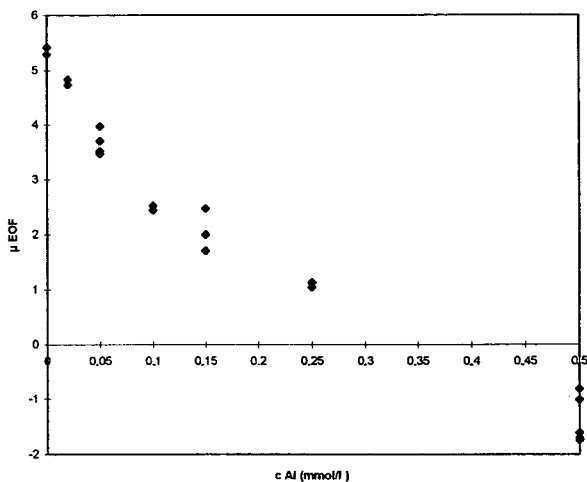


Fig. 3. Dependence of the EOF ( $\mu$  in  $10^{-8} \text{ V}^{-1} \text{ s}^{-1} \text{ m}^2$ ) on the aluminium-salt concentration, measured in Tris buffer, pH 7.4, 50 mmol/l. Mobility measurements were performed at least in triplicate.



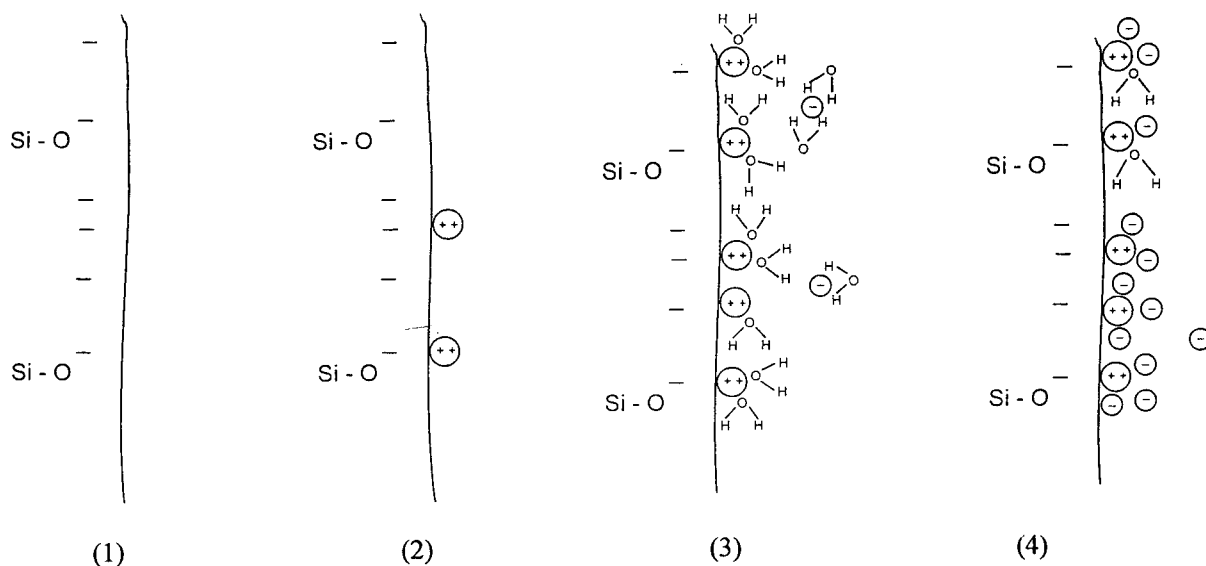


Fig. 4. Interpretation of results shown in Figs. 1–3. For details see text.

anode (iii). If the salt concentration is increased further, no additional adsorption of cations takes place, because all the binding sites are already saturated. The EOF towards the anode is not increased further. On the contrary, at high concentrations the anions displace the solvating water molecules on the surface of the cations [2,16]. A salt layer begins to form on the capillary surface. The surface charge and the EOF decrease again (iv).

The shape of the curves obtained with different metal salts depends on their affinity to the silica surface and the solubility of the cations.

### 3.3. Comparison with earlier investigations

Many investigations have analysed the dependence of the zeta potential on the concentration of various metal salts. The results obtained here are in agreement with earlier measurements, concerning the influence of aluminium and barium concentrations on the zeta potential of different glass surfaces ([17,18]; Table 1). Thus, the behaviour of other metal salts in CE can be predicted from older studies as well. Data about lithium ([14], p. 405), sodium [14,17], potassium, silver, magnesium, calcium, strontium, copper,

lead, mercurium, uranium, lanthanum, cerium and thorium salts are available ([14,17–19]; Table 1). However, significant effects of alkaline ions were only observed at high concentrations, and only the influence of potassium ions was investigated at these relevant concentrations.

The precision can be estimated by comparing data from different authors about the same ion. There are significant deviations, probably caused by different pH values, impurities of the reagents, different instrumentation to measure streaming potentials, heterogeneous glass materials, different capillary histories and equilibration statuses. Nevertheless, the concentration range in which different metal ions may be useful to control the EOF can be estimated.

The expected EOF mobility,  $\mu_{\text{EOF}}$ , can be simply calculated from the  $\zeta$  potential by:

$$\mu_{\text{EOF}} = -\frac{\epsilon\zeta}{\eta} \quad (6)$$

Assuming a permittivity  $\epsilon$  of  $7.08 \cdot 10^{-10} \text{ A s V}^{-1} \text{ m}^{-1}$  and a viscosity  $\eta$  of  $1 \cdot 10^{-3} \text{ N m}^{-2} \text{ s}$  for the electrolyte,  $7.08 \cdot 10^{-8} \text{ V}^{-1} \text{ s}^{-1} \text{ m}^2$  corresponds to a  $\zeta$  potential of 100 mV [20]. The data of Figs. 1–3 were incorporated into Table 1 using this relationship.

Table 1

The influence of different metal ions on the  $\zeta$  potential depending on the ion concentration  $c$ . Data of earlier publications are compared with the data shown in Figs. 1–3

Ion	Investigated $c$ range (mmol/l)	$\zeta$ potential range (mV) observed	$c$ (mmol/l) where $\zeta$ becomes 0 mV	$c$ (mmol/l) causing half of the maximal effect	$c$ (mmol/l) causing the maximal effect	Ref.
K <sup>+</sup>	0.01–1	–140–110		0.16	1	[14], p. 405 <sup>a</sup>
K <sup>+</sup>	0.05–10	–5.3––1.8 <sup>b</sup>		0.95	10	[14], p. 538 <sup>b</sup>
K <sup>+</sup>	0–1	–350––4			1	[18] <sup>a</sup>
K <sup>+</sup>	0–100	<sup>c</sup>	100	0.27	100	[17] <sup>c,d</sup>
K <sup>+</sup>	0–0.39	<sup>c</sup>		0.14	0.39	[17] <sup>c,e</sup>
Ag <sup>+</sup>	0–40	<sup>c</sup>	40	0.047	40	[17] <sup>c,d</sup>
Mg <sup>2+</sup>	0–18	–53––31		9	18	[14], p. 405 <sup>a</sup>
Ca <sup>2+</sup>	0–18	–53––25		7	18	[14], p. 405 <sup>a</sup>
Str <sup>2+</sup>	0–18	–53––22		7	18	[14], p. 405 <sup>a</sup>
Ba <sup>2+</sup>	0–18	–53––20		6	18	[14], p. 405 <sup>a,f</sup>
Ba <sup>2+</sup>	10 <sup>–3</sup> –10	–115–0	10	0.33	10	[14], p. 405 <sup>a,f</sup>
Ba <sup>2+</sup>	0.02–10	–4.7––1.0 <sup>b</sup>		0.78	10	[14], p. 538 <sup>b</sup>
Ba <sup>2+</sup>	0.01–1	–139––1.1			1	[18] <sup>a</sup>
Ba <sup>2+</sup>	0–250	–60–+7 <sup>g</sup>	>100	ca. 50	250	Fig. 2
Hg <sup>2+</sup>	0–0.03	<sup>c</sup>		3.8 · 10 <sup>–3</sup>	0.01	[17] <sup>c,d,h</sup>
Zn <sup>2+</sup>	0–60	–66–+31 <sup>g</sup>	3	1.5	25	Fig. 1
UO <sub>2</sub> <sup>2+</sup>	0–1	<sup>c</sup>	1	0.05	1	[17] <sup>c,d</sup>
Pb <sup>2+</sup>	5 · 10 <sup>–3</sup> –5					[19] <sup>i</sup>
Cu <sup>2+</sup>	0.13–10					[19] <sup>i</sup>
Al <sup>3+</sup>	0–0.5	–350–+1.4	8 · 10 <sup>–4</sup>		3 · 10 <sup>–3</sup>	[18] <sup>a</sup>
Al <sup>3+</sup>	0–0.5	–75–+24 <sup>g</sup>	0.35	0.2	0.5	Fig. 3
Al <sup>3+</sup>	0–0.1	<sup>c</sup>	0.1	4.5 · 10 <sup>–3</sup>	0.1	[17] <sup>c,d</sup>
Al <sup>3+</sup>	0–1.6 × 10 <sup>–3</sup>	<sup>c</sup>	1.6 · 10 <sup>–3</sup>	2.4 · 10 <sup>–4</sup>	1.6 · 10 <sup>–3</sup>	[17] <sup>c,e</sup>
La <sup>3+</sup>	2 × 10 <sup>–3</sup> –10	–5.2–+0.2 <sup>b</sup>	8.7	0.18	10	[14], p. 538 <sup>b</sup>
La <sup>3+</sup>	0.01–1	–30–+20	0.25	0.1	1	[14], p. 405 <sup>a</sup>
Ce <sup>3+</sup>	0–0.44	<sup>c</sup>		8.6 · 10 <sup>–3</sup>	0.44	[17] <sup>c,d</sup>
Th <sup>4+</sup>	10 <sup>–3</sup> –1	+45–+160		2 · 10 <sup>–3</sup>	0.1	[14], p. 405 <sup>a</sup>
Th <sup>4+</sup>	0–0.01	<sup>c</sup>	0.01	2.7 · 10 <sup>–3</sup>	0.01	[17] <sup>c,d</sup>
Th <sup>4+</sup>	0–3.8 · 10 <sup>–3</sup>	<sup>c</sup>	1.9 · 10 <sup>–3</sup>	4.4 · 10 <sup>–4</sup>	3.8 · 10 <sup>–3</sup>	[17] <sup>c,e</sup>

<sup>a</sup> Chlorides were used;  $\zeta$  potential obtained by measuring streaming potentials. Type of the glass capillary not specified, nor pH of solutions.

<sup>b</sup>  $\zeta$  potential of SiO<sub>2</sub> gel; nitrates were used. pH of solutions not specified.

<sup>c</sup> The absolute values of the  $\zeta$  potential were not determined. However, the given data can be considered as proportional to the  $\zeta$  potential.

<sup>d</sup> Chlorides, nitrates and sulphates were used; type of the glass capillary not specified, nor pH of solutions.

<sup>e</sup> Chlorides, nitrates and sulfates were used; capillary from fused-silica, pH of solutions not specified.

<sup>f</sup> Different measurement series.

<sup>g</sup> 7.08 · 10<sup>–8</sup> V<sup>–1</sup> s<sup>–1</sup> m<sup>2</sup> corresponds to a  $\zeta$  potential of 100 mV [20]; compare text and Eq. 6.

<sup>h</sup> The author states that the measurements with mercurium “were not performed with the same care like the others”. Nevertheless “it seems to be clear that there are strong effects caused by mercurium ions.”

<sup>i</sup> Cited in [14], p. 405.

Positively charged surfactants provide another possibility to control the EOF and to reverse the charge of silica surfaces [3,4]. The properties of alkylamines [21] and alkyltrimethylammonium salts [22,23] were studied systematically. These

cations are monovalent. Charge reversal becomes possible by the formation of hemimicelles at the silica surface.

In most cases these cationic surfactants also influence the electrophoretic mobility considera-

bly [22]. The hemimicelles offer additional binding sites for the adsorption of analytes. Moreover, the formation of hemimicelles depends strongly on the pH. Therefore, control of the EOF using cationic surfactants is less attractive. The use of metal ions may provide a good alternative for a number of applications.

### 3.4. Reproducibility of the EOF

The experiments were reproducible when zinc or barium salt was added to the buffer. The %C.V. of the migration time was always below 2% and typically below 1%. The investigations of zinc salt were repeated on two capillaries of the same batch. The results were nearly identical in both series. Therefore, these metal ions are useful to control the EOF for method development. The characteristics of barium-salt-containing buffers were studied more thoroughly at different pH values.

The deviations were much higher (>10% C.V.) when aluminium salt was added. The EOF decreased from run to run at all concentrations under investigation, independent of the EOF direction. It is possible that aluminium, which is a Lewis acid, catalyses the hydrolysis of the silica glass. This would lead to a gel-like structure on the surface, and thus the EOF would slow down (compare [24]).

### 3.5. Control of the EOF by addition of barium salts to buffers of various pH

Next, control of the EOF was investigated regarding reproducibility and influences of pH and of other ions. Four buffer pH values were selected between 5 and 9.2. Different amounts of barium salts were added. The EOF depends on the total buffer ion concentration. Thus, the buffers were adjusted using sodium salts to achieve comparable experimental conditions. The molarity of the anions was kept constant within a series, as well as the total amount of positive charge from metal ions: to vary the experimental conditions, each mmol of  $\text{Ba}^{2+}$  was replaced by 2 mmol of  $\text{Na}^+$ . In this way the

conductivity remained very similar within a series. However, the ionic strength could not be kept constant at the same time.

Different total ion concentrations at the same pH were also tested, and the influence of the capillary was investigated on two capillaries from different batches (Table 2). If barium ions were the only metal ionic compound of the buffer (%Ba = 100%), no EOF was detectable within 1 h ( $t_{\text{EOF}} > 60$  min, thus  $\mu_{\text{EOF}} < 2 \cdot 10^{-9} \text{ V}^{-1} \text{ s}^{-1} \text{ m}^2$ ), except at pH 5.05. Here a signal of the EOF marker occurred after 8 min, corresponding to a mobility of  $1.17 \cdot 10^{-8} \text{ V}^{-1} \text{ s}^{-1} \text{ m}^2$ .

The mobilities given in Table 2 are the averages of three measurements. The maximal deviations from this average were typically less than 2%. Exceptions are given as footnotes.

Good reproducibility was achieved in most cases. However, in some cases it was poor, especially when borate buffers were investigated. Secondary effects may result when borate ions bind to the surface. Generally, an equilibration time of 30 min was sufficient for measurements of the EOF in Tris buffer. This equilibration time had to be increased with aluminium-containing buffers. The reproducibility of some of the experiments could be improved by longer equilibration times. In general, more information is required about equilibration processes and equilibration times to obtain sufficient reproducibility.

However, a number of general conclusions are possible. No charge reversal was observed at barium concentrations up to 32 mmol/l. After this concentration, though, the EOF mobility dropped to almost zero, independently of the buffer pH. The relationship between barium concentration and EOF mobility depends decisively on the buffer pH. The mobilities obtained in Tris buffer (Fig. 2) and imidazole buffer (Table 2, pH 6.95) are very similar.

The effect of the barium ions is more pronounced at higher pH. Here the EOF is faster in the absence of barium salts, but it also decreases more sharply if barium salts are added. At rather low barium concentrations (2 mmol/l), the EOF is slower in alkaline than in neutral or acidic buffers.

The EOF can be controlled by mixtures of

Table 2

The dependence of the EOF on the buffer pH and the barium ion concentration, given as percentage of positive charge from metal ions contributed by barium [ $\%Ba = 100\% \cdot 2c_{Ba^{2+}} / (2c_{Ba^{2+}} + c_{Na^+})$ ]

%Ba	$\mu_{EOF}$ ( $10^{-8} \text{ V}^{-1} \text{ s}^{-1} \text{ m}^2$ ) at pH					
	5.05 <sup>a</sup>	6.95 <sup>b</sup>	8.5 <sup>d</sup>	8.5 <sup>e</sup>	9.2 <sup>g,h</sup>	9.2 <sup>g,i</sup>
0	3.45	4.55	6.20	5.50	6.20	6.38
6.25	4.03	3.82	4.70	3.72	2.12	4.13
12.5	3.58	3.70	3.70	2.82	2.95	1.70 <sup>j</sup>
25	3.12	3.15	2.92	2.20	1.80	1.23 <sup>j</sup>
50	2.53	2.78	2.07	0.93 <sup>f</sup>	0.57	≈0.6
62.5	2.41	3.45 <sup>c</sup>	1.17	1.00	0.75	0.63 <sup>j</sup>

EOF marker: acetanilide, effective column length: 30 cm, overall length: 37 cm; separation voltage: 20 kV. Typical total metal ion concentration corresponding to  $Me^+$ : 32 mmol/l (compare Experimental).

<sup>a</sup> Acetate buffer, 48 mmol/l; average of 2nd and 3rd injection.

<sup>b</sup> Imidazole buffer, 40 mmol/l; average of 2nd and 3rd injection.

<sup>c</sup> One injection only.

<sup>d</sup> Borate buffer, 60 mmol/l ( $c_{Me^+} = 10.48$  mmol/l); average of 3 injections.

<sup>e</sup> Borate buffer, 171.7 mmol/l ( $c_{Me^+} = 30$  mmol/l); average of 3 injections.

<sup>f</sup> Maximal deviations of 4% from measurement to measurement.

<sup>g</sup> Borate buffer, 60 mmol/l; two different capillary batches.

<sup>h</sup> Average of 3 injections, maximal deviation: 8%.

<sup>i</sup> Average of 2nd and 3rd injection.

<sup>j</sup> Average of 2nd and 3rd injection, maximal deviation: 6.5%.

barium and sodium salts. The competition of the ions at the surface decreases the effect of the barium ions on the surface charge. A similar effect, the competition of cationic surfactants and sodium ions, has been observed by other authors [21]. The EOF depends more on the absolute barium concentration than on the ratio of sodium and barium ions.

#### 4. Conclusions

The dependence of the zeta potential on metal-salt concentrations has become clear. The effects are in principle similar for different salts, but the concentration ranges in which these effects are observed differ. The affinity to the silica surface depends strongly on the type of metal ion.

The results presented here are in good agreement with earlier findings. Thus, information about other useful metal salts for CE can be easily adapted from earlier publications.

The possibility of using barium salts as buffer

additives was demonstrated. The EOF was measured at different pH values.

Barium salts are effective reagents to suppress the EOF even at high pH values.

#### Acknowledgements

We thank Mr. G. Walter for the construction of the laboratory-built instrument. We are grateful to Beckman Instruments, especially to Dr. C. Nutzhorn, for supporting these measurements.

#### References

- [1] O. Stern, Z. Electrochem., 30 (1924) 508.
- [2] H.-J. Jacobasch and H. Kaden, Z. Chem., 23 (1983) 81.
- [3] H. Wätzig, Habilitation Thesis, Würzburg, 1994.
- [4] H. Wätzig and C. Dette, Pharmazie, 49 (1994) 83.
- [5] C. Dette and H. Wätzig, J. Chromatogr. A, in press.
- [6] J. Porath, J. Chromatogr., 443 (1988) 3.
- [7] H.J. Issaq, G.M. Janiki, I.Z. Atamna, G.M. Muschik and J. Lukszo, J. Liq. Chromatogr., 15 (1992) 1129.

- [8] F.-T. Chen, C.-M. Liu, Y.-Z. Hsieh and J.C. Sternberg, *Clin. Chem.*, 37 (1991) 14.
- [9] R.A. Mosher, *Electrophoresis*, 11 (1990) 765.
- [10] H. Kajiwara, H. Hirano and K. Oono, *J. Biochem. Biophys. Meth.*, 22 (1991) 263.
- [11] H. Kajiwara, *J. Chromatogr.*, 559 (1991) 345.
- [12] F.S. Stover, B.L. Haymore and R.J. McBeath, *J. Chromatogr.*, 470 (1989) 241.
- [13] Y.-M. Liu and S.-J. Sheu, *J. Chromatogr.*, 600 (1992) 370.
- [14] *Gmelins Handbuch der Anorganischen Chemie*, Vol. 15 (Silizium), Part B, Verlag Chemie, Weinheim, 8th ed., 1959.
- [15] J.A. Lux, H.-F. Yin and G. Schomburg, *Chromatographia*, 30 (1990) 7.
- [16] D.G. Hall, *J. Chem. Soc. Faraday Trans. 2*, 76 (1980) 1254.
- [17] G. von Elissaoff, *Z. Phys. Chem.*, 79 (1912) 385.
- [18] H.R. Kruyt, *Kolloid-Z.*, 22 (1918) 81.
- [19] P. Tuorila, *Kolloidchem. Beih.*, 27 (1928) 44.
- [20] F. Foret, L. Krivankova and P. Bocek, *Capillary Zone Electrophoresis*, Verlag Chemie, Weinheim, 1993, p. 45.
- [21] D.W. Fuerstenau, *J. Phys. Chem.*, 60 (1956) 981.
- [22] T. Kaneta, S. Tanaka and M. Taga, *J. Chromatogr. A*, 653 (1993) 313.
- [23] T. Kaneta, S. Tanaka and H. Yoshida, *J. Chromatogr.*, 538 (1991) 385.
- [24] T.-L. Huang, *Chromatographia*, 35 (1993) 395.





ELSEVIER

Journal of Chromatography A, 716 (1995) 107–113

JOURNAL OF  
CHROMATOGRAPHY A

# Capillary electrochromatography of small molecules in polyacrylamide gels with electroosmotic flow

Chuzo Fujimoto<sup>a,\*</sup>, Jun Kino<sup>a</sup>, Hirokazu Sawada<sup>b</sup>

<sup>a</sup>*Department of Chemistry, Hamamatsu University School of Medicine, Hamamatsu 431-31, Japan*

<sup>b</sup>*Department of Materials Science, Toyohashi University of Technology, Toyohashi 441, Japan*

## Abstract

Traditionally, polyacrylamide gels have been used as sieving media for the separation of macromolecules such as proteins and polynucleotides. Since these analytes are electrically charged, they can migrate under an applied electric field. In an attempt to separate uncharged analytes, acrylamide (AA)-2-acrylamido-2-methyl-1-propane-sulfonic acid (AMPS) copolymers and AA-N,N'-methylenebisacrylamide (BIS)-AMPS copolymers were prepared. These copolymers are clear, UV-transparent gels and give electroosmosis due to the dissociation of the sulfo group. The preparation of the new gels in capillary tubes yielded the separation of comparatively small molecules, which is probably based on a molecular sieving effect.

## 1. Introduction

Since the advent of capillary electrophoresis (CE, originally called capillary zone electrophoresis) in 1979–83 [1–3], several variants have emerged as powerful methods for analyzing complex mixtures in nanoliter volumes or less. At the HPCE '94 Symposium, Knox [4] gave recommended names for the various capillary electroseparation (CES) systems. According to this proposal, CES is grouped into two general classes: those whose separation process is primarily based on electrophoresis and those whose separation is primarily based on the difference in partitioning between two phases.

CE and capillary gel electrophoresis (CGE) fall in the former group and capillary electrochromatography (CEC) and capillary micellar electrochromatography (CMEC, originally

termed micellar electrokinetic chromatography and often called micellar electrokinetic capillary chromatography) in the latter. It is recommended that the term CGE is used to describe the process whereby ionic analytes are separated in a gel-filled capillary [4]. CGE has been devoted primarily to the separation of large molecules such as proteins and DNA fragments. In CGE, separation is based on molecular size differences by restricted migration of analytes throughout the gel matrix. CMEC is capable of separating both neutral species and ions, unlike CE, which is a separation technique for ionic analytes only. The CMEC separation is based on the differential partitioning of analytes between the micelle (pseudo-stationary phase) and the aqueous phase.

The principle of CEC is the same as that of high-performance liquid chromatography, except that propulsion of a liquid through a column is effected by the application of an electric field

\* Corresponding author.

rather than pressure. Columns can be either a tube packed with a conventional HPLC packing material (or sub- $\mu\text{m}$  particles [5]) or an open-tubular column. Analytes are separated according to their different partitioning ratios between a mobile phase and a stationary phase. The term pressurized (flow) electrochromatography has also been used to describe an HPLC technique which applies pressure in combination with an electrical field [4,6].

Here, we report CEC separations of small organic compounds on columns containing non-particle packing materials. In preliminary studies [7,8], we have shown that the separation of charged, low-molecular mass compounds can be improved by using capillary columns filled with linear polyacrylamides without electroosmotic flow (EOF). In this work, we explored the variation of migration time with the concentration of polyacrylamide in detail since it seems to provide a starting-point to an understanding of the separation mechanism underlying the CEC separations of neutral compounds on charged columns which will be described here. Next, polyacrylamide gels of various composition were prepared using acrylamide (AA),  $N,N'$ -methylenebisacrylamide (BIS) and 2-acrylamido-2-methyl-1-propanesulfonic acid (AMPS) through linear and cross-linking procedures. The dissociation of the AMPS built in the polymer makes the generation of EOF possible, which in turn allows the electrokinetic injection and separation of neutral compounds and ionic compounds. Finally, we draw the conclusion that restricted migration of analytes through pores in the polymer network (a physical gel or chemical gel) play a role in the separation mechanism, as in usual CGE.

## 2. Experimental

### 2.1. Apparatus

Separations were performed using a laboratory-made system, consisting of a Model HCZE-30PN0.25 (Matsusada Precision Devices, Kusatsu, Japan) high-voltage power supply, a

Model 870-CE (Jasco, Tokyo, Japan) UV detector, 4-ml volume reservoirs and fused-silica tubing of 0.075 mm I.D. (or 0.10 mm) and 0.375 mm O.D. (GL Science, Tokyo, Japan).

The high-voltage end of the system was enclosed in a Plexiglas box equipped with an interlock system. Sample solutions were injected electrokinetically. All experiments were done at ambient temperature.

### 2.2. Chemicals

Distilled, deionized water, purified with an Autosil WG 23 system (Yamato, Tokyo, Japan), was used in the preparation of buffers. AA, BIS, ammonium peroxydisulfate (APS) and  $N,N,N',N'$ -tetramethylethylenediamine (TEMED) were purchased from Nacalai Tesque (Kyoto, Japan), 3-trimethoxysilylpropyl ester, AMPS, alcohols and ketones from Tokyo Kasei Kogyo (Tokyo, Japan), tris(hydroxymethyl)aminomethane (Tris) from Merck (Darmstadt, Germany) and boric acid from Kishida Chemical (Osaka, Japan).

### 2.3. Column preparation

The capillaries were internally treated with 3-trimethoxysilylpropyl ester in the manner described by Hjertén [9]. Polymerization of acrylamide monomers was initiated by APS, catalyzed by TEMED and accomplished in the capillary with 100 mM Tris–boric acid. All columns were pre-electrophoresed until the baseline of the detector remained stable.

Throughout this work, the following definitions are used to represent the gel composition:

$$\%T = 100(a + b + c)/V \quad (1)$$

$$\%C = 100b/(a + b + c) \quad (2)$$

where  $a$ ,  $b$  and  $c$  are the mass (g) of AA, BIS and AMPS, respectively, and  $V$  (ml) is the volume [10]. The AMPS content,  $\%S$ , is defined here as

$$\%S = 100\gamma/(\alpha + \beta + \gamma) \quad (3)$$

where  $\alpha$ ,  $\beta$ , and  $\gamma$  are the molarity of AA, BIS and AMPS, respectively.



### 3. Results and discussion

#### 3.1. Separation of charged molecules on linear polyacrylamide columns without EOF

Fig. 1A shows the ability of a linear polyacrylamide column to separate small organic compounds. Dansylated (Dns) amino acids were chosen as representatives of small molecules. The test solutes appears as a single peak in the electropherogram when separated in a free solution column [7,8]. For comparison, the separation of the test mixture was performed using a buffer solution which contained 10.0% (w/v) acrylamide monomer but no APS (and no

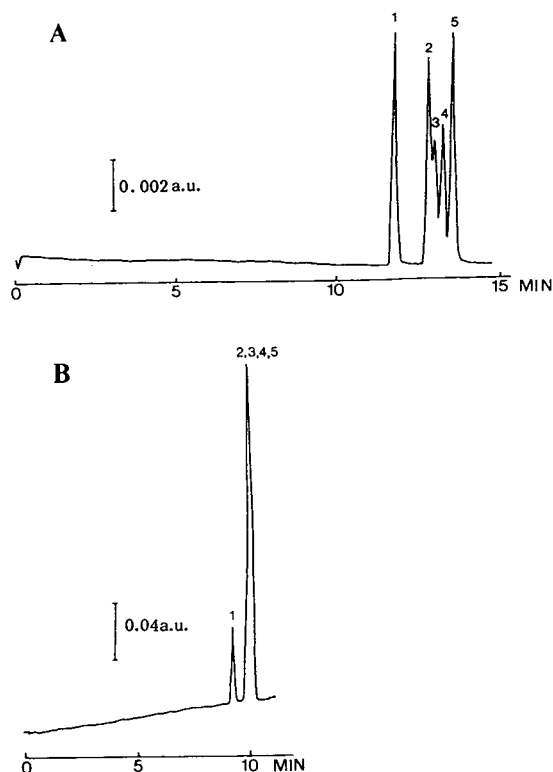


Fig. 1. Separation of dansylated amino acids (A) in linear polyacrylamide and (B) in acrylamide monomer solution capillaries. Conditions: buffer, 100 mM Tris–150 mM boric acid; capillary, 40.0 cm  $\times$  0.075 mm I.D. (15.0 cm effective length); applied voltage, 8.0 kV; detection wavelength, 254 nm. Peaks: 1 = Dns-Ala; 2 = Dns-Val; 3 = Dns-Leu, 4 = Dns-Ile; 5 = Dns-Phe. Note no EOF in either of these columns.

TEMED). The result is shown in Fig. 1B, where the electropherogram remains the same in appearance as that in the free solution column. These results suggest the participation of a polymer network in the separation shown in Fig. 1A.

The size selectivity of polyacrylamide columns can be tested by means of a Ferguson plot [11,12]. Fig. 2 shows the Ferguson plots for dansylated amino acids on columns containing linear polyacrylamides between 0 and 15.0 %T. Slight deviations from linearity can be seen in the plots. Such a phenomenon has already been observed for DNA restriction fragments [13]. The slope for each component was calculated by least squares analysis in the range of 3.0–8.0 %T, and listed in Table 1. The slope is steeper for larger molecules, suggesting the size separation mechanism.

In CES, a higher electric field strength offers the advantages of enhanced efficiency and reduced analysis time unless an excessive Joule heating is reached. On the basis of the equations

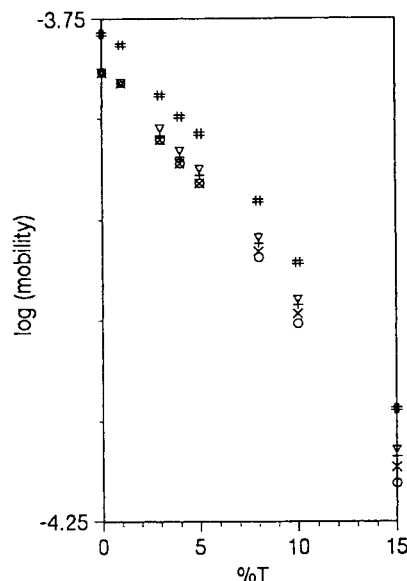


Fig. 2. Ferguson plot showing the dependence of the logarithm of the mobility of dansylated amino acids on %T. Solutes: # = Dns-Ala;  $\nabla$  = Dns-Val; + = Dns-Leu;  $\times$  = Dns-Ile;  $\circ$  = Dns-Phe. Conditions as in Fig. 1 except the column I.D., 0.10 mm.

Table 1  
Results of linear regression

Compound	Slope	Correlation coefficient
Dns-Ala	-0.0484	0.997
Dns-Val	-0.0499	0.999
Dns-Leu	-0.0500	0.999
Dns-Leu	-0.0505	0.999
Dns-Phe	-0.0541	0.999

Conditions: capillary, 40.0 cm  $\times$  0.10 mm I.D. (15.0 cm effective length); buffer, 100 mM Tris-150 mM boric acid (pH 8.2); applied voltage, 8.0 kV; detection wavelength, 220 nm.

derived by Wieme [14] and Liu et al. [15], the plate height ( $H$ ) for CEC using the polyacrylamide gel columns may be described by

$$H = h^2/(12L) + l^2/(12L) + d/R + 2D/v + (1 - R)d^2v/D \quad (4)$$

where  $h$  is the initial width of a sample plug,  $L$  is the column length,  $l$  is the detector observation length,  $d$  is the distance of a channel between fibers,  $R$  is the relative zone velocity,  $D$  is the diffusivity of a solute in the buffer and  $v$  is the velocity of the mobile phase. This expression, if it is to be general, must include the thermal contributions [5,16]. If the mobile phase velocity is proportional to the applied field strength ( $E$ ), the dependence of  $H$  on applied field strength can best be seen by writing Eq. 4 as

$$H = A + B/E + CE \quad (5)$$

where  $A$ ,  $B$  and  $C$  are constants with respect to field changes. Fig. 3 shows current and plate height of as a function of the applied field strength in both a column containing a straight buffer and a column containing 10.0 %T linear polyacrylamide. The current produced within the polyacrylamide column is significantly smaller than that produced within the straight buffer-containing column, probably owing to the higher

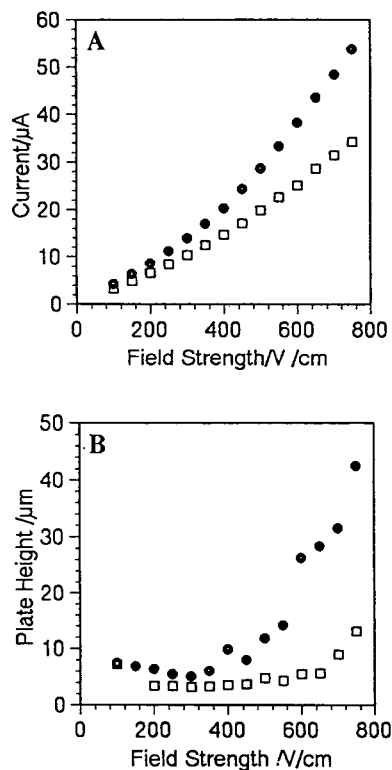


Fig. 3. Effect of field strength on current and plate height for (●) free solution and (□) 10 %T linear polyacrylamide columns. Conditions: buffer, 100 mM Tris-150 mM boric acid; capillary, 40.0 cm  $\times$  0.075 mm I.D. (15.0 cm effective length); detection wavelength, 254 nm; solute, Dns-Ala; injection, electromigration for 5 s at 2.0 kV.

viscosities in the former column. On the other hand, the column efficiencies are much higher with the polyacrylamide-filled column, indicating the anticonvective nature of the physical gel. The minimum plate height is obtained at ca. 300 V/cm. It is likely that beyond this field, the contribution to the plate height from Joule heating is sufficiently large to reduce the influence of the contributions from the others. Based on the success of these studies, we separated a mixture of 12 dansylated amino acids at the maximum field strength. The solutes were resolved and eluted within 17 min, as shown in Fig. 4.

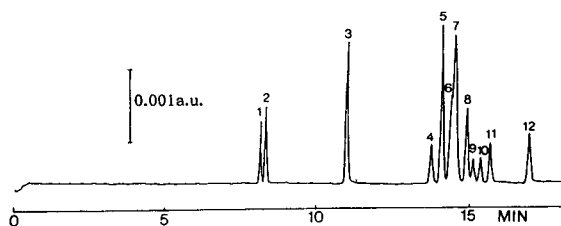


Fig. 4. Separations of 12 dansylated amino acids on a 10 %T linear polyacrylamide column. Conditions: buffer, 100 mM Tris–150 mM boric acid; capillary, 60.0 cm  $\times$  0.075 mm I.D. (30.0 cm effective length); applied voltage, 18.0 kV; detection wavelength, 254 nm; injection, electromigration for 5 s at 2.0 kV. Peaks: 1 = Dns-Asp; 2 = Dns-Glu; 3 = Dns-OH; 4 = Dns-Ala; 5 = Dns-Pro; 6 = Dns-Hyp; 7 = Dns-Thr; 8 = Dns-Val; 9 = Dns-Leu; 10 = Dns-Ile; 11 = Dns-Phe; 12 = Dns-Trp.

### 3.2. Separation of uncharged molecules on linear and cross-linked polyacrylamide columns with EOF

We expected that the traveling of uncharged compounds through a polyacrylamide column would be allowed by the introduction of ionizable functional groups into the network. For this purpose, AMPS, which has a sulfo group, was copolymerized with AA or an AA–BIS mixture. The gels should be negatively charged in a wide range of pH. Under an applied electric field, the solvent (i.e. the mobile diffuse layer) moves since the charge is fixed into the gel. Figs. 5–8 show typical chromatograms of CEC separations

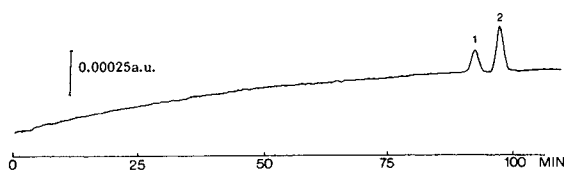


Fig. 5. Separation of a mixture of acetone and acetophenone on an AA–AMPS copolymer column. Conditions: buffer, 100 mM Tris–150 mM boric acid; capillary 65.0 cm  $\times$  0.075 mm I.D. (50.0 cm effective length); %T, 10.0; %S, 2.4; applied voltage, 13.0 kV; detection wavelength, 254 nm; injection, electromigration for 5 s at 13.0 kV. Peaks: 1 = acetone (0.5% in buffer), 2 = acetophenone (5 ppm in buffer).

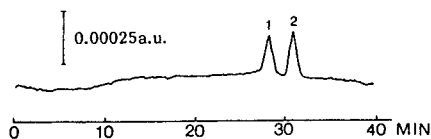


Fig. 6. Separation of a mixture of acetone and acetophenone on an AA–BIS–AMPS copolymer column. Conditions: buffer, 100 mM Tris–150 mM boric acid; capillary 65.0 cm  $\times$  0.075 mm I.D. (15.0 cm effective length); %T, 6.0; %C, 3.3; %S, 2.4; applied voltage, 13.0 kV; detection wavelength, 254 nm; injection, electromigration for 5 s at 13.0 kV. Peaks: 1 = acetone (0.5% in buffer), 2 = acetophenone (5 ppm in buffer).

of uncharged compounds on linear (10.0 %T, 2.4 %S) and cross-linked (6.0 %T, 3.3 %C, 2.4 %S and 12.0 %T, 5.0 %C, 7.8 %S) polyacrylamide columns with electro-osmotic flow (EOF). Since every solute is essentially neutral under the conditions used, these figures indicate that they are introduced into and move through the column by EOF.

It is not surprising that the copolymerized acrylamide is not extruded from the capillary by the EOF, by which the migration of the solutes through the column is effected. One might

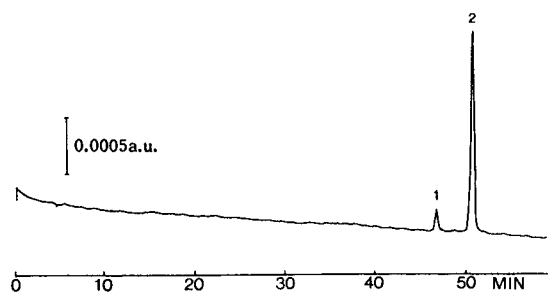


Fig. 7. Separation of a mixture of benzyl alcohol and cinnamyl alcohol on an AA–BIS–AMPS copolymer column. Conditions: buffer, 100 mM Tris–100 mM boric acid; capillary, 69.2 cm  $\times$  0.075 mm I.D. (59.5 cm effective length); %T, 12.0; %C, 5.8; %S, 7.8; applied voltage, 20.0 kV; detection wavelength, 254 nm; injection, electromigration for 5 s at 20.0 kV. Peaks: 1 = benzyl alcohol (0.23% in buffer); 2 = cinnamyl alcohol (0.015% in buffer).

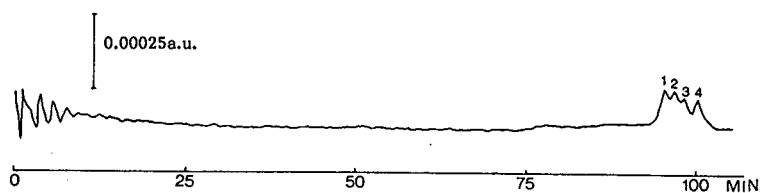


Fig. 8. Separation of a mixture of ketones on an AA-BIS-AMPS copolymer column. Conditions: buffer, 100 mM Tris–150 mM boric acid; capillary, 65.0 cm  $\times$  0.075 mm I.D. (50.0 cm effective length); %T, 6.0; %C, 3.3; %S, 2.4; applied voltage, 23.0 kV; detection wavelength, 254 nm; injection, electromigration for 5 s at 13.0 kV. Peaks: 1 = acetone; 2 = 2-butanone; 3 = methyl *n*-propyl ketone; 4 = 2-hexanone; 1% each in buffer.

Table 2  
Reproducibility of migration times ( $n = 5$ )

Parameter	Linear polyacrylamide <sup>a</sup>		Cross-linked polyacrylamide <sup>b</sup>	
	Acetone	Acetophenone	Acetone	Acetophenone
Average time (min)	39.76	40.32	27.89	30.23
Standard deviation	0.09	0.10	0.07	0.09
R.S.D. (%)	0.23	0.25	0.24	0.29

<sup>a</sup> Conditions: capillary, 65.0 cm  $\times$  0.075 mm I.D. (50.0 cm effective length); %T, 10.0; %S, 4.9; buffer, 100 mM Tris–150 mM boric acid (pH 8.2); applied voltage, 13.0 kV; detection wavelength, 254 nm.

<sup>b</sup> Conditions: capillary, 65.0 cm  $\times$  0.075 mm I.D. (15.0 cm effective length); %T, 6.0; %C, 3.3; %S, 2.4; other conditions as for linear polyacrylamide.

question the stability of these columns. The reproducibilities of the migration times of acetone and acetophenone were examined on linear and cross-linked polyacrylamide columns. The reproducibility data are given in Table 2. It is apparent that both columns give good reproducibilities. However, we found that the migration times of the test solutes slowly decreased on linear polyacrylamide columns. Therefore, the cross-linked polyacrylamide columns are the more favorable choice.

In summary, the introduction of dissociative functional groups into polyacrylamide gels permitted the separation of uncharged molecules. The stability of the cross-linked polyacrylamide columns studied here is as good as that of common polyacrylamide gel columns without EOF. From data presented here and elsewhere [17], we suspect that the separation of such small molecules is made mainly according to their size.

## Acknowledgements

C.F. greatly acknowledges the Asahi Glass Foundation and the Research Foundation of Hamamatsu University School of Medicine for financial support of this work.

## References

- [1] S. Hjertén, *J. Chromatogr.*, 270 (1983) 6.
- [2] J.W. Jorgenson and K.D. Lukacs, *Anal. Chem.*, 53 (1981) 1298.
- [3] F.E.P. Mikkers, F.M. Everaerts and Th.P.E.M. Verheggen, *J. Chromatogr.*, 160 (1979) 11.
- [4] J.H. Knox, paper presented at the 6th International Symposium on High Performance Capillary Electrophoresis, San Diego, CA, 1994, No. 045; *J. Chromatogr. A*, 680 (1994) 3.
- [5] J.H. Knox and I.H. Grant, *Chromatographia*, 24 (1987) 135.

- [6] Th. Eimer and K.K. Unger, paper presented at the 6th International Symposium on High Performance Capillary Electrophoresis, San Diego, CA, 1994, No. 043.
- [7] C. Fujimoto, H. Sawada, and K. Jinno, *J. High Resolut. Chromatogr.*, 17 (1994) 107.
- [8] C. Fujimoto and H. Sawada, *Bunseki Kagaku*, 44 (1995) 75.
- [9] S. Hjertén, *J. Chromatogr.*, 347 (1985) 191.
- [10] S. Hjertén, *Arch. Biochem. Biophys.*, Suppl. 1 (1962) 147.
- [11] K.A. Ferguson, *Metabolism*, 13 (1964) 1985.
- [12] A.T. Andrews, *Electrophoresis—Theory, Techniques, and Biochemical and Clinical Applications*, Clarendon Press, Oxford, 2nd ed, 1986, Ch. 4, p. 93.
- [13] D.N. Heiger, A.S. Cohen and B.L. Karger, *J. Chromatogr.*, 516 (1990) 33.
- [14] R.J. Wieme, in E. Heftmann (Editor), *Chromatography—A Laboratory Handbook of Chromatographic and Electrophoretic Methods*, Van Nostrand Reinhold, New York, 3rd ed., 1975, Ch. 10, p. 228.
- [15] J. Liu, V. Dolnik, Y.-Z. Hsieh and M. Novotny, *Anal. Chem.*, 64 (1992) 1328.
- [16] E. Grushka, R.M. McCormick and J.J. Kirkland, *Anal. Chem.*, 61 (1989) 241.
- [17] C. Fujimoto, in preparation.





ELSEVIER

Journal of Chromatography A, 716 (1995) 115–122

JOURNAL OF  
CHROMATOGRAPHY A

# Capillary zone electrophoresis with indirect UV detection applying a UV-absorbing counter ion

J. Collet, P. Gareil\*

*Laboratoire d'Electrochimie et de Chimie Analytique (URA CNRS 216), Ecole Nationale Supérieure de Chimie de Paris, 11 rue Pierre et Marie Curie, 75231 Paris Cedex 05, France*

## Abstract

The method of choice for the determination of non-UV-absorbing ions in capillary zone electrophoresis (CZE) usually consists in applying indirect UV detection with a non-UV-absorbing counter ion and a UV-absorbing co-ion (chromophore). Nevertheless, the use of chromogenic species with a sign of charge opposite to that of the analyte has recently been mentioned with regard to its principle but has not yet given rise to practical development. In this paper, the indirect UV detection of cations using anionic chromophores (benzoate, anisate) and cationic buffers (Tris, ethanolamine) is described. Based on the use of Kohlrausch's regulation function, a new equation for the response factor ( $k_i$ ) has been derived. Depending on the absolute mobility of the analyte ion relative to that of the co-ion, both negative and positive peaks can be observed. The separation of some alkali metal ions and quaternary ammonium ions was used to confirm the dependence of  $k_i$  on the absolute mobilities of the three components of the system (analyte ion, co-ion and counter ion). In addition, the peak shape of a weak analyte (ammonium ion) is also presented as a function of pH. From these results, it can be shown that using the proper pH, a higher efficiency can be reached by matching the effective mobility of the UV-transparent co-ion more closely to those of the analyte ions.

## 1. Introduction

In 1989, Foret et al. [1] provided a set of rules towards method development for the indirect UV detection of non-absorbing ions using charge displacement of an absorbing co-ion as a principal constituent of the background electrolyte. Since then, this mode of detection has become very popular in CZE, especially for the determination of inorganic anions and cations [2,3]. Relevant additional theoretical aspects were also published [4–7]. However, Foret et al. [1] also recognized the feasibility of detecting cations ( $K^+$ ,  $Li^+$ ) with an anionic chromophore (sor-

bate), but little attention has been paid to the development of practical applications. Nevertheless, the mathematical model, using the eigenvector approach, that was formulated by Poppe [7] for the simulation of indirect absorbance electropherograms was of sufficiently general scope to account for both counter ionic and co-ionic chromophores. While this work was under way, Beckers [8], assuming only the presence of fully ionized monovalent ionic components, shed light on the different approaches for UV detection in CZE: the detection of positive and negative peaks (dips) was discussed with respect to the UV absorbance or transparency of the analyte and of the electrolyte co-ion and counter ion. The appearance of system peaks

\* Corresponding author.

occurring with electrolytes containing two co-ions was also displayed.

In this paper, we report similar observations for the indirect UV detection of strong (alkali metal, quaternary ammonium ions) or weak ( $\text{NH}_4^+$ ) analytes applying a UV-transparent co-ion and a UV-absorbing counter ion. Both theoretical and experimental aspects of this original mode of detection are presented using response factor calculations, derived from the well known Kohlrausch's regulation function (KRF) [9]. Relative merits and drawbacks of the KRF approach are exemplified for the description of some indirect UV detection systems.

## 2. Theoretical

### 2.1. Strong electrolytes

Starting with Kohlrausch's regulation function, it holds for strong and multivalent electrolytes [10] that

$$\sum_i \frac{Z_i C_i}{m_i} = \omega \quad (1)$$

where  $Z_i$  is the absolute value of the charge of component  $i$ ,  $C_i$  its concentration and  $m_i$  the absolute value of its mobility ( $m_i \geq 0$ );  $\omega$  states the numerical value of KRF that is supposed to be locally invariant with time. For a background electrolyte AB composed of a co-ion A and a counter ion B applied to the electrophoresis of a sample ion  $i$ , it follows that

$$\frac{Z_A C_A^E}{m_A} + \frac{Z_B C_B^E}{m_B} = \frac{Z_A C_A^S}{m_A} + \frac{Z_B C_B^S}{m_B} + \frac{Z_i C_i^S}{m_i} \quad (2)$$

The superscripts E and S refer to the carrier electrolyte AB zone and the sample zone, respectively. In Eq. 2 we assume that the contributions from  $\text{H}^+$  and  $\text{OH}^-$  to KRF are negligible at an intermediate pH. We also assume that the mobilities  $m_A$ ,  $m_B$  and  $m_i$  are constant regardless of the zone E or S.

Electroneutrality demands that

$$Z_A C_A^E = Z_B C_B^E \quad (3)$$

and

$$Z_A C_A^S + Z_i C_i^S = Z_B C_B^S \quad (4)$$

Substituting Eqs. 3 and 4 into Eq 2 results in

$$C_B^E = C_B^S - k_i \cdot \frac{Z_i}{Z_B} \cdot C_i^S \quad (5)$$

with

$$k_i = \frac{m_B}{m_A + m_B} \left( 1 - \frac{m_A}{m_i} \right) \quad (6)$$

In the case of a UV-transparent solute  $i$ , a UV-transparent co-ion A and a UV-absorbing counter ion B, the application of Beer's law leads to the following expressions for the absorbance of the carrier electrolyte,  $A^E$ :

$$A^E = \varepsilon_B l C_B^E = \varepsilon_B l C_B^S - \varepsilon_B l k_i \cdot \frac{Z_i}{Z_B} \cdot C_i^S \quad (7)$$

and for the absorbance of the sample zone,  $A^S$ :

$$A^S = \varepsilon_B l C_B^S \quad (8)$$

Combination of Eqs. 7 and 8 yields

$$\Delta A = A^S - A^E = \varepsilon_B l k_i \cdot \frac{Z_i}{Z_B} \cdot C_i^S \quad (9)$$

where  $\varepsilon_B$  is the molar absorptivity of component B (chromophore) and  $l$  the optical path length. It may be seen from Eq. 9 that  $k_i$  represents the response factor of the sample ion  $i$ . Depending on the sign of  $k_i$ , both negative peaks (for  $m_i < m_A$ ) and positive peaks (for  $m_i > m_A$ ) can be observed in the electropherogram. Finally,  $m_i = m_A$  leads to  $k_i = 0$  (no peak). This model was previously described by Beckers [8] for monovalent ions. In the present work, as far as multivalent ions are considered, it ensues that (i)  $\Delta A$  is proportional to  $Z_i$ , (ii)  $\Delta A$  is in inverse proportion to  $Z_B$  and (iii)  $\Delta A$  is independent of  $Z_A$ .

By analogy with Ackermans' treatment [4], it can be shown that the measured peak area of a



solute ion  $i$  ( $A_i$ ) is directly proportional to the concentration  $c_i^S$ , the charge  $Z_i$ , the migration time  $t_i$  and the response factor  $k_i$ . In other words, it can be expected that the relationship between  $A_i/C_i Z_i t_i$  and  $k_i$  is linear, passing through the origin.

## 2.2. Weak electrolytes

The question of whether KRF can be applied to weak electrolytes is of great relevance for a correct interpretation of indirect UV detection profiles. It has already been pointed out by Poppe [7] that KRF is not suitable for components in acid–base equilibrium, and in cases where pH variations between analyte and electrolyte zones may occur. If pH cannot be carefully controlled during the separation process, then the apparent charges of weak constituents are no longer constant in Eq. (2). As a consequence, the use of KRF should be theoretically restricted to strong electrolytes. Unfortunately, this case does not correspond to the current practical situation, where weak analytes dictate the choice of weak electrolyte components for adequate buffering capacity. In the present investigation, we examined the relative merits and limitations of the KRF approach for the modelling of some indirect UV detection systems.

## 3. Experimental

Measurements were carried out with an Applied Biosystems (Santa Clara, CA, USA) Model 270A capillary electrophoresis system equipped with a 72 cm long (50 cm to the detector cell)  $\times$  50  $\mu$ m I.D. fused-silica capillary column. All experiments were performed at 30°C, at constant voltage, under normal polarity (anode at the inlet). Samples were introduced hydrodynamically by application of vacuum. Data were recorded on a Spectra-Physics (San Jose, CA, USA) Model 4400 integrator. Chemicals used as electrolyte components and test solutes were of analytical-reagent grade.

## 4. Results and discussion

### 4.1. Strong analytes

In order to verify the relationship between the response factor  $k_i$  and the mobilities of the three components of the system (solute ion  $i$ , co-ion A and counter ion B) (Eq. 6), the separation of seven fully ionized cations [potassium, barium, sodium, lithium, tetraethylammonium (TEA), tetrapropylammonium (TPA) and tetrabutylammonium (TBA)] was achieved employing 15 mM potassium–benzoate buffer, 15 mM sodium–benzoate buffer or 10 mM Tris–anisate buffer (displayed in Fig. 1 as systems 1, 2 and 3, respectively). As shown in electropherogram 1.1, all components are detected as dips, because  $m_i < m_A$  for all solutes  $i$  (see Tables 1 and 2). The potassium peak is absent in system 1 ( $m_i = m_A$ ). In system 2, only four solute ions give negative dips (lithium, TEA, TPA, TBA), whereas positive peaks are obtained for those (potassium, barium) satisfying the condition  $m_i > m_A$ . In addition, and as a consequence of electromigration dispersion, fronting or tailing peaks are observed for solutes having a mobility higher or lower (respectively) than the mobility of the co-ion, so that peaks at a time change their polarity and asymmetry in accordance with  $m_i$  with respect to  $m_A$  values. Then it is readily apparent that the major limitation of this detection mode for quantitative analysis lies in the fact that the maximum efficiency is obtained when the response factor is zero.

The results presented in systems 1 and 2, in which all solutes and electrolyte co-ions are strong electrolytes, are in good agreement with the previous treatment of Beckers [8]. More interesting, however, is the description of system 3 (10 mM *p*-anisic acid adjusted to pH 8.24 by adding Tris). In contrast to systems 1 and 2, where the buffering capacity was controlled by the counter ion, the pH is now governed by the co-ion (Tris). Since the pH chosen is close to the  $pK_a$  of Tris, it follows that the effective mobility of Tris is about half of its absolute mobility, ca.  $15.2 \cdot 10^{-5} \text{ cm}^2 \text{ V}^{-1} \text{ s}^{-1}$ . This calculation includes corrections for temperature and ionic strength

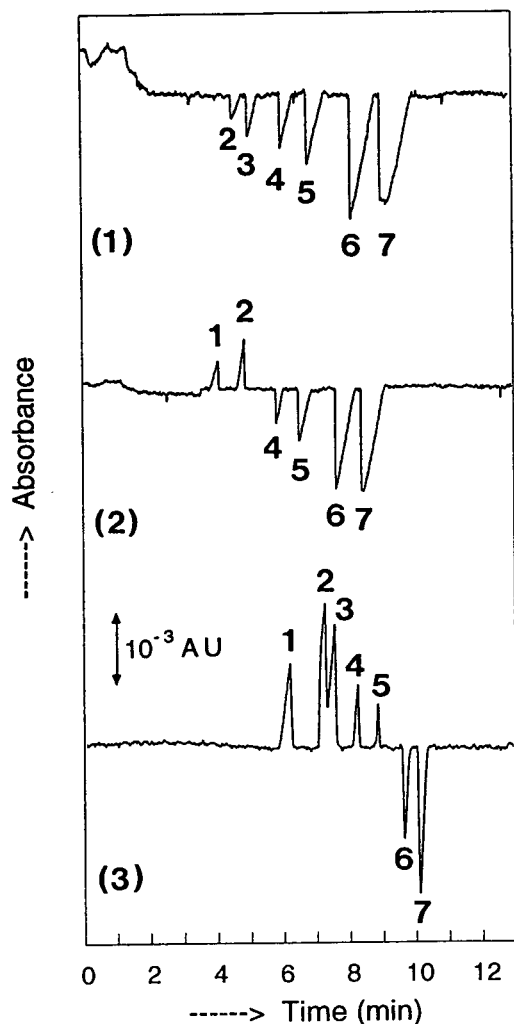


Fig. 1. Zone electrophoretic separations of seven fully ionized UV-transparent cations applying indirect UV detection with a chromogenic counter ion. Fused-silica capillary, 72 cm  $\times$  50  $\mu$ m I.D. (effective length 50 cm). Temperature, 30°C. Peaks: 1 = potassium; 2 = barium; 3 = sodium; 4 = lithium; 5 = tetraethylammonium (TEA); 6 = tetrapropylammonium (TPA); 7 = tetrabutylammonium (TBA). Pressure injection for 5 s. System 1: carrier electrolyte, 15 mM benzoic acid adjusted to pH 4.60 by adding KOH. Sample: aqueous solution of 2 mM of each ion, except for sodium (4 mM). Wavelength, 254 nm. Applied voltage, +15 kV. System 2: 15 mM benzoic acid adjusted to pH 4.60 by adding NaOH. Other conditions as in system 1. System 3: 10 mM *p*-anisic acid adjusted to pH 8.24 by adding tris [tris(hydroxymethyl) aminomethane]. Sample: aqueous solution of 0.5 mM of each ion, except for sodium (1 mM). Wavelength, 270 nm. Applied voltage, +7.5 kV. See text for further explanations.

Table 1

Electrophoretic mobilities ( $10^{-5}$  cm<sup>2</sup> V<sup>-1</sup> s<sup>-1</sup>) of the test compounds as determined in this work using electrolyte systems 1, 2 and 3 (see Fig. 1)

Solute ion	System 1	System 2	System 3
K <sup>+</sup>	—	71.7 (0.5)	71.0 (0.5)
Ba <sup>2+</sup>	61.8 (0.5)	55.7 (0.2)	52.1 (0.1)
Na <sup>+</sup>	51.0 (0.3)	—	47.8 (0.2)
Li <sup>+</sup>	41.1 (0.3)	40.4 (0.2)	38.5 (0.1)
TEA <sup>+</sup>	33.3 (0.2)	33.0 (0.2)	31.6 (0.1)
TPA <sup>+</sup>	24.1 (0.2)	24.1 (0.1)	24.0 (0.1)
TBA <sup>+</sup>	19.1 (0.2)	19.3 (0.1)	20.0 (0.1)

Temperature: 30°C. Average values were calculated from four successive experiments. Standard deviations are given in parentheses.

(Table 2). On the other hand, it appears from Fig. 1 (3) that the inversion point of the signal polarity is located between the TEA peak ( $m_i = 31.6 \cdot 10^{-5}$  cm<sup>2</sup> V<sup>-1</sup> s<sup>-1</sup>) and the TPA dip ( $m_i = 24.0 \cdot 10^{-5}$  cm<sup>2</sup> V<sup>-1</sup> s<sup>-1</sup>) (Table 1), suggesting that the condition for signal polarity inversion is still related to the absolute mobility of the co-ion, rather than to its effective mobility.

This observation also led us to consider that the expression for the response factor  $k_i$  (Eq. 6) could still be valid introducing the absolute mobility of co-ion A,  $m_A^0$ . In effect, if the ratio  $A_i/c_i z_i t_i$ , calculated from experimentally measured ( $t_i, A_i$ ) and known ( $c_i, z_i$ ) values, is plotted against response factors  $k_i$  (Fig. 2), calculated as stated above, the expected linear fitting is obtained for systems 1, 2 and 3. Noteworthy is the correct prediction for the divalent barium peak ( $Z_i = 2$ ). More important, the linearity of these plots and the zero intercepts are fairly good in comparison with the results obtained by Ackermans et al. [4] with a UV-absorbing co-ion. This can be explained by the fact that in the present system where a UV-absorbing counter ion is applied, a larger range of response factors can be explored ( $0 \leq k_i \leq 0.8$  in system 1 and  $-0.7 \leq k_i \leq 0.1$  in system 2) compared with that exploited in Ref. [4] ( $0.7 \leq k_i \leq 1.1$  in the best case). A comparison of these response factor values also suggests that the best sensitivity is generally obtained when a UV-absorbing co-ion

Table 2

Estimated absolute mobilities ( $10^{-5} \text{ cm}^2 \text{ V}^{-1} \text{ s}^{-1}$ ) derived from the literature, assuming an average correction factor of  $2\%/^{\circ}\text{C}$  and using the Debye–Hückel equation for the correction of ionic strength

Ion	From literature (25°C, infinite dilution)	After correction for temperature (30°C) and ionic strength ( $\mu$ )
Tris	29.5 [11]	30.5 ( $\mu = 10 \text{ mM}$ )
Ethanolamine	44.3 [11]	44.5 ( $\mu = 10 \text{ mM}$ )
$\text{NH}_4^+$	76.1 [12]	78.6 ( $\mu = 10 \text{ mM}$ )
Anisate	30.0 [13]	28.8 ( $\mu = 10 \text{ mM}$ )
Benzoate	33.6 [11]	31.6 ( $\mu = 15 \text{ mM}$ )

is applied (the usual case for indirect absorbance detection), because of the higher values of  $k_i$  that can be reached in this situation.

The slopes of the plots of  $A_i/c_i z_i t_i$  versus  $k_i$  are given in Fig. 2. In agreement with Eq. 9 showing that  $\Delta A$  is proportional to  $\varepsilon_B$ , the slopes obtained with the potassium–benzoate and sodium–benzoate carrier electrolytes are nearly identical (53.6 and 49.3). Using the Tris–anisate system, the slope is about four times increased because of the higher molar absorptivity of anisate. From the preceding results, it can be inferred that predictions from KRF still remains valid with strong analytes and electrolytes containing either weak counter or co-ions.

#### 4.2. Weak analytes

In the theoretical section, we discussed the problem of whether KRF is applicable to cases with acid–base equilibria involving both the sample and the carrier electrolyte constituents. Fig. 3 shows an electropherogram of four strong monovalent cations and weakly acidic ammonium ion obtained by using 10 mM *p*-anisic acid adjusted to pH 9.90 with ethanolamine. Two important features can be emphasized from this separation: first,  $\text{NH}_4^+$  gives a positive peak, as if its response factor were controlled by absolute mobilities. In fact, the absolute mobility ( $m_i^0$ ) of  $\text{NH}_4^+$  in the present conditions was estimated from the experiments to be  $78.6 \cdot 10^{-5} \text{ cm}^2 \text{ V}^{-1} \text{ s}^{-1}$  and the absolute mobility of ethanolamine ( $m_A^0$ ) (fully protonated form) is  $44.5 \cdot 10^{-5} \text{ cm}^2$

$\text{V}^{-1} \text{ s}^{-1}$  (Table 2). Hence the condition  $m_i^0 > m_A^0$  still results in a positive response factor for  $\text{NH}_4^+$ . Second, the detection of  $\text{NH}_4^+$  is accompanied by a high efficiency (about 270 000 theoretical plates in Fig. 3), giving rise to some questions.

In order to clarify this crucial point, a set of additional experiments was carried out at different pH values ranging from 8.51 to 10.20 using 10 mM ethanolamine–anisate as background electrolyte and  $\text{NH}_4^+$  as a test solute. The influence of pH on the ammonium peak shape is shown in Fig. 4 and the corresponding measured efficiencies are plotted in Fig. 5. These experimental findings can be better understood in comparing the effective mobility values of  $\text{NH}_4^+$  and ethanolamine. Based on absolute mobility (Table 2) and acidity constant estimations accounting for the actual values of temperature and ionic strength, it turns out that the calculated effective mobility of  $\text{NH}_4^+$  is higher than that of ethanolamine until pH 10.0, beyond which the two values remain almost equal (Fig. 6). It can be seen that the optimum efficiency for  $\text{NH}_4^+$  is reached when the effective mobility of the ammonium ion matches the effective mobility of ethanolamine. Curiously, this behaviour is not observed for TBA and TPA, which exhibited strong tailings in Figs. 1(3) and 3, although the basic theory predicts that fronting peaks should be expected in a situation for which the effective mobility of the analyte ion is superior to that of the background electrolyte co-ion. In our opinion, this apparent contradiction lays the stress on the limited ability of Kohlrausch's regulation function to deal with such complicated systems.

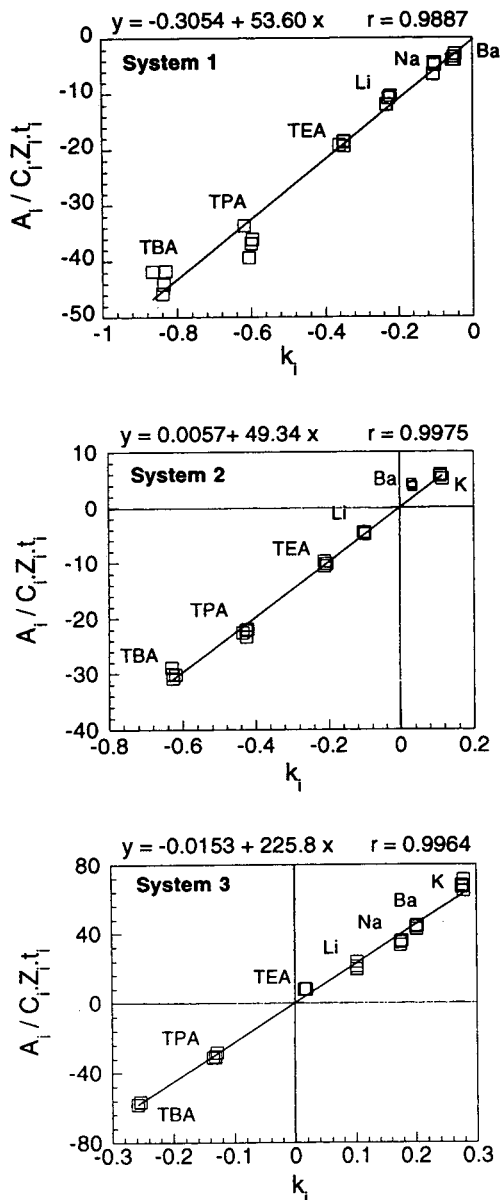


Fig. 2. Plots of  $A_i / c_i z_i t_i$  (arbitrary units) versus  $k_i$  associated with the experiments illustrated in Fig. 1.  $t_i$ ,  $A_i$ , migration times and peak areas, respectively, measured experimentally;  $c_i$ ,  $z_i$ , analyte concentrations and charges, respectively (known values);  $k_i$ , response factor calculated according to Eq. 6 using absolute values of absolute mobilities from this work (Table 1) or the literature (Table 2). System 1,  $m_A^0 = 71.7$  and  $m_B^0 = 31.6$ ; system 2,  $m_A^0 = 51.0$  and  $m_B^0 = 31.6$ ; system 3,  $m_A^0 = 30.5$  and  $m_B^0 = 28.8$  (all values in  $10^{-5} \text{ cm}^2 \text{ V}^{-1} \text{ s}^{-1}$ ). For solute ions,  $Z_i = 1$  except for barium ( $Z_i = 2$ ). For the chromophores,  $Z_B = 1$  in all cases. Data were collected from four successive injections.

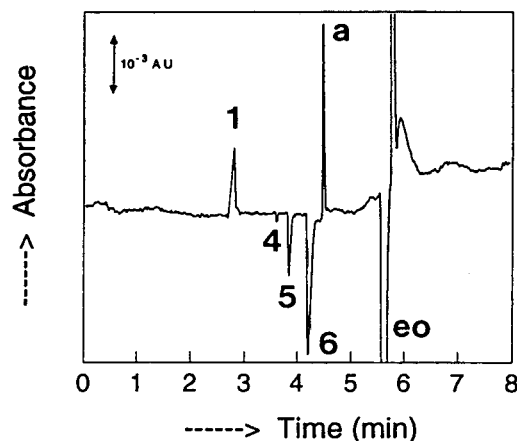


Fig. 3. Electropherogram of a mixture of potassium (1), lithium (4), tetraethylammonium (5), tetrapropylammonium (6) and ammonium (a) ions (0.5 mM each, pressure injection time 5 s) in the indirect UV absorption mode. Carrier electrolyte, 10 mM *p*-anisic acid adjusted to pH 9.90 by adding ethanolamine. Wavelength, 270 nm. Applied voltage, +15 kV. eo, signal produced by the electroosmotic flow.

## 5. Conclusion

This work was undertaken in order to provide further insight into the feasibility of detecting cationic solutes with an anionic chromophore. This alternative mode of indirect UV detection permits the simultaneous detection of cations and anions during a single run. It also allows a larger choice of non-UV-absorbing co-ions in comparison with that otherwise afforded by the limited list of chromophores suitable for indirect UV detection in CZE.

Supplementing the recent results published by Beckers [8], some important features were highlighted for weak electrolytes in this work. First, it can be recognized that the signal polarity is governed by an absolute mobility difference between the analyte ion and the co-ion, whereas a direct and intuitive viewpoint would have considered an effective mobility difference. Then, in agreement with the general concept of electromigration dispersion, we have experimentally demonstrated that the peak shape of a weak analyte is dependent on the effective mobility of the analyte ion relative to that of the co-ion. Taking advantage of this observation, sensitivity

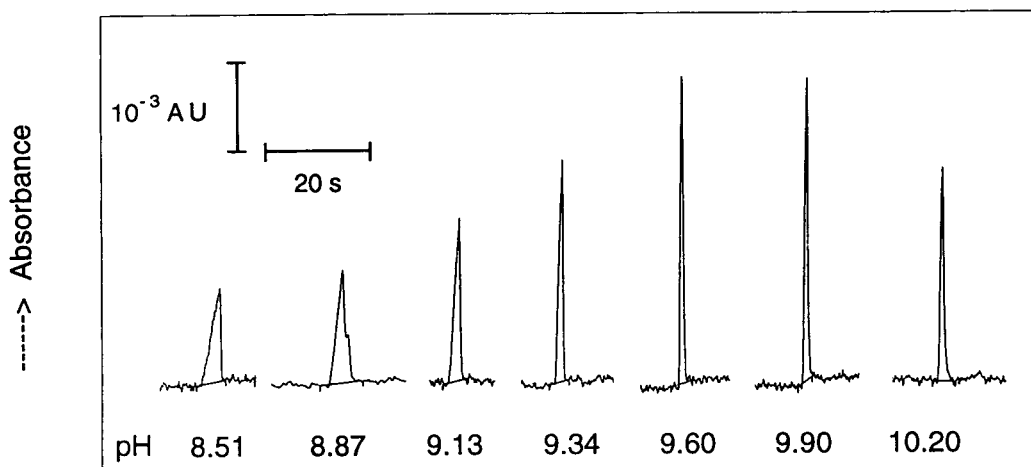


Fig. 4. Influence of pH on ammonium peak shape using 10 mM ethanolamine–anisate carrier electrolyte. Applied voltage, +30 kV. Detector rise time, 0.1 s. Other experimental conditions as in Fig. 3.

(related to peak efficiency) can be further improved by a proper choice of pH or employing complexing agents in order to minimize electromigration dispersion [15–17]. For example, 270 000 theoretical plates were reached for ammonium ion under the conditions described.

Finally, quantitative aspects of indirect UV detection were also displayed using response

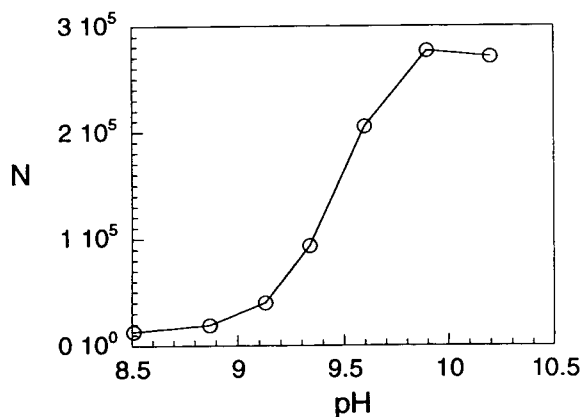


Fig. 5. Number of theoretical plates ( $N$ ) for the ammonium peak as a function of pH. Conditions as in Fig. 4.  $N$  was determined from the usual relationship  $N = 5.54(t_m/\omega)^2$ , where  $t_m$  is the migration time and  $\omega$  the peak width at half-height. Average values of  $N$  were calculated from three successive experiments.

factor ( $k_i$ ) calculations. As pointed out by Ackermans et al. [4], the relationship defined for  $k_i$  could be successfully applied to the development of universal calibration procedures for indirect UV detection in CZE, whatever chromogenic

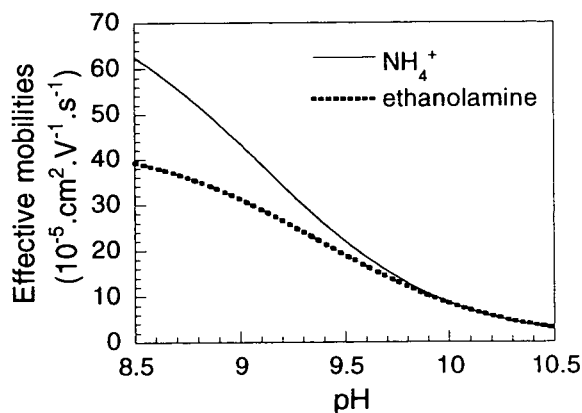


Fig. 6. Theoretical variations of the effective mobilities of ammonium and ethanolamine ions as a function of pH, accounting for an ionic strength of 10 mM and a temperature of 30°C. The  $pK_a$  and  $m^0$  values retained were as follows: for  $NH_4^+$ ,  $pK_a = 9.09$  (from Ref. [14]) and  $m^0 = 78.6 \cdot 10^{-5} \text{ cm}^2 \text{ V}^{-1} \text{ s}^{-1}$  (from Table 2); for ethanolamine,  $pK_a = 9.37$  (from Ref. [14], assuming a correction for temperature of about  $-0.03 \text{ p}K_a \text{ unit}/^\circ\text{C}$ ) and  $m_A^0 = 44.5 \cdot 10^{-5} \text{ cm}^2 \text{ V}^{-1} \text{ s}^{-1}$  (from Table 2). Considering weak bases, effective mobilities are defined as  $m = m^0 / (1 + 10^{pH - pK_a})$ .

species plays the role of co-ion or of counter ion. This aspect is under investigation.

## References

- [1] F. Foret, S. Fanali, L. Ossicini and P. Bocek, *J. Chromatogr.*, 470 (1989) 299.
- [2] F. Foret, S. Fanali, A. Nardi and P. Bocek, *Electrophoresis*, 11 (1990) 780.
- [3] J. Romano, P. Jandik, W.R. Jones and P.E. Jackson, *J. Chromatogr.*, 546 (1991) 411.
- [4] M.T. Ackermans, F.M. Everaerts and J.L. Beckers, *J. Chromatogr.*, 549 (1991) 345.
- [5] M.W.F. Nielen, *J. Chromatogr.*, 588 (1991) 321.
- [6] T. Wang and R.A. Hartwick, *J. Chromatogr.*, 607 (1992) 119.
- [7] H. Poppe, *Anal. Chem.*, 64 (1992) 1908.
- [8] J.L. Beckers, *J. Chromatogr. A*, 679 (1994) 153.
- [9] F. Kohlrausch, *Ann. Phys. (Leipzig)*, 62 (1897) 209.
- [10] S. Hjertén, L.-G. Öfverstedt and G. Johansson, *J. Chromatogr.*, 194 (1980) 1.
- [11] T. Hirokawa, M. Nishino, N. Aoki, Y. Kiso, Y. Sawamoto, T. Yagi, J.I. Akiyama, *J. Chromatogr.*, 271 (1983) D1.
- [12] P. Bocek, M. Deml, P. Gebauer and V. Dolnik, in Radola (Editor) *Analytical Isotachopheresis (Electrophoresis Library, Vol. 1)*, VCH, Weinheim, 1988.
- [13] R.C. Weast (Editor), *Handbook of Chemistry and Physics*, CRC Press, Boca Raton, FL, 1988.
- [14] D.D. Perrin, *Dissociation Constants of Organic Bases in Aqueous Solutions*, Butterworths, London, 1972.
- [15] A. Weston, P.R. Brown, P. Jandik, W.R. Jones and A.L. Heckenberg, *J. Chromatogr.*, 593 (1992) 289.
- [16] G.W. Tindall, D.R. Wilder and R.L. Perry, *J. Chromatogr.*, 641 (1993) 163.
- [17] T.-I. Lin, Y.-H. Lee and Y.-C. Chen, *J. Chromatogr. A*, 654 (1993) 167.



ELSEVIER

Journal of Chromatography A, 716 (1995) 123–133

JOURNAL OF  
CHROMATOGRAPHY A

# Post-column reaction system for fluorescence detection in capillary electrophoresis

Ruohua Zhu<sup>1</sup>, Wim Th. Kok\*

Laboratory for Analytical Chemistry, University of Amsterdam, Nieuwe Achtergracht 166, 1018 WV Amsterdam, Netherlands

## Abstract

A system for post-column derivatization in capillary electrophoresis has been developed and evaluated. In this system, reagent is added through a porous tube connecting the separation capillary with a reactor capillary. The reagent solution is driven by a regulated air pressure applied on the separation capillary inlet and the reagent vessel simultaneously. The system has been applied for the fluorescence detection of amino acids using *o*-phthalaldehyde as reagent. The reactor capillary geometry and flow-rates were optimized with respect to sensitivity and separation efficiency on the basis of measured reaction rate constants. A ten-fold increase in sensitivity could be obtained by using "bubble-cell" capillaries instead of normal fused-silica capillaries for detection.

Amino acids were separated in a pH 9.7 borate buffer. Plate numbers in the order of 100 000 to 150 000 were obtained. Detection limits were typically between  $2 \cdot 10^{-6}$  and  $4 \cdot 10^{-6}$  mol l<sup>-1</sup>, or 0.05 to 0.1 pmol injected. The method was applied to the determination of free amino acids in urine samples.

## 1. Introduction

In the last decade it has amply been shown that capillary electrophoresis (CE) provides an unparalleled efficiency for separations in the liquid phase. An exponentially growing number of research papers on CE has been published in the literature [1]. The bottleneck for a widespread use of CE in routine applications is now the detection. Due to the inherently small volume scale of CE, the technique still can not compete with the alternative separation method of liquid chromatography (LC) with respect to detection sensitivity. With on-column UV-Vis absorption detection the limits of detection are

usually not far below  $10^{-5}$  mol l<sup>-1</sup> [2]. An improvement of the sensitivity of UV-Vis detection has been sought in the use of "extended light path" detection cells [3–6], some of which are now commercially available. Other research groups have worked on the development and application of alternative detection modes which are more suited for miniaturization, such as electrochemical detection [7–12] or laser-induced fluorescence (LIF) detection [13–17].

With the latter technique so far the lowest detection limits have been obtained, with the ultimate limit of one molecule coming within reach [18]. However, there are some obvious drawbacks of LIF detection. Apart from the high costs and limited lifetime of most lasers that give enough power and stability in the interesting wavelength range, the fact that for a particular laser only one or a few spectral lines are avail-

\* Corresponding author.

<sup>1</sup> On leave from the Taiyuan Teachers College, Taiyuan, China.

able is probably the most important one. Therefore, instruments using conventional incoherent light sources for the excitation in fluorescence detection are also still being developed. Although Albin et al. [16] found detection limits with different lamps of one or two orders of magnitude higher than with a laser source, later work from the group of Dovichi [19] showed that with appropriate focusing of excitation and emission light, using microscope objectives, still very low detection limits can be obtained.

Since not many compounds show strong native fluorescence, for most applications of fluorescence detection in CE derivatization of the compounds of interest will be required. As in LC, derivatization can be performed before (pre-column) or after (post-column) the separation. For the choice between the two methods similar arguments are valid as in chromatography, considering for instance the rate and optimal conditions for the reaction, the possible occurrence of multiple reaction products or the stability of the derivatives. While pre-column derivatization procedures from LC can often be applied directly in CE, the transfer of post-column technology from LC to CE is not an easy task. First, the small volume scale of CE makes the construction of a suitable post-column reaction system technically difficult. Secondly, because of the high separation efficiency of CE, the requirements in terms of peak broadening, not only in volume units but also in time units, are much more stringent than in LC.

Different approaches have been studied in the development of a post-column system for CE. One is the free-solution approach [20]. Here, the separation capillary ends in a relatively large, grounded cuvette with the reagent. In this setup the detection volume is not restricted physically but by appropriate focusing of the excitation light close to the separation capillary exit. To preserve the separation efficiency a sheath flow of reagent can be applied to sweep out the analyte zones from the illuminated detection volume. This approach seems technically simple but requires careful focusing of the light beam. Also, its application is restricted to very fast derivatization reactions, since longer reaction

times can only be realized at the expense of a strong zone dilution.

In the other approach, capillaries are used as reactor and detection cell. The reagent solution can be added to the separation medium either by pressure or by electroosmotic processes. Jorgenson and co-workers developed a post-column reactor consisting of coaxial capillaries [21,22]. A small O.D. separation capillary was fixed inside a 100  $\mu\text{m}$  I.D. capillary which served as the reactor. A relatively high sheath flow of reagent was driven by helium pressure. By the group of Zare [23] a cross- or tee-shaped connector was developed through which the reagent could be added with little extra zone broadening. The reagent was driven by the pressure induced by a height difference. Albin et al. [16] used electroosmosis to drive the reagent-separation buffer mixture through a reaction capillary by placing the grounded electrode after the reaction capillary. The reagent was introduced through a small gap between the separation and the reaction capillary.

Neither the addition of the reagent by pressure nor that by electroosmotic processes is trivial. In a pressure-driven system precautions must be taken to prevent laminar flow in the separation capillary, while zone broadening by laminar flow in the reaction capillary is unavoidable. In an electroosmotic-driven system the flow-rate of the reagent solution cannot simply be regulated by the diameter ratio of the separation and the reaction capillaries, as has been suggested [16]. In principle, in the absence of leakage currents, the electroosmotic volumetric flow-rate does not change with the diameter of the capillary. In a wider piece of capillary, the advantage of a larger cross-section is exactly counteracted by a lower local field strength; since the current is the same everywhere, the field strength is inversely proportional to the cross-section. Therefore, an extra independent voltage source would be required to control the reagent flow freely.

In our opinion a post-column reaction system in CE will only be used in routine analysis in the future when its operation is simple. Separation and reaction conditions should be easily controlled and capillaries easily installed and



changed. In our laboratory we have studied the design and development of such a system. To be able to work without microscope and micro-manipulator, a capillary reactor system was chosen. Although realizing that the performance of fluorescence detection with post-column derivatization in terms of detection limits is mainly dependent on the optical system, in the preliminary experiments presented here an LC detector was used with only minor modifications. Experimental parameters affecting zone widths and sensitivities were studied. The derivatization of amino acids with *o*-phthalaldehyde (OPA) and 2-mercaptoethanol (2-ME) was studied as a model system.

## 2. Theory

Apart from the technical problems to be solved, the zone broadening caused by different reaction systems will determine the choice between them. With typical migration times of 10–15 min and plate numbers of 200 000–300 000 in CE, peak standard deviations  $\sigma$  are usually in the range 1–2 s. When, arbitrarily, a 25% decrease of the plate number by the post-column system is accepted, the peak-width contribution of the post-column system ( $\sigma_{\text{PCR}}$ ) should be limited to approximately 0.5–1.0 s. In first instance this zone broadening depends on the time required for the derivatization reaction to proceed to a certain degree of completion. Although in post-column systems a reaction yield of close to 100% is not necessary, to gain as much as possible in sensitivity a high yield is desirable. Since in practice the reagent is always in excess, the reaction kinetics can be described by a pseudo-first-order rate constant  $k_1$ :

$$Y = 1 - \exp(-k_1 t_R) \quad (1)$$

where  $Y$  is the yield of the reaction and  $t_R$  the reaction time. The reaction time, which should be chosen on the basis of known or measured rate constants, is set by the volumetric flow-rate of the reaction mixture and the volume of the reactor up to the detection position.

In a pressure-driven system, the zone broadening by the laminar flow in the reaction capillary can be described by the well-known Taylor–Aris equation, which can be written as

$$\sigma^2 = \frac{d_c^2}{96D} t_R \quad (2)$$

where  $\sigma^2$  is the increase in the zone variance (in  $\text{s}^2$ ),  $d_c$  the diameter of the reaction capillary and  $D$  the diffusion coefficient of the (derivatized) analyte ion. In Table 1 some examples are given of the maximally allowed reaction times with different capillary diameters. In principle, the length of the reaction capillary is not of importance. If for practical reasons a certain length has to be used, the actual reaction time and the resulting zone broadening can be decreased by increasing the reagent flow. Of course, this is accompanied by dilution of the analyte zones.

It seems obvious to use very narrow reaction capillaries to confine the zone broadening. However, with a lamp fluorescence detector with limited focusing possibilities, the illuminated volume, and with that the sensitivity, will decrease when the diameter of the capillary at the detection spot is decreased.

In an electroosmotic-driven system, the osmotic flow with its flat profile will not contribute to the zone broadening. Here, however, the reaction dispersion contribution has to be considered. In general, a derivatization reaction will change the charge or size of the analyte ion, giving a difference in the electrophoretic velocity between the non-reacted analyte and the de-

Table 1  
Maximum reaction times for various capillary diameters in a pressure-driven post-column reaction system

$d_c$ ( $\mu\text{m}$ )	$t_{\text{R,max}}$ (s) <sup>a</sup>	
	$\sigma_{\text{PCR}} = 0.5$ s	$\sigma_{\text{PCR}} = 1.0$ s
25	27	108
50	7	27
75	3	12
100	2	7

<sup>a</sup> Calculated for a compound with  $D = 7 \cdot 10^{-10} \text{ m}^2 \text{ s}^{-1}$ .

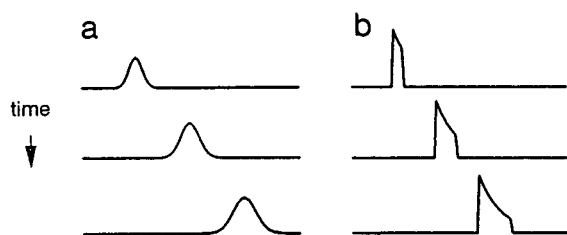


Fig. 1. The increase of the peak width in the reaction capillary by (a) laminar flow in a pressure-driven post-column reaction system and (b) reaction dispersion in a voltage-driven system.

derivatization product in the reaction capillary. In Fig. 1 the zone-broadening effect of the flow profile in pressure-driven post-column reaction systems and that of the differential migration in voltage-driven systems are shown schematically. The zone-broadening contribution of the reaction dispersion is given by

$$\sigma^2 = \frac{1}{k_1^2} \left( \frac{\Delta\mu_{\text{eff}}}{\mu_{\text{eff,P}}} \right)^2 \frac{1 - 2\exp(k_1 t_R) + \exp(2k_1 t_R) - (k_1 t_R)^2 \exp(k_1 t_R)}{[\exp(k_1 t_R) - 1]^2} \quad (3)$$

where  $t_R$  is the reaction time for the analyte,  $\mu_{\text{eff,P}}$  the effective mobility of the derivatization product (including the electroosmotic contribution) and  $\Delta\mu_{\text{eff}}$  the difference in effective mobility between the non-reacted and the reacted species. For relatively short reaction times ( $k_1 t_R \leq 1$ ) the zone broadening is approximately

$$\sigma^2 = \frac{1}{12} \left( \frac{\Delta\mu_{\text{eff}}}{\mu_{\text{eff,B}}} \right)^2 t_R^2 \quad (4)$$

For long reaction times ( $k_1 t_R > 5$ ) the zone broadening approaches a constant value, given by

$$\sigma^2 = \frac{1}{k_1^2} \left( \frac{\Delta\mu_{\text{eff}}}{\mu_{\text{eff,P}}} \right)^2 \quad (5)$$

In Fig. 2 calculated zone-broadening contributions for pressure- and voltage-driven systems are shown as a function of the reaction time. A comparison of the performances of pressure- and

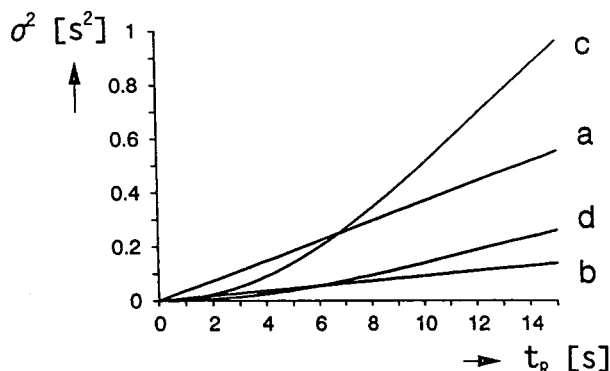


Fig. 2. Dependency of the zone broadening in a post-column reaction system on the reaction time. (a,b) Pressure-driven with a reaction capillary diameter of (a) 50 and (b) 25  $\mu\text{m}$ . (c,d) Voltage-driven with a relative mobility change ( $\Delta\mu/\mu$ ) of (c) 30% and (d) 15%.

voltage-driven post-column systems is difficult, since the first is mainly determined by the reactor diameter and the second by the chemistry of the derivatization reaction. However, as a general rule it can be stated that voltage-driven systems have an advantage when a low reaction yield ( $k_1 t_R < 1$ ) is acceptable, while a pressure-driven system is preferable for the highest sensitivities. For the latter reason we have chosen to develop a pressure-driven system.

### 3. Experimental

#### 3.1. Apparatus

Kinetic experiments were carried out with a one-line flow-injection setup, using a Spectroflow 400 HPLC pump (ABI, Ramsey, NJ, USA) and a Rheodyne injector with a 5- $\mu\text{l}$  loop and coiled 0.3 mm I.D. PTFE tubing as reactor. By varying the flow-rate and the reactor length, the reaction time could be varied from 1.5 to 100 s. Detection was carried out with a Shimadzu (Tokyo, Japan) RF-530 fluorometer with a xenon lamp and a standard quartz flow cell. The detector was set at an excitation wavelength of 345 nm and an emission wavelength of 455 nm. In these experiments a strip-chart recorder and a Hewlett-Pac-

kard (Waldbronn, Germany) 3394A integrator were used.

For capillary electrophoresis, a PRINCE (Lauer Labs, Emmen, Netherlands) system was used. Samples were introduced hydrodynamically. A Fug (Rosenheim, Germany) HCN 35-35000 high-voltage source was controlled from the PRINCE. Standard fused-silica capillaries were obtained from Polymicro Technologies (Phoenix, AZ, USA). Bubble-cell capillaries were a gift from Hewlett-Packard. For fluorescence detection, the flow cell of the RF-530 detector was removed and replaced by a homemade capillary holder. Approximately 2 mm of the polymer coating of the capillary was burned off to make a detection window. The coating close to the detection window was painted black. Detector signals were stored and processed on a PC with an A/D converter and the Caesar 3.1 integration package for CE (Lauer Labs).

### 3.2. Chemicals and solutions

OPA and sodium tetraborate were obtained from Merck (Darmstadt, Germany), other chemicals from Aldrich (Brussel, Belgium). All chemicals were of analytical-grade purity and were used without further purification. Solutions were prepared with doubly distilled water.

For the electrophoretic separations sodium tetraborate buffers were used, adjusted to the desired pH with sodium hydroxide. A 25 mg/ml stock solution of OPA in methanol was stored at 4°C in the dark. The reagent solution used in CE experiments was prepared fresh each day by diluting 1.5 ml of the OPA stock solution, 18  $\mu$ l of mercaptoethanol, 12.5 ml of a 0.1 mol l<sup>-1</sup> borax buffer (pH 10) and 5 ml methanol to 25 ml with water. All solutions were degassed with helium before use.

### 3.3. The post-column reaction system

In Fig. 3 the setup used for post-column reaction detection is shown schematically. A reagent vessel, with a total volume of approximately 1 ml, was manufactured from Kel-F. The separation and reaction capillaries could be fixed

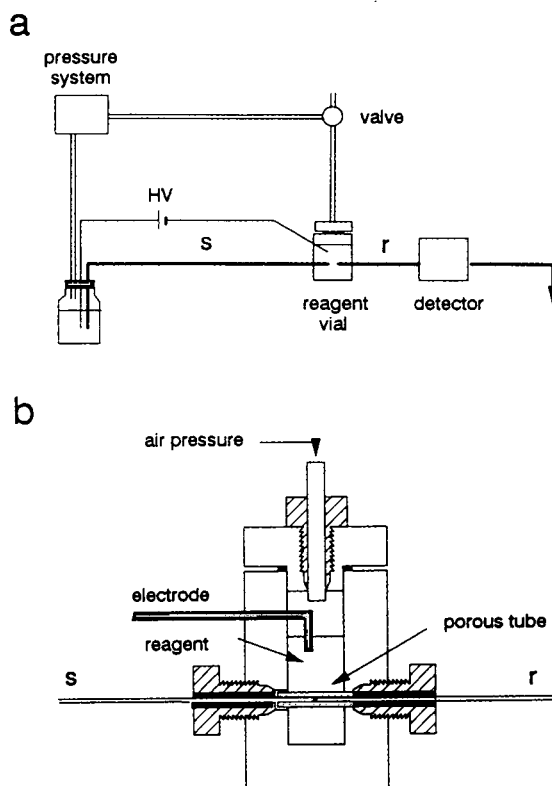


Fig. 3. Scheme of the post-column reaction system (a) with cross-section of the reagent vessel (b, not on scale). HV: high-voltage source; s: separation capillary; r: reaction capillary.

with fingertight fittings into a tube of porous PTFE (3.5 mm O.D., 0.35 mm I.D.) inside the reagent vessel, with a minimal gap between them. Reagent was driven by air pressure through the porous tube into the gap between the two capillaries. The pressure on the air-tight vessel was provided by the injection system of the PRINCE apparatus. Connections were made from 1 mm I.D. PEEK tubing. To prevent Pousseuille flow in the separation capillary, the pressure was applied simultaneously on the reaction vessel and on the inlet vial of the electrophoresis capillary during the separation. Furthermore, the inlet vial and reaction vessel are positioned at the same height.

To provide the possibility of hydrodynamic injection, an electrically actuated low-volume

gas-valve, controlled from the PRINCE, was inserted in the air-pressure line. Before injection the gas valve was switched, so that the connection to the PRINCE is closed, and the connection to the reagent vessel opened to ambient air. During analysis the valve connected the reagent vessel with the PRINCE. Because of the change of the pressurized air volume by the instrumental modification, the pressure system had to be recalibrated before use.

A platinum wire through the vessel wall, in contact with the reagent solution, served as the (grounded) electrode for the high voltage.

## 4. Results and discussion

### 4.1. Kinetics of the OPA reaction

Kinetic data on the OPA reaction of the common amino acids have been published by Svedas et al. [24] and Meyer et al. [25]. It was shown that the reaction is second order in the amino acid and OPA concentrations, with rate constants between 20 and 100 mol<sup>-1</sup> l s<sup>-1</sup> for most amino acids. For a further study of the kinetics and rate optimization, flow-injection experiments have been performed with some exemplary amino acids. A small (5 μl) sample plug was introduced in a reagent solution stream, and the reaction time was varied by changing the flow-rate and/or the length of the reaction coil. Fluorescence signals were recorded. The peak areas obtained were corrected for the varying hold-up time in the detector cell by division through the measured flow-rate. Since in all experiments the reagent concentration was in large excess, the proceeding of the reaction could be described as a pseudo-first-order process, with a yield as described by Eq. 1. When  $A'$  is the corrected peak area at a certain reaction time and  $A'_{\max}$  the maximum value obtained at long reaction times, a plot of  $\ln(1 - A/A_{\max})$  versus  $t_R$  should give a straight line through the origin with a slope equal to  $-k_1$ . Fig. 4 gives examples of the kinetic curves and the linearized plots obtained. Only for lysine this approach did not work, due to the relatively fast degradation

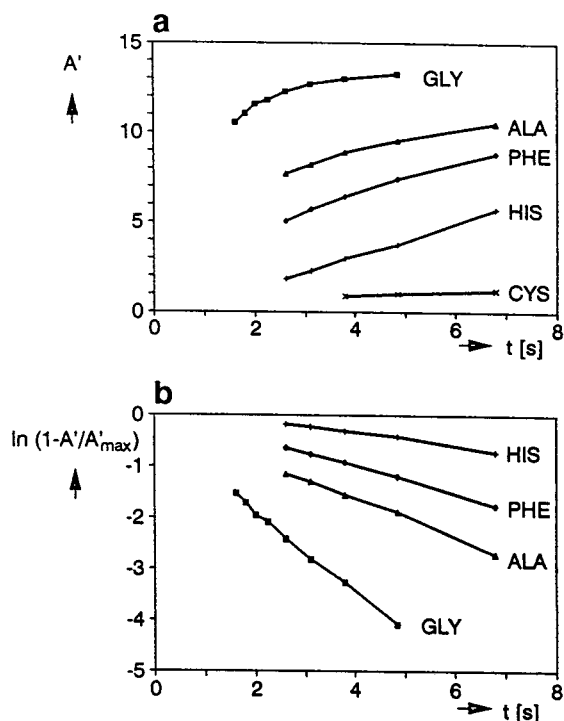


Fig. 4. Measurement of the kinetics of the OPA reaction of amino acids. (a) Kinetic curves; (b) linearized plots. Used was 5 mmol l<sup>-1</sup> OPA and 2-ME in a pH 10 solution; 5 μl of 10<sup>-4</sup> mol l<sup>-1</sup> of amino acids injected.

of the reaction product. For all other amino acids examined the pseudo-first-order rate constant was proportional to the OPA concentration in the range from 1 to 10 mmol l<sup>-1</sup>. Calculated second-order rate constants showed a fair agreement with literature values, except for glycine, for which a higher rate has been reported [24], and for cysteine, which reacted much slower in our experiments. At OPA concentrations higher than 10 mmol l<sup>-1</sup> the maximum fluorescence intensities were decreased.

The 2-ME concentration appeared to be not critical within the range 1–5 mmol l<sup>-1</sup>. At higher 2-ME concentrations the reaction rates and the maximum fluorescence intensities dropped. Optimum pH values were between 9 and 10, depending on the amino acid tested. The addition of up to 20% (v/v) methanol or ethanol to the reagent mixture increased the rate constants slightly. The addition of sodium dodecylsulphate

(SDS) to the reagent did not influence the rate constants nor the fluorescence intensities significantly. However, SDS appeared to stabilize the OPA–lysine reaction product when the pH was 9 or lower, so that kinetic analysis became possible. With an SDS concentration of 20 mmol l<sup>-1</sup>, a relatively high rate constant (93 mol<sup>-1</sup> l s<sup>-1</sup>) was measured for lysine at a pH of 9. In Table 2 measured rate constants for a number of amino acids are given.

Acknowledging that the (first-order) rate constants as given in Table 2 represent approximately optimum conditions, it is clear that for most amino acids a reaction time of 5–10 s is required in a post-column system to obtain optimal sensitivity. From Table 1 it can be seen that in that case the reaction capillary diameter should not exceed 50 μm.

#### 4.2. Reactor capillary geometry and pressure control

In the choice of the reaction capillary diameter the contradicting requirements in terms of zone broadening and sensitivity should be met. The relative sensitivities of the detector in use obtained with different capillaries were determined by measuring the fluorescence of 10<sup>-4</sup> to 5 · 10<sup>-4</sup> mol·l<sup>-1</sup> quinine sulphate solutions in 0.05 mol l<sup>-1</sup> sulphuric acid. Large plugs of the quinine sulphate solution were injected in a pressure-driven flow to eliminate effects of sample volume and dilution. Conventional capillaries with a 2-

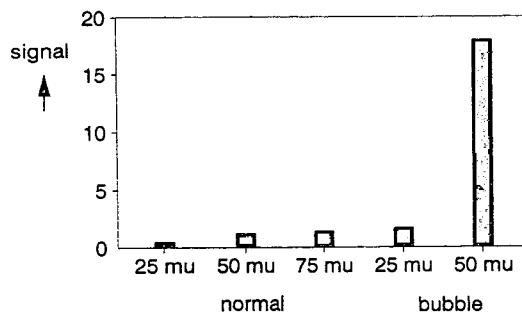


Fig. 5. Relative fluorescence intensities of quinine sulphate solutions obtained with various normal and “bubble-cell” fused-silica capillaries.

mm detection window and Hewlett-Packard “bubble-cell” capillaries were tested. The results are given in Fig. 5. The data in this figure are only indicative; especially with conventional capillaries the variance of the sensitivity was large due to small changes in the exact position of the capillary in the capillary holder. Still, it was clear that with the bubble-cell capillaries approximately a ten-fold increase of the sensitivity could be obtained compared to the conventional capillaries with the same inner diameter. Therefore, in further experiments a 50-μm bubble-cell capillary was used as reactor.

Since in the system as developed the air pressure used to drive the reagent solution is applied simultaneously on the reaction vessel and the capillary inlet, the flat electroosmotic flow profile in the separation capillary is expected not to be affected. We have found that this expectation comes true except when very wide (100 μm) separation capillaries were combined with narrow (25 or 50 μm) reaction capillaries and high reagent flow-rates. In this case migration times shorter than expected and increased zone widths were found. This was probably caused by the flow resistance of the porous tube over the connection between the two capillaries. The resulting pressure drop over the separation capillary causes a laminar flow superimposed on the electroosmotic flow in the direction of the reagent vessel. With 50 or 75 μm I.D. separation capillaries migration times were found to be not dependent on the reagent flow-

Table 2

Pseudo-first-order and second-order rate constants of the reaction of OPA with selected amino acids at pH 10

Amino acid	$k_1$ (s <sup>-1</sup> ) <sup>a,b</sup>	$k_2$ (mol <sup>-1</sup> l s <sup>-1</sup> ) <sup>b</sup>
Gly	0.77	153
Ala	0.36	72
Phe	0.26	52
His	0.15	31
Cys	0.02	4
Lys <sup>c</sup>	0.46	93

<sup>a</sup> [OPA] = 5 mmol l<sup>-1</sup>.

<sup>b</sup> [2-ME] = 5 mmol l<sup>-1</sup>.

<sup>c</sup> pH 9, 20 mmol l<sup>-1</sup> SDS added.

rate, so that the laminar flow in the separation capillary is apparently negligible here. In further experiments generally 75  $\mu\text{m}$  I.D. separation capillaries were used.

Since there is no electric field in the reaction capillary, the flow-rate in it can be described by Poiseuille's law. The total flow is comprised of the reagent flow and the electroosmotic flow from the separation capillary. Therefore, a minimum pressure  $P_{\text{min}}$  is required before the reagent solution can enter the reaction capillary (see Fig. 6). When a lower pressure is applied, the electrophoretic buffer will partly flow into the reaction vessel. When it is assumed that there is no electroosmosis in the porous tube,  $P_{\text{min}}$  is the pressure required to drive the electroosmotic flow from the separation capillary through the reaction capillary:

$$P_{\text{min}} = 32\eta\mu_{\text{os}} \Delta V \frac{L_2 d_1^2}{L_1 d_2^4} \quad (6)$$

where  $\eta$  is the solution viscosity,  $\mu_{\text{os}}$  the electroosmotic mobility,  $\Delta V$  the applied voltage and  $L_1$ ,  $L_2$ ,  $d_1$  and  $d_2$  the lengths and diameters of the separation and reaction capillaries, respectively. Experimental and calculated values of  $P_{\text{min}}$  were in fair agreement. For instance, using a 90 cm  $\times$  75  $\mu\text{m}$  separation capillary with an applied voltage of 20 kV and a 22 cm  $\times$  50  $\mu\text{m}$  reaction capillary, the calculated value of  $P_{\text{min}}$  was 94 mbar, while the lowest pressure that yielded fluorescence signals in practice was 90 mbar. This shows that the electroosmotic effects in the porous PTFE tube are indeed small.

With respect to sensitivity it would be best to

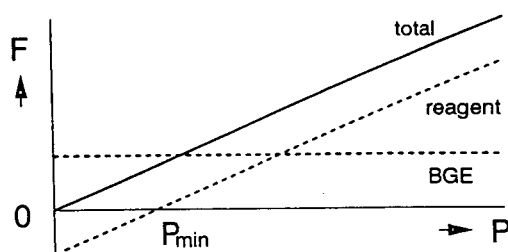


Fig. 6. Theoretical dependency of the reagent flow-rate on the applied pressure.

use a low reagent flow-rate to minimize zone dilution, and to adapt the reactor length according to the desired reaction time. However, with the detector used in this study, at least 11 cm of reaction capillary was required up to the detection window. Therefore, relatively large reagent flows were used. As shown in Fig. 7, an increase in the reagent flow results in an increase of the observed plate numbers and a decrease in the peak area. In further experiments, a pressure of 180 mbar was used, giving a buffer/reagent flow ratio of approximately 1:1 and a reaction time of 15 s. Under these conditions plate numbers were typically between 110 000 and 140 000 for negatively charged amino acids.

#### 4.3. Separation of amino acids

Borate buffers were examined as background electrolyte (BGE) for the separation of the common amino acids. It was found that the plate numbers obtained depended on the concentration of the buffer; the highest efficiency was obtained with a buffer concentration of 0.015 mol  $\text{l}^{-1}$ . The influence of the buffer pH on the

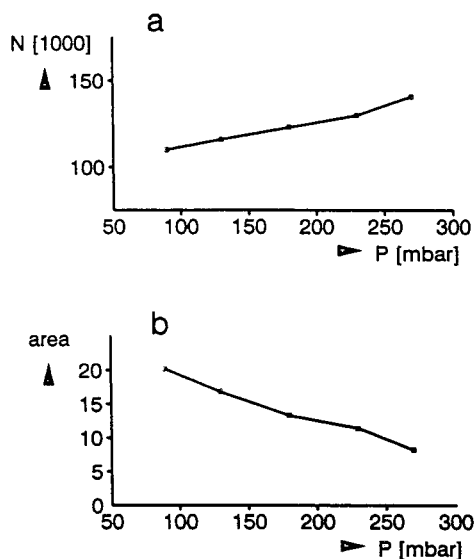


Fig. 7. Influence of the applied pressure on the plate number (a) and area (b) of the Ala peak. Separation capillary: 90 cm  $\times$  75  $\mu\text{m}$ ; reaction capillary: 22/11 cm  $\times$  50  $\mu\text{m}$ . Applied voltage 20 kV.

migration times was studied, with pH values between 9.3 and 10. Although changes of the selectivity and of the order of the peaks with the pH were found, a complete separation of all natural primary amino acids could not be realized at any pH in this simple buffer system. For instance, at pH 9.7 Ala could not be separated from Ile and Met not from Tyr. Still, at a pH of 9.7 the major amino acids found in urine samples could be separated. The peak of Lys showed tailing. Lys and Arg could be separated by addition of  $0.01 \text{ mol l}^{-1}$  SDS to the buffer, while the separation of the other amino acids was not affected by SDS. The resulting electropherogram is shown in Fig. 8a. For comparison, amino acids

derivatized with OPA shortly before the separation were analyzed under otherwise similar experimental conditions (Fig. 8b). It is clear that the derivatization has a considerable influence on the mobilities of the amino acids, and that a large part of the separation selectivity is lost with pre-column derivatization. It should be noted, however, that the separation conditions had been optimized for the underivatized compounds. Note that the unstable lysine derivative is not visible in the electropherogram. For the other amino acids the sensitivities obtained with pre- or post-column derivatization were of the same order of magnitude.

With the post-column reaction system, using  $10^{-4} \text{ mol l}^{-1}$  standard mixtures of amino acids, retention times were found to be reproducible within 0.5% and peak areas within 4.5% ( $n = 7$ ). Peak areas were linear with the sample concentration in the range from  $5 \cdot 10^{-6}$  to  $10^{-3} \text{ mol l}^{-1}$ , although at concentrations higher than  $2 \cdot 10^{-4} \text{ mol l}^{-1}$  peak distortion by overloading became visible. Detection limits, calculated for a signal-to-noise ratio of 2, ranged from  $2 \cdot 10^{-6}$  to  $4 \cdot 10^{-6} \text{ mol l}^{-1}$ , or 0.05 to 0.1 pmol injected.

Urine samples could be analyzed without any sample pretreatment except dilution (1 to 10) with distilled water. In Fig. 9 electropherograms are shown of a urine sample and a standard mixture of amino acids which are usually present in urine samples in appreciable concentrations ( $>5 \cdot 10^{-5} \text{ mol l}^{-1}$ ). Peaks in the electropherograms of the urine samples could be identified on basis of their migration times and by spiking with a standard mixture. The amino acid concentrations found in urine samples from healthy volunteers were within the normal range [26]. In all urine electropherograms a large, unidentified peak appeared at a migration time of 11.3 min.

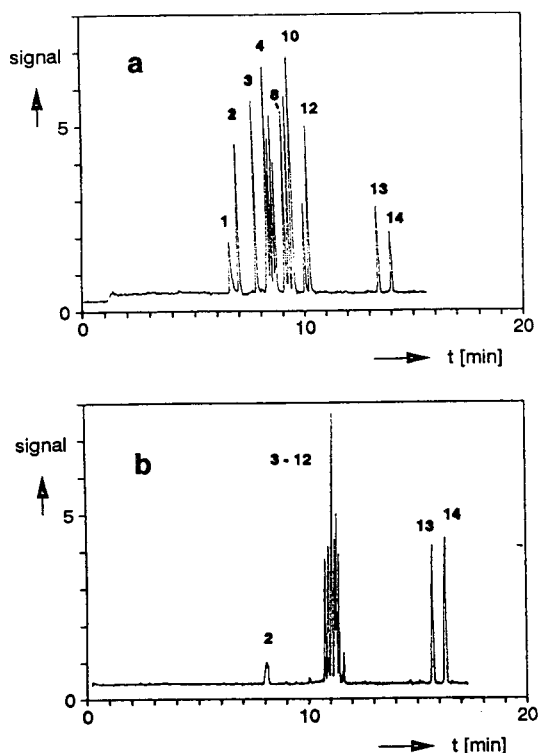


Fig. 8. Electropherograms of an amino acid standard mixture with (a) post-column or (b) pre-column derivatization with OPA. BGE:  $0.015 \text{ mol l}^{-1}$  borate,  $0.01 \text{ mol l}^{-1}$  SDS, pH 9.7. Applied pressure 180 mbar. Other conditions as in Fig. 7. Concentration of amino acids  $5 \cdot 10^{-5} \text{ mol l}^{-1}$  each. Peaks: 1 = Lys; 2 = Arg; 3 = AIBA; 4 = Ala; 5 = Leu; 6 = Val; 7 = Trp; 8 = Gly; 9 = Phe; 10 = Met; 11 = Thr; 12 = Ser; 13 = Glu; 14 = Asp.

## 5. Conclusions

In this study it has been shown that with a relatively simple pressure-driven post-column reaction system for CE, plate numbers in the order of 100 000 to 150 000 can be obtained. By applying a regulated air pressure on the capillary

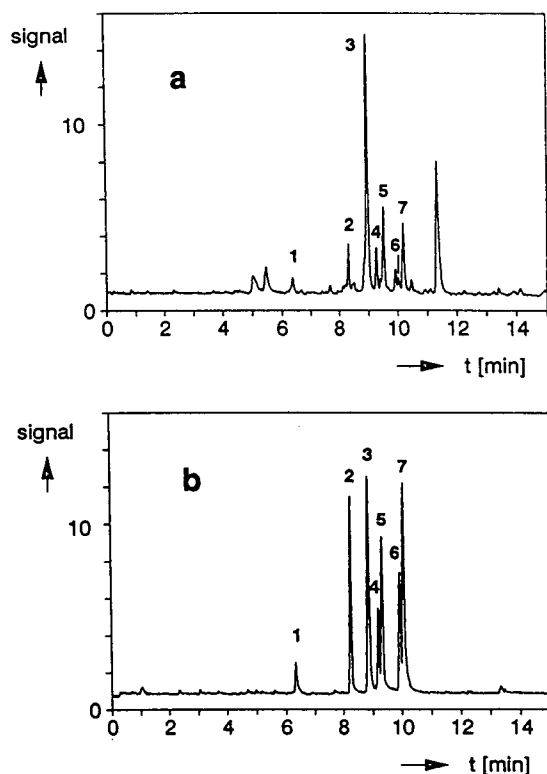


Fig. 9. Electropherograms of (a) a urine sample diluted 1:10, and (b) a  $10^{-4}$  mol  $l^{-1}$  standard mixture of amino acids. Experimental conditions as in Fig. 8. Peaks: 1 = Lys; 2 = Ala; 3 = Gly; 4 = His; 5 = Tyr; 6 = Thr; 7 = Ser.

inlet and the reagent vessel simultaneously during electrophoresis, the reagent flow-rate could be controlled without introducing laminar flow in the separation capillary. Since the experimental results followed the theoretical predictions closely, the conditions to obtain the optimal compromise between sensitivity on one hand and zone broadening on the other can easily be found.

For the fast reaction between amino acids and OPA studied in this work, a short reaction capillary, giving reaction times of 5–10 s, would have been sufficient. Since with the modified LC detector as used here a minimum capillary length is required, part of the sensitivity had to be traded in to keep the zone broadening within limits. Improvements in this respect can be

expected with an optical system specially designed for CE, possibly based on fibre optics.

Detection limits (LODs) found in our work were in the order of 50 to 100 fmol injected both with post-column and with pre-column derivatization. These LOD values are approximately one order of magnitude higher than those reported for OPA derivatives by Albin et al. [16], who also used a xenon lamp as excitation source. Therefore, we believe that an appreciable gain in sensitivity can still be obtained by an improvement of the optical system. Work in this direction is now being carried out in our laboratory.

## References

- [1] C.A. Monning and R.T. Kennedy, *Anal. Chem.*, 66 (1994) 280R.
- [2] G.J.M. Bruin, G. Stegeman, A.C. van Asten, X. Xu, J.C. Kraak and H. Poppe, *J. Chromatogr.*, 559 (1991) 163.
- [3] J.P. Chervet, R.E.J. van Soest and M. Ursum, *J. Chromatogr.*, 543 (1991) 439.
- [4] M. Albin, P.D. Grossman and S.E. Moring, *Anal. Chem.*, 65 (1993) 489A.
- [5] D.N. Heiger, *High Performance Capillary Electrophoresis—An Introduction*, Hewlett-Packard, Waldbronn, 1992.
- [6] S. Kim, W. Kim and J.H. Hahn, *J. Chromatogr. A*, 680 (1994) 109.
- [7] R.A. Wallingford and A.G. Ewing, *Anal. Chem.*, 59 (1987) 1762.
- [8] X. Huang, R.N. Zare, S. Sloss and A.G. Ewing, *Anal. Chem.*, 63 (1991) 189.
- [9] Y.F. Yik, H.K. Lee, S.F.Y. Li and S.B. Khoo, *J. Chromatogr.*, 585 (1991) 139.
- [10] T.J. O'Shea, R.D. Greenhagen, S.M. Lunte, M.R. Smyth, D.M. Radzik and N. Watanabe, *J. Chromatogr.*, 593 (1992) 305.
- [11] L.A. Colon, R. Dadoo and R.N. Zare, *Anal. Chem.*, 65 (1993) 476.
- [12] W.Th. Kok and Y. Sahin, *Anal. Chem.*, 65 (1993) 2497.
- [13] E. Gassmann, J.E. Kuo and R.N. Zare, *Science*, 230 (1985) 813.
- [14] Y.F. Chung and N.J. Dovichi, *Science*, 242 (1988) 562.
- [15] B. Nickerson and J.W. Jorgenson, *J. High Resolut. Chromatogr. Chromatogr. Commun.*, 11 (1988) 878.
- [16] M. Albin, R. Weinberger, E. Sapp and S. Moring, *Anal. Chem.*, 63 (1991) 417.
- [17] L. Hernandez, J. Escalona, N. Joshi and N. Guzman, *J. Chromatogr.*, 559 (1991) 183.
- [18] D.Y. Chen, H.P. Swerdlow, H.R. Harke, J.Z. Zhang and N.J. Dovichi, *J. Chromatogr.*, 559 (1991) 237.



- [19] E. Arriaga, D.Y. Chen, X.L. Cheng and N.J. Dovichi, *J. Chromatogr. A*, 652 (1993) 347.
- [20] D.J. Rose, Jr., *J. Chromatogr.*, 540 (1991) 343.
- [21] D.J. Rose, Jr. and J.W. Jorgenson, *J. Chromatogr.*, 447 (1988) 117.
- [22] B. Nickerson and J.W. Jorgenson, *J. Chromatogr.*, 480 (1989) 157.
- [23] S.L. Pentoney, Jr., X.H. Huang, D.S. Burgi and R.N. Zare, *Anal. Chem.*, 60 (1988) 2625.
- [24] V.-J.K. Svedas, I.J. Galaev, I.L. Borisov and I.V. Berezin, *Anal. Biochem.*, 101 (1980) 188.
- [25] M.W. Meyer, V.R. Meyer and S. Ramseyer, *Chirality*, 3 (1991) 471.
- [26] *Wissenschaftliche Tabellen Geigy*, Ciba-Geigy, Basel, 1977.



# Integrated optical detection cell based on Bragg reflecting waveguides

Thomas Delonge, Henning Fouckhardt\*

*Technische Universität Braunschweig, Institut für Hochfrequenztechnik, Abt. Optoelektronik, Postfach 3323, D-38023 Braunschweig, Germany*

## Abstract

In modern capillary electrophoresis systems with optical detection, the light beam is usually transmitted through the capillary crosswise. The disadvantages of this system are the small absorbent path length and the large amount of stray light. A new concept for a planar integrated optical detection cell with light guided in the liquid a defined length between 1 mm and 1 cm along the capillary is proposed. Using ARROWS (anti-resonant reflecting optical waveguides) or high-reflecting  $\text{TiO}_2$ - $\text{SiO}_2$  layers (Bragg layers), low-loss waveguiding can be established with confinement of the wave energy within the liquid exceeding 95%. Advantages of this system are an increased path length and a high signal-to-noise ratio while maintaining small inner dimensions below  $20 \mu\text{m} \times 20 \mu\text{m}$ . The stray light may be easily suppressed by masks on either side of the light path, which can be used as input slits for a spectrometer.

## 1. Introduction

Modern analytical systems use capillaries with an inner diameter of about  $50$ – $100 \mu\text{m}$ . Thinner capillaries promise an increased detection speed, better selectivity and smaller amounts of both solution and solvent. In most available capillary systems, the light is transmitted through the capillary crosswise. The light is either monochromatic for single-wavelength detection or emitted from a broadband source for spectral detection with a typical wavelength range from  $190$  to  $600 \text{ nm}$ . In order to have sufficient transparency for short UV wavelengths, the capillary material is usually fused silica ( $\text{SiO}_2$ ).

The major disadvantages of this set-up are the short path length which is given by the inner

diameter of the capillary and the large amount of “false” or “stray” light (Fig. 1), i.e. light going through the capillary wall instead of the fluid and entering the detecting element. This light decreases the signal-to-noise ratio and the dynamic range of the detector.

The attributes of a new sensor should be an increased path length and an effective reduction

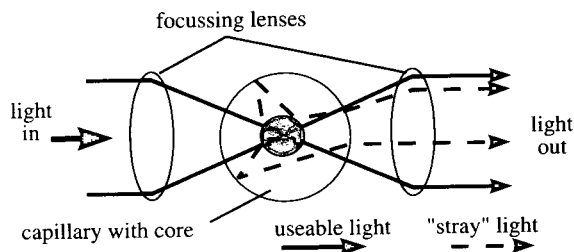


Fig. 1. Standard cross-capillary detection: disadvantages are a short path length and a large amount of stray light.

\* Corresponding author.

of false light while maintaining a small inner diameter.

## 2. Standard approaches

One commercially used approach to increasing the path length is to widen the capillary locally to a bubble (Hewlett-Packard). This widening is limited to three to five times the inner diameter of the capillary and the problem of the false light remains.

Another solution is to guide the light within the solvent in the direction of the column by normal Fresnel reflections [1,2]. However, this leads to significant losses. A further approach might be to guide the light in the capillary wall by total internal reflection at the wall/analyte interface. The interaction between the light and the analyte takes place only by the small evanescent fields extending into the liquid. This requires long interaction lengths. Yet another solution would be to guide the light within the liquid along the capillary, but with a low-loss waveguiding mechanism. For chromatographic detection the analyte is usually dissolved in water; this aqueous medium has a lower refractive index than fused silica. To achieve total reflection, either a solvent with a higher refractive index than the material of the capillary (e.g., salt solutions with Teflon PFA or PFE) or coating of the inner wall of the capillary with a low-index material can be chosen.

In the first case, there are two disadvantages: the aqueous salt solution is undesirable in many analytical measurements and the Teflon materials mentioned above are not sufficiently transparent at shorter UV wavelengths. In the second case, the coating material used is an amorphous fluoropolymer, Teflon AF, which has a lower refractive index than the aqueous solution. The disadvantage of this system is a high loss at lower wavelengths between 190 and 230 nm.

In the following, we present a waveguiding concept for analytical applications which ensures low-loss waveguiding, but allows the application of capillaries with walls having a higher refractive index than the liquid.

## 3. ARROW-Bragg waveguiding

The principle of the Bragg waveguides [3,4] is a reflection at the interfaces of layers with alternating higher and lower refractive indices, which bound the actual core of the waveguide. The refractive indices of the layers may be lower than, equal to or even higher than the refractive index of the core.

The design of the thicknesses of the layers can be carried out with standard methods such as the transfer-matrix method [5] combined with optimization algorithms. Using the transfer-matrix method, the complex propagation constant of the eigenmodes of a planar system with arbitrarily stacked layers can be calculated. In first order, the real part of the propagation constant determines the field and intensity profile and the imaginary part of the propagation constant determines the attenuation related to the propagation length. With this information, the transmission of the examined structure can be calculated.

A special class of Bragg waveguides are the anti-resonant reflecting optical waveguides (ARROWs) [6,7]. The principle of the ARROW is shown in Fig. 2. In the case of the Bragg reflecting waveguide, the core with the lowest refractive index of the structure is surrounded by

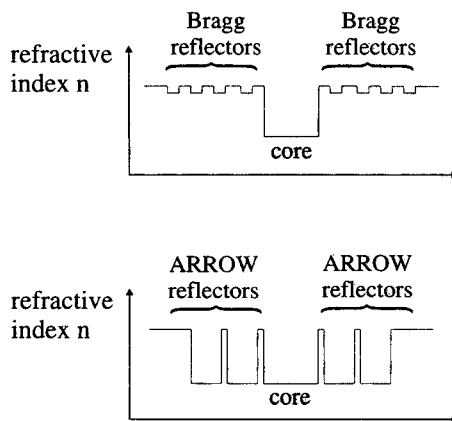


Fig. 2. Principles of Bragg and ARROW waveguides. Top: Bragg waveguides on both sides of the core made of layers with alternating higher and lower refractive indices. Bottom: ARROW waveguide with even-numbered reflectors on both sides of the core having a refractive index comparable to the refractive index of the core.

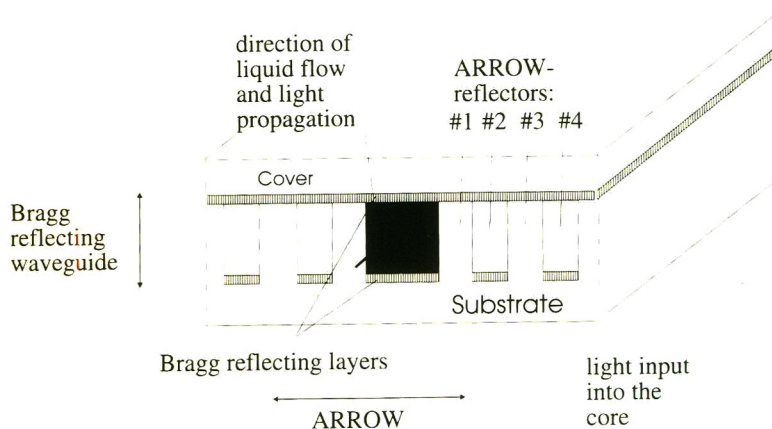


Fig. 3. Integrated optical detection cell as a combined Bragg–ARROW waveguide. In the horizontal direction the waveguiding is established by an ARROW structure; in the vertical direction Bragg layers are used.

thin layers of media with alternating higher and lower refractive indices. All reflection layers have a higher refractive index than the core. Here we use pairs of layers made of  $\text{TiO}_2$  and

$\text{SiO}_2$ . The refractive indices of the materials are wavelength dependent. For the considered wavelength region between 180 and 600 nm, the refractive indices lie in the ranges  $n = 1.7\text{--}4.3$  ( $\text{TiO}_2$ ) and  $n = 1.45\text{--}1.58$  ( $\text{SiO}_2$ ). We stress, however, that any material which can be deposited on the substrate can be used. The substrate itself should be transparent for high coupling of the light into the core.

The thicknesses of the Bragg reflecting layers depend on the core width, the refractive indices and the wavelength range. The principle of the ARROW is based on reflecting the light back into the core by specially designed pairs of coupled Fabry–Perot reflectors. The first reflector, turned to the core, consists of an arbitrary material with a higher refractive index than that of the core. The even-numbered reflectors on both sides of the core have a refractive index comparable to that of the core. For the highest reflection (anti-resonance), the thickness of these reflectors should be an odd multiple of half the thickness of the core. Fig. 3 depicts a cross-sectional view of an integrated absorption sensor with a combined ARROW–Bragg reflecting waveguide. In the horizontal direction waveguiding is achieved by an ARROW structure and in the vertical direction by Bragg reflecting layers. The core is filled with the fluid to be analysed; the even-numbered ARROW reflectors at both sides of the core are filled with a fluid with a

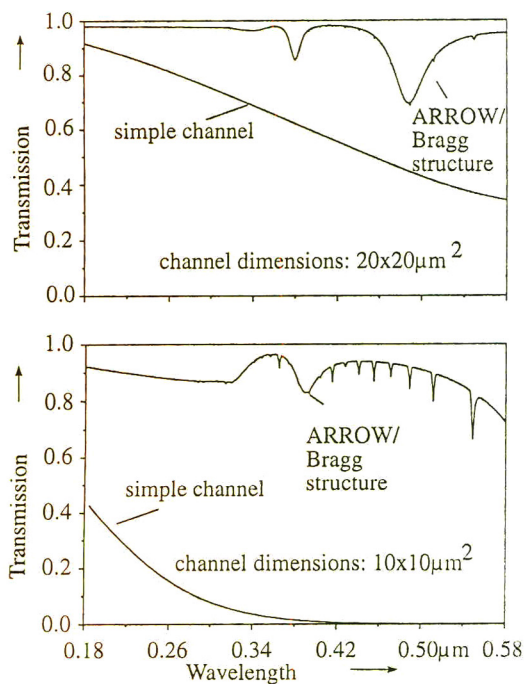


Fig. 4. Transmission of the combined ARROW–Bragg structure compared with a simple channel with cross-sectional dimensions of  $20\ \mu\text{m} \times 20\ \mu\text{m}$  and  $10\ \mu\text{m} \times 10\ \mu\text{m}$ . The absorbent path length is 1 cm.

refractive index comparable to that of the core.

Fig. 4 gives the calculated transmission of the ARROW–Bragg structure and a simple channel (waveguiding by Fresnel reflections according to Manz et al. [1] and Verpoorte et al. [2]). The path length is 1 cm and the cross-sectional dimensions of the structure are  $10\ \mu\text{m} \times 10\ \mu\text{m}$  and  $20\ \mu\text{m} \times 20\ \mu\text{m}$ , respectively. The combined ARROW–Bragg structure offers a significantly higher transmission than the simple channel, especially at higher wavelengths and smaller dimensions. For cross-sectional dimensions of  $20\ \mu\text{m} \times 20\ \mu\text{m}$  the gain in transmission is up to a factor of 2. The difference between the transmission of the two concepts increases drastically when the dimensions are reduced further. The second part of Fig. 4 shows the calculated transmission for cross-sectional dimensions of  $10\ \mu\text{m} \times 10\ \mu\text{m}$ . The transmission of the simple channel is lower than 10% for wavelengths over 300 nm while the transmission of the combined ARROW–Bragg waveguide is higher than 70%

over the whole wavelength region between 180 and 580 nm. At 350 nm the transmission is enhanced by a factor of 15, which leads to a significantly higher signal-to-noise ratio (by a factor of ca. 4 for this wavelength). The sharp dips in the transmission characteristic are related to the resonant states of the horizontal ARROW structure and can be suppressed by an appropriate calibration. Moreover, the stray light can be easily suppressed by masks on one or both sides of the end facets of the detection cell, which increases the signal-to-noise ratio and the dynamic range even further.

#### 4. Fabrication

The described structure is well suited for planar integration on different kinds of substrates. The technology will be the same as used for microelectronics, micromechanics or integrated optics. Combined with hybrid integration

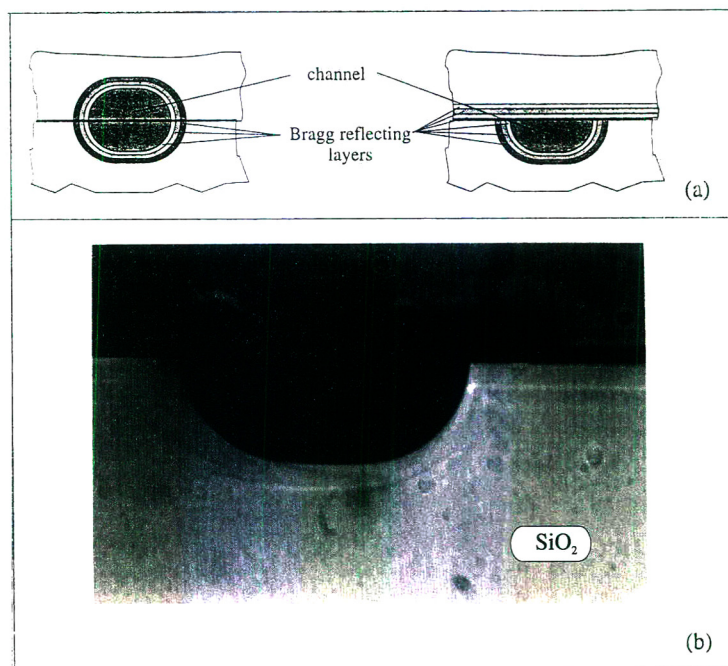


Fig. 5. (a) Alternative structures with waveguiding by Bragg reflecting layers in all dimensions and (b) photograph of a wet-chemically etched semi-cylindrical channel with a depth of  $10\ \mu\text{m}$  and a width of  $30\ \mu\text{m}$ .

of photodetectors, micromechanical pumps and valves, this structure opens the door to an analysis system on a single chip.

The channels in the substrate and cover are formed by standard processes, e.g., photolithographic structuring of resists spun on to the surface of the substrate with a subsequent wet, plasma or ion etching. The Bragg reflecting layers can be deposited by evaporation or, in the case of crystalline substrates, by epitaxial growth. The substrate and cover are fixed together by gluing or anodic bonding.

The horizontal ARROW structure requires a sophisticated structuring based on ion-etching techniques. A simpler method is wet chemical etching. Owing to the isotropic character of the fused silica, only (nearly) cylindrical-shaped channels are possible. In this case, the waveguiding has to be established by Bragg reflectors only. A typical structure is shown in Fig. 5 (in the photograph without Bragg layers). The etched substrate has a width of 30  $\mu\text{m}$  and a depth of 10  $\mu\text{m}$ . A channel can be formed either by using a symmetrical structure as superstrate or by using a simple plate as cover. The Bragg reflecting layers may be deposited by thermal evaporation of solids or chemical vapour deposition.

## 5. Conclusion

We have presented a new concept for an integrated-optical detection cell for capillary

electrophoresis and liquid chromatography. The detection cell offers low-loss waveguiding within the analyte especially when small cross-sectional dimensions of the channel are desired. The concept is based on ARROW and/or Bragg reflecting structures, which are well suited for planar integration of a CE system "on a chip". Although the concept presented requires greater technological effort than standard cross-column detection, it promises a substantially higher sensitivity owing to the increased path length and the high transmission combined with reduced stray light.

## References

- [1] A. Manz, D.J. Harrison, E. Verpoorte and H.M. Widmer, *Adv. Chromatogr.*, 33 (1993) 1–65.
- [2] E. Verpoorte, A. Manz, H. Lüdi, A.E. Bruno, F. Maystre, B. Kratinger, H.M. Widmer, B.H. van der Schoot and N.F. de Rooij, *Sensors Actuators B*, 6 (1992) 66–70.
- [3] P. Yeh, A. Yariv and C.-S. Hong, *J. Opt. Soc. Am. A*, 67 (1977) 423–438.
- [4] P. Yeh, A. Yariv and C.-S. Hong, *J. Opt. Soc. Am. A*, 67 (1977) 438–448.
- [5] J. Chilwell and I. Hodgkinson, *J. Opt. Soc. Am. A*, 1 (1984) 742–753.
- [6] M.A. Duguay, Y. Kokobun, T.L. Koch and L. Pfeiffer, *Appl. Phys. Lett.*, 49 (1986) 13–15.
- [7] Y. Kokobun, T. Baba and T. Sakaki, *Electron. Lett.*, 22 (1986) 892–983.







ELSEVIER

Journal of Chromatography A, 716 (1995) 141–156

JOURNAL OF  
CHROMATOGRAPHY A

# Optimum conditions for preparative operation of capillary zone electrophoresis

A. Cifuentes, X. Xu, W.Th. Kok, H. Poppe\*

*Amsterdam Institute for Molecular Studies (AIMS), Laboratory for Analytical Chemistry, University of Amsterdam, Nieuwe Achtergracht 166, 1018 WV Amsterdam, Netherlands*

## Abstract

The possibilities to use capillary zone electrophoresis (CZE) as a preparative tool have been studied, mostly from a theoretical point of view. The preparative performance of CZE is quantitated by the production rate, the amount of analyte that can be purified per unit of time. The production rate available with CZE is shown to depend in the first place on the chemical characteristics of the analyte–buffer combination. A figure of merit can be defined for a buffer system, describing its susceptibility to analyte overloading. Methods to find an optimal buffer system are referred to. It is shown that the loadability of the system is inversely proportional to the plate number required for the separation.

A second important factor for the maximum production rate is shown to be the thermal management of the instrumental system. The average increase of the solution temperature and the non-uniform migration velocity by temperature differences within the solutions are discussed. It is shown that in practical cases the temperature rise of the solutions will be the main limiting factor when high fields are used. With low fields, which in general give a higher production rate, siphoning of the solution becomes the dominant limitation for the production rate.

With cylindrical capillaries the highest production rate that can be obtained under practical conditions is in the order of  $5 \cdot 10^{-13}$  mol s<sup>-1</sup>. Experimental and theoretical results indicate that with rectangular capillaries the production rate can be increased by a factor of three.

## 1. Introduction

Capillary zone electrophoresis (CZE) is typically a miniaturized separation method. The paper by Jorgenson and Lukacs that set the whole technique off [1], clearly states the reasons for choosing a miniaturized system. The strong electric field one needs for obtaining a high speed of separation, in conjunction with the requirement to buffer both the pH and the conductivity of the carrier solution, inevitably leads to a large power dissipation per unit

volume. This can only be accommodated when the cross-sectional area of the electrophoretic duct is small, as otherwise the increase in temperature becomes too large. The common use of fused-silica as the tube material as well as the choice of inner diameters in the range of 10–100  $\mu\text{m}$  are the practical consequence of this thermal management problem.

As indicated, strong electric fields are desirable; the length of the ducts is therefore commonly in the range 0.1 to 1 m. With the maximum total voltage drop being limited for practical reasons to a few tens kilovolt, separation times in the order of 10 min can be obtained.

\* Corresponding author.

With these choices, the volume scale of the experiment is set: Typically, a 50  $\mu\text{m}$  I.D. tube with a length of 0.5 m, and a volume ( $V_d$ ) of approximately 1  $\mu\text{l}$  is used, in which 100 000 theoretical plates ( $N$ ) are generated. This leads to a volume standard deviation ( $\sigma_{V,i}$ ) of the zone on elution of 3 nl. The sample concentrations one can use without undesired loss of resolution are limited by the so-called electromigration dispersion, EMD (this is maybe more properly indicated as concentration overload, but the term EMD is now quite generally used). When analyte concentrations are not small compared to the concentration of electrolytes in the buffer, both the pH and the conductivity in the zone will differ from that in the initial carrier liquid. This results in a dependence of migration rate on analyte concentration, distorting the symmetrical zones, eventually into triangular shaped peaks.

This upper concentration limit is rather low, for two reasons. In the first place a price has to be paid for the high efficiency so easily accessible in CZE. The above-mentioned 100 000 plates lead to a time standard deviation ( $\sigma_{t,i}$ ) of solutes that equals 1/300 times the residence time ( $t_r$ ) of a compound. It follows that a relative change in the migration rate of this order of magnitude already will be visible as peak distortion and loss of resolution in the electropherogram. Without further detailed considerations one may therefore assume, guessing that a 10% analyte–buffer concentration ratio would lead to 1% change in migration rate, that analyte concentrations must be not much larger than 1/30 of the carrier electrolyte concentration.

In the second place, the carrier concentration itself cannot be chosen very high, because of the above-mentioned thermal management problem. Thus, one hardly finds in contemporary literature carrier solutions more concentrated than 0.03 mol/l. Therefore, total amounts that can pass the CZE instrument without serious zone distortion, are in the order of

$$\begin{aligned}\sqrt{2\pi} \cdot \sigma_{V,i} \cdot c_{i,\text{max}} &= 2.5 \cdot 3 \text{ nl} \cdot 1/30 \cdot 0.03 \text{ mol/l} \\ &= 8 \cdot 10^{-12} \text{ mol}.\end{aligned}$$

The pico-, femto- and attomole detection limits

reported for CZE have to be considered in this context. A picomole sensitivity is not so much of an effective advertisement for the technique when one realizes that this is also about the maximum the technique can effectively separate. That is, with picomole sensitivity peaks will either be distorted or suffer from a bad  $S/N$  ratio.

The analytical use of CZE is certainly hampered by this limitation, but the on-column detection, with simple UV absorption as well as with sophisticated electrochemical detectors and laser-based optical devices, has been improved to such an extent in the last ten years that many applications are possible with this miniaturized separation system.

The case of CZE forms an exquisite demonstration of the resolution–speed–capacity triangle once proposed by Scott and Kucera [2]. Without requirements on the capacity of the system one could have 40 kV across a 1-cm tube with 1  $\mu\text{m}$  I.D., and separations in much less than a second.

## 2. Results and discussion

### 2.1. Production rate

Despite the miniaturized character of CZE, there is much interest [3–6] in the preparative operation of the technique, e.g., for the isolation of DNA fragments, drugs, peptides and proteins.

The production rate ( $T_i$ ) can be defined as the amount of material  $i$  (in mol) that can be collected in purified form per time unit, averaged over a multiple of the separation time (or repetition time when regeneration of the system is required). This concept may appear slightly inappropriate in the present context, as it is associated strongly with preparative chromatography and technological ‘unit operations’ with an incomparably larger scale. Nevertheless, it is a useful concept as it applies to cases of repetitive operation as well as single separations. In the latter case  $T_i$  is just the ratio of amount collected and the run time. However, there might be cases where instrumental, physical or chemical con-

ditions would be such that repeated operation of a fast and small system would result in better productivity than one operation of a larger, slower system.

In analyzing the production rate we follow basically the same approach as has been used long ago by us in the case of preparative liquid chromatography (PLC) [7]. The mass flow,  $f_i(t)$  (mol/s), at the exit of the system (index  $e$ ) at time  $t$  is given by

$$f_i(t) = \frac{1}{4} \pi d_c^2 \cdot c_{e,i}(t) \cdot \mu_i E \quad (1)$$

where  $d_c$  is the inner diameter of the capillary,  $c_{e,i}$  is the concentration at the end of the capillary,  $\mu_i$  is the electrophoretic mobility (with the electroosmotic mobility  $\mu_{eo}$  included), and  $E$  is the strength of the electric field. The production rate  $T_i$  is found by averaging  $f_i$  over time. When  $c_{\max,i}$  is the maximum of  $c_{e,i}$  and the peak is a Gaussian with a time standard deviation  $\sigma_{t,i}$ , the total amount collected in one run is equal to

$$\sqrt{2\pi} \cdot \frac{1}{4} \pi d_c^2 \cdot c_{\max,i} \cdot \mu_i E \cdot \sigma_{t,i} \quad (2)$$

and  $T_i$  is found after dividing by the run time. For the latter we take the residence time of the component in question,  $t_{R,i}$ , the difference being only in a numerical factor that depends on the particular mixture composition at hand, the set of mobilities and/or the time needed for regeneration of the system.

The same reasoning can be applied to other peak shapes, e.g., the triangular one that occurs when EMD determines peak broadening. One can even use the same Eq. 2, as the condition that the zones have a Gaussian shape, required to warrant the exact validity of Eq. 2, is not very strict. For other shapes one arrives at factors other than  $\sqrt{2\pi}$  or 2.51, in Eq. 2. For those cases we define  $\sigma_{t,i}$  as the square root of the centralized, normalized second time moment, e.g. the width/ $\sqrt{12}$  for a block-shaped zone, or full width/ $\sqrt{18}$  for a zone shaped as a rectangular triangle. For these two cases, simple algebra yields values of 3.46 and 2.12, respectively. As we are looking for general guidelines rather than precise quantitative relations, Eq. 2

is regarded as valid for all peak shapes of interest, including ones with triangular shape.

The result for  $T_i$  is:

$$T_i = \sqrt{2\pi} \cdot \frac{1}{4} \pi d_c^2 \cdot c_{\max,i} \cdot \mu_i E \cdot \sigma_{t,i} / t_{R,i} \quad (3)$$

which can also be written as:

$$T_i = \sqrt{2\pi} \cdot \frac{1}{4} \pi d_c^2 \cdot c_{\max,i} \cdot \mu_i E \cdot N_{\text{req}}^{-1/2} \quad (4)$$

The required plate number for the separation of the mixture at hand,  $N_{\text{req}}$ , is considered as a constant. Its value is determined by the relative mobilities of the components of interest and those possibly interfering with them. Eq. 4 shows that improving  $T_i$  amounts to increasing  $c_{\max,i}$ ,  $d_c$  (or the cross-section area  $A$  in cases where the electrophoretic duct is not cylindrical) and  $E$ . While doing so, however, the plate number should remain at least equal to the required plate number.

In the following it is assumed that the system is always operated at the maximum voltage available. Other parameters, such as the dimensions of the capillary and the type and concentration of the buffer (but not the pH, which is usually dictated by the nature of the sample mixture, and the selectivities required for good separation) can then be varied in order to obtain a maximum production rate.

Most of the equations used, often taken from literature, contain  $E$  as variable. As will be shown later, strong fields lead to small  $d_c$  values and small productivities; at weak fields the production rate is much higher, but the run times may become excessive. In view of the latter fact we found it more attractive from the practical point of view to take the run time ( $t_R$ ) as the independent variable in graphs and tables. When the total voltage ( $\Delta V$ ) and  $t_R$  are known or assumed, the field strength and the capillary length can be calculated from:

$$L = (\mu_i \Delta V t_R)^{1/2} \quad (5)$$

$$E = (\Delta V / (\mu_i t_R))^{1/2} \quad (6)$$

However, in the equations these relations are usually not substituted, because that would lead to an unfamiliar form of many equations known from earlier work. Thus, all expressions con-

taining  $E$  and  $L$  should be interpreted with  $E$  and  $L$  given by Eqs. 5 and 6.

## 2.2. Chemical decisions

### *The electromigration dispersion, EMD, constant*

Plate number, column diameter and field strength as occurring in Eq. 4 are strongly interrelated because of the thermal management problem discussed in a later section. The variable  $c_{\max,i}$ , the maximum concentration of the target compound at the end of the duct, on the other hand, lends itself to straightforward discussion.

When resolution has to be preserved, the zone concentrations in CE must stay below a limit set by the EMD. The migration rate of a solute in its zone turns out to be dependent on the concentration, as a result of changes in conductivity (affecting the migration rate via changes in electric field) and, with protolyzing solutes, changes in pH, affecting the migration rate by changes in the effective mobility of the component.

The phenomenon, especially when caused by conductivity changes, has been investigated for non-protolyzing solutes and buffers by Mikkers et al. [8] and for weak acids and bases by Foret et al. [9]. The effect of pH changes has received little attention; recently, Beckers [10] applied a numerical procedure to obtain insight into this phenomenon. In our own work it has become possible to describe and predict this effect in two ways:

- (a) A numerical computer program [11], based on eigenvector description of the transport process, allows to predict the migration rate as a function of solute concentration, and to predict peak shapes. This approach applies to rather complicated electrophoretic systems, with solute and buffer components having up to five protolytic equilibrium stages, and up to four independent buffer constituents.
- (b) Recently [12], we found analytic solutions for the transport of monofunctional acids or bases in buffers based on monofunc-

tional acids or bases, taking into account the conductivity effect as well as the pH-shift effect.

Results of the two approaches are numerically the same. Together with the results cited above [8–12] they yield a common result of general importance. In this work we will restrict the discussion to cases of relatively small overload, such that extreme effects as, e.g., peak splitting, described and explained by Ermakov et al. [13], do not occur. If, moreover, the pH ranges between 3 and 11, the migration rate can be described with good accuracy, by the expression:

$$\mu_{\text{app},i} = \mu_{\text{eff},i}(1 + \beta_{\text{EMD},i}c_i/c_b) \quad (7)$$

where  $c_b$  is some convenient measure for the concentration of the buffer mixture.

Before discussing this equation, a few notes on the nomenclature are in order. The index 'eff' refers to the averaging of mobilities over the various acid/base forms of the solute, at infinite dilution of the compound for the type and pH of the buffer used. The index 'app' refers to the migration rate of the zone. To obtain  $\mu_{\text{app}}$ , the migration velocity is divided by the field in the blank buffer. This  $\mu_{\text{app}}$  is not a genuine mobility, but it is a highly convenient variable to work with. The difference between  $\mu_{\text{app}}$  and  $\mu_{\text{eff}}$  reflects the change in electric field brought about by the change in conductivity within the zone, as well as the local change due to the pH shift, which is indeed a genuine change in mobility. We apologize in passing to those people who prefer to use the index 'app' for inclusion of the electroosmotic flow (EOF); we could not think of another convenient descriptive index. As the presence of EOF does not impair the reasoning in this paper as long as all mobilities are understood to include it, we decided to use this symbol.

The parameter  $\beta_{\text{EMD},i}$  is dimensionless. It describes the 'sensitivity' of the solute–buffer combination to electromigration dispersion. As an illustration we give one expression for a case where it can be derived easily for a 1:1 non-

protolyzing buffer ( $A^+$ ,  $B^-$ ) with a non-protolyzing solute ( $I^+$ ). Then  $\beta_{EMD,i}$  is given by:

$$\beta_{EMD,i} = \frac{(\mu_B - \mu_I)(\mu_A - \mu_I)}{(-\mu_A + \mu_B)\mu_I} \quad (8)$$

where the  $\mu$  values are signed quantities. This is easily derived from the treatment presented by Mikkers et al. [8].

Another case where an explicit expression can be found, is that of a weak univalent acid or base as a solute in a buffer consisting of an univalent acid or base with an appropriate counter ion, as will be described in Ref. [12]. An important qualitative result from this work is that buffer conditions can be optimized to make  $\beta_{EMD,i}$  approach zero, even if the mobilities do not match, by virtue of the cancelation of conductivity and pH-shift effects. Still, for the majority of practical solute–buffer combinations one has to resort to the numerical approach.

#### Peak shape under EMD conditions

The description of the triangular peak shape obtained under overload conditions is a long-standing result of the theoretical efforts in electrophoresis [8–10]. We shall therefore give only a brief account, just to put the derivations in our symbols.

Let us assume that the velocity of molecules  $i$  is described by:

$$u_i = u_{0,i} + \alpha c_i \quad (9)$$

an equation that seems equivalent to Eq. 7; the reasons for this re-formulation will become clear in the sequel.

The transport equation in CZE can be written as

$$\frac{dc_i}{dt} = -\frac{dJ_i}{dz} = \frac{-d(u_i \cdot c_i)}{dz} \quad (10)$$

where  $J_i$  is the mass flux of component  $i$ .

The migration rate of a point in the diffuse boundary with constant concentration,  $u_{i,diff}$ , i.e., the migration rate as we ‘see’ it, can be found by:

$$\begin{aligned} u_{i,diff} &= \left( \frac{dz}{dt} \right)_{c_i} = -\frac{dc_i/dt}{dc_i/dz} = \frac{d(u_i c_i)/dz}{dc_i/dz} \\ &= \frac{u_i dc_i/dz + c_i du_i/dc_i \cdot dc_i/dz}{dc_i/dz} \\ &= u_i + \alpha c_i + \alpha c_i = u_{0,i} + 2\alpha c_i \end{aligned} \quad (11)$$

The factor 2 in Eq. 11 reflects the difference between the species and boundary velocity. It seems that this point, well known since the work of Helfferich and Klein [14] for chromatography, has not been formulated explicitly in electrophoresis. Depending on the way the zone profile is derived, this can matter. A prediction of peak shape is usually and correctly [15] obtained by applying Eq. 9 directly to the *steep* boundary (where species velocity equals boundary velocity). The profile is then obtained by drawing a straight line between the point found and the one corresponding to  $u_{i,0}$ . This procedure is rather awkward and error-prone, since the maximum concentration usually varies on migration, and one thus has to integrate the velocity to obtain the travelled distance. Also, for long injection plugs that are still partially ‘intact’, this procedure becomes rather counter-intuitive. We prefer, as in earlier papers, to find the slope of the diffuse boundary directly, and this has to be done with Eq. 11. Note that the velocity of the steep boundary  $u_{shock}$  equals

$$u_{i,shock} = u_i + \alpha c_i \quad (12)$$

which makes clear why a rectangular injection plug eventually transforms into a rectangular triangle. With an  $\alpha$ -value of the same sign as  $u_i$ , for instance the steep boundary at some point (in an infinite column) will be caught up by the faster moving diffuse boundary.

For triangular zones the position of the steep boundary is most easily found by applying the integral mass balance to find  $c_i$ ; the area under the curve must match the injected amount. However, this discussion is not necessary in this paper.

It follows from all this that, indeed, Eq. 9 is not equivalent with Eq. 7. However, Eq. 11 is, with  $\beta_{EMD,i} = 2\alpha/u_i \cdot c_b$ . We will further work with Eq. 7, and not use Eqs. 9–12.

It is now possible to draw conclusions about the maximum  $c_i$  value admissible in (preparative) CE experiments. The plate number,  $N$ , originally a measure for real dispersion, is used here as an expression for the required sharpness of separation. It therefore prescribes also the maximum admissible 'electromigration dispersion'.

The zero-concentration end of the diffuse boundary is eluted at a time:

$$t_{R,i,0} = L/(\mu_{\text{eff},i} \cdot E) \quad (13)$$

The peak maximum is eluted at a time:

$$t_{R,i,c} = L/(\mu_{\text{eff},i}(1 + \beta_{\text{EMD},i}c_{i,\text{max}}/c_b) \cdot E) \quad (14)$$

The difference is the peak width in terms of the full width of the triangle; it is to a high degree of accuracy equal to:

$$\begin{aligned} \Delta t_{R,i} &= L/(\mu_{\text{eff},i}E) \cdot (\beta_{\text{EMD},i} \cdot c_{\text{max},i}/c_b) \\ &= t_{R,i} \cdot (\beta_{\text{EMD},i} \cdot c_{\text{max},i}/c_b) \end{aligned} \quad (15)$$

A difficulty left is that the description of resolution is usually based on the assumption of Gaussian peaks, while the peaks here are triangular. As in the introduction, we (roughly) take as  $\sigma_{\text{EMD},i}$  the square root of the second moment. The factor between  $\Delta t_{R,i}$  and  $\sigma_{\text{EMD},i}$  is, as stated before,  $\sqrt{18} \approx 4.243$ . Assuming (for the moment) that the freedom to allow peaks to be broad can be consumed entirely by the overloading, i.e. neglecting real dispersion, etc., one has:

$$\sigma_{\text{EMD},i} = \frac{1}{4.243} \Delta t_{R,i} \quad (16)$$

$$t_{R,i}/\sigma_{\text{EMD},i} = \sqrt{N_{\text{req}}} \quad (17)$$

leading to

$$c_{\text{max},i} = 4.243/(\sqrt{N_{\text{req}}} \cdot \beta_{\text{EMD},i}) \cdot c_b \quad (18)$$

Working via the second moment may provoke some doubts. Therefore, we also approach the matter more directly. It is generally recognized that resolution 4 (a distance of 4 standard deviations between the peak medians) gives acceptable separation. With two triangular peaks having the same sign and degree of shape deformation, Eq. 16 implies that with resolution 4, the

distance of the maxima is 4/4.243 times the full width of one zone. Thus, a few percent overlap occurs, as one would have with Gaussian zones with the same resolution. We therefore feel confident that the different shapes do not affect the validity of our conclusions.

Eq. 18, although not contradicting any intuitive guesses about the matter, is important as it allows some quite general conclusions:

1. The loadability in terms of concentration is directly proportional to the buffer concentration.
2. It is inversely proportional to the square root of the required plate number; the more difficult the separation, the smaller is the loadability.
3. Once one has determined the mobilities of the mixture components, and from that the required plate number, the loadability can be predicted 'ab initio', since with the methods described in the references mentioned,  $\beta_{\text{EMD},i}$  can be calculated.

The parameter  $\beta_{\text{EMD},i}$  allows to compare the usefulness of various buffer systems for separations where the compound  $i$  is critical: the smaller  $\beta_{\text{EMD},i}$  the better. Note that in  $\beta_{\text{EMD},i}$  the choice of the buffer concentration (by virtue of the 'relative' definition of it in Eq. 7), does not play a role. It is therefore necessary to discuss the choice of  $c_b$  separately.

#### Choice of buffer concentration $c_b$

In subsequent sections it will be discussed that often the product  $d_c^2 E^2 \kappa$ , where  $\kappa$  is the conductivity of the buffer solution, has to stay below an upper limit. In fact this product is a direct measure for the thermal dissipation in the lumen. Clearly,  $\kappa$  can be written as:

$$\kappa = \Lambda_b c_b \quad (19)$$

where  $\Lambda_b$  and  $c_b$  are the 'convenient measures' of the mean molar conductivity and concentration, respectively, of the buffer (in this paper, of the counter ion of the buffer).

The higher  $c_b$ , the higher  $c_{\max,i}$  can be, according to Eq. 18. However, high values for  $c_b$  preclude adjusting  $d_c$  and  $E$  to high values, when the product  $d_c^2 E^2 \kappa_b$  should not increase above an upper limit.

Therefore, at a given value of the electric field  $E$ , the maximum value of  $\kappa$ , and as a result, the maximum values of  $c_b$  and  $c_{\max,i}$ , are inversely proportional to  $d_c^2$ . Substituting this into Eq. 4 shows that *the production rate is unaffected by the choice of the buffer concentration*. What is gained in  $c_{\max,i}$  by higher buffer concentrations, is lost as a result of the smaller admissible  $d_c$  values. We note that Knox [16] reached quite another conclusion, which we believe is due to an incorrect assessment of the production rate.

Our conclusion holds, of course, only within reasonable limits. For instance, extremely high  $c_b$  values would require correspondingly high  $c_i$  values, which may be impossible due to limited solubility of a component  $i$ . Also, in very strong buffers the mobilities become unpredictable. On the other hand, extremely low  $c_b$  values would require large diameters for exploitation, which may be inaccessible due to gravity-induced convection and experimental limitations. Yet another exception occurs when siphoning effects become predominant (see below under 'Case III').

A final point is the influence of the conductivity, related to  $c_b$  via Eq. 19. The smaller the proportionality constant  $\Lambda_b$  the better, as this allows larger diameters at a given value for  $E$ . Thus the final 'figure of merit',  $\Gamma_{b,i}$ , for a buffer system for a solute  $i$  is not  $\beta_{\text{EMD},i}$ , but rather its product with the mean molar conductivity,  $\Lambda_b$ :

$$\Gamma_{b,i} = \beta_{\text{EMD},i} \cdot \Lambda_b. \quad (20)$$

As an example we provide in Table 1 data on the figure of merit of various buffer systems for the electrophoresis of a simple weak acid HZ with a  $\text{p}K_a$  of 4.7. It is supposed that the purification of HZ has to be carried out at a pH of 5. The buffers compared are of the anion–acid type (e.g. acetate–acetic acid), the cation–base type (e.g. ammonium–amine) and of the two basic–acid type, with different  $\text{p}K_a$  values.

The calculations show that an ideal buffer system of the anion–acid type exists in theory, giving no electromigration dispersion at all with a  $\text{p}K_a$  of approximately 4.5.

With a cation–base type of buffer there is always some electromigration dispersion; it can be minimized by choosing a buffer with a low  $\text{p}K_a$  value.

With the two basic–acid buffer the EMD is always relatively high; when this buffer is to be used a compound with a  $\text{p}K_a$  value of 5.3 gives the best results for this particular example. From Table 1 it is also clear that it is by no means straightforward to find the optimum buffer system for a cation.

### 2.3. Column design

#### *Choice of $d_c$ , $L$ and $E$ for cylindrical capillaries*

As stated in the introduction, the conductive removal of the heat electrically generated in the lumen forms one of the limitations to the production rate. How large a temperature rise in the liquid can be tolerated, however, is not straightforward. One also has to distinguish between the elevation of the mean temperature on one hand and the thermal gradients in the lumen on the other hand.

The average temperature elevation may give rise to thermal decomposition of solutes, loss in efficiency due to enhanced longitudinal diffusion and badly reproducible results when the heat exchange is not constant. Radial gradients in the lumen may give rise to loss in efficiency as a result of non-uniform migration [17,18], in extreme cases also via gravity-induced convection. The mode of thermostating and other experimental conditions determine which of the above effects will set the limit to the increase in  $d_c$  and  $E$ , desirable for improving the production rate. Treating all cases does not appear to be very useful. We will restrict the discussion to three cases, which in our opinion are the most appropriate, and broadly speaking, lead to the same conclusions. These are:

*Case I.* The average temperature elevation  $\Delta T_{\max}$  is the limiting factor.

Table 1  
Figure of merit  $\Gamma_b$  for the purification of a weak monobasic acid HZ

Type	Buffer $pK_a$	$I_a$ counter ion (mol/l)	$\Lambda_b$ [ $\Omega^{-1} m^{-1}$ ] /(mol/l)]	$\beta_{EMD,Aci}$	$\Gamma_b$ [ $\Omega^{-1} m^{-1}$ ] /(mol/l)]
HA/A1-	3.9	0.0278	11.5	2.02	23.51
HA/A1-	4.1	0.0266	11.5	1.05	12.20
HA/A1-	4.3	0.0250	11.5	0.42	4.89
HA/A1-	4.5	0.0228	11.5	0.01	0.20
HA/A1-	4.7	0.0200	11.6	-0.24	-2.78
HA/A1-	4.9	0.0167	11.6	-0.40	-4.69
HA/A1-	5.1	0.0133	11.6	-0.50	-5.90
HA/A1-	5.3	0.0100	11.6	-0.57	-6.69
HA/A1-	5.5	0.0072	11.6	-0.61	-7.20
HA/A1-	5.7	0.0050	11.6	-0.64	-7.56
HA/A1-	5.9	0.0034	11.7	-0.67	-7.84
HA/A1-	6.1	0.0022	11.7	-0.68	-8.09
B/BH1+	3.9	0.0022	11.7	1.20	14.12
B/BH1+	4.1	0.0034	11.6	1.21	14.18
B/BH1+	4.3	0.0050	11.6	1.23	14.33
B/BH1+	4.5	0.0072	11.6	1.25	14.60
B/BH1+	4.7	0.0100	11.6	1.29	15.06
B/BH1+	4.9	0.0133	11.6	1.36	15.80
B/BH1+	5.1	0.0167	11.5	1.46	16.97
B/BH1+	5.3	0.0200	11.5	1.62	18.84
B/BH1+	5.5	0.0228	11.5	1.87	21.78
B/BH1+	5.7	0.0250	11.5	2.27	26.39
B/BH1+	5.9	0.0267	11.5	2.89	33.59
B/BH1+	6.1	0.0278	11.5	3.85	44.72
B/BH1+	6.3	0.0286	11.5	5.32	61.67
HA-/A2-	3.9	0.0855	13.9	-31.60	-439.59
HA-/A2-	4.1	0.0832	13.8	-17.49	-242.41
HA-/A2-	4.3	0.0799	13.7	-9.92	-136.75
HA-/A2-	4.5	0.0754	13.6	-5.70	-77.93
HA-/A2-	4.7	0.0697	13.5	-3.34	-45.28
HA-/A2-	4.9	0.0632	13.3	-2.09	-27.90
HA-/A2-	5.1	0.0562	13.0	-1.50	-19.66
HA-/A2-	5.3	0.0497	12.7	-1.33	-17.10
HA-/A2-	5.5	0.0441	12.5	-1.48	-18.64
HA-/A2-	5.7	0.0396	12.2	-1.96	-24.17
HA-/A2-	5.9	0.0364	12.0	-2.92	-35.31
HA-/A2-	6.1	0.0341	11.9	-4.74	-56.61
HA-/A2-	6.3	0.0326	11.8	-8.54	-100.98

Conditions: Solute HZ with a  $pK_a$  of 4.7 at a buffer pH of 5.0. Total buffer concentration 0.03 mol/l. Ionic mobilities ( $10^{-9} m^2 s^{-1} V^{-1}$ ) are:  $\mu_{Z-} = -60$ ;  $\mu_{A-} = -50$ ;  $\mu_{BH+} = 50$ ;  $\mu_{A2-} = -75$ ,  $\mu_{counter-ion} = \pm 70$ .

*Case II.* The non-uniformity plate height contribution is dominant.

*Case III.* The siphoning contribution to the plate height is dominant.

*Case I.* Average temperature elevation limited to  $\Delta T_{max}$ , e.g., 10 K.

The average temperature elevation  $\Delta T$  is in first-order approximation proportional to the



square of the tube diameter and to the power density:

$$\Delta T = r_{\text{tot}} \cdot d_c^2 \cdot A_b c_b E^2 \quad (21)$$

where the proportionality constant  $r_{\text{tot}}$  is the heat transfer resistance. As treated in some detail by Knox and Grant [18] and Grushka et al. [19],  $r_{\text{tot}}$  is built up of three main contributions, corresponding to the heat transfer resistance of the lumen, the wall and the surrounding thermostating medium:

$$r_{\text{tot}} = r_{\text{lum}} + r_{\text{wall}} + r_{\text{thm}} \quad (22)$$

As shown by many workers [16,17,19],  $r_{\text{lum}}$  and  $r_{\text{wall}}$  can be easily predicted:

$$r_{\text{lum}} = 1/(16k_s) \quad (23)$$

$$r_{\text{wall}} = 1/(8k_{\text{wall}}) \cdot \ln(d_o/d_c) \quad (24)$$

Here  $k_s$  and  $k_{\text{wall}}$  are the thermal conductivities of the solution and wall, respectively, and  $d_o$  is the outer diameter of the tube.

Unfortunately,  $r_{\text{thm}}$ , which is by far the largest contribution in practice (see e.g., discussion by Ermakov and Righetti [20]), cannot be calculated easily. It depends on the diameter of the tube, and in a complicated fashion on the flow regime and the properties of the thermostating fluid. It is therefore probably better to approach the matter from the experimental point of view. Since  $\Delta T$ -values are experimentally easily accessible via the voltage–current ratio, there are various sources of data on this point.

Bruin et al. [21] found an experimental value of  $r_{\text{thm}} = 4.2$ , using air thermostating and capillaries of 50  $\mu\text{m}$  I.D. and 335  $\mu\text{m}$  O.D., while Nielsen et al. [22] found a value of  $r_{\text{thm}} = 4.1$  with forced air convection and capillaries of 75  $\mu\text{m}$  I.D. and 360  $\mu\text{m}$  O.D.

Standard texts on heat transfer [23,24], as well as the discussions by Knox et al. [16,25], make clear that a constant value for  $r_{\text{thm}}$  (i.e. a constant Nusselt number [24–26]) is very unlikely. It could only occur when heat transport by pure conduction in the thermostating fluid takes place over a distance having a fixed proportion to the tube diameter. The fluid moves either because of the thermostating fan or by natural,

gravity-induced convection. The larger the diameter and/or the fluid velocity, the more heat is transported by convection and the smaller will be the  $r_{\text{thm}}$  values.

Although there are useful treatments of these effects available in chemical engineering science, these are not used in this paper. The reason is that we believe that the thermal conditions of a CE capillary are much too complicated to make such a treatment useful. The most important point here is the longitudinal non-uniformity. Two parts of the tubes (in the buffer vials) are in fact liquid-thermostatted, three parts at least (in both vials and in the detector) are in stagnant air and the remainder is in an air or liquid bath with a flow being non-uniform in intensity and direction across the tube length. In some instruments even half of the capillary may not be under proper thermostating. Longitudinal gradients, likely in all CE equipment with liquid- or air-thermostating, affect the electroosmotic flow, thereby inducing parabolic components in the velocity and giving rise to additional non-uniformity dispersion [27,28].

We shall work in the sequel with a constant value of 5.0 K/(W/m) for  $r_{\text{tot}}$ , a rough average of experimental values.

Eq. 22 can be then solved for the maximum  $d_c$  allowed when temperature increase is limiting:

$$d_c^2 = \Delta T_{\text{max}}/5.0/(E^2 A_b c_b) \quad (25)$$

Since the production rate is proportional to  $d_c^2 E$ , it will be inversely proportional to  $E$  and therefore increase with  $t_R^{1/2}$  when the maximum voltage is applied:

$$T_{i,\text{thm}} = E \cdot E^{-2} \approx \text{const.} \cdot E^{-1} \approx \text{const.} \cdot t_R^{1/2} \quad (26)$$

Summarizing, it is, irrespective of the conductivity of the buffer, always better to work at low electric fields and long run times, which allows large diameters, such that the larger  $d_c^2$  more than compensates the smaller  $E$ .

A strategy blindly following this conclusion, however, could lead into the range where the non-uniformity  $H$ -contribution predominates dispersion.

*Case II. Non-uniformity plate height contribution becomes dominant.*

The expression for the plate height with non-uniform migration velocity caused by radial temperature differences within the solutions has been derived by several authors [17–19,29], and can be written as

$$H_{\text{nu}} = \frac{1}{384} \frac{d_c^2 \Delta u_i^2}{D_i u_i} \quad (27)$$

where  $D_i$  is the diffusion coefficient of  $i$ , and  $\Delta u_i$  is difference in migration velocity over the parabolic profile between centre and wall region.

The latter quantity is equal to:

$$\begin{aligned} \Delta u_i &= \delta_i \cdot \Delta T_{\text{lum}} \cdot \mu_i E \\ &= \delta_i d_c^2 \Lambda_b c_b E^3 \mu_i / (16k_s) \end{aligned} \quad (28)$$

where  $\delta_i$  is the relative change in mobility per degree Kelvin. Substitution leads to

$$H_{\text{nu}} = \frac{1}{98\,304} \cdot \frac{\delta_i^2 (\Lambda_b c_b)^2}{D_i k_s^2} \cdot \mu_i \cdot d_c^6 \cdot E^5 \quad (29)$$

The total plate height equals:

$$H_{\text{tot}} = 2D_i/u_i + H_{\text{nu}} = 2D_i/(E\mu_i) + H_{\text{nu}} \quad (30)$$

The requirement to have  $N$  plates necessitates a length equal to  $N \cdot H$ . The length is also tied up to the field strength and the total voltage across the tube:  $\Delta V = L \cdot E$ . The voltage may be a limiting factor; 20 000 V is as taken as an (arbitrary) practical upper limit. The result,  $N \cdot H = \Delta V/E$ , leads with Eqs. 32 and 33 to an expression that can be solved for  $d_c$ . When the peak-height contribution of the axial diffusion is included, the maximum value of  $d_c^2$  can be expressed as:

$$d_c^2 = \left( \frac{\Delta V}{N_{\text{req}}} - \frac{2D_i}{\mu_i} \right)^{1/3} \left( \frac{98\,304 D_i k_s^2}{\delta_i^2 \Lambda_b^2 c_b^2 \mu_i} \right)^{1/3} / E^2 \quad (31)$$

When the required plate number is not close to the limiting value, the  $2D_i/\mu_i$  term in Eq. 31 is negligible.

Surprising in Eq. 31 is that the allowable diameter is simply inversely proportional to the applied electric field. The first factor at the right

hand side of Eq. 34 reflects the concept of the ‘ultimate plate number’, given for CZE by  $\Delta V \cdot \mu_i / (2D_i)$ , as discussed by Knox [16] and Kennedler and Schwer [30]. When the required  $N$  approaches this number, the difference given approaches zero; there is no ‘room’ for allowing any non-uniformity  $H$ -contribution and the diameter must go to zero (it does so slowly, though, because of the 1/6 exponent). When the difference becomes negative, the separation is impossible.

The production rate  $T_i$ , being proportional to  $d_c^2 c_b E$ , is in this case inversely proportional to the field strength  $E$  and therefore increasing with  $t_R^{1/2}$ . However, Eq. 31 shows that now  $T_i$  increases with  $c_b^{1/3}$ . When the average temperature increase of the solution was the limiting factor (Case I), the buffer conductivity could be traded in for the capillary cross-section without consequences for the production rate. In the case that the zone broadening by temperature differences in the solution is the limiting factor (Case II), the production rate can be increased by using more concentrated buffers in narrower capillaries. The gain in  $T_i$  is not strong, going up with  $c_b^{1/3}$  only.

It must be noted, as has been done before by Knox and Grant [16] and Ermakov and Righetti [20], that this contribution to  $H$  is usually not of large significance: before it could really become important, the buffer often boils.

*Case III. Siphoning contribution to the plate height becomes dominant.*

The above expressions point to the use of longer run times and lower fields, which permits to use larger capillary diameters, with an improvement in production rate in proportion to the square root of  $t_R$ . Some other limitations then come in sight. One could be the development of gravity-induced natural convection due to density differences in the thermally non-uniform liquid, a phenomenon that plagued electrophoretic experiments in free solution in the early days [31]. Before this happens, however, the longitudinal siphoning flow in the tube resulting from the unavoidable hydrostatic pressure imbalance may spoil the separation. In the following

we will assume that 1 mm ‘water head’ ( $\Delta P = 10$  Pa) pressure difference will be unavoidable.

The mean solvent velocity induced by siphoning,  $v_{\text{sip}}$ , follows from the Poisson equation:

$$v_{\text{sip}} = \frac{d_c^2 \Delta P}{32 \eta L} \quad (32)$$

The parabolic velocity profile, superimposed on the regular electrophoretic migration, will again lead to an Aris–Taylor-type dispersion effect. Following a similar reasoning as used in Refs. [17,18,29], we find for the plate height contribution by siphoning:

$$H_{\text{sip}} = \frac{d_c^6 \Delta P^2}{98\,304 \eta^2 L^2 D_i E \mu_i} \quad (33)$$

In a way similar to what we have done in Case II a maximum capillary diameter can be found:

$$d_c = \left( \frac{1}{N_{\text{req}}} - \frac{2D_i}{\Delta V \mu_i} \right)^{1/6} \left( \frac{98\,304 \eta^2 \Delta V^3 D_i \mu_i}{\Delta P^2 E^2} \right)^{1/6} \quad (34)$$

As in Eq. 31, the diffusion term  $2D_i/(\Delta V \mu_i)$  in the right-hand side of Eq. 34 often can be neglected.

The equation shows that the allowable diameter is proportional to  $E^{-1/3}$ . The production rate  $T_i$ , being proportional to  $E d_c^2$ , goes up with  $E^{1/3}$ , quite contrary to what happens in Cases I and II, where a beneficial effect of a low electric field was predicted. Since siphoning does not depend on the conductivity  $\kappa$  of the solution, in this case the production rate simply increases with  $c_b$ .

### Combination of three limitations Circular capillaries

Depending on the conditions, one, two or in exceptional cases all three of the limitations are in effect. As each limitation in the above sections was expressed in terms of the maximum value of  $d_c$  compatible with the preset requirements on  $t_R$  and  $N$ , the limitation leading to the smallest  $d_c$  value determines the ultimate production rate.

In Figs. 1 and 2 we have plotted the maximum diameters, according to Eqs. 25, 31 and 34,

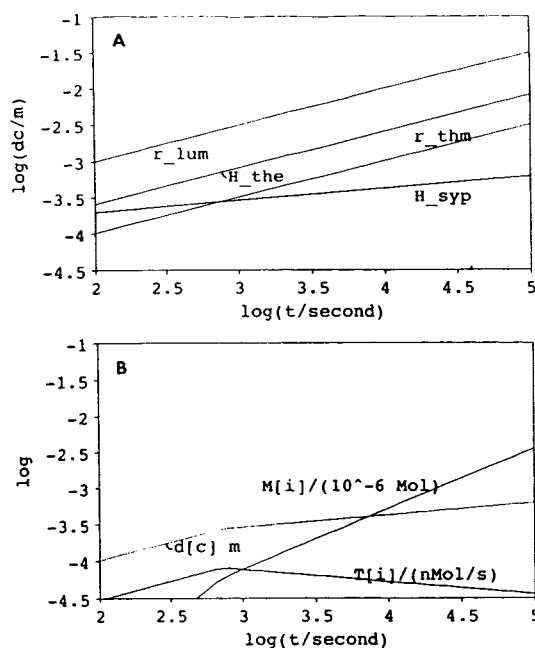


Fig. 1. (A) Maximum diameters for a circular capillary ( $\log d_c/m$ ), according to Eqs. 25, 31 and 34. Conditions: required plate number  $N = 200\,000$ .  $\Delta V = 20$  kV,  $c_b = 0.003$ ,  $\beta_{\text{EMD},i} = 0.1$ ,  $\Delta P = 10$  Pa and  $\Delta T_{\text{max}} = 10$  K,  $\mu_i = 30 \cdot 10^{-9} \text{ m}^2 \text{ s}^{-1} \text{ V}^{-1}$ ,  $D_i = 10^{-9} \text{ m}^2/\text{s}$ ,  $\eta = 10^{-3} \text{ kg m}^{-1} \text{ s}^{-1}$ ,  $\delta_i = 0.023$ ,  $r_{\text{thm}} = 5.0 \text{ K}/(\text{W}/\text{m})$ . Line indicators: ‘ $r_{\text{lum}}$ ’: maximum diameter to keep  $\Delta T$  in lumen below 10 K; ‘ $H_{\text{the}}$ ’: maximum diameter to keep plate height due to thermal non-uniformity sufficiently low to obtain required plate number (Eq. 34); ‘ $r_{\text{thm}}$ ’: maximum diameter to keep  $\Delta T$  in air bath below 10 K; ‘ $H_{\text{syp}}$ ’: maximum diameter to keep plate height due to siphoning sufficiently low to obtain required plate number (Eq. 37). (B) Production rate  $T_i$  (plotted as  $\log[T_i/(\text{nmol}/\text{s})]$ ), amount in single run,  $M_i$ , (plotted as  $\log M_i/\mu\text{mol}$ ) and maximum diameter  $d_c$  [plotted as  $\log(d_c/m)$ ] as a function of run time.

found for conditions and requirements that appeared appropriate:  $\Delta V = 20$  kV,  $c_b = 0.003$ ,  $\beta_{\text{EMD},i} = 0.1$ ,  $\Delta P = 10$  Pa and  $\Delta T_{\text{max}} = 10$  K, with (overall) mobility of  $\mu_i = 30 \cdot 10^{-9} \text{ m}^2 \text{ s}^{-1} \text{ V}^{-1}$ .

The diffusion coefficient  $D_i$  was taken as  $10^{-9} \text{ m}^2/\text{s}$ , and the viscosity as  $10^{-3} \text{ kg m}^{-1} \text{ s}^{-1}$ , while  $\delta_i$  was assumed to be 0.023.

Fig. 1 applies to the case when  $N = 200\,000$  plates are required, close to the theoretical limit of 300 000 for  $\Delta V = 20\,000$  V. In Fig. 1A it is seen that the two limitations of importance are those

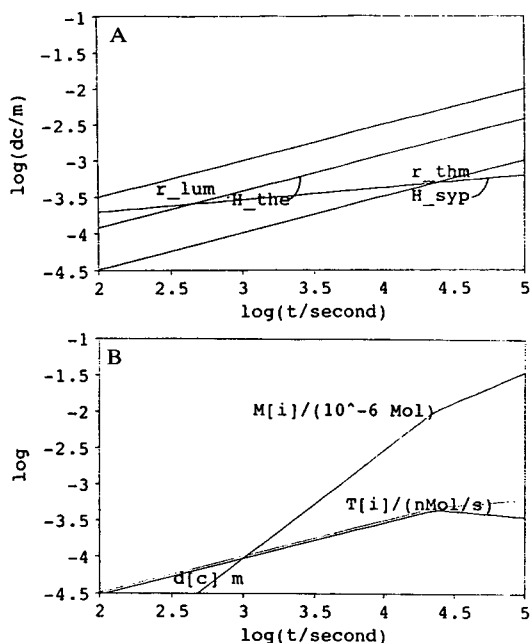


Fig. 2. (A) Maximum diameters, for a circular capillary, according to Eqs. 25, 31 and 34. Conditions:  $c_b = 0.03$ . Other conditions as in Fig. 1. (B) As in Fig. 1.

of the absolute temperature increase (' $r_{thm}$ '), set here at 10 K, and the siphoning effect (' $H_{sip}$ '). The first limitation is important at fast runs at high field, forcing the use of small diameters, the second being important at long run times and weak fields, with corresponding increase in admissible diameters. The 'break-even' point lies at  $t_R = 800$ , corresponding to a field  $E$  of 30 000 V/m, with a diameter  $d_c$  of 280  $\mu\text{m}$  and a tube length of 0.7 m.

As explained above, when accepting longer run times, one enters the range of the siphoning limitation. The admissible diameter goes up with  $t_R$  only slowly, not fast enough to compensate for the slower operation of the system. As can be seen in Fig. 1B, from the break-even point on the production rate goes down, although the production per run keeps increasing at a slower pace. In this realm it is better to repeat faster runs, rather than to try to devise an experiment where the required material can be collected in one run.

It is important to be aware of the strong

dependence of these relations on the parameters chosen for the calculations. The most important one is probably the  $c_b$  value, for which a rather low value was chosen here (0.003 mol/l). A ten times higher value would move down the ' $r_{thm}$ '-line in Fig. 1A over half a log unit. When the choice would have been to work at the lower end of the  $t_R$  scale, left of the 'break-even' point (rather close to common CE-conditions), the net effect would be zero: Although the diameter goes down, this is exactly compensated by the larger concentration loadability of the more concentrated buffer.

However, the ' $H_{sip}$ ' line would stay in the same position. The 'break-even' point therefore would move to higher  $t_i$  values. This is shown in Fig. 2 where a ten times higher buffer concentration was chosen than in Fig. 1. A higher maximum production rate is found when the time required for a simple run is not limited and the optimum value of the capillary length can be used, the production rate increases with  $c_b^{3/4}$ . The final limit of the production rate in this case will be set by changes of the selectivities found in high-ionic strength solutions or by the limited solubility of the buffer or the analyte.

Another parameter with a strong influence is  $\beta_{EMD,i}$ . The assumed value, 0.1, is about the best one can expect under carefully tuned buffering conditions. Since the production rate is directly proportional to its inverse, the absolute values of  $T_i$  and  $M_i$ , as given in the figures, can turn out to be much smaller in practical situations, e.g., where the buffer choice has not been carried out with extreme care, or when it is simply impossible to tune the buffer to the requirements in various critical parts of the electropherogram.

In Fig. 3 the results are shown when a lower value (50 000) for the required plate number is assumed. Compared to Fig. 1, the lines representing the limitations on  $d_c$  have moved up, that for the temperature increase more strongly than that for the siphoning effect. As a result, the 'break-even' point has moved to the right. The maximum production rate is increased with a factor of approximately seven, obtained at an optimal run time for a single run, which is approximately three times longer. This increase

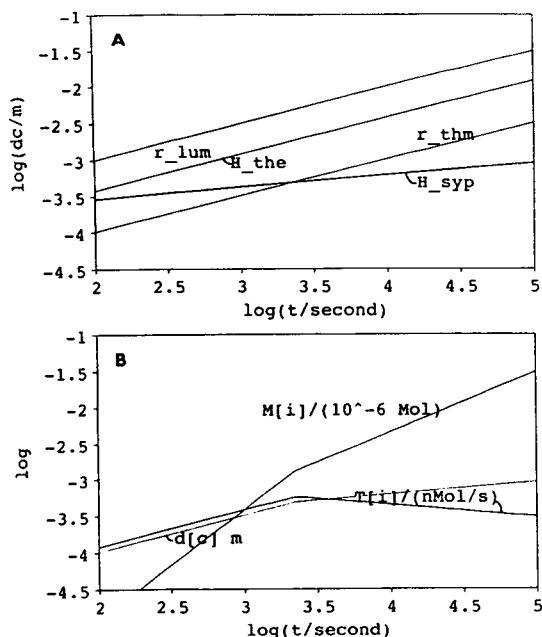


Fig. 3. (A) Maximum diameters, for a circular capillary, according to Eqs. 25, 31 and 34. Conditions: required plate number  $N = 50\,000$ . Other conditions as in Fig. 1. (B) As in Fig. 1.

of  $T_i$  with the looser demands on the separation sharpness can be explained by two factors. First, the maximum concentration of the analyte as well as the peak volume are increased, both proportional with  $N^{-1/2}$ , as has been shown in previous sections. This gives already a factor of four in the production rate going from 200 000 to 50 000 for  $N_{\text{req}}$ . The second factor is the shift of the maximum towards the more advantageous low fields and long run times. This generally gives an extra gain proportional to  $N^{-1/4}$ . In this particular example the gain is even larger because with  $N_{\text{req}} = 200\,000$  the allowed plate height is partially already consumed by the axial diffusion term.

#### Rectangular ducts.

The cylindrical configuration is experimentally convenient. However, from the point of view of heat conduction it is the worst configuration possible. For all of the three main resistances to heat transfer, i.e., in the lumen (lum), the wall

and the thermostating medium (thm), the Nusselt number is larger [28] for flat rectangular ducts having the same cross-sectional area. Thus, all of the above conclusions apply equally well to such a design, with suitable adjustment of the constants.

The thermal effects and dispersion in so-called rectangular (rather ellipsoidal) fused-silica capillaries have been studied theoretically [32–34], as well as experimentally [27,35]. In such a channel, with dimensions  $2a$  by  $2b$ , with  $a < b$  and  $\phi = b/a$ , the thermal effect ('r\_lum') and the dispersion connected with it ('H\_the') are controlled [32–34] mainly by the height of the channel, i.e.  $2a$ . This provides an important feature of the rectangular columns compared to the circular tubing, since by increasing the width,  $b$ , of the rectangular capillary while keeping the height,  $a$ , constant, the sample capacity is improved without affecting the efficiency due to thermal effects. Moreover, by keeping the same height,  $a$ , the heat dissipation remains constant, which allows to maintain the same separation voltage, without losing analysis speed.

In Fig. 4 the mean temperature rise in the lumen for a circular and a rectangular column against the electric field is shown. The temperature rise was calculated from the variation between the experimental electric current and the

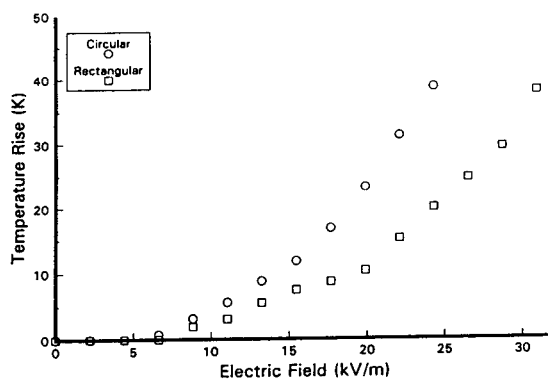


Fig. 4. Temperature rise against the electric field for a circular and a rectangular capillary (modified from Ref. [25]). Conditions: 0.05 M 3-(cyclohexylamino)-1-propanesulfonic acid (CAPS) buffer, pH 10.4. Capillaries: circular 200  $\mu\text{m}$  I.D. and rectangular 500  $\times$  50  $\mu\text{m}$ , both with the same total length (90.5 cm).

hypothetical one that would be obtained if no thermal effects were present, and assuming that a 2% variation in the electric current is equivalent to a temperature rise of 1 K. Results show that the temperature rise is larger in the circular capillary than in the rectangular one. This is partly due to the larger cross-sectional area of the circular column (25% larger). However, at higher voltages the difference in current is much larger than 25%. Also, Fig. 4 demonstrates that for the same temperature rise the rectangular capillary allows a higher run voltage. Moreover, the higher the voltage applied, the larger the difference between both capillaries.

In view of these promising experimental results, we found it attractive to repeat the exercises documented in Fig. 1 for parameter values that appear to apply to such rectangular ducts. We assumed rectangular cross-sections (although they were in reality not quite so) and applied the numerical values found in Ref. [34] for the non-uniformity dispersion, the pressure-induced flow and the dissipation-induced temperature rise in the lumen. Equations equivalent to Eqs. 25, 31 and 34 allowed us to calculate the effects denoted by 'r\_lum', 'H\_the' and 'H\_sip' for such channels.

For the air-bath temperature drop, 'r\_thm', we had to make a similar wild guess as we were forced to make in the case of circular tubes. Based on our own results, we decided to use  $r_{thm} = 5.0 \text{ K}/(\text{W}/\text{m})$ , equal to the value assumed for circular ones. It is likely that the value in fact could be lower, but this choice has the additional advantage that there is no ill-justified bias towards the rectangular geometry.

The results are shown in Figs. 5 and 6. For  $d_c$  we used 'equivalent' values, i.e.  $d_c$  is the diameter of a circular tube having the same cross-sectional area. In Fig. 5 the width-to-height ratio was 10, close to the value estimated for the ellipsoidal capillaries ( $50 \times 500 \mu\text{m}$ ) used in some of our earlier experiments [28].

Comparison of this figure with Fig. 1 in the first place shows that the limiting factors 'r\_thm' and 'H\_sip' are the same. With the choice of  $r_{thm}$  being equal, the 'r\_thm' branches in the plots are identical; for the outside dissipation the geome-

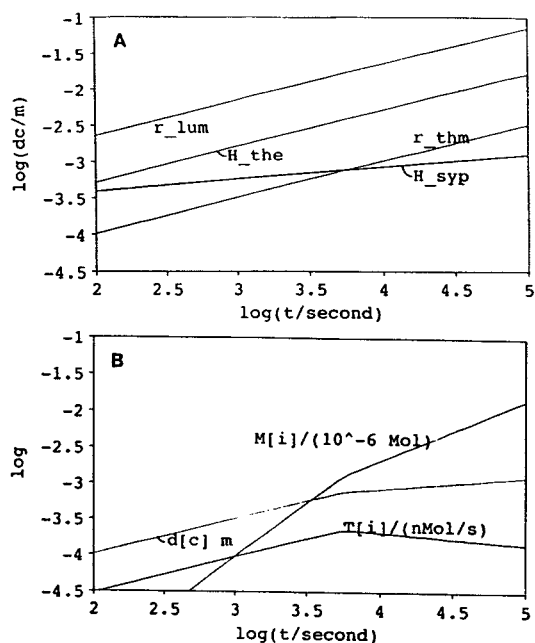


Fig. 5. (A) Maximum equivalent diameters,  $d_c = \sqrt{4/\pi}$  area, for a rectangular capillary, according to Eqs. 25, 31 and 34. Conditions: required plate number  $N = 200\,000$ . Width to height ratio of rectangular channel  $\phi = 10$ . Other conditions as in Fig. 1. (B) As in Fig. 1.

try of the inner channel is not important. Thus, on the left side all the plots are identical. The 'H\_the' plot lies at higher values for the rectangular tubes (as elaborately discussed in Ref. [34]), but that is irrelevant since this effect never sets a limit to the production rate.

The difference between Fig. 5 on the one hand and Fig. 1 on the other resides in the smaller influence of the siphoning effect. The low flow permeability of the flattened channel, leading to small velocities at the head pressure of 10 Pa, allows to go to larger areas (equivalent  $d_c$ ) without serious deterioration of the efficiency. For instance, in Fig. 5A it can be seen that the 'break-even' point between 'r\_thm' and 'H\_sip' is at about  $t_R = 6000 \text{ s}$ , with ' $d_c$ ' =  $700 \mu\text{m}$ , while for a circular capillary the values are  $t_R = 800 \text{ s}$  and  $d_c = 250 \mu\text{m}$ . An improvement of about a factor of three in the production rate  $T_i$  is the result. It should be noted that ' $d_c$ ' here is an

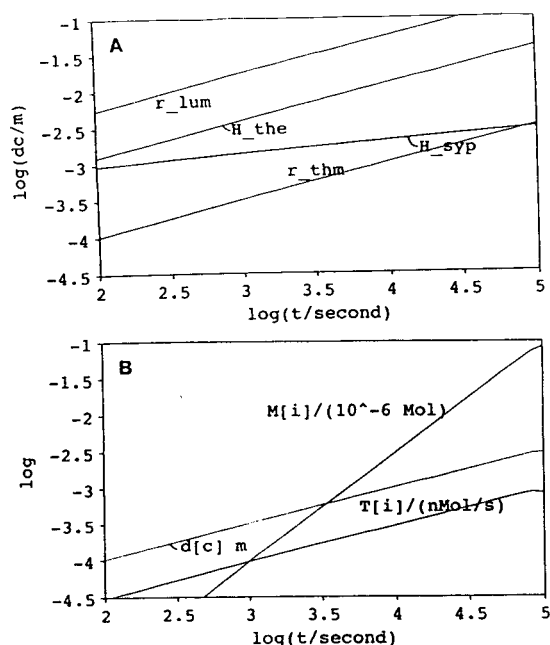


Fig. 6. (A) Maximum equivalent diameters,  $d_c = \sqrt{4/\pi}$  area, for a rectangular capillary, according to Eqs. 25, 31 and 34. Conditions: required plate number  $N = 200\,000$ . Width to height ratio of rectangular channel  $\phi = 64$ . Other conditions as in Fig. 1. (B) As in Fig. 1.

'equivalent' value;  $700\ \mu\text{m}$  corresponds for  $\phi = 10$  to dimensions of about  $200 \times 2000\ \mu\text{m}$ .

In Fig. 6 it is shown that a further increase of the production rate can be obtained when rectangular capillaries with  $\phi = 64$  were available. However, the predicted optimum in  $T_i$  lies rather far away from contemporary CE conditions, with a run time of  $80\,000\ \text{s}$  and a capillary height and width of  $340$  and  $22\,000\ \mu\text{m}$ . It is doubtful whether the extrapolation of our insights in CE behaviour to such dimensions is justified. Certainly, experimental work would be needed to verify this.

### 3. Conclusions

This work was undertaken in order to derive general guidelines for optimization of CE, under the constraint of a fixed required plate number,

when production per time unit is important. It is therefore appropriate to summarize the conclusions, and to indicate further research directions. The most important aspect is the choice of the background electrolyte (BGE). With acid-base-type sample constituents (the majority of the cases), manipulation of the pH can lead to the best 'selectivity' (ratio of mobilities), for which the required plate number is as low as possible. Production rate is directly proportional to  $1/N$ . When the pH has been decided upon, it may be worthwhile to investigate various buffer systems with this pH value, in order to keep the electromigration dispersion (EMD) as low as possible. A low EMD allows the use of high concentration loads. Analytical expressions as well as numerical procedures are available to predict EMD. The optimization of the geometry amounts to increasing the diameter as far as possible. At low accepted run times, using short tubes, this is limited by the absolute temperature rise in the lumen. Accepting longer run times it is possible to increase the diameter, and to improve the production rate, roughly by a factor of  $\sqrt{10}$  for a ten times longer run time. This approach finds, as far as we can see, its end when the siphoning in wider tubes affects the efficiency significantly. The point where this happens is in the range of practical CE conditions for high plate numbers and low buffer concentrations. For small plate numbers and higher buffer concentrations the points lie outside the range where predictions about CE conditions are believed to be reliable.

Keeping within the realistic range, the theoretical results for a preparative CE system can be compared with those obtained in a typical analytical-scale CE system. As has been pointed out in the introduction, in an analytical system with a  $0.03\ \text{mol/l}$  buffer concentration, typically  $8 \cdot 10^{-12}\ \text{mol}$  of analyte can be purified in 10 min, giving a production rate of approximately  $10^{-14}\ \text{mol/s}$ . With the same buffer concentration in Fig. 2B a maximum production rate of  $5 \cdot 10^{-13}$  is predicted, a factor of 50 higher than for the analytical system. The time for a single run to obtain this result is approximately 6 h.

Rectangular or ellipsoidal shaped capillaries have important promises for the increase of

sample capacity and production rate. The main reason is that the smaller flow permeability (for the same area) allows to increase the area without development of pressure-induced flow. If conditions can be found where external heat transfer is also better in these capillaries, the prospects would be even better.

## References

- [1] J.W. Jorgenson and K.D.A. Lukacs, *Anal. Chem.*, 53 (1981) 1298–1302.
- [2] R.P.W. Scott and P. Kucera, *J. Chromatogr. Sci.*, 12 (1974) 473–485.
- [3] A. Guttman, A.S. Cohen, D.N. Heiger and B.L. Karger, *Anal. Chem.*, 62 (1990) 137–141.
- [4] D.J. Rose and J.W. Jorgenson, *J. Chromatogr.*, 438 (1988) 23–29.
- [5] C. Schwer and F. Lottspeich, *J. Chromatogr.*, 623 (1992) 345–355.
- [6] K.D. Altria and Y.K. Dave, *J. Chromatogr.*, 633 (1993) 221–225.
- [7] A.W.J. de Jong, H. Poppe and J.C. Kraak, *J. Chromatogr.*, 148 (1978) 127–141.
- [8] F.E.P. Mikkers, F.M. Everaerts and Th.P.E.M. Verheggen, *J. Chromatogr.*, 169 (1979) 1–10.
- [9] F. Foret, S.F. Ossicini and P. Bocek, *J. Chromatogr.*, 470 (1989) 299–308.
- [10] J.L. Beckers, *J. Chromatogr. A*, 693 (1995) 347.
- [11] H. Poppe, *Anal. Chem.*, 64 (1992) 1908–1919.
- [12] X. Xu, W.T. Kok and H. Poppe, in preparation.
- [13] S.V. Ermakov, M.Y. Zhukov, L. Capelli and P.G. Righetti, *Anal. Chem.*, 66 (1994) 4034.
- [14] F. Helfferich and G. Klein, *Multicomponent Chromatography*, Marcel Dekker, New York, 1970.
- [15] F.E.P. Mikkers, F.M. Everaerts and Th.P.E.M. Verheggen, *J. Chromatogr.*, 169 (1979) 11–20.
- [16] J.H. Knox, *Chromatographia*, 26 (1988) 329–337.
- [17] R. Virtanen, *Acta Polytech. Scand.*, 123 (1974) 1–67.
- [18] J.H. Knox and I.H. Grant, *Chromatographia*, 24 (1987) 135–143.
- [19] E. Grushka, R.M. McCormick and J.J. Kirkland, *Anal. Chem.*, 61 (1989) 241–246.
- [20] S.V. Ermakov and P.G. Righetti, *J. Chromatogr. A*, 667 (1994) 257.
- [21] G.J.M. Bruin, P.P.H. Tock, J.C. Kraak and H. Poppe, *J. Chromatogr.*, 517 (1990) 557–572.
- [22] R.J. Nielsen, A. Paulus, A.S. Cohen, A. Guttman and B.L. Karger, *J. Chromatogr.*, 480 (1989) 111–127.
- [23] R.H. Perry and C.H. Chilton, *Chemical Engineers' Handbook*, McGraw-Hill, Tokyo, 1973.
- [24] S.T. Hsu, *Engineering Heat Transfer*, Van Nostrand, New York, 1963.
- [25] J.H. Knox and K.A. McCormack, *Chromatographia*, 38 (1994) 215–221.
- [26] R. Hilpert, *Forsch. Gebiete Ingenieurw.*, 4 (1933) 215.
- [27] J.K. Towns and F.E. Regnier, *Anal. Chem.*, 64 (1992) 2473–2478.
- [28] A. Cifuentes and H. Poppe, *Electrophoresis*, in press.
- [29] G.D. Roberts, P.H. Rhodes and R.S. Snyder, *J. Chromatogr.*, 480 (1989) 35.
- [30] E. Kenndler and C. Schwer, *Anal. Chem.*, 63 (1991) 2499–2502.
- [31] S. Hjertèn, *Chromatogr. Rev.*, 9 (1967) 122–219.
- [32] R. Aris, *Proc. Roy. Soc. A*, 252 (1959) 538–550.
- [33] M.J.E. Golay, *J. Chromatogr.*, 216 (1981) 1–8.
- [34] A. Cifuentes and H. Poppe, *Chromatographia*, 39 (1994) 391–404.
- [35] Z. Ryšlavy, P. Boček, M. Deml and J. Janák, *J. Chromatogr.*, 144 (1977) 17.



# Analysis of protein fractions by micropreparative capillary isoelectric focusing and matrix-assisted laser desorption time-of-flight mass spectrometry

F. Foret<sup>1</sup>, O. Müller, J. Thorne, W. Götzinger, B.L. Karger\*

*Barnett Institute, Northeastern University, Boston, MA 02115, USA*

---

## Abstract

In this study, the use of capillary isoelectric focusing (cIEF) as a micropreparative tool for protein analysis by matrix-assisted laser desorption time-of-flight mass spectrometry (MALDI-TOF-MS) is demonstrated. A newly designed, automated, collection interface equipped with a fiber-optic UV detector and a sheath flow connection was employed for collection of protein fractions. Multiple fractions were collected during a single cIEF run and further analyzed by MALDI-TOF-MS for mass assignment. The feasibility of the method was tested with a mixture of model proteins with different isoelectric points and molecular masses, and with variants of human hemoglobins differing in  $pI$ , but with negligible difference in  $M_r$ . Some practical considerations of the collection procedure and subsequent TOF analysis are presented.

---

## 1. Introduction

Capillary isoelectric focusing (cIEF), as originally introduced by Hjertén and Zhu [1], is an important tool for the analysis and characterization of proteins. Recently, cIEF has become a rugged technique for fast, highly efficient separation of minute amounts of samples [2–5]. Since the quantity of sample used for cIEF matches the requirement for modern peptide mapping, sequencing procedures and mass spectrometric analysis [6], cIEF can be an attractive purification tool. The coupling of this CE approach with mass spectrometry is especially interesting, given the potential for fast analysis, high sensitivity

and high accuracy of the mass determination. In addition, structural information can be obtained through MS–MS experiments [7].

In this work, the feasibility of off-line coupling capillary isoelectric focusing with matrix-assisted laser desorption time-of-flight mass spectrometry (MALDI-TOF-MS) is investigated. In principle, an advantage of the off-line arrangement is that only part of the collected fraction may be necessary for the MS analysis while the rest can be used for further analysis. Alternatively, on-line procedures may also be considered.

cIEF has two inherent advantages for this application. First, the cIEF separation is not affected by the molecular mass of the separated molecules. Differences in the isoelectric points of the proteins are the sole basis for the separation. The coupling of cIEF to MALDI-TOF-MS therefore represents a true orthogonal method,

---

\* Corresponding author.

<sup>1</sup> On leave from the Institute of Analytical Chemistry, Brno, Czech Republic.

the latter of which separates on the basis of the mass, where singly (or doubly) charged species are generally obtained in the vapor phase. A second advantage of cIEF stems from its concentrating capabilities, since the entire volume of the capillary can be filled with the sample–ampholyte mixture. During focusing, individual proteins form narrow zones with concentrations orders of magnitude higher than in the original sample, which can be exploited for preparative purposes.

In current practice, cIEF is a two-step process [1–5]. First, a pH gradient with sample proteins focusing at the point where they have no net charge ( $\text{pH} = \text{pI}$ ) is established. During this step, the current drops to 10% or less of the initial value. Second, mobilization of the focused zones past the detection point takes place with the applied field on. (Focusing and mobilization have sometimes been combined into one step.) Several different mobilization procedures have been described, including the use of salt and/or zwitterions [8], electroosmotic [9] and/or pressure [5] flow. In this work, we have utilized pressure mobilization with no electroosmotic flow; after the focusing step the content of the capillary is forced to move by lifting the anodic end of the separation column. High voltage simultaneously counter-balances zone broaden-

ing due to the parabolic flow profile [5]. The advantage of the pressure mobilization approach is that all zones move with the same velocity which leads to a linear change in pH with time.

Since the resolving power of cIEF is high [10], care must be taken to use an interface that maintains this resolving potential. In this study we have used an off-line combination utilizing our recently developed collection interface for CE [11]. This design includes a sheath liquid at the exit of the CE capillary to transport the sample zones into collection capillaries. The sheath liquid allows maintenance of the electric field while pressure mobilization occurs. After collection, the selected protein fractions are mixed with the MALDI matrix and subjected to TOF-MS analysis.

## 2. Experimental

### 2.1. Capillary isoelectric focusing

cIEF was performed with a laboratory-made instrument consisting of a high-voltage power supply (CE 1000, Spellman, Plainview, NY, USA) and a collection interface with an UV detector, as described below (Fig. 1). Fused-silica capillaries of 40 cm  $\times$  360  $\mu\text{m}$  O.D.  $\times$  75

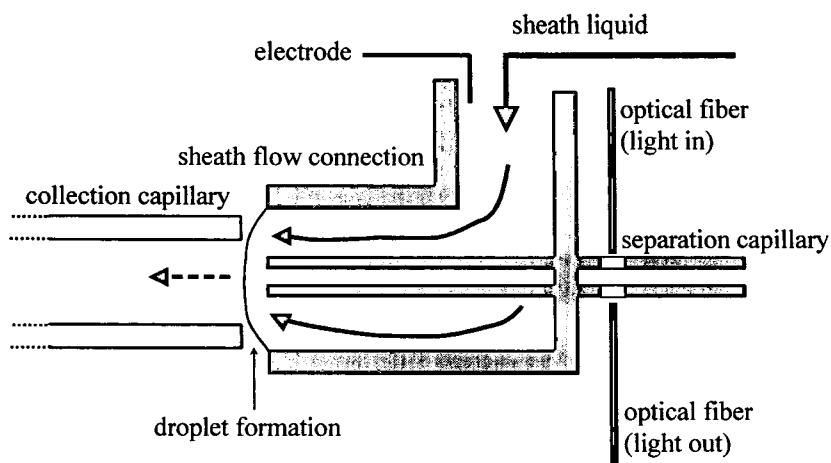


Fig. 1. Schematic diagram of the sheath flow interface consisting of a sheath flow tee connection, optical fibers close to the exit end of the separation capillary and a set of collection capillaries. Note that in actual practice the electrode is separated from the sheath flow by a membrane [11].

$\mu\text{m}$  I.D. (Polymicro Technologies, Phoenix, AZ, USA) deactivated with a newly developed hydrolytically stable coating were used [12]. The exit end of the separation capillary was attached to the tip of the collection interface. A sheath liquid, consisting of the cathodic buffer, provided electrical contact and a means for transporting species to the collection capillaries. The ground electrode (negative pole) of the power supply was separated from the stream of the collection buffer by a semipermeable membrane to prevent any changes in the buffer composition [11]. The injection end of the capillary was inserted into the electrode reservoir containing acetic acid solution (anolyte, pH 2.9), whereas the exit end was fastened in a tee connection and rinsed by a flow of ammonium hydroxide (catholyte, pH 10.9 sheath liquid). Prior to the separation, the column was entirely filled with the sample–ampholyte solution. Focusing was accomplished by applying 10 kV for 2 min followed by 13 min at 30 kV. The focusing step was monitored as a decrease in the electric current flowing through the capillary. Once a plateau was reached (typically in 15 min, with residual current less than 2  $\mu\text{A}$ ), the focused zones were then mobilized by raising the injection side by 5 cm, in the case of standard proteins, and 8 cm, in the case of hemoglobin (Hb) variants. This step resulted in a hydrodynamic flow of 22 nl/min (standard proteins) and 35 nl/min (Hb variants) which was measured during calibration runs using fluorescein as a marker. The high voltage was applied during mobilization to maintain the focused zones and thus counterbalance band broadening due to parabolic flow.

## 2.2. Collection procedure

The sheath flow interface used for sample collection (Fig. 1) is discussed in detail elsewhere [11]. In short, it consisted of a fiber optic-based UV detector operating at 254 nm with detection 10 mm before the exit of the capillary, a sheath liquid collection interface, and a stepper motor-driven/computer-controlled rotor holding 60 collection capillaries (20  $\mu\text{l}$  volume, Idaho Tech-

nologies, Moscow, ID, USA). A syringe pump (Model 341B; Sage Instruments, Boston, MA, USA) was used to supply the ammonium hydroxide solution, which served as the collection buffer to the sheath liquid interface at a flow-rate of 12  $\mu\text{l}/\text{min}$ . The mobilized protein zones were detected by the on-column fiber-optic UV detector. Upon detection, the exit times were calculated, and a collection capillary was automatically positioned close (ca. 200  $\mu\text{m}$ ) to the sheath flow connection at the appropriate time for sample collection. Protein fractions which eluted in the sheath liquid were transported by capillary action into the collection capillaries. Alternatively, when closely spaced proteins were detected, the stepper motor was programmed in 10-s increments. The detector signal was digitized by an A/D converter, and the collection procedure was controlled by a 486 IBM-compatible computer. The software was written in the laboratory in the LabView (National Instruments, Austin, TX, USA) environment. The collected fractions were either stored as solutions in the collection capillaries or as essentially salt free solids after evaporation of the ammonium hydroxide solution.

## 2.3. MALDI-TOF-MS

All mass spectra were obtained on a Bruker Reflex TOF mass spectrometer (Bruker Instruments, Billerica, MA, USA), operated in either the linear or reflectron mode, as specified in the text. A saturated solution of sinapinic acid in 0.1 M trifluoroacetic acid–acetonitrile (60:40, v/v) was used as the matrix for MALDI. A pulsed nitrogen laser was operated at 337 nm (50  $\mu\text{J}$ , 5 ns), and the signal was accumulated and averaged over 50–100 shots. Two different sample preparation procedures were employed. After the collection of standard proteins, 2  $\mu\text{l}$  of the sample fractions were directly deposited onto the probe and allowed to evaporate. Sinapinic acid (2  $\mu\text{l}$ ) was added to the dried fractions for creation of a crystalline matrix. For the collected hemoglobin variant fractions, the sheath liquid was evaporated to dryness, the samples were

stored in the freezer ( $-20^{\circ}\text{C}$ ) and then redissolved in  $2\ \mu\text{l}$  of the MALDI matrix.

#### 2.4. Chemicals

cIEF was performed using 1% (1:1:1, v/v) mixture of Pharmalyte (Sigma, St. Louis, MO, USA), Ampholine (Sigma) and Servalyte (Serva, Hauppauge, NY, USA).

Samples of myoglobin (horse heart), carbonic anhydrase I (human erythrocytes) and II (bovine erythrocytes),  $\beta$ -lactoglobulin A (bovine milk) (Sigma) were dissolved in the carrier ampholyte mixture at a concentration of 0.05 mg/ml. A second sample of a mixture of human hemoglobin variants A, C, S, F (Isolab, OH, USA) was dissolved in the above carrier ampholyte solution to a final concentration of 0.08 mg/ml. All protein samples were used as received without further purification.

Water solutions of 0.3% ammonium hydroxide and 0.5% acetic acid (both from Fisher, Pittsburgh, PA, USA) were used as catholyte and anolyte, respectively. All solutions were passed through a  $0.2\text{-}\mu\text{m}$  syringe filter (Gelman, Ann Arbor, MI, USA) or centrifuged prior to use. Sinapinic acid, trifluoroacetic acid and acetonitrile, used for the preparation of the MALDI matrix, were obtained from Sigma.

### 3. Results and discussion

The purpose of this work is to demonstrate the feasibility of collecting multiple fractions from a cIEF separation followed by MALDI-TOF-MS analysis. Because of the focusing effect and the high resolving power, cIEF is especially attractive for preparative purposes. However, there are two main problems for collecting multiple bands from a single cIEF separation. First, it is desirable to apply the focusing voltage during mobilization in order to minimize band broadening. Our recently developed sheath flow collection device [11] decouples one electrode efficiently from the end of the capillary, allowing collection of many fractions without disrupting the electrical circuit. Mobilization is accom-

plished by raising the anodic buffer reservoir; separated proteins elute in droplets formed by the sheath buffer.

The second problem is the determination of the exact exit time of individual bands. In the case of cIEF, the exit time cannot be calculated on-line with the present single-optical-fiber arrangement, because the exact location of a protein zone at the beginning of the mobilization step is unknown. Therefore, a separate calibration step to determine the flow velocity has been performed prior to each run. For this purpose, the injection end of the capillary was inserted into a vial containing a fluorescein solution ( $10^{-4}\ \text{M}$ ) and raised to the appropriate level (5 or 8 cm). The calibration revealed a run to run deviation of ca. 2–3% in the flow velocity. This was mainly due to difficulties in reproducibly manually setting the height of the capillary. In the future this problem could be overcome by detecting on-line with two sets of optical fibers which would allow accurate on-line determination of the hydrodynamic flow velocity. In addition, reproducible instrumental control of the pressure may be utilized. Nevertheless, the potential for multiple fraction collection for cIEF separations is demonstrated in the following examples.

The UV trace in Fig. 2 shows a cIEF separation of a standard protein mixture consisting of myoglobin ( $pI\ 7.2$ ), carbonic anhydrase I ( $pI\ 6.6$ ), carbonic anhydrase II ( $pI\ 5.9$ ) and  $\beta$ -lactoglobulin A ( $pI\ 5.1$ ). Under the given experimental conditions, sharp, well resolved peaks were detected. It is to be noted that a 1:1:1 (v/v) mixture of three different ampholytes was used in Fig. 2. Considering that each commercial ampholyte mixture is prepared by a different synthetic procedure and contains different buffer components, it is reported that mixing different brands increases the uniformity of the pH gradient as the number of ampholytes in a given pH range increases [13]. It is worth noting that detection close to the capillary end enables the cIEF separation to be performed without additives such as N,N,N',N'-tetramethylethylenediamine (TEMED) [14], as only a fraction of the pH gradient (2.5% for the given experimental

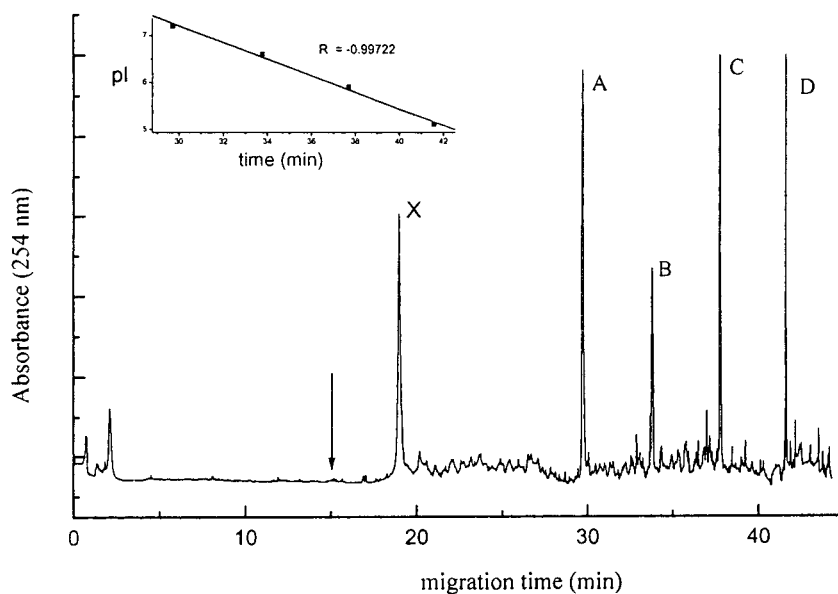


Fig. 2. cIEF separation of (A) myoglobin ( $pI$  7.2), (B) carbonic anhydrase I ( $pI$  6.6), (C) carbonic anhydrase II ( $pI$  5.9) and (D)  $\beta$ -lactoglobulin A ( $pI$  5.1). Inset: plot of migration time vs.  $pI$ . Conditions: 40 cm (39 cm to detector)  $\times$  75  $\mu$ m I.D. capillary, coated; for more detailed description of buffer system, mobilization and collection see text.

conditions) cannot be detected. Since detection was carried out at 254 nm, ampholyte constituents could be observed, resulting in a relatively noisy baseline. The first peak, marked X, stems from differences in UV absorbance and/or change in refractive index of the ampholyte constituents. The total amount of individual proteins was 88 ng (2–5 pmol, depending on the molecular weight of a protein), as a result of the internal volume of the separation capillary (1.8  $\mu$ l) and protein concentration (0.05 mg/ml). The inset of Fig. 2 shows a plot of  $pI$  vs. migration time in minutes. With the given set of electrolytes, a linear relation with a high correlation coefficient is achieved, as found by others over wider pH ranges [5]. Under these experimental conditions, the  $pI$  of unknown proteins can be calculated with high precision. Collection of cIEF fractions allows subsequent protein analysis such as Edman sequencing, peptide mapping or MS analysis to achieve additional information.

A sheath flow collection device provided automatic collection of each protein zone, resulting in a collected volume of 13  $\mu$ l for each fraction.

The peak widths at the baseline of the standard protein mixture were up to 20 s. Because the protein zones were widely spaced, the collection window was set at 65 s to ensure complete collection of each band. This window took into account the deviation in the hydrodynamic flow velocity, resulting from the manual lifting of the capillary. For exact identification of each protein, the collected fractions were subjected to MS analysis.

Since initial experiments indicated that mixing of the collected fractions directly with the matrix (1:10, v/v) in a separate vessel resulted in poor crystal formation and low ion current, a different approach for sample preparation was applied. Prior to the TOF analysis, 2  $\mu$ l (ca. 450–750 fmol, assuming full recovery) of each fraction were placed on the MALDI target. After evaporation of the ammonium hydroxide, 2  $\mu$ l of the matrix were added for crystal formation. (It is to be noted that this approach leaves 11  $\mu$ l (collected volume 13  $\mu$ l) of the collected protein for additional analysis such as Edman sequencing. In cases involving a lower sample concentration,

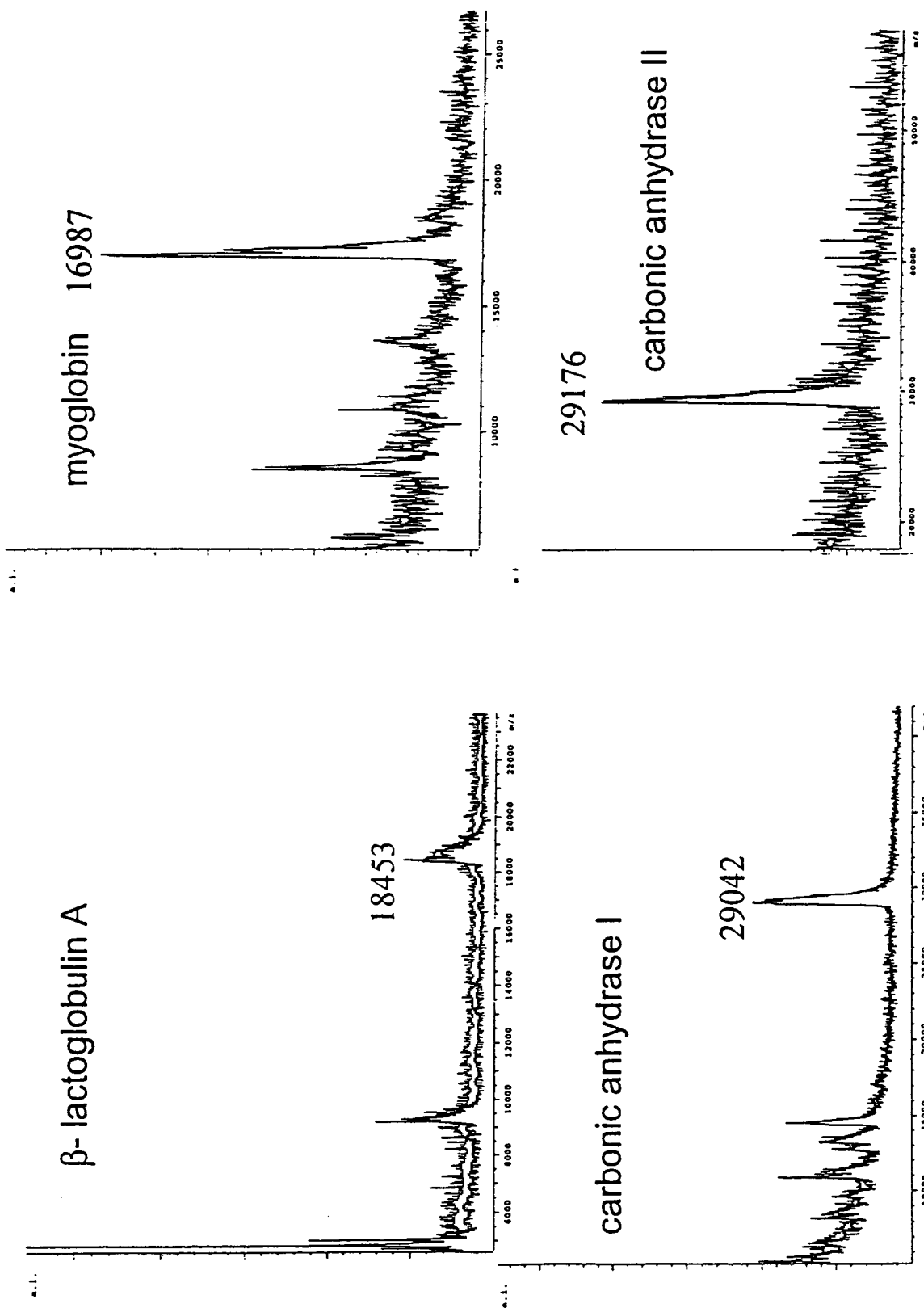


Fig. 3. MALDI-TOF-MS spectra of standard proteins collected during separation shown in Fig. 1. For details see text. a.i. = arbitrary intensity.

Table 1  
Molecular mass determinations for standard proteins used for cIEF MALDI-TOF-MS

Protein	pI (Ref. [5])	$M_r$ (Ref. [6])	$M_r$ (exp.)	Accuracy (%)
Myoglobin	7.2	16 950	16 987	0.2
Carbonic anhydrase I	6.6	28 781	29 042	0.9
Carbonic anhydrase II	5.9	29 151	29 176	0.09
$\beta$ -Lactoglobulin A	5.1	18 365	18 453	0.5

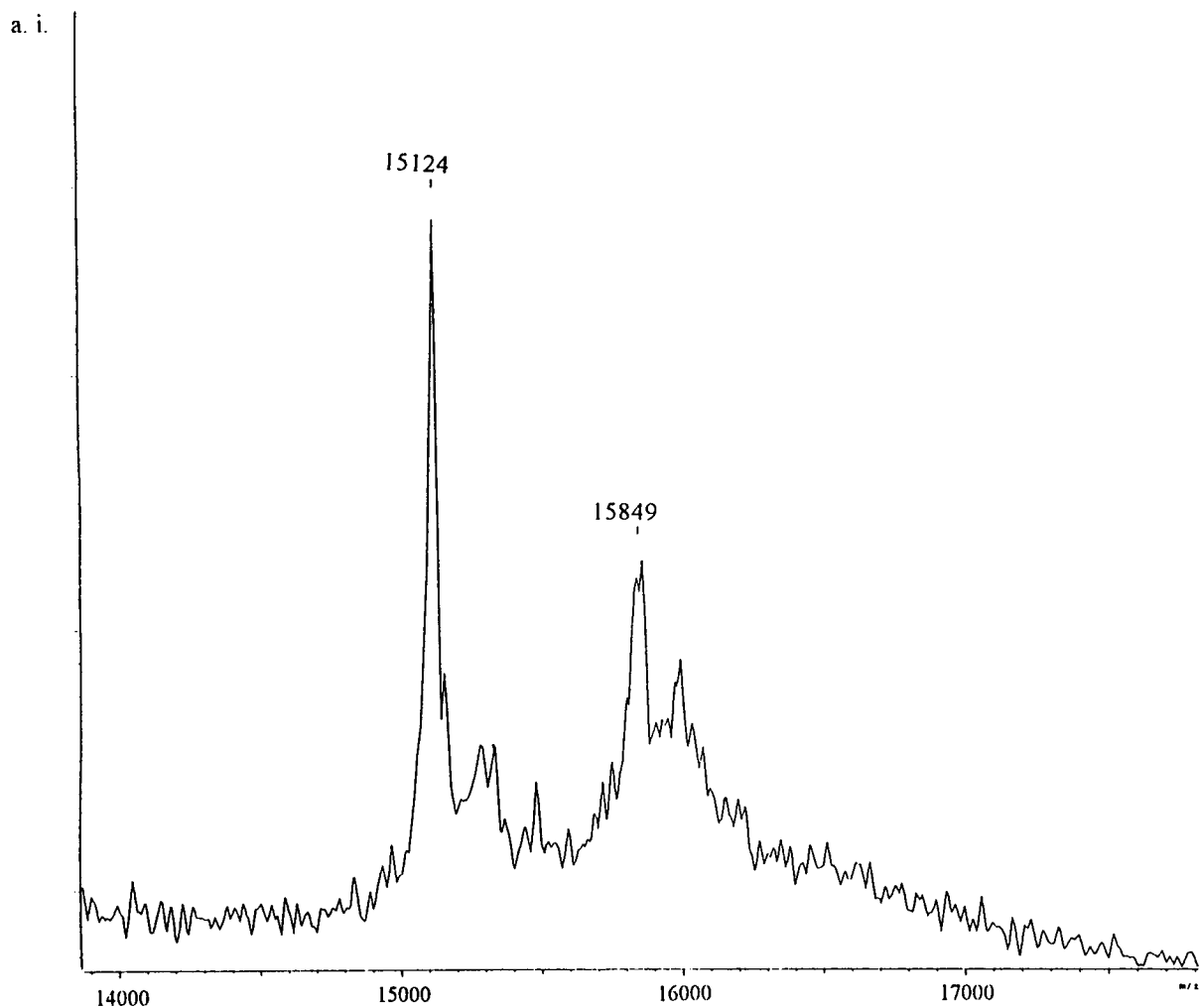


Fig. 4. MS spectrum of a standard mixture of hemoglobin variants (HbA, HbF, HbS and HbC). For details see text. a.i. = arbitrary intensity.

the entire collected volume could be evaporated in order to further concentrate the sample.) Fig. 3 shows the resulting TOF mass spectra. Although low sample amounts were analyzed, the precision of the molecular mass determination was still satisfactory and comparable to that typically obtained for CE–MALDI-TOF-MS experiments [15]. The measured and expected molecular masses, and mass accuracies are listed in Table 1. The mass accuracy was <1% and in most cases better than 0.5%. In addition, the isoelectric points were determined with a precision of 0.1 pI units. The off-line coupling of CE and MS therefore allows the determination of two independent parameters which are important for protein characterization.

The capability of the device was demonstrated by collecting multiple fractions from a standard hemoglobin mixture (HbA, HbF, HbS and HbC). In this case, the proteins did not significantly vary in molecular mass but in isoelectric point due to a single or a few amino acid substitutions in the polypeptide chain [16]. As shown in Fig. 4, the MALDI-TOF-MS spectrum of a standard hemoglobin mixture (no cIEF) displays only two major peaks, with molecular masses centered at 15 124 and 15 849. Although hemoglobin contains four subunits, only the individual chains and their matrix adducts (+200  $m/z$ ) could be detected in the mass spectrometer upon ionization. The molecular masses of the Hb variant chains did not differ significantly (see Table 2) making their differentiation by MALDI-TOF-MS difficult if not impossible. It is to be noted that the results for Figs. 4 and 5 utilized the reflectron mode of the TOF, which permitted up to an order of magnitude higher

resolution than measurements in the linear mode.

The UV trace of the cIEF separation of the hemoglobin variants is shown in Fig. 5. The changes in amino acids are sufficient for baseline resolution of the four variants by cIEF [17]. As an example, the substitution of glutamic acid in position 6 by basic lysine in the  $\beta$ -chain of HbC changes the isoelectric point by 0.5 pH units compared to normal HbA (Table 2). At the same time the change in molecular mass is less than 16 Da (ca. 0.1%).

For the cIEF collection, the capillary was filled with 140 ng (2 pmol total) of the hemoglobin mixture containing the four different variants A, F, S and C. Since the proteins had closely spaced bands, collection of individual peaks was difficult, given the deviation of the flow velocity of 2–3%. In order to isolate each of the variants, it was decided to collect over a 2-min time range in 10-s steps (2  $\mu$ l each collected volume). This collection procedure could easily be achieved with the appropriate programming of the collection device in combination with the sheath flow connection. The dry fractions were redissolved in the MALDI matrix just before the mass measurement. The amount collected and taken for the MALDI-TOF-MS experiment was ca. 500 fmol. The inset in Fig. 5 shows the mass spectrum of the fraction collected in the specified interval. It is to be noted that the mass spectrum of Hb C is virtually the same as that of the Hb standards (Fig. 4). Every collected fraction was submitted to MS analysis and the resulting MS spectra showed the same trace in all samples containing a Hb variant. Furthermore, the pattern of fraction collections coincided with the

Table 2  
Characteristics of Hb variants

Variant	Mutation	$\Delta MW_r$	pI
A	$\alpha_2\beta_2$ , wild type adult hemoglobin	—	6.95
F	$\alpha_2\gamma_2$ , wild type fetal hemoglobin	128	7.0
S	$\alpha_2\beta_2^{6\text{Glu}\rightarrow\text{Val}}$ , adult hemoglobin	30	7.2
C	$\alpha_2\beta_2^{6\text{Glu}\rightarrow\text{Lys}}$ , adult hemoglobin	0.9	7.45



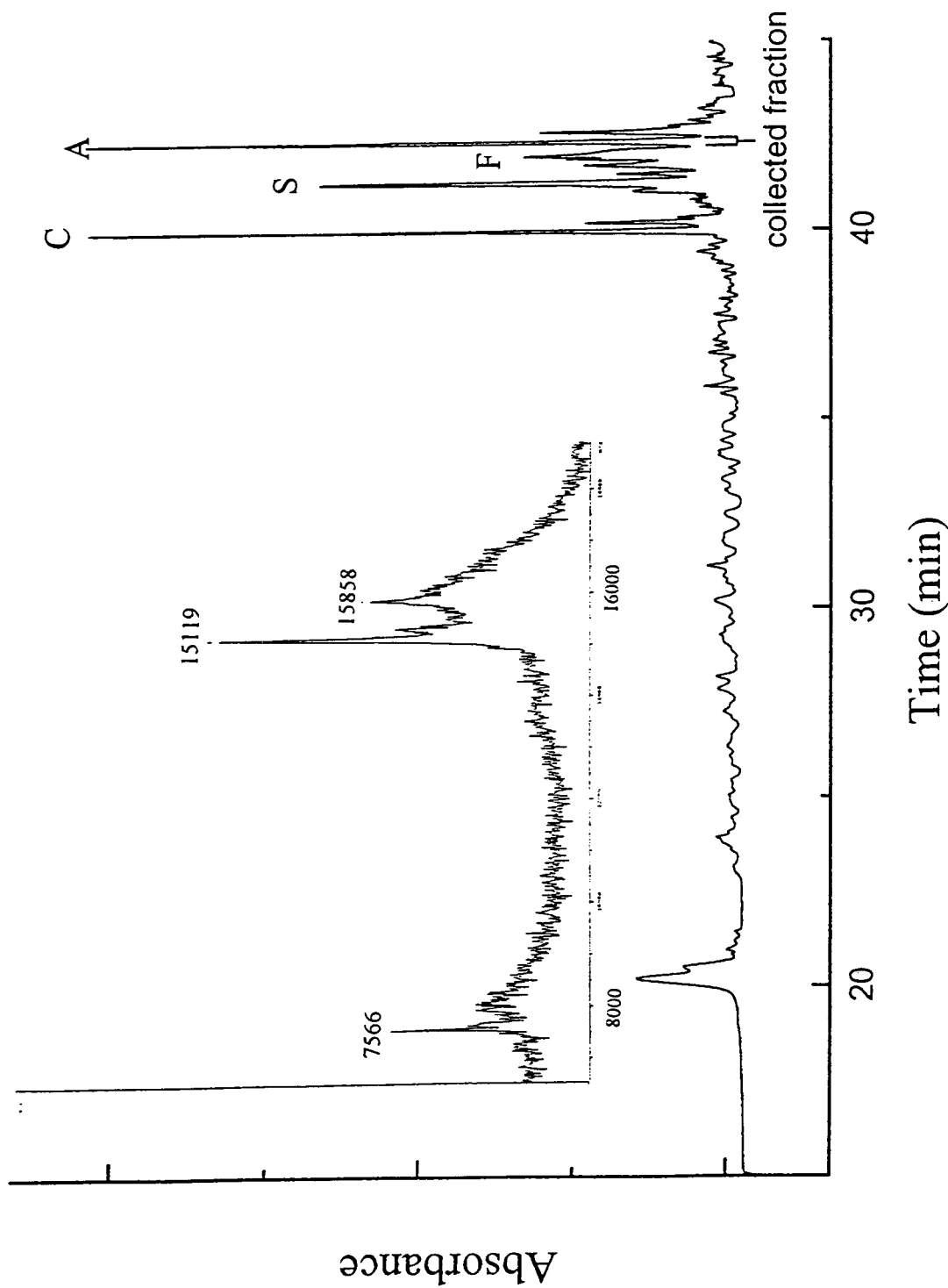


Fig. 5. cIEF separation of hemoglobin variants A (pI 6.95), F (pI 7.0), S (pI 7.2) and C (pI 7.45). Inset: MALDI-TOF-MS analysis of the specified collected variant, conditions as in Fig. 4. Conditions: as in Fig. 2, collection interval: 10 s, in predefined steps.

UV trace of the cIEF separation. Therefore, the mass spectrum identified the collected species as hemoglobin, but could not provide sufficient information to distinguish between different mutants. The complementary of cIEF and MALDI-TOF-MS is clearly shown in this example.

#### 4. Conclusions

The new sheath flow collection device was shown to be a useful tool for collecting multiple protein fractions from cIEF and subsequent MALDI-TOF-MS analysis. Because of the focusing effect of proteins into narrow zones, cIEF is effective for preparative purposes. Since the separation is based solely on the difference in isoelectric points and MALDI-TOF-MS analysis is based on differences in molecular masses, this approach, combining two orthogonal separation principles, has potential for two-dimensional protein analysis [18]. Thus, one can envision the potential for complex protein mixture analysis at the trace level. Note that these same two separation principles are used in two-dimensional gel electrophoresis [19]. In the future, the reproducibility of flow variation can be improved by precisely applying a positive pressure for mobilization and/or using two sets of optical fiber detectors for on-line flow velocity determination. In addition, on-line collection on MALDI targets will also be possible.

#### Acknowledgements

The authors acknowledge NIH GM15847 for support of this work. The authors also gratefully acknowledge Bruker Instruments for assistance in the MALDI-TOF-MS measurements. Contribution 641 from the Barnett Institute.

#### References

- [1] S. Hjertén and M.D. Zhu, *J. Chromatogr.*, 346 (1985) 265–270.
- [2] J.-L. Liao and R. Zhang, *J. Chromatogr. A*, 684 (1994) 143–148.
- [3] F. Kilár and S. Hjertén, *Electrophoresis*, 10 (1989) 23–29.
- [4] S. Kyiohito and B.L. Karger, *Anal. Chem.*, 66 (1994) 9–15.
- [5] S.M. Chen and J.E. Wiktorowicz, *Anal. Biochem.*, 206 (1992) 84–90.
- [6] R.D. Smith, J.H. Wahl, D.R. Goodlett and S.A. Hofstadler, *Anal. Chem.*, 65 (1993) A574–A584.
- [7] J.A. Loo, J.P. Quinn, S.I. Ryu, K.D. Henry, M.W. Senko and F.W. McLafferty, *Proc. Natl. Acad. Sci. U.S.A.*, 89 (1992) 286–289.
- [8] M. Zhu, R. Rodriguez and T. Wehr, *J. Chromatogr.*, 559 (1991) 479–488.
- [9] J.R. Mazzeo and I.S. Krull, *J. Chromatogr.*, 606 (1992) 291–296.
- [10] X.W. Yao and F.E. Regnier, *J. Chromatogr.*, 632 (1993) 185–193.
- [11] O. Müller, F. Foret and B.L. Karger, presented at the 7th International Symposium on High Performance Capillary Electrophoresis, Würzburg, 29 January–2 February 1995, poster p-634.
- [12] W. Götzinger, B.L. Karger, P. Shieh and N.H.C. Cooke, presented at the 7th International Symposium on High Performance Capillary Electrophoresis, Würzburg, 29 January–2 February 1995, poster p. 637.
- [13] C. Simpson, in F. Franks (Editor), *Characterization of Proteins*, Humana Press, Clifton, NJ, 1988, Ch. 12.
- [14] M. Zhu, R. Rodriguez, T. Wehr and C. Siebert, *J. Chromatogr.*, 608 (1992) 225–237.
- [15] W. Weinmann, C.E. Parker, L.J. Deterding, D.I. Papac, J. Hoyes, M. Przybylski and K.B. Tomer, *J. Chromatogr. A*, 680 (1994) 353–361.
- [16] H.F. Bunn and B.G. Forget, *Hemoglobin: Molecular, Genetic and Clinical Aspects*, Saunders, Philadelphia, PA, 1986, Ch. 4, p. 61.
- [17] S. Molteni, H. Frischknecht and W. Thormann, *Electrophoresis*, 15 (1994) 22–30.
- [18] R. Grimm, G. Ross and F. Bek, presented at the 7th International Symposium on High Performance Capillary Electrophoresis, Würzburg, 29 January–2 February 1995, poster p. 633.
- [19] B.D. Hames and D. Rickwood (Editors), *Gel Electrophoresis of Proteins – A Practical Approach*, IRL Press, Oxford, 1990.

# Capillary zone electrophoresis at subzero temperatures

## I. Separation of the *cis* and *trans* conformers of small peptides

Stacey Ma, Franka Kálmán, András Kálmán, Frank Thunecke, Csaba Horváth\*

Department of Chemical Engineering, Yale University, New Haven, CT 06520, USA

### Abstract

The *cis*–*trans* conformers of two dipeptides, Phe–Pro and Leu–Pro, and two opioid heptapeptides containing one or two proline residues were separated by capillary zone electrophoresis (CZE) in borate buffer at low temperatures down to  $-17^{\circ}\text{C}$ . At temperatures near ambient, the relaxation time of the *cis*–*trans* isomerization is on the time-scale of minutes for the dipeptides and thus commensurate with the migration times in CZE under usual operating conditions. The conformers of both dipeptides could be separated with baseline resolution below  $10^{\circ}\text{C}$  in neat aqueous 100 mM sodium borate (pH 8.4). The conformer peaks on the electropherograms were identified by using authentic samples of the *cis* and *trans* forms of Phe–Pro and Leu–Pro that were obtained by reversed-phase HPLC at  $0^{\circ}\text{C}$ , validated by NMR spectroscopy and stored in liquid nitrogen. The interplay of the electrophoretic migration and on-column isomerization reaction in CZE of Phe–Pro under various conditions was analyzed in the light of the Damköhler number ( $Da$ ). The results showed that besides employing low temperature increasing the voltage and/or decreasing the capillary length also reduce the magnitude of  $Da$  to bring about the separation of interconverting species. In this work the use of low temperature in this work was preferred due to the experimental simplicity. The separation of *cis*–*trans* conformers of two opioid heptapeptides was carried out by CZE at subzero temperatures with aqueous sodium borate containing 23% (v/v) glycerol at pH\* 11.3 as measured with a glass electrode. The two conformers of Tyr–Pro–Phe–Asp–Val–Val–Gly–NH<sub>2</sub> were baseline separated at  $-12^{\circ}\text{C}$  and the four conformers of Tyr–Pro–Phe–Gly–Tyr–Pro–Ser–NH<sub>2</sub> due to the presence of two peptidyl–proline bonds in the molecule, were also resolved at  $-12^{\circ}\text{C}$ . From the electrophoretic mobilities, the hydrodynamic radii of the *cis*–*trans* conformers of the dipeptides Phe–Pro and Leu–Pro were estimated. In both cases, the *trans* isomers had 1.3 times greater Stokes radii than the *cis* conformers. This agrees with the observed migration order and molecular modeling results. The hydrodynamic radii of the Phe–Pro conformers were smaller than those of the Leu–Pro isomers despite the lower molecular mass of the latter. The results demonstrate that CZE is suitable for measuring certain molecular properties and suggest that the methods introduced here are applicable to the study of other systems of interconverting conformers.

### 1. Introduction

Peptides containing proline residues, but at the N-terminus, are known to exist in both the

*cis* and *trans* conformations due to the rigidity of the peptidyl–proline bond [1,2]. *Cis* and *trans* proline dipeptides [3–6] were first separated more than 12 years ago by reversed-phase chromatography at subambient temperatures, where the rate of interconversion is slow enough not to

\* Corresponding author.

interfere with the separation. Recently, even subzero temperatures [7,8] were used for the HPLC separation of the *cis*–*trans* conformers of certain biologically active tetra- and heptapeptides.

In this work we examined the separation of *cis* and *trans* peptide conformers by capillary zone electrophoresis (CZE), a high-performance analytical tool that offers new avenues to the rapid separation of closely related substances. Another advantageous feature of CZE is that the interpretation of the migration data is not encumbered by interactions with a stationary phase as is the case with the retention data in HPLC. This makes the precision instruments for CZE analysis eminently suitable for the measurement of molecular properties and other physico-chemical data.

At ambient temperature, the relaxation time for the *cis*–*trans* peptide isomerization reactions investigated so far is on the time-scale of minutes. Consequently, the separation of the conformers by CZE requires the use of either very short capillaries and a specially designed instrument or the employment of subambient/subzero temperatures by simple modification of readily available instrumentation. Albeit the significance of temperature control in CZE has been well recognized [9], the technique is almost exclusively practiced at ambient or near-to-ambient temperatures and only very recently was the separation of certain heterocyclic nitrosamines performed at 5°C [10]. No experiments by CZE at subzero temperatures have been reported.

On the other hand, in conventional gel electrophoresis, subzero temperatures as low as –30°C were employed for investigation of interacting biological systems that are rapid on the time-scale of separation. Ligand binding and subunit exchange within hemoglobin [11] were studied by electrofocusing at –5 to –10°C with ethylene glycol in the polyacrylamide gel. Hybrids of human and sickle cell hemoglobin and partially oxidized human carboxyhemoglobin [12] were separated by both gel electrophoresis and isoelectric focusing using aqueous DMSO at –20 to –30°C. Recently, Harrington and Zewart [13] carried out slab gel electrophoresis at tem-

peratures as low as –20°C to enhance the separation efficiency by the application of high voltage without surpassing the permissible current level.

On the basis of our earlier experience with on-column *cis*–*trans* isomerization and separation in HPLC [3–6], we have chosen to operate our CZE instrument at temperatures sufficiently low to separate the *cis*–*trans* conformers of two dipeptides and two opioid heptapeptides [14,15]. The separation of the heptapeptide isomers required temperatures as low as –12°C, therefore particular attention was paid to the choice of the antifreeze. The dimensionless Damköhler number was used to analyze the complex interplay of the first-order reversible reaction and the electrophoretic migration behavior of the *cis*–*trans* conformers and guidelines were established for the optimization of the separation. Authentic samples of both the *cis* and *trans* conformers of Phe–Pro and Leu–Pro, purified by RP-HPLC and validated by NMR spectroscopy, were used for the identification of the conformer peaks in CZE. The mobilities of the conformers were used to estimate their drag coefficients and thus to assess the differences in their three-dimensional molecular structures. The results obtained by this molecular electrophoretic approach are compared with those attained by HPLC measurements.

## 2. Experimental

### 2.1. Chemicals

Optically pure dipeptides L-Phe–L-Pro and L-Leu–L-Pro were purchased from Sigma (St. Louis, MO, USA). The opioid heptapeptides Tyr–Aib–Phe–Asp–Val–Val–Gly–NH<sub>2</sub> (Aib = aminoisobutyric acid), Tyr–Pro–Phe–Asp–Val–Val–Gly–NH<sub>2</sub> and Tyr–Pro–Phe–Gly–Tyr–Pro–Ser–NH<sub>2</sub> were donated by Dr. Ralf Schmidt (Laboratory of Chemical Biology and Peptide Research, Clinical Research Institute of Montreal, Montreal, Quebec, Canada).

Analytical-reagent grade phosphoric acid and sodium hydroxide and HPLC-grade methanol

were supplied by Fisher (Pittsburgh, PA, USA), sodium borate ( $\text{Na}_2\text{B}_4\text{O}_7 \cdot 10\text{H}_2\text{O}$ ) by Mallinckrodt (Paris, KY, USA), boric acid and anhydrous glycerol by J.T. Baker (Phillipsburg, NJ, USA). Potassium hydrogenphthalate (pH 4.01) and potassium phosphate (pH 7.00) buffer standards for calibration of the pH meter were obtained from Baker and potassium carbonate (pH 10.00) buffer standard from Brand-Nu Laboratories (Meriden, CT, USA). Deionized water was prepared using a NanoPure purification system (Barnstead, Boston, MA, USA) and used throughout.

## 2.2. Capillary zone electrophoresis

CZE experiments were performed by using a P/ACE 2200 capillary electrophoresis unit (Beckman, Fullerton, CA USA). The temperature control unit of the instrument was assisted by an external cooling system, a Model RTE-4DD refrigerated bath (NESLAB, Portsmouth, NH, USA), which accommodated a heat exchanger coil for the coolant fluid. The heat exchanger was placed in the coolant recirculation line between the pump and the cartridge containing the capillary. The bath was filled with ethylene glycol for operation at subzero temperatures. The coolant temperature, measured at the outlet of the cartridge by an Omega thermocouple (Stamford, CT, USA) with a precision of  $0.1^\circ\text{C}$ , was taken as the operating temperature. The capillary electrophoresis unit thus modified was kept and operated in a cold room at  $7^\circ\text{C}$ . The software for control of the instrument and data processing was the Microsoft Windows version 3.0 of P/ACE. Fused-silica capillaries of  $375\ \mu\text{m}$  O.D. and  $50\ \mu\text{m}$  I.D. with polyimide cladding were obtained from Quadrex (New Haven, CT, USA). A narrow segment of the outer coating was removed to open a window for UV-Vis detection at 214 nm. In most experiments, the capillary length and the pertinent migration distances were 370 and 300 mm, respectively.

Sodium borate buffer (pH 8.4) was prepared by adjusting the pH of 25 mM aqueous sodium borate solution with 100 mM boric acid. For operation at subzero temperatures, 77 parts of 50

mM aqueous boric acid solution were mixed with 23 parts of glycerol and 1 M NaOH was added to the solution to give a glass electrode reading of  $\text{pH}^*$  11.3 with a calomel reference electrode (Fisher). By addition of glycerol, the freezing point of the medium is depressed to about  $-20^\circ\text{C}$  [16].

The samples were dissolved in the buffer at a concentration of ca. 1 mg/ml and injected depending on the temperature over a period from 1 to 8 s at 0.5 p.s.i. (1 p.s.i. = 6894.76 Pa). Between runs the capillary was flushed with at least five column volumes of the buffer at an inlet pressure of 20 p.s.i. The reproducibility of peak height in six experiments was found to be better than 3.2% (R.S.D.). The electroosmotic flow was measured by acrylamide as the neutral marker with a reproducibility of the migration time better than 0.5% R.S.D. (four experiments).

## 2.3. HPLC

For preparative chromatography, a unit assembled from an LDC/Milton Roy (Rivera Beach, FL, USA) ConstaMetric III metering pump, Milton Roy SpectraMonitor variable-wavelength detector and an injection valve with a  $20\text{-}\mu\text{l}$  sample loop (Rheodyne, Cotati, CA, USA) was employed. Chromatograms were obtained with a LDC/Milton Roy CI 10 integrator. A  $250 \times 4.6\ \text{mm}$  I.D. column packed with  $5\text{-}\mu\text{m}$  UltraSpher ODS RP-18 (Beckman) was jacketed and connected to a NESLAB RTE-4DD refrigerated circulating bath suitable for operation at temperatures as low as  $-30^\circ\text{C}$ . The eluent was a mixture of methanol–50 mM monobasic sodium phosphate solution (30:70, v/v). Before use, the pH reading with the glass electrode was adjusted to 6.0 with 1 M NaOH and the solution was filtered and degassed. The peptides were dissolved in the eluent at a concentration of  $60\ \text{mg}\ \text{ml}^{-1}$ . The chromatographic experiments were performed isocratically at a flow-rate of  $0.5\ \text{ml}\ \text{min}^{-1}$  and at a detection wavelength of 280 nm. The fractions containing pure conformers were collected in liquid nitrogen [8] and then subjected to CZE measurements.

### 3. Results and discussion

#### 3.1. CZE at subambient/subzero temperatures

The apparent mobility of the migrant molecules,  $\mu_{\text{app}}$ , is the sum of  $\mu_{\text{e eo}}$ , the electroosmotic flow coefficient, and  $\mu_{\text{ep}}$ , the electrophoretic mobility of the migrant. Since under our experimental conditions the corresponding velocities have opposite signs,  $\mu_{\text{app}}$  is given by

$$\mu_{\text{app}} = \mu_{\text{e eo}} - \mu_{\text{ep}} \quad (1)$$

The magnitude of  $\mu_{\text{e eo}}$  is determined by the properties of the electrophoretic system as

$$\mu_{\text{e eo}} = \frac{\varepsilon \varepsilon_0 \zeta}{\eta} \quad (2)$$

where  $\zeta$  is the zeta potential at the inner wall of the capillary,  $\varepsilon_0$  is the permittivity of the vacuum,  $\varepsilon$  is the dielectric constant and  $\eta$  is the viscosity of the medium. On the other hand, the electrophoretic mobility,  $\mu_{\text{ep}}$ , depends on the migrant's molecular properties and for spherical molecules is given by

$$\mu_{\text{ep}} = \frac{ze}{6\pi\eta R_{\text{hd}}} \quad (3)$$

where  $z$  is the characteristic charge,  $R_{\text{hd}}$  is the hydrodynamic (Stokes) radius and  $e$  is the unit charge.

The current,  $I$ , is proportional to the conductivity of the background electrolyte,  $\kappa$  so that

$$I = \kappa E A_c \quad (4)$$

where  $E$  is the applied electric field and  $A_c$  is the cross-sectional area of the capillary tube. The conductivity depends on the mobility,  $\mu_i$ , of the individual ions,  $i$ , present in the background electrolyte [17] as

$$\kappa = \sum_i z_i F c_i \mu_i \quad (5)$$

where  $F$  is the Faraday constant and  $c_i$  is the concentration of the ion  $i$ .

According to Eqs. 2, 3 and 5, the mobilities of the migrants and background ions are expected to change with temperature mainly owing to changes in the viscosity of the medium. Under

the experimental conditions used in this study, the temperature dependence of the viscosity can be described by the Andrade equation [18]:

$$\eta = A \exp\left(\frac{B}{T}\right) \quad (6)$$

where  $A$  and  $B$  are empirical constants for a given liquid and  $T$  is the absolute temperature. If the dependence of the dielectric constant and the zeta potential on  $T$  is negligible, according to Eqs. 2 and 6 the electroosmotic flow coefficient is related to the temperature by

$$\ln \mu_{\text{e eo}} = C_m - \frac{B}{T} \quad (7)$$

where  $C_m$  is constant under our experimental conditions. *Mutatis mutandis*, Eq. 7 holds also for logarithm of the electrophoretic mobility,  $\mu_{\text{ep}}$ .

The temperature dependence of the conductivity is given by

$$\ln \kappa = C_k - \frac{B}{T} \quad (8)$$

where  $C_k$  is a constant determined by the ionic strength and molecular dimensions of the background ions. According to Eqs. 7 and 8, both the logarithmic conductivity and electrophoretic flow coefficient are linear functions of the reciprocal temperature with slopes representing properties of the electrophoretic medium.

In order to test Eqs. 7 and 8, electroosmotic flow coefficient and conductivity data were measured in neat aqueous borate (pH 8.4) and 50 mM borate buffer containing 23% (v/v) glycerol (pH\* 11.3). The results are plotted in Fig. 1 against the operating temperature in the range from 1 to 50°C (dashed lines) and from -17 to 40°C (solid lines), respectively. Since all plots are straight lines with correlation coefficients better than 0.99, the data strongly support the validity of Eqs. 7 and 8. As expected, the two pairs of lines representing the mobility and conductivity data obtained in the same medium have almost identical slopes. For parameter  $B$  in neat aqueous borate buffer, we obtain a mean value of 1802 K, which compares well with the literature value of 1844 K for water [16]. With

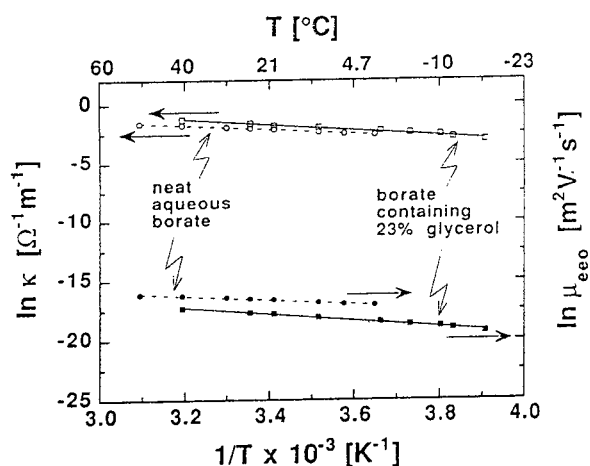


Fig. 1. Plots of the electroosmotic flow coefficient,  $\mu_{\text{eeo}}$ , and the conductivity,  $\kappa$ , of the medium against the temperature. ( $\circ$ )  $\kappa$  and ( $\bullet$ )  $\mu_{\text{eeo}}$  with neat aqueous 100 mM sodium borate buffer (pH 8.4) in the range 1–50°C; ( $\square$ )  $\kappa$  and ( $\blacksquare$ )  $\mu_{\text{eeo}}$  with aqueous 50 mM sodium borate containing 23% (v/v) glycerol (pH\* 11.3) in the range from –17 to 40°C. Capillary, 37 cm  $\times$  50  $\mu\text{m}$  I.D.; voltage, 30 kV; detector setting, 214 nm; marker for electroosmotic flow, acrylamide.

the aqueous glycerol mixture, the average value of  $B$  is 2610 K and thus significantly higher than that shown above for the neat aqueous buffer. Since at 20°C the respective viscosities of water and the 23% (v/v) water–glycerol mixture are 1.0 and 1.9 CP [19], the findings in this study are consistent with the Lewis–Squires postulate [20] that the sensitivity of the viscosity of liquids to temperature changes depends primarily on the magnitude of the liquid viscosity. Therefore, the higher the viscosity of the liquid, the greater is the change on temperature variation and therefore the larger is  $B$ .

The molecular diffusivity,  $D_{\text{m}}$ , has a stronger dependence on the temperature than the viscosity does, as seen from the following expression valid for spherical molecules:

$$D_{\text{m}} = \frac{RT}{6\pi\eta R_{\text{hd}}} \quad (9)$$

where  $R$  is the gas constant. In CZE, when longitudinal molecular diffusion is the only factor contributing to zone dispersion, then the separation efficiency in terms of theoretical plates

[21–24] is given by

$$N = \frac{zFV}{2RT} \quad (10)$$

where  $N$  is the number of theoretical plates and  $V$  is the applied voltage. According to Eq. 10, the separation efficiency increases with decreasing temperature. The enhancement of efficiency at subzero temperatures can be clearly seen in Fig. 2, which depicts two electropherograms of the opioid heptapeptide Tyr–Aib–Phe–Asp–Val–Val–Gly–NH<sub>2</sub> obtained with the glycerol–aqueous borate buffer (pH\* 11.3) at –12 and

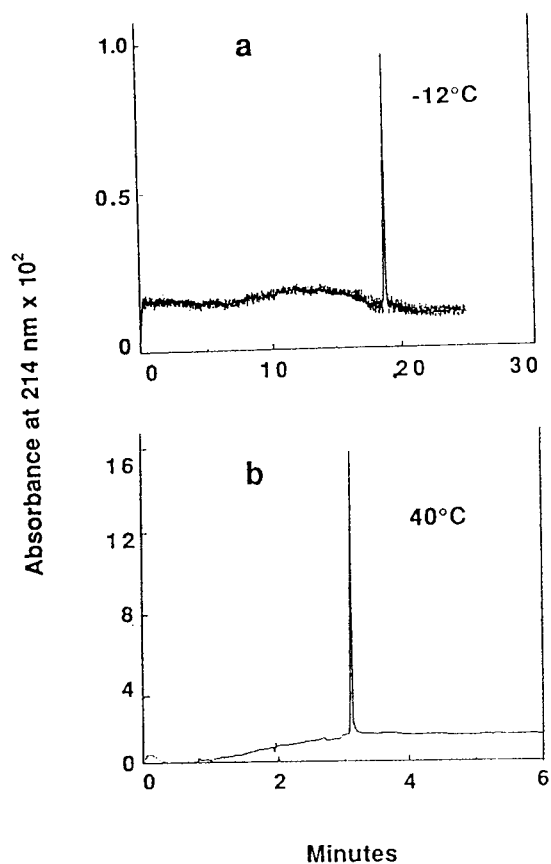
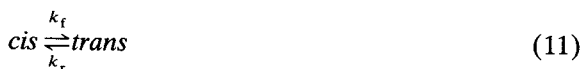


Fig. 2. Electropherograms of Tyr–Aib–Phe–Asp–Val–Val–Gly–NH<sub>2</sub> obtained at –12 and 40°C. Capillary, 37 cm  $\times$  50  $\mu\text{m}$  I.D.; buffer, aqueous 50 mM sodium borate containing 23% glycerol (pH\* 11.3); voltage, 30 kV; detector setting, 214 nm. (a) Temperature, –12°C; current, 9  $\mu\text{A}$ ; (b) temperature, 40°C; current, 47  $\mu\text{A}$ .

40°C. The peak sharpness is nearly the same in the two electropherograms, although the migration time is about six times longer at -12°C than at 40°C.

### 3.2. Interplay of electrophoretic migration and reaction

The *cis-trans* isomerization of the dipeptides has been treated [2] as a reversible first-order reaction:



where  $k_f$  is the rate constant for the forward and  $k_r$  for the reverse reaction. The equilibrium constant,  $K_m$ , is given by

$$K_m = \frac{[trans]}{[cis]} = \frac{k_f}{k_r} \quad (12)$$

and the relaxation time,  $\tau$ , for the reaction is

$$\tau = \frac{1}{k_f + k_r} = \frac{1}{k_f \left(1 + \frac{1}{K_m}\right)} \quad (13)$$

The Arrhenius equation describes the temperature dependence of the reaction rate as

$$k = A_k \exp\left(-\frac{E_a}{RT}\right) \quad (14)$$

where  $A_k$  is the pre-exponential factor and  $E_a$  is the activation energy for isomerization.

The interplay of migration and reaction is governed by the dimensionless Damköhler number,  $Da$ , which is defined as the ratio of the residence time of the migrant in the capillary,  $t_R$ , to the relaxation time of the reaction,  $\tau$ . In capillary electrophoresis,  $Da$  can be expressed as

$$Da = \frac{t_R}{\tau} = k_f \left(1 + \frac{1}{K_m}\right) \frac{l}{v_{app}} \quad (15)$$

where  $l$  is the pertinent migration length of the capillary and  $v_{app}$  is the apparent velocity of the migrant. The latter is given by the relationship

$$v_{app} = \mu_{app} E = \mu_{app} \frac{V}{L} \quad (16)$$

where  $L$  is the total length of the capillary. By combining Eqs. 1-3, 15 and 16, we obtain

$$Da = k_f \left(1 + \frac{1}{K_m}\right) \frac{lL}{V \left(\epsilon \epsilon_0 \zeta - \frac{ze}{6\pi R_{hd}}\right)} \cdot \eta \quad (17)$$

As the viscosity and the rate constants are related to temperature by Eqs. 6 and 14, respectively, the  $Da$  can be further expressed as

$$Da = C \cdot \frac{lL}{V} \exp\left(\frac{B - E_a/R}{T}\right) \quad (18)$$

where

$$C = \left(1 + \frac{1}{K_m}\right) \frac{A_k A}{\epsilon \epsilon_0 \zeta - \frac{ze}{6\pi R_{hd}}} \quad (19)$$

Examination of Eqs. 18 and 19 shows that the magnitude of  $Da$  is determined roughly by four factors. The parameter  $C$  encompasses the properties of the tube wall, the migrant molecules and some kinetic properties and thus it represents the chemical nature of the system. The other factors are the pertinent tube length,  $l$ , and the electric field strength,  $V/L$ . The exponential term represents the effect of temperature on the kinetics of the reaction and on the viscosity of the medium.

The enthalpy change for the *cis-trans* isomerization of the dipeptides is close to zero in aqueous media [25,26], thus the equilibrium constant changes very little with temperature. Assuming that the dielectric constant, the zeta potential of the capillary inner wall and the molecular properties of the peptides are also invariant with temperature, the parameter  $C$  can be considered constant. According to Eq. 18, in this case the magnitude of the Damköhler number increases exponentially with the reciprocal of temperature and is proportional to the approximate capillary length squared and inversely proportional to the applied voltage. From the results in the literature [3-5] and the above discussion, it follows that the separation of interconverting species is facilitated at low Damköhler numbers. Since the kinetics are determined by the chemical nature of the system, the other avenues to lowering  $Da$  are based on the somewhat conflict-



ing conditions: the capillary length is short, the temperature is low and the voltage is high.

### 3.3. Electrophoretic behavior of phenylalanyl-proline and leucyl-proline

The dipeptides Phe-Pro and Leu-Pro were chosen to study the interplay of electrophoretic migration and reversible *cis-trans* isomerization, since the conformers of both peptides are reasonably stable below 15°C. Further, authentic samples of each conformer were available from low-temperature HPLC and subsequently validated by NMR spectroscopy [8]. Throughout this study, the operating conditions, except the temperature and capillary length, were kept constant. Thus, changes in the Damköhler number were brought about by varying one or both of these parameters.

### Effect of temperature and capillary length

Electropherograms of Phe-Pro and Leu-Pro obtained at 5, 25 and 40°C with 100 mM aqueous sodium borate buffer (pH 8.4) are shown in Fig. 3. As can be seen, the electrophoretic pattern undergoes significant changes within this temperature range. At 5°C, each dipeptide yielded two baseline-separated peaks believed to be the *cis* and *trans* conformers. At 25°C, the resolution was poor and the height ratios of the conformer peaks were different from those at 5°C. Finally at 40°C, each peptide yielded only a single, sharp peak.

In order to investigate the effect of the capillary length on the separation, experiments were carried out at 5°C by using 37, 57 and 97 cm long capillaries of 50  $\mu\text{m}$  I.D. and the electropherograms are depicted in Fig. 4. It can be seen that baseline separation was obtained only with the shortest tube; the electropherograms obtained

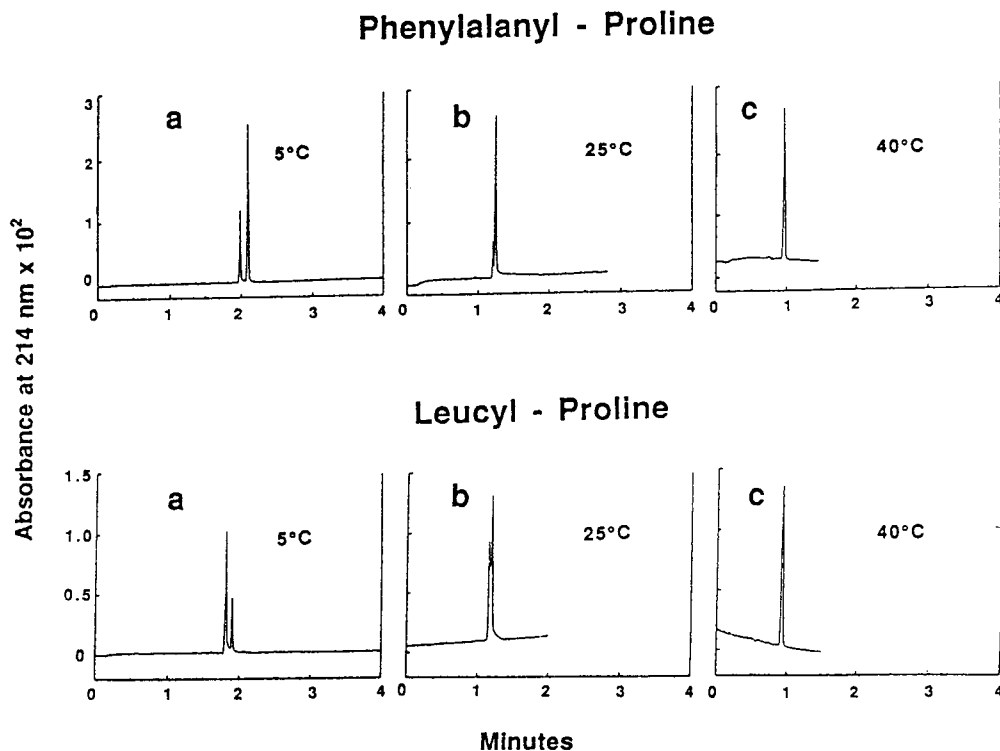


Fig. 3. Effect of temperature on the separation of *cis* and *trans* conformers of Phe-Pro and Leu-Pro. Capillary, 37 cm  $\times$  50  $\mu\text{m}$  I.D.; buffer, neat aqueous 100 mM sodium borate (pH 8.4); voltage, 30 kV; detector setting, 214 nm. (a) Temperature, 5°C; current, 13  $\mu\text{A}$ ; (b) temperature, 25°C; current, 22  $\mu\text{A}$ ; (c) temperature, 40°C; current, 29  $\mu\text{A}$ .

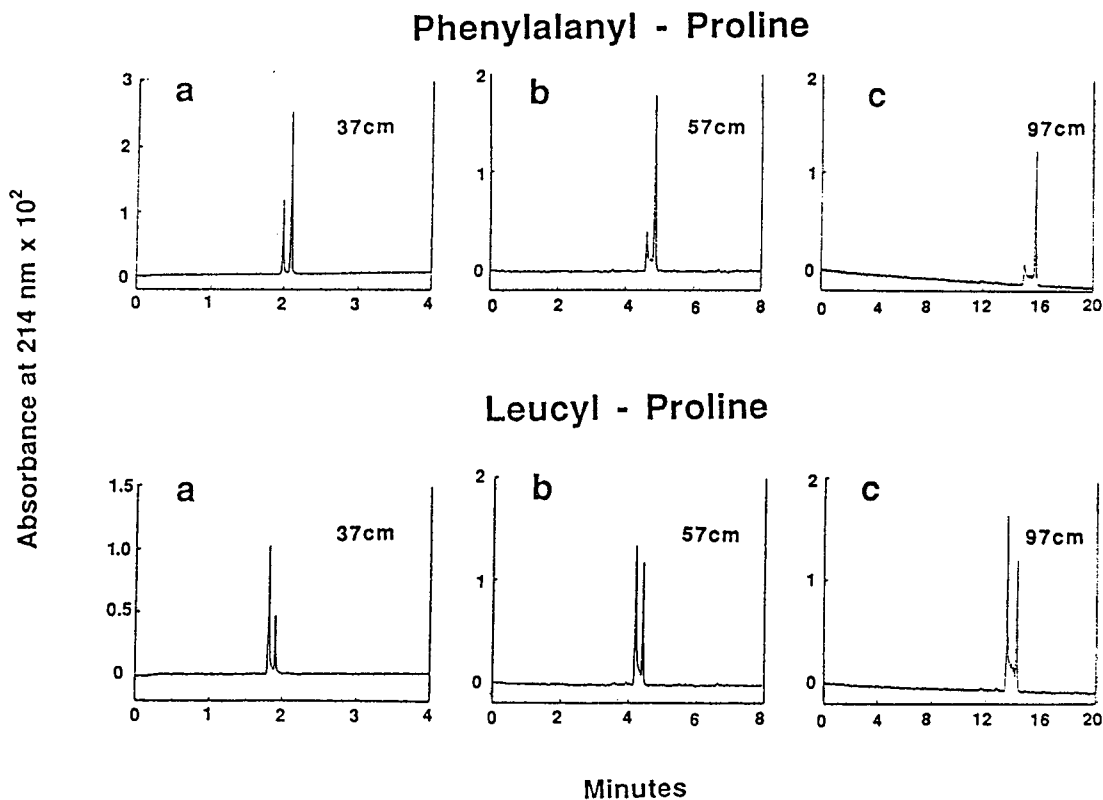


Fig. 4. Separation of the *cis-trans* conformers of Phe-Pro and Leu-Pro with 50  $\mu\text{m}$  I.D. capillaries of different lengths. Buffer, 100 mM sodium borate buffer (pH 8.4); voltage, 30 kV; temperature, 5°C; detector setting, 214 nm. (a) Length, 37 cm; current, 13  $\mu\text{A}$ ; (b) length, 57 cm; current, 9  $\mu\text{A}$ ; (c) length, 97 cm; current, 5  $\mu\text{A}$ .

with the 57 and 97 cm long capillaries show that the migration times were greatly increased and concomitantly the two peaks were not resolved owing to the intervening reaction zone.

In order to identify the conformer peaks, authentic *cis* and *trans* conformers separated by RP-HPLC, collected and kept in liquid nitrogen and validated by NMR spectroscopy, were used since CZE experiments precluded the collection of the isolated conformers in amounts sufficiently large for NMR measurements. Typical chromatograms from the RP-HPLC experiments at 0°C are shown in Fig. 5. The pure conformers isolated in such experiments were subjected to CZE in aqueous sodium borate buffer (pH 8.4) at 11°C. The migration times of the authentic conformers and those of peaks A and B in Fig. 6 are listed in Table 1. Comparison of the migra-

tion times in Table 1 shows that the two baseline-resolved peaks A and B obtained in the CZE of the dipeptides are indeed the *trans* and *cis* conformers, respectively.

The electrophoretic behavior depicted in Figs. 3 and 4 is readily explained in the light of the Damköhler number defined in Eq. 15. The measurement of both the equilibrium constant  $K_m$  and the forward rate constant  $k_f$  for the *cis-trans* interconversion by different methods under conditions employed in HPLC and CZE is described in a forthcoming paper [27]. The following parameters were obtained by the "stop-flow" method for the isomerization of Phe-Pro in the neat aqueous sodium borate buffer: the forward reaction rate constant  $k_f$  at 10°C is  $1.42 \cdot 10^{-4} \text{ s}^{-1}$ , the equilibrium constant  $K_m$  is 0.37 and the activation energy  $E_a$  is 19.4

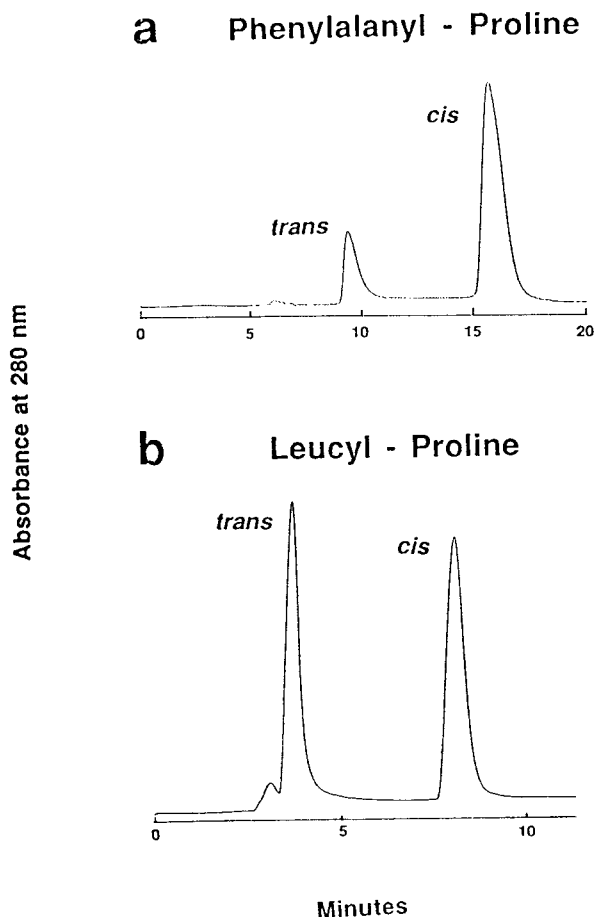


Fig. 5. Chromatographic separation of the *cis*-*trans* conformers of (a) Phe-Pro and (b) Leu-Pro at 0°C by RP-HPLC. Column, 250 × 4.6 mm I.D., 5- $\mu$ m UltraSpher ODS; detector setting, 280 nm; flow-rate, 0.5 ml min<sup>-1</sup>; mobile phase, 50 mM phosphate buffer-methanol (70:30, v/v) (pH\* 6.00).

kcal mol<sup>-1</sup>. With the above data and the measured migration times, the Damköhler numbers were calculated by using Eq. 15 and the results are presented in Table 2. As can be seen, the Damköhler number ranges from 0.03 to 1.8 under the conditions investigated and decreases with decrease in temperature and/or the capillary length, as predicted from Eq. 18.

The interference between migration and reaction is conveniently measured by  $\lambda$ , the relative amount of the substance in the reaction zone between the two peaks as illustrated in Fig. 7, which shows the dependence of  $\lambda$  on  $Da$ . When

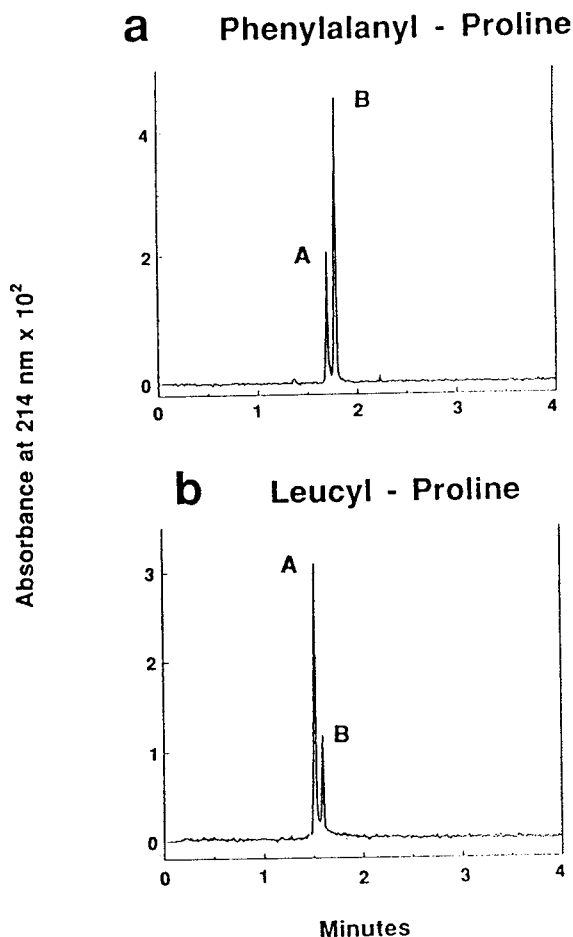


Fig. 6. Electropherograms of (a) Phe-Pro and (b) Leu-Pro showing the peaks of the *cis*-*trans* isomers identified by using authentic conformers isolated by cryochromatography. Capillary, 37 cm × 50  $\mu$ m I.D.; buffer, neat aqueous 100 mM sodium borate (pH 8.4); voltage, 30 kV; current, 16  $\mu$ A; temperature, 11°C; detector setting, 214 nm.

$Da > 0.5$ , the isomerization is rapid on the time-scale of migration and the *cis*-*trans* conformers elute as a single peak. When  $Da < 0.1$ , the isomerization is sufficiently slow for the interference to be negligible and the two conformers are separated with baseline resolution. In the range  $0.1 < Da < 0.5$ , there is an intervening plateau region between the peaks with concomitant deterioration of the separation efficiency.

Such *cis*-*trans* interconversion together with other on-column reactions, e.g., oxidation, ag-

Table 1

Migration times of the authentic *cis* and *trans* conformers and of peaks A and B obtained from each dipeptide by CZE as shown in Fig. 6

Dipeptide	Migration time, $t_R$ (min)			
	Peak A	<i>trans</i>	Peak B	<i>cis</i>
Phe-Pro	1.669	1.677	1.760	1.750
Leu-Pro	1.545	1.557	1.614	1.598

Capillary, 37 cm  $\times$  50  $\mu$ m I.D.; buffer, 100 mM sodium borate (pH 8.4); voltage, 30 kV; current, 16  $\mu$ A; temperature, 11°C.

glomeration, complexation and different kinds of isomerization, have been observed to interfere with the separation not only in CZE [10] and slab gel electrophoresis [11,12] but also in HPLC [28], where the degree of interference was expressed by the Damköhler number [3]. The critical range of  $Da$ , where the interference of the on-column reaction with the separation leads to the formation of an inter-peak reaction zone or to additional band broadening at the least, varies with the chromatographic system used and the kinetics of the reaction. However, in general such untoward phenomena are not expected to occur according to the literature [28] when  $Da < 0.1$  or  $Da > 50$ . The critical  $Da$  range in CZE, however, must be narrower than in HPLC owing to the much higher plate numbers achievable in

Table 2

Damköhler numbers characterizing the interplay of the *cis-trans* isomerization and the electrophoretic migration of Phe-Pro at different temperatures and in capillaries of different lengths under the experimental conditions

Damköhler number, $Da$	Operating temperature, $T$ (°C)	Capillary length, $L$ (cm)	Migration time, $t_R$ (min)	Forward rate constant, $k_f$ ( $10^{-4}$ s $^{-1}$ )	Relaxation time, $\tau$ (min)
0.034	5	37	2.09	0.73	61.88
0.059	10	37	1.88	1.42	31.69
0.080	5	57	5.00	0.73	61.88
0.096	16	37	1.56	2.77	16.26
0.135	20	37	1.38	4.39	10.25
0.206	25	37	1.21	7.68	5.86
0.256	5	97	15.80	0.73	61.88
0.507	35	37	1.03	22.25	2.02
0.790	40	37	0.96	36.92	1.22
1.823	50	37	0.85	96.97	0.46

Capillary ID, 50  $\mu$ m; buffer, 100 mM sodium borate, pH 8.4; voltage, 30 kV.

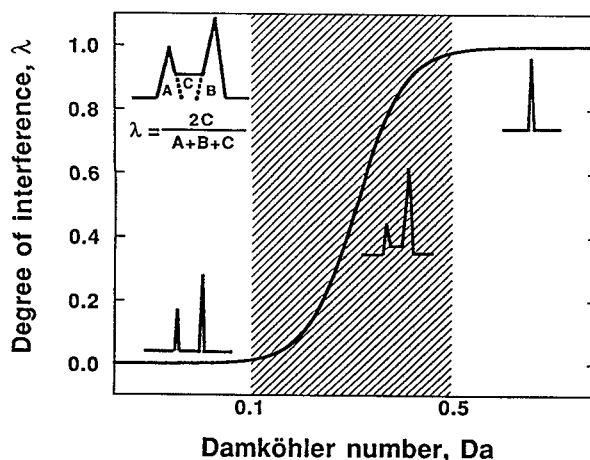


Fig. 7. Schematic illustration of the degree of interference,  $\lambda$ , by on-column *cis-trans* isomerization on the separation of *cis*- and *trans*-Phe-Pro as function of the Damköhler number.

CZE. Indeed, with the *cis-trans* isomerization of Phe-Pro, no interference of the separation by the reaction was observed outside the range  $0.1 < Da < 0.5$ .

#### Effect of molecular structure: charge and size

Fig. 6 shows electropherograms of the *cis-trans* conformers of Phe-Pro and Leu-Pro obtained by CZE at 11°C with 100 mM sodium borate buffer (pH 8.4) at 810 V/cm. It is intriguing to attempt an interpretation of the observed

electrophoretic behavior in terms of the molecular properties of the dipeptides [29]. For such an analysis, first the electrophoretic mobilities of the migrants have to be evaluated. It should be noted that under the conditions of our experiments, they are negatively charged and therefore migrate electrophoretically towards the anode against the counteracting electroosmotic flow, the coefficient,  $\mu_{\text{e eo}}$ , of which is 4–8 times greater than the  $\mu_{\text{ep}}$  values of the peptides listed in Table 3. As a consequence, the apparently faster migrating sample component in Fig. 6 has the lower electrophoretic mobility.

Our goal is to estimate from the electrophoretic mobilities the Stokes radii of the four dipeptides assuming that the electrophoretic mobility of such small peptides can be expressed by Eq. 3 as a function of their characteristic charge and size. The *cis*–*trans* conformers of each dipeptides share the same molecular mass and ionogenic functions. However, they have significantly different electrophoretic mobilities, as seen in Table 3. This finding suggests that the drag coefficient of the molecules is strongly affected by the conformation of the peptide.

Similar observations have also been reported on the electrophoretic behavior of the *cis*–*trans* isomers maleic and fumaric acid [30] and the latter was found to have the lower electrophoretic mobility. By assuming that the characteristic charges of the two isomers are essentially the same, the authors concluded that fumaric acid, the *trans* isomer, has a greater hydrodynamic radius than maleic acid. In our case, we used the Henderson–Hasselbach equation with  $\text{p}K_{\text{a}}$  val-

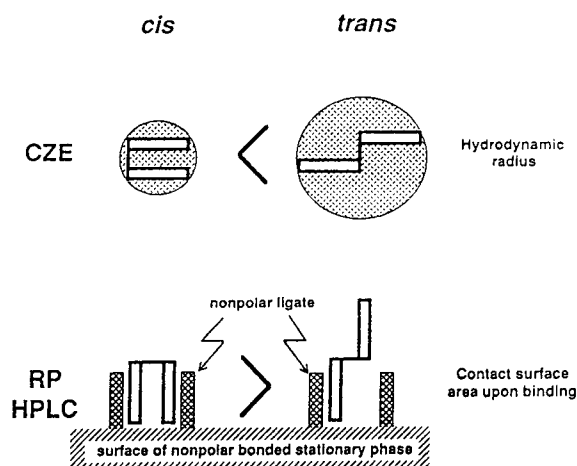


Fig. 8. Illustration of the putative origin of selectivity for the *cis* and *trans* dipeptide conformers in CZE and RP-HPLC. The *trans* isomer has a larger Stokes radius than the *cis* form and therefore has lower electrophoretic mobility in CZE. In HPLC, the *trans* form is less retained because its contact surface with the ligates of the non-polar bonded stationary phase is smaller than that of the *cis* isomer.

ues of the amino acids adjusted for microenvironmental effects [31] to estimate the electrostatic charges of the dipeptide conformers, and the results are presented in Table 3. With the  $z$  values, which are of course the same for a given *cis*–*trans* pair, the Stokes radii of each conformer were calculated from their mobilities by Eq. 3 and are also shown in Table 3. For both dipeptides, the *trans* conformers are larger than the *cis* conformers in terms of the hydrodynamic radii, as illustrated schematically in Fig. 8. Thus the slightly smaller size of the *cis* conformers is

Table 3  
Properties of the *cis* and *trans* conformers of Phe–Pro and Leu–Pro

Peptides	Molecular mass	Electrophoretic mobility, $\mu_{\text{ep}}$ ( $10^{-9} \text{ m}^2 \text{ V}^{-1} \text{ s}^{-1}$ )	$\mu_{\text{cis}}/\mu_{\text{trans}}$	Characteristic charge, $z$	Stokes radius, $R_{\text{hd}}$ (Å)
<i>cis</i> -Phe–Pro	262.3	11.07	1.20	–0.83	4.87
<i>trans</i> -Phe–Pro	262.3	9.24	1.20	–0.83	5.84
<i>cis</i> -Leu–Pro	228.3	7.47	1.34	–0.61	5.31
<i>trans</i> -Leu–Pro	228.3	5.57	1.34	–0.61	7.12

Electrophoretic mobilities were calculated by Eq. 1 from data measured in 100 mM sodium borate (pH 8.4) at 11°C and the Stokes radii were calculated by Eq. 3. The charges on the peptides were calculated from the adjusted  $\text{p}K_{\text{a}}$  values of the amino acid residues [31] by the Henderson–Hasselbach equation.

likely to be responsible for their higher mobility. Higher molecular mass, however, does not necessarily mean a larger hydrodynamic radius, as seen from the properties of the corresponding conformers in Table 3. Despite their higher molecular masses, the Phe-Pro isomers were found to have smaller Stokes radii than the Leu-Pro conformers. Since these results are contingent upon the accuracy of the  $pK_a$  values, their further refinement is essential to advance the accuracy of such calculations.

The *cis-trans* conformers of numerous dipeptides were separated by reversed-phase chromatography [3–6] and the selectivity of the chromatographic system was attributed to differences in the hydrophobic surface areas of the conformers. For the two dipeptides in the present study, by careful examination of the appropriate molecular models, the *trans* conformer was found to have the smaller hydrophobic contact areas upon binding. The illustration in Fig. 8 of

the hypothetical binding of the *cis* and *trans* dipeptides to the alkyl chains at the surface of non-polar bonded phases reflects the experimental observation that the retention times of the *trans* isomers are shorter than those of the corresponding *cis* conformers.

#### 3.4. Subzero CZE of opioid heptapeptides with one or more proline residues

The *cis-trans* conformers of the dipeptides Phe-Pro and Leu-Pro were successfully separated at temperatures above 0°C, as was shown in Figs. 3, 4 and 6. Comparable separations of isomeric opioid heptapeptides, however, required subzero temperature and the use of glycerol as an “antifreeze” in the sodium borate buffer. This is illustrated in Fig. 9 by the electropherograms of Tyr-Pro-Phe-Asp-Val-Val-Gly-NH<sub>2</sub>, which has a single peptidyl-proline bond and therefore is expected to have two

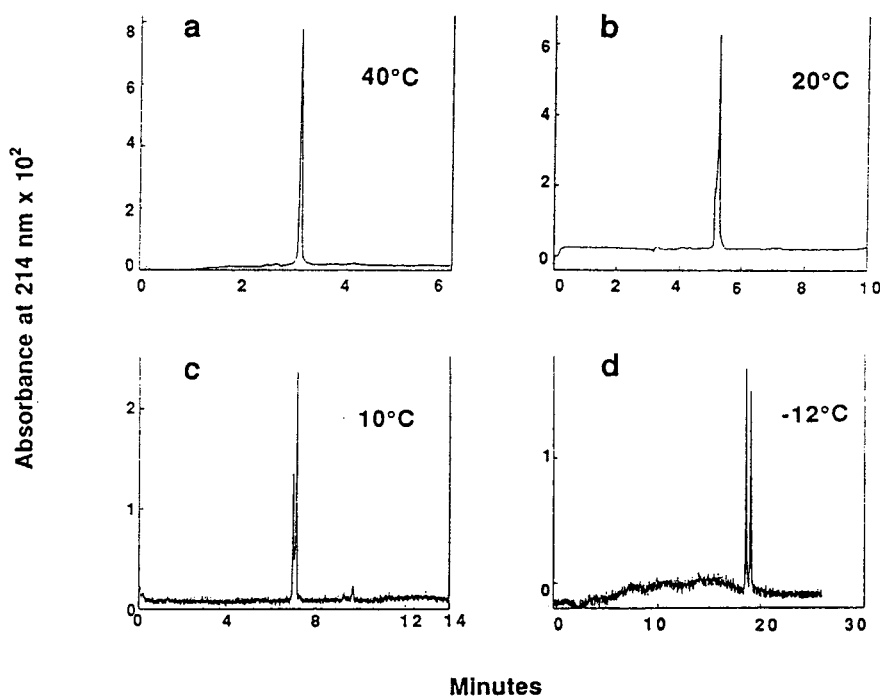


Fig. 9. Electropherograms of Tyr-Pro-Phe-Asp-Val-Val-Gly-NH<sub>2</sub> obtained at various temperatures. Capillary, 37 cm  $\times$  50  $\mu$ m I.D.; buffer, aqueous 50 mM sodium borate containing 23% glycerol (pH\* 11.3); voltage, 30 kV; detector setting, 214 nm. (a) Temperature, 40°C; current, 47  $\mu$ A; (b) temperature, 20°C; current, 30  $\mu$ A; (c) temperature, 10°C; current, 23  $\mu$ A; (d) temperature, -12°C; current, 9  $\mu$ A.

relatively stable conformers. A mixture of 77% (v/v) borate buffer and 23% (v/v) glycerol was the electrophoretic medium (the reading of the pH meter with glass electrode was  $\text{pH}^* 11.3$ ) and the effect of temperature on the electrophoretic behavior is shown in Fig. 9. The heptapeptide yields only a single sharp peak at  $40^\circ\text{C}$  (Fig. 9a), but on lowering the temperature, a shoulder appears at the leading edge of the peak at  $20^\circ\text{C}$  (Fig. 9b). The shoulder becomes a sharp peak at the front of the main peak at  $10^\circ\text{C}$ , as depicted in Fig. 9c. With further decrease in temperature, this sharp peak increases and at  $-12^\circ\text{C}$  it becomes taller than the “main” peak and the two are separated with baseline resolution (Fig. 9d).

In order to elucidate the effect of the glycerol content of the electrophoretic medium on the separation of the *cis-trans* peptide isomers at low temperatures, Phe-Pro was also subjected to CZE in the aqueous-organic mixture described above and the electropherograms obtained at

four different temperatures are shown in Fig. 10. The peptide yielded only a single peak at  $40^\circ\text{C}$ , but on lowering the temperature the two conformers gradually emerged as individual peaks and were separated with baseline resolution at  $10^\circ\text{C}$ . In neat aqueous borate, the electrophoretic migration behavior of Phe-Pro was essentially the same as in the medium containing glycerol and, as seen in Fig. 6, the separation of the conformers was also completed on lowering the temperature to  $11^\circ\text{C}$ . Comparison of the two cases suggests that the presence of the glycerol has no major effect on the chemical nature of the system. On the other hand, Fig. 10c and d confirm that the resolution improved with further decrease in temperature and reveal that the effect of glycerol is mainly due to imparting to the medium the high viscosity that is responsible for the much improved separation efficiency by virtue of a concomitant decrease in diffusivity and the much longer migration rates.

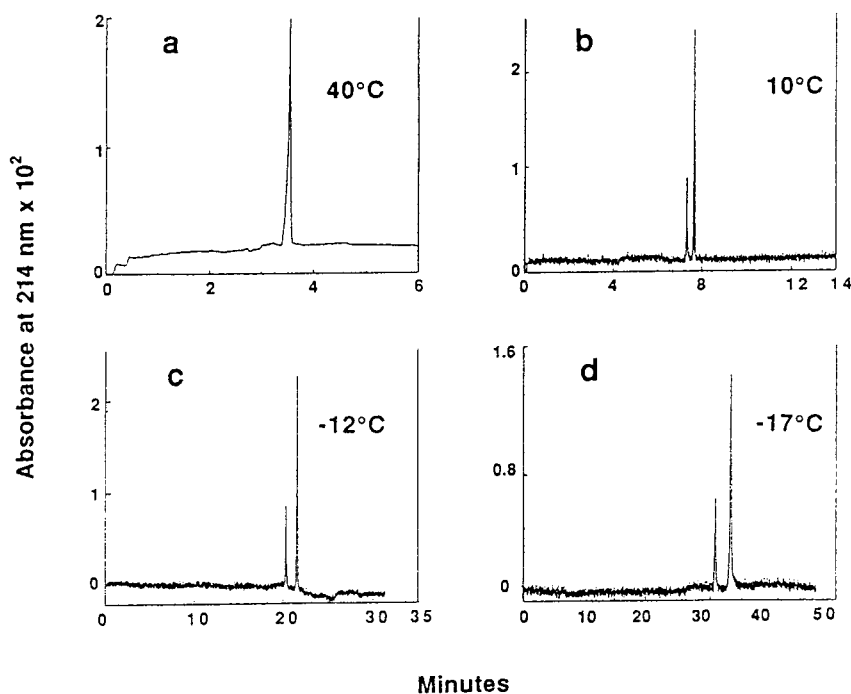


Fig. 10. Electropherograms of Phe-Pro obtained at various temperatures. Capillary, 37 cm  $\times$  50  $\mu\text{m}$  I.D.; buffer, aqueous 50 mM sodium borate containing 23% glycerol ( $\text{pH}^* 11.3$ ); voltage, 30 kV; detector setting 214 nm. (a) Temperature,  $40^\circ\text{C}$ ; current, 47  $\mu\text{A}$ ; (b) temperature,  $10^\circ\text{C}$ ; current, 23  $\mu\text{A}$ ; (c) temperature,  $-12^\circ\text{C}$ ; current, 9  $\mu\text{A}$ . (d) temperature,  $-17^\circ\text{C}$ ; current, 7  $\mu\text{A}$ .

The effect of temperature on the resolution of the *cis*–*trans* isomers of different peptides in the same electrophoretic medium can be assessed by comparing Figs. 9 and 10, which illustrate the respective electropherograms of the heptapeptide and Phe–Pro obtained in the same medium containing 23% (v/v) glycerol. It is seen that the Phe–Pro isomers could be resolved at 10°C, whereas the separation of the *cis* and *trans* forms of the heptapeptide required –12°C. The temperature, at which the *cis*–*trans* peptide forms are completely resolved under otherwise fixed conditions, could be used as a practical measure of the difficulty associated with the separation. This temperature measured with a fixed electrophoretic system could be used to rank interconverting peptides according to their kinetics. In turn, by using a suitable peptide standard and different media, the temperature of complete resolution would be a characteristic of media effects.

It is recalled that the Damköhler number is an

exponential function of the reciprocal temperature and depends roughly on the capillary length squared. Therefore, reducing the capillary length offers an alternative to lowering the temperature in order to diminish  $Da$  and thus improve the separation of the conformers. Computer simulations are in progress to shed light on the effect of temperature and capillary length on the separation of such interconverting species over a wide range of conditions.

Up to now, we have examined the CZE of peptides containing a single proline residue. In the following, we report results with the electrophoretic migration behavior of the opioid heptapeptide Tyr–Pro–Phe–Gly–Tyr–Pro–Ser–NH<sub>2</sub>, which has two peptidyl–proline bonds and consequently should have, at sufficiently low temperatures, four relatively stable conformers: *cis*–*cis*, *cis*–*trans*, *trans*–*cis* and *trans*–*trans*. CZE experiments were conducted with the 50 mM aqueous sodium borate–glycerol mixture (pH\* 11.3). Again, at 40°C a single peak is obtained, as

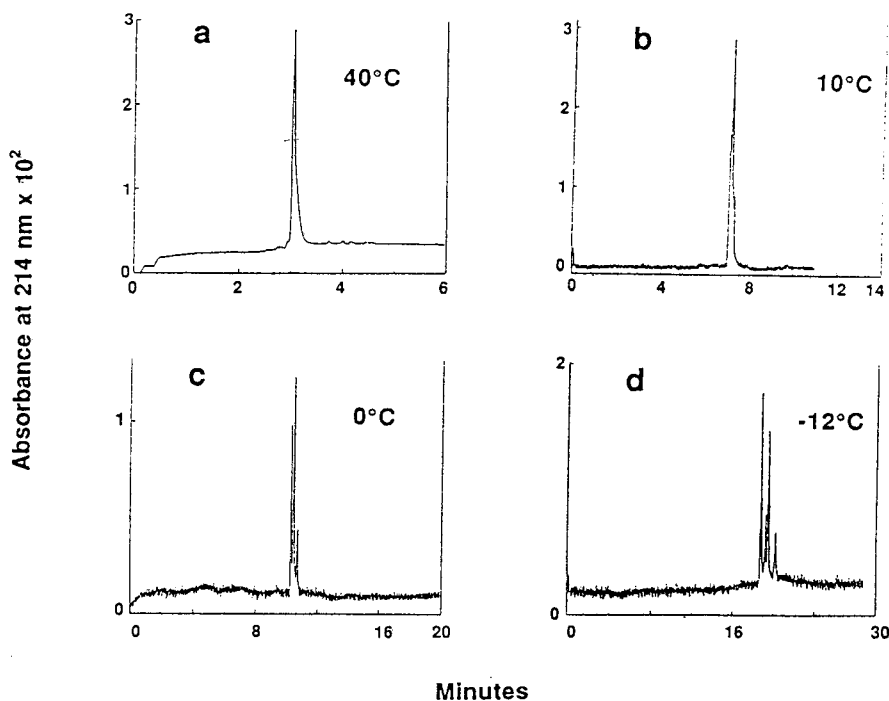


Fig. 11. Electropherograms of Tyr–Pro–Phe–Gly–Tyr–Pro–Ser–NH<sub>2</sub> obtained at various temperatures. Capillary, 37 cm × 50 μm I.D.; buffer, aqueous 50 mM sodium borate containing 23% glycerol (pH\* 11.3); voltage, 30 kV; detector setting, 214 nm. (a) Temperature, 40°C; current, 47 μA; (b) temperature, 10°C; current, 23 μA; (c) temperature, 0°C; current, 17 μA; (d) temperature, –12°C; current, 9 μA.



shown in Fig. 11a. With decreasing temperature, the peak gradually broadens until several small peaks appear to arise at 10°C as depicted in Fig. 11b. With further decrease in temperature to 0°C, the peaks become more pronounced, as illustrated in Fig. 11c, and at –12°C the four peaks are almost resolved except for the inter-peak reaction zone near the baseline, as seen in Fig. 11d. Further decrease in the temperature to –17°C resulted in a long residence time and concomitantly the resolution of the four conformers deteriorated.

The results demonstrate that CZE can be a highly efficient tool for the separation of *cis-trans* peptide conformers at sufficiently low temperatures, at least when the peptides are small in size and contain no polar amino acid near the proline residue. As an analytical separation method, CZE competes very favorably with HPLC owing to its much higher resolving power, which comes to be even higher at low temperatures, but the latter technique is far superior when large quantities of the pure isomers are to be isolated for further use.

Besides being high-performance techniques for the separation of labile sample components in non-analytical applications, both HPLC and CZE can be used for physico-chemical measurements that provide insight into distinct features of the molecular architecture of the substances under investigation. These approaches are, therefore, appropriately referred to as molecular chromatography and molecular electrophoresis.

The enhanced separation efficiency at subambient/subzero temperatures provides further incentives to use CZE not only for the separation of *cis-trans* conformers of peptides or other reacting samples, but also to carry out analytical CZE at low temperatures in general. This approach is being further pursued in our laboratory to explore the potential of cryoelectrophoresis at temperatures down to –50°C.

#### Acknowledgements

We thank the Alexander von Humboldt Foundation for financial support in the form of a Feodor–Lynen Fellowship for F.K. and the

foundation of German Chemical Industry for providing a Habilitation Scholarship for F. Th. A.K. is grateful to the Halász Foundation for financial support. This work was funded by grant GM No. 20993 from National Institute of Health, US Public Health Service.

#### References

- [1] H.L. Maia, K.G. Orrell and H.N. Rydon, *Chem. Commun.*, (1971) 1209.
- [2] J.F. Brandts, H.R. Halvorson and M. Brennan, *Biochemistry*, 14 (1975) 4953.
- [3] W.R. Melander, J. Jacobson and Cs. Horváth, *J. Chromatogr.*, 234 (1982) 269.
- [4] J. Jacobson, W. Melander, G. Vaisnys and Cs. Horváth, *J. Phys. Chem.*, 88 (1984) 4536.
- [5] W.R. Melander, H.J. Lin, J. Jacobson and Cs. Horváth, *J. Phys. Chem.*, 88 (1984) 4527.
- [6] D.E. Henderson and Cs. Horváth, *J. Chromatogr.*, 368 (1986) 203.
- [7] D.E. Henderson and J.A. Mello, *J. Chromatogr.*, 499 (1990) 79.
- [8] A. Kálmán, F. Thuncke, Cs. Horváth, R. Schmidt and P.W. Schiller, *J. Chromatogr. A*, in press.
- [9] R.J. Nelson and D.S. Burgi, in J.P. Landers (Editor), *Handbook of Capillary Electrophoresis*, CRC Press, Ann Arbor, MI, 1994, pp. 549–563.
- [10] G.M. Janini, G.M. Muschik and H.J. Issaq, *J. High Resolut. Chromatogr.*, 17 (1994) 753.
- [11] C.M. Park, *Ann. N.Y. Acad. Sci.*, 209 (1973) 237.
- [12] M. Perrella, A. Heyda, A. Mosca and L. Rossi-Bernardi, *Anal. Biochem.*, 88 (1978) 212.
- [13] M.G. Harrington and T.E. Zewert, *Electrophoresis*, 15 (1994) 195.
- [14] P.W. Schiller, G. Weltrowska, T.M.D. Nguyen, C. Lemieux, N.N. Chung, B.J. Marsden and B.C. Wilkes, *J. Med. Chem.*, 34 (1991) 3125.
- [15] R. Schmidt, A. Kálmán, N.N. Chung, C. Lemieux, Cs. Horváth and P.W. Schiller, *Int. J. Pept. Protein Res.*, in press.
- [16] R.C. Weast, *Handbook of Chemistry and Physics*, Chemical Rubber Co., Cleveland, OH, 49th ed., 1968.
- [17] I.N. Levine, *Physical Chemistry*, McGraw-Hill, New York, 3rd ed., 1988, pp. 467–511.
- [18] E.N. da C. Andrade, *Nature*, 125 (1930) 582.
- [19] G.J. Janz and R.P.T. Tomkins, *Nonaqueous Electrolytes Handbook I*, Academic Press, New York, 1972, p. 99.
- [20] R.C. Reid, J.M. Prausnitz and B.E. Poling, *The Properties of Gases and Liquids*, McGraw-Hill, New York, 4th ed., 1987, p. 439.
- [21] J.C. Giddings, *Sep. Sci.*, 4 (1969) 181.
- [22] J.W. Jorgenson and K.D. Lukacs, *Anal. Chem.*, 53 (1981) 1298.

- [23] J.C. Giddings, *J. Chromatogr.*, 395 (1987) 19.
- [24] J.C. Giddings, *J. Chromatogr.*, 480 (1989) 21.
- [25] L.N. Lin and S.F. Brandts, *Biochemistry*, 18 (1979) 43.
- [26] H.N. Cheng and F.A. Bovey, *Biopolymers*, 16 (1977) 1465.
- [27] F. Thuncke, A. Kálmán, F. Kálmán, S. Ma and Cs. Horváth, presented at the 14th American Peptide Symposium, Columbus, OH, 18–23 June 1995, P745.
- [28] Cs. Horváth, in H. Kalász and L.S. Ettre (Editors), *Proceedings of Chromatography '85*. Akadémiai Kiadó, Budapest, 1986, pp. 1–18.
- [29] Z. Deyl, in Z. Deyl, F.M. Everaerts, Z. Prusík and P.J. Svendsen (Editors), *Electrophoresis*, Elsevier, Amsterdam, 1979, pp. 45–66.
- [30] R.R. Chadwick and J.C. Hsieh, *Anal. Chem.*, 63 (1991) 2377.
- [31] E.C. Rickard, M.M. Strohl and R.G. Nielsen, *Anal. Biochem.*, 197 (1991) 197.

# Use of negatively charged sulfobutyl ether- $\beta$ -cyclodextrin for enantiomeric separation by capillary electrophoresis

Claudia Desiderio, Salvatore Fanali\*

*Istituto de Cromatografia del CNR, Area della Ricerca di Roma, P.O. Box 10, 00016 Monterotondo Scalo (Rome), Italy*

## Abstract

A newly modified charged  $\beta$ -cyclodextrin (sulfobutyl ether- $\beta$ -cyclodextrin) was investigated as a chiral selector in capillary electrophoresis in a study of the enantiomeric separation of a variety of underivatized anionic and cationic compounds of pharmaceutical interest and uncharged phenyl alcohols and dansyl-amino acids. Owing to the presence of four sulfonic groups, the chiral selector is negatively charged at all pH values used (2.5–9) and the complexation caused an increase in migration time for each compound studied. At a relatively low pH (2.5) the chiral selector could only be used at low concentration (0.1–0.5 mg/ml) for basic compounds, whereas at higher pH (6–9) the modified cyclodextrin in the concentration range 0–20 mg/ml was used. The concentration of the chiral selector, the distance from the aromatic group of the asymmetric centre of the analytes and the chemical composition and pH of the background electrolyte influenced the complexation, selectivity and resolution. Good enantiomeric separation was obtained for terbutaline at all pH values studied, whereas for other racemic compounds, warfarin, acenocoumarol, promethazine, bupivacaine and some dansyl-amino acids and phenyl alcohols, the pH range 6–9 was effective for optimizing the chiral resolution. Non-polar substituent groups on the asymmetric carbon of the analytes seem to enhance the complexation and the stereoselectivity.

## 1. Introduction

The analysis of chiral drugs is a very important field of application, especially in pharmaceutical science, because very often the two enantiomers possess different pharmacological and toxicological properties. Thus rapid, sensitive and high-resolution separation methods need to be optimized for chiral purity control of drugs, pharmacokinetic and/or medical studies, etc.

Analytical methods so far used for chiral separations include high-performance liquid chromatography (HPLC) [1–3], thin-layer chromatography (TLC) [4], gas chromatography

(GC) [5–7] and, more recently, capillary electrophoresis (CE) [8–15].

Capillary electrophoresis, which has the above-mentioned characteristics, is becoming very popular for enantiomeric separations mainly using the direct separation method [14]. Among the different separation mechanisms and chiral selectors used in CE, inclusion complexation by cyclodextrin (CD) forming labile diastereoisomeric complexes during the run exhibited successful stereoselective effects, allowing the chiral separation of a wide number of compounds [16].

Among the native CD ( $\alpha$ -,  $\beta$ - and  $\gamma$ -) used in CE for chiral resolution,  $\beta$ -CD proved to be the most versatile resolving agent, probably owing to its cavity dimensions, able to accommodate a

\* Corresponding author.

wide range of analytes. Unfortunately, its use is limited owing to its relatively low solubility [1.8% (w/v) in aqueous buffer].

Primary and secondary hydroxy groups of the CDs can be modified chemically, leading to CDs with properties different from the native compounds, e.g., increased solubility, different conformation, different dimensions and additional stereoselective bondings.

Chargeable cyclodextrins, first introduced by Terabe [10], represent an interesting field of research in chiral separation by CE [13,17–21]. As previously investigated [19,20], the use of a chiral selector with its own mobility, opposite to that of the electrosmotic flow, showed a strong resolving power, also at very low concentration. Further, the ion-pairing interaction can be advantageously used for the inversion of migration of the two separated enantiomers [13,21].

The aim of this work was to investigate the utility of the negatively charged sulfobutyl ether- $\beta$ -CD derivative (SBE- $\beta$ -CD) on the enantiomeric separation by capillary electrophoresis of several basic and acidic compounds of pharmaceutical interest, including antihypertensive, anticoagulant, antihistaminic, anaesthetic and bronchodilator underivatized drugs and several uncharged phenyl alcohols. The effect of the concentration of the chiral selector added to the background electrolyte (BGE) and the effect of the pH of the BGE on the effective mobility, resolution and selectivity were examined.

## 2. Experimental

### 2.1. Chemicals and reagents

All solvents used were of HPLC or analytical-reagent grade and were purchased from Carlo Erba (Milan, Italy). Phosphoric acid (85%), sodium hydroxide and tris(hydroxymethylaminomethane) (Tris) were obtained from Carlo Erba and hydrochloric acid (30%) and borax (sodium tetraborate) from Merck (Darmstadt, Germany). Sulfobutyl ether- $\beta$ -cyclodextrin was kindly provided by Perkin-Elmer (San Jose, CA, USA). Warfarin, promethazine, pindolol racemic

standard compounds, D,L-2-phenyl-2-butanol (2-Ph-2B), (S)-(-)-1-phenyl-1-butanol (1-Ph-1B), (R)-(+)-1-phenyl-1-butanol, (S)-(+)-1-phenyl-1,2-ethanediol (1-Ph-1,2-diol), (R)-(-)-1-phenyl-1,2-ethanediol, ( $\pm$ )-1-phenyl-1-propanol (1-Ph-1P), (S)-(+)-2-methoxy-2-phenylethanol (2-Me-2-PhE), (R)-(-)-2-methoxy-2-phenylethanol and ( $\pm$ )- $\alpha$ -ethylphenethyl alcohol ( $\alpha$ -Et-PhEt) were purchased from Aldrich (Steinheim, Germany) and (R)-(+)- and (S)-(-)-1-phenylethanol (1-PhEt) from Fluka (Buchs, Switzerland). Racemic acenocoumarol was purchased as a commercial pharmaceutical preparation. Terbutaline, propranolol, atenolol, oxprenolol, bupivacaine, metoprolol were obtained from Sigma (St. Louis, MO, USA). Stock standard solutions ( $10^{-3}$  M) of the standard compounds were prepared in methanol and then diluted using 10 mM of buffer (pH 6) in order to obtain  $10^{-4}$  M working standard solutions for injection.

### 2.2. Instrumentation

Electrophoretic experiments were carried out using a Biofocus 3000 automated capillary electrophoresis apparatus (Bio-Rad Labs., Hercules, CA, USA), equipped with a multi-wavelength UV detector. The output detector wavelength was 206 nm. Electrophoretic runs were performed in uncoated fused-silica capillaries of 40 cm  $\times$  50  $\mu$ m I.D. (35.5 cm effective length) (Polymicro Technologies, Phoenix, AZ, USA) and 50 cm  $\times$  50  $\mu$ m I.D. (45.5 cm effective length) (Bio-Rad). The capillaries were positioned into a Bio-Rad user assembler cartridge after removing the polyimide layer (about 0.5 cm). Injections were made by the pressure method applying 5 p.s.i. s at the anodic end of the capillary. A constant voltage of 15 kV was applied for the electrophoretic runs. In order to obtain good data reproducibility, washings between runs consisted of four purge cycles: water (50 s), followed by 0.1 M sodium hydroxide (50 s), then water (60 s) and BGE (60 s). Background electrolytes of pH 2.5 and 6 were prepared from concentrated phosphoric acid solution (85%, w/v) titrated with NaOH to the final pH value, the final concentration being 50 mM,

while 50 mM Tris-HCl and 50 mM sodium tetraborate-phosphoric acid buffers were used for experiments at pH 8 and 9, respectively.

Electroosmotic flow was measured by detecting for each sample injection the methanol peak as electroosmosis marker.

### 3. Results and discussion

#### 3.1. Separation of basic and acidic compounds

Several basic compounds of pharmaceutical interest, namely pindolol, propranolol, oxprenolol, atenolol, metoprolol, promethazine, bupivacaine and terbutaline, were analysed by CE using phosphate buffer of pH 2.5. Under the operating conditions, all the analytes were positively charged and moved as a single peak to the cathode. For the study of enantiomeric separation, a new modified  $\beta$ -CD, sulfobutyl ether- $\beta$ -CD, was added to the BGE.

As can be seen in Fig. 1, the sulfobutyl ether- $\beta$ -CD possesses four modified hydroxyl groups at position 6 through an ether bond with a butyl chain and with a sulfonic group at the end. The presence of the sulfonic group makes the CD derivative negatively charged at any commonly used pH in CE and more soluble in aqueous buffer in comparison with the parent compound. Owing to its charge, the SBE- $\beta$ -CD moved in the opposite direction to the analytes. Different amounts of the chiral selector, in the range 0.1–5 mg/ml, were added to the BGE at pH 2.5 and the racemic samples were injected separately for the electrophoretic runs. Among the basic drugs studied, only racemic terbutaline was resolved

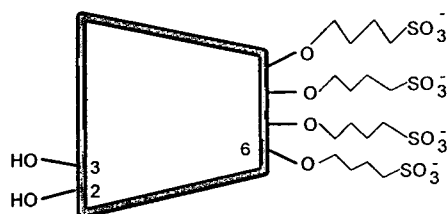


Fig. 1. Structure of sulfobutyl ether- $\beta$ -cyclodextrin (SBE- $\beta$ -CD).

into its enantiomers. The enantiomeric separation of the other compounds was not successful because broad peaks were obtained with increasing concentration of SBE- $\beta$ -CD. This effect was probably due to both strong electrostatic interactions between negatively charged CD-analytes and adsorption on the capillary wall. Further, electromigration dispersion and polydispersive effects arising from multiple species in the SBE- $\beta$ -CD [22] should be taken into account. The tailing recorded for basic compounds confirmed previous findings [19], hence the use of CD concentrations higher than 0.5 mg/ml was not possible, hindering further studies.

Preliminary experiments using a phosphate buffer of pH 6 and containing different amounts of SBE- $\beta$ -CD were successful for the enantiomeric separation of several compounds with good peak shapes even at concentrations of chiral selector higher than 0.5 mg/ml. Thus a phosphate buffer of pH 6 was selected for further investigations of both basic and acidic analytes (for their structures, see Fig. 2), the former moving to the detector by the electroosmotic flow. In this study, the concentration of SBE- $\beta$ -CD added to the BGE was in the range 0–20 mg/ml.

Fig. 3a and b show the electropherograms of the separation of racemic terbutaline into its enantiomers at pH 2.5 and 6, respectively, with 0.2 and 1 mg/ml of SBE- $\beta$ -CD, respectively. Good enantiomeric resolution was achieved under both experimental conditions, but with a noticeable decrease in migration time at pH 6.

The effective mobility, resolution factor and selectivity were calculated using the following equations:

$$\mu_a = \mu_e + \mu_{eof} \quad (1)$$

$$R = 2 \cdot \frac{t_2 - t_1}{w_2 + w_1} \quad (2)$$

$$S = \frac{\Delta\mu}{\mu_m} \quad (3)$$

where  $\mu$ ,  $R$  and  $S$  represent the mobility, resolution factor and selectivity, respectively, a stands for apparent, e for effective and eof indicates the electroosmotic flow;  $\Delta\mu$  and  $\mu_m$  are

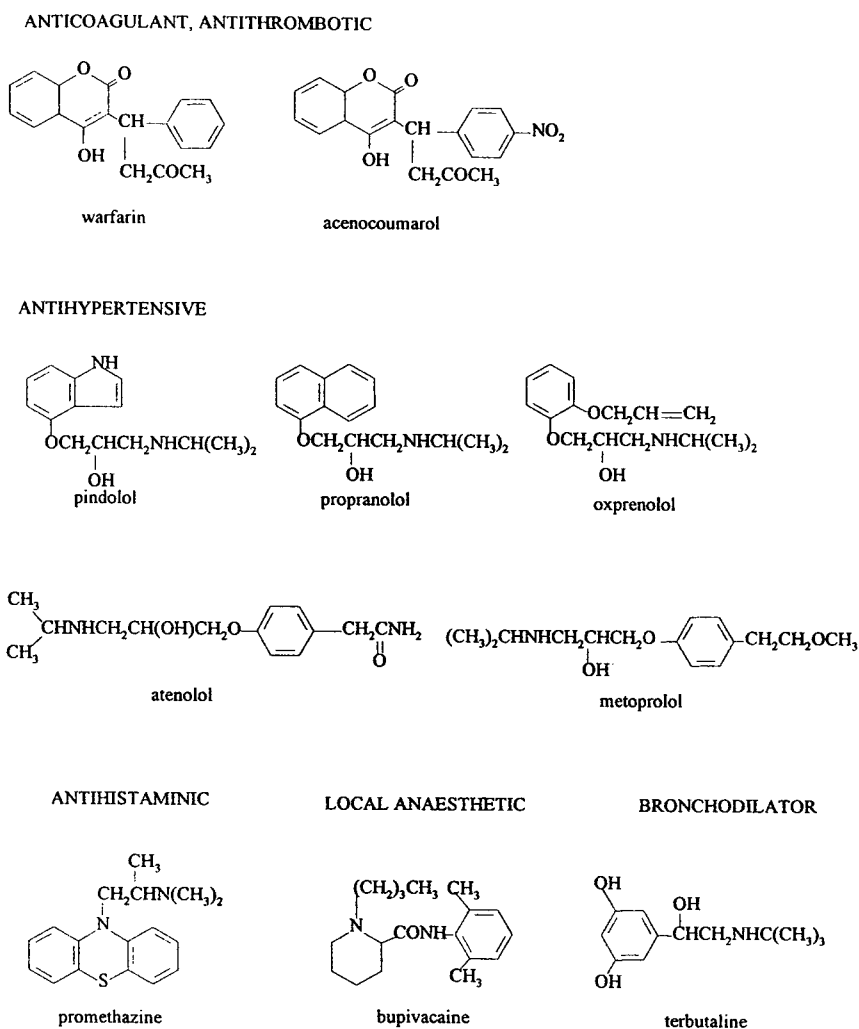


Fig. 2. Structures of the studied compounds of pharmaceutical interest.

the difference in effective mobilities of the two enantiomers and their media, respectively.

The migration times of the analytes were influenced by the concentration of modified CD; a general increase in migration time with increasing CD concentration was recorded owing to the complexation effect towards the analytes.

As can be seen in Fig. 4, both the analytes and chiral selector were carried towards the detector by the electroosmotic flow; the negatively charged CD forming diastereoisomeric complexes caused a retardation of all compounds studied. The apparent mobility ( $\mu_a$ ) for basic

and acidic analytes is a combination of the mobility of free and complexed analyte and of the electroosmotic flow. In the case of cationic compounds, the effective mobility ( $\mu_e$ ) was positive and in some instances dropped to a negative value when the concentration of SBE- $\beta$ -CD was increased. For acidic analytes the sign of the mobility was always negative, i.e., they were migrating behind the electroosmotic flow.

Fig. 5 shows the effect of the concentration of SBE- $\beta$ -CD, added to the BGE at pH 6, on the effective mobility of the studied underivatized drugs. Owing to the strong complexation, inver-

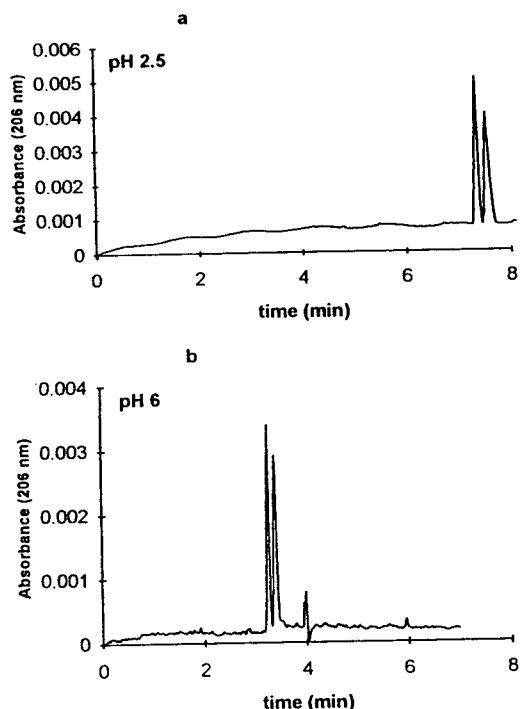


Fig. 3. Electropherograms of the enantiomeric separation of racemic terbutaline. Capillary, 40 (35.5) cm  $\times$  0.05 mm I.D. (uncoated). The concentration of SBE- $\beta$ -CD was 0.2 mg/ml and 1 mg/ml dissolved in 50 mM phosphate buffer at pH (a) 2.5 and (b) 6.0, respectively. The concentration of terbutaline was  $10^{-4}$  M injected by pressure at 5 p.s.i. s. Applied voltage, 15 kV.

sion of mobility was obtained for promethazine at 1 mg/ml, propranolol at 3 mg/ml, metoprolol at 6 mg/ml, pindolol and terbutaline at 10 mg/ml

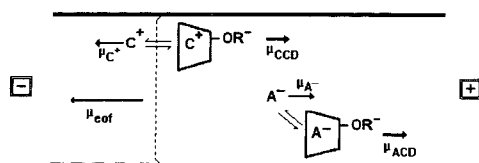


Fig. 4. Electrophoretic separation mechanism of cationic and anionic analytes using a negatively charged cyclodextrin.

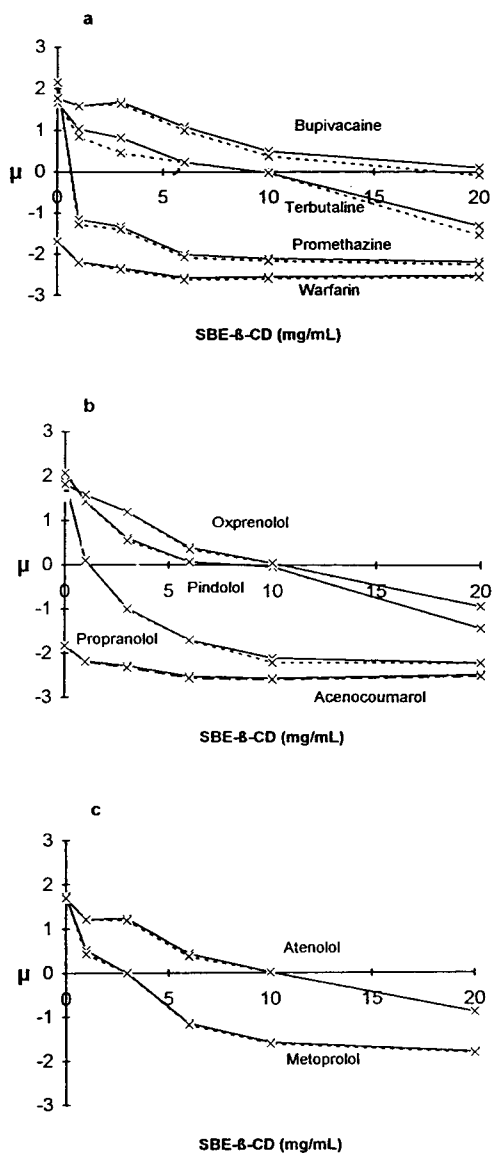


Fig. 5. Effect of the concentration of sulfobutyl ether- $\beta$ -cyclodextrin (SBE- $\beta$ -CD) on the effective mobility of the studied compounds of pharmaceutical interest. Background electrolyte, 50 mM phosphate buffer (pH 6) containing different concentrations of chiral selector; capillary (uncoated), 50 cm  $\times$  0.05 mm I.D. For other experimental conditions, see Table 1.

ml and oxprenolol, bupivacaine and atenolol at 20 mg/ml. Hence the complexation order, based on the decrease or increase in  $\mu_e$  for cationic and anionic drugs, respectively, was estimated to be

promethazine > propranolol > metoprolol > terbutaline = pindolol > bupivacaine > oxprenolol > atenolol > warfarin = acenocoumarol.

Table 1 gives the calculated resolution factor and selectivity when the analytes were run at pH 6 and the BGE contained increasing concentrations of chiral selector.

Enantiomeric resolution was achieved for warfarin, acenocoumarol, promethazine, metoprolol and terbutaline when the lowest concentration of chiral selector was used (1 mg/ml). At this concentration baseline resolution was obtained only for the former compound (terbutaline), while 3 mg/ml of SBE- $\beta$ -CD were necessary for acenocoumarol and warfarin, 6 mg/ml for promethazine and 10 mg/ml for bupivacaine. Poor enantiomeric resolution was obtained for metoprolol, oxprenolol, atenolol, pindolol and propranolol ( $R < 0.5$ ).

Relatively high selectivity was recorded for terbutaline, metoprolol and promethazine when 1 mg/ml of SBE- $\beta$ -CD was added to the BGE, whereas for oxprenolol and atenolol a higher concentration of modified CD was necessary in order to obtain comparable results. The increase in the concentration of the chiral selector caused

a decrease in selectivity for promethazine, terbutaline and metoprolol; for the other analytes the reverse occurred except for warfarin and acenocoumarol, which showed a maximum of  $S$  at 3 mg/ml of CD.

These results indicate the importance of the concentration of the chiral selector for the optimization of the baseline enantiomeric separation of racemic warfarin, acenocoumarol, promethazine and bupivacaine using different concentrations of SBE- $\beta$ -CD.

Fig. 6 shows the electropherograms of the enantiomeric separation of racemic warfarin, acenocoumarol, promethazine and bupivacaine using the BGE at pH 6 with SBE- $\beta$ -CD.

In order to study the dependence of the effective mobilities and resolution on pH, phosphate buffer (pH 6), Tris-HCl buffer (pH 8) and borate-phosphate buffer (pH 9) containing 20 mg/ml SBE- $\beta$ -CD were used. On increasing the buffer pH from 6 to 9, in the absence of a chiral agent, almost all the investigated drugs still exhibited their cationic or anionic behaviour with lower mobilities, close to the electroosmotic flow in some cases, probably in accord with their  $pK_a$  values. Electroosmotic flow (EOF) measurement, using methanol as EOF marker, revealed

Table 1

Effect of the concentration of sulfobutyl ether- $\beta$ -cyclodextrin (SBE- $\beta$ -CD) on the resolution ( $R$ ) and selectivity ( $S$ ) of racemic compounds of pharmaceutical interest ( $\mu_c$ :  $10^{-4}$  cm<sup>2</sup> V<sup>-1</sup> s<sup>-1</sup>)

Compound	SBE- $\beta$ -cyclodextrin (mg/ml)									
	1		3		6		10		20	
	$R$	$S$	$R$	$S$	$R$	$S$	$R$	$S$	$R$	$S$
(1) Warfarin	<0.5	0.009	1.09	0.017	1.35	0.015	1.69	0.016	2.11	0.016
(2) Acenocoumarol	0.63	0.009	1.09	0.017	1.40	0.016	1.59	0.012	2.13	0.012
(3) Promethazine	<0.5	0.098	0.78	0.051	1.28	0.034	1.45	0.028	2.00	0.027
(4) Bupivacaine	–	–	<0.5	0.030	1.0	0.086	1.36	0.273	–	–
(5) Terbutaline	1.56	0.191	nm	nm	nm	nm	nm	nm	5.10	0.161
(6) Pindolol	–	–	<0.5	0.087	–	–	–	–	–	–
(7) Metoprolol	<0.5	0.189	–	–	<0.5	0.026	<0.5	0.019	<0.5	0.011
(8) Propranolol	–	–	<0.5	0.020	<0.5	0.006	–	–	–	–
(9) Oxprenolol	–	–	–	–	<0.5	0.108	–	–	–	–
(10) Atenolol	–	–	<0.5	0.033	<0.5	0.150	–	–	–	–

Capillary, 50 (45.5) cm  $\times$  0.05 mm I.D. (uncoated); background electrolyte, 50 mM phosphate buffer (pH 6) supplemented with the appropriate concentration of chiral selector; applied voltage, 15 kV (constant); injection, pressure 5 p.s.i. of  $10^{-4}$  M racemic compounds.



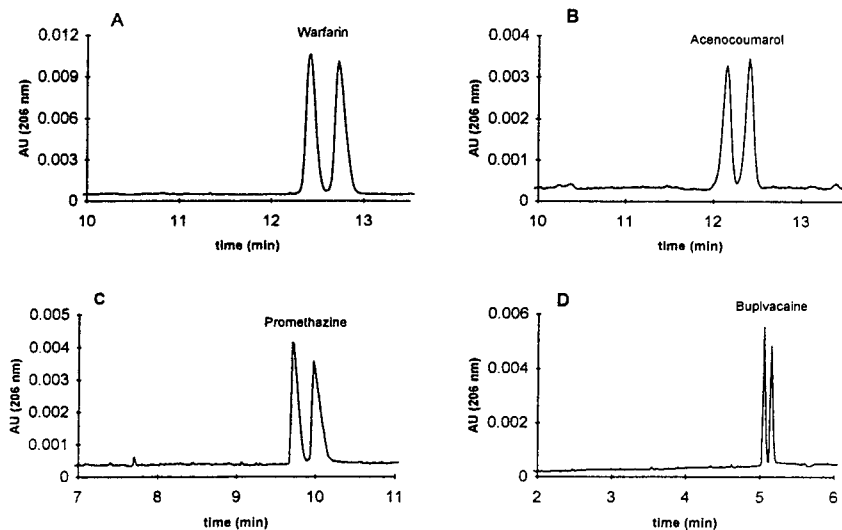


Fig. 6. Electropherograms of the baseline enantiomeric separation of racemic warfarin, acenocoumarol, promethazine and bupivacaine. Background electrolyte, 50 mM phosphate buffer (pH 6) containing SBE- $\beta$ -CD (A, B and C, 6 mg/ml; D, 10 mg/ml); capillary, 50 (45.5) cm  $\times$  0.05 mm I.D. For other experimental conditions, see Table 1.

an increase in  $\mu_{\text{eof}}$  from  $5 \cdot 10^{-4}$  to  $7 \cdot 10^{-4}$   $\text{cm}^2 \text{V}^{-1} \text{s}^{-1}$ . In the presence of the chiral agent, the electroosmosis increased slowly, from  $3.98 \cdot 10^{-4}$  to  $5.27 \cdot 10^{-4}$   $\text{cm}^2 \text{V}^{-1} \text{s}^{-1}$ .

Table 2 gives the effective mobilities, resolution and selectivity of the drugs at different pH values.

An increase in the pH of the BGE did not influence the enantiomeric resolution of propranolol, bupivacaine and oxprenolol (no resolution at any pH using 20 mg/ml SBE- $\beta$ -CD). For the other compounds studied a general decrease in  $R$  on increasing the pH was recorded, except for atenolol and pindolol, which showed resolution only at pH 9.

From the effective mobilities, we can conclude that at pH 6 the complexation is generally higher than at other pH values (the absolute value of  $\mu_e$  generally decreased with increase in pH); terbutaline exhibited the highest value at pH 8.

Under the operating experimental conditions, only terbutaline showed a relatively high value of selectivity ( $S = 0.161$  at pH 6) that decreased with increase in pH.

The use of a BGE at pH 9 (with 20 mg/ml of chiral selector) but with different chemical

composition (Tris-HCl instead of borate-phosphate) was less effective for chiral recognition for all the racemic analytes studied. To explain the different behaviour of the SBE- $\beta$ -CD using the two buffers we have to consider that the electroosmotic flow with Tris electrolyte was higher than with borate ( $5.27 \cdot 10^{-4}$  and  $4.02 \cdot 10^{-4}$   $\text{cm}^2 \text{V}^{-1} \text{s}^{-1}$ , respectively) and consequently lower migration times were recorded. Comparing the effective mobilities using the two BGEs (results not shown), the different chemical composition caused an increase in absolute effective mobility, using borate buffer, for warfarin, acenocoumarol and bupivacaine, whereas for other analytes a decrease was observed. The better results obtained with borate are probably due to the effect of the counter ion on the selective stability of the inclusion complex and to the longer time spent by the two enantiomers in the CD cavity during the electrophoretic process.

### 3.2. Enantiomeric separation of uncharged compounds

Several phenyl alcohol derivatives (for their structures, see Fig. 7) were selected as un-

Table 2

Effective mobilities, resolutions and selectivities obtained for pharmaceutical compounds at different pH using 20 mg/ml SBE- $\beta$ -CD as chiral selector

Compound	pH					
	6		8		9	
	$\mu_1$ R	$\mu_2$ S	$\mu_1$ R	$\mu_2$ S	$\mu_1$ R	$\mu_2$ S
(1) Warfarin	-2.23	-2.57	-2.18	-2.01	-2.17	-2.19
	2.11	0.016	1.00	0.037	1.12	0.009
(2) Acenocoumarol	-2.48	-2.51	-2.34	-2.37	-2.22	-2.25
	2.13	0.012	1.4	0.013	1.52	0.013
(3) Promethazine	-2.20	-2.36	-2.06	-2.12	-2.04	-2.07
	2.00	0.027	1.7	0.029	1.78	0.015
(4) Bupivacaine	0.11	-0.08	-1.06	—	-1.10	—
	nm	nm	—	—	—	—
(5) Terbutaline	-1.31	-1.54	-1.35	-1.56	-1.05	-1.21
	5.10	0.161	5.40	0.144	5.00	0.142
(6) Pindolol	-1.43	—	-1.28	—	-1.11	-1.13
	—	—	—	—	0.90	0.018
(7) Metoprolol	-1.80	-1.82	-1.75	-1.77	-1.50	—
	<0.5	0.011	<0.5	0.011	—	—
(8) Propranolol	-2.21	—	-2.17	—	-1.81	—
	—	—	—	—	—	—
(9) Oxprenolol	-0.93	—	-1.08	—	-0.62	—
	—	—	—	—	—	—
(10) Atenolol	-0.89	—	-0.86	—	-0.78	-0.82
	—	—	—	—	<0.5	0.050
EOF	3.98		5.27		4.02	

Applied voltage 15 kV. For other experimental conditions, see text and Table 1.  $\mu$ :  $10^{-4}$  cm<sup>2</sup> V<sup>-1</sup> s<sup>-1</sup>.

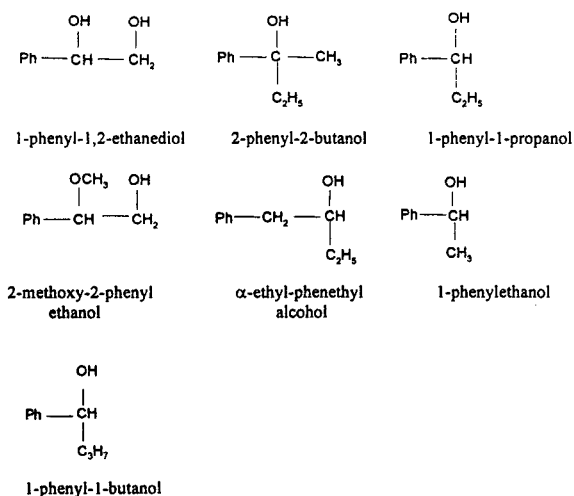


Fig. 7. Structures of the uncharged phenyl alcohols studied.

charged samples in order to study the effect of SBE- $\beta$ -CD on complexation and enantiomeric separation. The racemic mixtures were separately injected for the electrophoresis using a BGE of pH 6, where they were carried to the detector by the relatively strong electroosmotic flow.

The addition of SBE- $\beta$ -CD to the BGE caused a general increase in migration time for all the analytes studied owing to both complexation and a decrease in the electroosmotic flow.

Table 3 shows the effect of the concentration of SBE- $\beta$ -CD in the BGE at pH 6 on the effective mobility, resolution and selectivity of the studied uncharged compounds.

An increased concentration of the chiral selector caused a reduction in the electroosmotic flow, probably due to an increase in the viscosity

Table 3

Effect of the concentration of SBE- $\beta$ -CD on the effective mobility (expressed as  $\mu_e \times 10^{-4} \text{ cm}^2 \text{ V}^{-1} \text{ s}^{-1}$ ), resolution ( $R$ ) and selectivity ( $S$ ) of uncharged racemic phenyl alcohols

Compound	SBE- $\beta$ -CD (mg/ml)									
	1		2		6		10		20	
	$\mu_1$ $R$	$\mu_2$ $S$	$\mu_1$ $R$	$\mu_2$ $S$	$\mu_1$ $R$	$\mu_2$ $S$	$\mu_1$ $R$	$\mu_2$ $S$	$\mu_1$ $R$	$\mu_2$ $S$
2-Phenyl-2-butanol	-0.89	–	-1.60	-1.70	-1.65	-1.73	-1.19	-1.26	-1.92	-1.96
	–	–	<0.5	0.061	1.30	0.047	1.35	0.057	1.40	0.051
1-Phenylethanol	-0.46	–	0.79	–	-0.66	–	-0.11	–	-0.28	–
	–	–	–	–	–	–	–	–	–	–
$\alpha$ -Ethylphenethyl alcohol	-0.74	-0.79	-1.06	–	-1.74	–	-1.72	-1.74	-1.94	-1.95
	<0.5	0.065	–	–	–	–	<0.5	0.012	0.65	0.005
1-Phenyl-1-butanol	-0.72	–	-1.28	–	-1.40	-1.45	-0.90	-0.94	-0.83	-0.86
	–	–	–	–	<0.5	0.035	<0.5	0.043	0.79	0.035
1-Phenyl-1,2-ethanediol	-0.35	–	-0.71	–	-0.39	–	-0.11	–	-0.86	-0.93
	–	–	–	–	–	–	–	–	<0.5	0.078
1-Phenyl-1-propanol	-0.30	–	-0.43	–	-1.16	–	-1.17	-1.22	-1.79	-1.82
	–	–	–	–	–	–	1.09	0.041	1.09	0.017
2-Methoxy-2-phenylethanol	-0.38	–	-0.47	–	-1.42	–	-1.35	–	-1.78	-1.80
	–	–	–	–	–	–	–	–	<0.5	0.010
EOF	4.32	–	4.52	–	3.76	–	3.72	–	3.11	–

Capillary, 40 (35.5) cm  $\times$  0.05 mm I.D. (uncoated); background electrolyte, 50 mM phosphate buffer (pH 6) with the appropriate concentration of chiral selector. The concentration of injected racemic compounds was  $10^{-4}$  M. For other experimental conditions, see Table 1.  $\mu$ :  $10^{-4} \text{ cm}^2 \text{ V}^{-1} \text{ s}^{-1}$ .

of the BGE. Enantiomeric separation was achieved for all the compounds studied except for 1-phenylethanol and the resolution was strongly influenced by the concentration of the modified cyclodextrin. Baseline separation was obtained only for the two enantiomers of 2-phenyl-2-butanol and 1-phenyl-1-propanol when 6 and 20 mg/ml SBE- $\beta$ -CD were used, respectively, while relatively good resolution was obtained for 1-phenyl-1-butanol ( $R = 0.8$ ) and  $\alpha$ -ethylphenethyl alcohol ( $R = 0.65$ ) with 20 mg/ml of chiral selector. 1-Phenyl-1,2-ethanediol and 2-methoxy-2-phenylethanol were poorly resolved with 20 mg/ml of modified CD.

The enantiomeric resolution was generally influenced by the concentration of SBE- $\beta$ -CD in the BGE and the maximum value was obtained at 20 mg/ml for all the compounds studied.

The chiral resolution capability of SBE- $\beta$ -CD towards the compounds studied was found to be 2-Ph-2B > 1-Ph-1P > 1-Ph-1B >  $\alpha$ -Et-PhEt > 1-Ph-1,2-diol = 2-Me-2-PhE. The higher enantiomeric separation obtained for 2-Ph-2B and 1-Ph-1P in comparison with the other uncharged analytes is due to the different substituent groups

on the asymmetric carbon, responsible for the stereoselective interactions with the chiral selector, causing the formation of stereoisomers with different stability constants. The presence of one ethyl substituent plays a very important role in the stereoselectivity (2-Ph-2B and 1-Ph-1P). In fact, when this group was replaced with a methyl or propyl group (1-PhE and 1-Ph-1B), the resolution was completely lost or decreased, respectively. The explanation for such behaviour is not easy to find without other studies, e.g., NMR spectroscopy, too difficult to perform mainly owing to the nature of the chiral selector (traces of other substituted CD are present). Anyway, we can consider that the  $\text{C}_2\text{H}_5$  group can either be accommodated in the CD cavity and/or bind with the butyl spacer of the CD. The former could be considered when a comparison is made with a methyl group (less hydrophobic than an ethyl group), but not with the propyl, in which case we could expect an improvement in resolution. This assumption is also supported by the lower resolution of 1-Ph-1,2-diol and 2-Me-2-PhE where the  $\text{CH}_2\text{OH}$  group (less hydrophobic than  $\text{C}_2\text{H}_5$ ) was present. Finally, the position of

the asymmetric centre influenced the enantiomeric separation; in fact, in the case of  $\alpha$ -Et-PhE, the resolution was lower than for 2-Ph-2B, 1-Ph-1P and 1-Ph-1B but higher than for 1-Ph-1,2-diol and 2-Me-2-PhE.

Three buffer systems of pH 6, 8 and 9, supplemented with 20 mg/ml of chiral selector, were tested in order to study the effect of pH on the enantiomeric resolution of 2-phenyl-2-butanol, 1-phenylethanol,  $\alpha$ -ethyl-phenethyl alcohol, 1-phenyl-1-butanol and 1-phenyl-1,2-ethanediol. Table 4 gives the resolutions and selectivities obtained at different pH values. The data shown here at pH 6 are not the same as those in Table 3 because a longer capillary (50 cm) was used.

An increase in pH led to an increase in the electroosmotic flow. The resolution increased with increase in the pH of the BGE for 2-Ph-2B and 1-Ph-1,2-diol whereas it decreased for the other compounds. 1-Phenylethanol was poorly resolved at pH 8 ( $R < 0.5$ ).

The migration order was verified by spiking the racemic mixtures with the separate enantiomers commercially available for 1-phenyl-1-butanol and 1-phenyl-1,2-ethanediol. In both cases the (+)-antipodes moved with shorter

migration times than the (–)-antipodes, indicating that the former was less complexed by the SBE- $\beta$ -CD. As an example, Fig. 8 shows the electropherograms for the enantiomeric separation of some phenyl alcohols using a BGE of pH 9 and containing 20 mg/ml of chiral selector.

### 3.3. Enantiomeric separation of dansyl-amino acids

The electrophoretic separation of several amino acid derivatives, namely Phe, Glu, Val, nor-Val, Leu, nor-Leu, Thr, Trp, Ser, Asp and Met, in a BGE of pH 8 and in the absence of SBE- $\beta$ -CD revealed that all these compounds moved behind the electroosmotic flow, clearly exhibiting a negative charge.

The addition of SBE- $\beta$ -CD to the BGE caused an increase in migration times for all the compounds studied owing to the complexing effect of the chiral additive. Satisfactory enantiomeric resolution was obtained for Leu, nor-Leu, Phe, Met and Trp, whereas Asp, Thr and Val were poorly resolved ( $R < 0.5$ ) but Glu not at all.

As can be seen in Table 5, the absolute effective mobility and resolution increased on

Table 4  
Effect of the pH of the background electrolyte on the effective mobility, resolution and selectivity of phenyl alcohols

Compounds	pH					
	6		8		9	
	$\mu_1$ R	$\mu_2$ S	$\mu_1$ R	$\mu_2$ S	$\mu_1$ R	$\mu_2$ S
2-Phenyl-2-butanol	-1.93	-1.99	-2.05	-2.10	-1.92	-1.96
	1.94	0.031	1.18	0.024	2.12	0.021
1-Phenylethanol	-1.30	–	-1.31	-1.33	-1.24	–
	–	–	<0.5	0.015	–	–
$\alpha$ -Ethylphenethyl alcohol	-2.65	-2.67	-2.09	-2.10	-1.92	-1.93
	0.76	0.007	<0.5	0.005	<0.5	0.005
1-Phenyl-1-butanol	-2.37	-2.41	-1.94	-1.98	-1.85	-1.89
	1.47	0.017	1.30	0.021	1.28	0.021
1-Phenyl-1,2-ethanediol	-1.18	–	-0.91	–	-1.21	-1.26
	–	–	–	–	1.35	0.040
EOF	3.94		4.33		3.97	

Capillary, 50 (45.5) cm  $\times$  0.05 mm I.D. (uncoated); applied voltage, 15 kV (constant).  $\mu$ :  $10^{-4}$  cm<sup>2</sup> V<sup>-1</sup> s<sup>-1</sup>.

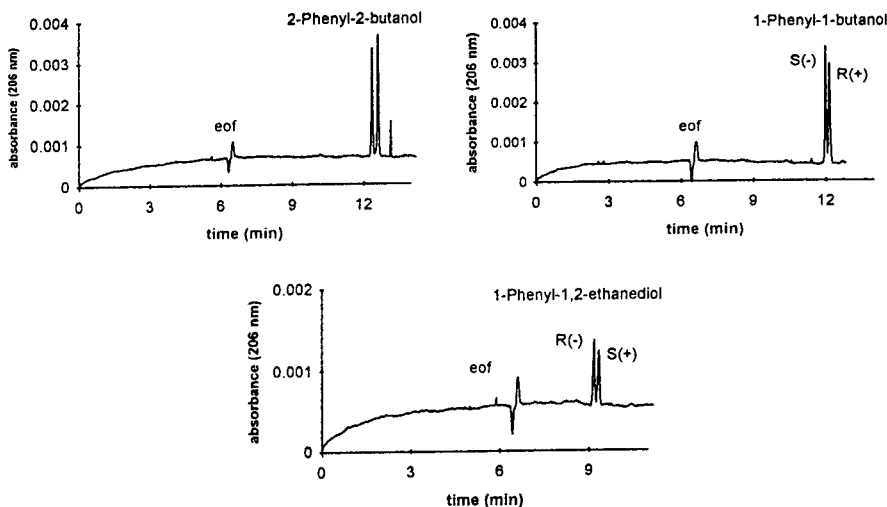


Fig. 8. Electropherograms of the enantiomeric separation of 2-phenyl-2-butanol, 1-phenyl-1-butanol and 1-phenyl-1,2-ethanediol. Background electrolyte, 50 mM borate buffer (pH 9) containing 20 mg/ml of SBE- $\beta$ -CD; capillary, 50 (45.5) cm  $\times$  0.05 mm I.D.; applied voltage, 15 kV, 63  $\mu$ A; injection, 5 p.s.i.  $\cdot$  s of  $10^{-4}$  M racemic standard.

increasing the concentration of the chiral selector added to the BGE. In some cases an increase in  $\mu_e$  was observed up to certain concentration of SBE- $\beta$ -CD and then a decrease (Asp, Thr, Leu), clearly showing a lower complexing effect of the CD in comparison with the other analytes.

The maximum resolution was obtained using 20 mg/ml of modified cyclodextrin for the separated enantiomers, except for Thr, which was poorly resolved only at 10 mg/ml. The resolution order at 20 mg/ml of chiral selector was found to be nor-Leu > Phe > Leu > Met > nor-Val > Trp > Val = Ser = Asp.

Our results indicate that the chiral recognition, also in the case of dansyl-amino acids, is influenced by both the concentration of the chiral selector and the nature of the chain bound to the asymmetric carbon of the amino acid derivative. In fact, amino acids with non-polar chains were better resolved than the others. The migration order was verified by spiking the racemic analytes with their pure *L*-enantiomer and in all cases the *D*-enantiomer moved faster than the *L*-isomer, clearly indicating that the former was the most complexed analyte.

As an example, Fig. 9 shows the enantiomeric

separation of several racemic dansyl-amino acids using a BGE of pH 8 and containing different concentrations of chiral selector.

Experiments performed at pH 6 and 9 revealed that a lower pH (6) allowed higher resolution to be obtained for Leu, Trp, Val, nor-Val and Met, whereas at pH 9 the resolution generally decreased. For Asp a change in the pH of the BGE caused no noticeable modification of resolution.

Although the SBE- $\beta$ -CD was effective for the enantiomeric separation of most of the amino acid derivatives studied, it was not able to separate the racemic mixtures from one another, and further studies are necessary in order to solve this problem, e.g., using surfactant additives to the chiral BGE.

#### 4. Conclusions

Capillary zone electrophoresis using a new chiral selector, sulfobutyl ether- $\beta$ -cyclodextrin, shows great promise for chiral separations of several classes of enantiomers. The complexation, resolution and selectivity are influenced by

Table 5

Effect of the concentration of SBE- $\beta$ -cyclodextrin on effective mobility ( $\mu$ ), resolution ( $R$ ) and selectivity ( $S$ ) of several dansyl-amino acids

Dansyl-amino acids	SBE- $\beta$ -CD (mg/ml)											
	0		1		3		6		10		20	
	$\mu_2$ $R$	$\mu_1$ $S$	$\mu_2$ $R$	$\mu_1$ $S$	$\mu_2$ $R$	$\mu_1$ $S$	$\mu_2$ $R$	$\mu_1$ $S$	$\mu_2$ $R$	$\mu_1$ $S$	$\mu_2$ $R$	$\mu_1$ $S$
Phe	-2.05	-	-2.01	-2.03	-2.10	-2.17	-2.29	-2.37	-2.23	-2.36	-2.47	-2.56
	-	-	<0.5	0.010	1.39	0.033	1.78	0.034	3.84	0.057	3.89	0.036
Trp	-1.69	-	-1.90	-	-1.96	-	-2.12	-2.16	-2.11	-2.15	-2.36	-2.40
	-	-	-	-	-	-	0.92	0.019	1.25	0.019	1.28	0.017
Met	-1.73	-	-1.94	-	-1.93	-	-2.02	-2.05	-2.03	-2.07	-2.29	-2.36
	-	-	-	-	-	-	0.72	0.015	1.45	0.019	1.87	0.030
Asp	-3.33	-	-3.38	-	-3.26	-	-3.27	-	-3.19	-	-3.09	-3.10
	-	-	-	-	-	-	-	-	-	-	<0.5	0.003
Glu	-3.24	-	-3.16	-	-3.14	-	-3.18	-	-3.10	-	-2.79	-
	-	-	-	-	-	-	-	-	-	-	-	-
Val	-1.82	-	-2.04	-	-1.96	-	-2.11	-	-2.16	-	-2.36	-2.37
	-	-	-	-	-	-	-	-	-	-	<0.5	0.004
nor-Val	-1.90	-	-1.96	-	-1.98	-	-2.17	-2.22	-2.06	-2.11	-1.32	-2.37
	-	-	-	-	-	-	0.93	0.023	1.70	0.024	1.69	0.021
Leu	-1.68	-	-1.92	-	-1.96	-2.03	-2.20	-2.28	-2.42	-2.53	-2.21	-2.30
	-	-	-	-	1.00	0.035	1.40	0.036	2.5	0.044	3.54	0.040
nor-Leu	-1.81	-	-2.25	-	-1.98	-2.03	-2.20	-2.29	-2.18	-2.25	-2.45	-2.53
	-	-	-	-	0.64	0.025	1.79	0.040	2.50	0.020	4.28	0.032
Ser	-2.00	-	-2.14	-	-2.00	-	-2.07	-	-2.03	-	-2.24	-2.25
	-	-	-	-	-	-	-	-	-	-	<0.5	0.004
Thr	-1.73	-	-1.93	-	-1.89	-	-2.08	-	-2.24	-2.25	-1.97	-
	-	-	-	-	-	-	-	-	<0.5	0.004	-	-
EOF	5.54		5.24		4.94	4.91	-	-	4.60		4.26	

Conditions: capillary, 50 (45.5) cm  $\times$  0.05 mm I.D.; background electrolyte, 50 mM phosphate buffer (pH 8) with the appropriate concentration of modified cyclodextrin; applied voltage, 18 kV; injection, 5 p.s.i. of  $10^{-4}$  M racemic mixtures.  $\mu$ :  $10^{-4}$  cm<sup>2</sup> V<sup>-1</sup> s<sup>-1</sup>.

the amount of SBE- $\beta$ -CD added to the background electrolyte, and the pH of the BGE and the substituent groups on the asymmetric carbon of the analytes. The modified CD being negatively charged, ion-pairing interactions have to be considered in order to optimize the electrophoretic separation mechanism when basic analytes have to be separated into their enantiomers. Owing to this effect, basic compounds exhibited strong complexation and in several instances the mobility was reversed. This effect can be advantageously used in order to reverse

the migration order, which is important when a minor component has to be determined in an enantiomeric mixture. However, the coulombic interaction between the SBE- $\beta$ -CD seems not to be fundamental for the chiral recognition, as demonstrated by the good chiral resolution obtained when negatively charged compounds were studied (warfarin and acenocoumarol). The composition of the chiral BGE has to be chosen so as to avoid a pH and concentration of SBE- $\beta$ -CD such that the mobility of the two enantiomers is close to the electroosmotic flow in order

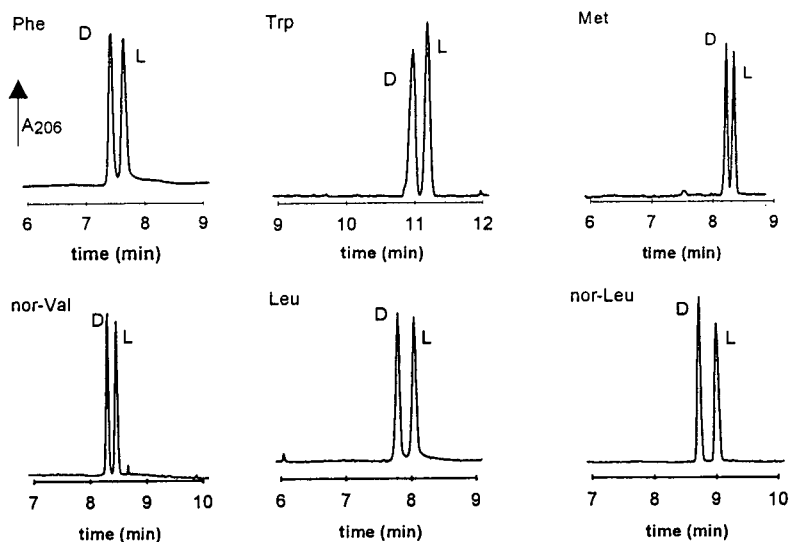


Fig. 9. Electropherograms of the enantiomeric separation of dansyl-amino acids using a BGE of pH 8 (50 mM Tris-HCl) and containing different concentrations of SBE- $\beta$ -CD (Phe, 3 mg/ml; Leu, 6 mg/ml; nor-Leu, nor-Val and Met, 10 mg/ml; and Trp, 20 mg/ml). Capillary, 50 cm  $\times$  0.05 mm I.D.; applied voltage, 18 kV; injection, 5 p.s.i.  $\cdot$  s of  $10^{-4}$  M racemic compounds.

to select the optimum experimental conditions. The CE method is easy and not expensive to perform in comparison with other analytical

methods where expensive columns are needed, e.g., HPLC; in fact, the volume of the capillary is only of the order of nanolitres or microlitres.

Table 6

Effect of the pH of the BGE on resolution ( $R$ ) and selectivity ( $S$ ) of enantiomeric separation of dansyl-amino acids

Dansyl-amino acids	pH					
	6		8		9	
	$R$	$S$	$R$	$S$	$R$	$S$
Phe	4.00	0.035	3.89	0.036	3.44	0.026
Trp	1.89	0.016	1.28	0.017	1.00	0.014
Met	2.96	0.017	1.87	0.030	1.82	0.019
Asp	<0.50	0.003	<0.50	0.003	0.56	0.004
Glu	—	—	—	—	—	—
Val	0.95	0.012	<0.50	0.004	<0.50	0.005
nor-Val	2.71	0.035	1.69	0.021	1.76	0.023
Leu	4.37	0.035	3.54	0.040	2.75	0.032
nor-Leu	3.68	0.032	4.28	0.032	2.27	0.028
Ser	<0.50	0.004	<0.50	0.004	—	—
Thr	—	—	—	—	—	—

Experimental conditions as in Table 5 except the applied voltage, 15 kV, 64  $\mu$ A, at pH 9.

## Acknowledgement

Thanks are due to Perkin-Elmer Applied Biosystems Division (Foster City, CA, USA) for providing the sulfobutyl ether- $\beta$ -cyclodextrin.

## References

- [1] J. Debowski, D. Sybilska and J. Jurczak, *J. Chromatogr.*, 282 (1983) 83.
- [2] T.J. Ward and D.W. Armstrong, *J. Liq. Chromatogr.*, 9 (1986) 407.
- [3] G. Blaschke, *J. Liq. Chromatogr.*, 9 (1986) 341.
- [4] D.W. Armstrong, J.R. Faulkner, Jr., and S.M. Han, *J. Chromatogr.*, 452 (1988) 323.
- [5] F. Kobor and G. Schomburg, *J. High. Resolut. Chromatogr.*, 16 (1993) 693.
- [6] C.P. Granville, B. Gehrcke, W.A. Konig and I.W. Wainer, *J. Chromatogr.*, 622 (1993) 21.
- [7] M. Jung, S. Mayer and V. Schurig, *LC · GC Mag. Sep. Sci.*, 12 (1994) 458.
- [8] J. Snopek, I. Jelinek and E. Smolkova-Keulemansova, *J. Chromatogr.*, 438 (1987) 211.
- [9] A. Guttman, A. Paulus, A.S. Cohen, N. Grinberg and B.L. Karger, *J. Chromatogr.*, 448 (1988) 41.
- [10] S. Terabe, *Trends Anal. Chem.*, 8 (1989) 129.
- [11] S. Fanali, *J. Chromatogr.*, 474 (1989) 441.
- [12] S. Terabe, H. Shibata and Y. Miyashita, *J. Chromatogr.*, 480 (1989) 403.
- [13] T. Schmitt and H. Engelhardt, *Chromatographia*, 37 (1993) 475.
- [14] S. Fanali and P. Bocek, *Electrophoresis*, 11 (1990) 757.
- [15] C. Desiderio, Z. Aturki and S. Fanali, *Electrophoresis*, 15 (1994) 864.
- [16] S. Fanali, M. Cristalli, R. Vespalec and P. Bocek, in A. Chrambach, M.J. Dunn and B.J. Radola (Editors), *Advances in Electrophoresis*, VCH, Weinheim, 1994, p. 1.
- [17] A. Nardi, A. Eliseev, P. Bocek and S. Fanali, *J. Chromatogr.*, 638 (1993) 247.
- [18] T. Schmitt and H. Engelhardt, *J. High Resolut. Chromatogr.*, 16 (1993) 525.
- [19] B. Chankvetadze, G. Endresz and G. Blaschke, *Electrophoresis*, 15 (1994) 804.
- [20] C. Dette, S. Ebel and S. Terabe, *Electrophoresis*, 15 (1994) 799.
- [21] Z. Aturki and S. Fanali, *J. Chromatogr. A*, 680 (1994) 137.
- [22] I.S. Lurie, R.F.X. Klein, T.A. Dal Cason, M.J. LeBelle, R. Brenneisen and E. Weinberger, *Anal. Chem.*, 66 (1994) 4019.





ELSEVIER

Journal of Chromatography A, 716 (1995) 197–205

JOURNAL OF  
CHROMATOGRAPHY A

# Buffer effects in the desionoselective/ionoselective/ duoselective separation selectivity model-assisted optimization of the capillary electrophoretic separation of enantiomers I. Low-pH phosphate buffers

Robert L. Williams, Gyula Vigh\*

*Department of Chemistry, Texas A&M University, College Station, TX 77843-3255, USA*

## Abstract

The complexation of aromatic permanently charged anions by  $\beta$ -cyclodextrin in capillary electrophoresis has been studied using phosphate background electrolytes in which the pH was varied from 2.0 to 3.6. The complex formation constants and ionic mobilities proved independent of the pH, indicating that the electrophoretically determined parameters of the multiple equilibria-based separation selectivity model (DID model) are meaningful and should be suitable for the optimization of enantiomer separations. Therefore, the effective mobilities of the enantiomers of  $\alpha$ -methoxy- $\alpha$ -trifluoromethyl phenylacetic acid, suspected to belong to the families of ionoselective or duoselective separations, were measured as a function of pH and  $\beta$ -cyclodextrin concentration in the  $2 < \text{pH} < 4$  and  $0 < c_{\text{CD}} < 15 \text{ mM}$  ranges in phosphoric acid-based background electrolytes. The effective mobilities were fitted to the DID model to extract the respective acid dissociation and complex formation constants and ionic mobilities. Peak resolution for the duoselective separation was calculated with these parameters as a function of pH and the  $\beta$ -cyclodextrin concentration of the background electrolyte, as well as the dimensionless electroosmotic flow coefficient. The shapes of the predicted and observed peak resolution curves agreed well, demonstrating that the DID model can be used for the optimization of the CE separations of enantiomers.

## 1. Introduction

Over the last few years the tools available for the quantitative description of peak resolution in the cyclodextrin-mediated capillary electrophoretic (CE) separations of enantiomers [1–10] have improved significantly. First, a resolution equation has been proposed which describes

peak resolution,  $R_s$ , as a function of the effective part of the applied potential, separation selectivity, and the effective charge of the analyte [1], as well as the dimensionless electroosmotic flow [2]. Second, equilibrium models have been presented to describe the mobility of the enantiomers as a function of the cyclodextrin (CD) concentration [3–5] of the background electrolyte (BGE). Subsequently, it was shown that not only the CD concentration, but also the hydronium ion concentration of the BGE plays a crucial role in the

\* Corresponding author.

success of the separation, and the desionoselective/ionoselective/duoselective separation selectivity model (DID model) was introduced [6–10] to aid in the rational selection of the optimum separation conditions.

It was demonstrated that the acid dissociation and complex formation constants, as well as the ionic mobilities of the free and cyclodextrin-complexed enantiomers can be determined from three simple sets of CE experiments [2,6–10]. The first set has to be carried out in the absence of CD by varying the pH of the BGE and evaluation of the measured mobilities yields the  $pK_a$  and  $\mu^0$  values. In the second set of experiments, the CD concentration is varied while pH is kept constant at a value where the analyte is fully ionized. This set of experiments yields the complexation constants for the dissociated forms of the analyte. In the third set, the CD concentration is varied again while the pH is kept constant at a value where the analyte is about one third ionized. This set of experiments, together with the previously determined constants, yields the complexation constants for the non-dissociated forms of the analyte.

Some concerns were expressed [11] about the possible effects that the competitively binding BGE components might have on the complexation constants one can obtain from CE mobility measurements as the pH of the background electrolyte is changed from a value where the analyte is fully dissociated to a value where the analyte is only one third dissociated. The present paper addresses this concern in the case of one of the most frequently used CE buffering systems, the phosphate buffer, and shows the utility of the DID model and the experimentally determined model parameters in the optimization of the separation of the enantiomers of a weak acid analyte that displays duoselective separation behavior.

## 2. Experimental

A diode-array detector equipped P/ACE 5500 system (Beckman Instruments, Fullerton, CA,

USA) was used for the mobility measurements, with the detector electrode kept at high positive potential. The thermostating cartridge temperature was 37°C. Untreated, 25  $\mu\text{m}$  and 50  $\mu\text{m}$  I.D., 180  $\mu\text{m}$  O.D. (40.7 cm from injector to detector, 47.4 cm total length) fused-silica capillaries (Polymicro Technologies, Phoenix, AZ, USA) and 50  $\mu\text{m}$  I.D., 375  $\mu\text{m}$  O.D. coated capillaries with a neutral coating (eCAP Neutral Capillary, P/N 477441, Beckman Instruments) and an amine coating (eCAP Amine Capillary, P/N 477430, Beckman Instruments) were used for the separations. The field strength was varied between 100 and 256 V/cm to maintain power dissipation levels below 500 mW/m.

BGEs of 100 mM balanced cation-concentration [2,8–10] were prepared by weighing the required amount of LiOH (Aldrich, Milwaukee, WI, USA) into the volumetric flask and adjusting the pH of the solution with phosphoric acid (Aldrich) in such a way that the total cation concentration (hydronium ion concentration plus lithium ion concentration) remained constant.  $\beta$ -Cyclodextrin (American Maize Products, Hammond, IN, USA) was used as chiral resolving agent. To minimize the risk of cyclodextrin hydrolysis at very low pH values (hydrolysis half-life at pH = -0.133 and 40°C: 48 days [14]), the BGEs were freshly prepared before use. The test solutes included *p*-toluenesulfonic acid (PTSA) and 4-ethylbenzene sulfonic acid (EBSA) (Aldrich) as permanently charged anionic markers,  $\alpha$ -methoxy- $\alpha$ -trifluoromethyl phenylacetic acid (MTPA) (a generous gift from H. Billiet, Technical University of Delft, Netherlands) as chiral probe, and benzyl alcohol as the electroosmotic flow marker. The initial 0.3-min long potential rise time of the P/ACE 5500 was taken into account in the calculation of the correct mobility values [12].

The parameters of the mobility equation were evaluated with the TableCurve 2D software package (Jandel Scientific, San Rafael, CA, USA). They were then used to calculate the mobility, effective charge, selectivity and resolution surfaces with the Origin Ver. 3.5 software package (MicroCal, Northampton, MA, USA) running on a 486DX4 100 MHz 20 MB RAM

personal computer (ARM Computers, San Jose, CA, USA).

### 3. Results and discussions

#### 3.1. Formation constants for the cyclodextrin complexes of permanently charged anions in $2.0 < \text{pH} < 3.6$ phosphate BGEs

According to Ref. [1], the effective mobility of an analyte can be described as a linear combination of the ionic mobilities and the mole fractions of all possible forms of the species present. For a permanently charged anion,  $\text{P}^-$ , which complexes with CD, the effective mobility,  $\mu_{\text{P}}^{\text{eff}}$ , becomes:

$$\mu_{\text{P}}^{\text{eff}} = \frac{\mu_{\text{P}^-}^0 + \mu_{\text{PCD}^-}^0 K_{\text{PCD}^-} [\text{CD}]}{1 + K_{\text{PCD}^-} [\text{CD}]} \quad (1)$$

where  $\mu_{\text{P}^-}^0$  and  $\mu_{\text{PCD}^-}^0$  are the ionic mobilities of the free and the complexed forms of  $\text{P}^-$ ,  $K_{\text{PCD}^-}$  is the formation constant for the cyclodextrin complex of  $\text{P}^-$ , and  $[\text{CD}]$  is the cyclodextrin concentration, respectively. When the analytical concentration of  $\text{P}^-$  is much smaller than the analytical concentration of CD, and the BGE components do not complex strongly with CD, or when the analytical concentration of the BGE components is high [6], the analytical concentration of CD,  $c_{\text{CD}}$  can be used instead of  $[\text{CD}]$ . If it can be shown that the  $\mu_{\text{PCD}^-}^0$  and  $K_{\text{PCD}^-}$  values for a series of weakly binding permanently charged anions remain constant in cation concentration-balanced [2] phosphate BGEs of varying pH, the  $K$  and  $\mu^0$  values of the more strongly binding analyte enantiomers will also remain independent of the pH of the phosphate BGE and be suitable for the optimization of the resolution of the enantiomers.

Thus, a series of phosphate BGEs were prepared with pH values varying between 2.0 and 3.6.  $\beta$ -Cyclodextrin was dissolved in these BGEs to obtain twelve different CD concentrations in the 0 to 15 mM range. The  $\mu_{\text{P}}^{\text{eff}}$  effective mobilities of the two aromatic sulfonate test solutes,

PTSA and EBSA, were determined from  $\mu_{\text{P}}^{\text{obs}}$ , their observed mobilities, and  $\mu_{\text{eo}}$ , the coefficient of the electroosmotic flow, as:

$$\mu_{\text{P}}^{\text{obs}} = \mu_{\text{P}}^{\text{eff}} + \mu_{\text{eo}} \quad (2)$$

The  $\mu_{\text{P}}^{\text{eff}}$  values (at least five replicate measurements at each cyclodextrin concentration level) were then fitted to Eq. 1 to calculate parameters  $\mu_{\text{PCD}^-}^0$  and  $K_{\text{PCD}^-}$  as listed in Table 1. The  $K_{\text{PCD}^-}$  values are small (about 100) for PTSA, moderate for EBSA (about 330). There is no clearly discernible trend in either the  $\mu_{\text{PCD}^-}^0$  or the  $K_{\text{PCD}^-}$  values as pH is increased from 2.0 to 3.6. This indicates that the components of the phosphate buffer have a negligible effect on the ionic mobilities and complex formation constants of even the weakly binding PTSA. Consequently, the DID model and its parameters should be suitable for the optimization of the separation of enantiomers whenever the  $K$  values are at least 100 or larger.

#### 3.2. Formation constants for the cyclodextrin complexes of the MTPA enantiomers

A previous CE study on the separation of the enantiomers of nine mandelic acid analogs [13] found that only the enantiomers of MTPA and 2-phenylpropionic acid could be separated with  $\beta$ -cyclodextrin as resolving agent. Since these separations occurred at high pH, well above the expected  $\text{p}K_{\text{a}}$  values of the acids, according to the DID separation selectivity model the separations must behave as either *ionoselective* or *duoselective* separations [2,6–10]. (In an *ionoselective* separation, only the dissociated forms of the enantiomers complex selectively. In a *duoselective* separation, both the dissociated and the non-dissociated forms of the enantiomers complex selectively [2,6–10].) Therefore, it was of interest to see if this suspected separation type assignment, based on a limiting  $\text{p}K_{\text{a}}$  value (less than 6) and a single resolution value, was correct because, if so, the separation can be optimized very simply.

According to Refs. [2,6–10], the effective

Table 1  
Complex formation constants and ionic mobilities for permanently charged anions in phosphate BGEs at different pH values

Solute	pH	$\mu_P^0$ ( $\cdot 10^{-5}$ cm <sup>2</sup> /Vs)	$\mu_{PCD^-}^0$ ( $\cdot 10^{-5}$ cm <sup>2</sup> /Vs)	$K_{PCD^-}$
PTSA	2.0	32.6 ± 0.1	7.3 ± 0.4	90 ± 6
	2.5	32.1 ± 0.1	7.8 ± 0.3	102 ± 5
	2.9	32.1 ± 0.1	7.8 ± 0.6	106 ± 6
	3.6	32.1 ± 0.1	7.6 ± 0.7	95 ± 6
EBSA	2.0	30.6 ± 0.1	8.7 ± 0.2	323 ± 6
	2.5	29.9 ± 0.1	8.1 ± 0.1	316 ± 9
	2.9	30.0 ± 0.1	8.2 ± 0.2	337 ± 10
	3.6	30.1 ± 0.1	8.4 ± 0.2	341 ± 16

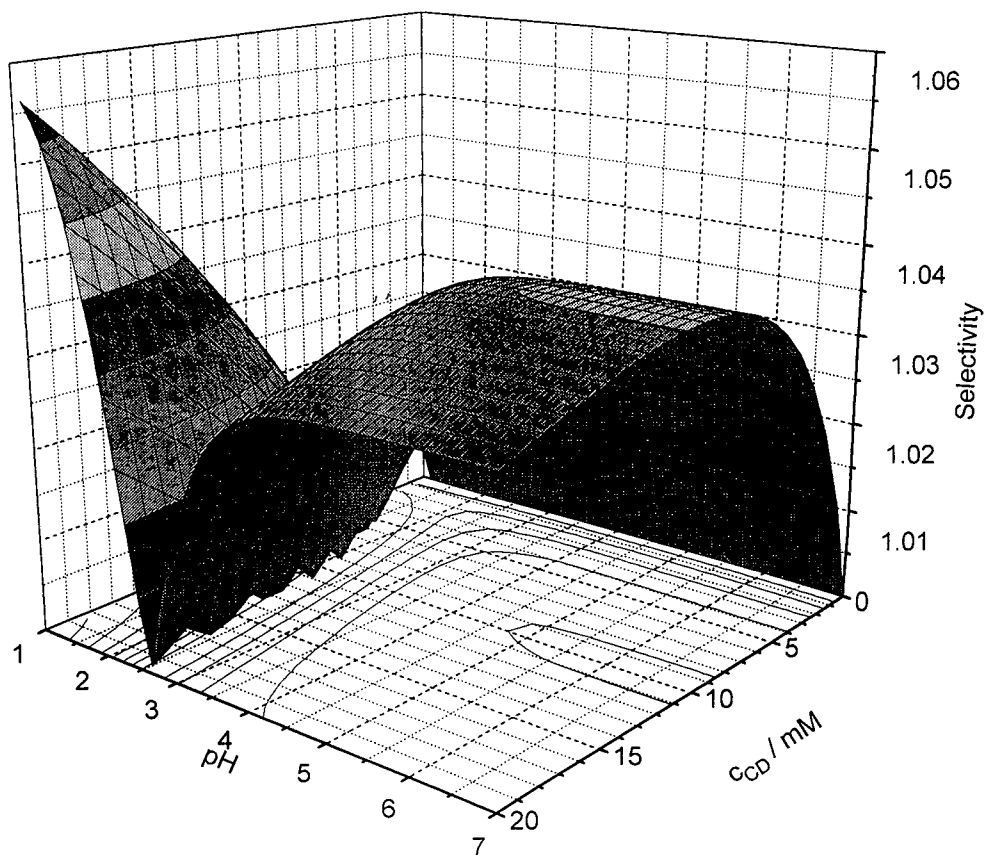


Fig. 1. Selectivity surface for the separation of the enantiomers of MTPA as a function of the  $\beta$ -cyclodextrin concentration and the pH in 100 mM cation concentration-balanced phosphate BGEs. The surface was calculated with Eq. 5 and the constants in Table 2.

Table 2  
Estimated model parameter values for MTPA

$\mu_-^0$ ( $10^{-5}$ cm <sup>2</sup> /Vs)	25.0 ± 0.2
$10^2 K_a$	3.1 ± 0.1
pK <sub>a</sub>	1.5
$\mu_{\text{RCD}^-}^0$ ( $10^{-5}$ cm <sup>2</sup> /Vs)	7.1 ± 0.2
$\mu_{\text{SCD}^-}^0$ ( $10^{-5}$ cm <sup>2</sup> /Vs)	7.4 ± 0.2
$K_{\text{RCD}^-}^0$	127 ± 4
$K_{\text{SCD}^-}^0$	149 ± 4
$K_{\text{HRCD}}$	1257 ± 19
$K_{\text{HS CD}}$	1292 ± 15

mobility of a weak acid *R*-enantiomer,  $\mu_{\text{R}}^{\text{eff}}$ , is:

$$\mu_{\text{R}}^{\text{eff}} = \frac{\mu_-^0 + \mu_{\text{RCD}^-}^0 - K_{\text{RCD}^-}[\text{CD}]}{1 + K_{\text{RCD}^-}[\text{CD}] + \frac{[\text{H}_3\text{O}^+]}{K_a}(1 + K_{\text{HRCD}}[\text{CD}])} \quad (3)$$

where  $\mu_-^0$  and  $\mu_{\text{RCD}^-}^0$  are the ionic mobilities of the fully dissociated free and CD-complexed

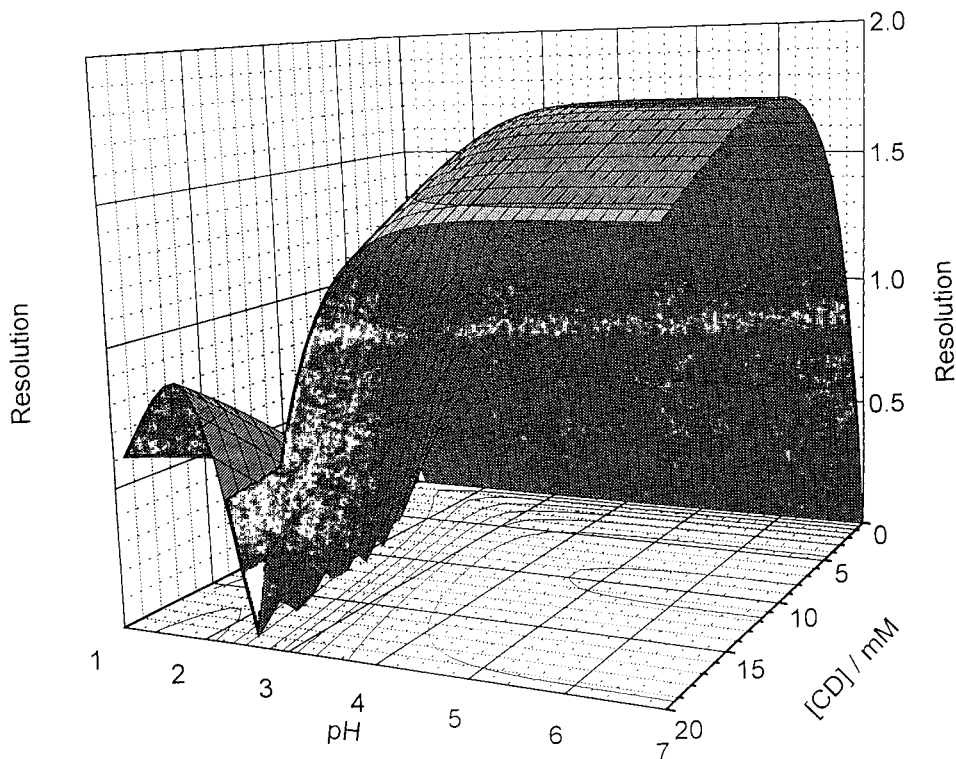


Fig. 2. Peak resolution surface for the separation of the enantiomers of MTPA as a function of the  $\beta$ -cyclodextrin concentration and the pH in 100 mM cation concentration-balanced phosphate BGEs. The surface was calculated with Eq. 6 and the constants in Table 2 for  $\beta = 0$  and  $E = 265$  V/cm,  $T = 310$  K, and  $l = 40.7$  cm.

enantiomers,  $K_a$  is the acid dissociation constant of the enantiomer,  $K_{\text{RCD}^-}$  and  $K_{\text{HRCD}}$  are the formation constants for the cyclodextrin complexes of the dissociated and non-dissociated forms of the enantiomer, and  $[\text{H}_3\text{O}^+]$  and  $[\text{CD}]$  are the hydronium ion and cyclodextrin concentrations. The parameters in Eq. 3 have been determined as outlined in the Introduction, and described in detail in [2,6–10]. The results, shown in Table 2, indicate that the separation of the enantiomers of MTPA belongs to the family of duoselective separations ( $K_{\text{RCD}^-} \neq K_{\text{SCD}^-}$ ,  $K_{\text{HRCD}} \neq K_{\text{HSCD}}$ , and  $\mu_{\text{RCD}^-}^0 \neq \mu_{\text{SCD}^-}^0$ ), as expected on the basis of the single-pH resolution data in [13].

### 3.3. Separation selectivity and peak resolution surfaces

Once the  $K$  values are known, the absolute value of effective charge of the enantiomer,  $Z_{\text{R}}^{\text{eff}}$ , can be calculated as [2]:

$$Z_{\text{R}}^{\text{eff}} = \frac{Z_{-}^0 + Z_{\text{RCD}^-}^0 - K_{\text{RCD}^-}[\text{CD}]}{1 + K_{\text{RCD}^-}[\text{CD}] + \frac{[\text{H}_3\text{O}^+]}{K_a}(1 + K_{\text{HRCD}}[\text{CD}])} \quad (4)$$

where  $Z_{-}^0$  and  $Z_{\text{RCD}^-}^0$  are the absolute values of

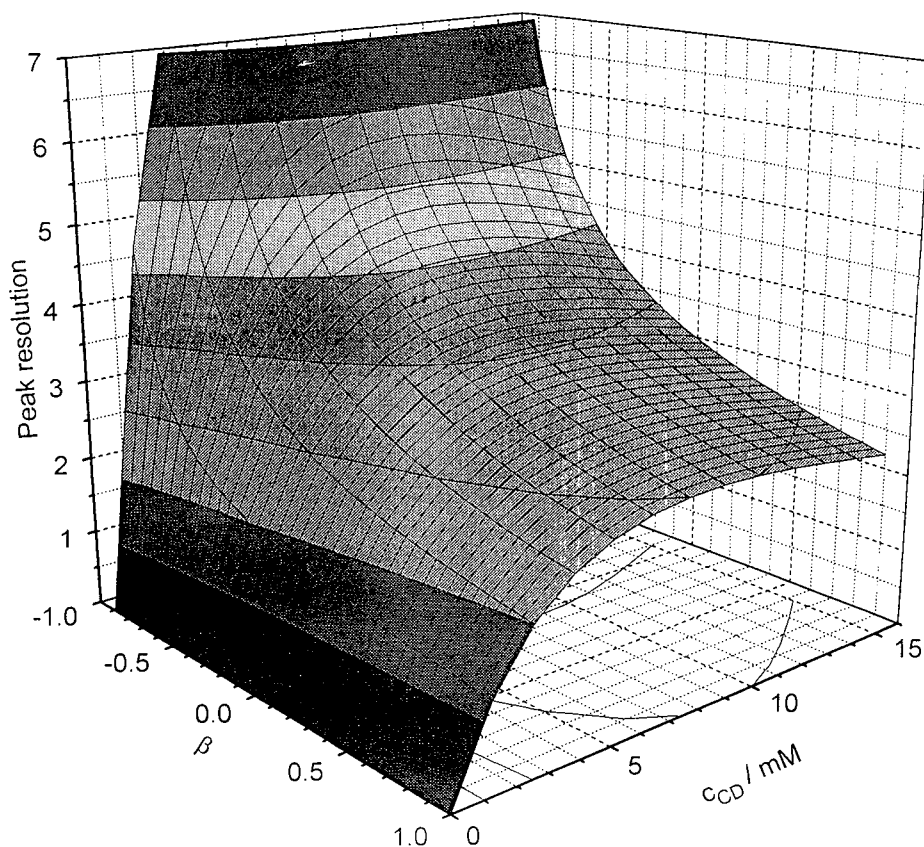


Fig. 3. Peak resolution surface for the separation of the enantiomers of MTPA as a function of pH and  $\beta$  in 100 mM cation concentration-balanced phosphate BGEs. The surface was calculated with Eq. 6 and the constants in Table 2 for  $c_{\text{CD}} = 15$  mM,  $E = 265$  V/cm,  $T = 310$  K, and  $l = 40.7$  cm.

the ionic charges of the fully dissociated free and CD-complexed enantiomers, respectively. Separation selectivity,  $\alpha$ , the ratio of the effective mobilities of the two enantiomers, can be calculated as [6]:

$$\alpha = \frac{\mu_{-}^{0} + \mu_{\text{RCD}}^{0} - K_{\text{RCD}}[\text{CD}]}{\mu_{-}^{0} + \mu_{\text{SCD}}^{0} - K_{\text{SCD}}[\text{CD}]} \frac{1 + K_{\text{SCD}}[\text{CD}] + \frac{[\text{H}_3\text{O}^+]}{K_a}(1 + K_{\text{HSCD}}[\text{CD}])}{1 + K_{\text{RCD}}[\text{CD}] + \frac{[\text{H}_3\text{O}^+]}{K_a}(1 + K_{\text{HRCD}}[\text{CD}])} \quad (5)$$

assuming, for the sake of discussion, that the *S*-enantiomer is the less mobile enantiomer. If  $\alpha$

and  $Z^{\text{eff}}$  are known, peak resolution can be obtained [2,8–10] as:

$$R_s = \sqrt{\frac{E l e_0}{8 k T} \frac{\text{abs}(\alpha - 1) \sqrt{\text{abs}(\alpha + \beta)} \sqrt{\text{abs}(1 + \beta)} \sqrt{Z_{\text{R}}^{\text{eff}} Z_{\text{S}}^{\text{eff}}}}{\sqrt{\text{abs}[(\alpha + \beta)^3] Z_{\text{R}}^{\text{eff}} + \sqrt{\alpha \text{abs}[(1 + \beta)^3] Z_{\text{S}}^{\text{eff}}}}}, \quad (6)$$

where  $E$  is the field strength,  $l$  the effective length of the capillary,  $e_0$  the electric charge,  $k$  the Boltzman constant,  $T$  the absolute temperature, and  $\beta$  the dimensionless electroosmotic flow coefficient, defined as:

$$\beta = \frac{\mu_{\text{eo}}}{\mu_{\text{S}}^{\text{eff}}} \quad (7)$$

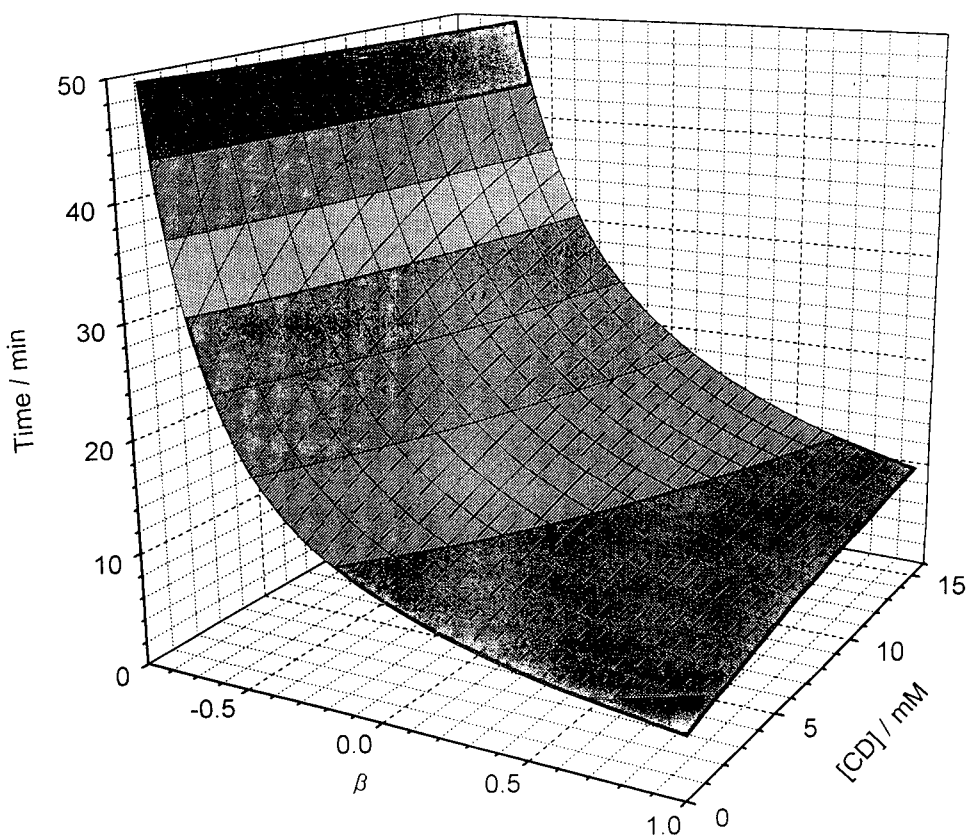


Fig. 4. Separation time surface for the resolution of the enantiomers of MTPA as a function of pH and  $\beta$  in 100 mM cation concentration-balanced phosphate BGEs. The surface was calculated with Eq. 6 and the constants in Table 2 for  $c_{\text{CD}} = 15 \text{ mM}$ ,  $E = 265 \text{ V/cm}$ ,  $T = 310 \text{ K}$ , and  $l = 40.7 \text{ cm}$ .

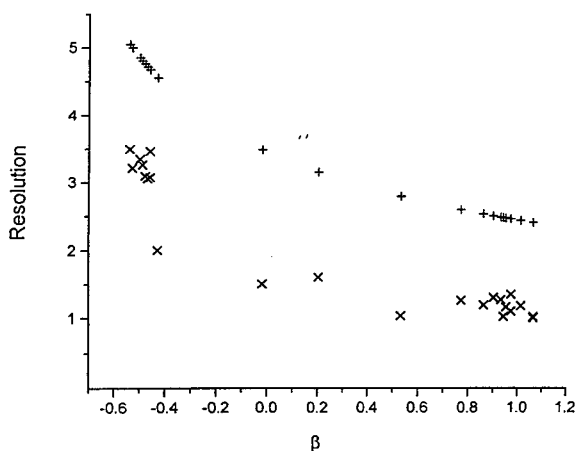


Fig. 5. Comparison of the predicted (symbol +) and measured (symbol  $\times$ )  $R_s$  values for MTPA as a function of  $\beta$  in 100 mM cation concentration-balanced phosphate, 15 mM  $\beta$ -cyclodextrin BGEs. The measured values were obtained using  $E = 265$  V/cm, with  $\beta$  values varying in the  $-0.6$  to  $1.06$  range.

The separation selectivity surface for MTPA is shown in Fig. 1 as a function of  $c_{CD}$  and pH. When the pH is at least 1 unit above the  $pK_a$ , selectivity passes a maximum as a function of  $c_{CD}$ . If the CD concentration is kept constant close to the solubility limit,  $c_{CD} = 15$  mM, and pH is decreased from 3.6, selectivity first remains constant, then decreases, becomes unity, then

the migration order reverses and  $\alpha$  increases again. The features of this selectivity surface agree with the theoretically predicted features of a *duoselective* enantiomer separation [6].

The peak resolution surface calculated for  $\beta = 0$  (no electroosmotic flow) is shown in Fig. 2. The two lobes of the resolution surface are separated by an  $R_s = 0$  valley in the vicinity of the  $pK_a$  value. On the primary lobe, above the  $pK_a$ , there is an  $R_s$  maximum at  $c_{CD} = 10$  mM. The separation is rugged in terms of the pH variable. On the secondary lobe,  $R_s$  increases as  $c_{CD}$  is increased toward the solubility limit. However, as pH is decreased further,  $R_s$  passes through a local maximum at  $pH = 1.75$  because the effective charge is lost. The migration order is opposite on the two lobes. The  $R_s$  surface in Fig. 2 agrees with the theoretically predicted resolution surface of a *duoselective* separation and indicates that the enantiomers can be readily separated as long as the pH is kept at least one pH unit above the  $pK_a$ .

Since the separation is superior on the primary lobe, it is instructive to see the effects of varying  $\beta$  on both  $R_s$  and the separation time. For this calculation  $E = 256$  V/cm and  $c_{CD} = 15$  mM were chosen, and  $\beta$  was varied in the  $-1$  to  $1$  range. As it can be seen in Fig. 3,  $R_s$  improves dramatically as one approaches the  $\beta = -1$  value. However, the separation time also increases

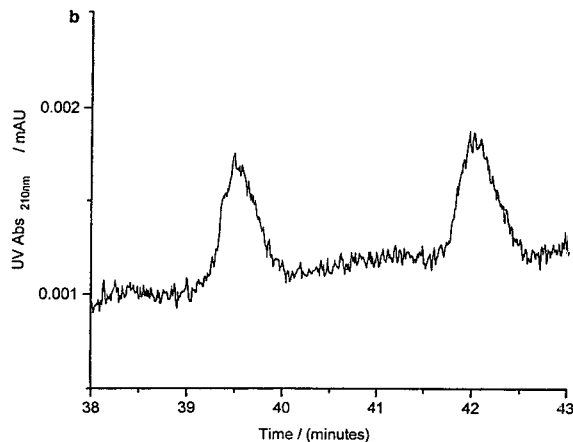
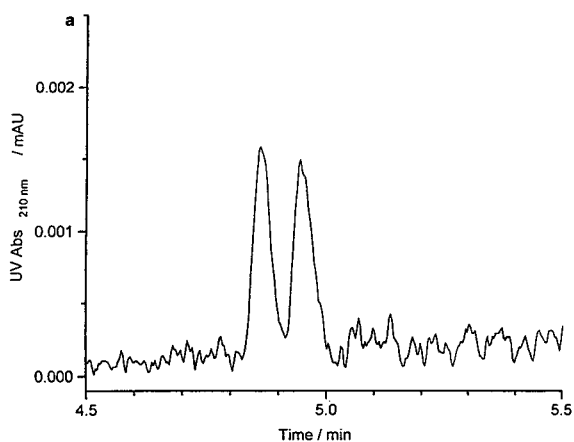


Fig. 6. Electropherograms of an MTPA sample, obtained in 100 mM cation concentration-balanced phosphate, pH 3.6, 15 mM  $\beta$ -cyclodextrin BGEs, with  $\beta = 1.06$  (a) and  $\beta = -0.6$  (b),  $E = 256$  V/cm.



dramatically (Fig. 4). A good compromise could be obtained by selecting a  $\beta = -0.6$  value: compared to  $\beta = 1$ ,  $R_s$  can be more than doubled for a four- to five-fold increase in the separation time.

In Fig. 5 the theoretically predicted (symbol +) and actually measured (symbol  $\times$ )  $R_s$  values are compared for different dimensionless electroosmotic flows ( $\beta$ ). Both curves follow the same trend, but the measured  $R_s$  values are about 20 to 30% lower, because the shape of the analyte peak is distorted by electromigration dispersion. The electropherograms of MTPA at  $\beta = -0.6$  and 1.06 are compared in Fig. 6.

#### 4. Conclusions

The complexation equilibria-based DID model was used to describe the mobilities of permanently charged anions and MTPA as a function of the cyclodextrin concentration and pH of phosphate BGEs. The complex formation constants and ionic mobilities of the permanently charged anions remain constant while the pH of the phosphate BGE is varied in the 2.0 to 3.6 range. This indicates that the formation constants obtained for the moderately or strongly complexing analyte enantiomers are also independent of the pH of the phosphate buffer and can be used for optimization of the separation. The separation of MTPA represents a duoselective enantiomer separation, because all four complexation constants are different. Rugged separations can be achieved on the primary lobe of the resolution surface (at pH values at least one unit above the  $pK_a$  of MTPA). By selecting negative  $\beta$  values around the  $-0.6$  level,  $R_s$  can be easily doubled at the cost of quadrupled separation time. The measured peak resolution values are 20–30% lower than the theoretically predicted ones, because the separation is plagued by electromigration dispersion. Nevertheless, the DID model can be used both for the rationalization of the migration behavior of the

MTPA enantiomers and the selection of the optimum separation conditions.

#### Acknowledgements

Partial financial support by the National Science Foundation (CHE-8919151), the Texas Coordination Board of Higher Education Advanced Research Program (Project Number 010366-016), Beckman Instruments (Fullerton, CA, USA), the WR Johnson Pharmaceutical Research Institute (Springfield, PA, USA), and the Dow Chemical Company (Midland, MI, USA) is gratefully acknowledged. American Maize Products Corporation (Hammond, IN, USA) is acknowledged for the donation of the  $\beta$ -cyclodextrin samples.

#### References

- [1] W. Friedl and E. Kenndler, *Anal. Chem.*, 65 (1993) 2003.
- [2] Y.Y. Rawjee and Gy. Vigh, *Anal. Chem.*, 66 (1994) 619.
- [3] S.A.C. Wren and R.C. Rowe, *J. Chromatogr.*, 603 (1992) 235.
- [4] S.A.C. Wren and R.C. Rowe, *J. Chromatogr.*, 609 (1992) 363.
- [5] S.A.C. Wren and R.C. Rowe, *J. Chromatogr.*, 635 (1993) 113.
- [6] Y.Y. Rawjee, D.U. Staerk and Gy. Vigh, *J. Chromatogr.*, 635 (1993) 291.
- [7] Y.Y. Rawjee, R.L. Williams and Gy. Vigh, *J. Chromatogr. A*, 652 (1993) 233.
- [8] Y.Y. Rawjee, R.L. Williams and Gy. Vigh, *J. Chromatogr. A*, 680 (1994) 599.
- [9] Y.Y. Rawjee, R.L. Williams, L. Buckingham and Gy. Vigh, *J. Chromatogr. A*, 688 (1994) 273.
- [10] M.E. Biggin, R.L. Williams and Gy. Vigh, *J. Chromatogr. A*, 692 (1995) 319.
- [11] Poster Discussion Session at HPLC'94 Symposium, Minneapolis, MN, May 23–27, 1994.
- [12] B.A. Williams and Gy. Vigh, *Anal. Chem.*, 67 (1995) 3079.
- [13] F.E. Valko, H.A.H. Billiet, J. Frank and K.Ch.A.M. Luyben, *J. Chromatogr. A*, 678 (1994) 139.
- [14] M.L. Bender and M. Komiyama, *Cyclodextrin Chemistry*, Springer Verlag, Berlin, 1978, p. 9.



# Evaluation of the parameters determining the performance of electrochromatography in packed capillary columns

Beate Behnke, Edgar Grom, Ernst Bayer\*

*Institut für Organische Chemie, Universität Tübingen, Auf der Morgenstelle 18, 72076 Tübingen, Germany*

---

## Abstract

Electrochromatography is a variant of reversed-phase liquid chromatography performed in capillary columns whereby transport of the eluent is accomplished by applying an electric field across the length of the column. Column-length restrictions arising from resistance to flow encountered with conventional pumping are absent in electrochromatography, allowing separation in capillaries packed with 1.5- $\mu\text{m}$  stationary phases up to 50 cm, thus rendering efficiencies of more than 100 000 plates per column. Practical problems, however, have restricted the number of successful applications reported. A number of parameters determining the electrochromatographic performance are investigated: eluent, frits, packed columns and optional supplementary pressure. These factors are investigated separately and then combined stepwise. With thoroughly degassed eluent, frits made of sintered silica gel, and the use of supplementary pressure, stable and reproducible conditions may be readily obtained.

---

## 1. Introduction

High-performance liquid chromatography (HPLC) and capillary electrophoresis (CE) are methods which have been well evaluated and are now routinely used for a wide range of applications. Electrochromatography, on the other hand, is a new technique that can be considered as a combination of these two methods: reversed-phase liquid chromatography is performed in packed columns with an electric field applied across the length of the column.

The retention of neutral molecules is determined purely by chromatographic parameters, while the retention of charged analytes is additionally influenced by electrophoresis. Tsuda [1] used this approach for tuning the selectivity in HPLC separations of charged analytes. He also

described the problem of excessive Joule heat, which results in bubble formation, and proposed overcoming this effect by the application of pressure.

Another approach to avoiding the problems related to heat development is the miniaturization of the inner diameter of the capillary column to provide increased heat dissipation. While Tsuda used columns of 200–500  $\mu\text{m}$  inner diameter (I.D.), recent work on electrochromatography has been performed using capillary columns of 50–100  $\mu\text{m}$  I.D. [2–9].

An important effect of the electric field is the transport of the eluent by electroosmotic flow, thus rendering the pressure of HPLC unnecessary. The phenomenon of electroosmotic flow provides a two-fold advantage over conventional pumped systems. First, the efficiency of the separation increases by a factor of approximately two as a consequence of the flat flow profile.

---

\* Corresponding author.

Secondly, the electroosmotic flow is independent of the particle size of the stationary phase over a wide range, thus giving access to the high efficiency obtainable in 0.5-m columns packed with 1.5- $\mu\text{m}$  particles [2–6].

Despite the enormous potential offered by this method, relatively few successful applications have been reported so far, mainly because of the difficulty in obtaining stable flow conditions in purely electro-driven systems. To date, few have approached these problems. In this paper we report our investigations upon the parameters influencing the electrochromatographic performance.

## 2. Experimental

### 2.1. Preparation of the frits

Three different types of frits are produced for testing in electrochromatographic columns. The first is formed by in situ polymerization of a potassium silicate solution with formamide according to the method of Cortes et al. [10]. The potassium silicate solution is prepared by adding 1.3 g potassium hydroxide and 2.4 g silicon dioxide to 12 ml water. Thermostating for 2 h at 70°C yields a clear liquid. The solution is diluted in a ratio of 1:6 with formamide, resulting in a viscous liquid which begins to harden after ca. 10 min. During this time a small plug of this liquid is drawn by vacuum into the appropriate position inside the capillary. The material is completely polymerized after 1 h at 120°C.

Another type of frit is prepared by tapping the tip of a capillary into spherical silica gel (Gromsil, particle diameter  $d_p = 5 \mu\text{m}$ ; Grom, Herrenberg, Germany) which is wetted with potassium silicate solution. The frit is sintered using an electrically heated hot iron wire.

The third type of frit is formed by sintering pure silica gel (Gromsil,  $d_p = 5 \mu\text{m}$ ). It is filled into the capillary column either by slurry packing or by tapping the end of the capillary into silica gel wetted with water.

The frits were tested for mechanical stability by flushing the capillary with water and applying

pressure. The pressure is increased in steps of 25 bar and each step lasts 30 s.

### 2.2. Slurry packing of the capillary columns

Fused-silica capillaries of 50, 100 and 150  $\mu\text{m}$  I.D. and 360  $\mu\text{m}$  O.D. were obtained from Polymicro Technology (Phoenix, AZ, USA). For preparation of the packed capillary columns, only the frits consisting of sintered spherical silica gel were used. The slurry of either reversed-phase material (GromSil ODS-2,  $d_p = 1.5 \mu\text{m}$ ) or silica gel (GromSil,  $d_p = 5 \mu\text{m}$ ) in acetone (1:10, w/v) is ultrasonicated for 5 min and transferred into a stainless-steel slurry chamber (25 mm  $\times$  1 mm I.D.). The capillary protruded about 2 mm into the chamber, which was placed into an ultrasonic bath during packing. The slurry was pumped into the capillary at 400 bar using a liquid chromatographic pump (Model S1100; Sykam, Gilching, Germany).

A packed capillary column is prepared in the following steps. First, a temporary frit is produced by tapping an end of the capillary into silica gel wetted with water, drying for 12 h at room temperature and sintering. After packing the capillary with silica gel, the final outlet frit is formed by sintering at a distance of approximately 15 cm from the end of the capillary. The temporary end-frit is then cut-off and the capillary emptied on both sides of the final outlet-frit by flushing with water under ultrasonification. Removal of the polyimide coating by the electrical heater allows on-column UV absorbance detection. Packing of the capillary with the reversed-phase particles is followed by removal of ca. 1 cm stationary phase by heating the tip of the capillary, thus causing rapid solvent evaporation and ejection of slurry. Finally, this end of the capillary is filled up with silica gel and the inlet-frit sintered after drying.

### 2.3. Apparatus

The electrochromatographic system consists of a modular capillary electrophoresis system (Grom, Herrenberg, Germany). It can be combined with a HPLC system (Sykam, Gilching, Germany) for flushing and pressurizing the

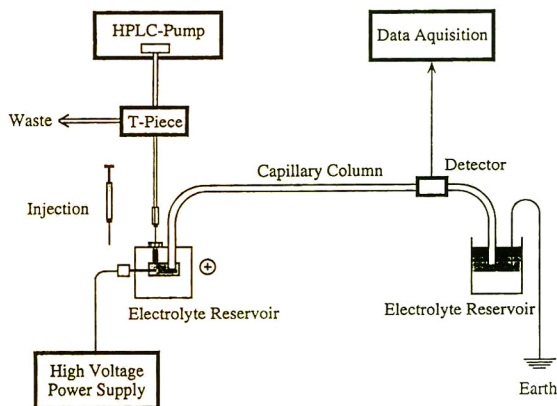


Fig. 1. Schematic representation of the setup for pressurized electrochromatography.

packed capillary columns as shown in Fig. 1. A T-piece and a capillary column of 50  $\mu\text{m}$  I.D. and 30 cm length are used for solvent splitting. A Chromatopack C-R6A (Shimadzu, Kyoto, Japan) is used for data processing.

#### 2.4. Electrochromatography

Pressurized electrochromatography is carried out in capillary columns of 100  $\mu\text{m}$  I.D. packed to a length of 15 cm (GromSil ODS-2,  $d_p = 1.5 \mu\text{m}$ ), 150 bar supplementary pressure and 20 kV. The overall length is 40 cm.

On-column UV absorbance detection (254 nm) is performed 0.1 cm behind the frit. The mobile phase is 80% acetonitrile–20% buffer containing 5 mM sodium phosphate at pH 8. Samples are injected electrokinetically for 5 s at a voltage of 10 kV.

The chemicals for eluent preparation were purchased from Merck (Darmstadt, Germany) and were of research grade.

### 3. Results and discussion

#### 3.1. A practical approach to electrochromatography

Electrochromatography in packed capillary columns should ideally provide stable and reproducible electroosmotic flow without interfer-

ing with detection. In practice, it is often hampered by several phenomena such as variation of the electric current, the electroosmotic flow velocity or the detection signal. These effects can increase, causing the detection noise to rise until current and electroosmotic flow finally break down. When the capillary column is flushed, bubbles are swept out which have formed inside the capillary column.

To overcome these problems we investigated some of the factors determining stability and reproducibility of the electrochromatographic performance. The electrochromatographic system is split into the factors eluent, frits, columns and optional supplementary pressure. These are tested separately for suitable performance and then combined stepwise to obtain an appropriate system.

#### 3.2. Degassing of the eluent

An eluent composition similar to those described in [3,4] with 80% acetonitrile and 5 mM phosphate buffer at pH 8 was chosen to test the eluent in an open tubular column of 150  $\mu\text{m}$  I.D. This diameter is large compared with those used in other electro-driven systems, thus problems related to insufficient heat dissipation are likely to occur; however, it provides a sensitive system for the investigation of related phenomena.

Degassing of the eluent proved to be the crucial factor in this test system. Insufficient degassing led to increased baseline drift, unstable current and finally breakdown of electroosmotic flow as a result of bubble formation. These symptoms can be overcome by thoroughly degassing the eluent. The best results are obtained by a combination of purging with helium and applying vacuum under ultrasonication.

#### 3.3. Selection of appropriate frits

The ideal frit should have sufficient mechanical stability to withstand the pressure of the packing procedure, should be easily prepared and, most importantly, must not interfere with the electrochromatographic process. Three different types of frits, described in the Experimental section, are evaluated.

The frit prepared by condensation of potassium silicate and formamide displayed the best mechanical properties. Even with pressures up to 400 bar it was not possible to remove it from its position in the capillary column. The frit is easily prepared and can be placed at any desired position inside the capillary column. It has a three-dimensional network of connected channels forming pores of ca. 1  $\mu\text{m}$  diameter [10]. Thus, both good mechanical stability and sufficient permeability to the eluent are provided. However, current and baseline signal were unstable under electrochromatographic conditions.

The same problems, although not as severe, are encountered with frits made by sintering spherical silica gel wetted with potassium silicate. In addition, these have only moderate mechanical stability, being displaced at pressures above 100 bar.

It is presumed that these problems originate in the freshly polymerized silicate surface which is common to both systems. The formation of a homogenous electrical double-layer on the surface area is presumably disturbed. The electron micrograph of this frit (Fig. 2A) shows silica gel spheres connected and partly covered by the silicate polymer. The covering is inhomogeneous so that irregular channels are formed. This observation coincides with results of Rebscher and Pyell [8] using similar frits made of silica gel and potassium silicate. They measured band-broadening in electrochromatography and explained the high contribution of the inlet frit by inhomogeneities of the flow within the frits.

The frit prepared by sintering of pure spherical silica gel proved to be better suited for the electrochromatographic system. It allows stable conditions of electroosmotic flow and a stable baseline. The electron micrograph of this frit (Fig. 2B) shows a section of packed particles. The silica gel spheres are melted together at their contact points. Unfortunately, the sintering of the frit destroys the polyimide coating, making these parts of the column susceptible to breakage. Frits of this type are removed by pressures in excess of 50 bar in capillaries of 150  $\mu\text{m}$  I.D., so that care must be exercised during the slurry packing of these capillary columns. Fortunately, the stability of the frits increases

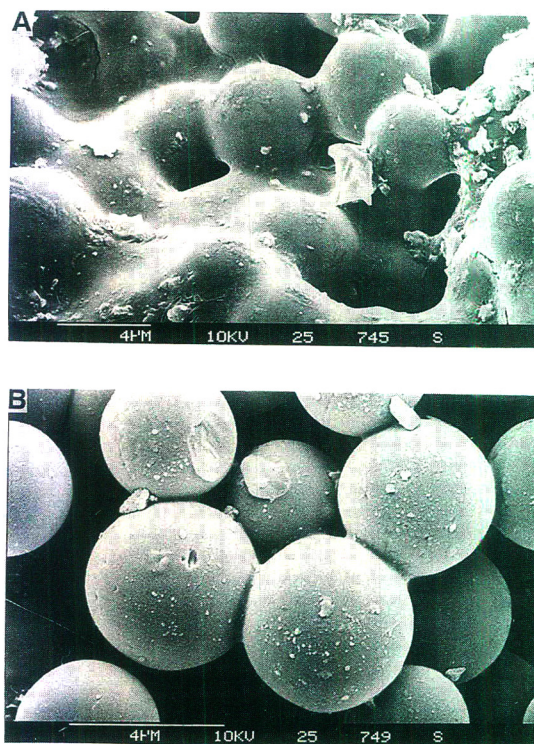


Fig. 2. Electron micrographs of frits used in packed capillary columns. (A) Sintering spherical silica gel that is wetted with potassium silicate solution yields packed spheres covered with irregular layers of polymer coating. (B) The spheres in a packing of silica gel are melted to each other by sintering with an electrical heater. During the preparation for the electron micrograph small fragments of polish fell onto the frit. In addition, a silica sphere broke off, leaving marks where it had been attached (see centre of the upper part).

with decreasing I.D., so that capillaries of 50  $\mu\text{m}$  I.D. with sintered silica gel frits can be flushed at pressures up to 400 bar without removal of the frits. The preparation of these frits within the column requires several steps.

In spite of the laborious preparation, well-packed columns and satisfactory electrochromatographic performance are obtained with these frits.

#### 3.4. Design of the chromatographic columns

In packed capillary columns for liquid chromatography in both the pressure and electro-driven

mode or in combinations of these, the stationary phase of slurry-packed columns must be contained between two frits: the outlet frit prevents removal of the particles when using the pump, while the inlet frit retains the particles which would otherwise migrate upstream in an electrical field as a result of their negative charge. On-column UV detection requires a detection window behind the packing material. The alternative in-column detection as described in [9] results in decreased sensitivity because of light scattering.

These requirements can be satisfied by two different column designs: a coupled and an uncoupled system, as shown in Fig. 3. The coupled system consists of two capillary columns connected by a Teflon tube. The chromatographic column is filled over its full length and limited by two frits. It is adjoined to an open tubular capillary which carries the detection window ca. 5 mm behind the connection to the outlet frit. With this setup the packed columns are readily prepared. In the case of breakage at the window, the open tubular capillary is easily exchanged. Unfortunately, the use of this system is restricted to a low electrical field strength in our experimental setup. The capillary is fastened by a metal support in the detection device of the capillary electrophoresis system. A current to the photocell arises at an electrical field strength higher than  $10 \text{ kV m}^{-1}$ . This prevents the application of higher field strengths in our setup because of an increase in detection noise. This effect can probably be reduced by the use of an

insulating material as support in the detection device.

The uncoupled column system consists of a single fused-silica capillary. Here, the outlet frit is several centimetres from the end of the capillary, and directly behind the outlet frit is the detection window. The minimized dead volume between the chromatographic column and the detection window reduces band-broadening. Disadvantages include the more difficult preparation of the columns and the susceptibility to mechanical breakage at the detection window. Despite these drawbacks, this column design is considered superior for capillary electrochromatography.

### 3.5. Electrochromatographic performance

Without supplementary pressure, electrochromatographic analysis of neutral compounds (alkylbenzenes) in capillary columns of  $100 \mu\text{m}$  I.D. is moderately successful. Separations with a reduced plate height of 1.6 for butylbenzene are obtainable with an optimized buffer (5 mM phosphate). Both higher and lower salt concentrations produced unstable electrochromatographic conditions. Knox and Grant [3] investigated the dependency of the buffer salt concentration on the reduced plate height with a  $40 \mu\text{m}$  I.D. packed capillary column. They described a minimum at ca. 4 mM phosphate buffer and increasing plate height with lower or higher concentrations. Corresponding to this, we observed that with columns of  $50 \mu\text{m}$  I.D., electrochromatographic analysis is possible over a wider range of buffer concentrations than with the  $100\text{-}\mu\text{m}$  column. However, phenomena like variance of current and temperature inside the column as indicated by a baseline drift still occurred in numerous separations. Thus, with this approach no satisfactory reproducible results are obtained.

### 3.6. Pressurized electrochromatography

The problems associated with electrochromatography driven solely by electroosmotic flow can be overcome by applying pressure to the

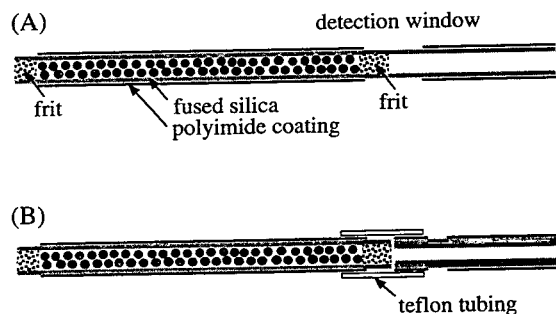


Fig. 3. Packed capillary columns for electrochromatography and micro-HPLC as (A) an uncoupled and (B) a coupled system.

system so that electrochromatographic separations can be performed under stable and reproducible conditions [1,5,6]. This can be accomplished by two different approaches.

Smith and Evans [5] pressurized the buffer reservoirs of their capillary electrophoresis system on both the inlet and outlet sides by approximately 40 bar.

However, it is advantageous to couple an HPLC system to the capillary electrophoresis setup, allowing the capillary column to be pressurized up to 400 bar. This is necessary for filling the capillary column with solvent and for changing the eluent when a different composition is required or when the electroosmotic flow breaks down by bubble formation due to insufficient heat dissipation. Furthermore, a gradient elution mode can easily be realized [6]. Injection can be accomplished both electrokinetically and by pressure. In contrast to electrokinetic injection, injection by pressure does not discriminate the analytes according to their charge, and the

injected sample amount is independent of the charge of the sample molecules.

In pressurized electrochromatography, thorough degassing is less important than in pure electrochromatography: purging with helium is found to be sufficient. Furthermore, analyses can be performed over a wider range of buffer and modifier concentrations [6].

A separation of alkylbenzoates is shown in Fig. 4. The analysis was carried out in a capillary column packed to a length of 15 cm with 1.5- $\mu\text{m}$  stationary phase; 50 000 plates are obtained for pentylbenzoate within 4 min analysis time. The flow velocity of 3 mm s<sup>-1</sup> is far higher than that of 0.4 mm s<sup>-1</sup> obtained by application of the same pressure but without an electrical field. It is apparent that the eluent is transported primarily by electroosmotic flow and that the pressure has merely a stabilizing function.

#### 4. Conclusion

Several parameters influencing the electrochromatographic performance are evaluated and experimental conditions are described to overcome the major problems encountered so far related to electrochromatography, opening this powerful separation technique to a wide field of applications.

#### Acknowledgements

The authors gratefully acknowledge the valuable practical assistance of Ingrid Enss, Rigo Herrmann and Hans-Joachim Gaus and the advice of Shigang Zhang for the preparation of the silicate-formamide frit.

#### References

- [1] T. Tsuda, *LC·GC*, 5 (1992) 32.
- [2] J.H. Knox and I.H. Grant, *Chromatographia*, 24 (1987) 135.
- [3] J.H. Knox and I.H. Grant, *Chromatographia*, 32 (1991) 317.

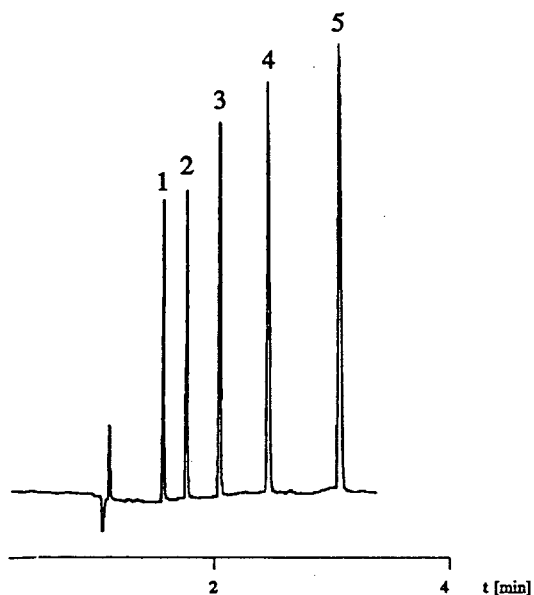


Fig. 4. Separation of alkylbenzoates by pressurized electrochromatography. The column of 100  $\mu\text{m}$  I.D. is packed for a length of 15 cm with 1.5- $\mu\text{m}$  reversed-phase particles. Other conditions as described in the Experimental section. The peaks 1–5 correspond to methyl-, ethyl-, propyl-, butyl- and pentylbenzoate, respectively.



- [4] H. Yamamoto, J. Baumann and F. Erni, *J. Chromatogr.*, 593 (1992) 313.
- [5] N.W. Smith and M.B. Evans, *Chromatographia*, 38 (1994) 649.
- [6] B. Behnke and E. Bayer, *J. Chromatogr. A*, 680 (1994) 93.
- [7] T. Eimer and K. Unger, Packed Fused Silica Capillaries in Electrochromatography, Lecture presented at the 6th International Symposium on High Performance Capillary Electrophoresis, San Diego, CA, 31 January–3 February 1994.
- [8] H. Rebscher and U. Pyell, *Chromatographia*, 38 (1994) 737.
- [9] S. Li and D.K. Lloyd, *Anal. Chem.*, 65 (1993) 3684.
- [10] H.J. Cortes, C.D. Pfeiffer, B.E. Richter and T.S. Stevens, *J. High Resolut. Chromatogr. Chromatogr. Commun.*, 10 (1987) 446.





ELSEVIER

Journal of Chromatography A, 716 (1995) 215–220

JOURNAL OF  
CHROMATOGRAPHY A

# Analysis by capillary electrophoresis–laser-induced fluorescence detection of oligosaccharides produced from enzyme reactions

Xiaochun Le, Christine Scaman, Yanni Zhang, Jianzhong Zhang,  
Norman J. Dovichi\*, Ole Hindsgaul, Monica M. Palcic  
*Department of Chemistry, University of Alberta, Edmonton, Alb. T6G 2G2, Canada*

## Abstract

Six structurally similar, fluorescently labeled oligosaccharides were baseline resolved by capillary electrophoresis (CE); laser induced fluorescence (LIF) detection gave detection limits of 50 molecules for the oligosaccharides. A simple design of the LIF detector that incorporates the advantages of high sensitivity, stability and ease of operation is described. The system was used to monitor enzyme products formed during the incubation of yeast cells with  $\alpha$ -D-Glc(1 $\rightarrow$ 2) $\alpha$ -D-Glc(1 $\rightarrow$ 3) $\alpha$ -D-Glc-O(CH<sub>2</sub>)<sub>8</sub>CONHCH<sub>2</sub>CH<sub>2</sub>NHCO-tetramethylrhodamine. This fluorescent trisaccharide is enzymatically hydrolyzed to fluorescent disaccharide, monosaccharide and the free linker arm that is used to conjugate the saccharides with the fluorophore tetramethylrhodamine.

## 1. Introduction

Oligosaccharides play important roles in many biological functions [1–3]. The formation of oligosaccharides results from a complex series of glycosyltransferase (synthetic) and glycosidase (hydrolytic) enzymatic reactions. Alternation of these enzyme activities can result in a change in the formation or amounts of the complete oligosaccharide chain. Such changes are associated with a number of diseases, especially cancer [4–8]. Assay of the activity of these enzymes and determination of the oligosaccharides are essential to an understanding of their roles in biology.

Conventionally, enzyme assays of glycosyltransferases have often been carried out by using radiochemical methods, gel-permeation, ion-exchange and affinity chromatography and enzyme linked immunosorbent assay [9–15]. Many of

these assays involve tedious procedures and are consequently time consuming. In addition, these assays usually require the use of large amounts of sample and are applicable only to relatively high levels of enzyme.

Capillary electrophoresis combined with laser-induced fluorescence detection (CE–LIF) has been shown to be a powerful technique, which combines the efficient separation offered by CE and the exquisite sensitivity of LIF [16–21]. A minute amount of sample can be analyzed by CE–LIF because of the small sample volume requirement. Therefore, CE–LIF is an ideal technique for assaying enzyme activity in situations where the amount of substrate or enzyme is limited.

Previous work by our group [22] has demonstrated the capability of CE–LIF in assaying two enzymes, fucosyltransferase and  $\alpha$ -fucosidase. Well characterized and purified enzymes were used to react with fluorescently tagged substrates

\* Corresponding author.

under well defined conditions. CE was used to separate the substrate from the enzyme product and postcolumn LIF was followed to detect the fluorescent compounds. More recently, we have successfully used CE–LIF to monitor biosynthetic transformations of a tetramethylrhodamine-labeled derivative of N-acetylglucosamine in crude microsomal extracts that were prepared from the cell line HT-29 (human colon adenocarcinoma) [23]. The technique allowed us to determine minor enzyme products in the presence of major amount of unreacted substrate.

In this work, we extended the application of CE–LIF to the determination of enzyme substrate and products in intact cells. Products formed from the  $\alpha$ -glucosidase I and II reactions are monitored after a fluorescently labeled trisaccharide,  $\alpha$ -D-Glc(1 $\rightarrow$ 2) $\alpha$ -D-Glc(1 $\rightarrow$ 3) $\alpha$ -D-Glc-O(CH<sub>2</sub>)<sub>8</sub>CONHCH<sub>2</sub>CH<sub>2</sub>NHCO-tetramethylrhodamine (-TMR) is incubated with *Saccharomyces cerevisiae* (baker's yeast). We also describe a simple design of an LIF detector using a postcolumn sheath flow cuvette and demonstrate the baseline resolution and sensitive detection of structurally similar oligosaccharides.

## 2. Experimental

### 2.1. Materials

Fluorescently labeled oligosaccharides were prepared as described previously [23,24]. Stock solutions including 0.1 M Na<sub>2</sub>HPO<sub>4</sub> (Fisher Scientific, Nepean, ON, Canada), 0.1 M borate (Fisher Scientific), 0.1 M sodium dodecyl sulfate (BDH, Toronto, ON, Canada) and 0.1 M phenylboronic acid (Sigma, St. Louis, MO, USA), were prepared in deionized water (Barnstead NANOpure system) and filtered with a 0.2- $\mu$ m pore size disposable filter (Nalgene, Cleveland, OH, USA). The electrophoresis running buffer was prepared by mixing these stock solutions to final concentrations of 10 mM each of Na<sub>2</sub>HPO<sub>4</sub>, borate, sodium dodecyl sulfate (SDS) and phenylboronic acid (pH 9.3). All other reagents were of analytical-reagent grade.

### 2.2. Capillary electrophoresis system

The electrophoresis was driven by a Spellman (Plainview, NY, USA) CZE 1000R high-voltage power supply. The separation voltage, injection voltage and injection time were controlled by a Macintosh Quadra 650 computer, with a program written in LabVIEW (National Instruments, Austin, TX, USA). Separation was carried out in a 42 cm  $\times$  10  $\mu$ m I.D.  $\times$  144  $\mu$ m O.D. fused-silica capillary (Polymicro, Phoenix, AZ, USA) at an electric field of 400 V/cm. The high-voltage injection end of the capillary was held in a Plexiglas box equipped with a safety interlock. The other end of the capillary was placed inside a sheath flow cuvette detector and was held at ground potential. For optimum separation, the running buffer was composed of 10 mM each of phosphate, borate, phenylboronic acid, and SDS at pH 9.3. The sheath fluid was identical with the running buffer and was gravity fed from a 250-ml wash bottle. The sheath fluid level was arranged to be 5 cm higher than the level in the waste reservoir. This arrangement maintained a smooth sheath flow through the cuvette.

### 2.3. Laser-induced fluorescence detection system

A postcolumn LIF detector using a sheath flow cuvette (Fig. 1) was constructed on an optical bread board (Newport, Irvine, CA, USA). A 1.0-mW helium–neon laser (Melles Griot, Nepean, ON, Canada) with a wavelength of 543.5 nm was used as the excitation source. The beam was focused with a 5 $\times$  microscope objective (Melles Griot) into a sheath flow cuvette. The sheath flow cuvette was used as the fluorescence detection cell, as described elsewhere [16–18]. Briefly, the cuvette was constructed with high optical quality quartz, and had 1-mm thick walls, a 200- $\mu$ m square inner chamber and a length of 2 cm. The quartz cuvette was mounted in a locally constructed stainless-steel body. A capillary was inserted into the cuvette such that the laser beam was illuminated approximately 20  $\mu$ m below the tip of the capillary. The coating on the detector end of the capillary was removed to reduce any

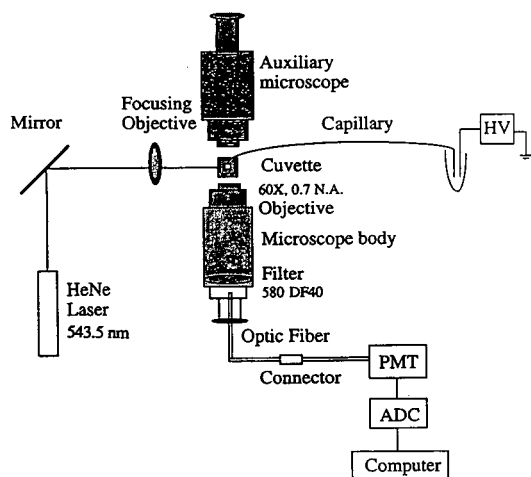


Fig. 1. Schematic diagram of a modified postcolumn laser-induced fluorescence detector for capillary electrophoresis.

possible scattering of laser light. Fluorescence was collected at right-angles with respect to the laser beam by using a high numerical aperture (0.7 NA), 60 $\times$  microscope objective Model 60X-LWD (Universe Kogaku, Oyster Bay, NY, USA). The fluorescence was spectrally filtered with a band-pass filter (580DF40; Omega Optical, Brattleboro, VT, USA) and imaged on to a SELFOC fiber collimator (p-type; NSG America, Somerset, NJ, USA) that consisted of an optical fiber and two grin lenses, one on each end of the optical fiber [25]. The diameter of the grin lens was 2 mm. The fluorescence was propagated through the fiber collimator and was detected with an R1477 photomultiplier tube (PMT) (Hamamatsu, Bridgewater, NJ, USA). The output from the PMT was digitized by a National Instruments board in a Macintosh Quadra 650 computer.

It is necessary to align a tightly focused laser beam with a small-diameter sample stream so that the fluorescence passes through a high numerical aperture objective and is detected by the PMT. In the present optical design, the alignment can be optimized very easily and quickly. An auxiliary microscope was placed opposite the collection optic and used to assist

the alignment. During the alignment process, the bulkhead connector (Radiant Communications, Plainfield, NJ, USA) between the two fiber collimators was disconnected. When light from a flashlight illuminates the end of the fiber collimator, light travels back through the optical system in a path that is the reverse of the fluorescence. A small, bright spot representing the image of the fiber collimator is projected through the collection optic. The auxiliary microscope is focused on this bright image of the fiber collimator. The position of the laser beam and the sheath flow cuvette are then adjusted to superimpose the projected image of the fiber collimator with the fluorescence from the sample stream. When the images superimpose, the system is in alignment. The sheath flow cuvette and the laser beam focusing objective are each mounted on a set of three-axis translation stages, and thus their positions can be adjusted with ease and precision. The system is compact and very stable.

#### 2.4. Incubation of yeast cells and preparation of spheroplasts

*Saccharomyces cerevisiae* (baker's yeast, Fleischman) was grown on Sabouraud dextrose agar plates (Difco) at 37°C and then stored at 4°C. A typical colony was inoculated into 1 ml of sterile Sabouraud dextrose medium and grown at room temperature with shaking overnight (ca. 17 h). A subsample of 200  $\mu$ l was transferred into a sterile microfuge tube and pelleted. Old medium was removed and fresh medium was added to the pelleted cells along with sterile filtered trisaccharide,  $\alpha$ -D-Glc(1 $\rightarrow$ 2) $\alpha$ -D-Glc(1 $\rightarrow$ 3) $\alpha$ -D-Glc-O(CH<sub>2</sub>)<sub>8</sub>CONHCH<sub>2</sub>CH<sub>2</sub>NHCO-TMR, from a 10 mM stock solution. The final concentration of the trisaccharide substrate in the culture was 50  $\mu$ M. Tubes were covered with aluminium foil and incubated at 25°C for 5 h with shaking. At the end of the incubation period, cells were pelleted and the supernatant was removed. A subsample of the supernatant was saved for analysis by capillary electrophoresis. Cells were then transferred to the surface of a 0.22  $\mu$ m, 47 mm diameter cellulose filter

(Micron Separations) and washed under vacuum with ca. 500 ml of phosphate-buffered saline (PBS). Cells were washed off the filter into a test-tube with PBS and pelleted. A sample of the PBS supernatant was taken for capillary electrophoresis to determine if all free trisaccharide substrate had been removed. Control cells were prepared in the same manner except that no trisaccharide substrate was added.

The intact PBS-washed cells were used to generate spheroplasts with the following procedure [26,27]. Cells were washed twice with a high-ionic-strength buffer, 25 mM Tris-HCl (pH 7.5)–2.0 M sorbitol, and then incubated at 37°C in 40  $\mu$ l of the same buffer containing 770 U per 100  $\mu$ l of lyticase (*Arthrobacter luteus*,  $\beta$ 1–3 glucanase; Sigma). After a 2-h incubation at 37°C, most of the cells were converted into spheroplasts, as determined by visual inspection of a sample under a microscope. Spheroplasts were lysed by adding a buffer containing 10 mM borate and 10 mM SDS and by sonicating for 1 h in a water-bath ultrasonic cleaner (Branson, Shelton, CT, USA). The sample was subjected to CE-LIF analysis.

### 2.5. Determination of oligosaccharides by CE-LIF

Samples were electrokinetically injected on to a 10  $\mu$ m I.D. capillary typically by applying a 500–1000-V potential for 5 s. To reduce contamination, the capillary tip was first rinsed in a vial containing running buffer before the capillary was placed in the vial containing the buffer used for electrophoresis analysis. The separation was performed at room temperature. Peak identity in the electropherogram was obtained by comparing the migration time of the analyte in the sample with those of the standards. Further confirmation of the enzyme products was achieved by analysis of the co-injected standard compound and the reaction mixture. Co-elution of an analyte and the standard compound provided evidence that the reaction mixture contained that standard compound.

### 3. Results and discussion

Fig. 2 shows two electropherograms obtained from the analysis of a mixture of six fluorescently labeled sugars and the linker arm. Each component in the standard mixture was  $10^{-10}$  M (for the top trace) and  $10^{-9}$  M (for the bottom trace). The separation capillary (42 cm  $\times$  10  $\mu$ m I.D.) has a total volume of 33 nl. Electrokinetic injection at 500 V for 5 s corresponds to the introduction of ca. 5.5 pl of the standard mixture. Therefore, ca. 350 (top trace) and 3500 (bottom trace) molecules of each compound

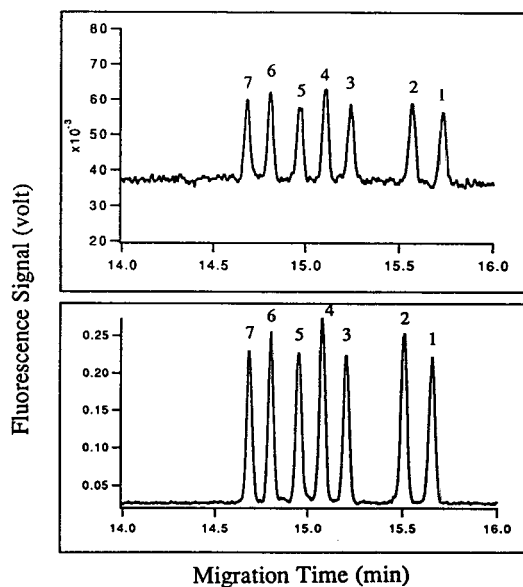


Fig. 2. CE-LIF of six fluorescently labeled saccharides (peaks 2–7) and the linker arm (peak 1). Capillary, 42 cm  $\times$  10  $\mu$ m I.D.  $\times$  144  $\mu$ m O.D.; running buffer, 10 mM phosphate-borate-phenylboronic acid-SDS; running voltage, 16.8 kV (400 V/cm); injection time, 5 s; injection voltage, 500 V; injection volume, 5.5 pl; concentration of each component,  $10^{-10}$  M (top) and  $10^{-9}$  M (bottom). Peaks: 1 = HO(CH<sub>2</sub>)<sub>8</sub>CONHCH<sub>2</sub>CH<sub>2</sub>NHCO-TMR (linker arm: -O-TMR); 2 = N-acetyl- $\beta$ -D-glucosaminide-O-TMR (GlcNAc-O-TMR); 3 =  $\beta$ Gal(1 $\rightarrow$ 3) $\beta$ GlcNAc-O-TMR (Lewis C); 4 =  $\beta$ Gal(1 $\rightarrow$ 4) $\beta$ GlcNAc-O-TMR (LacNAc); 5 =  $\alpha$ Fuc(1 $\rightarrow$ 2) $\beta$ Gal(1 $\rightarrow$ 4) $\beta$ GlcNAc-O-TMR (H-Type II); 6 =  $\beta$ Gal(1 $\rightarrow$ 4)[ $\alpha$ Fuc(1 $\rightarrow$ 3)] $\beta$ GlcNAc-O-TMR (Lewis X); 7 =  $\alpha$ Fuc(1 $\rightarrow$ 2) $\beta$ Gal(1 $\rightarrow$ 4)[ $\alpha$ Fuc(1 $\rightarrow$ 3)] $\beta$ GlcNAc-O-TMR (Lewis Y).

were injected for these analyses. The detection limit calculated according to Knoll's method [28] is ca. 80 yoctomol ( $8 \times 10^{-23}$  mol), or 50 molecules of the TMR-labeled saccharides.

Compounds **3** and **4** are two disaccharide isomers, as are compounds **5** and **6**. The structural differences between these compounds are minor, especially after the saccharides have been labeled with the relatively large TMR fluorophore. The baseline resolution of these compounds shown in Fig. 2 demonstrates the excellent separation efficiency, which is achieved by using an optimized buffer solution containing borate, phenylboronic acid, phosphate and SDS. The combination of borate and phenylboronic acid is used to enhance the resolution; the complexation of sugar hydroxyl groups with borate [29,30] and phenylboronic acid enhances the mobility differences between the labeled saccharides.

Fig. 3 demonstrates an application of the CE-LIF system to the analysis of enzyme products generated in intact yeast cells. The top electropherogram was obtained from the injection of lysed spheroplasts, formed from cells incubated for 5 h with the trisaccharide  $\alpha$ -D-Glc(1 $\rightarrow$ 2) $\alpha$ -D-Glc(1 $\rightarrow$ 3) $\alpha$ -D-Glc-O(CH<sub>2</sub>)<sub>8</sub>CONHCH<sub>2</sub>CH<sub>2</sub>NHCO-TMR. Most of this substrate was converted into linker arm (L) and intermediate disaccharide (D) and monosaccharide (M). Prior to spheroplast formation, the yeast cells were thoroughly washed with PBS, and these compounds were not found to be present at detectable levels in the PBS wash solution. This indicates that the compounds detected after spheroplast lysis originating from inside the cells. Monitoring of the intact yeast cells, using confocal laser scanning microscopy, also confirmed the uptake of the fluorescent trisaccharide by yeast cells after an incubation period (results not shown). The trisaccharide substrate is stable in aqueous solution. The hydrolysis products observed arise from the sequential activity of  $\alpha$ -glucosidase I and II inside the yeast, which act specifically on  $\alpha$ -D-Glc(1 $\rightarrow$ 2) and  $\alpha$ -D-Glc(1 $\rightarrow$ 3) linkages, respectively [31,32]. Using the present technique, we

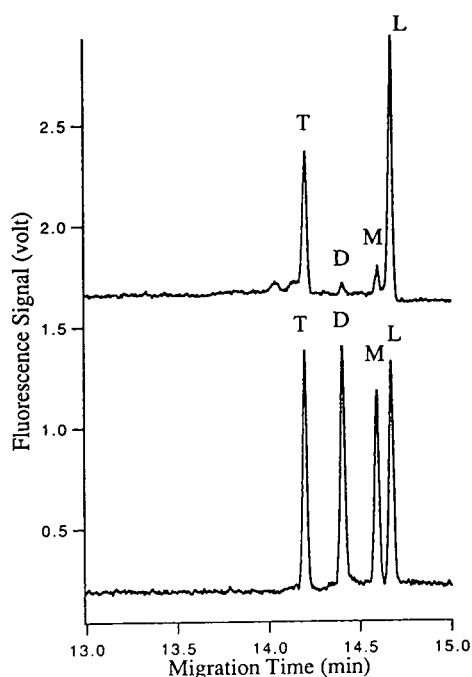


Fig. 3. Electropherograms obtained from the analysis of lysed yeast spheroplasts (top) and a standard solution containing  $10^{-9}$  M of each component (bottom). Peaks: T =  $\alpha$ -D-Glc(1 $\rightarrow$ 2) $\alpha$ -D-Glc(1 $\rightarrow$ 3) $\alpha$ -D-Glc-O(CH<sub>2</sub>)<sub>8</sub>CONHCH<sub>2</sub>CH<sub>2</sub>NHCO-TMR; D =  $\alpha$ -D-Glc(1 $\rightarrow$ 3) $\alpha$ -D-Glc-O(CH<sub>2</sub>)<sub>8</sub>CONHCH<sub>2</sub>CH<sub>2</sub>NHCO-TMR; M =  $\alpha$ -D-Glc-O(CH<sub>2</sub>)<sub>8</sub>CONHCH<sub>2</sub>CH<sub>2</sub>NHCO-TMR; L = H-O(CH<sub>2</sub>)<sub>8</sub>CONHCH<sub>2</sub>CH<sub>2</sub>NHCO-TMR.

are able to determine both the major and minor enzyme products in a single analysis.

The capability of the technique is not limited to the oligosaccharides described in this paper. The instrumentation and the general methodology presented here should be applicable to the assay of other enzymes and fluorescent substrates.

#### Acknowledgements

This work was supported by a Strategic Grant (STR 149003 to O.H., N.J.D. and M.M.P.) from the Natural Sciences and Engineering Research

Council of Canada. A studentship (to Y.Z.) from the Alberta Heritage Foundation for Medical Research and a Killam Post-doctoral Fellowship (to X.L.) are gratefully acknowledged.

## References

- [1] T.W. Rademacher, R.B. Parekh and R.A. Dwek, *Annu. Res. Biochem.*, 57 (1988) 785–838.
- [2] V. Ginsberg and P.W. Robbins (Editors), *Biology of Carbohydrates*, Vol. 3, JAI Press, Greenwich, CT, 1991.
- [3] A. Kobata, *Acc. Chem. Res.*, 26 (1993) 319–324.
- [4] L. Warren, C.A. Buck and P. Tuszynski, *Biochim. Biophys. Acta*, 516 (1978) 97–127.
- [5] S. Hakomori, *Annu. Rev. Immunol.*, 2 (1984) 103–126.
- [6] J.W. Dennis, S. Laferte, C. Waghorne, M.L. Breitman and R.S. Kerbel, *Science*, 236 (1987) 582–585.
- [7] S. Hakomori and R. Kannagi, *J. Natl. Cancer Inst.*, 71 (1983) 231–251.
- [8] R. Kleene and E.G. Berger, *Biochim. Biophys. Acta*, 1154 (1993) 283–325.
- [9] T.A. Beyer, J.E. Sadler, J.I. Rearick, J.C. Paulson and R.L. Hill, *Adv. Enzymol.*, 52 (1981) 23–175.
- [10] J.A. Voynow, T.F. Scanlin and M.C. Glick, *Anal. Biochem.*, 168 (1988) 367–373.
- [11] R.D. Cummings, *Methods Enzymol.*, 230 (1994) 66–86.
- [12] A. Kobata, *Methods Enzymol.*, 230 (1994) 200–208.
- [13] J.U. Baenziger, *Methods Enzymol.*, 230 (1994) 237–249.
- [14] S.C. Crawley, O. Hindsgaul, G. Alton, M. Pierce and M.M. Palcic, *Anal. Biochem.*, 185 (1990) 112–117.
- [15] L.M. Keshvara, S. Gosselin and M.M. Palcic, *Glycobiology*, 3 (1993) 416–418.
- [16] Y.F. Cheng and N.J. Dovichi, *Science*, 242 (1988) 562–564.
- [17] Y.F. Cheng, S. Wu, D.Y. Chen and N.J. Dovichi, *Anal. Chem.*, 62 (1990) 496–503.
- [18] D.Y. Chen and N.J. Dovichi, *J. Chromatogr. B*, 657 (1994) 265–269.
- [19] J. Liu, O. Shirota, D. Wiesler and M. Novotny, *Proc. Natl. Acad. Sci. U.S.A.*, 88 (1991) 2302–2306.
- [20] M. Stefansson and M. Novotny, *Anal. Chem.*, 66 (1994) 1134–1140.
- [21] Z.E. Rassi, *Adv. Chromatogra.*, 34 (1994) 177–250.
- [22] J.Y. Zhao, N.J. Dovichi, O. Hindsgaul, S. Gosselin and M.M. Palcic, *Glycobiology*, 4 (1994) 239–242.
- [23] Y. Zhang, X. Le, N.J. Dovichi, C.A. Compston, M.M. Palcic, P. Diedrich and O. Hindsgaul, *Anal. Biochem.*, 227 (1995) 368–376.
- [24] I. Neverova, C. Scaman, O.P. Srivastava, R. Szweda, I.K. Vijay and M.M. Palcic, *Anal. Biochem.* 222 (1994) 190–195.
- [25] J.Z. Zhang, Ph.D. Thesis, University of Alberta, Edmonton, 1994.
- [26] D. Lohr, in I. Campbell and J.H. Duffus (Editors), *Yeast: a Practical Approach*, IRL Press Washington, DC, 1988, pp. 125–145.
- [27] A.H. Rose and F.J. Veazey, in I. Campbell and J.H. Duffus (Editors), *Yeast: a Practical Approach*, IRL Press, Washington, DC, 1988, pp. 255–275.
- [28] J.E. Knoll, *J. Chromatogr. Sci.*, 23 (1985) 422–425.
- [29] S. Honda, S. Iwase, A. Makino and S. Fujiwara, *Anal. Biochem.*, 176 (1989) 72–77.
- [30] S. Hoffstetter-Kuhn, A. Paulus, E. Gassmann and H.M. Widmer, *Anal. Chem.*, 63 (1991) 1541–1547.
- [31] R.D. Kilker, Jr., B. Saunier, J.S. Tkacz and A. Herscovics, *J. Biol. Chem.*, 256 (1981) 5299–5303.
- [32] B. Saunier, R.D. Kilker, Jr., J.S. Tkacz, A. Quaroni and A. Herscovics, *J. Biol. Chem.*, 257 (1982) 14155–14161.



# Nanomolar determination of aminated sugars by capillary electrophoresis

Yanni Zhang, Edgar Arriaga, Paul Diedrich, Ole Hindsgaul, Norman J. Dovichi\*  
*Department of Chemistry, University of Alberta, Edmonton, Alb. T6G 2G2, Canada*

## Abstract

A procedure is described for the determination of aminated monosaccharides at nanomolar concentrations by derivatization with the fluorogenic reagent 3-(*p*-carboxybenzoyl)quinoline-2-carboxyaldehyde (CBQCA) to produce a fluorescent derivative that can be identified and detected by capillary electrophoresis with laser-induced fluorescence detection. Labeling conditions that favor the formation of the CBQCA-aminated sugar derivative over secondary fluorescent products were chosen. Samples as dilute as  $1.0 \times 10^{-9}$  M 1-glucosamine were analyzed. The results can be extended to other aminated monosaccharides since they showed similar reaction yields on labeling. The capability for the analysis of mixtures of aminated sugars was also demonstrated. Five labeled aminated sugars were separated by capillary electrophoresis using a running buffer containing a mixture of phenyl boronate and borate. The detection scheme was based on a low-scattering sheath flow cuvette as a postcolumn detector and two photomultiplier tubes that have mutually excluded wavelength ranges to prevent the water Raman band from contributing to the background signal. The system had a limit of detection of 75 zeptomol of fluorescently labeled 1-glucosamine.

## 1. Introduction

The structural complexity of carbohydrates complicates the establishment of a relationship between their structure and their biological function. Determination of the structure of the saccharide moiety in biomolecules such as glycoproteins, proteoglycans and polysaccharides requires a technique that allows the identification of the individual monosaccharides and determines how they are linked to each other. Selective enzymatic cleavage of complex carbohydrates can be used to determine how monosaccharides are interconnected to form carbohydrates. In addition, a separation and identifica-

tion technique for monosaccharides that is compatible with the enzymatic cleavage is required.

Separation and identification methods for monosaccharides, such as high-performance liquid chromatography, gas chromatography and thin-layer chromatography, usually require large samples [1]. Ideally, determination of carbohydrate structure requires the handling and analysis of samples in very small volumes. For example, if complex carbohydrates or monosaccharides from a single cell are to be analyzed, a technique that provides high sensitivity and low detection limits such as capillary electrophoresis with laser-induced fluorescence detection (CE-LIF) is required.

CE-LIF is a useful technique for the trace analysis of biological molecules such as DNA,

\* Corresponding author.

proteins, peptides and carbohydrates [2,3]. However, CE–LIF analyses of saccharides are often more difficult than analyses of other biomolecules, since saccharides do not have a net charge (except for acidic saccharides). Thus, direct separation of saccharides by CE is not possible. The use of borate as a complexing agent in the separation buffer facilitates the formation of carbohydrate–borate complexes that are charged; thus, electrophoretic separation is possible [4–12].

Another difficulty in analyzing carbohydrates by CE–LIF is the lack of a native fluorophore in the molecule, making it necessary to attach a fluorescent tag to the molecule. Some procedures for fluorescent labeling of saccharides use direct attachment of an amine-containing fluorescent tag to the reducing hydroxyl of the saccharide. Reagents such as 2-aminopyridine (AP), 5-aminonaphthalene-2-sulfonate (ANS) and 7-amino-1,3-naphthalenedisulfonate (ANTS) can be conjugated to the anomeric carbon of the saccharide through reductive amination using sodium cyanoborohydride [13–16]. ANTS is an attractive reagent since it fluoresces at longer wavelengths than AP and ANS and it provides the labeled saccharide with three negative charges that contribute to labeled-saccharide electrophoretic mobility while AP and ANS provide no and one negative charge to the labeled saccharide, respectively. Other procedures require reduction of the hydroxyl group at the anomeric carbon to form a primary amine, followed by labeling with an amine-reactive probe. Liu et al. [17] added a primary amino group to the anomeric carbon by reacting the saccharide in the presence of sodium cyanoborohydride and excess of ammonium.

In general, fluorescent labeling reactions for saccharides require extremely high concentrations of the saccharide and the labeling reagent. Zhao et al. [12], despite attaining the lowest limit of detection for an aminated sugar monomer ever reported (60 molecules), used 1 mM 5-carboxytetramethylrhodamine succinimidyl ester to label 20 mM aminated sugar. Since the level of some carbohydrates found in biological samples is submicromolar, the labeling scheme

should be effective at those levels. In addition, high concentrations of fluorescent labeling reagents can result in overlapping reagent peaks in the electropherograms. Hence techniques that allow labeling of carbohydrates at submicromolar levels and do not result in electropherograms containing reagent peaks are required to handle many biological samples.

Novotny and co-workers introduced the use of 3-(*p*-carboxybenzoyl)quinoline-2-carboxyaldehyde (CBQCA) as a fluorogenic reagent to label monosaccharides and also polysaccharides that have been previously aminated [17–19]. This approach offers the advantage that the reagent does not fluoresce unless it reacts with an amine group. Thus, electropherograms are free of reagent peaks that in other cases may overlap with the saccharide derivative peaks. Using CBQCA for labeling aminated sugars, excitation with 457-nm radiation from an argon ion laser and on-column detection, Liu et al. [8] reported a limit of detection (LOD) in the sub-attomole range.

Here we report a method for CBQCA labeling of monosaccharides and demonstrate the labeling of  $10^{-9}$  M 1-glucosamine. The CBQCA derivative of 1-glucosamine is then detected by CE–LIF. The highly sensitive detection scheme is based on the selection of an alternative excitation wavelength that minimizes interference from water Raman scatter. The CE separation of five aminated monosaccharides based on the formation of charged complexes with borate and phenyl boronate is presented to illustrate the compatibility among the labeling technique, CE separation and LIF detection.

## 2. Experimental

### 2.1. Instrument

The CE–LIF instrument has been described elsewhere [20]. Non-derivatized capillaries (180  $\mu\text{m}$  O.D., 50  $\mu\text{m}$  I.D. or 142  $\mu\text{m}$  O.D., 10  $\mu\text{m}$  I.D.) were used for the separation. A CZE 1000R high-voltage power supply (Spellman, Plainview, NY, USA) with a maximum output of

29 kV provided a positive high voltage at the injection end (cathodic mode). Usually, CBQCA derivatives of aminated sugars (maximum excitation at 456 nm) are excited with 442-nm radiation from a He–Cd laser or 457-nm radiation from an argon ion laser and the emission is detected at 552 nm [8,9]. In our experiment, fluorescence was excited with 488-nm radiation from a multiple-wavelength argon ion laser (INNOVA 99-4; Coherent, Palo Alto, CA, USA) set at 30 mW. The detector was arranged in order to eliminate the water Raman band (577–596 nm) associated with excitation with 488-nm radiation. Detection was based on light collection by two R1477 photomultiplier tubes (Hamamatsu, Middlesex, NJ, USA). A dichroic beam splitter, 590DRLP@45 (Omega Optical, Brattleboro, VT, USA), reflected light with wavelengths shorter than 590 nm (reflected channel) and transmitted light with wavelengths longer than 590 nm (transmitted channel). Reflected light was sent through a 535DF35 bandpass filter (transmission range 515–555 nm; Omega Optical) before reaching the reflected channel photomultiplier tube. For the transmitted channel, light was transmitted through a 635DF55 bandpass filter (transmission range 605–685 nm; Omega Optical) before reaching the photomultiplier tube. The PMT outputs were digitized using an NB-MIO-16X-18 input/output board (National Instruments, Austin, TX, USA). The digitized signals were summed to obtain a combined signal that includes fluorescence in the 515–555 and 605–685 nm ranges and excludes light from 552.5 to 607.5 nm. The water Raman band is in the range 577–596 nm, which is effectively blocked by this detector configuration, resulting in a lower background and improved limits of detection.

## 2.2. Preparation of sugar derivatives

Glucose, galactose, mannose, and fucose were reductively aminated to produce their 1-amino-1-deoxy-D-alditols. 2-Amino-2-deoxy-D-glucitol was synthesized by reduction of N-acetylglucosamine. Their synthesis has been described elsewhere [12]. In this paper, the alditols will be

referred to as 1-glucosamine, 1-galactosamine, 1-mannosamine, 1-fucosamine and 2-glucosamine.

## 2.3. CBQCA labeling reaction

Stock solutions ( $1.0 \cdot 10^{-2}$  M) of the sugar derivatives were prepared in 0.185 M sodium hydrogencarbonate (BDH, Toronto, ON, Canada) and stored at 4°C. Dilutions for labeling reactions were made with HPLC-grade water (Fisher Scientific, Nepean, ON, Canada). Dilutions for electrokinetic injections were made with 10 mM sodium borate (Fisher Scientific) and 10 mM sodium dodecyl sulfate (BDH) buffer (BS buffer). A 10 mM stock solution of CBQCA (Molecular Probes, Eugene, OR, USA) was prepared in methanol and stored at –20°C. Potassium cyanide (Molecular Probes) was dissolved in HPLC-grade water to obtain a 0.20 M stock solution and stored at 4°C.

The labeling reaction mechanism has been described elsewhere [18]. The reaction starts with the nucleophilic attack of cyanide on CBQCA and then the amine group is incorporated and participates in the formation of a quinoline ring; the resulting derivative has highly fluorescent properties compared with the unreacted CBQCA reagent. The labeling reaction was performed by mixing 5–10  $\mu$ l of a dilution of the aminated sugar in HPLC-grade water, 10  $\mu$ l of the CBQCA stock solution and an aliquot of methanol (or phosphate buffer) to make up 23  $\mu$ l. Then 2  $\mu$ l of 50 mM cyanide were added to the mixture. The 25  $\mu$ l of reaction mixture contained 4 mM CBQCA, 4 mM cyanide and  $10^{-4}$ – $10^{-9}$  M aminated sugar. After vortex mixing, the mixture was incubated in the dark for 2–10 h. The mixture was vortex mixed every 30 min. A blank was prepared by replacing the aminated sugar aliquot with water. The reaction mixtures could be stored at –20°C for 1 week without noticeable degradation.

The effect of pH on the labeling reaction was determined by using 100 mM phosphate buffer instead of methanol to make the reaction volume 25  $\mu$ l. The reaction mixture contained 4 mM

CBQCA and 2 mM cyanide and the reaction was carried out for 4 h.

#### 2.4. Separation

Prior to electrokinetic injection, CBQCA derivatives of aminated sugars were diluted to  $2.0 \cdot 10^{-7}$  M in BS buffer. This concentration is based on a 100% yield for the labeling reaction. For concentrations  $\leq 2.0 \cdot 10^{-7}$  M, no dilution was performed prior to injection.

Separation buffers were prepared from stock solutions of 0.556 M sodium dodecyl sulfate, 0.20 M sodium phosphate dibasic acid (Fisher), 0.20 M sodium borate and 0.10 M phenylboronic acid (Sigma, St. Louis, MO, USA). The pH was adjusted with 1.1 M sodium hydroxide (BDH). Although several buffers were investigated for use in the separation, the buffer selected for the separation contained 50 mM phenylboronic acid,

20 mM phosphate dibasic acid and 20 mM borate (pH 9).

### 3. Results and discussion

#### 3.1. Selection of labeling reaction conditions

The conditions for the labeling reaction were optimized using 1-glucosamine. The conditions required to maximize the reaction yield depended on the concentration of 1-glucosamine. For samples with high concentrations of 1-glucosamine (e.g.,  $10^{-4}$  M), the labeling reaction had its highest yield when 6 mM CBQCA and 8 mM cyanide were used. On the other hand, samples with low 1-glucosamine concentrations (e.g.,  $10^{-9}$  M) could not be detected by CE-LIF when these concentrations of CBQCA and cyanide were used. Samples with low concen-

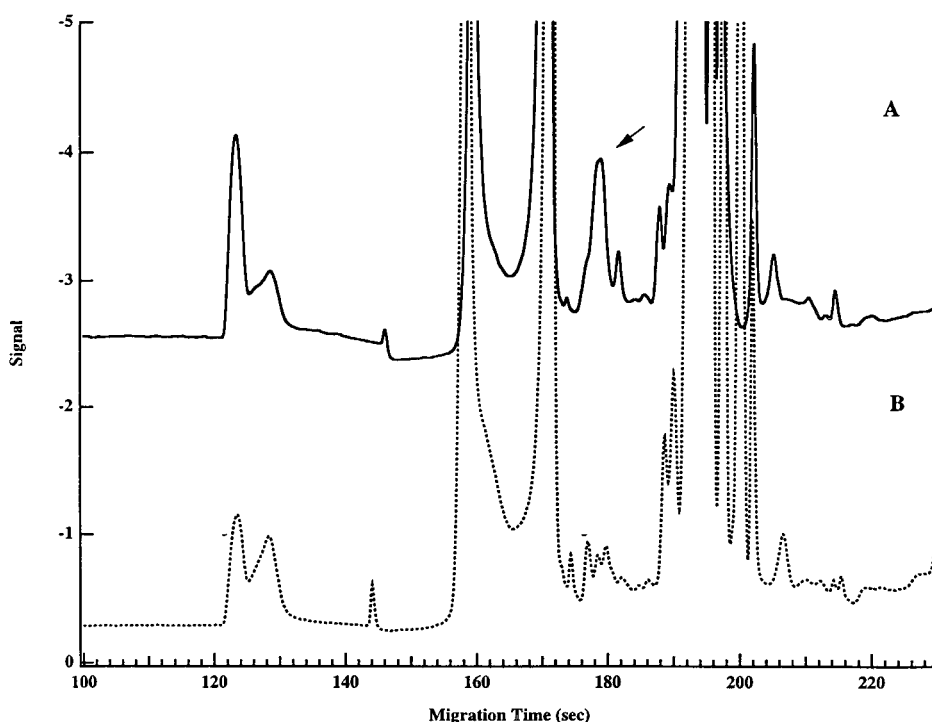


Fig. 1. Electropherogram of a fluorescently labeled sample containing (A)  $10^{-9}$  M 1-glucosamine and (B) a reaction blank. Reaction conditions: (A)  $10^{-9}$  M 1-glucosamine–4 mM CBQCA–4 mM KCN for 10 h at room temperature; (B) 4 mM CBQCA–4 mM KCN for 10 h at room temperature. Separation conditions: 41.5 cm  $\times$  50  $\mu$ m I.D. capillary; running buffer, 10 mM borate–10 mM SDS; 400 V/cm. Injection conditions: 2500 V for 5 s.

trations of 1-glucosamine had their highest yield when 4 mM CBQCA and 4 mM cyanide were used in the labeling reaction.

Fig. 1A shows an electropherogram of a sample containing  $1.0 \cdot 310^{-9}$  M 1-glucosamine that was labeled with CBQCA and detected by CE-LIF. The blank peaks attributed to secondary reactions between CBQCA and cyanide (Fig. 1b) are much larger than the peak of the CBQCA derivative of 1-glucosamine. It has been observed that cyanide can induce condensation of two aromatic aldehydes to form an  $\alpha$ -hydroxy ketone; many condensation products are possible [21]. Formation of cyanohydrins is another possible explanation for the secondary peaks that appear in the electropherograms [22]. However, the peak of the CBQCA derivative elutes in a region, 170–190 s, where the electropherogram baseline is relatively flat. If the concentrations of CBQCA or cyanide used in the labeling reaction are higher than 4 mM each, the baseline is irregular in the elution region of the CBQCA derivative, making its detection impossible at this low concentration. A method to eliminate the fluorescent secondary products for the labeling reaction of insulin B with FQ (a fluorogenic reagent that has similar chemistry to CBQCA) could be a good alternative to obtain cleaner electropherograms [23].

The pH of the labeling reaction has been known to affect the yield of the CBQCA labeling reactions of different amine-containing molecules. Amino acids and small peptides have their highest reaction yield when the labeling reaction is carried out at pH 8.5–9.5; reaction yields for larger peptides are pH insensitive [18] and sugar reaction yields are highest at pH 7.0 [9]. The yield of the 5-h labeling reaction of  $10^{-4}$  M 1-glucosamine with CBQCA varied with pH. For pH 7.1, 8.0 and 9.0 the relative yield was  $0.5 \pm 0.1$ ,  $1.0 \pm 0.1$  and  $0.6 \pm 0.1$ , respectively. If no phosphate buffer was used to regulate the pH in the sample, the reaction yield was about 40 times lower. Despite the low reaction yield when the reaction mixture lacks phosphate buffer, samples with low concentrations of 1-glucosamine (e.g.,  $10^{-9}$  M) were labeled without addition of such buffer. Since samples containing low concen-

trations of 1-glucosamine cannot be diluted prior to injection, the presence of phosphate buffer results in an unstable baseline around the elution time of the CBQCA derivative of 1-glucosamine in addition to tailing of the peak. To compensate for the slow kinetics when no phosphate buffer is used, the reaction time was extended to 10 h.

### 3.2. Sample concentration range for labeling of 1-glucosamine

Samples containing  $1.0 \cdot 10^{-4}$ – $1.0 \cdot 10^{-9}$  M 1-glucosamine were labeled using 4 mM CBQCA and 4 mM cyanide; these reagent concentrations allowed labeling of 1-glucosamine over the whole concentration range. The labeling reaction was carried out at room temperature for 10 h without using phosphate buffer in the reaction mixture. Fig. 2 shows a plot of signal intensity corrected for dilution versus concentration of 1-glucosamine in the sample prior to derivatization. The non-linearity at the low end of the concentration range is attributed to the presence of methanol in the sample. As the 1-glucosamine concentration was decreased, less dilution was required prior to injection, resulting in higher concentrations of methanol in the injected dilution. The presence of methanol resulted in an increased local electric field during injection and a resultant increase in the amount of sample injected.

### 3.3. Limit of detection for CBQCA-labeled 1-glucosamine

The LOD (three times the standard deviation of the background) for the fluorescently labeled sugar is calculated from the injection volume [24] and the total concentration of fluorescently labeled aminated sugar. The LOD for fluorescently labeled 1-glucosamine is 75 zeptomol and  $4.5 \cdot 10^{-11}$  M 1-glucosamine (based on a labeling reaction of  $10^{-4}$  M and diluted to  $5 \cdot 10^{-7}$  M prior to injection). This estimate is conservative, since it assumes 100% labeling of the aminated sugar. This LOD is more than one order of magnitude lower than those reported by Novotny's group for the labeling of monosac-

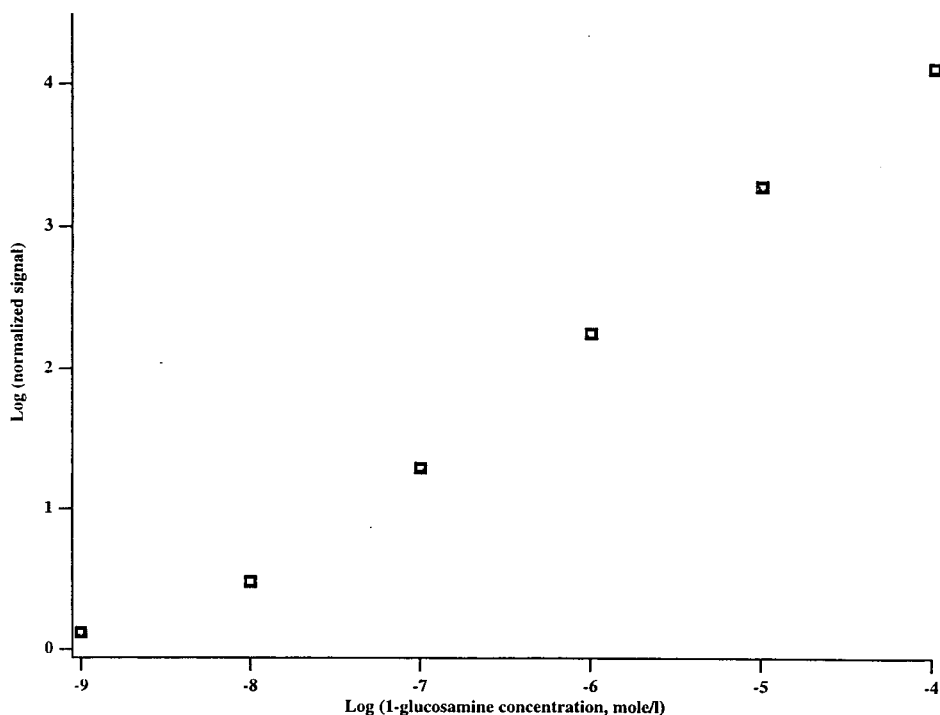


Fig. 2. Concentration range of 1-glucosamine for an effective labeling reaction. Reaction conditions:  $10^{-9}$ – $10^{-4}$  M 1-glucosamine–4 mM CBQCA–4 mM KCN for 5 h at room temperature. Separation conditions as in Fig. 1. Injection conditions: prior to injection (2500 V for 5 s) samples were diluted to  $1.0 \cdot 10^{-8}$  M (labeled and unlabeled) 1-glucosamine, except for labeling reaction samples containing  $10^{-9}$ – $10^{-8}$  M 1-glucosamine.

charides with CBQCA (2.3 attomol for 1-mannosamine, 1.3 attomol for 1-glucosamine, 0.5 attomol for 1-galactosamine [8] and 240 attomol for 1-galactosamine) [9]. The improvement in the LOD reported here is attributed to the use of a sheath flow cuvette with low light scattering as a postcolumn detector, which results in low background and elimination of the main water Raman band from the background through improved spectral filtering. Novotny's group used the 457-nm radiation from an argon ion laser for excitation since it has better overlap with the absorption profile of the derivative; however, the wavelength of the water Raman band coincides with the maximum fluorescence, increasing the background signal.

#### 3.4. Reaction yield for different aminated sugars

As expected, the yield of the CBQCA labeling reaction for the five aminated sugars studied

here is not the same. Fig. 3 shows the electropherograms of the CBQCA derivative of the five different aminated sugars labeled, injected and separated under identical conditions. The relative yields were calculated from the relative area under the peak for each aminated sugar. The highest yield was observed for 1-fucosamine (100%) and the lowest for 1-mannosamine (26%). The yields for 1-galactosamine, 2-glucosamine, and 1-glucosamine were 91%, 84% and 66%, respectively. These results suggest that limits of detection for the other aminated sugars will be of the same order of magnitude as for 1-glucosamine.

#### 3.5. Separation of CBQCA derivatives of five aminated sugars

The five aminated sugars investigated, 1-glucosamine, 1-mannosamine, 1-fucosamine, 1-galactosamine and 2-glucosamine, form CBQCA

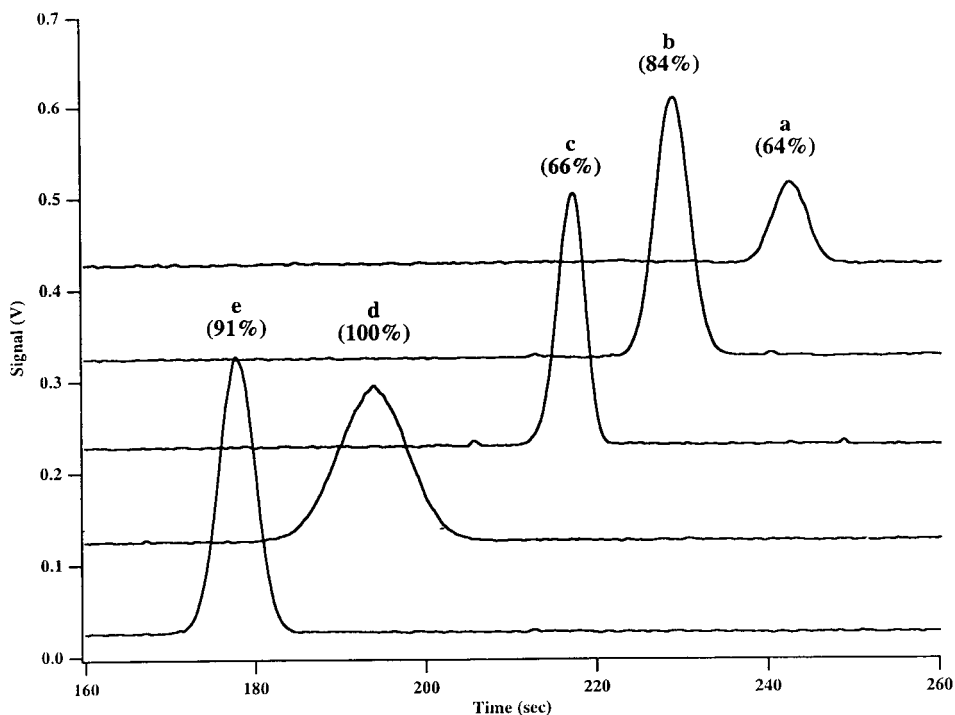


Fig. 3. Comparison of the electropherograms for five aminated monosaccharides labeled under identical conditions. (a) 1-Mannosamine; (b) 2-glucosamine; (c) 1-glucosamine; (d) 1-fucosamine; (e) 1-galactosamine. The time axis does not represent the migration time since peak positions have been offset. Relative area under the peak is indicated in parentheses. Reaction conditions: monosaccharides ( $10^{-4}$  M) were labeled individually; 4 mM CBQCA–2 mM KCN (pH 7.1) for 2 h at  $50^{\circ}\text{C}$ . Separation conditions as in Fig. 1 except for 49.6-cm long capillary. Injection conditions: samples were diluted to  $1.0 \cdot 10^{-6}$  M (labeled and unlabeled) aminated monosaccharide prior to injection (1000 V for 5 s).

derivatives that are expected to have similar electrophoretic mobilities since they have similar molecular masses and the same net charge. They cannot be resolved in a conventional electrophoretic separation based on mass-to-charge ratio. However, if borate or phenylboronate is added to the running buffer, the derivatives can be separated since borate and phenylboronate complex with the CBQCA derivatives. Borate complexation is due to the interaction of hydroxyl groups in the sugar moiety with tetrahydroxyborate ions  $\text{B}[\text{OH}]_4^-$ , one of the borate species present at pH 8–12 [4,5]. The charge of the complex is proportional to its formation constant. For example, favorable configurations (with high formation constants) such as the *cis*-oriented pair of hydroxyl groups at C-2 and C-4 and the *cis*-1,2-diol configuration of the monosaccharide will have a greater net charge. Differ-

ences in mass-to-charge ratio for the various complexes allow for their electrophoretic separation.

The use of borate in the running buffer for the separation of monosaccharides or their derivatives has been used by several workers [5,8,9,11]. However, based on their electropherograms, complete separation of the five aminated sugars used here was not achieved. Evidence that the use of phenylboronate in the running buffer allows better separations of monosaccharides has also been published by Zhao et al. [12] for derivatives of aminated sugars labeled with 5-carboxytetramethylrhodamine succinimidyl ester. They reported the separation of the derivatives of 1-glucosamine, 2-glucosamine, 1-mannosamine, 1-galactosamine, 2-galactosamine, and 1-fucosamine.

Here, the separation of the CBQCA deriva-

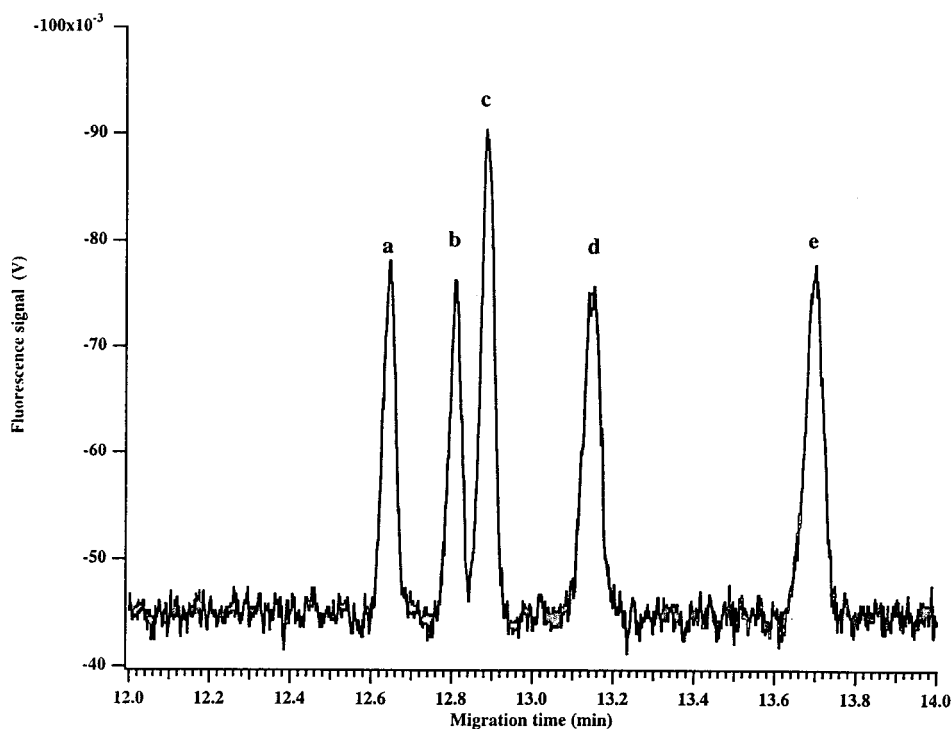


Fig. 4. Separation of five CBQCA derivatives of monosaccharides. (a) 1-Mannosamine; (b) 2-glucosamine; (c) 1-glucosamine; (d) 1-fucosamine; (e) 1-galactosamine. Reaction conditions: monosaccharides ( $1 \cdot 10^{-4} M$ ) were labeled individually, 4 mM CBQCA–4 mM KCN for 5 h at room temperature. Separation conditions: 72.5 cm  $\times$  10  $\mu$ m I.D. capillary; running buffer, 20 mM phosphate–50 mM phenylboronate–20 mM borate; 400 V/cm. Injection conditions: samples were diluted to  $2.0 \cdot 10^{-7} M$  (labeled and unlabeled) aminated monosaccharide prior to injection (2.5 kV for 5 s).

tives of 1-glucosamine, 2-glucosamine, 1-mannosamine, 1-galactosamine and 1-fucosamine was possible with the running buffer 50 mM phenylboronate–20 mM phosphate–20 mM borate. Fig. 4 shows the separation of the CBQCA derivatives of the five aminated sugars. In separations using 30 mM (or lower) phenylboronate, the CBQCA derivatives for 1-glucosamine and 2-glucosamine were not resolved. Use of higher concentrations of borate (in the absence of phenylboronate) did not allow the complete separation of the five aminated sugars. At present, no information on the interaction of boronate with carbohydrates is available. The complex stability is expected to be different for boronate complexation than it is for borate, since the bulky phenyl group would introduce some steric hindrance. The interaction of the hydroxyl groups in the sugar moiety with trihy-

droxyboronate,  $B(Ph)(OH)_3$  would increase the mass of the monosaccharide but it would not affect the charge of the monosaccharide. Competitive equilibrium between boronate and borate for the monosaccharide would increase the structural differences among the different monosaccharide complexes, resulting in a better separation. Competitive borate and phenylboronate complexation may prove to be useful for the separation of other monosaccharides and oligosaccharides.

#### 4. Conclusions

Samples with concentrations as low as  $1.0 \cdot 10^{-9} M$  1-glucosamine or other aminated monosaccharides can be fluorescently tagged using CBQCA as a fluorogenic reagent. This sensitivi-



ty results from the selection of labeling conditions that favor the formation of the CBOCA sugar derivative over the secondary fluorescent products. Further improvement comes from the use of a fluorescent detector with low background signals. The separation of five basic aminated sugars using a mixture of phenylboronate and borate in the separation buffer was also demonstrated. These results illustrate a promising methodology for the separation and identification of very low levels of monosaccharides.

### Acknowledgements

We thank Scott Delinger for his insightful comments. This work was supported by a Strategic Grant (STR 149003) from the Natural Sciences and Engineering Research Council of Canada. Y.Z. gratefully acknowledges a post-graduate fellowship from the Alberta Heritage Foundation for Medical Research. O.H. and N.J.D. acknowledge Steacie fellowships from NSERC.

### References

- [1] S.C. Churms, *J. Chromatogr.*, 500 (1990) 555–583.
- [2] C.A. Monnig and R.T. Kennedy, *Anal. Chem.*, 66 (1994) 280R–314R.
- [3] W.G. Kuhr and C.A. Monnig, *Anal. Chem.*, 64 (1992) 389R–407R.
- [4] M. Stefansson and D. Westerlund, *J. Chromatogr.*, 632 (1993) 195–200.
- [5] S. Hoffstetter-Kuhn, A. Paulus, E. Gassmann and H.M. Widmer, *Anal. Chem.*, 63 (1991) 1541–1547.
- [6] S. Honda, S. Iwase, A. Makino and S. Fujiwara, *Anal. Biochem.*, 176 (1989) 72–77.
- [7] S. Honda, A. Makino, S. Susuki and K. Takehi, *Anal. Biochem.*, 191 (1990) 228–234.
- [8] J. Liu, O. Shiota, D. Wiesler and M. Novotny, *Proc. Natl. Acad. Sci. U.S.A.*, 88 (1991) 2302–2306.
- [9] J. Liu, S. Osamu and M. Novotny, *Anal. Chem.*, 63 (1991) 413–417.
- [10] W. Nashabeh and Z. El Rassi, *J. Chromatogr.*, 514 (1990) 57–64.
- [11] W. Nashabeh and Z. El Rassi, *J. Chromatogr.*, 536 (1991) 31–42.
- [12] J.Y. Zhao, P. Diedrich, Y. Zhang, O. Hindsgaul and N.J. Dovichi, *J. Chromatogr. A*, 657 (1994) 307–313.
- [13] P. Jackson, *Biochem. J.*, 270 (1990) 705–713.
- [14] P. Jackson and G.R. Williams, *Electrophoresis*, 12 (1991) 94–96.
- [15] M. Stefansson and M. Novotny, *Anal. Chem.*, 66 (1994) 1134–1140.
- [16] M. Stefansson and M. Novotny, *Carbohydr. Res.*, 258 (1994) 1–9.
- [17] J. Liu, O. Shiota and M. Novotny, *J. Chromatogr.*, 559 (1991) 223–235.
- [18] J. Liu, Y.-O. Hsieh, D. Wiesler and M. Novotny, *Anal. Chem.*, 63 (1991) 408–412.
- [19] J. Sudor and M. Novotny, *Proc. Natl. Acad. Sci. U.S.A.*, 90 (1993) 9451–9455.
- [20] D. Figeys, E. Arriaga, A. Renborg and N.J. Dovichi, *J. Chromatogr. A*, 669 (1994) 205–216.
- [21] P.J.M. Kwakman, H. Koelewijn, I. Kool, U.A.T. Brinkman and G.J. De Jong, *J. Chromatogr.*, 511 (1990) 155–166.
- [22] E.A. Arriaga, Y. Zhang and N.J. Dovichi, *Anal. Chim. Acta*, in press.
- [23] D.M. Pinto, E.A. Arriaga, S. Sia and N.J. Dovichi, *Electrophoresis*, 16 (1995) 534–540.
- [24] X. Huang, M. Gordon and R. Zare, *Anal. Chem.*, 60 (1988) 375–377.



# Sensitive determination of sugars by capillary zone electrophoresis with indirect UV detection under highly alkaline conditions

X. Xu, W.Th. Kok, H. Poppe\*

*Laboratory of Analytical Chemistry, University of Amsterdam, Nieuwe Achtergracht 166, 1018 WV Amsterdam, Netherlands*

---

## Abstract

The separation with capillary zone electrophoresis and indirect UV detection of underivatized sugars was studied. It was found that the high pH of the background electrolyte which was required for the separation resulted in a strong increase of the low-frequency noise and baseline instability with indirect detection. It was shown that the baseline instability is related to the Joule heat production and insufficient thermostating of the capillary. Detection could be strongly improved by using narrow (25  $\mu\text{m}$ ) capillaries and low voltages, and by instrumental measures to promote a uniform heat dissipation along the capillary. The low-frequency noise and baseline disturbances were found also to depend on the type of monitoring and counterions in the background electrolyte. By optimization of the experimental conditions the workable pH range for the separation could be extended to 13. After optimization, limits of detection of approximately 0.05  $\text{mmol l}^{-1}$  were obtained. Calibration plots were linear up to concentrations of 5  $\text{mmol l}^{-1}$ . The reproducibility of migration times was within 0.4%; peak areas were reproducible within 4%. The method developed was applied to the analysis of culture medium samples.

---

## 1. Introduction

Methods for sugar analysis have found applications in many fields, such as biology, biochemistry, medicine, pharmacy and food production and control. Commonly used approaches include gas-liquid chromatography (GC) and high-performance liquid chromatography (HPLC) [1]. GC has been the method of choice when high sensitivity was required. However, this technique necessitates time-consuming derivatization procedures to convert the carbohydrates into volatile derivatives. Therefore, GC has largely been substituted by HPLC [2,3]. Underivatized sugars can be separated on different HPLC column

types, such as reversed-phase, amino-modified silica gel or cation-exchange resins, with either low-wavelength UV or refractive-index detection. A short column lifetime, insufficient separation efficiency and lack of sensitivity of detection are the major drawbacks of these HPLC methods [4]. In order to achieve better separation and detection, laborious pre- or post-column derivatization or sample preparation methods were often required in HPLC [5–7]. Sensitive analysis of underivatized carbohydrates can be obtained by ion chromatography with a sodium hydroxide mobile phase, normally at  $\text{pH} \geq 13$ , using pulsed amperometric detection (PAD) [8]. Investigation showed, however, that amino acids can be detected by PAD and often coelute with sugars, interfering with the sugar determi-

\* Corresponding author.

nation, and should be removed from the sample with an anion–cation-exchange pre-column [9].

In recent years, capillary electrophoresis (CE), with its simple instrumentation, high separation efficiency, rapid analyses and low sample and reagent consumption, offers an alternative to HPLC in many analytical fields. The separation and detection of sugars in CE, however, are difficult because of the absence of readily ionizable functional groups and chromophore systems in mono-, di- and oligosaccharides. Moreover, the very hydrophilic property of sugars prevents the use of micellar separation systems. Different strategies have been described in the literature to solve these problems. (a) By dynamic formation of negatively charged complexes between sugars and borate at pH 8–10, a relatively low increase (2–20 fold) in UV absorbance of underivatized sugars at 195 nm has been observed [10]. However, detection at such a low wavelength is non-selective and may suffer from the interference of charged substances such as amino acids, peptides and proteins that are present with the sugars in the sample [11]. (b) By labeling sugars with a charged chromophoric or fluorophoric group through pre-column derivatization, a significant increase in sensitivity and improved separation have been achieved [12,13]. Recently, several derivatization approaches have been evaluated. It was found that a number of di- and trisaccharides as well as aldonic acids still could not be derivatized successfully [14]. (c) With an electrochemical detector, underivatized sugars can be detected sensitively by a pulsed-potential technique with a gold electrode [15] or at a constant detection potential with copper-based electrodes [16,17]. A high pH (12–13) solution is necessary for the separation as well as for the detection. (d) Sugars are weakly acidic, having a  $pK_a$  value in the range from 12 to 13. By ionizing sugars at high pH and adding a UV absorbing or fluorescent monitoring ion to the separation buffer, a charge displacement between sugars and the chromophore or fluorophore is observed that allows the indirect detection of sugars. Generally, the resolution of sugars is improved at a higher pH. With indirect UV detection, the highest utilizable pH was

reported to be pH 12.1 and the detection limit was relatively high ( $0.5 \text{ mmol l}^{-1}$ ) [18]. By increasing the pH, the sensitivity decreased rapidly, due to increasing competition of hydroxide ions in the displacement of the chromophore. With indirect laser-induced fluorescence detection [19], the utilizable pH range was even lower, being limited to around pH 11.5. According to the theory with respect to the detection limit in indirect fluorescence detection, a lower concentration of the fluorophore (in a certain range) gives a lower detection limit [20]. Normally, indirect fluorescence detection is performed with fluorophore concentrations below  $1 \text{ mmol l}^{-1}$ . At such low concentrations, the competition of hydroxide ions with the monitoring ions is more pronounced with rising pH.

In our recent study on noise, using indirect detection, which will be presented in another paper [21], it was found that low-frequency noise, drift and wavy baseline disturbances, as well as disturbances resembling real peaks, increased with an increasing conductivity of the background electrolyte (BGE) and led to a dramatic decrease in sensitivity and in the quantitative reliability. At pH values above 12, necessary for the separation of underivatized sugars, the conductivity increases exponentially with the pH, thereby limiting the detection possibilities for sugars.

In the work presented here, we have tried to extend the buffer pH value for indirect UV detection to 13 without compromising with the sensitivity, mainly by solving the noise problems. The method developed has been applied for the analysis of sugars in tissue culture media also containing a number of neutral and charged substances, including amino acids or proteins.

## 2. Experimental

### 2.1. Apparatus

Two CE systems have been used and compared: an ABI Capillary Electrophoresis System, Model 270A-HT (Foster City, CA, USA), and a system PRINCE (Lauer Labs, Emmen, Nether-

lands), with a Spectroflow 757 (ABI, Ramsey, NJ, USA) or a Spectra 100 (Linear, Reno, NV, USA) UV detector. The UV detector was operated at 256, 267 or 310 nm when using sorbic acid, riboflavin or 3,4-dimethoxycinnamic acid as monitoring ions, respectively.

Fused-silica capillaries of 25  $\mu\text{m}$  I.D. and 350  $\mu\text{m}$  O.D. (Polymicro Technologies, Phoenix, AZ, USA) were used, with a tube length of 78 cm when using the ABI system or ABI detector and 63 cm when using the Linear detector, with a 50-cm distance from the injection end to the detection window. The window for the on-column detector cell was created by burning off a small section (ca. 0.4 mm) of the polyimide coating.

## 2.2. Capillary zone electrophoresis

Experiments were carried out at room temperature (18.5°C). The fluctuation of the temperature is  $\pm 1^\circ\text{C}$  per day and  $\pm 0.1^\circ\text{C}$  per run. A new capillary was filled with BGE for at least 10 h before use. Samples were injected hydrodynamically at 167 mbar for 10 s (ABI) or at 145 mbar for 12 s (PRINCE). Electrophoresis was carried out at a voltage of +10 kV for 30 min, unless stated otherwise. After each electrophoretic run, the capillary was flushed with the BGE at 668 mbar for 9 min and at 1500 mbar for 3.5 min when using the ABI system and the modular PRINCE system, respectively. The anode buffer was replaced after 10 runs.

Electropherograms were recorded with a sample rate of 10 Hz and analyzed on a 486 DX66 PC with an appropriate ADC card and interface, using the electrophoresis data processing software CAESAR 3.0 (Lauer Labs). Analyte concentrations were quantitated by peak area.

## 2.3. Chemicals and solutions

Maltose monohydrate was obtained from Merck (Darmstadt, Germany). Sucrose, D-(+)-glucose, D-(-)-fructose, riboflavin, lithium hydroxide monohydrate (label content >90%, titration value 87.23%) and sorbic acid were purchased from BDH (Laboratory Chemicals

Division, Poole, UK) and 3,4-dimethoxycinnamic acid (DMC) from Fluka (Buchs, Switzerland). RPMI-1640 culture medium (pH 8.6) was obtained from Sigma (Poole, UK). In some cases 10% (v/v) fetal calf serum (FCS, pH 8.4) was added to the medium. Deionized water was used for the preparation of all solutions.

BGE solutions were prepared by dissolving appropriate amounts of hydroxide and monitoring compounds (sorbic acid, riboflavin or DMC) and adding distilled water to one litre, giving final concentrations of 31, 46, 63 and 109  $\text{mmol l}^{-1}$  of the hydroxides and 12  $\text{mmol l}^{-1}$  of the monitoring ions. The buffers were stored in polyethylene containers in the dark at 4°C and filtered through a 0.45- $\mu\text{m}$  filter (Millipore) before use.

Stock solutions of sugars of 20  $\text{mmol l}^{-1}$  in distilled water and RPMI media with and without 10% fetal calf serum were stored at  $-20^\circ\text{C}$  and were thawed before use. After dilution of the samples with distilled water they were used without filtering.

## 3. Results and discussion

### 3.1. Noise reduction by instrumental optimization

Since most sugars have a  $\text{pK}_a$  value between 12 and 13, a high pH of the electrolyte is required for their separation [15–18]. The conductivity of the medium increases with the pH and the resulting high electrophoretic currents are accompanied with baseline instabilities and low signal-to-noise ratios with indirect UV detection. According to our studies on noise with indirect UV detection, low-frequency noise and baseline disturbances are closely related to an insufficient and non-uniform heat dissipation along the capillary. Since the Joule heat development in the separation capillary is proportional to the electrophoretic current, we have tried to decrease the noise problems by using small-diameter capillaries. A decrease of the capillary inner diameter from the standard 50  $\mu\text{m}$  to 25  $\mu\text{m}$  resulted in a decrease of the current by a

factor of four and of the low-frequency noise by a factor of ten, while the peak heights remained virtually the same when the ABI detector was used (see Fig. 1). The independence of the sensitivity on the capillary diameter was found to be a special feature of the ABI detector; with the Linear detector the signals were substantially lower when 25- $\mu\text{m}$  capillaries were used. The noise could be reduced further by using 10- $\mu\text{m}$  capillaries. However, with these very narrow inner diameters blocking of the capillary became a frequent problem and flushing times became unacceptably long. Therefore, 25- $\mu\text{m}$  capillaries were used in subsequent work. Reduction of the electrophoretic current by reducing the applied voltage also resulted in a more stable baseline, of

course at the expense of short analysis times (Fig. 2).

The importance of the thermostating of the capillary was shown by comparing the results obtained with different instruments. In Fig. 3a, the electropherogram obtained with the ABI

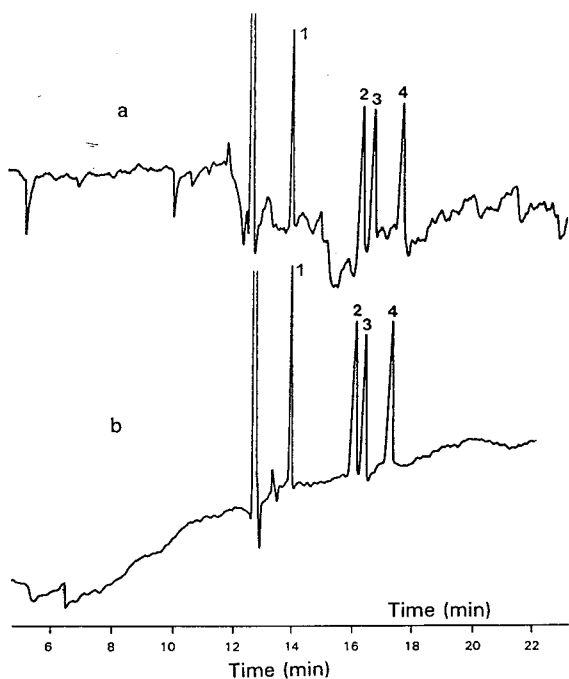


Fig. 1. Influence of the inner diameter of the capillary on baseline noise. Instrument: ABI system; capillary: 110 cm total length and 90 cm to the detection point; injection: 167 mbar for 2.5 and 10 s using 50- $\mu\text{m}$  (a) and 25- $\mu\text{m}$  (b) capillaries, respectively; separation: 25 kV, 35  $\mu\text{A}$  (a), 11  $\mu\text{A}$  (b); BGE: 12  $\text{mmol l}^{-1}$  sorbate–63  $\text{mmol l}^{-1}$  NaOH; sample: standard mixture of 2.5  $\text{mmol l}^{-1}$  of sugars. Peaks: 1 = sucrose, 2 = maltose, 3 = glucose, 4 = fructose.

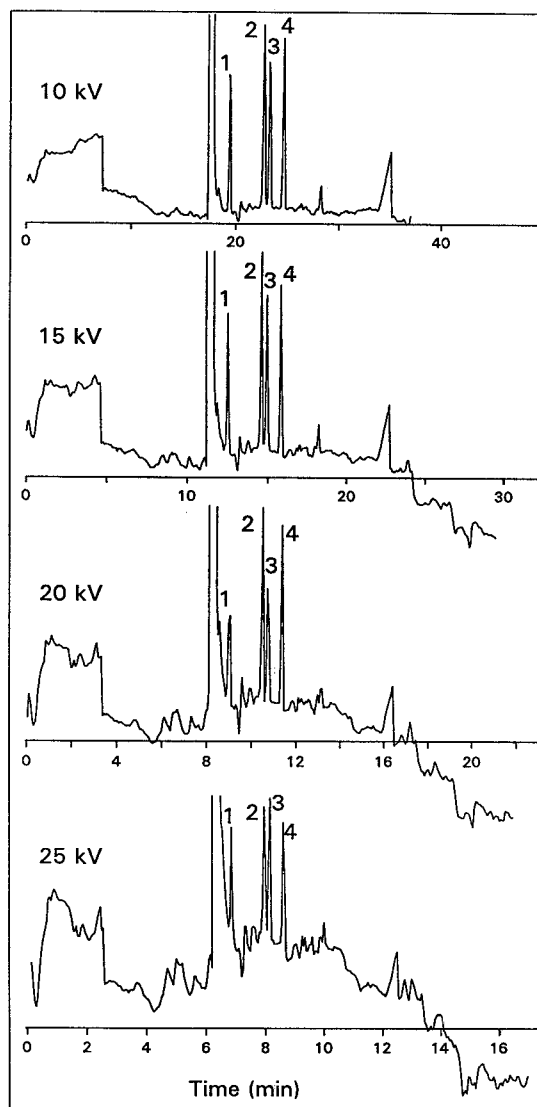


Fig. 2. Influence of the separation voltage on baseline noise. Instrument: modular PRINCE system; BGE: 12  $\text{mmol l}^{-1}$  riboflavin–63  $\text{mmol l}^{-1}$  LiOH; sample: standard mixture of 1.0  $\text{mmol l}^{-1}$  of sugars as in Fig. 1.

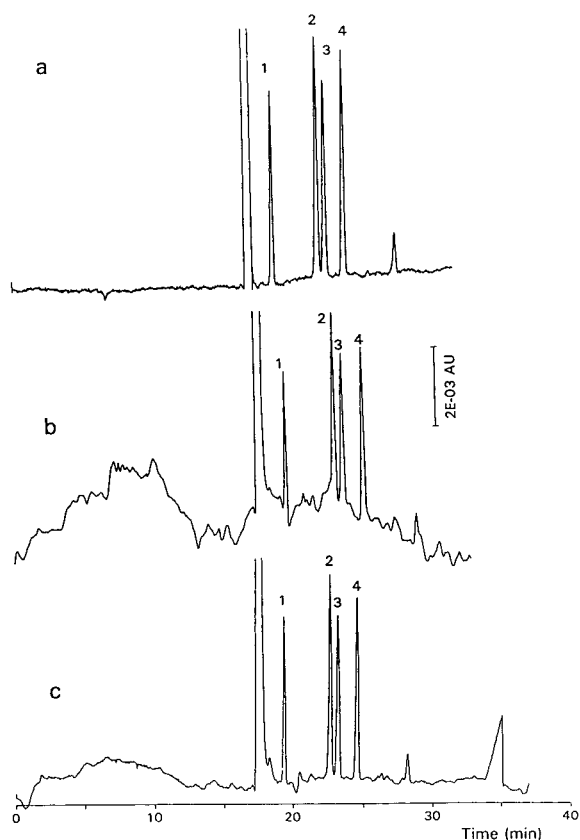


Fig. 3. Comparison of the detection sensitivities obtained with different CE systems and detectors, and the influence of thermostating of the capillary on noise and disturbances of the baseline. Instrument: (a) ABI system, (b) normal PRINCE system, (c) PRINCE system with thermostating of the capillary using sponge sleeves; BGE: 12 mmol l<sup>-1</sup> riboflavin–63 mmol l<sup>-1</sup> LiOH; sample: standard mixture of 1.0 mmol l<sup>-1</sup> of sugars as in Fig. 1.

system is shown. With the ABI apparatus approximately 84% of the effective length of the capillary is placed in the ventilated, thermostatted area of the instrument and 10% of the length in the detector area. By making an opening of 2 cm diameter between the ventilation and the detector chambers the noise could be slightly reduced further. In Fig. 3b, the electropherogram obtained with the modular PRINCE system is shown. With this apparatus in its standard configuration only 30% of the capillary length is in the thermostatted chamber. A substantial

improvement of the baseline stability could be realized by shielding the parts of the capillary exposed to ambient air with sponge sleeves (Fig. 3c).

Working at temperatures above ambient intensified the baseline instability (Fig. 4). When the temperature was increased from 22 to 40°C, the low-frequency noise and drift increased by a factor of approximately ten. Again, this can be explained by the non-uniform thermostating conditions along the capillary.

### 3.2. Optimization of the BGE composition

In Fig. 5, the influence of the hydroxide concentration of the BGE on the resolution of the sugars is shown. It is clear that an increase of the pH gives a better separation. A baseline separation of maltose and glucose was obtained at hydroxide concentrations of 63 mmol l<sup>-1</sup> and higher.

The influence of the BGE composition on the sensitivity for the sugars tested was first studied with the help of a computer simulation program for CZE developed in our laboratory [22,23]. The results indicated that the p*K*<sub>a</sub> value, the

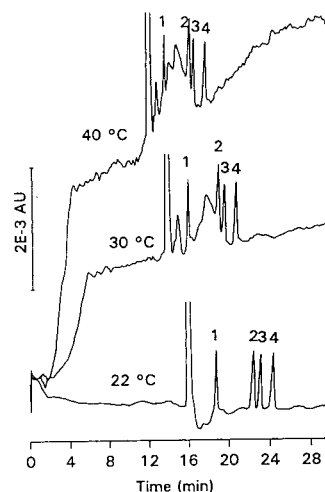


Fig. 4. Influence of the working temperature on the noise, disturbances and separation. Instrument: ABI system; BGE: 12 mmol l<sup>-1</sup> sorbate, 63 mmol l<sup>-1</sup> NaOH; standard mixture of 1.0 mmol l<sup>-1</sup> of sugars as in Fig. 1.

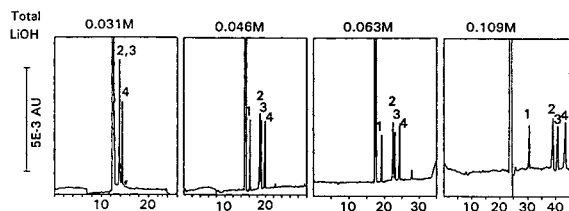


Fig. 5. Influence of the hydroxide concentration of the BGE on the resolution of the sugars. Instrument: ABI system; BGE: 12 mmol l<sup>-1</sup> riboflavin + LiOH; standard mixture of 1.0 mmol l<sup>-1</sup> of sugars as in Fig. 1.

ionic mobility and the concentration of the monitoring ion to be used will have little influence on the displacement ratios (sensitivities) and electromigration dispersion obtained at high pH values. Sorbic acid ( $\epsilon = 27\,000$  at 256 nm), DMC ( $\epsilon = 27\,000$  at 310 nm) and riboflavin ( $\epsilon = 30\,000$  at 267 nm) were tested experimentally as monitoring compounds. Indeed, it was found that the sensitivities for the sugars were virtually the same with these monitoring ions. Also it was found (with riboflavin as monitoring ion) that the sensitivities did not depend on the monitoring-ion concentration in the range from 6 to 15 mmol l<sup>-1</sup> with a hydroxide concentration of 63 mmol l<sup>-1</sup>. However, the low-frequency noise and baseline disturbances strongly depended on the type of monitoring ion, especially when an instrument with insufficient thermostating capability was used (Fig. 6). The instability of the baseline increased with increasing mobility of the monitoring ion (sorbate > DMC > riboflavin).

According to the simulation programme an influence of the counterion mobility on the sensitivities is expected, with a higher mobility leading to higher displacement ratios. We found experimentally that the sensitivities using sodium hydroxide in the BGE were approximately two times higher than with lithium hydroxide. However, the choice of the counterion type also influences the baseline stability. Apparently, the chemical composition of the BGE controls the way in which temperature differences and changes along the capillary are translated into absorbance differences. Of the counterions tested [tetrabutyl ammonium (TBA), tetramethyl ammonium (TMA), lithium, sodium and potassium], lithium ions gave the most stable baseline,

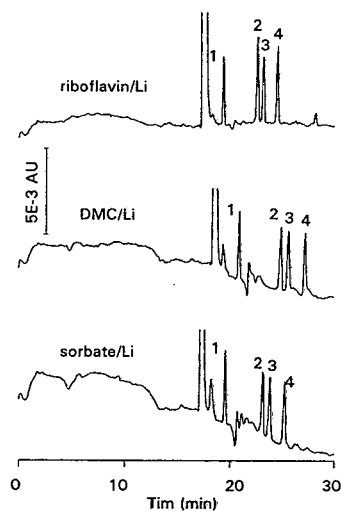


Fig. 6. Influence of the monitoring ion on noise and baseline disturbances. Instrument: PRINCE system; BGE: 12 mmol l<sup>-1</sup> monitoring ion, 63 mmol l<sup>-1</sup> LiOH; standard mixture of 1.0 mmol l<sup>-1</sup> of sugars as in Fig. 1.

irrespective of the monitoring ion used (Fig. 7). The choice of the counterion did not influence the separation behaviour of the sugars. The electroosmotic flow-rate, however, depended strongly on the counterion type (TBA > TMA > K > Na > Li).

Generally, up to three system disturbances were observed in the electropherograms. One is the water system peak appearing just before the sucrose peak, representing the electroosmotic flow-rate. A second system disturbance appears as a triangular peak after the sugar peaks. The migration time of this peak depends on the counterion type. Since its migration time increases with the length of the capillary after the detector window, it appears as if it originates from the end of the capillary. A third system disturbance is visible as a baseline shift before the electroosmotic peak. It appears in the electropherograms after approximately four runs from the same buffer vials. Therefore, this disturbance is probably related to the change of the buffer composition in the inlet or outlet vials due to the electrochemical reaction taking place at the electrodes. None of the system disturbances interfered with the determination of the sugars tested.



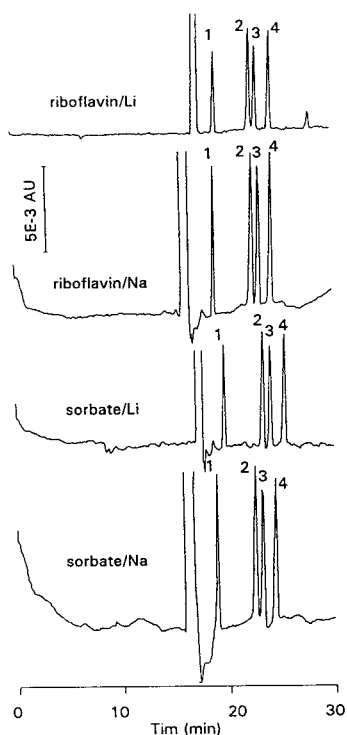


Fig. 7. Influence of the counterion on noise and baseline disturbances. Instrument: ABI system; BGE:  $12 \text{ mmol l}^{-1}$  monitoring ion,  $63 \text{ mmol l}^{-1}$  hydroxides; standard mixture of  $1.0 \text{ mmol l}^{-1}$  of sugars as in Fig. 1.

### 3.3. Analytical performance

From the optimization studies described above, a BGE containing  $63 \text{ mmol l}^{-1}$  LiOH and  $12 \text{ mmol l}^{-1}$  riboflavin and the PRINCE system

were selected for the evaluation of the analytical performances of the method developed in this paper, unless stated otherwise.

The sample pH did not influence peak shapes and area counts from pH 7 to pH 12.2. Thus, samples can normally be injected or diluted with water. The maximum loading capacity of the capillary without loss of resolution was determined. The limit was 3 nl, corresponding to a zone length of 5 mm or injection at 145 mbar for 12 s. The plate number was approximately 110 000 for all four sugars at concentrations of  $0.5 \text{ mmol l}^{-1}$ . Regression parameters of the calibration lines for the four sugars tested are listed in Table 1.

The upper limits of the linear range of calibration for the sugars were determined to be at least  $5 \text{ mmol l}^{-1}$ . Above it, because of the concentration overloading effect, maltose and glucose were not baseline separated.

The limits of detection (LOD) for fructose as a function of the LiOH and NaOH concentrations obtained using the ABI systems are given in Fig. 8. It is seen that sensitivity can be gained by using Na. By choosing Na, however, efficient dissipation of heat becomes more crucial.

A standard mixture of sugars was analyzed repeatedly, using the same vial for the anode electrolyte. The results for the reproducibility of the migration times are given in Table 2. As is clear from the table, the reproducibility of the migration times of the sugars is excellent, since the relative standards deviations were found

Table 1  
Regression parameters and limits of detection (LOD)

Calibration lines	Sucrose	Maltose	Glucose	Fructose
Regression parameters <sup>a</sup>				
<i>a</i>	0.0422	0.0693	0.0529	0.0539
<i>b</i>	-0.00074	-0.0017	-0.0068	-0.00097
<i>r</i> <sup>2</sup>	0.99994	0.99994	0.99990	0.99995
LOD ( $\text{mmol l}^{-1}$ ) <sup>b</sup>	0.06	0.04	0.05	0.055

<sup>a</sup> Here *a* and *b* are the constants in the calibration line  $y = ax + b$ , where *x* is the concentration of the analyte in  $\text{mmol l}^{-1}$  and *y* is the peak area, and *r*<sup>2</sup> is the correlation coefficient of the regression line with  $n = 7$ .

<sup>b</sup> Obtained using a signal-to-noise ratio of 3.

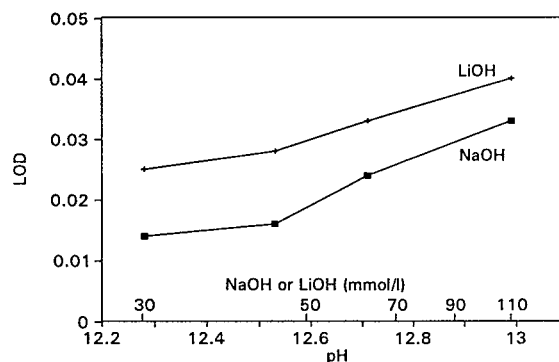


Fig. 8. Limit of detection (LOD) of fructose as a function of the hydroxide concentration. Instrument: ABI system; BGE: 12 mmol l<sup>-1</sup> riboflavin + NaOH or LiOH.

within the range from 0.1 to 0.9% for ten consecutive injections. The reproducibility of the peak areas ( $n = 10$ ) was also acceptable, with relative standard deviations between 1 and 4% (Table 3). However, after approximately 20 injections a change in the peak areas for all sugars was observed. This can be explained as

the result of a change in the anode electrolyte composition, due to the electrochemical reaction taking place at the electrode. Therefore, it is recommended to change the anode solution after every ten injections.

Over a period of nine days a standard mixture of sugars was injected repeatedly using the same capillary. In between, various experiments had been performed with RPMI-media with and without calf serum. The reproducibility of the electroosmotic peak migration time was within 1.5%. Peak areas showed a change of -2 to -7% over nine days. Riboflavin is a photo-sensitive compound and must be kept in a dark and cool place. Separate etching procedures for the capillary appeared not to be necessary. A short flushing step after each run was sufficient.

### 3.4. Application to culture medium

RPMI-1640 medium contains more than 40 compounds, including almost all naturally existing amino acids, vitamins, organic acids and

Table 2  
Reproducibility of the migration times with a standard mixture of sugars (1.0 mmol l<sup>-1</sup>)

Peak	Migration times (min, mean $\pm$ S.D. <sup>a</sup> )		
	First 10 runs	Second 10 runs	Third 10 runs
Sucrose	19.46 $\pm$ 0.08	20.03 $\pm$ 0.17	20.22 $\pm$ 0.22
Maltose	22.89 $\pm$ 0.07	23.54 $\pm$ 0.19	23.71 $\pm$ 0.04
Glucose	23.52 $\pm$ 0.07	24.16 $\pm$ 0.21	24.32 $\pm$ 0.04
Fructose	24.89 $\pm$ 0.05	25.26 $\pm$ 0.20	25.72 $\pm$ 0.04
Electroosmotic flow	17.61 $\pm$ 0.05	18.17 $\pm$ 0.15	18.37 $\pm$ 0.02

<sup>a</sup> S.D. = standard deviation.

Table 3  
Reproducibilities of peak areas with a standard mixture of the sugars (1.0 mmol l<sup>-1</sup>)

Sugars	Measured concentration (mmol l <sup>-1</sup> , mean $\pm$ S.D. <sup>a</sup> )		
	First 10 runs	Second 10 runs	Third 10 runs
Sucrose	0.98 $\pm$ 0.02	0.97 $\pm$ 0.03	0.93 $\pm$ 0.01
Maltose	0.99 $\pm$ 0.04	0.96 $\pm$ 0.02	0.92 $\pm$ 0.02
Glucose	1.02 $\pm$ 0.02	1.01 $\pm$ 0.02	0.97 $\pm$ 0.04
Fructose	0.99 $\pm$ 0.03	0.97 $\pm$ 0.02	0.94 $\pm$ 0.02

<sup>a</sup> S.D. = standard deviation.

Table 4  
Recovery of sugars added to culture media

Sugar	Concentration (mmol l <sup>-1</sup> )			Recovery (%)
	Present	Spiked	Found	
<i>RPMI-1640</i>				
Sucrose	0	1.0	0.98 ± 0.02	97.8 ± 2
Maltose	0	1.0	1.00 ± 0.03	103.3 ± 3
Glucose	1.16 ± 0.03	1.0	2.15 ± 0.05	99.1 ± 5
Fructose	0	1.0	0.98 ± 0.02	98.2 ± 2
<i>RPMI-1640 + 10% FCS</i>				
Sucrose	0	1.0	1.01 ± 0.01	100.1 ± 1
Maltose	0	1.0	1.01 ± 0.02	101.1 ± 2
Glucose	1.07 ± 0.02	1.0	2.10 ± 0.05	103.8 ± 5
Fructose	0.054 ± 0.004	1.0	1.09 ± 0.02	103.2 ± 2

Mean ± S.D. for three injections.

inorganic salts. The concentration of D-glucose in the medium is 2 g l<sup>-1</sup> (ca. 11 mmol l<sup>-1</sup>). To some of the samples, 10% fetal calf serum was added to resemble the protein fraction of possible cultures.

The recovery of the sugars from the medium was studied by comparing peak areas obtained

with and without spiking standard mixtures to the medium. Recoveries were found to be between 98 and 104% for all sugars (Table 4).

In Fig. 9, electropherograms obtained with ten times diluted RPMI media, with and without the addition of 10% fetal calf serum are shown. From these electropherograms and recovery

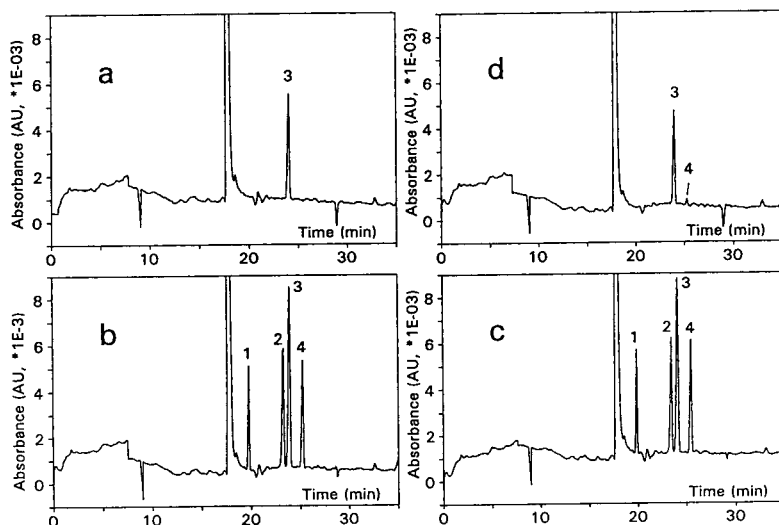


Fig. 9. Electropherograms obtained with RPMI culture media diluted with water (dilution factor 1:9): (a) RPMI-1640; (b) RPMI-1640 spiked with 1.0 mmol l<sup>-1</sup> of the sugars as in Fig. 1; (c) RPMI-1640 + 10% FCS; (d) RPMI-1640 + 10% FCS spiked with the sugars as in (b).

studies it is clear that: (1) the presence of the RPMI medium does not change the electrophoresis of the sugars; (2) the RPMI medium does not contain components (in significant concentrations) interfering with the sugar determination; (3) the addition of calf serum to the RPMI medium does not influence the electrophoretic process, and does not contain components (in significant concentrations) interfering with the sugar determination except for a small amount of fructose.

The fact that the serum proteins do not change the electroosmotic flow, as has been observed frequently in other applications of CE, may be explained by the high pH of the separation solution. At high pH absorption of proteins to the fused-silica surface of the capillary is not very likely. Moreover, the capillary wall is constantly etched by the solution during analysis.

#### 4. Conclusions

The method developed for determination of low-molecular-mass sugars by capillary zone electrophoresis is sensitive, quantitative, reproducible and robust. Joule heat and non-uniform thermostating of the capillary are the main sources of the low-frequency noise and baseline disturbances. Moreover, the noise is influenced by the composition of the BGE. Thus, riboflavin and lithium were found to be the preferred monitoring and counterions, respectively. Both compounds had the lowest mobility of the compounds tested, which provides an explanation for the reduced noise problems observed. By reducing the low-frequency noise and the baseline disturbances, the pH of the BGE can be increased to 13 without major loss of sensitivity. The detection limits obtained with the optimized system are approximately 25 times lower at pH 12.3 when using a riboflavin–NaOH BGE and one order of magnitude lower at higher pH

(12.6–13) when using a riboflavin–LiOH BGE, compared to results cited in the literature [18].

#### References

- [1] S.C. Churms, *J. Chromatogr.*, 500 (1990) 555–583.
- [2] K. Kakehi and S. Honda, *J. Chromatogr.*, 379 (1986) 27–25.
- [3] K. Robards and M. Whitelaw, *J. Chromatogr.*, 373 (1968) 81–110.
- [4] M. Verzele, G. Simoens and F. Van Damme, *Chromatographia*, 23 (1987) 292–300.
- [5] R.A. Femia and R. Weinberger, *J. Chromatogr.*, 402 (1987) 127–134.
- [6] D.B. Gomis, M.D.G. Alvarez, J.J.M. Alonso and A.N. Vallina, *Chromatographia*, 25 (1988) 701–706.
- [7] E.C. Conrad, *Food Technol.*, 30 (1976) 84–92.
- [8] R.D. Rockling and C.A. Pohl, *J. Liq. Chromatogr.*, 6 (1983) 1577–1590.
- [9] J.D. Lamb, G.S. Myers and N. Edge, *J. Chromatogr. Sci.*, 31 (1993) 353–357.
- [10] S.H. Kuhn, A. Paulus, E. Gassmann and H.M. Widmer, *Anal. Chem.*, 63 (1991) 1541–1547.
- [11] A.M. Arentoft, S. Michaelsen and H. Sørensen, *J. Chromatogr. A*, 652 (1993) 517–524.
- [12] W. Nashabeh and Z.E. Rassi, *J. Chromatogr.*, 600 (1992) 279–287.
- [13] C. Chiesa and C. Horváth, *J. Chromatogr.*, 645 (1993) 337–352.
- [14] P.J. Oefner, A.E. Vorndran, E. Grill, C. Huber and G.K. Bonn, *Chromatographia*, 34 (1992) 308–316.
- [15] W.Z. Lu and R.M. Cassidy, *Anal. Chem.*, 65 (1993) 2878–2881.
- [16] L.A. Colon, R. Dadoo and R.N. Zare, *Anal. Chem.*, 65 (1993) 476–481.
- [17] X. Huang and W. Th. Kok, *J. Chromatogr. A*, 716 (1995) 347.
- [18] A.E. Vorndran, P.J. Oefner, H. Scherz and G.K. Bonn, *Chromatographia*, 33 (1992) 163–168.
- [19] T.W. Garner and E.S. Yeung, *J. Chromatogr.*, 515 (1990) 639–644.
- [20] W.G. Kuhr and E.S. Yeung, *Anal. Chem.*, 60 (1988) 2642–2646.
- [21] X. Xu, W.Th. Kok and H. Poppe, in preparation.
- [22] H. Poppe, *Anal. Chem.*, 64 (1992) 1908–1919.
- [23] G.J.M. Bruin, G. Stegeman, A.C. van Asten, X. Xu, J.C. Kraak and H. Poppe, *J. Chromatogr.*, 559 (1991) 163–181.



ELSEVIER

Journal of Chromatography A, 716 (1995) 241–257

JOURNAL OF  
CHROMATOGRAPHY A

# Separation of 8-aminonaphthalene-1,3,6-trisulfonic acid-labelled neutral and sialylated N-linked complex oligosaccharides by capillary electrophoresis

Antje Klockow<sup>a,b</sup>, Renato Amadò<sup>b</sup>, H. Michael Widmer<sup>a</sup>, Aran Paulus<sup>a,\*</sup>

<sup>a</sup>*Ciba, Corporate Analytical Research, CH-4002 Basle, Switzerland*

<sup>b</sup>*Swiss Federal Institute of Technology (ETH Zürich), Institute of Food Science, CH-8092 Zürich, Switzerland*

## Abstract

Complex oligosaccharides, both neutral and sialylated, were derivatized with 8-aminonaphthalene-1,3,6-trisulfonic acid (ANTS) and separated by capillary electrophoresis. The derivatization reaction was carried out in a total reaction volume of 2  $\mu$ l. The separated peaks were detected by laser-induced fluorescence detection using the 325-nm line of a He–Cd laser. Concentration and mass detection limits of  $5 \cdot 10^{-8}$  M and 500 amol, respectively, could be achieved. The limiting step for higher sensitivity is not the detector performance, however, but the chemistry with a derivatization limit of  $2.5 \cdot 10^{-6}$  M. Two labelling protocols were established, one with overnight reaction at 40°C and the other with a 2.5-h derivatization time at 80°C. Neutral oligosaccharides could be labelled with either protocol. However, sialylated oligosaccharides hydrolysed when labelled at 80°C. Low nanomole to picomole amounts of oligomannose-type and complex-type oligosaccharide mixtures were derivatized and separated in less than 8 min with excellent resolution using a phosphate background electrolyte at pH 2.5. The linear relationship between the electrophoretic mobility and the charge-to-mass ratios of the ANTS conjugates was used for peak assignment. Further, the influence of the three-dimensional structure of the complex oligosaccharides on their migration behaviour is discussed. The suitability of the ANTS derivatization and the subsequent separation for the analysis of complex oligosaccharide patterns is demonstrated with oligosaccharide libraries derived from ovalbumin and bovine fetuin. For peak assignment the patterns are compared with those of the oligomannose and the complex-type oligosaccharide mixtures. The separation efficiency of 120 000 theoretical plates and analysis times of less than 10 min are superior to those with state-of-the-art chromatographic methods and other capillary electrophoresis separation methods. A migration time difference of 0.06 min was found to be sufficient for the baseline separation of complex oligosaccharides.

## 1. Introduction

Complex oligosaccharides as found in the glycan moieties of glycoproteins typically consist of 8–14 monosaccharide units. Composed of only seven different glycosidic monomers, they

are characterized by a wide variety of different intermolecular glycosidic bonds, resulting in an enormous multitude of possible structures. In glycoproteins, complex carbohydrates can be linked to the polypeptide chain via an O-glycosidic bond to the hydroxyl group of a serine or threonine residue or via an N-glycosidic bond formed with the side-chain of an asparagine

\* Corresponding author.

residue. Complex carbohydrates are involved in a number of biological recognition processes such as cell–cell interactions, cell development, cell differentiation, hormone–receptor and antigen–antibody interactions [1,2]. In addition, glycosylation increases the proteolytic resistance of proteins. A number of therapeutic proteins are produced by recombinant techniques in mammalian cells. Because these proteins are often expressed with glycan moieties which affect their biological activity, lifetime and specificity, control of correct glycosylation of these drugs is a very important issue [3].

It is generally accepted that the specificity and activity of glycoproteins are determined not only by the amino acid sequence of the protein part but also by the composition and structure of its glycan moieties. In contrast to proteins and nucleic acids, where the molecular alphabet has been deciphered, the “sugar language” of complex carbohydrates remains a challenging scientific problem because of the considerable structural diversity of complex carbohydrates.

The limited amount of sample released from purified glycoproteins adds to the analytical demand for highly sensitive and selective methods. In general, amino acid sequence information can be obtained with 10 pmol of purified protein. This also limits the amount of oligosaccharides available for further analysis. If all carbohydrate can be completely derivatized in 10  $\mu$ l, the concentration detection limit of the analytical method has to be lower than  $10^{-6}$  M while still allowing the selective separation of closely related solutes.

Several electrophoretic and chromatographic techniques have been used for the determination of mono- and oligosaccharide mixtures, with high-performance anion-exchange chromatography combined with pulsed amperometric detection (HPAEC–PAD) as the state-of-the-art method. However, with a mass detection limit of ca. 10 pmol [4], corresponding to a concentration detection limit of  $10^{-6}$  M, HPAEC–PAD is short of the sensitivity necessary for complex carbohydrate analysis in bioresearch applications.

Capillary electrophoresis (CE) evolved as a promising alternative in carbohydrate analysis

with respect to fast and highly efficient separations. Since neutral carbohydrates lack both charge and chromophores for CE analysis, several strategies have been discussed for the on-column detection of carbohydrates after CE separation. The on-column complexation with borate results in a 2–20-fold increase in the UV signal at 195 nm, thus allowing detection at a millimolar level [5]. With indirect photometric detection using sorbic acid, detection limits in the higher micromolar ( $10^{-4}$ – $10^{-5}$  M) range could be achieved [6–8]. Amperometric detection has recently been reported to allow selective detection at the  $10^{-6}$  M level for reducing and non-reducing carbohydrates [9]. However, similarly to refractive index detection in CE, the applicability of which to carbohydrate analysis has been demonstrated [10], amperometric detection is not yet commercially available for CE and consequently is limited in its use for most biochemical laboratories.

Precolumn derivatization therefore seems to be the most promising approach for the sensitive detection of carbohydrates. Several labelling procedures for carbohydrates for sensitive UV and/or fluorescence detection have been described in the literature. The most frequently used procedure for reducing carbohydrates consists in their reductive amination with a chromophore or fluorophore containing a primary amino group, such as 2-aminopyridine [11], *p*-amino- or ethyl-*p*-aminobenzoic acid [12,13] or 4-aminobenzonitrile [14]. A base-catalysed condensation for reducing carbohydrates with the active hydrogens of 3-methyl-1-phenyl-2-pyrazolin-5-one (MPP) was developed by Honda et al. [15]. UV detection of 2-aminopyridine-, *p*-aminobenzoic acid- or MPP-labelled carbohydrates resulted in detection limits of  $(4–8) \cdot 10^{-6}$  M [15,16]. UV detection limits reported to date are therefore insufficient to detect labelled glycoprotein-derived oligosaccharides even if purification, release and labelling can be performed on a theoretical level.

The lowest concentration detection limit of  $10^{-9}$  M was reported using laser-induced fluorescence (LIF) detection of 3-(4-carboxybenzoyl)-2-quinolinecarboxyaldehyde (CBQCA) carbohy-

drate derivatives [17]. CBQCA reacts with aminoglycans, which are formed by reductive amination of carbohydrates with ammonia. This two-step labelling procedure is also hampered by a narrow range of molar excess of label to obtain the maximum derivatization yield [18]. However, LIF detection schemes provide the hope of achieving the submicromolar detection limits necessary for glycoprotein-derived oligosaccharides when suitable labels and optimized labelling conditions can be worked out.

Separation in CE relies on charge and size differences. As the majority of carbohydrates lack readily ionizable groups, their electrophoretic separation is difficult. An approach frequently used to overcome this difficulty is the complexation of the carbohydrate with borate at high pH, forming anionic species [5]. Under these conditions, a strong electroosmotic flow (EOF), generated at the negatively charged inner capillary wall, drives all solutes from the cathodic injection side towards the detector. Labels carrying pH-independent charges would allow more flexibility in the choice of electrolyte composition as for pH and additives.

As positive charges tend to adsorb on the negatively charged capillary wall of an unmodified fused-silica capillary, a negatively charged label is preferred. Labelling strategies involving derivatives of aromatic sulfonic acids such as 7-aminonaphthalene-1,3-disulfonic acid (ANDS) and 8-aminonaphthalene-1,3,6-trisulfonic acid (ANTS) seem to be very promising, since the corresponding carbohydrates derivatives are highly charged even at low pH, which is important with respect to the optimization of resolution.

The resolution of two compounds in any separation system depends on the efficiency, given by the number of theoretical plates and the selectivity of the solutes measured by the difference in their migration velocity [19]. In CE, migration velocity is the vectorial sum of electroosmotic ( $\mu_{eo}$ ) and electrophoretic ( $\mu_{ep}$ ) mobility. With an increase in electroosmotic flow (EOF) under otherwise identical conditions, the resolution of two solutes decreases because the difference in migration times decreases. Op-

timum resolution can be achieved by balancing the EOF against the electrophoretic migration velocity of the solutes. At a highly acidic pH, the electrophoretic migration velocity of the negatively charged ANDS- or ANTS-labelled carbohydrates is larger than the small EOF in fused-silica capillaries. This allows fast and high-resolution separations.

The derivatization of reducing carbohydrates with ANTS was first described by Jackson [20] for use in slab gel electrophoresis. Applications of ANTS [21–23] and ANDS [24] labelling procedures to mono- and oligosaccharides with subsequent CE separations were published recently.

In this work, the ANTS labelling scheme was applied to the determination of glycoprotein-derived complex oligosaccharides. Mass and concentration limits with He–Cd laser LIF detection were investigated, especially with respect to the minimum sample amount that can be derivatized and detected. Rapid and high-resolution CE separations of oligomannose- and complex-type oligosaccharide mixtures are demonstrated. The influence of charge and mass of the ANTS-labelled oligosaccharides on their elution order is discussed. Finally, oligosaccharide libraries, released from ovalbumin and fetuin, were ANTS labelled and separated by CE. A complete interpretation of the complex library pattern was not possible with the available data; however, by comparison of the migration data with those for purified standard complex oligosaccharides and by establishing mobility versus charge-to-mass ratio relationships, tentative peak assignments were made.

## 2. Experimental

### 2.1. Chemicals

All complex oligosaccharide standards and glycoprotein oligosaccharide libraries were supplied by Oxford Glyco Systems (Abingdon, UK). The derivatization reaction was carried out with ANTS, purchased from Molecular Probes (Eugene, OR, USA), sodium cyanoborohydride

(NaCNBH<sub>3</sub>) and acetic acid from Sigma (Buchs, Switzerland) and dimethyl sulfoxide (DMSO) from Fluka (Buchs, Switzerland). Sodium dihydrogenphosphate (NaH<sub>2</sub>PO<sub>4</sub>) and the sodium hydroxide for the background electrolyte were supplied by Merck (Darmstadt, Germany) and Fluka.

## 2.2. Instrumentation

CE separations were performed on a P/ACE 2100 system (Beckman, Fullerton, CA, USA), equipped with an LIF module. The original Ar ion laser was replaced with a He–Cd laser (Omnichrome, Chino, CA, USA), which was connected to the P/ACE instrument detector via a UV-transmissible optical fibre (Laaber Faser-optik, Munich, Germany). The ANTS-labelled carbohydrates were excited with the 325-nm line of the He–Cd laser with ca. 2 mW. Collimated fluorescence radiation was passed through a 520-nm bandpass filter.

## 2.3. Electrophoresis

All separations were carried out in 50  $\mu\text{m}$  I.D. capillaries with an overall length of 27 cm and an effective separation length of 20 cm with 50 mM phosphate background electrolyte titrated to pH 2.5 and 2 M hydrochloric acid. Since under these conditions the EOF is smaller ( $1.25 \cdot 10^{-5} \text{ cm}^2/\text{V}\cdot\text{s}$ ) than the electrophoretic mobility of triply negatively charged carbohydrates [ $(12\text{--}19) \cdot 10^{-5} \text{ cm}^2/\text{V}\cdot\text{s}$ ], the power supply polarity was reversed with the anodic side at the detector. Between runs the capillary was flushed with 100 mM sodium hydroxide and background electrolyte for 2 min each.

Throughout all experiments, the capillaries were thermostated at 25°C. The injections at the cathodic end of the capillary were performed hydrodynamically. An injection pressure of 35 mbar and injection times of 2, 3 and 6 s resulted in injection volumes of 4, 6 and 12 nl, respectively.

## 2.4. Derivatization procedure

The optimization of the derivatization reaction was described in a previous paper [21]. For the

carbohydrates analysed in this study, two different sets of conditions were used, one for overnight reaction at low temperature (standard conditions) and one at elevated temperature (fast conditions). In both sets, 5  $\mu\text{g}$  of complex oligosaccharide, corresponding to ca. 3 nmol, or 50  $\mu\text{g}$  of a glycoprotein oligosaccharide library were dissolved in 1  $\mu\text{l}$  of a 0.15 M ANTS solution in acetic acid–water (3:17 v/v). In the standard procedure with very mild derivatization conditions, 1  $\mu\text{l}$  of a 1 M NaCNBH<sub>3</sub> solution in DMSO was added to the ANTS–carbohydrate solution. After vortex mixing, the reaction mixture was incubated in a heating block at 40°C for 15 h. When a faster derivatization time was required, the ANTS–carbohydrate solution was heated to 80°C. After 30 min of preincubation, the NaCNBH<sub>3</sub> was added. The derivatization was complete within 2.5 h. Prior to injection, the samples were diluted 100–200-fold.

## 2.5. N-Linked oligosaccharides

The complex oligosaccharides used in these experiments were exclusively of the N-linked type. All N-linked oligosaccharides share the same pentasaccharide core structure M<sub>3</sub>GN<sub>2</sub> (see Table 1), which attaches the oligosaccharides to the asparagine residue of the polypeptide. This core element is extended through the attachment of a number of monosaccharides in different branching patterns. Based on compositional similarities, these carbohydrates are classified as oligomannose- or high-mannose-, hybrid- and complex-type structures. In oligomannose-type oligosaccharides, only mannose is attached to the pentasaccharide core. In the complex-type structures, the core is extended by the addition of various monosaccharides such as N-acetylglucosamine, galactose or sialic acid, but not mannose. The hybrid-type oligosaccharides contain mannose residues in the  $\alpha$ -(1,6) branch of the core element and residues other than mannose in the  $\alpha$ -(1,3) branch.

The oligosaccharides investigated in this study are all of the oligomannose- or complex-type structure (see Table 1). According to the supplier, all carbohydrate samples were released from a defined glycoprotein by hydrazinolysis



Table 1  
N-Linked complex oligosaccharides

Oligomannose type

$  \begin{array}{c}  \text{M}\alpha 1 \quad \diagdown \quad 6 \\  \text{M}\alpha 1 \quad \diagup \quad 3 \quad \text{M}\alpha 1 \quad \diagdown \quad 6 \\  \text{M}\alpha 1 \quad \diagup \quad 3 \quad \text{M}\alpha 1 \quad \diagdown \quad 6 \\  \text{M}\alpha 1 \quad \diagup \quad 3  \end{array}  $	$  \text{M}\beta 1 - 4\text{GN}\beta 1 - 4\text{GN}  $	<p><b>MAN5</b> (<math>M_r = 1235</math>) <i>Oligomannose 5</i></p>	
$  \begin{array}{c}  \text{M}\alpha 1 \quad \diagdown \quad 6 \\  \text{M}\alpha 1 \quad \diagup \quad 3 \quad \text{M}\alpha 1 \quad \diagdown \quad 6 \\  \text{M}\alpha 1 - 2\text{M}\alpha 1 \quad \diagup \quad 3  \end{array}  $	$  \text{M}\beta 1 - 4\text{GN}\beta 1 - 4\text{GN}  $	<p><b>MAN6</b> (<math>M_r = 1398</math>) <i>Oligomannose 6</i></p>	
$  \left[ \begin{array}{c}  \text{M}\alpha 1 \quad \diagdown \quad 6 \\  \text{M}\alpha 1 \quad \diagup \quad 3 \quad \text{M}\alpha 1 \quad \diagdown \quad 6 \\  \text{M}\alpha 1 - 2\text{M}\alpha 1 \quad \diagup \quad 3  \end{array} \right]  $	$  \text{M}\beta 1 - 4\text{GN}\beta 1 - 4\text{GN}  $	<p><b>MAN7</b> (<math>M_r = 1560</math>) <i>Oligomannose 7</i></p>	
$  \left[ \begin{array}{c}  \text{M}\alpha 1 \quad \diagdown \quad 6 \\  \text{M}\alpha 1 \quad \diagup \quad 3 \quad \text{M}\alpha 1 \quad \diagdown \quad 6 \\  \text{M}\alpha 1 - 2\text{M}\alpha 1 \quad \diagup \quad 3  \end{array} \right]  $	$  \text{M}\beta 1 - 4\text{GN}\beta 1 - 4\text{GN}  $	<p><b>MAN8</b> (<math>M_r = 1398</math>) <i>Oligomannose 8</i></p>	
$  \begin{array}{c}  \text{M}\alpha 1 - 2\text{M}\alpha 1 \quad \diagdown \quad 6 \\  \text{M}\alpha 1 - 2\text{M}\alpha 1 \quad \diagup \quad 3 \quad \text{M}\alpha 1 \quad \diagdown \quad 6 \\  \text{M}\alpha 1 - 2\text{M}\alpha 1 - 2\text{M}\alpha 1 \quad \diagup \quad 3  \end{array}  $	$  \text{M}\beta 1 - 4\text{GN}\beta 1 - 4\text{GN}  $	<p><b>MAN9</b> (<math>M_r = 1398</math>) <i>Oligomannose 9</i></p>	
<p>Neutral complex type</p>	$  \begin{array}{c}  \text{G}\beta 1 - 4\text{GN}\beta 1 - 2\text{M}\alpha 1 \quad \diagdown \quad 6 \\  \text{G}\beta 1 - 4\text{GN}\beta 1 - 2\text{M}\alpha 1 \quad \diagup \quad 3 \quad \text{M}\alpha 1 \quad \diagdown \quad 6 \\  \text{G}\beta 1 - 4\text{GN}\beta 1 - 2\text{M}\alpha 1 \quad \diagup \quad 3  \end{array}  $	$  \text{M}\beta 1 - 4\text{GN}\beta 1 - 4\text{GN}  $	<p><b>NA2</b> (<math>M_r = 1642</math>) <i>Asialo-, galactosylated bi-antennary</i></p>
$  \begin{array}{c}  \text{G}\beta 1 - 4\text{GN}\beta 1 - 2\text{M}\alpha 1 \quad \diagdown \quad 6 \\  \text{GN}\beta 1 - 4\text{M}\beta 1 - 4\text{GN}\beta 1 - 4\text{GN} \\  \text{G}\beta 1 - 4\text{GN}\beta 1 - 2\text{M}\alpha 1 \quad \diagup \quad 3  \end{array}  $	$  \text{M}\beta 1 - 4\text{GN}\beta 1 - 4\text{GN}  $	<p><b>NA2B</b> (<math>M_r = 1845</math>) <i>Asialo-, galactosylated bi-antennary, with bisecting GN</i></p>	

(Continued on p. 246)

Table 1 (continued)

	$  \begin{array}{c}  \text{G}\beta\text{1} \text{---} 4\text{GN}\beta\text{1} \text{---} 2\text{M}\alpha\text{1} \begin{array}{l} \diagdown 6 \\ \diagup 3 \end{array} \\  \text{G}\beta\text{1} \text{---} 4\text{GN}\beta\text{1} \text{---} 2\text{M}\alpha\text{1} \begin{array}{l} \diagdown 6 \\ \diagup 3 \end{array}  \end{array}  $	$  \begin{array}{c}  \text{F}\alpha\text{1} \\    \\  \text{M}\beta\text{1} \text{---} 4\text{GN}\beta\text{1} \text{---} 4\text{GN}  \end{array}  $	<b>NA2F</b> ( $M_r = 1788$ ) <i>Asialo-, galactosylated bi-antennary, core-substituted with fucose</i>
	$  \begin{array}{c}  \text{G}\beta\text{1} \text{---} 4\text{GN}\beta\text{1} \text{---} 2\text{M}\alpha\text{1} \begin{array}{l} \diagdown 6 \\ \diagup 3 \end{array} \\  \text{G}\beta\text{1} \text{---} 4\text{GN}\beta\text{1} \begin{array}{l} \diagdown 4 \\ \diagup 2 \end{array} \\  \text{G}\beta\text{1} \text{---} 4\text{GN}\beta\text{1} \begin{array}{l} \diagdown 4 \\ \diagup 2 \end{array}  \end{array}  $	$  \begin{array}{c}  \text{M}\beta\text{1} \text{---} 4\text{GN}\beta\text{1} \text{---} 4\text{GN}  \end{array}  $	<b>NA3</b> ( $M_r = 2005$ ) <i>Asialo-, galactosylated tri-antennary</i>
	$  \begin{array}{c}  \text{G}\beta\text{1} \text{---} 4\text{GN}\beta\text{1} \begin{array}{l} \diagdown 6 \\ \diagup 2 \end{array} \\  \text{G}\beta\text{1} \text{---} 4\text{GN}\beta\text{1} \begin{array}{l} \diagdown 6 \\ \diagup 2 \end{array} \\  \text{G}\beta\text{1} \text{---} 4\text{GN}\beta\text{1} \begin{array}{l} \diagdown 4 \\ \diagup 2 \end{array} \\  \text{G}\beta\text{1} \text{---} 4\text{GN}\beta\text{1} \begin{array}{l} \diagdown 4 \\ \diagup 2 \end{array}  \end{array}  $	$  \begin{array}{c}  \text{M}\alpha\text{1} \begin{array}{l} \diagdown 6 \\ \diagup 3 \end{array} \\  \text{M}\alpha\text{1} \begin{array}{l} \diagdown 6 \\ \diagup 3 \end{array} \\  \text{M}\beta\text{1} \text{---} 4\text{GN}\beta\text{1} \text{---} 4\text{GN}  \end{array}  $	<b>NA4</b> ( $M_r = 2373$ ) <i>Asialo-, galactosylated tetra-antennary</i>
	$  \begin{array}{c}  \text{GN}\beta\text{1} \begin{array}{l} \diagdown 6 \\ \diagup 2 \end{array} \\  \text{GN}\beta\text{1} \begin{array}{l} \diagdown 6 \\ \diagup 2 \end{array} \\  \text{GN}\beta\text{1} \begin{array}{l} \diagdown 4 \\ \diagup 2 \end{array} \\  \text{GN}\beta\text{1} \begin{array}{l} \diagdown 4 \\ \diagup 2 \end{array}  \end{array}  $	$  \begin{array}{c}  \text{M}\alpha\text{1} \begin{array}{l} \diagdown 6 \\ \diagup 3 \end{array} \\  \text{M}\alpha\text{1} \begin{array}{l} \diagdown 6 \\ \diagup 3 \end{array} \\  \text{M}\beta\text{1} \text{---} 4\text{GN}\beta\text{1} \text{---} 4\text{GN}  \end{array}  $	<b>NGA4</b> ( $M_r = 1724$ ) <i>Asialo-, agalacto-, tetra-antennary</i>
Sialylated complex type	$  \begin{array}{c}  \text{NAc2} \text{---} 3/6\text{G}\beta\text{1} \text{---} 4\text{GN}\beta\text{1} \text{---} 2\text{M}\alpha\text{1} \begin{array}{l} \diagdown 6 \\ \diagup 3 \end{array} \\  \text{NAc2} \text{---} 3/6\text{G}\beta\text{1} \text{---} 4\text{GN}\beta\text{1} \text{---} 2\text{M}\alpha\text{1} \begin{array}{l} \diagdown 6 \\ \diagup 3 \end{array}  \end{array}  $	$  \begin{array}{c}  \text{M}\beta\text{1} \text{---} 4\text{GN}\beta\text{1} \text{---} 4\text{GN}  \end{array}  $	<b>A2</b> $M_r = 2224$ <i>Di-sialylated-, galactosylated bi-antennary</i>
	$  \begin{array}{c}  \text{NAc2} \text{---} 3/6\text{G}\beta\text{1} \text{---} 4\text{GN}\beta\text{1} \text{---} 2\text{M}\alpha\text{1} \begin{array}{l} \diagdown 6 \\ \diagup 3 \end{array} \\  \text{NAc2} \text{---} 3/6\text{G}\beta\text{1} \text{---} 4\text{GN}\beta\text{1} \begin{array}{l} \diagdown 4 \\ \diagup 2 \end{array} \\  \text{NAc2} \text{---} 3/6\text{G}\beta\text{1} \text{---} 4\text{GN}\beta\text{1} \begin{array}{l} \diagdown 4 \\ \diagup 2 \end{array}  \end{array}  $	$  \begin{array}{c}  \text{M}\alpha\text{1} \begin{array}{l} \diagdown 6 \\ \diagup 3 \end{array} \\  \text{M}\alpha\text{1} \begin{array}{l} \diagdown 4 \\ \diagup 2 \end{array} \\  \text{M}\beta\text{1} \text{---} 4\text{GN}\beta\text{1} \text{---} 4\text{GN}  \end{array}  $	<b>A3</b> $M_r = 2881$ <i>Tri-sialylated, galactosylated tri-antennary</i>

NAc = N-acetylneuraminic acid, G = galactose, GN = N-acetyl-glucosamine, M = mannose, F = fucose.

and subsequently purified by various chromatographic procedures [25].

### 3. Results and discussion

The derivatization scheme for complex oligosaccharides is based on the reductive amination of the reducing carbonyl group of the oligosaccharide with the primary amino group of a chromophore or fluorophore. The primary reaction product is a Schiff base, which is subsequently reduced (and stabilized) to a secondary amine by sodium cyanoborohydride (Fig. 1).

#### 3.1. Derivatization sensitivity and minimum sample amount

In a previous study [21], maltose was used as a model carbohydrate to establish optimum label-

#### *N*-LINKED OLIGOSACCHARIDE DYE

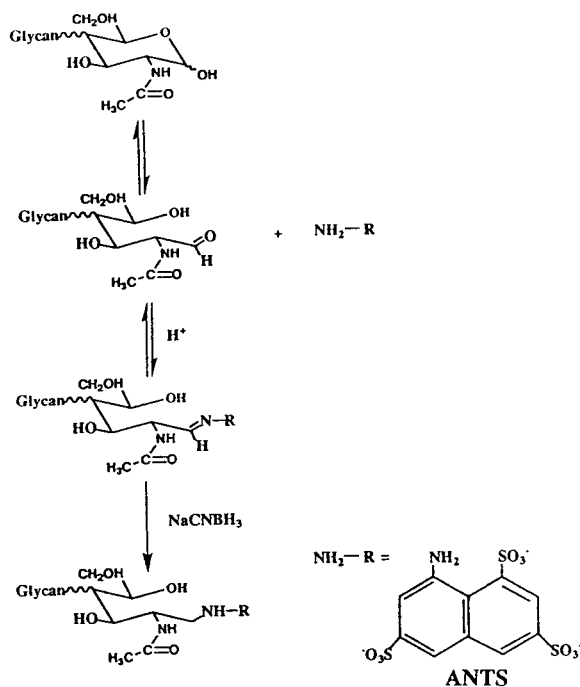


Fig. 1. Reaction scheme for the derivatization of complex oligosaccharides by reductive amination.

ling conditions with respect to derivatization time, temperature and acetic acid concentration. Using volumes as small as 2  $\mu$ l and low nanomolar amounts of carbohydrate in the derivatization reaction, a concentration detection limit (LOD) of  $5 \cdot 10^{-8}$  M could be achieved with LIF detection, using the 325-nm line of a He-Cd laser. This corresponds to a mass detection limit of 500 amol injected, assuming a 10-nl injection volume. Both concentration and mass detection limits were found to be dependent on the molecular mass of the oligosaccharide, since the overall derivatization yield decreases slightly with increasing size of the oligosaccharide. For the present study, the optimum conditions found for maltose were transferred to complex oligosaccharides yielding the same mass and concentration sensitivities.

Mass and concentration detection limits for labelled solutes are in general determined by serial dilutions of derivatization reactions carried out at the milli- or micromolar level for both reactants. However, in a biochemistry laboratory not only the detector performance but also the minimum amount of sample that can be labelled and detected after derivatization is of interest. Therefore, a series of ANTS derivatizations of two complex oligosaccharides, NA2 and NA3 (for structures see Table 1), were carried out. The absolute amounts ranged from 500 to 12 pmol, corresponding to 1  $\mu$ g–25 ng total carbohydrate. Fig. 2 demonstrates that as little as 25 pmol (50 ng) of NA3 could be detected after ANTS labelling. For the smaller NA2, the minimum amount of 12 pmol (20 ng) was even lower, because the reaction yield is higher with smaller carbohydrates.

Since for the experiment all carbohydrates were in a final volume of 10  $\mu$ l prior to injection, the concentration of the complex carbohydrate can be calculated to be  $(1.2\text{--}2.5) \cdot 10^{-6}$  M. This is what we call the derivatization limit of the ANTS labelling of oligosaccharides. The derivatization limit is of practical importance since it takes detector performance and reaction efficiency into account. The concentration detection limit of  $5 \cdot 10^{-8}$  M with the LIF detection system is 1.5 orders of magnitude better than the

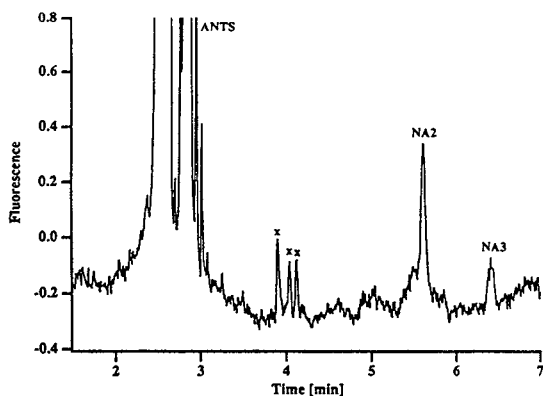


Fig. 2. Derivatization limit for complex oligosaccharides. Derivatization and separation of 25 pmol of NA2 and NA3. CE conditions: electrolyte, 50 mM phosphate (pH 2.5); capillary, 27 cm (20 cm effective length)  $\times$  50  $\mu$ m I.D.; voltage, 10 kV; temperature, 25°C; injection time, 6 s; He–Cd laser with LIF detection: excitation at 325 nm, emission at 520 nm.  $\times$  = Unknown peaks, generated from the ANTS label during derivatization.

lowest carbohydrate concentration of  $1.2 \cdot 10^{-6}$  M that can currently be derivatized with ANTS. This means that the detector potential is not yet fully utilized, because the chemistry is the limiting factor and procedures for labelling at the submicromolar level are not commonly available.

With an injection volume of 10 nl, an absolute amount of 25 fmol per peak is introduced into a capillary. In contrast, the lowest detectable amount of complex carbohydrates reported with slab gel electrophoresis is 5 pmol per band of ANTS conjugate [20].

### 3.2. Sialylated oligosaccharides

Complex oligosaccharides carrying sialic acid residues attached to the end of the antennae, such as A2 or A3 (Table 1), are of special interest, because the degree of sialylation of the glycan moieties is believed to be responsible for the microheterogeneity of glycoproteins [26]. Therefore, a method capable of differentiating complex carbohydrates according to the number of sialic acid residues incorporated would allow at least a first assessment of native microheterogeneity.

Since the  $\alpha$ -(2,3) and  $\alpha$ -(2,6) linkages of the

sialic acids are sensitive to hydrolysis, special attention should be paid during the optimization of the derivatization procedure. Because the reductive amination is acid catalysed, the presence of acetic acid in the reaction mixture was evaluated with respect to the stability of the sialic acid residues during the derivatization of sialylated carbohydrates. In addition, temperature and reaction time were also investigated.

Experiments with neutral oligosaccharides demonstrated their stability under reaction conditions in the presence of 15% acetic acid at 40°C for at least 15 h. To evaluate the influence of the acetic acid on the stability of the sialylated oligosaccharides, an A3 sample was labelled in the presence of 15% acetic acid, whereas in a control experiment acetic acid was omitted. The electropherograms for both A3 samples look almost identical, with one main peak followed by two smaller ones (see Fig. 3a). If sialic acid is hydrolysed during the labelling reaction, one would expect to see also the non-sialylated species. Therefore, the neutral “analogon” of A3, NA3, was labelled under standard conditions. In the acidic buffer medium, the A3 samples with a molecular mass of 3291 migrate faster than the corresponding smaller NA3 with a mass of 2417. The migration times of 5.63 and 5.90 min for A3 and 7.19 min for NA3 (Fig. 3a) clearly demonstrate that additional negative charges from the sialic acid accelerate the migration of the larger A3.

Although the electropherograms obtained after labelling in the presence or absence of acetic acid show identical products, the derivatization yield is vastly different. The A3 sample labelled in the presence of 15% acetic acid resulted in a tenfold larger peak area compared with the control sample without acetic acid. It seems that acetic acid is an important catalyst in the derivatization of reducing carbohydrates by reductive amination. The mechanism of this catalytic effect is not clear as, owing to the dissociation of the sulfonic acid groups of ANTS, the reaction solution has an almost identical pH (pH 1.6 and 1.8, respectively) in the presence or absence of acetic acid. Therefore, acetic acid cannot act as an acidic catalyst as it is completely protonated under these conditions.

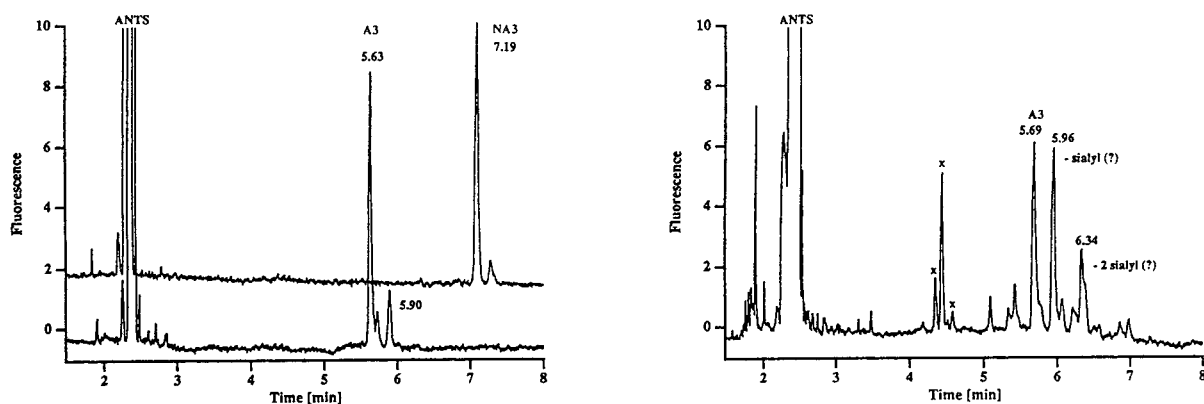


Fig. 3. Electropherogram of (a, left) the neutral triantennary oligosaccharide NA3 and its trisialylated analogon A3 derivatized with ANTS at 40°C for 15 h and (b, right) the sialylated A3 derivatized with ANTS at 80°C for 2.5 h. CE conditions as in Fig. 2, except injection time, 3 s.

Labelling optimization with maltose demonstrated that with an increased temperature of 80°C the reaction time could be reduced to 2.5 h if the cyanoborohydride was added in a second step after 30 min [21]. With neutral complex oligosaccharides no degradation was observed on heating to 80°C. In Fig. 3, A3 was labelled under standard conditions (40°C, 15 h, Fig. 3a) and fast conditions (80°C, 2.5 h, Fig. 3b). A comparison of the two electropherograms reveals sample degradation of the sialylated oligosaccharide at 80°C, since not just one major peak but at least three main peaks can be observed. Most likely these peaks are generated through desialylation of the A3 molecule.

### 3.3. Standard mixtures

An oligomannose-type and a complex-type oligosaccharide mixture were prepared to characterize the separation system. The oligomannoses were derivatized as a mixture, containing MAN5 to MAN9, and as purified samples MAN5, MAN8 and MAN9. The complex-type mixture was made up by mixing the individually labelled oligosaccharides.

#### Oligomannose-type panel

The separation of the five oligomannose-type carbohydrates is shown in Fig. 4. The solutes migrate in order of increasing molecular mass, with the smaller MAN5 eluting first and the

larger MAN9 last. The peak to peak mass difference is 162, equivalent to the mass of one anhydrous mannose residue. All solutes carry the same three negative charges from the ANTS label.

For peak identification, individual oligomannose standards were labelled and injected and their migration times were compared with those of the mixture. In this way, MAN5, MAN8 and MAN9 could be clearly assigned. Given the regular, oligomeric nature of the sample, the two major peaks between MAN5 and MAN8 were assigned to MAN6 and MAN7.

According to electrophoretic theory, an ion or particle migrates in free solution in an electrical field with an electrophoretic mobility,  $\mu_{ep}$ , that is proportional to its electrical charge,  $q$ , and inversely proportional to viscosity,  $\eta$ , and its hydrodynamic radius,  $R$  [27]:

$$\mu_{ep} = q/6\pi\eta R \quad (1)$$

Although Eq. 1 holds true only for small, symmetrical, spherical ions in infinite dilution, it can also be applied to larger solutes. As the hydrodynamic radius is related to the size and molecular mass, the charge-to-mass ratio,  $q/M$ , of a solute should be proportional to its electrophoretic mobility in free solution electrophoresis.

For all complex carbohydrates used in this work, Table 2 lists the molecular masses of the

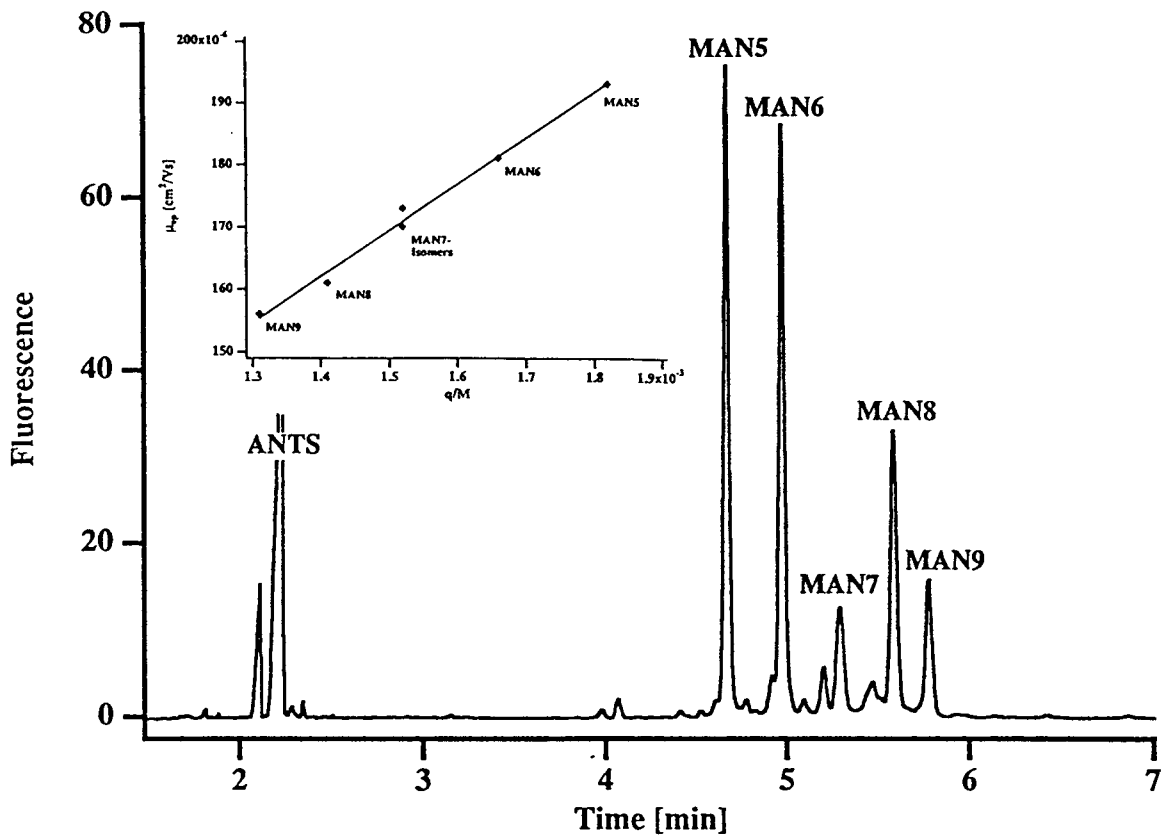


Fig. 4. Separation of ANTS-labelled oligomannose-type oligosaccharides MAN5 to MAN9. CE conditions as in Fig. 2. Sample: 50  $\mu\text{g}$  per 2  $\mu\text{l}$  of derivatized MAN mixture, 250  $\mu\text{g}/\text{ml}$  injected. Inset:  $\mu_{\text{ep}}$  versus  $q/M$  relationship for the MAN5–9 ANTS derivatives:  $y = 5.839 \cdot 10^{-5} + 0.074 \cdot x$ ,  $r = 0.995$ .

Table 2

Electrophoretic mobilities ( $\mu_{\text{ep}}$ ) and charge-to-mass ratios of various neutral and sialylated N-linked oligosaccharides

Oligosaccharide	Mass (g/mol)	+ANTS (g/mol)	Charge	Charge/mass $\times 10^{-3}$	$t_{\text{M}}$ (min)	$\mu_{\text{ep}}$ ( $10^{-5} \text{ cm}^2/\text{V} \cdot \text{s}$ )
MAN5	1235	1645	-3	1.82	4.67	19.3
MAN6	1398	1808	-3	1.66	4.97	18.1
MAN7	1560	1970	-3	1.52	5.20/5.29	17.3/17.0
MAN8	1722	2132	-3	1.41	5.58	16.1
MAN9	1884	2294	-3	1.31	5.78	15.6
NGA4	1724	2134	-3	1.41	5.66	15.9
NA2	1642	2052	-3	1.46	5.77	15.6
NA2B	1845	2255	-3	1.33	5.85	15.4
NA2F	1788	2198	-3	1.36	5.99	15.0
NA3	2005	2415	-3	1.24	6.69	13.7
NA4	2373	2783	-3	1.08	7.31	12.3
A2	2224	2634	-5	1.90	5.10	17.6
A3	2881	3291	-6	1.82	5.41	16.6

pure and ANTS-labelled carbohydrates, the number of charges, assuming  $-3$  for ANTS and  $-1$  for each sialic acid, the charge-to-mass ratio,  $q/M$ , the migration time,  $t_m$ , in the pH 2.5 phosphate background electrolyte and the electrophoretic mobility,  $\mu_{ep}$ . The data for the oligomannose-type carbohydrates including the assumed assignments of MAN6 and MAN7 are plotted as  $\mu_{ep}$  versus  $q/M$  in the inset in Fig. 4 and yield a linear relationship with  $y = 5.839 \cdot 10^{-5} + 0.074x$ ,  $r = 0.995$ . Since all oligomannose-type carbohydrates are neutral, having the same number of three negative charges originating from the ANTS label, their migration order is according to the increasing number of mannose residues. A higher charge-to-mass ratio is therefore equivalent to a lower molecular mass. The linear  $\mu_{ep}$  versus  $q/M$  relationship thus confirms the peak assignment of MAN6 and MAN7. This result compares favourably with a recently published separation without labelling [28].

MAN7 and MAN8 can exist as stereoisomers (see Table 1), as confirmed by the specifications of the supplier through HPAEC–PAD analysis. The additional mannose in MAN7, compared with MAN6, can be attached to one of the three branches. However, only two isomers should be present in the sample, in a ratio of 3:7 [29]. The electropherogram also exhibits two peaks in a 3:7 ratio just where the MAN7 should be, adding more evidence to the assignment. Because of the MAN7 isomers, two dots appear in the  $\mu_{ep}$  versus  $q/M$  curve.

A similar argument could be made for MAN8; however, according to the HPAEC–PAD reference chromatogram, both isomers exist only in a ratio smaller than 1:10, resulting in a main peak with a slight shoulder. Without purified isomers, it seems difficult to assign the small preceding peak of MAN8, which could well be a reaction side-product.

A similar attempt to describe the electrophoretic mobility–molecular size relationship appeared recently. Oefner and Chiesa [30] adapted a model developed by Offord [31] for proteins and peptides, with the electrophoretic mobility being inversely proportional to (molecular mass) $^{-2/3}$ . However, the experimentally deter-

mined mobilities do fit the simple and straightforward relationship described above. Additionally, the more complicated model does not take the charge influence into account, a serve limitation for describing the migration behaviour of sialylated complex carbohydrates.

#### Complex-type panel

Fig. 5 shows the separation of six different neutral bi-, tri- and tetraantennary (NA2, NA2B, NA2F, NA3, NA4, NGA4) and two sialylated (A2, A3) complex-type oligosaccharides in the pH 2.5 phosphate background electrolyte in less than 8 min. The sialylation in A2 and A3 accounts for two and three additional negative charges compared with the neutral analogues NA2 and NA3. The additional charges result in higher charge-to-mass ratios and therefore faster migration, despite the increase in molecular mass. The largest neutral oligosaccharides, NA4, has the longest migration time, 7.31 min.

As discussed for the homologous series of oligomannoses, the principal separation mechanism for this set of complex-type oligosaccharides is the difference in the charge-to-mass ratio. However, the strict linear  $\mu_{ep}$  versus  $q/M$  relationship cannot be applied here. As shown in Table 1, the two complex oligosaccharides, NA2B and NA2F, differ in their composition but not in the number of sugar residues. The bisect-

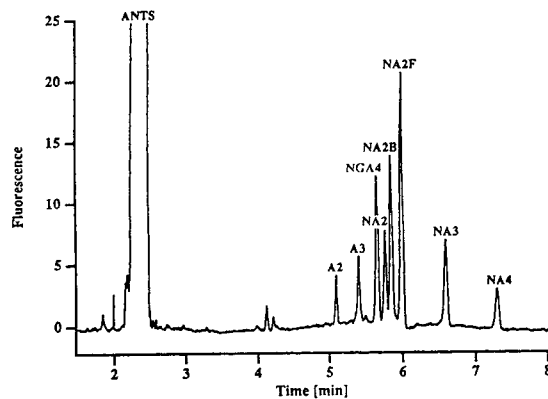


Fig. 5. CE separation of sialylated (A) and neutral (NA) complex-type oligosaccharides. CE conditions as in Fig. 2; oligosaccharide concentration, 3.8–6.1  $\mu M$ .

ing N-acetylglucosamine (GN) in the NA2B is substituted by a fucose (F) residue in the core of the NA2F. This results in a difference in molecular mass of only 57. The corresponding charge-to-mass ratios of  $1.33 \cdot 10^{-3}$  and  $1.36 \cdot 10^{-3}$  for NA2B and NA2F (Table 2), respectively, are not reflected in the separation. Surprisingly, NA2B and NA2F can be well separated, with the larger NA2B migrating in front of NA2F (Fig. 5).

The same is true for the pair NGA4 and NA2, which also contain the same number of sugar residues but differ in composition. NA2 with a charge-to-mass ratio of  $1.46 \cdot 10^{-3}$  migrates more slowly than NGA4, which has a charge-to-mass ratio of only  $1.41 \cdot 10^{-3}$ . On the other hand carbohydrates with a larger mass difference, such as NA2 and NA2B ( $\Delta M = 203$ ), show less resolution than the NA2B–NA2F and the NGA4–NA2 pairs. These two examples demonstrate that the migration behaviour of these complex carbohydrates is affected not only by their charge-to-mass ratio.

It can be assumed that the distinct three-dimensional structure, determined by the steric position of the sialic acids, the glycosidic linkages, the  $\alpha/\beta$  anomericity and the variety of branching, causes a deviation from a simple  $\mu_{ep}$  versus  $q/M$  relationship, which assumes spherical solutes without preferential arrangement in the electrical field. The assumed influence of the three-dimensional structure brings additional selectivity to the separation. The high resolution is a result of a high separation power of at least 120 000 theoretical plates, and the selectivity provided mainly by a  $\mu_{ep}$  versus  $q/M$  dependence, which is applicable only to a series of

homologous compounds, mediated by assumed stereochemical effects. Therefore, even small differences in molecular mass can be sufficient to obtain baseline or close to baseline resolution for the separation of complex oligosaccharides in a very simple separation system.

#### Trisialylated oligosaccharide (A3)

The linear  $\mu_{ep}$  versus  $q/M$  relationship can also be used to explore if the three peaks generated during labelling of A3 at elevated temperature could possibly result from a desialylation process (Fig. 3b). The plot of  $\mu_{ep}$  versus  $q/M$  (calculated values in Table 3) shows a similar linear dependence as demonstrated for the oligomannose-type carbohydrates. The migration times of A3 and NA3 in this data set are not identical with those in Table 2, because of a slight change in EOF over several weeks. However, within one set of experiments, all data are consistent. The corresponding linear equation ( $y = 5.618 \cdot 10^{-5} + 0.0566x$ ) has a high correlation coefficient  $r$  of 0.994. Therefore, the three peaks in Fig. 3b at 5.69, 5.96 and 6.34 min can be assigned to A3 with three, two and one sialic acid, respectively. Complete desialylation of A3 does not occur under the reaction conditions, as no peak is present at the migration time of NA3 (7.20 min), which represents the asialo form of A3. The migration time of NA3 could be predicted with the values for the tri-, bi- and monosialylated species and verified by an independent experiment.

The  $\mu_{ep}$  versus  $q/M$  dependence also allows the assignment of one of the additional peaks that shows up in the separation of A3 (Fig. 3a). By comparing the migration time of the smaller

Table 3  
Electrophoretic mobilities ( $\mu_{ep}$ ) and charge-to-mass ratios of various neutral and sialylated N-linked oligosaccharides

Oligosaccharide	Mass (g/mol)	+ANTS (g/mol)	Charge	Charge/mass $\times 10^{-3}$	$t_M$ (min)	$\mu_{ep}$ ( $10^{-5}$ cm <sup>2</sup> /V·s)
A3	2881	3291	−6	1.82	5.69	15.8
−1 sialyl	2589	2999	−5	1.67	5.96	15.1
−2 sialyl	2297	2707	−4	1.48	6.34	14.2
−3 sialyl (NA3)	2005	2415	−3	1.24	7.20	12.5



peak with the  $\mu_{ep}$  values in Table 2, the signal at 5.90 min can be assigned to the A3 with only two sialic acid residues. That means that the original A3 sample is slightly degraded either during the derivatization or already during the isolation and purification process. Another batch of A3 showed the same pattern after derivatization.

### 3.4. Oligosaccharide libraries

After optimizing the derivatization conditions for neutral and charged oligosaccharide standards, the labelling procedure was applied to oligosaccharide libraries generated from two different glycoproteins, ovalbumin and fetuin. A 50- $\mu$ g amount of each library was used and labelled under standard conditions to avoid possible degradation. The fetuin sample, which contains a considerable number of highly charged complex carbohydrates, was labelled without acetic acid. After the derivatization, the reaction volume was made up to 20  $\mu$ l prior to injection.

#### Ovalbumin oligosaccharide library

Ovalbumin, found in hen egg white, is a glycoprotein with a molecular mass of 43 000, containing two possible N-glycosylation sites. Glycosylation accounts for only 3.5% of its mass [32]. The nine oligosaccharides structurally identified belong to either the oligomannose- or hybrid-type structures. Both types are present in ovalbumin in a ratio of ca. 1:1 [33].

Fig. 6a shows the separation of the ANTS-labelled ovalbumin-derived oligosaccharides. In less than 6.5 min, ten peaks could be clearly distinguished. As ovalbumin contains a considerable amount of oligomannose-type oligosaccharides, its carbohydrate pattern was matched with the oligomannose reference pattern (Fig. 6b).

An overlay of the two traces revealed that several peaks with identical migration times are found in the reference and the glycoprotein-derived trace. This could be further confirmed by co-injecting the ovalbumin library and the oligomannose panel. For the co-injection, the two samples were injected one after the other for

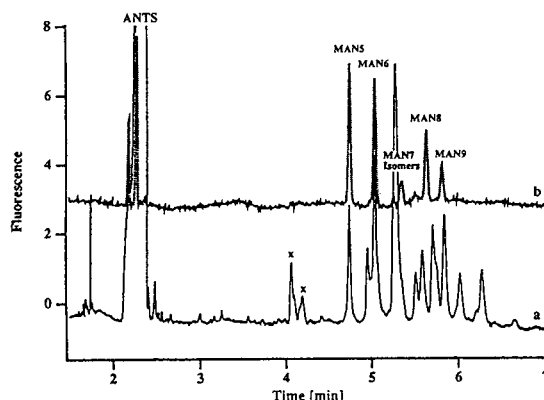


Fig. 6. Comparison of the ovalbumin oligosaccharide pattern (a) with the oligomannose type reference panel (b). CE conditions as in Fig. 2.

2 s. The migration times of double injected samples were independent of the injection order, confirming that co-injection does not bias against the first injected sample. The combined injection volume of  $2 \times 4$  nl corresponds to less than 0.4% of the total capillary volume.

Co-injection of ovalbumin-derived oligosaccharides and the oligomannose-type panel resulted in a co-migration of three of the first four signals of the ovalbumin-derived oligosaccharides with MAN5, MAN6 and MAN7 (Fig. 7). The unambiguous identification of MAN7 in the

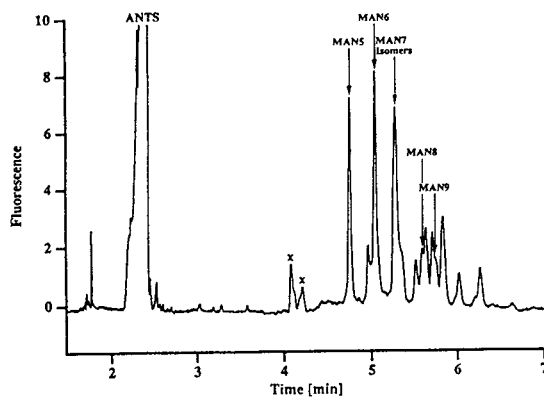


Fig. 7. Co-injection of oligomannose-type reference panel and the ovalbumin oligosaccharide library. CE conditions as in Fig. 2, except injection time, 2 s for each sample.

ovalbumin-derived pattern is not possible, since the concentration of MAN7 in the reference mixture is fairly low compared with the ovalbumin; however, the presence of MAN5 and MAN6 in the ovalbumin library can be ascertained. MAN8 produced a double peak at 5.64 min and migration of MAN9 increased the slight shoulder of an ovalbumin peak at 5.72 min, indicating that these two oligomannoses are not present in the ovalbumin oligosaccharide library. The other peaks in the ovalbumin library can be attributed to the hybrid-type oligosaccharides with eight to eleven carbohydrate residues [34]. A more detailed assignment of the peaks to distinct structures was not possible, since the corresponding oligosaccharide standards were not available.

Honda et al. [35] reported that the capillary electrophoretic separation of the ovalbumin oligosaccharide pool could resolve only five peaks in an acidic phosphate electrolyte [35]. The separation of aminopyridine-labelled carbohydrates is also based primarily on size differences. However, some of the oligomannose- and the hybrid-type oligosaccharides most likely contain the same number of monomers with only small differences in their total molecular masses. The five peaks represent five size classes defined by the number of carbohydrate residues. It is interesting that the ANTS separation system presented here has dramatically improved the resolving power and is able to distinguish clearly ten peaks.

The resolution,  $R_s$ , of two peaks is given by the following equation [19]:

$$R_s = \frac{1}{4} \sqrt{N} \cdot \frac{\Delta u}{\bar{u}} \quad (2)$$

where  $N$  = number of theoretical plates,  $\Delta u$  = difference in migration velocity of two solutes and  $\bar{u}$  = average migration velocity. The minimum difference in migration velocity of two solutes can be calculated by rearrangement:

$$\Delta u = 4R_s \cdot \frac{\bar{u}}{\sqrt{N}} \quad (3)$$

As the migration velocity  $u$  is related to the effective separation length  $l$  with migration time  $t$ , the migration velocity and migration time are inversely proportional at a constant separation length. With a minimum number of theoretical plates of 120 000 and an average migration time of 5.5–6.5 min, baseline resolution ( $R_s = 1$ ) is achieved with a difference in migration time of at least 0.06–0.08 min. This allows very small differences in solute mobility to be sufficient for separation. The first three oligomannose components of the ovalbumin differ by 0.3 min, allowing an easy separation. The other peaks attributed to the hybrid-type carbohydrates are separated with a resolution between 1.5 and 5. Only two shoulders on the MAN7 peak and MAN9 peak indicate that this separation system is not sufficient to resolve the ovalbumin sample completely into all its individual components.

#### *Bovine fetuin oligosaccharide library*

Bovine fetuin, the major glycoprotein in fetal calf serum, represents a highly glycosylated protein, containing O- and N-linked glycan moieties [36]. Bovine fetuin is known to contain a considerable amount of charged oligosaccharides. Among the N-linked glycans, six classes of complex carbohydrates can be distinguished in fetuin corresponding to zero, one, two, three, four and five sialic acid residues in the molecule. The major species are the di-, tri- and tetrasialylated oligosaccharides, most of them with a triantennary structure [37]. Biantennary structures have also been identified [34].

The separation of the ANTS-labelled oligosaccharide library of bovine fetuin is shown in Fig. 8. The electropherogram can be roughly divided into two parts. The first part is distinguished by very sharp but smaller peaks (2.8–4 min). The second part contains broader, but higher peaks (5–6.7 min). The fetuin library, prepared by hydrazinolysis, contains both N- and O-linked carbohydrate structures. Because O-linked reference carbohydrates were not commercially available, the oligosaccharide pattern was only compared with the N-linked carbohy-

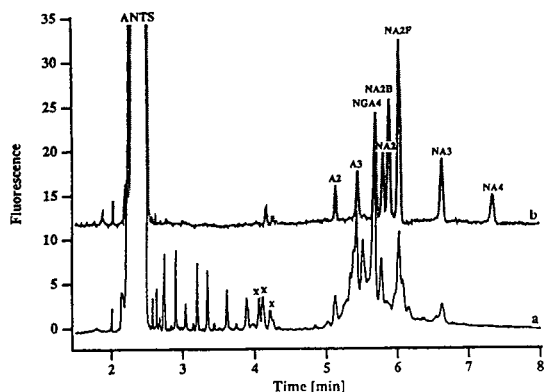


Fig. 8. Comparison of the fetuin oligosaccharide library (a) with the complex-type reference panel, including charged (A) and uncharged (NA) oligosaccharides (b). CE conditions as in Fig. 2.

drates of the complex reference panel. There is no match in the first part of the electropherogram, but the second part shows identical migration times in both electropherograms. A close inspection reveals the co-migration of six fetuin oligosaccharides with the A2, A3, NGA4, NA2, NA2F and NA3 reference oligosaccharides. This could also be confirmed by co-injection of the fetuin and the complex-type oligosaccharide mixture, similarly to the procedure described for ovalbumin.

Fetuin is known to contain the two neutral oligosaccharides, NA2 and NA3 [34], next to the A3 and its various isomeric forms, differing in the position of the sialic acid or the galactose linkages [37]. The two shoulders on the A3 peak in Fig. 8a could possibly be attributed to these isomeric forms.

The peaks in the fetuin panel having the same migration times as NGA4 and NA2F in the complex reference panel could possibly also originate from mono- and disialylated A3. The  $\mu_{ep}$  versus  $q/M$  curve would predict the same migration times. Therefore, a peak assignment is only tentative with the available data. Owing to the complexity of oligosaccharide structures, data from complementary methods will be neces-

sary for complete structural elucidation of oligosaccharide libraries.

#### 4. Conclusions

The ANTS labelling procedure was optimized to allow the electrophoretic separation and detection of both neutral and charged (sialylated) N-linked oligosaccharides under the same conditions. Whereas the neutral oligosaccharides proved to be stable under the conditions for standard and fast derivatization, sialylated oligosaccharides should be handled with care, especially with respect to temperature and acetic acid concentrations during the labelling reaction. Concentration detection limits of  $5 \cdot 10^{-8} M$  can be achieved with LIF detection using the 325-nm line of a He–Cd laser. The derivatization detection limit is of the order of a few micromolar, corresponding to absolute amounts of 10–20 pmol of complex oligosaccharide to be analysed. This is sufficient to work with glycoprotein-derived oligosaccharides.

Further improvements in the detection limit for complex oligosaccharides are not restricted by the detector performance, which is at least 1.5 orders of magnitude better than the derivatization limit. The limiting factor is the chemistry of the labelling reaction. New micromethods have to be developed to work on a microlitre scale, preferably with 1–5  $\mu l$ . The greatest challenge, however, will be to guarantee a quantitative reaction at the dilute concentrations of both solute and label. The mass and concentration detection limits have been pushed to levels unthinkable a few years ago, yet the chemistry to utilize this detection performance has not kept up.

With the current labelling, separation and detection methods, oligosaccharide libraries of various glycoproteins can be analysed, allowing a rapid screening of glycan patterns. With the high separation efficiency for ANTS conjugates and the influence of the molecular structure of the labelled oligosaccharides on their migration, excellent resolution can be achieved. This meth-

od is suitable as a quality control tool to assess the glycosylation of recombinant glycoproteins by comparison with reference libraries.

Peak identification in a separation technique relies on the availability of purified and characterized reference standards. The number of complex oligosaccharides commercially available is still small, but growing. New analytical methods such as that presented here will help to characterize samples purified by chromatographic methods. With a wider selection of complex oligosaccharides, available peak assignment will be facilitated. To compare migration times from run to run better, internal standards might be necessary to eliminate variations introduced by a changing EOF [38].

As the database grows, the interpretation of known and at present unknown oligosaccharide libraries will be possible. A better understanding of unexpected selectivity, presumably introduced by the distinct three-dimensional structure, will also help in an accurate peak assignment and in the correct prediction of migration order. However, as the shoulders in the bovine fetuin library pattern indicate, even the unprecedented selectivity of the current separation system might not be sufficient to resolve all complex oligosaccharides present in a glycan library because the structural variety might be too large.

ANTS derivatization combined with LIF detection has been demonstrated to be suitable as a screening method for the glycosylation pattern of glycoproteins. If the identification of single complex oligosaccharides in mixtures of released glycans can be further advanced, CE with its advantages in speed and resolution could become an effective and valuable tool in the structural elucidation of glycoproteins.

### Acknowledgements

The authors thank Drs. Ernst Gassmann and Beat Krattiger for valuable help with interfacing the He–Cd laser with the P/ACE system. Earlier versions of the manuscript were critically read and commented upon by Drs. Len Cummins (Isis Pharmaceuticals) and Gerard Bruin (Ciba).

### References

- [1] H. Schachter, *Trends Glycosci. Glycotechnol.*, 4 (1992) 241.
- [2] J.M. Paulson, *Trends Biochem. Sci.*, 14 (1989) 272.
- [3] M.W. Spellman, *Anal. Chem.*, 62 (1990) 1714.
- [4] M.R. Hardy and R.R. Townsend, *Proc. Natl. Acad. Sci. U.S.A.*, 85 (1988) 3289.
- [5] S. Hofstetter-Kuhn, A. Paulus, E. Gassmann and H.M. Widmer, *Anal. Chem.*, 63 (1991) 1541.
- [6] A. Klockow, A. Paulus, V. Figueiredo, R. Amadò and H.M. Widmer, *J. Chromatogr.*, 680 (1994) 187.
- [7] A.E. Vorndran, P.J. Oefner, H. Scherz and G.K. Bonn, *Chromatographia*, 33 (1992) 163.
- [8] T.W. Garner and E.S. Yeung, *J. Chromatogr.*, 515 (1990) 639.
- [9] L.A. Colon, R. Dadoo and R.N. Zare, *Anal. Chem.*, 65 (1993) 476.
- [10] A.E. Bruno, B. Krattiger, F. Mayestre and H.M. Widmer, *Anal. Chem.*, 63 (1991) 2689.
- [11] S. Honda, S. Iwase, A. Makino and S. Fujiwara, *Anal. Biochem.*, 176 (1989) 72.
- [12] E. Grill, C. Huber, P.J. Oefner, A.E. Vorndran and G.K. Bonn, *Electrophoresis*, 14 (1993) 1004.
- [13] A.E. Vorndran, E. Grill, C. Huber, P.J. Oefner and G.K. Bonn, *Chromatographia*, 34 (1992) 109.
- [14] H. Schwaiger, P.J. Oefner, C. Huber, E. Grill and G.K. Bonn, *Electrophoresis*, 15 (1994) 941.
- [15] S. Honda, S. Suzuki, A. Nase, K. Yamamoto and K. Kakehi, *Carbohydr. Res.*, 215 (1991) 193.
- [16] P.J. Oefner, A.E. Vorndran, E. Grill, C. Huber and G.K. Bonn, *Chromatographia*, 34 (1992) 308.
- [17] J. Liu, O. Shirota, W. Donald and M. Novotny, *Proc. Natl. Acad. Sci. U.S.A.*, 88 (1991) 2302.
- [18] P.J. Oefner, C. Chiesa, G. Bonn and C. Horváth, *J. Capillary Electrophoresis*, 1 (1994) 5.
- [19] J.C. Giddings, *Sep. Sci.*, 4 (1969) 181.
- [20] P. Jackson, *Biochem. J.*, 270 (1990) 705.
- [21] A. Klockow, H.M. Widmer, R. Amadò and A. Paulus, *Fresenius' J. Anal. Chem.*, 350 (1994) 415.
- [22] C. Chiesa and C. Horváth, *J.A Chromatogr.*, 66 (1993) 1134.
- [23] M. Stefanson and M. Novotny, *Anal. Chem.*, 66 (1994) 1134.
- [24] K.-B. Lee, S.-Y. Kim and R.L. Linhardt, *Electrophoresis*, 12 (1991) 636.
- [25] *Tools for Glycobiology*, Oxford Glyco Systems, Abingdon.
- [26] A.D. Tran, S. Park, P. Lisi, O.T. Huynh, R.R. Ryall and P.A. Lane, *J. Chromatogr.*, 542 (1991) 459.
- [27] P.D. Grossman, J.C. Colburn and H.H. Lauer, *Anal. Biochem.*, 179 (1989) 28.
- [28] D.E. Hughes, *J. Chromatogr.*, 657 (1994) 315.
- [29] Technical Note, Reference Panel Oligomannose-Type, Cat. No. RP-2500, Oxford Glyco Systems, Abingdon.
- [30] P.J. Oefner and C. Chiesa, *Glycobiology*, 4 (1994) 397.

- [31] R.E. Offord, *Nature*, 211 (1966) 591.
- [32] N. Tomiya, J. Awaya, M. Kurono, S. Endo, Y. Arata and N. Takahasi, *Anal. Biochem.*, 171 (1988) 73.
- [33] J.P. Landers, R.P. Oda, B.J. Madden and T.C. Spelsberg, *Anal. Biochem.*, 205 (1992) 115.
- [34] S. Suzuki, K. Kakehi and S. Honda, *Anal. Biochem.*, 205 (1992) 227.
- [35] S. Honda, A. Makino, S. Suzuki and K. Kakehi, *Anal. Biochem.*, 191 (1990) 228.
- [36] B. Bendiak, M. Harris-Brandts, S.W. Michnik, J.P. Carver and D.A. Cumming, *Biochem.*, 28 (1989) 6491.
- [37] R.R. Townsend, M.R. Hardy, D.A. Cumming, J.P. Carver and B. Bendiak, *Anal. Biochem.*, 182 (1989) 1.
- [38] P. Hermentin, R. Doenges, R. Witzel, C.H. Hokke, J.F.G. Vliegenhart, P. Kamerling, H.S. Conradt, M. Nimtz and D. Brazel, *Anal. Biochem.*, 221 (1994) 29.



# High-resolution capillary electrophoresis and polyacrylamide gel electrophoresis of heparins

Reinhard Malsch\*, Job Harenberg, Dieter. L. Heene

1st Department of Medicine, Medical University Clinic Mannheim, Theodor Kutzer Ufer, 68167 Mannheim, Germany

## Abstract

Heparin-oligosaccharides, low-molecular-mass heparins (LMMHs) and heparins were determined using high-resolution capillary electrophoresis (HPCE) and polyacrylamide gel electrophoresis (PAGE). The conditions for HPCE were 20 mM phosphate buffer (pH 3.5) and 20°C. The method was equivalent to that used previously with a borate–sodium dodecyl sulfate buffer (pH 8.8). Six LMMHs were determined using PAGE. The method showed a standard deviation of the average molecular mass from 6.4 to 19.8% and of their polydispersity from 0.7 to 10.2%. HPCE and PAGE revealed different important structural and compositional differences of heparins.

## 1. Introduction

Heparin is an endogenously occurring glycosaminoglycan with anticoagulant properties which has been applied for over half a century in clinical use. The major disaccharide sequences of heparin are established as an  $\alpha(1\rightarrow4)$ -linked L-iduronic acid 2-sulfate  $\rightarrow$  D-glucosamine N,6 disulfate (IdoA-2S  $\rightarrow$  GlcNS-6S) [1]. The highly sulfated glycosaminoglycan (DS = 2.0–2.5) is commonly determined by different electrophoretic methods; traditionally, heparin electrophoresis is performed by agarose gel electrophoresis using barium trimethylenediamines [2], which resolves a fast- and slow-moving heparin fractions. More information about the primary sequence of heparin is obtained by compositional analysis with high resolution and specificity using high-performance capillary electrophoresis (HPCE). The method is as efficient as the traditional SAX HPLC analysis [3,4]. More

detailed information about the secondary structure of heparin can be obtained by polyacrylamide gel electrophoresis (PAGE). This method gives detailed information about the degree of polymerization ( $D_p$ ), the average molecular mass and the distribution of molecular mass of heparin [5,6].

Recently, it has been demonstrated that the molecular mass of heparin is a crucial parameter for its pharmacodynamics. The anti-Xa activity is associated with the pentasaccharide sequence and the following structure: –GlcNAc(6-OSO<sub>3</sub>)–GlcA–GlcNSO<sub>3</sub>(3,6-di-OSO<sub>3</sub>)–IdoA(2-OSO<sub>3</sub>)–GlcNSO<sub>3</sub>(6-OSO<sub>3</sub>) [7,8]. The anti-IIa activity, which seems to be of importance for the anti-thrombotic activity of heparin, requires a saccharide chain of at least 18 saccharide units ( $M > 5800$ ) [9,10].

This paper describes and compares different electrophoretic methods for determining heparins. An HPCE method for the determination of heparins and heparin oligosaccharides is described. PAGE analysis with a new staining

\* Corresponding author.

method was developed and shows a better resolution of oligosaccharides resulting in a different molecular mass distribution and polydispersity for each heparin. The microheterogeneity of heparin macromolecules can be best performed using a combination of HPCE and PAGE.

## 2. Experimental

### 2.1. Heparins

The following unfractionated and low-molecular-mass heparins (LMMHs) were used: unfractionated sodium heparin (analytical-reagent grade), prepared from bovine lung, was obtained by Braun Melsungen (Germany), Braun-LMMH containing sodium chloride and water for injection from Braun Melsungen (Germany), Clexane containing water for injection from Nattermann (Cologne, Germany), Fragmin containing sodium chloride and water for injection from Kabi Pfrimmer (Erlangen, Germany), Fraxiparin containing calcium hydroxide and water for injection from Sanofi-Wintrop (Munich, Germany), Merckle LMMH (analytical-reagent grade) from Merckle (Ulm, Germany) Reviparin from Nordmark (Germany) and Mono Embolex was generously provided by Sandoz (Nürnberg, Germany).

Heparin-oligosaccharides prepared by synthesis, ranging from di- to dodecasaccharide, were generously provided by Dr. M. Petitou and Dr. L. Lormeau (Institut Choay, Paris, France).

Heparin-disaccharide standards (H-0895, H-8642, H-1145, H-9517, H-1020, H-9392 and H-9267) were obtained from Sigma (St. Louis, MO, USA). Heparinase I was generously supplied by Baxter Diagnostics (Deerfield, IL, USA) and chondroitinase ABC purified from *Proteus vulgaris* was obtained from Seikagaku (Tokyo, Japan).

### 2.2. Chemicals

Tris and Sephadex G-25 F were of research grade and were obtained from Sigma (Deisenhofen, Germany), glycerol from Merck (Darmstadt, Germany), 3-dimethylaminopropionitrile

(DNPN) from Fluka (Neu-Ulm, Germany) and acrylamide, N,N-methylenebisacrylamide, ethylenediaminetetraacetic acid and glycine of research grade from Serva (Heidelberg, Germany).

### 2.3. HPCE of heparin and heparin-oligosaccharides

The experiments were performed on a PACE System 2050 from Beckman Instruments (Fullerton, CA, USA), equipped with a variable-wavelength ultraviolet detector. System operation and data management were controlled using System Gold software (Beckman Instruments) running on an IBM personal computer. In both modes the samples were analysed using a 50 cm × 50 μm I.D. capillary cartridge (No. 727604) from Beckman Instruments.

The concentrations of the stock standard solutions were 1 mg/ml for heparin-disaccharides and 10 mg/ml for heparin-oligosaccharides and heparin preparations.

### 2.4. Normal polarity

The following conditions were used: data rate, 5 Hz; rise time, 1 s; range (AU), 0.05; polarity, direct; wavelength, 200 and 230 nm; time, 30 min; voltage, 18 kV; temperature, 25°C; injection, high pressure for 10 or 15 s; buffer system, 10 mM sodium tetraborate and 50 mM boric acid (pH 8.5 and 8.8).

### 2.5. Reversed polarity

The following conditions were used: data rate, 5 Hz; rise time, 1 s; range (AU), 0.2; polarity, indirect; wavelength, 200 and 230 nm; time, 60 min; voltage, 12 kV; temperature, 25°C; injection, high pressure for 15 s; buffer system, 20 mM sodium phosphate adjusted to pH 3.5 with hydrochloric acid.

### 2.6. Preparation of gradient polyacrylamide gels and electrophoresis

Gradient polyacrylamide resolving gels, 20–30% total acrylamide and 2–5% total N,N-



bisacrylamide (pH = 8.3), were prepared using a linear gradient maker from Hoefer Instruments (San Francisco, CA, USA). A stacking gel of 5% total acrylamide (pH 8.0) was prepared. Preconcentration of the samples was performed in the stacking gel at 20 V. Electrophoresis was performed for 4 h at 80 V. The gels were fixed and stained with 1% aqueous acridine orange solution. Destaining was carried out 24 h with gentle shaking using ethanol–water (20:80). The gels were scanned by a densitometer from Hirschmann Instruments (Traufkirchen, Germany) at 548 nm.

### 2.7. Determination of the average molecular mass by PAGE

Each gel was scanned at 548 nm with a densitometer and the data were transferred as an ASCII file to a Excel program. The oligosaccharides did not differ in resolution and absorbance. The molecular mass and polydispersity were calculated and displayed as mean  $\pm$  standard deviation.

## 3. Results

The electrophoretic methods for heparins are dependent on their structure, sequence, charge and mass of the molecule. HPCE, however, is a powerful method for the characterization of different heparins and low-molecular-mass heparins. PAGE analysis is suitable for determining the molecular mass distribution, the average molecular mass and the polydispersity, which are of importance for the effects of heparins.

### 3.1. HPCE analysis of heparin-disaccharides

Using enzymatic depolymerization, heparin was cleaved to heparin-disaccharides. These commercially available pure heparin-disaccharides with the structure  $\Delta$ UA 2X (1 $\rightarrow$ 4)  $\alpha$ -D-GlcNY6X were resolved and detected selectively at 230 nm. The migration time of the heparin-disaccharides was about 30–50% shorter than a 50  $\mu$ m than with a 75  $\mu$ m I.D. capillary.

Decreasing the voltage from 20 to 5 kV increased the separation between mono- and disulfated isomers. Consequently, the migration time increased. Increasing the temperature to 40°C resulted in a loss of resolution of the mono- and disulfated compounds.

### 3.2. Normal polarity

The heparin-disaccharides used were resolved within 8 min and migrated according to their sulfation. In the normal polarity mode the trisulfated heparin-disaccharide  $\Delta$ UA 2S (1 $\rightarrow$ 4)  $\alpha$ -D-GlcNHS6S was the slowest and the non-sulfated  $\Delta$ UA (1 $\rightarrow$ 4)  $\alpha$ -D-GlcNHAc the fastest component (Fig. 1). At concentrations between 20  $\mu$ g/ml and 1 mg/ml there was a linear correlation between the peak area and concentration, with correlation coefficient in the range  $r^2 = 0.98$ – $0.99$ .

### 3.3. Reverse polarity

On reversing the polarity, the order of migration changed completely. The analysis was performed in 44 min and resolved the heparin-disaccharides from each other. The migration order was reversed: the trisulfated heparin-disaccharide  $\Delta$ UA 2S (1 $\rightarrow$ 4)  $\alpha$ -D-GlcNS6S was the fastest and the non-sulfated  $\Delta$ UA (1 $\rightarrow$ 4)  $\alpha$ -D-GlcNHAc the slowest component (Fig. 2).

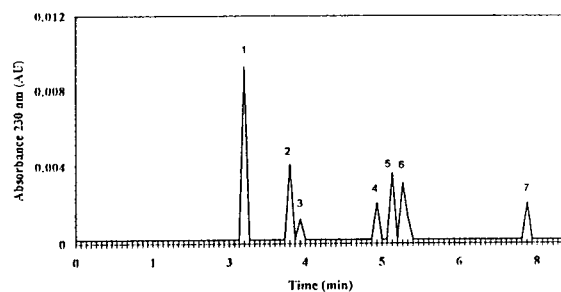


Fig. 1. HPCE separation of seven heparin-disaccharides using normal polarity. Peaks: 1 =  $\Delta$ UA (1 $\rightarrow$ 4)  $\alpha$ -D-GlcNHAc; 2 = monosulfated  $\Delta$ UA (1 $\rightarrow$ 4)  $\alpha$ -D-GlcNAc6X; 3 =  $\Delta$ UA 2S (1 $\rightarrow$ 4)  $\alpha$ -D-GlcNAc; 4 = disulfated  $\Delta$ UA 2S (1 $\rightarrow$ 4)  $\alpha$ -D-GlcNAc6S; 5 =  $\Delta$ UA (1 $\rightarrow$ 4)  $\alpha$ -D-GlcNS6S; 6 =  $\Delta$ UA 2S (1 $\rightarrow$ 4)  $\alpha$ -D-GlcNS; 7 = trisulfated disaccharide  $\Delta$ UA 2S (1 $\rightarrow$ 4)  $\alpha$ -D-GlcNS6S. The buffer system contained 10 mM borate and 50 mM SDS.

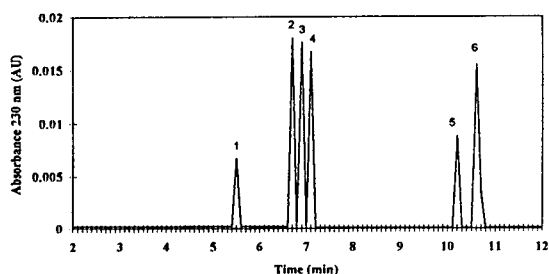


Fig. 2. HPCE separation of seven heparin-disaccharides using reverse polarity. Peaks: 1 = trisulfated  $\Delta$ UA 2S (1 $\rightarrow$ 4)  $\alpha$ -D-GlcNS6S; 2 = disulfated  $\Delta$ UA 2S (1 $\rightarrow$ 4)  $\alpha$ -D-GlcNS; 3 =  $\Delta$ UA (1 $\rightarrow$ 4)  $\alpha$ -D-GlcNS6S; 4 = disulfated  $\Delta$ UA 2S (1 $\rightarrow$ 4)  $\alpha$ -D-GlcNAc6S; 5 = monosulfated  $\Delta$ UA 2S (1 $\rightarrow$ 4)  $\alpha$ -D-GlcNAc; 6 =  $\Delta$ UA (1 $\rightarrow$ 4)  $\alpha$ -D-GlcNAc6X; 7 = non-sulfated disaccharide  $\Delta$ UA (1 $\rightarrow$ 4)  $\alpha$ -D-GlcNAc (44.4 min). The buffer contained 20 mM phosphate (pH 3.5). Rise time, 1 s; data rate, 5 Hz; range (AU), 0.02; polarity, direct; wavelength, 230 nm; time, 60 min; voltage, 12 kV; temperature, 25°C; injection, high pressure for 15 s.

At concentrations between 20  $\mu$ g/ml and 1 mg/ml there was a linear correlation between the peak area and concentration, with  $r^2 = 0.98$ – $0.99$ .

### 3.4. HPCE analysis of heparin-oligosaccharides

Heparin-oligosaccharides with the general structure IdoA2 (1 $\rightarrow$ 4)  $\alpha$ -D-GlcNY6X were analysed; they were detected at 200 nm using normal and reverse polarity. Their purity was confirmed using HPSEC and a peak purity check of the components [11]. The oligosaccharides migrated due to their mass and charge. The heparin-disaccharide (Fig. 3a) using was monosulfated, as was shown by co-injection experiments. Using reverse polarity, the heparin-disaccharides could be separated from tetra- and hexasaccharides. The hexasaccharides showed a shorter migration time than the heparin-tetrasaccharides.

An increase in the molecular mass of the heparin-oligosaccharides also increased the possibility of the simultaneous detection of heparin-oligosaccharides of different size and sulfation. Thus the large peak between 9 and 10 min of the heparin-oligosaccharides contains overlapped heparin-oligosaccharides. The oc-

tasaccharide was better resolved than the decasaccharide, which also illustrates the loss of resolution of longer heparin-oligosaccharides (Fig. 3). For higher oligosaccharides and a mixture of these, complete resolution was not possible.

In the normal mode, the migration of heparin-disaccharides interfered with higher oligosaccharides. Hence they could not be separated from tetrasaccharides and higher heparin-oligosaccharides (Table 1).

### 3.5. HPCE analysis of heparins and low-molecular-mass heparins

Different heparin preparations differ in their structure, molecular mass and sulfation [12]. All heparins and low-molecular-mass compounds used have similar degrees of sulfation, ranging from 2.1 to 2.3. The higher the sulfation of the compound, the shorter was the migration time. Chondroitin sulfates with a considerably lower degree of sulfation (1.1) showed longer migration times than heparins.

Changing the voltage or the pH of the buffer did not increase the resolution of heparin-disaccharides or those of heparins and of low-molecular-mass heparins. Heparins were detected at 200 nm. Modified heparins, produced by enzymatic cleavage or  $\beta$ -elimination, have an unsaturated uronic acid residue ( $\Delta$ UA) at their non-reducing end. Hence they exhibit an absorbance maximum at 230 nm and permit selective detection.

Heparin (4a, calcium salt) and heparin (4b, sodium salt) showed only minor differences in their resolution because their degree of sulfation and molecular mass were similar. The samples were of high purity and dissolved in water. The large peaks from 5.8 to 5.9 min could be attributed to the simultaneous detection of disulfated heparin-disaccharides, higher charged heparin chains and heparin-oligosaccharides of different lengths, whereas the peaks from 7.0 to 7.4 min co-migrated with monosulfated heparin-disaccharides. The peak areas, peak widths and migration times of the two heparin preparations differed.

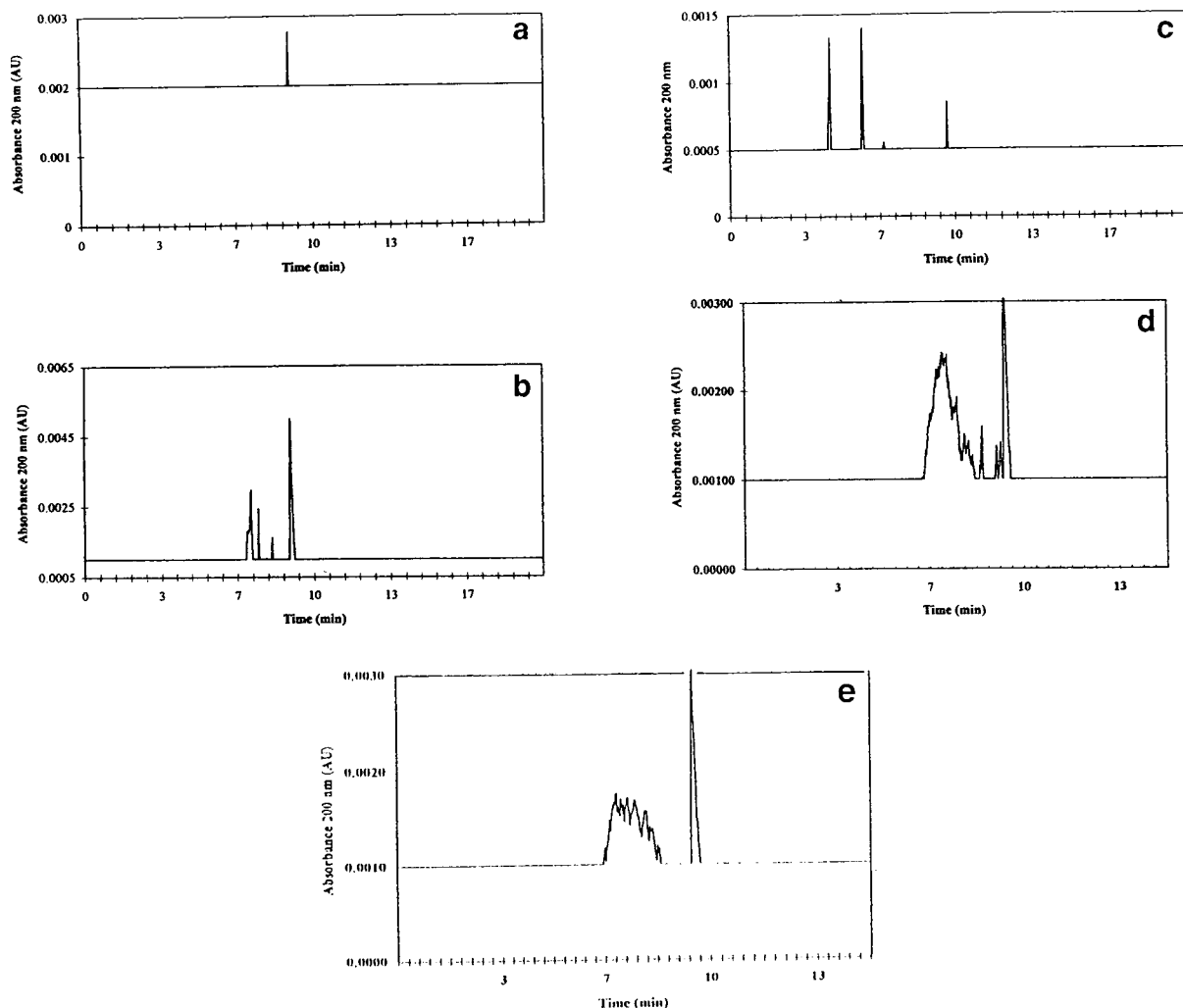


Fig. 3. Electropherograms of heparin-oligosaccharides of different chain length using reverse polarity. (a) Heparin-disaccharide; (b) heparin-tetrasaccharide; (c) heparin-hexasaccharide; (d) heparin-octasaccharide; (e) heparin-decasaccharide. The oligosaccharides migrate differently depending on their mass and charge. Experimental conditions: 20 mM phosphate buffer (pH 3.5), range (AU), 0.02; polarity, indirect; wavelength, 200 nm. For further conditions, see Experimental.

The simultaneous detection of heparin-oligosaccharides of different sizes and sulfation results in a characteristic electropherogram for each heparin preparation.

Fraxiparin (**4c**), Clexane (**4d**) and Fragmin (**4e**) reflect typical electropherograms of low-molecular-mass heparins. Compounds **4c** and **4e** have an end-terminal 2,5-anhydromannitol residue and similar molecular masses. The large

peak from 5.8 to 5.9 min could be assigned to the simultaneous detection of disulfated heparin-disaccharides and higher charged heparin chains and heparin-oligosaccharides of different lengths, whereas the peaks from 7.0 to 7.4 min co-migrated with monosulfated heparin-disaccharides. The peaks between 6.0 and 7.0 min are smaller heparin-oligosaccharides (tetrasaccharides). The peak areas, peak widths and

Table 1  
HPCE of heparin-oligosaccharides using normal polarity

Heparin-oligosaccharide	Migration time (min)	Peak area (AU)
Disaccharide	3.22	0.16
	3.89	0.56
	5.31	0.50
	5.73	0.14
Tetrasaccharide	3.37	0.19
	3.97	0.19
	4.32	0.09
	5.44	0.21
	5.72	0.10
Hexasaccharide	6.72	0.04
	3.12	0.18
	3.76	0.66
	4.04	0.59
	4.10	0.30
Octasaccharide	5.10	0.97
	3.01	0.26
	3.74	0.60
	4.16	0.18
Decasaccharide	5.00	0.48
	3.07	0.37
	3.72	0.91
	4.04	0.29
	5.00	0.73

The buffer system was 10 mM sodium tetraborate and 50 mM SDS (pH 8.8). Higher oligosaccharides were separated according to their charge and overlapped with lower oligosaccharides.

migration times of the two low-molecular-mass heparin preparations differed, however. Clexane (4d) is produced by  $\beta$ -elimination of a benzyl ester of heparin and contains an unsaturated uronic acid residue. The profile of this compound differs strongly from those of heparin and the other low-molecular-mass heparins.

Using reverse polarity for each heparin, a typical electropherogram was obtained (Fig. 4). This is due to the different structure, molecular mass and sulfation. Glycosaminoglycans structurally related to heparin show different migration profiles.

Using the normal polarity mode, no significant differences in the resolution were obtained for LMMH and heparins. The different migration times of the heparins did not correlate with their molecular mass or with the degree of sulfation.

### 3.6. PAGE– analysis of heparin-oligosaccharides

Heparins and LMMHs from different commercial sources were analysed by gradient PAGE using a modified Laemli system. The gels were stained using acridine orange. The sensitivity of the staining method ranged from 0.2 to 1.0  $\mu\text{g}$ . Defined heparin oligosaccharides ranging from di- to dodecasaccharide and heparin standards of molecular mass ranging from 11 000 to 21 000, which were prepared by HPSEC, were run by co-migration with LMMHs to standardize the PAGE. The equation obtained on plotting the  $R_F$  value ( $y$ ) versus the logarithm of the molecular mass ( $x$ ) was  $y = -0.30x + 1.81$  with  $r^2 = 0.99$ . These data indicated that the migration distance of the oligosaccharides in the gel was dependent on the molecular mass of the saccharide chains (Fig. 5).

### 3.7. PAGE analysis of heparins and low-molecular-mass heparins

An LMMH produced by nitrous acid showed defined bands ranging from tetra- to dodecasaccharide and could be used as an internal ladder of the molecular mass for PAGE [14]. The migration of their oligosaccharides corresponded to their molecular mass ( $r^2 > 0.98$ ). The bands showed a resolution of oligosaccharides of the LMMH that could be identified better than by staining with alcian blue or toluidine blue. Scanning the intensity of the bands at 548 nm, the average molecular mass  $M_m$  and the polydispersity ( $M_w/M_n$ ) of the LMMH were calculated.

The glycosaminoglycans samples were analysed by PAGE on five different days (Fig. 6). They showed a standard deviation of the average molecular mass  $M_m$  from 6.4 to 19.8% and of their polydispersity  $P$  from 0.7 to 10.2%. Table 2 shows the inequivalence of these heparins. For low-molecular-mass preparations  $M_n$  ranged from 3256 to 5107,  $M_m$  from 4629 to 9084 and  $M_z$  from 5291 to 11 354. The standard deviations of the LMMHs also differed significantly from 1.23 to 1.57 (Table 2). The polydispersity of the

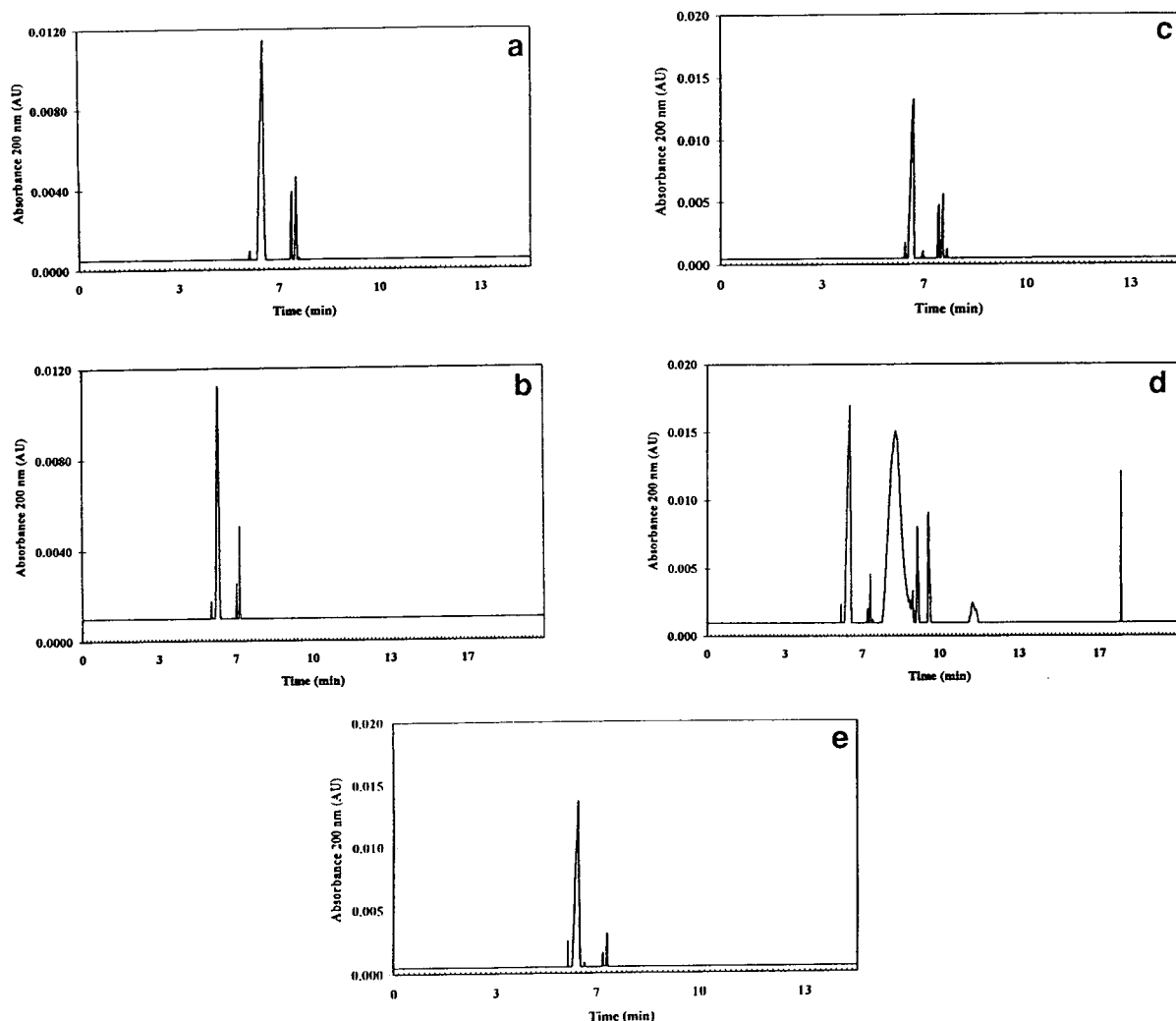


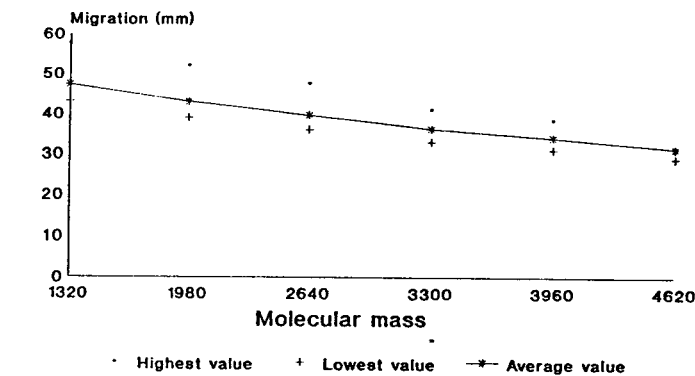
Fig. 4. Electropherograms of heparins and low-molecular-mass heparins. (a) Heparin (calcium) and (b) heparin (sodium) show only minor differences in their resolution because their sulfation and molecular mass were similar. (c) Fraxiparin; (d) Clexane and (e) Fragmin show electropherograms of low-molecular-mass heparins. Experimental conditions: 20 mM phosphate buffer (pH 3.5); range (AU), 0.02; polarity, indirect; wavelength, 200 nm. For further conditions, see Experimental.

compounds was always higher than 1.0, which represents an ideal homogeneous polymer.

#### 4. Discussion

Capillary zone electrophoresis of heparin-disaccharides was first described by Ampofo et al. [5]. The composition of heparin and heparin sulfate was determined with heparin-disaccha-

rides which were standardized by fast atom bombardment mass spectrometry. Two disaccharides,  $\Delta\text{UA (1}\rightarrow\text{4) GlcNS}$  and  $\Delta\text{UA 2S (1}\rightarrow\text{4) GlcNAc}$ , had very similar migration times and co-migrated on CZE analysis. The introduction of 50 mM SDS in 10 mM sodium borate without boric acid gave optimum resolution of the disaccharides used. The buffers described and the heparin-disaccharides were of the highest purity and were used to determine heparin-oligosac-



PAGE Analysis

Fig. 5. Migration of heparin-oligosaccharides in polyacrylamide gels. The migration in the gel was dependent on the molecular mass of the oligosaccharide. The gels contained 20–30% total acrylamide and 2–5% total N,N-bisacrylamide (pH 8.3). The electrophoresis was performed for 4 h at 80 V.

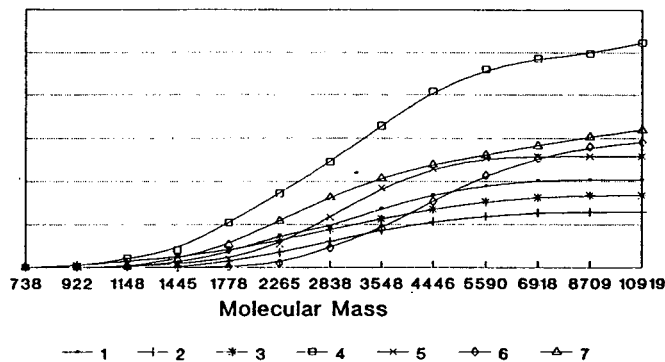


Fig. 6. Different molecular distributions of seven low-molecular-mass heparins using PAGE. For conditions, see Experimental.

Table 2

Inequivalence of the average molecular mass and polydispersity of heparins

Compound:	$M_m$	Polydispersity ( $P$ )
Heparin	11272 ± 837	1.48 ± 0.043
Clexane	4629 ± 208	1.27 ± 0.034
Fragmin	6441 ± 403	1.35 ± 0.094
Fraxiparin	5453 ± 1106	1.23 ± 0.019
LMMH-Braun	4774 ± 442	1.40 ± 0.027
LMMH-Merckle	9084 ± 186	1.37 ± 0.018
LMMH-Sandoz	5558 ± 186	1.57 ± 0.091
Reviparin	4903 ± 111	1.30 ± 0.033

PAGE was performed using a 20–30% total acrylamide and 2–5% total N,N-bisacrylamide (pH 8.3) linear gradient gel. Results are means of five runs ± S.D.

charides and heparins (see Experimental). Several standardized heparin-disaccharides also commercially available.

Reversing the polarity of the system gave a better resolution of longer oligosaccharides [13]. Tetrasaccharides of different structures were examined by Dam et al. [4] in the context of heparin that was cleaved by heparinases. The longer time of analysis, however, requires optimization, which was achieved by using a thinner capillary. Varying the applied voltage from 20 to 5 kV or the pH of buffer from 2.0 to 4.0 did not improve the resolution of heparin-oligosaccharides and heparins. The heparins used were of research quality and contained small amounts of ethanol (0.5–1%) and dermatan sulfate

(<1%). Contaminants in low-molecular-mass heparin preparations most likely represent synthetic precursors, although their identity is not known. It should be realized that, in general, detection based on UV absorption is much more sensitive for the synthetic substituents than for the end products, which may lead to an overestimation of contaminants.

Gradient PAGE has already been used for the determination of glycosaminoglycans [6]. Heparin and chondroitin sulfates in aqueous and endogenous fluids have been determined [7]. However, the method has not been run using smaller slab gels. This method needs a shorter run time, less material and buffer. Further, several slab gel units can be run in parallel. The method requires a molecular ladder to characterize the migration times.

Calculating the electrophoretic mobility may be a valuable parameter for characterizing various heparin-oligosaccharide fractions, because it is independent of voltage and the length of the gel. The mobility is dependent only on the buffer type, pH and temperature. This mobility can only be calculated for the resolving gel because the samples were first preconcentrated in the stacking gel. The difference in the voltage applied implies that the mobility would not be a better parameter than the migration time for characterizing the PAGE of the heparin oligosaccharides. The standard used (Reviparin) was an LMMH, which was produced by nitrous acid and showed clearly resolved bands that ranged from di- to tetradodecasaccharide.

A new staining procedure for glycosaminoglycans with acridine orange allowed a better resolution of the oligosaccharide bands compared with alcian blue (more defined bands could be detected). This difference may be due to the different molecular mass of alcian blue and acridine orange forming cation–anion complexes. Smaller molecules might be bound even by weaker interactions. The LMMHs were scanned five times on different days with a densitometer and their molecular mass was calculated as described previously [14].

The PAGE method presented could be automated to obtain more information about the

oligosaccharide composition of each heparin preparation.

A combination of PAGE and HPCE methods may be the best for the characterization of the different heparin preparations. PAGE analysis provides information about the composition of oligosaccharides fractions, which is most important with regard to the anticoagulant activity because the antifactor Xa, anti-thrombin activity and the neutralization of heparin require oligosaccharide chains of different chain length.

### Acknowledgements

This work was financially supported by the German Research Council (DFG), Grant Ha 1164/3-2, and the Faculty of Medicine, Mannheim, Germany.

### Abbreviations

GAGs, glycosaminoglycans; CZE, capillary zone electrophoresis; HPCE, high-performance capillary electrophoresis; HPSEC, high-performance size-exclusion chromatography; LMMH, low-molecular-mass heparin;  $D_p$ , degree of polymerization;  $P$ , polydispersity;  $M$ , average molecular mass;  $M_m$ , mass-average molecular mass;  $M_n$ , number-average molecular mass;  $M_z$ , z-average molecular mass; L-IdoA, L-iduronic acid; GlcNSO<sub>3</sub>, glucosamine N-sulfate; ΔUA, 4-deoxy-α-L-threo-hex-4-enopyranosyl uronic acid; GlcNAc, 2-deoxy-2-acetamidoglycopyranose; SAX, strong anion exchange; Am, anhydromannose; SDS, sodium dodecylsulfate.

### References

- [1] B. Casu, Adv. Carbohydr. Chem. Biochem., 43 (1985) 51–134.
- [2] P. Bianchini, H.B. Nader, H.K. Takahashi, B. Osima, A.H. Straus and C.P. Dietrich, J. Chromatogr., 196 (1980) 455.

- [3] H.B. Nader, H.K. Takahashi, J.A. Guimaães, C.P. Dietrich, P. Bianchini and B. Ozima, *Int. J. Biol. Macromol.*, 3 (1981) 356–360.
- [4] B.L. Damm, G.T. Overklift, B.W.M. Vermeulen, C.F. Fluitsma and G.W.K. van Dedem, *J. Chromatogr.*, 608 (1992) 297–309.
- [5] S.A. Ampofo, H.M. Wang and R.J. Linhardt, *Anal. Biochem.*, 199 (1991) 249–255.
- [6] K.G. Rice, M.K. Rottink and R.J. Linhardt, *Biochem. J.*, 244 (1987) 515–522.
- [7] R.J. Linhardt, D. Loganathan, A.A. Hakim, H.M. Wang, J.M. Walenga, D. Hoppensteadt and J. Fareed, *J. Med. Chem.*, 33 (1990) 1639–1645.
- [8] M. Petitou, P. Duchausson, I. Lederman, J. Choay and P. Sinay, *Carbohydr. Res.*, 179 (1988) 163–172.
- [9] J.M. Walenga, I. Bara, M. Petitou, M. Samama, J. Fareed and J. Choay, *Thromb. Res.*, 51 (1988) 23–33.
- [10] J. Hirsh and M.N. Levine, *Blood*, 1 (1992) 1–17.
- [11] J. Harenberg and J.X. de Vries, *J. Chromatogr.*, 261 (1983) 287–292.
- [12] R. Malsch and J. Harenberg, *Thromb. Haemostas.*, 70 (1993) 718–719.
- [13] A. Pervin, A.A. Hakim and R.J. Linhardt, *Anal. Biochem.*, 221 (1994) 182–188.
- [14] R. Malsch, J. Harenberg, M. Guerrini, G. Torri, B. Casu and D.L. Heene, *Sem. Thromb. Hemostas.*, 20 (1994) 135–143.





ELSEVIER

Journal of Chromatography A, 716 (1995) 269–277

JOURNAL OF  
CHROMATOGRAPHY A

## Capillary zone electrophoresis of organic acids in serum of critically ill children

Vladislav Dolník<sup>a,\*</sup>, Jana Dolníková<sup>b</sup>

<sup>a</sup>*Institute of Analytical Chemistry, Academy of Sciences of the Czech Republic, Veveří 97, CZ-611 42 Brno, Czech Republic*

<sup>b</sup>*Department of Anesthesiology, J.G. Mendel Faculty Children's Hospital, Černopolní 9, CZ-662 63 Brno, Czech Republic*

### Abstract

Capillary zone electrophoresis with indirect UV detection was found to be suitable for the determination of organic acids in serum. Serum can be analysed directly without any deproteination in a capillary coated with linear polyacrylamide. With 10 mM  $\epsilon$ -aminocaproic acid–10 mM mandelic acid (pH 3.8) as the operational electrolyte, anions such as pyruvate, phosphate, citrate, malate, acetoacetate and lactate can be determined in 12 min. In quantitative analysis, the calibration line for lactate is linear over the range 0–10 mM. The detection limit for citrate was 8  $\mu$ M. The effect of the chloride concentration on the migration times of minor peaks is discussed. The potential of the method was demonstrated by analysing sera from several critically ill children.

### 1. Introduction

A number of pathological states result in increases in the organic acid levels in blood. The increase in the level of some organic acids, so called acidaemia, can lead to a decrease in blood pH (i.e., acidosis), to acidotic coma and even to death. This is well described for lactic acidosis [1] and diabetic ketoacidosis [2,3]. The concentration of some acids need not necessarily influence the pH value of blood, but their values are related to some disorders, as shown for serum dicarboxylic acids in patients with Reye's syndrome [4], and have clinical significance as biochemical markers. For example, 2-ketoglutarate was shown to be a harbinger of hyperammonaemic coma [5]. In some cases, the con-

centration ratio between two organic acids gives more valuable information than the determination of a single acid: the concentration ratios of pyruvate to lactate [6,7] and acetoacetate to 3-hydroxybutyrate [8,9] are the best examples. The serum organic acid profiles, although studied by only few research groups, seem to be very promising for clinical chemistry [10,11].

Capillary electrophoresis has long been used for determination of organic acids in blood. Organic acids can be determined in serum directly by capillary isotachopheresis [12,13]. A good correlation has been found between the severity of disease and the isotachopheretic profile of serum organic acids [14]. Serum oxalate can be concentrated and detected by multi-column isotachopheresis [15]. Capillary isotachopheresis has been used for the determination of formate and glyoxalate in individuals intoxicated with methanol and ethylene glycol, respectively

\* Corresponding author. Present address: Molecular Dynamics, 928 E. Arques Avenue, Sunnyvale, CA 94086, USA.

[16,17]. Capillary zone electrophoresis can separate acid metabolites of phenylalanine in phenylketonuric urine [18] and organic acids in cerebrospinal fluid [19] and urine [20]. It has been used to separate lactate and pyruvate in a single erythrocyte [21].

This paper describes the use of capillary zone electrophoresis with indirect UV detection for the determination of serum organic acids in blood of critically ill children.

## 2. Experimental

Samples of blood (1 ml) were collected from selected paediatric patients by venipuncture. After coagulation of the blood, the samples were centrifuged for 10 min at 3000 rpm. Sera were collected and stored at  $-26^{\circ}\text{C}$  until analysis. In the initial experiments, sera were deproteinated by mixing with the same volume of acetone and centrifuged for 10 min at 10 000 rpm.

Vinylmagnesium bromide and furan were purchased from Aldrich (Milwaukee, WI, USA),  $\epsilon$ -aminocaproic acid,  $\beta$ -alanine and citramalic acid from Sigma (St. Louis, MO, USA) and mandelic, 2-ketoisocaproic, 2-ketocaproic, 2-ketomethylvaleric, 2-hydroxyphenylacetic, hippuric and phenylpyruvic acid from Fluka (Buchs, Switzerland). All other chemicals were obtained from Lachema (Brno, Czech Republic). Sodium acetoacetate was prepared by alkaline hydrolysis of ethyl acetoacetate [22].

A fused-silica capillary (75  $\mu\text{m}$  I.D., 360  $\mu\text{m}$  O.D.) was a gift from J&W Scientific (Folsom, CA, USA). The total length of the capillary was usually 60 cm with 45 cm to the detection window. The capillary was coated with linear polyacrylamide after previous vinylation of the capillary inner surface with vinylmagnesium bromide [23] so that the electroosmotic flow was completely eliminated. To prevent damage of the coating, the detection window was made by manually cutting off the polyimide layer [24].

The experiments were performed with a Crystal CE System, Model 310 (ATI Unicam, Cambridge, UK). Some experiments were performed with laboratory-made instrumentation [25]. A

Spectra 100 variable-wavelength detector (Thermo Separation Products, Palo Alto, CA, USA) was used to detect the separated zones. The highest sensitivity was found at a wavelength of 220 nm and therefore all analyses were monitored at this wavelength. The data were collected by using 4880 software (ATI Unicam) with reversed polarity of the signal.

## 3. Results and discussion

### 3.1. Selection of operational electrolyte

#### *Effect of pH*

The majority of organic acids of interest are weak acids with  $\text{p}K_{\text{a}}$  values in the range 2.5 (pyruvate) to 4.4 (3-hydroxybutyrate). Since it is well known that the best separation of weak acids and bases is achieved at pH values near to their  $\text{p}K_{\text{a}}$  values [12,18,26,27], this pH range represents the approximate pH interval in which the separation of the compounds of interest should be investigated. For indirect UV detection, a UV-absorbing co-ion is required, preferably with the  $\text{p}K_{\text{a}}$  value in the above estimated pH range. The initial experiments were performed with a model mixture; however, the electropherograms of real samples were found to be more useful for optimizing the separation conditions. Therefore, serum from a paediatric patient with severe respiratory insufficiency was used to find the optimum operational electrolyte. The identification of peaks was performed by simultaneous analysis of serum and the appropriate standards. The results are shown in Fig. 1. Since the polarity of the detection output was reversed, the non-UV-absorbing compounds provide positive peaks. The first peak behind the large skewed peak of chloride was not identified. It was shown, however, that it does not correspond to pyruvate, which is in this particular case overlapped by the chloride zone. The peak with a migration time of ca. 6 min corresponds to phosphate; as shown by detailed analysis, it also contains some other organic anions: 2-ketoglutarate, 2-ketoisovalerate (KIV), 2-ketomethylvalerate (KMV), etc. The next separated

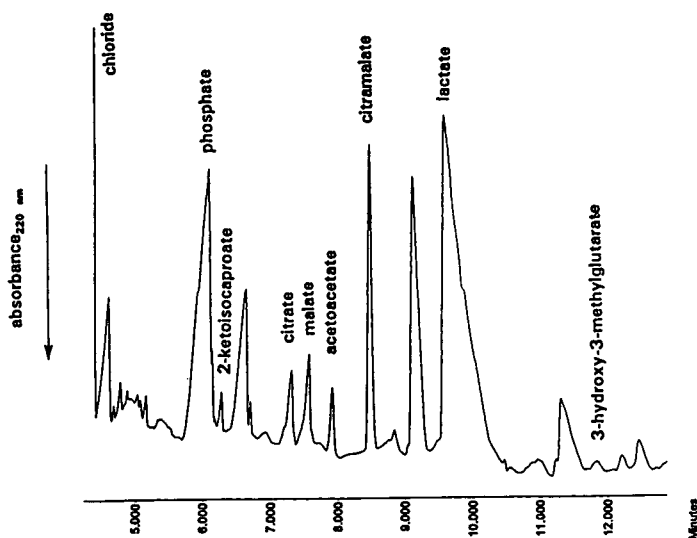


Fig. 1. Determination of acids in serum from a paediatric patient with respiratory insufficiency. Experimental conditions: linear polyacrylamide-coated capillary, 75  $\mu\text{m}$  I.D., 360  $\mu\text{m}$  O.D., total length 508 mm, effective length 413 mm; operational electrolyte, 10 mM  $\epsilon$ -aminocaproic acid–10 mM mandelic acid; voltage, –20 kV; detection, absorption at 220 nm. Undiluted serum sampled by pressure of 100 mbar for 6 s.

peak corresponds to 2-ketoisocaproate (KIC) and may contain glyoxalate. The next peak was not identified. The triplet of peaks with migration times between 7 and 8 min are citrate, malate and acetoacetate. The peak with a migration time of ca. 8.5 min was identified as citramalate. The skewed peak with a migration time of 9.8 min corresponds to lactate and the minor peak with a migration time of 11.8 min is 3-hydroxy-3-methylglutarate.

The effect of various operational electrolytes on the separation of the acids of interest is shown in Fig. 2. With an operational electrolyte containing 10 mM  $\epsilon$ -aminocaproic acid (EACA) and 10 mM 2-hydroxyphenylacetic acid (pH 4.35), several peaks of acids with higher  $\text{p}K_{\text{a}}$  appear in the electropherogram, including 3-hydroxybutyrate with a migration time of 15.8 min. However, the peaks between phosphate and lactate are only partially resolved (trace a). Trace b shows electropherogram of the test serum, when 10 mM  $\epsilon$ -aminocaproic acid (EACA)–10 mM mandelic acid (pH 3.83) was used as the operational electrolyte (this trace is almost identical with the electropherogram in

Fig. 1). The peaks between phosphate and lactate are well resolved, although the phosphate peak still contains some other acids. 3-Hydroxybutyrate has a migration time >35 min at this pH (not shown). When EACA ( $\text{p}K_{\text{a}} = 4.3$ ) is replaced with  $\beta$ -alanine ( $\text{p}K_{\text{a}} = 3.55$ ), so that the operational electrolyte contains 10 mM  $\beta$ -alanine–10 mM mandelic acid (pH 3.51), trace c is obtained. In this case, the migration times of lactate and other anions increase and the shape of their peaks is more deformed owing to electromigration dispersion. However, the separation in the vicinity of phosphate is not improved in comparison with trace b. The electropherogram of serum acids in the operational electrolyte 10 mM  $\beta$ -alanine–10 mM hippuric acid (pH 3.6) is shown as trace d. In this case, the migration times are not changed significantly, only the skewed shape of the slower peaks is reversed as a result of a higher mobility of the co-ion. Even more acidic operational electrolytes were tested (e.g., 10 mM picric acid). Unfortunately, the capillary frequently became plugged with these operational electrolytes, probably as a result of denaturation of serum proteins. We

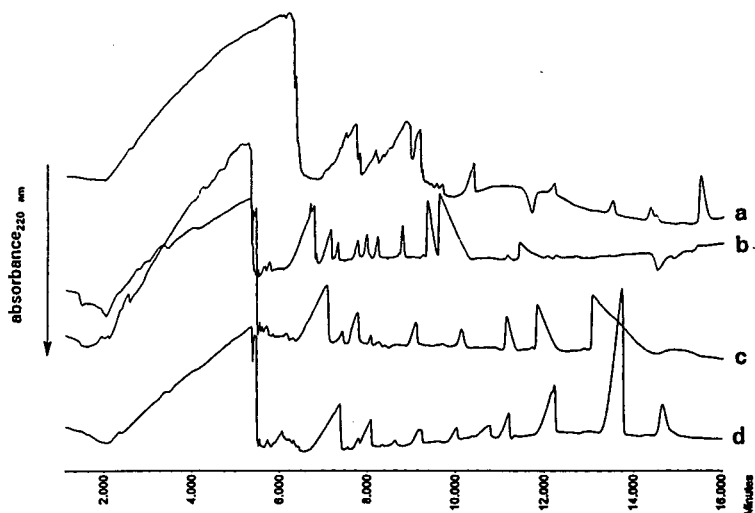


Fig. 2. Effect of pH of the operational electrolyte on the separation of serum acids. Experimental conditions: linear polyacrylamide-coated capillary, 75  $\mu\text{m}$  I.D., 360  $\mu\text{m}$  O.D., total length 550 mm, effective length 455 mm; operational electrolyte, (a) 10 mM  $\epsilon$ -aminocaproic acid–10 mM 2-hydroxyphenylacetic acid (pH 4.35); (b) 10 mM  $\epsilon$ -aminocaproic acid–10 mM mandelic acid (pH 3.83); (c) 10 mM  $\beta$ -alanine–10 mM mandelic acid (pH 3.51); (d) 10 mM  $\beta$ -alanine–10 mM hippuric acid (pH 3.6); voltage,  $-24$  kV; detection, absorption at 220 nm. Undiluted serum as in Fig. 1 sampled by pressure of 100 mbar for 6 s.

consider the possibility of determining serum acids directly without any previous deproteinization to be one of the major advantages of capillary electrophoresis and therefore more acidic operational electrolytes were not tested further.

Based on these results, the operational electrolyte containing  $\epsilon$ -aminocaproic acid as counter ion and mandelic acid as the UV-absorbing co-ion was used in all subsequent experiments. The main disadvantages when using this operational electrolyte are the long migration time of 3-hydroxybutyrate, especially in comparison with isotachopheresis, where all serum acids including 3-hydroxybutyric acid are determined in a reasonable time [12], and significant asymmetry of some peaks. However, preliminary experiments indicated that this problem may be solved by introducing a pH gradient or pH step into the separation capillary [28,29].

#### Effect of concentration

To achieve a reasonable detection sensitivity in capillary zone electrophoresis with indirect

UV detection, the co-ion of the operational electrolyte must absorb UV light, whereas the counter ion should be transparent at the given wavelength. The detected substance partially replaces the co-ion in its zone, which results in a reduced UV absorption when the  $\omega$ -function is kept constant.

The effect of the concentration of the operational electrolyte was investigated using an equimolar mixture of  $\epsilon$ -aminocaproic acid as counter ion and mandelic acid as co-ion, analysing the serum as above. The results are shown in Fig. 3. The concentration of the operational electrolyte determines the value of the  $\omega$ -function and thus the maximum concentration of chloride which can be reached in its zone. Because of this limit, the volume of the chloride zone and the migration time of the rear boundary of the chloride zone decrease with increasing electrolyte concentration.

For the detection sensitivity, it holds that the lower the concentration of the operational electrolyte, the higher is the relative concentration of the detected substances in their zones. Simul-

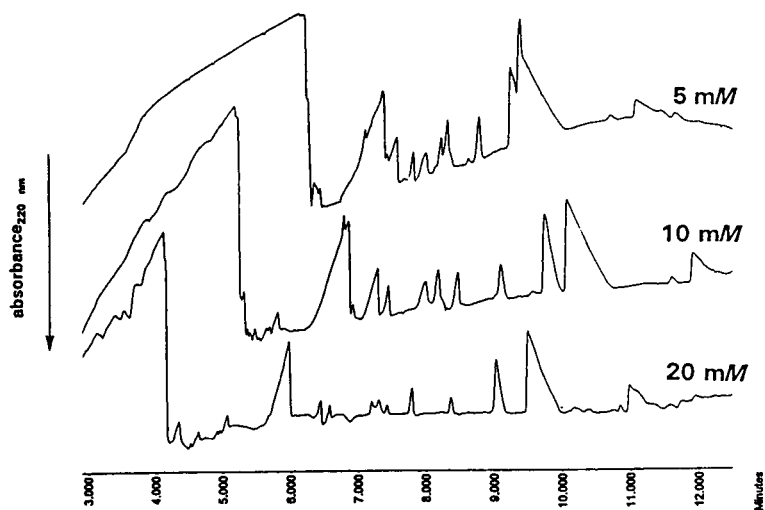


Fig. 3. Effect of concentration of the operational electrolyte on the separation of serum acids. Experimental conditions as in Fig. 2. Operational electrolyte, 5–20 mM  $\epsilon$ -aminocaproic acid–5–20 mM mandelic acid.

taneously, some disturbing effects such as noise and baseline drift are more pronounced at lower concentrations of the operational electrolyte. This is demonstrated in Fig. 3: in 5 mM operational electrolyte, a high detection sensitivity is achieved when a significant baseline drift is observed. In 20 mM operational electrolyte, the baseline drift is almost negligible, but the detection sensitivity is reduced. A concentration of 10 mM seems to be an acceptable compromise.

### 3.2. Effect of chloride concentration on migration times

Several effects of increasing concentration of the major compound (chloride) in the sample were observed which influence the migration of minor compounds. Chloride has a higher mobility than the co-ion (mandelate) so that during analysis there is a lower electric field strength in the chloride zone. At constant voltage, since the electric current is constant through the whole capillary, the electric field out of the chloride zone is higher than the average calculated value. An inhomogeneous electric field strength results in shorter migration times and higher absolute values of the apparent mobilities of the anions of

interest with increasing amount of injected chloride. The effect is demonstrated in Fig. 4 in the chloride concentration range 0–15 mM. (Obviously, a reversed effect of low-mobility anions can be expected and actually was observed in sera with a higher content of lactate.) When the concentration of chloride increases further, other effects appear. Starting from a certain amount of chloride, sample self-stacking occurs [30] and

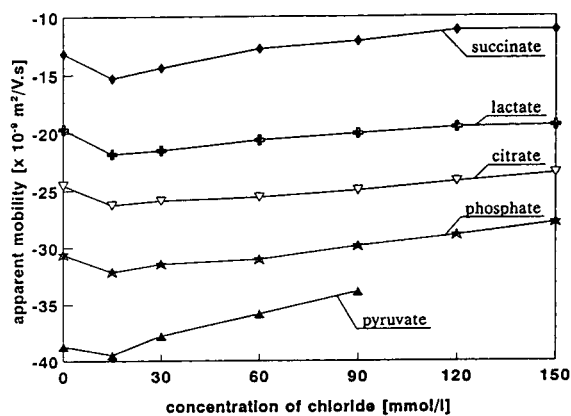


Fig. 4. Effect of concentration of chloride in sample on the apparent mobility of selected anions at constant voltage. Separation conditions as in Fig. 1. Apparent mobilities calculated as  $\mu_{app} = l_t l_{eff} / V t_m$ .

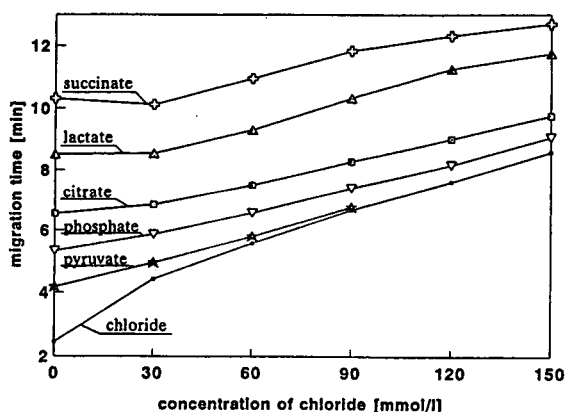


Fig. 5. Effect of concentration of chloride in sample on the migration times of selected anions at constant driving current. Experimental conditions: linear polyacrylamide-coated capillary, 75  $\mu\text{m}$  I.D., 360  $\mu\text{m}$  O.D., total length 600 mm, effective length 450 mm; operational electrolyte, 10 mM  $\epsilon$ -aminocaproic acid–10 mM mandelic acid; driving current,  $-11 \mu\text{A}$ ; detection wavelength, 220 nm. Model mixture sampled by pressure of 100 mbar for 6 s.

minor compounds are retained in the chloride zone. This is why the pyruvate peak does not appear in all runs. Some other effects can be expected which contribute to the mobility shift, such as a pH decrease in the chloride zone in comparison with the operational electrolyte and a lower electric field in the chloride zone. The larger the amount of chloride, the longer the compounds of interest stay in the mixed zone with chloride and, because of the lower pH value, they acquire lower ionization and, thus, a lower absolute value of the apparent mobility. Slower compounds with higher  $pK_a$  (e.g., succinate) leave the chloride zone sooner than those with lower  $pK_a$ , but the effect of slower pH (resulting in a more pronounced decrease in ionization) still influences their effective mobility. Simultaneously, the lower electric field strength in the chloride zone results in lower absolute values of the apparent mobilities of the anions of interest.

In the constant-current regime, the applied voltage varies during analysis, which is why migration times are used to describe the following experiments. In this case, the electric field strength out of the chloride zone is not affected

by the amount of chloride injected. However, at lower concentrations of chloride, we can see acceleration of slower anions (i.e., anions with higher  $pK_a$ , such as succinate and partially lactate) with increasing concentration of chloride (Fig. 5). This may be caused by faster migration of these anions in the zone of the original sample if this has higher pH. At higher concentrations of chloride, the same effects are observed as at constant voltage.

These effects have a significant practical impact: in samples of biological origin, the content of the major compound chloride varies, which results in variation of the migration times of the same compound when analyzing different samples. This has to be taken into account when identifying the particular peaks in the sample. Since the time period during which the zone stays in detector is also affected by mobility variations, these effects can also influence the quantitative analysis.

### 3.3. Quantitation and detection limit

Quantitative analysis was performed only for lactate and the calibration line is given in Fig. 6. It is linear in the range 0–10 mM. Although the lactate peaks are significantly skewed in the

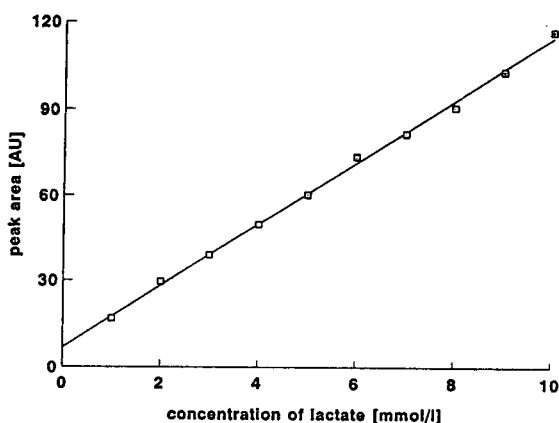


Fig. 6. Calibration graph for determination of lactate. Experimental conditions: linear polyacrylamide-coated capillary, 75  $\mu\text{m}$  I.D., 360  $\mu\text{m}$  O.D., total length 650 mm, effective length 500 mm; operational electrolyte, 10 mM  $\epsilon$ -aminocaproic acid–10 mM mandelic acid; voltage,  $-26 \text{ kV}$ ; detection wavelength, 220 nm. Samples injected by pressure of 100 mbar for 6 s.

operational electrolyte EACA–mandelic acid, the correlation coefficient of this line is 0.998. This permits the determination of lactate in real samples to be performed.

Of the minor anions found in sera, citrate was selected as a model compound for the determination of the detection limit. Citric acid was determined in the concentration range 1–10  $\mu\text{M}$ . The lowest concentration of citrate providing an observable peak was 8  $\mu\text{M}$ , and this value was taken as the detection limit.

### 3.4. Practical examples

We analysed sera from patients hospitalized in the Intensive Care Unit, J.G. Mendel Faculty Children's Hospital, Brno, during September–December 1994. Sera were analysed without prior deproteination. No significant plugging of the capillary by serum proteins precipitated during analysis was observed if the capillary was rinsed sufficiently between runs. Depending on the patients' condition, we found various acid profiles in the sera analysed. Typical peaks,

which were present in all the samples analysed, were phosphate and lactate. Pyruvate frequently did not appear in the electropherogram since it was overlapped by the chloride peak. Citrate, malate and acetoacetate, which form a triplet of peaks in the centre of the chloride–lactate area, were sometimes incomplete, as some of these anions (most frequently malate) were present at levels below the detection limit.

Fig. 7 shows two electropherograms of serum from the same patient suffering from meningoencephalitis and from a perforated duodenal ulcer and the resulting shock. Trace a corresponds to the analysis of the blood taken shortly after a repeated cardiopulmonary resuscitation. The large peak of lactate, resulting from insufficient oxygenation, which corresponds to a lactate concentration of 14.8 mM, confirms clearly the severity of the patient's state. Trace b corresponds to the analysis of blood taken 2 days later when the patient's state had stabilized; the peak of lactate is reduced, corresponding to a concentration of 2.1 mM. Two peaks migrating in front of lactate were not observed in trace a

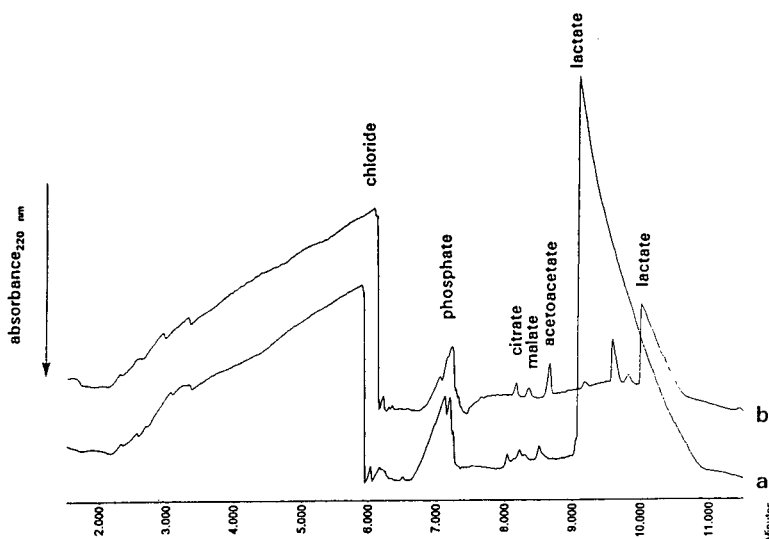


Fig. 7. Determination of acids in serum from a paediatric patient in shock. Experimental conditions: linear polyacrylamide-coated capillary, 75  $\mu\text{m}$  I.D., 360  $\mu\text{m}$  O.D., total length 600 mm, effective length 500 mm; operational electrolyte, 10 mM  $\epsilon$ -aminocaproic acid–10 mM mandelic acid; voltage, –24 kV; detection, absorption at 220 nm. Undiluted serum sampled by pressure of 100 mbar for 6 s. (a) Analysis after repeated cardiopulmonary resuscitation; (b) analysis 2 days later, when the patient's state had stabilized.

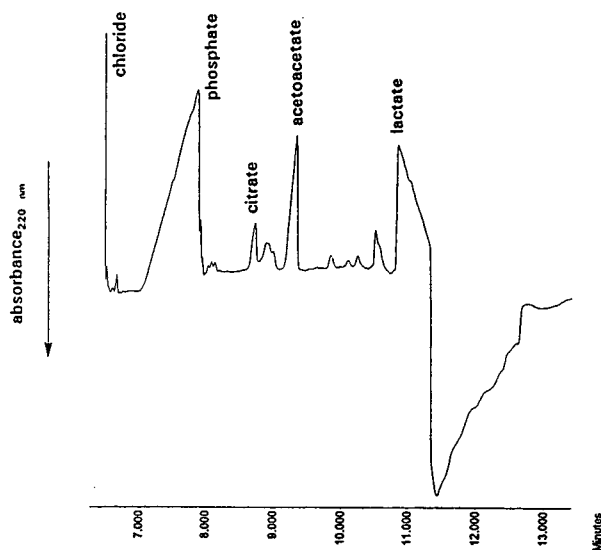


Fig. 8. Determination of acids in serum from a paediatric patient with respiratory insufficiency. Experimental conditions as in Fig. 7.

since they were probably overlapped by the lactate peak.

Fig. 8 shows an electropherogram of serum from a patient suffering from congenital heart malformation, bronchopneumonia, overall dystrophy and respiratory insufficiency. Several peaks are significant, e.g., the increased peak of acetoacetate and especially the UV-absorbing peak migrating behind lactate, which was not identified (hippurate migrates in model mixtures in this position; however, analysis of this sample at various pH values showed that this UV-absorbing peak is not hippurate).

Fig. 9 shows an electropherogram of serum from a patient with severe craniocerebral injury. There is a pair of unidentified peaks migrating in front of phosphate, several peaks co-migrating with phosphate and increased peaks of acetoacetate and lactate.

Analysis of serum from a patient with multiple trauma and brain injury is shown in Fig. 10. A large peak of phosphate dominates this electropherogram and obviously it is not clear how many compounds may be hidden by it. It is likely

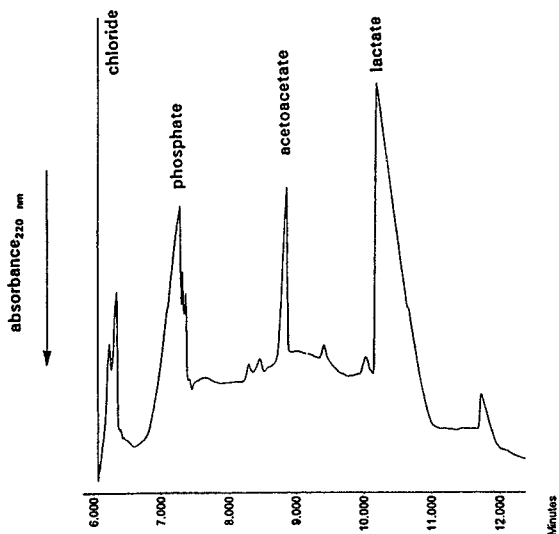


Fig. 9. Determination of acids in serum from a paediatric patient with severe head injury. Experimental conditions as in Fig. 7.

that phosphate is a minor compound in this peak. A similar profile was observed when analysing uraemic sera by capillary isotachopheresis [14].

#### 4. Conclusion

Capillary zone electrophoresis has been demonstrated to be a suitable method for the determination of organic acids in real samples of serum. It does not require deproteination of sera prior to analysis and provides valuable results in ca. 12 min.

#### Acknowledgements

The authors thank ATI Unicam, Cambridge, UK, and Chromspec, Prague, Czech Republic, for providing the full instrumentation for capillary electrophoresis. A gift of a silica capillary from J&W Scientific (Folsom, CA, USA) is also acknowledged. The authors thank Dr. Petr



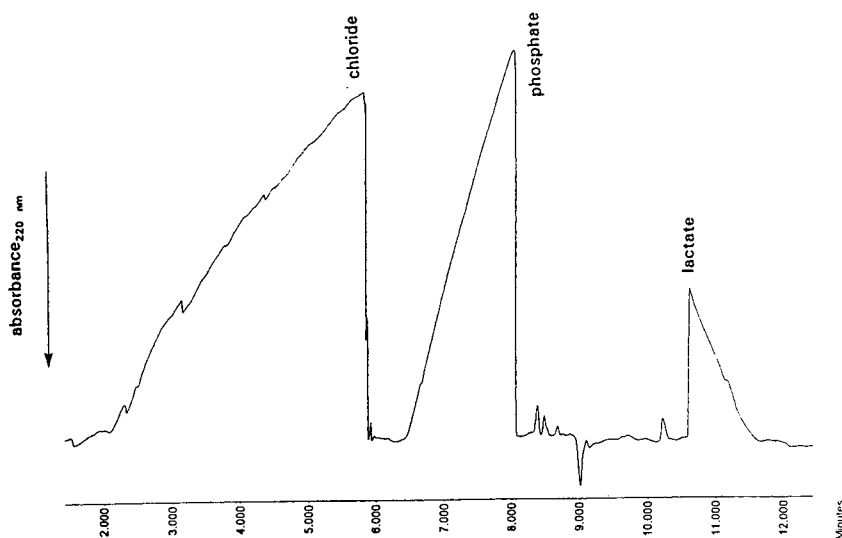


Fig. 10. Determination of acids in serum from a paediatric patient with multiple trauma. Experimental conditions as in Fig. 7.

Gebauer for discussions of the sample self-stacking phenomena.

## References

- [1] V.L. Hood and R.L. Tannen, *Mineral Electrolyte Metab.*, 9 (1983) 317.
- [2] P.W. Felts, *Med. Clin. North Amer.*, 67 (1983) 831.
- [3] M.A. Sperling, *Pediatr. Clin. North Am.*, 31 (1984) 591.
- [4] J.H. Tonsgard, *J. Pediatr.*, 109 (1986) 440.
- [5] M.L. Batshaw, M. Walser and S.W. Brusilow, *Pediatr. Res.*, 14 (1980) 1316.
- [6] S.H.G. Allen, R. Rahm and D.M. Shah, *Circ. Shock*, 11 (1983) 13.
- [7] P. Chariot, M. Monnet, M. Rohr, J.P. Jefaucheur, M.L. Dubreuillemaire, M. Chousterman and R. Gherardi, *Arthritis Rheum.* 37 (1994) 583.
- [8] M. Yamamoto, J. Tanaka, K. Ozawa and T. Tobe, *J. Surg. Res.*, 28 (1980) 124.
- [9] T. Tani, Y. Taki, H. Aoyama, A. Jikkoh, S. Arii, K. Ozawa and T. Tobe, *Life Sci.*, 35 (1984) 1177.
- [10] D. Issacher, J.F. Holland and C.C. Sweeley, *Anal. Chem.*, 54 (1982) 29.
- [11] G.F. Hoffmann, C.K. Seppel, B. Holmes, L. Mitchell, H.J. Christen, F. Hanefeld, D. Rating and W.L. Nyhan, *J. Chromatogr.*, 617 (1993) 1.
- [12] V. Dolník and P. Boček, *J. Chromatogr.*, 225 (1981) 455.
- [13] V. Dolník and P. Boček, *J. Clin. Chem. Clin. Biochem.*, 19 (1981) 654.
- [14] V. Dolník and V. Doležalová, unpublished results.
- [15] V. Dolník, M. Deml and P. Boček, *Electrophoresis*, 9 (1988) 839.
- [16] S. Øvrebø, D. Jacobsen and O.M. Sejersten, in J.C. Holloway (Editor), *Analytical and Preparative Isotachopheresis*, Walter de Gruyter, Berlin, 1984, p. 261.
- [17] S. Øvrebø, D. Jacobsen and O.M. Sejersted, *J. Chromatogr.*, 416 (1987) 111.
- [18] V. Dolník, *J. Microcol. Sep.*, 6 (1994) 63.
- [19] A. Hiraoka, J. Akai, I. Tominaga, M. Hattori, H. Sasaki and T. Arato, *J. Chromatogr. A*, 680 (1994) 243.
- [20] M. Shirao, R. Furuta, S. Suzuki, H. Nakazawa, S. Fujita and T. Maruyama, *J. Chromatogr. A*, 680 (1994) 247.
- [21] Q.F. Xue and E.S. Yeung, *J. Chromatogr. A*, 661 (1994) 287.
- [22] R.C. Kreuger, *J. Am. Chem. Soc.*, 74 (1952) 5536.
- [23] K.A. Cobb, V. Dolník and M. Novotny, *Anal. Chem.*, 62 (1990) 2478.
- [24] V. Dolník and M. Novotny, *Anal. Chem.*, 65 (1993) 563.
- [25] V. Dolník and L. Skurský, *J. Chromatogr. A*, 680 (1994) 455.
- [26] P. Boček, M. Deml, P. Gebauer and V. Dolník, *Analytical Isotachopheresis*, VCH, Weinheim, 1988.
- [27] V. Dolník, J. Liu, J.F. Banks, Jr., M.V. Novotny and P. Boček, *J. Chromatogr.*, 480 (1989) 321.
- [28] J. Pospíchal, M. Deml and P. Boček, *J. Chromatogr.*, 470 (1989) 43.
- [29] J. Sudor, J. Pospíchal, M. Deml and P. Boček, *J. Chromatogr.*, 545 (1991) 331.
- [30] P. Gebauer, W. Thormann and P. Boček, *J. Chromatogr.*, 608 (1992) 47.





ELSEVIER

Journal of Chromatography A, 716 (1995) 279–290

JOURNAL OF  
CHROMATOGRAPHY A

# Utilization of fluorescein sodium salt in laser-induced indirect fluorimetric detection

## II. Application to organic anions

A.M. Desbène<sup>a,b,\*</sup>, C.J. Morin<sup>a,b</sup>, N.L. Mofaddel<sup>a,b</sup>, R.S. Groult<sup>c</sup>

<sup>a</sup>Laboratoire d'Analyse des Systèmes Organiques Complexes, Université de Rouen, I.U.T., 43 Rue Saint Germain, 27000 Evreux, France

<sup>b</sup>I.F.R.M.P., Université de Rouen, 76134 Mont Saint Aignan Cedex, France

<sup>c</sup>Beckman France, 92 Chemin des Bourdons, 93220 Gagny, France

### Abstract

Previously, we have used the fluorescein sodium salt to generate the background signal in the indirect fluorimetric detection of inorganic cations (alkaline, alkaline earth metals and transition metals) separated by capillary zone electrophoresis (CZE). In this work, we report that the use of fluorescein sodium salt can be extended to the detection of organic anions. A study of the detection thresholds and of reproducibility (elution times and effective electrophoretic mobilities) was performed. As samples we used, on the one hand, a mixture of *n*-alkane sulfonates (from C<sub>1</sub> to C<sub>10</sub>) and, on the other hand, a mixture of carboxylic acids (from C<sub>1</sub> to C<sub>18</sub>). Under the optimal conditions, detection thresholds of about 700 to 800 ppb were obtained and the reproducibility of effective electrophoretic mobilities was characterized by a relative standard deviation of about 0.5%. Calibration curves were also established (correlation coefficients were found to be between 0.995 and 0.9998). Finally, we compared the evolution of the experimental response coefficients of these two series of samples as a function of alkyl chain length with theoretical response coefficients obtained from findings reported by Ackermans et al. [J. Chromatogr., 549 (1991) 345].

### 1. Introduction

High-performance capillary electrophoresis (HPCE) is a rapidly expanding separation technique which has been successfully used in a wide range of analytical problems involving both inorganic anions and cations and neutral or potentially ionizable molecules [1,2]. A disadvantage, however, is the lack of a sensitive, generally applicable detector. An interesting way of overcoming this drawback was to use indirect detec-

tion. Indirect detection is now widely used in capillary electrophoresis for the determination of both organic and inorganic compounds that do not possess a suitable detection property [3,4].

In ionic capillary electrophoresis, which is used for the determination of both anions [5–15] and cations [16–33], detection is essentially performed via indirect UV detection.

As laser-induced fluorimetric detection is now commercially available, we recently considered the development of a new electrophoretic system with which indirect fluorimetric detection could be used, and without detector modification.

\* Corresponding author.

Taking into account the characteristics of the laser associated with the commercial fluorimetric detector, we investigated the potential of the sodium salt of fluorescein as a fluorescent reagent in order to detect alkaline, alkaline earth and transition metals separated by capillary zone electrophoresis (CZE) [34]. In view of the very satisfactory results, we have now decided to extend this work to organic anions which have no chromophoric or fluorophoric group (*n*-alkane sulfonates and linear carboxylic acids) to study the sensitivity of indirect fluorimetric detection.

In the first instance, *n*-alkane sulfonates, which are consumed on a large scale in industrial and commercial formulations, were determined without derivatization in CZE. Various strategies had already been developed in indirect UV detection [5,35,36], with and without an electroosmotic flow reverser. Recently, with the aim of optimizing detector sensitivity, Shamsi and Danielson [36] tested various naphthalene sulfonates as chromophoric ions.

Determination of carboxylic acids in a similar way, to which much effort is being devoted since they are commonly used for the preparation of ionic and zwitterionic surfactants, is difficult because: (i) on the one hand, they are amphiphiles as a result of the strong polarity of the carboxylic group and of the weak affinity of their alkyl chain for water ( $> C_{12}$ ), (ii) on the other hand, they have no chromophoric group which would allow detection in the classical UV range.

A variety of techniques has been proposed for such analyses [37–46]; all, however, have drawbacks. For example, in gas-phase chromatography, derivatization is required to obtain satisfactory sensitivity or volatility. And absorption phenomena are a hazard, in particular with the techniques in which a solid stationary phase is used.

In such conditions, capillary electrophoresis has already been investigated as an alternative method. The carboxylic acids have been analyzed using isotachopheresis with hydro-alcoholic media [46,47], MEKC [48] and, in particular, CZE. With respect to this last technique, different detection methods have been reported: di-

rect UV detection at low wavelength [49], conductimetry [17–19] and, in by far the greatest number of studies, indirect UV detection [5,8,36,48,50,51].

Moreover, different systems have been proposed for the determination of mono-, di- and even tricarboxylic acids. In the case of polycarboxylic acids the electroosmotic flow has often been modified by the addition of cationic surfactant [5,8,48].

In view of the dearth of analyses for long-chain carboxylic acids (from  $C_8$  to  $C_{18}$ ), we undertook the study of their separation and of the potential of fluorimetric detection in this application. We used the electrophoretic medium based on the utilization of the fluorescein sodium salt that we had previously developed to analyze cations [34].

In order to establish its broader applicability, we tested this new electrophoretic medium in analyses to determine the whole range of commercially available *n*-alkane sulfonates, i.e. from  $C_1$  to  $C_{10}$ .

## 2. Experimental

### 2.1. Reagents

All solutions, electrolytes and standards were prepared using 18 M $\Omega$  water generated by an Alpha Q Laboratory water-purification system (Millipore, Bedford, MA, USA). The *n*-alkane sulfonates (purity  $> 98\%$ ) and linear carboxylic acids (purity  $> 98\%$ ) were obtained, respectively, from Aldrich (Aldrich France, La Verpillière, France) and from Janssen (Janssen Chimica, Noisy le Grand, France). Sodium tetraborate (99.999% purity), used for the preparation of buffers, was purchased from Aldrich France. The cosolvents used, on the one hand, to modify the electroosmotic flow and, on the other hand, to solubilize the long-chain carboxylic acids were all of RS grade for high-performance liquid chromatography (HPLC) and were purchased from Carlo Erba (Rueil Malmaison, France). In order to solubilize the longest carboxylic acids, a polyoxyethylenic surfactant resulting from the

condensation of ethylene oxide on a  $C_{12}$  fatty alcohol was used. This hexaethylene glycol mono-*n*-dodecyl ether (purity >99%) was purchased from Nikko (Nikko Chemicals, Tokyo, Japan). Finally, the fluorescein sodium salt providing the fluorescence background was purchased from Aldrich France. All chemicals were used without further purification.

## 2.2. Electrolyte and standard preparation

The electrolytes used were prepared from solutions made up fresh each day containing the sodium tetraborate buffer. After dilution, electrolytes were systematically degassed for 20 min using sonication and their pH was measured before use. All the vessels used for the preparation of the solutions to be analyzed and of the electrolytes were made of polypropylene (Polylabo Block, Strasbourg, France). The disposable sample vials were made of siliconized polypropylene and were also purchased from Polylabo Block. Finally, the dilutions were performed using Gilson electronic automatic pipettes (Gilson France, Villiers le Bei, France) equipped with disposable polypropylene cones.

## 2.3. Apparatus

All experiments were carried out on a P/ACE 2100 System (Beckman, Fullerton, CA, USA) fitted with an on-column Argon-laser-based fluorescence detector ( $\lambda_{\text{excitation}} = 488 \text{ nm}$ ,  $\lambda_{\text{emission}} = 520 \text{ nm}$ ) and monitored by PS/2 computer (IBM, Greenock, UK) using the PACE or GOLD 7.11 software (Beckman). Data collection was performed using the same software. Samples were loaded by pressure injection [injection pressure 3447.38 Pa (0.5 psi)] into a fused-silica capillary. Before use the following solutions were flushed through the capillary, in the order given: 0.1 M NaOH, water and finally the buffer solution. The untreated fused-silica capillaries were 50  $\mu\text{m}$  I.D. and 57 cm in length. Injections were done at the high-voltage anode and organic anions were eluted to the earthed electrode. Indirect fluorimetric detection was performed at  $\lambda = 520 \text{ nm}$  through the capillary at a distance of

50 cm from the inlet. Finally, the pH values of the electrolytes were measured using a Beckman Model  $\phi$  pH meter at the analysis temperature.

## 3. Results and discussion

In a previous study [34], we showed that the sensitivity of the detector response was a function of: (i) on the one hand, the pH of the electrophoretic medium, because of the nature of the fluorescent reagent used to generate the background signal, i.e. fluorescein; (ii) on the other hand, as also found by Yeung and Khur [4], the concentration of the fluorophoric agent (here, fluorescein).

In the present work, therefore, we systematically performed the separations of *n*-alkane sulfonates and of carboxylic acids in basic media (pH = 9), at a  $10^{-5} \text{ M}$  concentration of the sodium salt of fluorescein, i.e. under the best conditions with respect to the sensitivity of the detection system [34].

### 3.1. Analysis of a mixture of $C_1$ to $C_{10}$ *n*-alkane sulfonates

In order to optimize the separation of this complex mixture of surfactants we studied the influence of ionic strength on the electrophoretic behaviour of the analytes. The effect of buffer concentration was investigated in the range 2.5–30 mM, 2.5 mM being the minimum that gives a buffer effect. The evolution of the effective electrophoretic mobilities of the different *n*-alkane sulfonates as a function of the ionic strength of the electrophoretic medium is reported in Fig. 1.

This figure shows clearly that the selectivity of the electrophoretic system, which is measured by the difference between the effective electrophoretic mobilities of the analytes taken two by two [1,2], evolves only to a very small extent, or perhaps even not at all, as a function of ionic strength. However, whatever the *n*-alkane sulfonate, its effective electrophoretic mobility increases when the ionic strength of the electrolyte decreases. Considering that the aim of this study

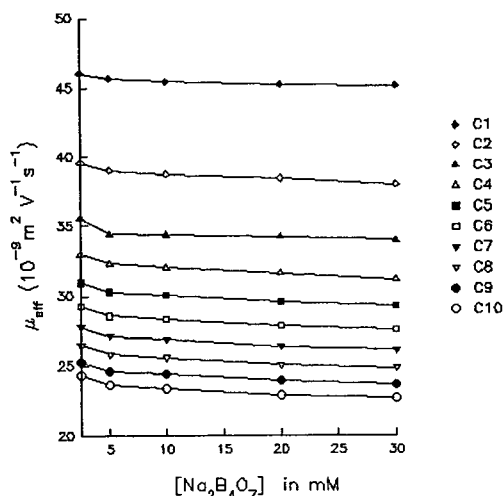


Fig. 1. Evolution of the effective electrophoretic mobilities of alkane sulfonates as a function of the borate concentration in the electrophoretic medium. Experimental conditions: fused-silica capillary: 57 cm  $\times$  50  $\mu$ m I.D.; electrolyte:  $\text{Na}_2\text{B}_4\text{O}_7$  buffer (pH = 9.2), [fluorescein] =  $10^{-5}$  M; temperature: 30°C; applied voltage: 30 kV.

was not only to separate the *n*-alkane sulfonates, but also to achieve the greatest possible sensitivity, a compromise optimum value of this parameter must exist.

(i) Retention must be sufficient for satisfactory separation of the analyte components to be obtained. Consequently, the electroosmotic flow must be perfectly adapted.

(ii) However, in our recent study [34], in which we reported for the first time the utilization of fluorescein as the fluorophore generating the background signal, we showed that the sensitivity of the detector response was greater at smaller ionic-strength values. To obtain optimum sensitivity, therefore, ionic strength should be minimal, whereas for optimum separation it should be maximal. After optimization, we found that the best compromise is obtained at a sodium borate concentration of 5 mM. Sodium tetraborate concentrations lower than this improve system efficiency and give shorter analysis times and maximal detector sensitivity. However, as a result of the almost constant selectivity as a function of the ionic strength, the discrimination of the longest-chain *n*-alkane sulfonates,

$\text{C}_9$  and  $\text{C}_{10}$  (which are the first eluted), is not sufficient. On the other hand, at borate concentrations greater than 5 mM, the discrimination between the different peaks corresponding to  $\text{C}_9$  and  $\text{C}_{10}$  is greater, and migration times increase as a result of the decreasing electroosmotic flow; this does not mean, though, that the peak-to-peak resolution is increased, because the system efficiency falls. Moreover, as mentioned above, using such conditions leads to a noticeable loss of sensitivity and to a degradation of the analysis quality.

We report in Fig. 2 the analysis of the ten *n*-alkane sulfonates under these optimal ionic-strength conditions. As can be seen from this figure, the resolution is satisfactory, with the exception of the  $\text{C}_9$ – $\text{C}_{10}$  pair. In order to obtain good resolution of all the components of this complex mixture we investigated the consequences of adding an organic cosolvent.

We studied the influence of the cosolvent on the detector sensitivity and on the electrophoretic behaviour of the *n*-alkane sulfonates, as it is known that such a strategy makes it possible to modify the electroosmotic flow [1,2]. We used

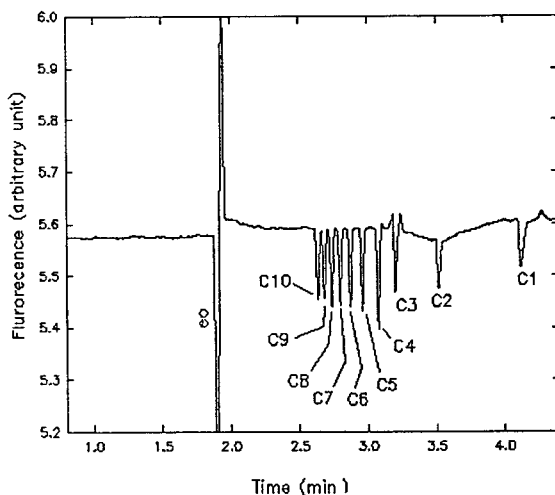


Fig. 2. Electropherogram corresponding to the analysis of the 10 *n*-alkane sulfonates in the optimal ionic-strength conditions (operating conditions identical to those reported in Fig. 1, except that the  $\text{Na}_2\text{B}_4\text{O}_7$  concentration is fixed at 5 mM).

essentially 2-propanol and acetonitrile, which are widely used in MEKC and are perfectly adapted to capillary electrophoresis.

To begin with, we verified that the addition of organic cosolvent (2-propanol, ethanol or acetonitrile) does not affect the sensitivity of the detector response. Whatever the solvent used, we did not observe any decrease in the background signal for a cosolvent percentage lower than 40%. Beyond this limit, baseline perturbations appear and the noise increases appreciably.

We then examined the influence of the nature and the percentage of organic cosolvent on the electrophoretic behaviour of the *n*-alkane sulfonates. We report in Fig. 3 the evolution of the peak-to-peak resolution of seven of the ten *n*-alkane sulfonates studied, as a function of the quantity of organic cosolvent, for two solvents possessing very different chemical characteristics: 2-propanol (Fig. 3a) and acetonitrile (Fig. 3b).

It can be seen clearly that, whichever of the cosolvents (2-propanol or acetonitrile) was used and whatever the *n*-alkane sulfonate pair analyzed, the resolution increased when the percentage of organic cosolvent increased. However, this improvement is not identical for all the

*n*-alkane sulfonate pairs. Moreover, it is greater in the case of 2-propanol. This applies most markedly in the case of the *n*-nonyl sulfonate–*n*-decyl sulfonate pair. In fact, these two compounds are not completely resolved in aqueous solutions and present the limiting resolution in the mixture analyzed. Therefore, it seems, at first sight, that 2-propanol should be used as the cosolvent. However, this conclusion is not totally correct because the change in the electroosmotic flow as a function of the cosolvent percentage differs according to the nature of the cosolvent, as shown in Fig. 4.

It can be seen clearly that the addition of acetonitrile in the electrophoretic buffer results in a smaller modification of the electroosmotic flow than the addition of 2-propanol or ethanol (which have similar behaviour). Consequently, it is possible to use higher amounts of organic cosolvent in the case of acetonitrile while maintaining satisfactory analysis times and detection sensitivity. Comparison of Figs. 3a and 3b shows that an equivalent resolution of the limiting pair (*n*-nonyl sulfonate–*n*-decyl sulfonate) is obtained with 10% of 2-propanol or 20% of acetonitrile. It would seem, then, that acetonitrile is the cosolvent required in order for the best res-

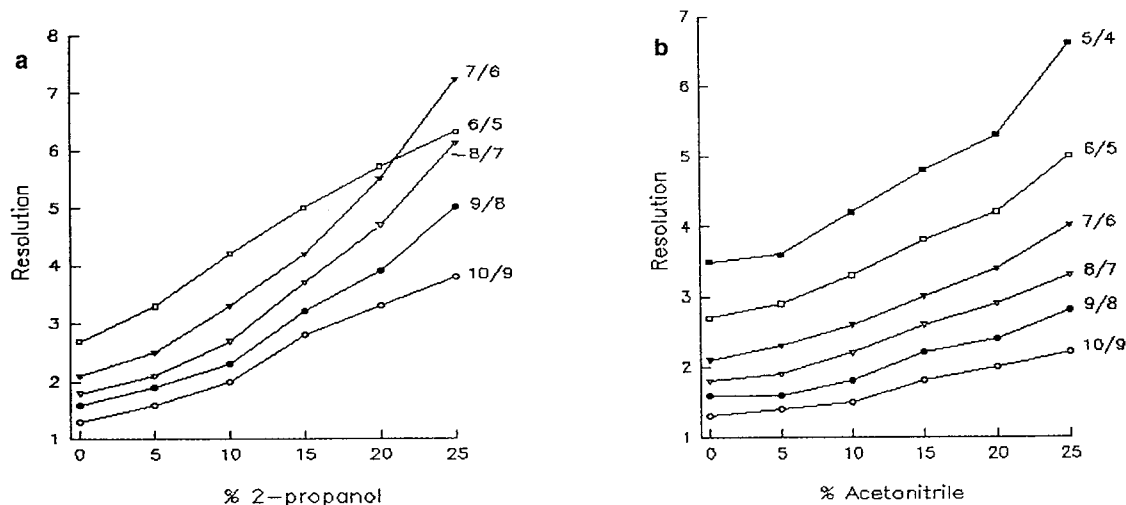


Fig. 3. Evolution of the peak-to-peak resolution as a function of the nature and percentage of the organic cosolvent in the electrolyte. (a) 2-Propanol, (b) acetonitrile. Operating conditions: fused-silica capillary: 57 cm  $\times$  50  $\mu$ m I.D.; electrolyte: 5 mM  $\text{Na}_2\text{B}_4\text{O}_7$ , at pH = 9.2, [fluorescein] =  $10^{-5}$  M; temperature: 30°C; applied voltage: 30 kV.

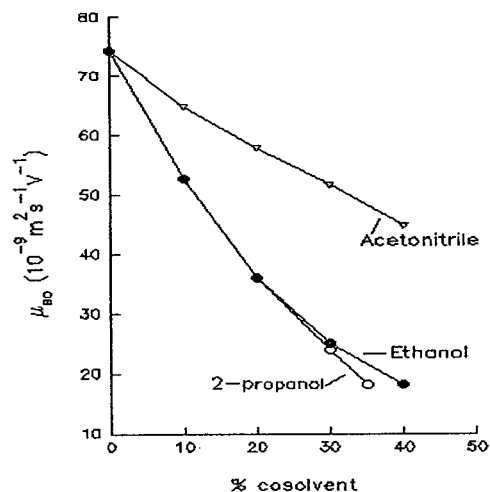


Fig. 4. Evolution of the electroosmotic flow as a function of the nature and the percentage of organic cosolvent added to the electrophoretic buffer. Operating conditions similar to those reported in Fig. 3.

olution/time unit ratio to be obtained. The comparison of the two electropherograms reported in Fig. 5, which were obtained using

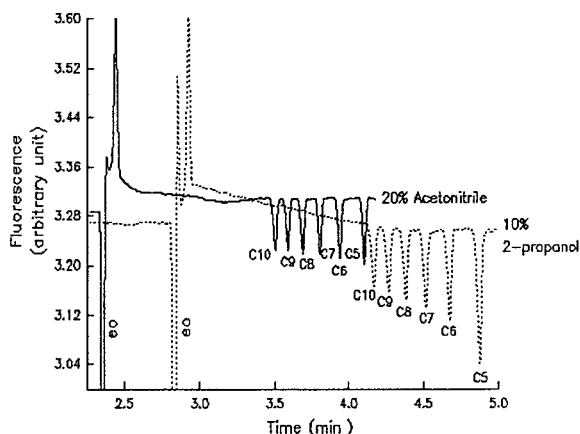


Fig. 5. Analysis of a mixture of alkane sulfonates containing all the homologous compounds from  $C_5$  to  $C_{10}$ . Operating conditions: fused-silica capillary: 57 cm  $\times$  50  $\mu$ m I.D.; electrolyte: 5 mM  $Na_2B_4O_7$ , at pH = 9.2, [fluorescein] =  $10^{-5}$  M; temperature: 30°C; applied voltage: 30 kV; detection:  $\lambda_{exc.} = 488$  nm,  $\lambda_{emis.} = 520$  nm; hydrodynamic injection: 1 s. Dashed line: 20% 2-propanol added in the electrophoretic buffer; solid line: 10% acetonitrile added in the electrophoretic buffer.

electrophoretic buffers containing respectively 10% 2-propanol and 20% acetonitrile, confirms the validity of this strategy.

Since the optimum conditions for the analysis of *n*-alkane sulfonates were being determined in order to obtain also the maximal sensitivity of the detector response, we studied the quantification of this complex mixture and we estimated the reproducibility, response coefficients and detection thresholds for some of the *n*-alkane sulfonates concerned.

The reproducibility of effective mobilities of the *n*-alkane sulfonates on which the analysis was performed was more than satisfactory: we obtained a relative standard deviation (R.S.D.) better than 0.5% from 19 independent analyses. Similarly, the reproducibility of retention times was quite acceptable: the R.S.D.s determined from 19 independent analyses were at most 1% and varied somewhat as a function of the *n*-alkane sulfonate being studied. Finally, the reproducibility of peak areas was greatly dependent on the dilution in the concentration range explored, i.e. from  $2.5 \cdot 10^{-4}$  to  $2 \cdot 10^{-3}$  M. Generally speaking, at an individual concentration of  $10^{-3}$  M for each *n*-alkane sulfonate, the R.S.D. obtained in peak areas was about 3%, and it reached 6% for  $2.5 \cdot 10^{-4}$  M concentration.

We established the response factors using the calibration curves obtained from the corrected peak areas. The number of independent analyses was from 6 to 10 for each dilution, depending on the *n*-alkane sulfonates being analyzed. We obtained satisfactory calibration curves between corrected areas of peaks and the corresponding concentrations. The analytical expressions of these calibration curves are reported in Table 1.

Except in the case of methane sulfonate (correlation coefficient of the linear regression = 0.995) the correlation coefficients are systematically equal to 0.9995. Moreover, an evolution of the response coefficients of *n*-alkane sulfonates as a function of their side-chain lengths is in evidence. The response coefficient increases with alkyl chain length, i.e. when the absolute electrophoretic mobility of the *n*-alkane sulfonates decreases. This behaviour is in perfect



Table 1

Calibration curves, response coefficients in indirect fluorimetric detection and effective electrophoretic mobilities for a number of the *n*-alkane sulfonates analyzed

<i>n</i> -Alkane sulfonates	Effective electrophoretic mobilities (m <sup>2</sup> s <sup>-1</sup> V <sup>-1</sup> )	Response coefficients	Intercept	Correlation
C <sub>10</sub>	23.1	3392	-0.05	0.9993
C <sub>9</sub>	24.1	3266	-0.002	0.9991
C <sub>8</sub>	25.3	3233	0.05	0.9998
C <sub>7</sub>	26.6	3081	0.04	0.9995
C <sub>6</sub>	28.0	3097	-0.02	0.9997
C <sub>5</sub>	29.7	3031	0.02	0.9997
C <sub>1</sub>	44.69	2484	0.01	0.995

agreement with the theoretical treatment of indirect detection developed by Ackermans et al. [51], that we have previously transposed to the indirect fluorimetric detection of cations, using the fluorescein sodium salt [34].

From this theoretical treatment of indirect detection it appears that the response coefficient must evolve as a function of the absolute or effective electrophoretic mobility of the anion being detected as:

$$C \cdot \frac{m_B^0 + m_X^0}{m_X^0}$$

where  $m_B^0$  and  $m_X^0$  are the respective absolute electrophoretic mobilities of the sodium ion and the anion being detected (here an alkane sulfonate), and  $C$  is a constant given by the ratio of the absolute electrophoretic mobility of the fluorescein anion to the sum of the absolute mobilities of the sodium cation and of the fluorescein anion.

It is therefore interesting to study the variation of the experimental response coefficients of the different *n*-alkane sulfonates being determined as a function of their effective electrophoretic mobility (see Table 1), and then to compare this variation to the computed theoretical variation for the same *n*-alkane sulfonates. This comparison is reported in Fig. 6. There is good agreement between the theoretical and the experimental estimations.

Finally, we completed this quantitative study by determining the detection thresholds of these organic anions using our electrophoretic system. These detection thresholds are about 700 ppb.

These results show that the electrophoretic system based on the utilization of fluorescein in a basic medium is suitable for the analysis of organic anions lacking chromophoric or fluorophoric groups, which at present can be detected routinely only by using indirect detection in capillary electrophoresis.

The analysis of only one mixture is not sufficient to assess objectively the potential of this new electrophoretic medium for the analysis of

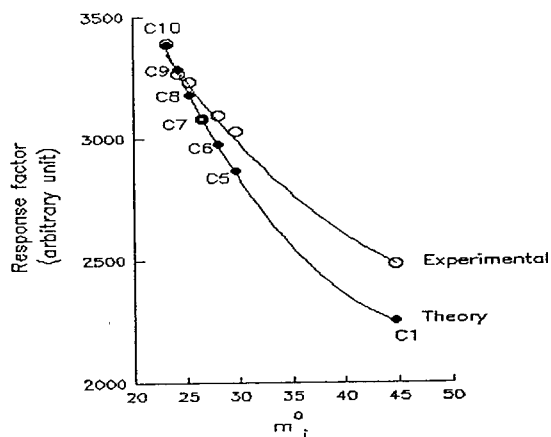


Fig. 6. Comparative study of the evolution of the theoretical and experimental response factors of *n*-alkane sulfonates as a function of their effective electrophoretic mobility.

such ions, and we used it to perform both qualitative and quantitative analyses of another mixture. We studied the analysis of carboxylic acids, with a view to concentrating on the mixtures containing both the carboxylic acids previously analyzed (from  $C_1$  to  $C_8$ ) [47,48] and carboxylic acids possessing longer chains, particularly the  $C_{16}$  and  $C_{18}$  carboxylic acids.

### 3.2. Analysis of a mixture of carboxylic acids containing all the homologues between $C_1$ and $C_{12}$ and the $C_{16}$ and $C_{18}$ carboxylic acids

This mixture is quite similar to the *n*-alkane sulfonates mixture, as it is totally ionized in basic medium, at a pH allowing the maximum sensitivity of the detector. Under these conditions, the first phase of the optimization procedure developed previously in this paper for *n*-alkane sulfonates can be transposed directly. Consequently, we started the optimization to resolve this complex mixture from the pH and ionic strength selected previously for the analysis of *n*-alkane sulfonates. The electropherogram obtained in these conditions is reported in Fig. 7.

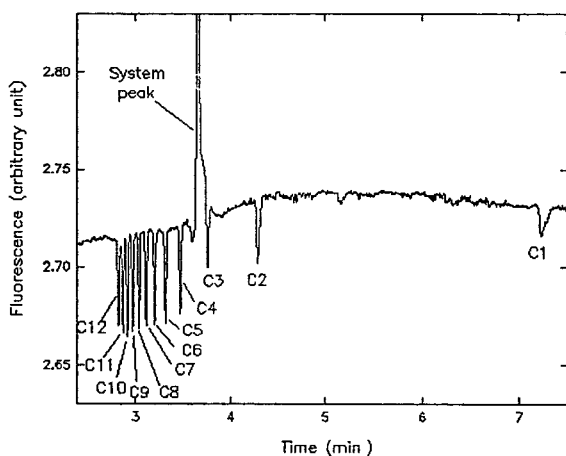


Fig. 7. Analysis of a mixture of carboxylic acids by capillary electrophoresis with laser-induced indirect fluorimetric detection. Experimental conditions: fused-silica capillary: 57 cm  $\times$  50  $\mu$ m I.D.; electrolyte: 5 mM  $\text{Na}_2\text{B}_4\text{O}_7$  at pH=9.2, [fluorescein] =  $10^{-5}$  M, temperature: 30°C; applied voltage: 30 kV; detection:  $\lambda_{\text{exc.}} = 488$  nm,  $\lambda_{\text{emis.}} = 520$  nm; hydrodynamic injection: 1 s.

Thus, it is possible to separate in about 7 min all the homologues of carboxylic acids from  $C_1$  to  $C_{12}$ , with a practically satisfactory resolution. Unfortunately, the analysis of carboxylic acids possessing chains longer than  $C_{12}$  is impossible using this electrophoretic buffer, because they are not soluble in this medium. As natural oils contain  $C_{16}$  and  $C_{18}$  carboxylic acids, both saturated and unsaturated, it was compulsory to develop operating conditions which would permit analysis for these acids to be performed.

To begin with, we attempted to solubilize these compounds using a non-ionic surfactant; if successful, this strategy could result in similar or even shorter analysis times. We used hexaethylene glycol mono-*n*-dodecyl ether ( $C_{12}E_6$ ), this having the longest hydrocarbon chain of the commercially available non-ionic surfactants of acceptable purity.

We then proceeded to study the evolution of resolution as a function of the concentration of this surfactant in the electrophoretic medium. The results are reported in Fig. 8.

These curves show that peak-to-peak resolution varies noticeably as a function of the  $C_{12}E_6$  concentration in the electrolyte. Moreover, this evolution is not monotonic; it presents either a

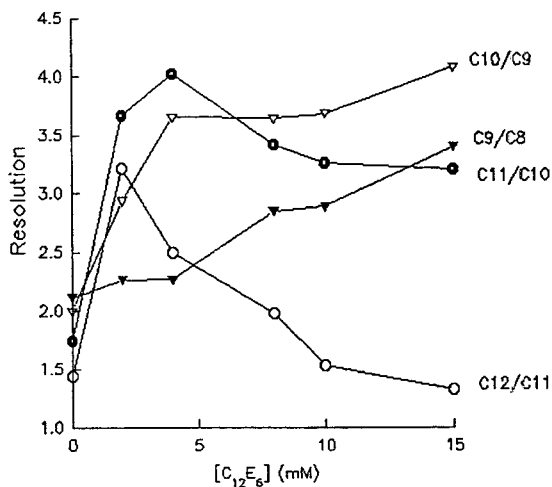


Fig. 8. Evolution of the resolution as a function of the non-ionic surfactant ( $C_{12}E_6$ ) concentration in the electrolyte in the case of some of the carboxylic acids from Fig. 7. Operating conditions similar to those reported in Fig. 7.

step or a maximum, depending on the pair of carboxylic acids being studied. The expectation was that there would be an optimal value of the  $C_{12}E_6$  concentration in the electrophoretic buffer which would permit maximal resolution per time unit. It can be seen from Fig. 8 that this optimal concentration of  $C_{12}E_6$  is low, about 1 mM or even lower. The evolution of the resolution in the case of the  $C_{11}$ – $C_{12}$  acids pair demonstrates this more than clearly (Fig. 8). In fact, in this case the optimal value is 0.2 mM. Below this value, the heaviest carboxylic acids (palmitic and oleic acids) are no longer solubilized, and the analysis becomes impossible. This analysis is also impossible at higher  $C_{12}E_6$  concentrations, for the following reasons: (i) the addition of non-ionic surfactant results in a sharp decline in the efficiency of the electrophoretic system; (ii) migration times decrease sharply with the addition of surfactant to the electrolyte.

The analysis of a carboxylic acids mixture containing particularly palmitic and oleic acids in the presence of non-ionic surfactant ( $C_{12}E_6$  at a 0.2 mM concentration) is reported in Fig. 9. This electropherogram shows that it is possible to analyze in about 3 min a mixture of carboxylic

acids containing all homologous compounds from  $C_7$  to  $C_{12}$ , and also palmitic and oleic acids. However, the resolution of the two latter compounds is only partial. This half-check is in fact encouraging: to our knowledge, this is the first analysis in CE of such heavy carboxylic acids. In an attempt to separate totally the pair palmitic–oleic acids, we considered dissolving them in the presence of organic solvents and analyzing them in CZE using an organic cosolvent. The less attractive feature of this strategy is a decrease in the electroosmotic flow, which is of greater or lesser importance depending on the solvent used (Fig. 4) and which lengthens the analysis time.

Among the solvents considered during the optimization of the separation of *n*-alkane sulfonates, only the two alcohols give efficient solubilization of the heaviest carboxylic acids. As we showed previously that the electroosmotic flow is modified to a greater extent by the addition of 2-propanol than by the addition of ethanol, we selected this latter cosolvent. As can be seen from Fig. 10, the addition of ethanol results in a noticeable improvement in the resolution. This increase is more marked in the case of the shortest-chain acids.

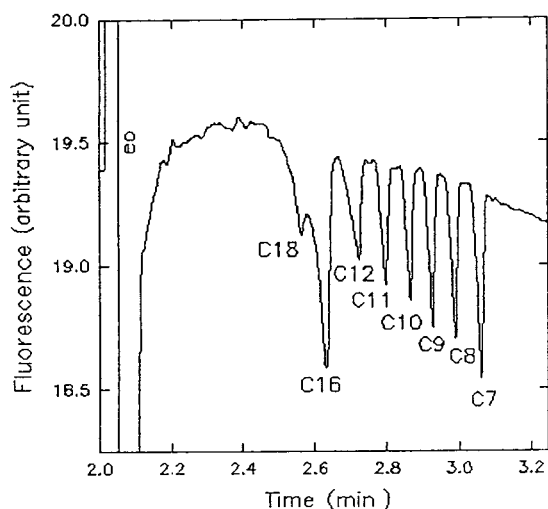


Fig. 9. Analysis of a mixture of fatty acids, containing in particular oleic and palmitic acids, in the presence of  $C_{12}E_6$ . Operating conditions similar to those reported in Fig. 7, except for the presence of  $C_{12}E_6$  (0.2 mM) and that the injection time was fixed at 3 s.

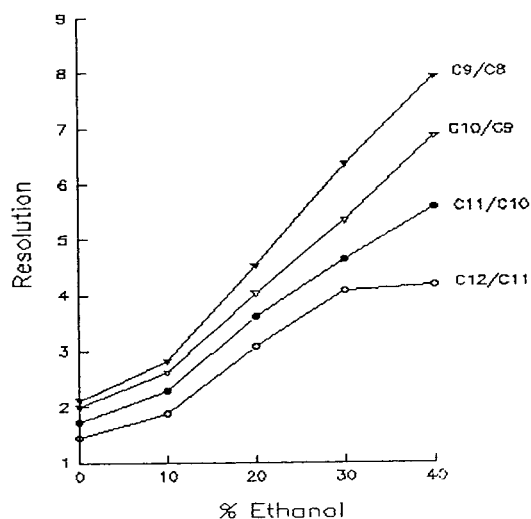


Fig. 10. Resolution in the analysis of some carboxylic acids as a function of the ethanol concentration in the electrolyte. Operating conditions similar to those reported in Fig. 7.

The limiting pair being the oleic and palmitic acids, this last result suggests that very high percentages of ethanol should be used. However, in order to keep the detector sensitivity at an acceptable level, ethanol addition could not exceed 40%. The electropherogram obtained with a mixture of  $C_7$  to  $C_{18}$  carboxylic acids under these operating conditions is reported in Fig. 11.

This electropherogram shows clearly that we were able to resolve correctly the whole of this mixture. However, this satisfactory resolution was obtained at the cost of a longer analysis time (20 min), due to the considerable retardation of the electroosmotic flow under these conditions. Obviously, this buffer also allows the separation of  $C_1$  to  $C_6$  carboxylic acids. Unfortunately, though, analysis of the whole distribution of carboxylic acids from  $C_1$  to  $C_{18}$  takes too long. It is therefore advisable to perform two separate analyses, using two different buffers: (i) a 5 mM  $Na_2B_4O_7$  buffer at pH = 9.2, with a fluorescein concentration of  $10^{-5}$  M, allows the separation of all the homologues from  $C_1$  to  $C_{11}$ ; (ii) a 5 mM  $Na_2B_4O_7$  buffer at pH = 9.2–EtOH (60:40, v/v), with a fluorescein concentration of  $10^{-5}$  M,

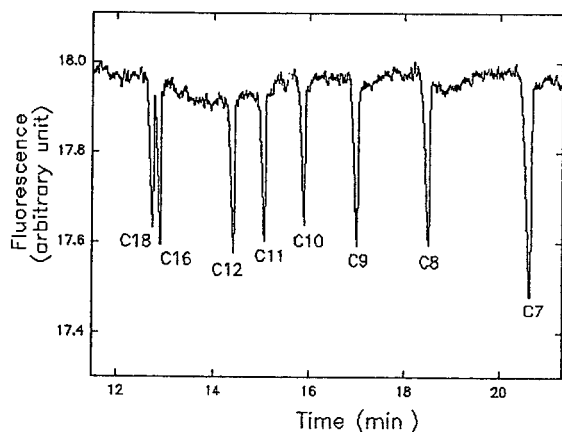


Fig. 11. Analysis by CZE of a mixture of fatty acids containing oleic and palmitic acids. Operating conditions: fused-silica capillary: 57 cm  $\times$  50  $\mu$ m I.D.; electrolyte: 5 mM  $Na_2B_4O_7$  at pH = 9.2–ethanol (60:40, v/v), [fluorescein] =  $10^{-5}$  M; temperature: 40°C; applied voltage: 30 kV; detection:  $\lambda_{exc.}$  = 488 nm,  $\lambda_{emis.}$  = 520 nm; hydrodynamic injection: 2 s.

allows the separation of the  $C_{10}$  to  $C_{18}$  homologous acids.

Then, having studied the quantitative aspect of this analysis, we evaluated the reproducibility of the method, the response factors and the detection thresholds.

Reproducibilities of migration times and of effective electrophoretic mobilities are quite satisfactory when analyses are performed using an electrolyte containing only the borate buffer and fluorescein. From 10 independent experiments we obtained an R.S.D. from 0.4 to 0.7% in the case of effective electrophoretic mobilities and from 0.9 to 1.1% for the migration times. On the other hand, in the presence of 40% ethanol, this reproducibility is somewhat worsened. Effectively, the R.S.D.s computed from 16 independent experiments are now respectively 2.2% for effective electrophoretic mobilities and 2.6% for migration times. As previously reported in the case of the *n*-alkane sulfonates, the reproducibility of peak areas is a function of the dilution of the solution analyzed. Its values vary from 4%, at a 2 mM concentration, to 10%, at a 0.1 mM concentration.

As shown in Table 2, in the concentration range explored, we obtained calibration curves with linear regression coefficients varying from 0.990 to 0.9991. The regression coefficients of calibration curves remained excellent when the electrolyte contained 40% ethanol. Once again, perfect agreement is observed between the theoretical and the experimental response coefficients (Table 2). In fact, the response factors increase with the length of the hydrocarbon chains, i.e. if the absolute or effective electrophoretic mobilities decrease.

To conclude this quantitative study, we determined the detection thresholds in the presence and in the absence of ethanol, and these were about 1 ppm.

#### 4. Conclusions

The indirect fluorimetric detection system based on the utilization of the sodium salt of fluorescein to provide the background signal

Table 2

Calibration curves, response coefficients in indirect fluorimetric detection and effective electrophoretic mobilities for a number of the carboxylic acids analyzed

Carboxylic acids	Effective electrophoretic mobilities ( $\text{m}^2 \text{s}^{-1} \text{V}^{-1}$ )	Response coefficients	Intercept	Correlation
C <sub>12</sub>	20.5	7544	0.09	0.9991
C <sub>11</sub>	21.3	7503	0.09	0.990
C <sub>10</sub>	22.2	7200	0.08	0.996
C <sub>9</sub>	23.2	7335	0.21	0.991
C <sub>8</sub>	24.3	7069	0.30	0.994
C <sub>6</sub>	26.9	6882	0.16	0.996
C <sub>5</sub>	28.5	6870	0.08	0.997
C <sub>4</sub>	30.5	6551	0.17	0.994
C <sub>2</sub>	38.6	6515	-0.28	0.992
C <sub>18</sub>	9.8	6094	0.09	0.998

(derived from a system developed previously to analyze inorganic cations) is perfectly adapted to the qualitative and quantitative analysis of organic anions. Analyses with quite acceptable reproducibilities, both of retentions and of quantitative measurements, can be performed. Moreover, this electrophoretic system is highly sensitive, with detection thresholds of a few hundred ppb.

However, if an organic cosolvent is added to the electrophoretic buffer, either to dissolve the analyte or to optimize the electroosmotic flow so that satisfactory resolution can be attained, this sensitivity is slightly decreased at higher cosolvent levels.

Finally, using a buffer rich in ethanol, this electrophoretic system allowed, for the first time, the analysis of heavy carboxylic acids such as oleic and palmitic acids. However, because of a relatively weak electroosmotic flow, the time taken for a single complete analysis of carboxylic acids from C<sub>1</sub> to C<sub>18</sub> was prohibitive. Under these conditions, it seems reasonable to analyze such complex mixtures by performing two distinct analyses, in different electrophoretic conditions: with a simple borate buffer to analyze for C<sub>1</sub> to C<sub>11</sub> acids, and with a borate buffer in the presence of organic cosolvent to determine the remaining compounds from C<sub>12</sub> to C<sub>18</sub>. In this way, analysis times remain quite acceptable.

Following these very encouraging results, we intend soon to apply this electrophoretic system to the analysis and detection of inorganic anions in capillary zone electrophoresis.

## References

- [1] S.F.Y. Li, *Capillary Electrophoresis—Principles, Practice and Applications*, Elsevier, Amsterdam, 1992.
- [2] R. Kuhn and S. Hoffstatter-Kuhn, *Capillary Electrophoresis: Principles and Practice*, Springer Verlag, Berlin, 1994.
- [3] E.S. Yeung, *Acc. Chem. Res.*, 22 (1989) 125.
- [4] E.S. Yeung and W.G. Kuhr, *Anal. Chem.*, 63 (1991) 275A.
- [5] J. Romano, P. Jandik, W. Jones and P. Jackson, *J. Chromatogr.*, 546 (1991) 411.
- [6] W. Jones and P. Jandik, *J. Chromatogr.*, 546 (1991) 445.
- [7] B. Wildman, P. Jackson, W. Jones and P. Alden, *J. Chromatogr.*, 546 (1991) 459.
- [8] B.F. Kenney, *J. Chromatogr.*, 546 (1991) 423.
- [9] S. Grocott, I. Jefferies, T. Bowser, J. Carnavale and P. Jackson, *J. Chromatogr.*, 602 (1992) 257.
- [10] K. Hargadon and B. McCord, *J. Chromatogr.*, 602 (1992) 241.
- [11] W. Buchberger and P. Haddad, *J. Chromatogr.*, 608 (1992) 59.
- [12] G. Bondoux, P. Jandik and W. Jones, *J. Chromatogr.*, 602 (1992) 79.
- [13] D. Salomon and J. Romano, *J. Chromatogr.*, 602 (1992) 219.
- [14] J. Nair and C. Izzo, *J. Chromatogr.*, 640 (1993) 445.

- [15] M. Harrold, M. Wojtusik, J. Riviello and P. Henson, *J. Chromatogr.*, 640 (1993) 463.
- [16] X. Huang, T. Pang, M.J. Gordon and R.N. Zare, *Anal. Chem.*, 59 (1987) 2747.
- [17] X. Huang, J.A. Luckey, M.J. Gordon and R.N. Zare, *Anal. Chem.*, 61 (1989) 766.
- [18] X. Huang, M.J. Gordon and R.N. Zare, *J. Chromatogr.*, 480 (1989) 285.
- [19] X. Huang, R.N. Zare, S. Sloss and A.G. Ewing, *Anal. Chem.*, 63 (1991) 189.
- [20] M. Aguilar, X. Huang and R.N. Zare, *J. Chromatogr.*, 480 (1989) 427.
- [21] M. Aguilar, A. Farran and M. Martinez, *J. Chromatogr.*, 635 (1993) 127.
- [22] F. Foret, S. Fanali, A. Nardi and P. Bocek, *Electrophoresis*, 11 (1990) 780.
- [23] L. Gross and E.S. Yeung, *Anal. Chem.*, 62 (1990) 427.
- [24] M. Chen and R. Cassidy, *J. Chromatogr.*, 602 (1992) 227.
- [25] A. Weston, P. Brown, P. Jandik, W. Jones and A. Heckenberg, *J. Chromatogr.*, 593 (1992) 289.
- [26] P. Jandik, W. Jones, A. Weston and P. Brown, *LC-GC*, 9 (1991) 634.
- [27] A. Weston, P. Brown, A. Heckenberg, P. Jandik and W. Jones, *J. Chromatogr.*, 602 (1992) 249.
- [28] M. Koberda, M. Kondowski, P. Younberg, W. Jones and A. Weston, *J. Chromatogr.*, 602 (1992) 235.
- [29] A. Weston, P. Brown, P. Jandik, A. Heckenberg and W. Jones, *J. Chromatogr.*, 608 (1992) 395.
- [30] W. Beck and H. Engelhardt, *Chromatographia*, 33 (1992) 313.
- [31] K. Bächmann, J. Boden and I. Haumann, *J. Chromatogr.*, 626 (1992) 259.
- [32] D. Swaile and M. Sepaniak, *Anal. Chem.*, 63 (1991) 179.
- [33] P. Morin, C. François and M. Dreux, *Analisis*, 22 (1994) 178.
- [34] P.L. Desbène, C. Morin, A.M. Desbène-Monvernay and R.S. Groult, *J. Chromatogr. A*, 689 (1995) 135.
- [35] S. Chen and D.J. Pietrzyk, *Anal. Chem.*, 65 (1993) 2770.
- [36] S.A. Shamsi and N.D. Danielson, *Anal. Chem.*, 66 (1994) 3757.
- [37] J.L. Iverson and A.J. Sheppard, *J. Chromatogr. Sci.*, 13 (1975) 505.
- [38] J. Krupcik, J. Hrivnak and J. Janak, *J. Chromatogr. Sci.*, 14 (1976) 4.
- [39] J.N. Shantha and G.E. Napolitano, *J. Chromatogr.*, 624 (1992) 37.
- [40] H.D. Drust, M. Milano, E.J. Kikta, S.A. Connelly and E. Grushka, *Anal. Chem.*, 47 (1975) 1797.
- [41] H. Miwa, C. Hiyama and M. Yamamoto, *J. Chromatogr.*, 321 (1985) 165.
- [42] Y. Yasaka, M. Tanaka, T. Shono, T. Tetsumi and J. Katakawa, *J. Chromatogr.*, 508 (1990) 133.
- [43] Y. Liu, F. Yang and C. Pohl, *J. Microcol. Sep.*, 2 (1990) 245.
- [44] C. de Jong and H.T. Badings, *J. High Resolut. Chromatogr.*, 13 (1990) 94.
- [45] Y. Tsuyama, T. Uchida and T. Goto, *J. Chromatogr.*, 596 (1992) 181.
- [46] M. Koval, D. Kaniansky, M. Hutta and R. Lacko, *J. Chromatogr.*, 325 (1985) 151.
- [47] T. Barth, *Anal. Chem.*, 59 (1987) 2232.
- [48] R. Szücs, J. Vindevogel and P. Sandra, *J. High Resolut. Chromatogr.*, 14 (1991) 692.
- [49] M. Shirao, R. Furuta, S. Suzuki, H. Nakazawa, S. Fujita and T. Maruyama, *J. Chromatogr. A*, 680 (1994) 247.
- [50] S. Hjerten, K. Elenbring, F. Kilar, A.J. Chen, C.J. Siebert and M. Zhu, *J. Chromatogr.*, 403 (1987) 47.
- [51] M.T. Ackermans, F.M. Everaerts and J.L. Beckers, *J. Chromatogr.*, 549 (1991) 345.



ELSEVIER

Journal of Chromatography A, 716 (1995) 291–301

JOURNAL OF  
CHROMATOGRAPHY A

# Capillary electrophoretic determination of organic acids with indirect detection

C.H. Wu, Y.S. Lo, Y.-H. Lee, T.-I. Lin\*

*Department of Chemistry, National Taiwan University, Taipei 10764, Taiwan*

## Abstract

Methods for the determination of several organic acids commonly found in foods and beverages, including oxalic, citric, acetic, tartaric, malic, succinic, lactic, carbonic, aspartic, glutamic, ascorbic and gluconic acids, by capillary electrophoresis (CE) with indirect absorbance detection were developed. Several absorbance providers, including chromate, *p*-hydroxybenzoate, phthalate, terephthalate, trimellitate and pyromellitate, were investigated for their suitability as background electrolytes (BGEs). CE was performed in the negative voltage (reverse polarity, detector towards anode) mode. The effects of pH and various additives on CE separations were evaluated. The BGE and pH each played a major role in affecting the selectivity and resolution of CE. All analytes except malate and succinate could be baseline resolved in one run by performing CE with 5 mM trimellitate (as the BGE)–1 mM tetradecyltrimethylammonium bromide at pH 9.0 in less than 10 min. On the other hand, the CE separation of the tri- and dicarboxylic acids and hydroxydicarboxylic acids (the first five) could best be obtained at pH 5.5 in 5 min. The precision of the method for most monoprotic analytes is typically less than 1% for the migration time and 1–4% for the peak area ( $n = 6$ ). The detection limit for most analytes is of the order of  $2.0 \cdot 10^{-6}$  M. The new methods developed are rapid, sensitive and quantitative and can be readily applied to real food samples for quantitative analysis.

## 1. Introduction

Organic acids are commonly present in foods, beverages, medicines and a variety of samples of analytical interest. The simultaneous determination of several organic acid constituents in samples can best be accomplished by chromatographic techniques, e.g., gas chromatography (GC), ion chromatography (IC) or high-performance liquid chromatography (HPLC), as has been amply demonstrated in the past [1,2].

The determination of organic acids in food samples by capillary electrophoresis (CE) was

first demonstrated [3] by using a commercial proprietary chemical reagent kit. The various advantages offered by the CE method include ease of sample preparation, low cost, automation and speed. A mixture of seven standards, including citric, tartaric, malic, succinic, acetic, lactic and butyric acids, can be separated in less than 15 min and detected (by the indirect UV absorbance method) at the 50  $\mu\text{g}/\text{ml}$  level. Since not all analytes exhibit high UV absorptivity, the indirect absorbance method has been welcomed as a universal means for the detection of non-absorbing analytes. In the indirect absorbance method, an absorbing co-ion [background electrolyte (BGE)], which provides a background

\* Corresponding author.

UV (or visible) absorbance, co-migrates with the mixture of analytes which do not absorb (at the wavelength that the detector was set for the BGE). When the analyte passes the detector, a negative absorbance peak appears. For analytes which do not absorb appreciably in the UV region, the indirect absorbance technique provides a universal detection scheme. Because for many analytes the indirect absorbance method affords good sensitivity, CE coupled with indirect UV absorbance detection has gained increasing popularity. CE methods have been successfully implemented for the determination of various organic acids in sugar refinery juices, fruit juices, foods and urine samples [4–7]. Various BGEs including chromate [4], benzoate [5], phthalate [6,7], 1,2,4-benzenetricarboxylate (trimellitate) [8,9], 1,2,4,5-benzenetetracarboxylate (pyromellitate) [10], 2,6-naphthalenedicarboxylate [11] and naphthalene mono-, di- and trisulfonates [12] have been investigated. Selectivity could be optimized to improve the CE resolution of organic acids via dynamic pH- and flow-gradient techniques [13]. The optimization of indirect UV detection and the injection technique for the CE of anions have also been addressed in several studies [14–21].

Previously, we have developed methods for the CE analysis of a mixture of twenty common amino acids with indirect absorbance detection [22]. In the present investigation, we employed the indirect detection method for the determination of anions, including acetate, lactate, succinate, malate, tartrate, glutamate, ascorbate, citrate, oxalate, gluconate, carbonate and aspartate, that are commonly found in foods and beverages. Several absorbance providers, including chromate, benzoate, *p*-hydroxybenzoate, phthalate, terephthalate, trimellitate and pyromellitate, were investigated for their suitability as background electrolytes (BGEs). CE could be performed by applying either positive voltage (towards the cathode) or reverse polarity; however, for the present analysis, we found that the reverse polarity mode gave better results. The effects exerted by pH and various additives on the selectivity and resolution of CE were evaluated. The new methods developed are

rapid, sensitive and quantitative and can be readily applied to real food samples for the determination of these analytes.

## 2. Experimental

### 2.1. Chemicals

Various organic and inorganic acids and BGEs, as either free acids or sodium salts, and electroosmotic flow (EOF) modifiers, all of analytical or reagent grade, were obtained from several suppliers. Various brands of beverage and food samples were purchased from local market stores. Doubly deionized water prepared with a Milli-Q system (Millipore, Bedford, MA USA) or doubly deionized, distilled water was used exclusively to prepare all solutions.

### 2.2. Samples, buffers and pH adjustment

Solutions of oxalic, citric, tartaric, malic, succinic, carbonic, acetic, lactic, aspartic, glutamic, ascorbic and gluconic acids (or sodium salts) were prepared, each at  $10^{-2}$  M. These solutions were mixed and diluted to 0.1 mM (pH adjusted to 7.0); the diluted mixture was used as the standard. Most real samples were diluted tenfold or more with 2 mM NaOH. After dilution, most real samples were near neutral, hence further pH adjustment was usually unnecessary. BGEs, including benzoic acid, *p*-hydroxybenzoic acid (PHBA), phthalic acid (PHA), terephthalic acid (TPA), trimellitic acid (TMA), pyromellitic acid (PMA) and sodium chromate, were prepared as 5 mM stock solutions; their pH values were adjusted to 5–10 with concentrated NaOH or HCl depending on the experiments. Cetyltrimethylammonium bromide (CTAB), dodecyltrimethylammonium bromide (DTAB), tetracycltrimethylammonium bromide (TTAB) and diethylenetriamine (DETA) were employed as EOF modifiers and their concentrations were varied from 0.2 to 5 mM. The pH of the buffer was checked periodically and readjusted when necessary. All samples and buffers were filtered



through 0.2- $\mu\text{m}$  membranes and degassed under vacuum for 10 min.

### 2.3. Electrophoretic procedures

CE experiments were carried out in a fully automated Spectra Phoresis Model 1000 instrument (Thermo Separation Products, Fremont, CA, USA) as described previously [23]. In most experiments, except in the electrophoretic mobility determination of BGEs, the detector wavelength was fixed at the optimum wavelength depending on the BGE used as specified in Table 1. In indirect detection, peaks in the electropherogram appear originally as negative peaks but are inverted to positive peaks by using the vendor's software. The separation capillaries (bare fused silica) from Polymicro Technologies (Phoenix, AZ, USA) were 75  $\mu\text{m}$  I.D. (365  $\mu\text{m}$  O.D.)  $\times$  43 cm (36 cm to the detector) for the determination of the mobilities of BGEs and 75  $\mu\text{m}$  I.D. (365  $\mu\text{m}$  O.D.)  $\times$  70 cm (63 cm to the detector) for the separation of analytes.

Procedures for capillary pretreatment, pre- and post-washings and a daily routine pre-washed sequence were similar to those reported previously [23]. Sample injection was effected in the hydrodynamic (HD) mode for 3 s. The separation run was carried out at  $-20$  kV constant voltage (except in the mobility determination experiment, in which a positive voltage was applied), at  $25^\circ\text{C}$  constant temperature and with a current of ca.  $20$   $\mu\text{A}$ . Between runs, the capillary was post-washed with deionized water for 5 min. Peak identification for each analyte was carried out by spiking with the known

standard, and the peak with increased height was identified.

### 2.4. Electrophoretic mobility determination

The mobilities of various BGEs under the specified CE conditions were determined in buffer solution containing  $10$  mM sodium phosphate (pH 8.0). A mixture of all BGEs,  $0.1$  mM each in deionized water, containing  $0.05\%$  dimethyl sulfoxide (DMSO) as a neutral marker, was injected in the HD mode for 1 s. The CE voltage applied was  $+20$  kV. Detection was effected by rapid scanning of absorbance from 200 to 350 nm, which allowed a positive identification of the background provider. The electroosmotic mobility,  $\mu_{\text{eo}}$ , and the electrophoretic mobility of the BGE,  $\mu_{\text{e}}$ , were calculated from the observed mobility,  $\mu_{\text{obs}}$ , using the equations described previously [22].

## 3. Results and discussion

### 3.1. Selection of suitable BGE and EOF modifier

Among the twelve acid analytes of interest here, only ascorbic acid absorbs strongly in the UV region above 200 nm ( $\epsilon_{\text{max}} = 8.2 \cdot 10^3$  l mol $^{-1}$  cm $^{-1}$  at 254 nm). All other analytes have molar absorptivities from 25 to 180 l mol $^{-1}$  cm $^{-1}$  at 220 nm. When selecting a BGE suitable for CE, the mobility and the molar absorptivity of the BGE must both be taken into consideration. In theory, the BGE with a mobility matching those of the majority of the analytes would give a

Table 1  
CE conditions for the various combinations of BGE-EOF modifier pairs

System	BGE	EOF modifier	pH	$\lambda$ (nm)
Chromate	5 mM chromate	0.5 mM TTAB	8.0	265
PMA	2 mM PMA	2 mM DETA	9.0	220
TMA	5 mM TMA	1 mM TTAB	9.0	220
PHA	5 mM PHA	0.5 mM TTAB	8.0	220
TPA	5 mM TPA	0.25 mM TTAB	9.0	240
Benzoate	5 mM benzoate	0.3 mM TTAB	8.0	220

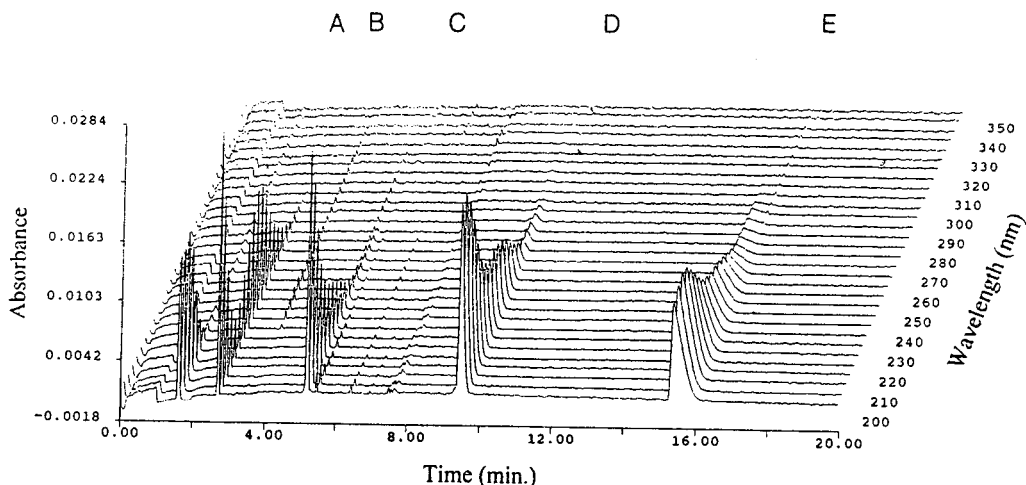


Fig. 1. Three-dimensional spectral view of CE separation of a mixture of four BGEs and the neutral marker. (A) DMSO; (B) PHBA; (C) PTA; (D) TMA; (E) PMA. Conditions as in the mobility determination (see Experimental for details).

better separation and resolution. The absorbance of the BGE should be high, and ideally should not overlap with those of the analytes. Fig. 1 shows a three-dimensional spectral scan of the CE of four selected BGEs to show their absorption spectral characteristics.

The electrophoretic mobilities for the various BGEs decreased in the following order: chromate > pyromellitate > trimellitate > terephthalate, phthalate > benzoate > *p*-hydroxybenzoate (Fig. 2, bottom). Chromate has the highest mobility, and is most suitable as the BGE for inorganic anions such as  $\text{Cl}^-$ ,  $\text{Br}^-$ ,  $\text{NO}_3^-$  and  $\text{SO}_4^{2-}$ . Its molar absorptivity is adequate in the region where the organic acids of

interest are transparent. However, for the slower moving organic acids, performing CE using chromate as the BGE would result in poorer resolution and these acids would appear as trailing peaks. Other ionized BGEs carry charges from  $-1$  (benzoate) to  $-4$  (pyromellitate). Since their absorption characteristics are similar, they can be paired together to provide a wider range of mobilities that can match better with the mobilities of the present analytes (Fig. 2, top). Among the present analytes, tartaric, malic and succinic acids at alkaline pH have mobilities that are close to each other. On the other hand, the mobilities for the two amino acids, ascorbic and gluconic acid, are not significantly different at

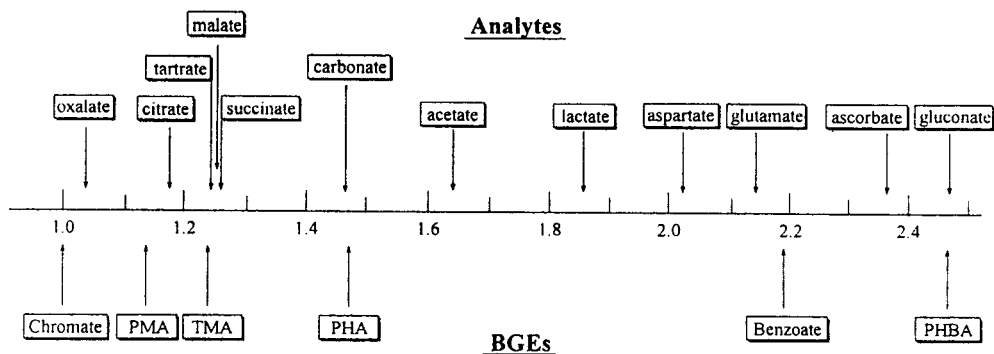


Fig. 2. Relative electrophoretic mobilities (with respect to chromate) of several BGEs and organic anions at pH 8.0.

acidic pH. Therefore, these analytes are most difficult to separate at the pH extremes. Trimellitate has a mobility that matches closest to those of the dicarboxylic acids; its transfer ratio is high, so it also offers better sensitivity [8]. Pyromellitate as the BGE would produce similar results to TMA. Phthalate, which has been a popular choice as a BGE in earlier studies, has a molar absorptivity that is not as high as that of PMA. Hence the sensitivity of phthalate is inferior to that of the latter. Terephthalate, although it has a higher molar absorptivity, suffers from a lack of resolving power for the analytes citrate, tartrate and malate.

In CE of anions, a negative voltage is applied and the analytes migrate towards the anode in the opposite direction to the EOF. The migration time of anions can be shortened significantly by decreasing the EOF with the addition of cationic surfactants (EOF modifiers), which neutralize the negative surface charges on the bare fused-silica capillary. Both TTAB and CTAB were fairly effective (see below), but TTAB gave slightly better results. DTAB could also be used, but it has a higher critical micelle concentration and thus required a higher concentration to be effective, which caused a higher current. PMA formed white precipitates with cationic surfactants (e.g., TTAB). In this case, hexamethonium hydroxide [10] or diethylenetriamine [7] must be substituted as the EOF modifier to be paired with PMA. Among the various combinations of BGE–EOF modifier pairs investigated (Table 1), the combined use of TMA as the BGE and TTAB as the EOF modifier appears to give the best separation.

### 3.2. CE Separation of organic acids

Fig. 3a shows a typical electropherogram of a mixture of the twelve organic acids (0.1 mM of each analyte) in 5 mM TMA–1 mM TTAB at pH 5.5. The faster migrating species, tri- and dicarboxylates, could well be separated in less than 6 min. However, at this pH, glutamate and ascorbate could not be baseline resolved and citrate appears as a smaller and broader peak. On the other hand, at alkaline pH (9.0), with

other CE conditions being the same, all except the three dicarboxylic acids, tartrate, malate and succinate, can be baseline resolved in less than 9.5 min (Fig. 3b). At, pH 9.0 the migration times of the analytes increase in the following order: (1) oxalate, (2) citrate, (3) tartrate, (4) malate, (5) succinate, (6) carbonate, (7) acetate, (8) lactate, (9) aspartate, (10) glutamate, (11) ascorbate and (12) gluconate. Note that the order of migration times also changes for citric acid at the two pHs. At acidic pH, the uncharged carbonic acid migrates too slowly to appear in the electropherogram. The migration time of the ion is strongly dependent on the electric charges that it carries and its mass. The tri- and diprotic acids migrate faster than all other acids because they carry more negative charges than the other analytes. Albeit carrying more negative charge, citrate trails behind oxalate, presumably because of its higher mass (see Table 2). Tartrate migrates faster than malate, and the latter is faster than succinate, since malate and tartrate carry one and two hydroxyls, respectively, while succinate has none. The faster mobility may be attributed to the presence of hydroxyl groups. Among the monocarboxylic acids, carbonate, acetate and lactate migrate in ascending order in accordance to their mass. Being zwitterions, aspartate and glutamate trail behind owing to the positive charges carried on the amine group. Ascorbate and gluconate move the slowest because of their higher masses. Note that because the mobility of TMA (as the BGE) is between those of citrate and succinate, the peak shape of these analytes appears to be symmetrical. However, those analytes which move slower than TMA have trailing peaks.

### 3.3. Effect of pH

The electrophoretic mobility of acids is strongly dependent on the pH of the running buffer, as contrasted in Fig. 3a and b. Table 2 gives the  $pK_a$  values for the BGEs and the analytes of interest which serve as a guide for manipulating the extent of ionization of these analytes by adjusting the pH. The effect of pH on the relative migration time of the twelve acids is

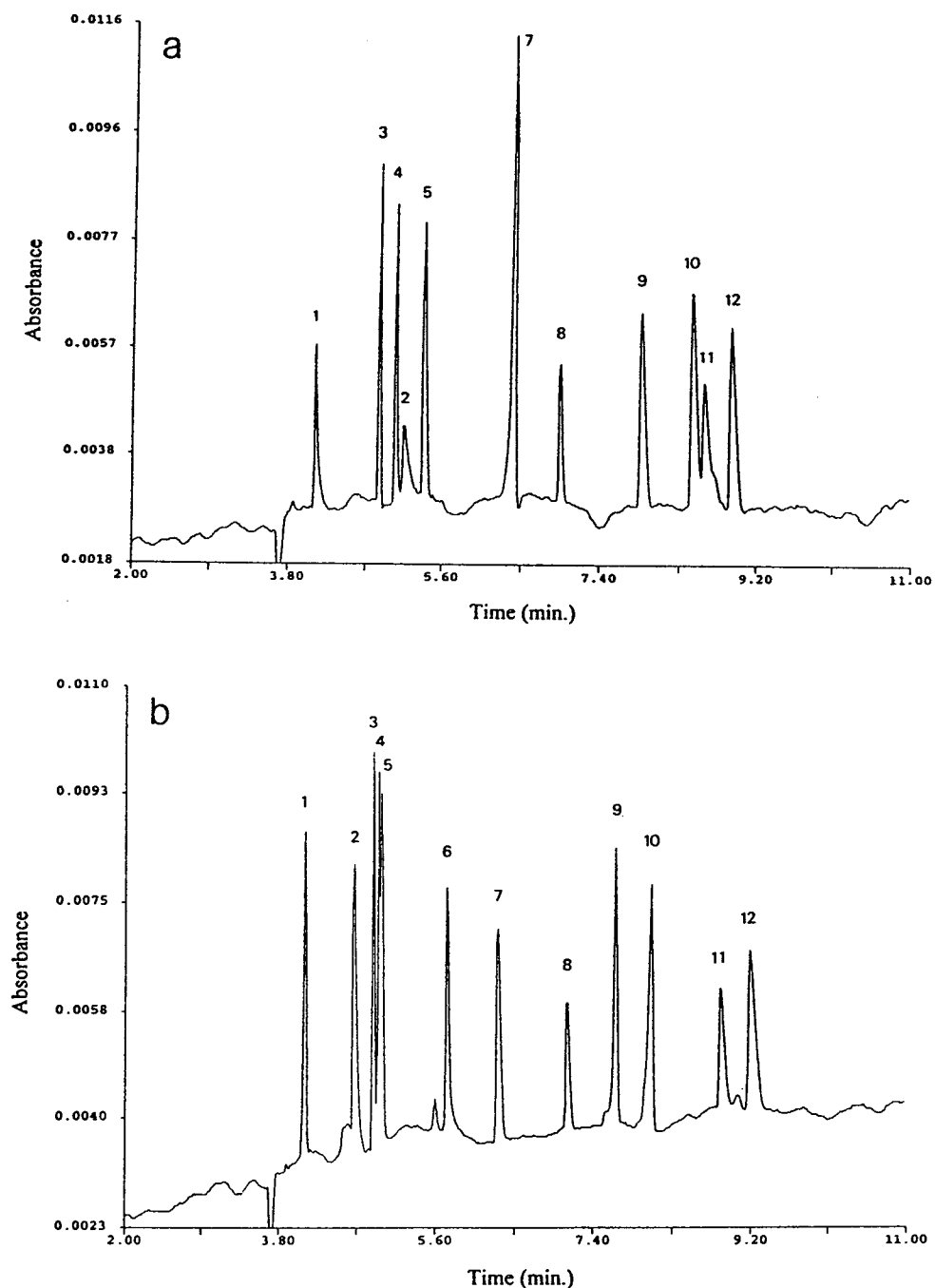


Fig. 3. Electropherograms of a mixture of the twelve anions (0.1 mM each) in 5 mM TMA–1 mM TTAB at (a) pH 5.5 and (b) pH 9.0. Migration order (peaks): 1 = oxalate; 2 = citrate; 3 = tartrate; 4 = malate; 5 = succinate; 6 = carbonate; 7 = acetate; 8 = lactate; 9 = aspartate; 10 = glutamate; 11 = ascorbate; 12 = gluconate.

Table 2  
Molecular masses and  $pK_a$  values of the various BGEs and analytes

Acid	$M_r$	$pK_{a1}$	$pK_{a2}$	$pK_{a3}$	$pK_{a4}$
Benzoic	122.1	4.19			
<i>p</i> -Hydroxybenzoic	138.1	4.48	9.32		
Phthalic	166.1	2.89	5.51		
Terephthalic	166.1	3.51	4.82		
Trimellitic <sup>b</sup>	210.1	2.42	3.71	5.01	
Pyromellitic <sup>b</sup>	254.2	1.87	2.72	4.30	5.52
Oxalic	90.1	1.23	4.19		
Citric	192.1	3.14	4.77	6.39	
Tartaric	150.1	2.98	4.34		
Malic	134.1	3.40	5.11		
Succinic	118.1	4.16	5.61		
Carbonic	62	6.35	10.33		
Acetic	60.1	4.76			
Lactic	90.1	3.08			
Aspartic	133.1	2.09	3.86	9.82	
Glutamic	147.1	2.19	4.25	9.67	
Ascorbic	176.1	4.10	11.79		
Gluconic	196.2	3.76			

<sup>a</sup> From Ref. [31], except where indicated.

<sup>b</sup> From Ref. [32].

shown in Fig. 4. At acidic pH, the pH affects the di- and triprotic acids most significantly. At pH 5.5, citric acid dissociates only two protons and migrates behind tartrate and malate but ahead of

succinate because of its heavier mass (Fig. 3a). As the pH is raised above the  $pK_{a3}$  of citric acid, citrate carries an extra negative charge and migrates ahead of tartrate and malate. Thus, a better separation can be obtained at pH 5.5 for the fast-moving polyacids. On the other hand, at alkaline pH (9.0), a better resolution could be achieved for carbonate and the slower moving amino acids, ascorbic and gluconic acid.

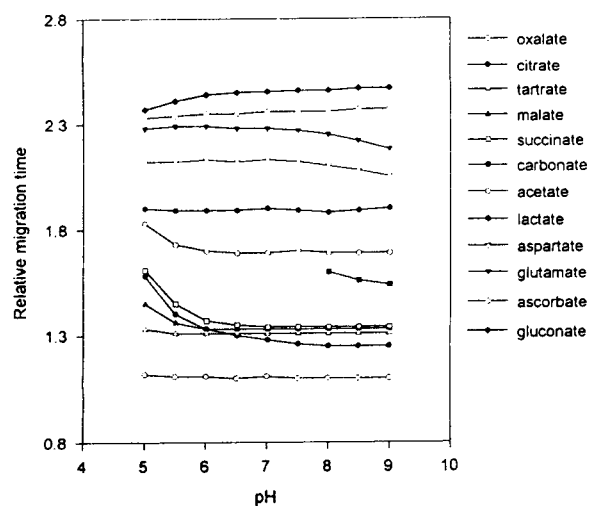


Fig. 4. Effect of pH on the relative migration times of the organic acids. Other conditions as in Fig. 3b.

### 3.4. Effects of EOF modifiers

Since in the CE of anions the analytes migrate towards the anode in the opposite direction to the EOF, adding cationic surfactants or alkylamines could neutralize the negative surface charges on the bare fused-silica capillary, thus reducing the EOF (as these compounds are often called EOF modifiers). Further, when enough modifiers are added to the running buffer, the direction of the EOF could be reversed, further facilitating the migration of anions. The migration time of anions can thus be shortened significantly. For TTAB, a concentration as low as

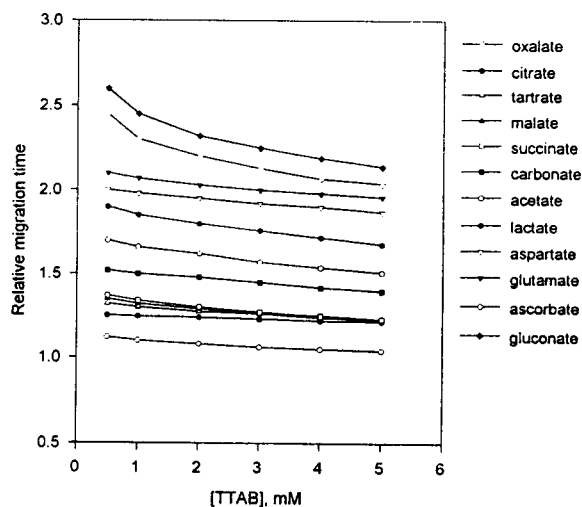


Fig. 5. Effect of TTAB concentration on the electrophoretic mobility of the organic acids in 5 mM TMA (pH 9.0). Other conditions as in Fig. 3b.

0.1 mM could reverse the EOF. On the other hand, when the concentration of the surfactant exceeds its critical micellar concentration (CMC), the effect of the surfactant concentration on modifying the EOF is less pronounced [22]. The effect of the concentration of TTAB from 0.5 to 5 mM on the relative migration time of the various analytes is shown in Fig. 5. It is apparent that when [TTAB] is above 2 mM, the separation for tartrate, malate and succinate become very poor. On the other hand, although

at 0.5 mM [TTAB] the separation for these three anions is better, the relative migration time is much longer and the baseline starts to drift. Therefore, we chose 1 mM TTAB as a compromise. However, in samples in which ascorbate and gluconate are both absent, the CE conditions could be set at a lower pH and a lower concentration of EOF modifier to optimize the separation of the diprotic acids.

### 3.5. Precision and linearity

The precisions [expressed in terms of relative standard deviation (R.S.D.)] of the present method for the various analytes are summarized in Table 3. The R.S.D.s for the migration times are typically less than 0.3% for all except three analytes (<1%). The R.S.D.s for the peak areas typically are less than 3%, except for citrate (3.8%). The R.S.D.s for the peak heights are slightly better (about 2%), except for citrate (5.4%). The linearity of the present method was investigated by analysing standard solutions containing a mixture of twelve analytes with known concentrations ranging from  $1.0 \cdot 10^{-5}$  M to 1.0 mM. From the electropherograms, either the peak area or the peak height is plotted against the concentration of the analyte to obtain the calibration graph for each analyte. Earlier studies have shown that in CE with indirect absorbance detection, the linearity of the cali-

Table 3  
Precision and linearity for the various analytes

Acid	R.S.D. (%)			Linearity		
	$t_m$	Area	Height	$a \times 10^5$	$b \times 10^4$	$R^2$
Oxalic	0.19	1.6	1.8	2.49	-0.04	0.9996
Citric	0.89	3.8	5.4	2.48	-1.04	0.9995
Tartaric	0.22	1.4	1.0	2.01	0.09	0.9992
Malic	0.20	2.0	1.2	1.97	0.013	0.9990
Acetic	0.22	2.7	1.7	1.55	0.27	0.9979
Lactic	0.24	1.4	1.4	1.32	0.12	0.9993
Aspartic	0.63	2.6	1.9	2.33	0.13	0.9995
Glutamic	0.73	2.5	2.3	2.83	0.15	0.9990
Ascorbic	0.26	2.9	1.9	2.73	-0.07	0.9998
Gluconic	0.30	2.3	1.8	2.50	0.2	0.9990

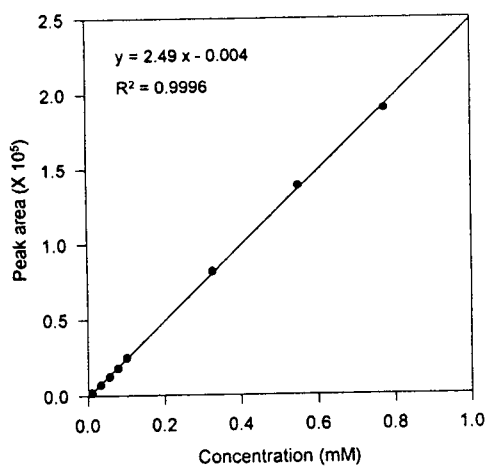


Fig. 6. Linearity of the calibration graph for oxalic acid (0.01–0.78 mM). Other conditions as in Fig. 3b.

bration spans only two orders of magnitude [24,25]. A typical calibration graph for the CE determination of oxalate is shown in Fig. 6. The data points from the calibration graphs were subjected to least-squares regression analysis and the slope  $a$ , intercept  $b$  and correlation coefficient  $R^2$  for the various analytes are given in Table 3. The linearity of the present method for most analytes is good, with correlation coefficients better than 0.999.

### 3.6. Analysis of real beverage samples

To demonstrate their practical applications, we applied the present CE methods to determine various organic acids in real beverage samples. These samples are classified into four types: "sports drink", nutrients-added drink, fruit juice (natural or artificial flavoured) and tea. Electropherograms of the four representative beverage samples are shown in Fig. 7. The concentrations of the organic acids of interest for the four samples are summarized in Table 4. Sports-drinks generally contain high concentrations of salts, chloride being a predominant anion. Citrate, lactate and ascorbate are also commonly found in these drinks. The contents of nutrients-added drinks vary; besides citrate, malate and ascorbate, the amino acids aspartate and glutamate are also commonly found. In most juices,

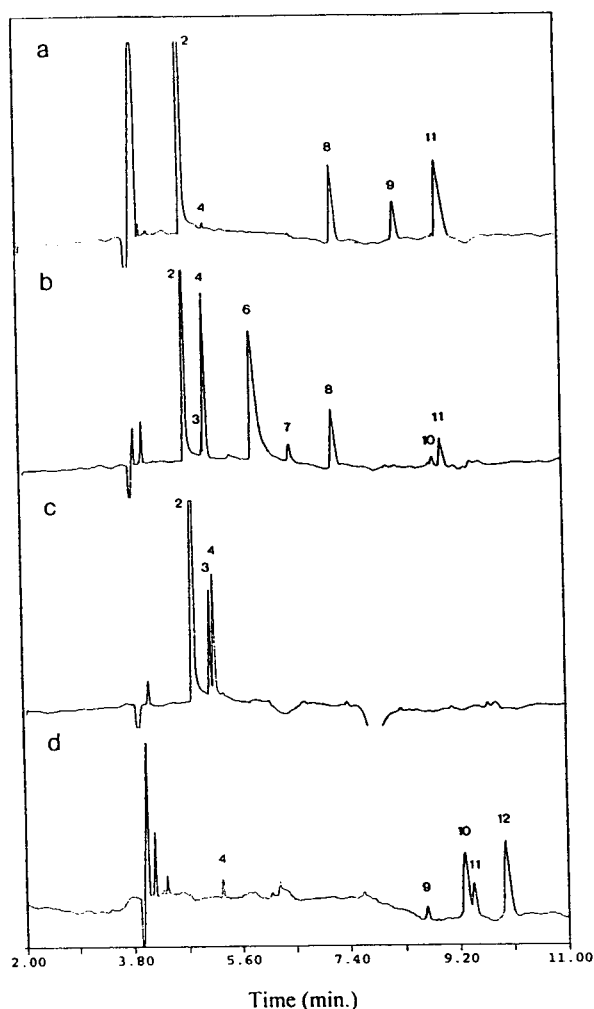


Fig. 7. Electropherograms of organic acids in real beverage samples: (a) sports-drink; (b) nutrients-added drink; (c) fruit juice; (d) tea. Other conditions as in Fig. 3b.

citrate is omnipresent, and in grape juice, tartaric acid is present in high concentration. Examination of the ingredient labels (quantitative data are unavailable) on the containers generally showed good agreement with the analyses by the CE method. The determination of vitamin C (ascorbic acid) is of special interest to the food and pharmaceutical industries because vitamin C is present in beverages, juices and medicines [26–29]. A common problem associated with the determination of vitamin C is the oxidation

Table 4  
Contents of the organic acids of interest found in representative beverage samples

Acid	Sample 1	Sample 2	Sample 3	Sample 4
Citric	13	9.5	13	0.42
Tartaric	0	0.13	1.5	0
Malic	0.014	3.2	1.9	0.057
Acetic	0	0.22	0	0
Lactic	1.1	2.8	0	0
Aspartic	0	0	0	0.051
Glutamic	0.54	0.023	0	0
Ascorbic	2.2	0.61	0	0.42
Gluconic	0	0	0	0.90

Samples: 1 = sports-drink; 2 = nutrients-added drink; 3 = artificial flavoured grape juice; 4 = honey tea. Concentrations in mM.

problem. Once dissolved, ascorbic acid is readily oxidized to dehydroascorbic acid, catalysed by air or light exposure [30]. Solutions of ascorbic acid should be freshly prepared and kept tightly capped in an amber-coloured bottle; solutions can be maintained for 12 h without obvious oxidation problems. Only the unoxidized form of ascorbate absorbs strongly in the UV region;

therefore, the indirect absorbance detection method was used to monitor the oxidation reaction of ascorbic acid. Fig. 8 shows CE analyses of ascorbic acid samples under various conditions. A freshly prepared ascorbate solution gives only a single peak (profile a). Even when kept in the dark, the solution is 45% oxidized after 18 h (profile b). After the solution has been exposed to air and light for 3 h, almost 80% of the ascorbate is oxidized (profile c). After 24 h, a negative peak appears. Hence the CE method is a valuable aid for checking freshness and for quality assurance.

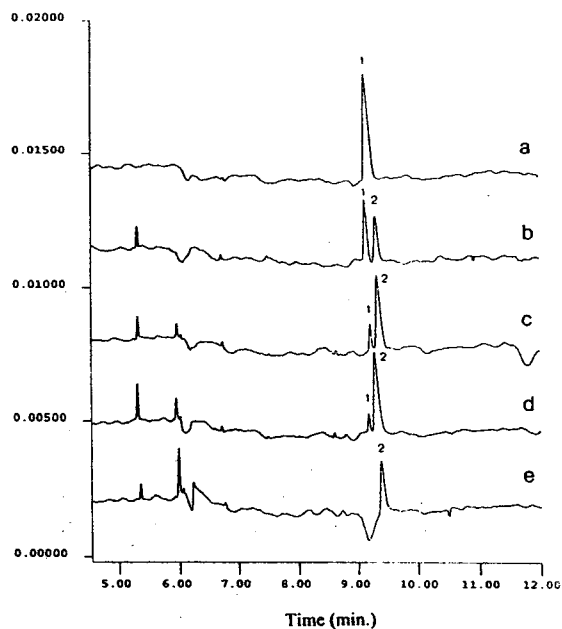


Fig. 8. Electrophoretic monitoring of the photocatalysed oxidation of 0.1 mM ascorbate: (a) fresh; (b) in the dark after 18 h oxidation; exposed to light and air after (c) 3 h, (d) 9 and (e) 24 h. Other conditions as in Fig. 3b.

#### 4. Conclusion

Organic acids, commonly found in beverages and juices (either naturally or artificially added), could be determined readily by CE with indirect absorbance detection. The CE separation was best performed with reverse polarity (towards the anode) using TMA (5 mM) as the BGE and TTAB (1 mM) as the EOF modifier. For the simultaneous determination of all analytes, the optimum pH is 9.0, at which all peaks except for malate and succinate are baseline resolved within 9.5 min. Alternatively, an acidic pH (5.5) could be used to improve the resolution of the diprotic acids but at the expense that glutamate and ascorbate peaks would not be baseline resolved. The CE methods developed here show very good



precision and linearity and could be readily applied to analyses of real food samples.

### Acknowledgement

This work was supported by a grant from the National Science Council, Republic of China (Taiwan).

### References

- [1] M.A. R. Rodriguez, M.L.V. Oderiz, J.L. Hernandez and J.S. Lozano, *J. Chromatogr. Sci.*, 30 (1992) 433.
- [2] J. Morris and J.S. Fritz, *LC·GC*, 11 (1993) 513.
- [3] B.F. Kenney, *J. Chromatogr.*, 546 (1991) 423.
- [4] B.J. Wildman, P.E. Jackson, W.R. Jones and P.G. Alden, *J. Chromatogr.*, 546 (1991) 459.
- [5] J. Romano, P. Jandik, W.R. Jones and P.E. Jackson, *J. Chromatogr.*, 546 (1991) 411.
- [6] S.P.D. Lalljie, J. Vindevogel and P. Sandra, *J. Chromatogr. A*, 652 (1993) 563.
- [7] L. Kelly and R.J. Nelson, *J. Liq. Chromatogr.*, 16 (1993) 2103.
- [8] S.M. Cousins, P.R. Haddad and W. Buchberger, *J. Chromatogr. A*, 671 (1994) 397.
- [9] W. Buchberger, S.M. Cousins and P.R. Haddad, *Trends Anal. Chem.*, 13 (1994) 313.
- [10] M.P. Harrold, M.J. Wojtusik, J. Riviello and P. Henson, *J. Chromatogr.*, 640 (1993) 463.
- [11] E. Dabek-Zlotorzynska and J.F. Dlouhy, *J. Chromatogr. A*, 671 (1994) 389.
- [12] S.A. Shamsi and N.D. Danielson, *Anal. Chem.*, 66 (1994) 3757.
- [13] H.-T. Chang and E.S. Yeung, *J. Chromatogr.*, 608 (1992) 65.
- [14] W. Buchberger and P.R. Haddad, *J. Chromatogr.*, 608 (1992) 59.
- [15] W.R. Jones and P. Jandik, *J. Chromatogr.*, 608 (1992) 385.
- [16] W.R. Jones, *J. Chromatogr.*, 640 (1993) 387.
- [17] J.B. Nair and C.G. Izzo, *J. Chromatogr.*, 640 (1993) 445.
- [18] P.E. Jackson and P.R. Haddad, *J. Chromatogr.*, 640 (1993) 481.
- [19] N.J. Benz and J.S. Fritz, *J. Chromatogr. A*, 671 (1994) 437.
- [20] S.A. Oehrle, *J. Chromatogr. A*, 671 (1994) 383.
- [21] M. Jimidar and D.L. Massart, *Anal. Chim. Acta*, 294 (1994) 165.
- [22] Y.-H. Lee and T.-I. Lin, *J. Chromatogr. A*, 680 (1994) 287.
- [23] T.-I. Lin, Y.-H. Lee and Y.-C. Chen, *J. Chromatogr. A*, 654 (1993) 167.
- [24] E.S. Yeung and W.G. Kuhr, *Anal. Chem.*, 63 (1991) 275A.
- [25] Y. Ma and R. Zhang, *J. Chromatogr.*, 625 (1992) 341.
- [26] M.C. Gennaro, C. Abrigo and E. Marengo, *Chromatographia*, 30 (1990) 311.
- [27] W.A. Behrens and R. Madere, *J. Liq. Chromatogr.*, 17 (1994) 2445.
- [28] E.V. Koh, M.G. Bissell and R.K. Ito, *J. Chromatogr.*, 633 (1993) 245.
- [29] M. Chiari and M. Nesi, G. Carrea P.G. Righetti, *J. Chromatogr.*, 645 (1993) 197.
- [30] M.B. Davies, J. Austin and D.A. Partridge, *Vitamin C. Its Chemistry and Biochemistry*, Royal Society of Chemistry, London, 1991.
- [31] D.R. Lide and H.P.R. Frederikse (Editors), *Handbook of Chemistry and Physics*, CRC Press, Boca Raton, FL, 75th ed., 1994.
- [32] A. Townshend, D.T. Burns, G.G. Guilbault, R. Lobinski, Z. Marczenko, E.J. Newman and H. Onihsi (Editors), *Dictionary of Analytical Reagents*, Chapman and Hall, London, 1st ed., 1993.



# Capillary zone electrophoresis in organic solvents: separation of anions in methanolic buffer solutions

Marcella Chiari<sup>a</sup>, Ernst Kenndler<sup>b,\*</sup>

<sup>a</sup>*Istituto di Chimica degli Ormoni, Consiglio Nazionale delle Ricerche, Via Mario Bianco 9, I 20131 Milan, Italy*

<sup>b</sup>*Institute for Analytical Chemistry, University of Vienna, Währingerstr. 38, A 1090 Vienna, Austria*

## Abstract

A tris(hydroxymethyl)aminomethane–acetate buffer system with methanol as solvent has been used at an apparent pH of 8.5 for the separation of six aromatic and aliphatic acids. Compared to pure aqueous buffer systems with various pH values (4.4, 5.5, 6.2 and 8.0) improved separation was obtained due to increased selectivity. This improvement is related to a specific shift in the  $pK_a$  values of the solutes in the organic solvent, and is interpreted by the concept of the transfer activity coefficient and the medium effect.

## 1. Introduction

Electrophoretic separations in nonaqueous and mixed aqueous–organic media deserve increased attention for several reasons. The advantages of performing capillary electrophoresis (CE) in organic solvents or in mixed-solvent systems are threefold: (i) most organic compounds exhibit greater solubility than water, (ii) changes in the effective mobilities may lead to greater selectivity and (iii) the electroosmotic flow is reduced [1,2]. Reduction of the electroosmotic flow can also influence the separation selectivity, and generally improves the reproducibility of the electrophoretic migration time.

The electrophoretic migration property of the solutes, governed by the ionic mobility, is influenced by organic solvents like methanol in two ways [3–8], affecting

(i) their actual mobility, due to changes in

the size of the solvated particle (and the viscosity of the bulk solution) and

(ii) their acid–base property, expressed by the  $pK_a$  value, thus determining the effective mobility at a given pH.

The second effect seems to be the most significant, because (in contrast to the actual mobilities) the dissociation constant,  $K_a$ , may change for different solvents by many orders of magnitude, and the mutual changes for the particular solutes are only weakly correlated, as shown for CE, specifically with respect to isotachopheresis of organic ions, in previous papers [9–11]. It should be mentioned that this change is different for different types of acids. It is very pronounced for acids of type HA, so-called neutral acids (those this paper deals with), but is less significant for  $HA^+$ -type cationic acids.

Only a few articles have been published reporting CE separations in pure organic or in mixed aqueous–organic solvents [8–24], most of them concerning isotachopheresis. The solvents

\* Corresponding author.

used were the lower alcohols, acetonitrile, dimethylsulfoxide, dimethylformamide, tetrahydrofuran, acetone or dioxan. In the present work we compare the separation of a mixture of aromatic and aliphatic acids in aqueous solutions with that obtained in pure methanol. The analytes selected in this work were chosen because their actual mobilities and  $pK$  values are similar in aqueous solution. This renders the separation of all components in a single run quite difficult, requiring complex optimization.

## 2. Experimental

### 2.1. Materials

Benzoic acid, *p*-toluenesulfonic acid, caffeic acid, *p*-hydroxycinnamic acid and 3-(trimethoxysilyl)propyl methacrylate (Bind Silane) were purchased from Aldrich (Steinheim, Germany). Methanol used as solvent had a water content of <0.05% (HPLC grade, Fluka, Buchs, Switzerland). *N*-Acryloylglycine (Immobiline,  $pK$  3.6) and *N*-acryloyl- $\gamma$ -aminobutyric acid (Immobiline,  $pK$  4.6) were purchased from Pharmacia LKB Biotechnology (Uppsala, Sweden). Ammonium peroxydisulfate and *N,N,N',N'*-tetramethylethylenediamine (TEMED) were obtained from Bio-Rad Labs (Richmond, CA, USA). Tris(hydroxymethyl)aminomethane (Tris) and 2-[*N*-morpholino]ethanesulfonic acid (MES) were from Sigma (St. Louis, MO, USA). Acryloylaminoethoxyethanol (AAEE) was synthesized as described by Chiari et al. [25].

### 2.2. Methods

Capillary zone electrophoresis (CZE) was performed in a Waters Quanta 4000 capillary electrophoresis system (Millipore, Milford, MA, USA). For the experiments 75  $\mu\text{m}$  I.D., 370  $\mu\text{m}$  O.D. capillaries purchased from Polymicro Technologies (Phoenix, AZ, USA) were used. The samples were loaded by hydrostatic pressure and the separations were carried out at ambient temperature (28 to 30°C). The detector was set at 254 nm.

### 2.3. Coating procedure

Capillaries coated with linear poly(AAEE) bonded through methacryloxypropyl silyl moieties were prepared according to a procedure described by Kilar and Hjerten [26] and modified as follows: the capillary was pretreated with 1 *M* NaOH for 5 h, then rinsed and flushed with 0.1 *M* HCl followed by NaOH (0.1 *M*). After 1 h it was rinsed with water and tetrahydrofuran (THF). Residual water was eliminated by connecting the capillary to a gas chromatographic oven at 120°C for 45 min under nitrogen flow. A 50% solution of  $\gamma$ -methacryloxypropyltrimethoxysilane in THF was then pulled through the capillary under pressure for 20 min and allowed to set for 12 h. After this treatment, the capillary was flushed extensively with THF and water, then filled with a 3% acrylamide solution containing the appropriate amount of catalyst (1  $\mu\text{l}$  TEMED and 1  $\mu\text{l}$  of 40% ammonium peroxydisulfate per ml of gelling solution) and degassed under vacuum (20 mmHg) for 40 min. Polymerization was allowed to proceed overnight at ambient temperature, after which the capillary was emptied by means of a syringe.

### 2.4. Separation conditions

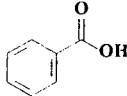
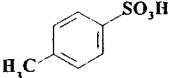
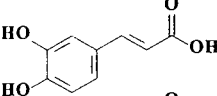
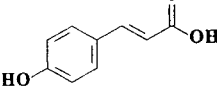
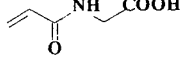
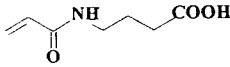
The mixture of components to be separated was injected into poly(AAEE)-coated capillaries (43 cm total length, 35 cm to the detector) using Tris–acetate (50 mM, pH 8.0), MES–Tris (50 mM, pH 6.2 and 5.5, respectively), and acetate–Tris (50 mM, pH 4.4) as pure aqueous running buffers. The same mixture was resolved in an uncoated capillary using a methanolic solution of Tris–acetate, where the concentrations of Tris and glacial acetic acid were 100 and 56 mM, respectively. The apparent pH of this solution was 8.5.

## 3. Results and discussion

### 3.1. Separation in aqueous solution

Electropherograms of the six components (see Table 1) were acquired in aqueous buffers at

Table 1  
Formulae and symbols

Name	Formula	Symbol
Benzoic acid		B
<i>p</i> -Toluenesulfonic acid		T
Caffeic acid		C
<i>p</i> -Hydroxycinnamic acid		H
N-Acryloylglycine		G
N-Acryloyl- $\gamma$ -aminobutyric acid		A

different pH values (4.4, 5.5, 6.2 and 8.0). Coated capillaries were used for the aqueous systems to reduce the electroosmotic flow and thus improve the reproducibility of the electrophoretic migration of the solutes. The pH value 4.4 falls within the range of  $pK$  values for the weak acids (3.6 to 4.6), and at pH 8.0 the solutes are fully dissociated. Typical electropherograms (obtained at the lowest and the highest pH, respectively) are shown in Figs. 1 and 2. In all the buffer systems, however, solutes co-migrate, except at pH 5.5; even at this pH, *p*-hydroxycinnamic and N-acryloyl- $\gamma$ -aminobutyric acid are not fully baseline-resolved.

The corresponding ionic mobilities, calculated from the electrophoretic data, are given in Table 2. The effective mobilities of the solutes increase with increasing pH of the buffer (except for the sulfonic acid, the mobility of which remains about constant due to its strong acidity) and reach a nearly constant value at high pH, namely that of the actual mobility. The scatter around the constant value can be attributed to the variation of the ionic strength of the buffer, and

to temperature effects. From the mobilities it can also be seen that the migration sequence varies with pH, specifically in the case of benzoic acid and N-acryloylglycine, which switch order with increasing pH. This effect is connected with the fact that benzoic acid is the weaker acid with the higher actual mobility.

### 3.2. Separation in methanolic solution

The electropherogram obtained in methanolic solution at an apparent pH of 8.5 is shown in Fig. 3. In contrast to the results obtained with the aqueous buffers, full resolution is observed. This is evidence of dramatic improvement in the separation selectivity, reflected by the greater difference in the mobilities of the components in the methanolic system. As stated in the Introduction the effective mobility (at a certain pH) is influenced very markedly by change in the  $pK$  value, often most dramatically for solvents other than water.

This variation in the  $pK_a$  values is explained

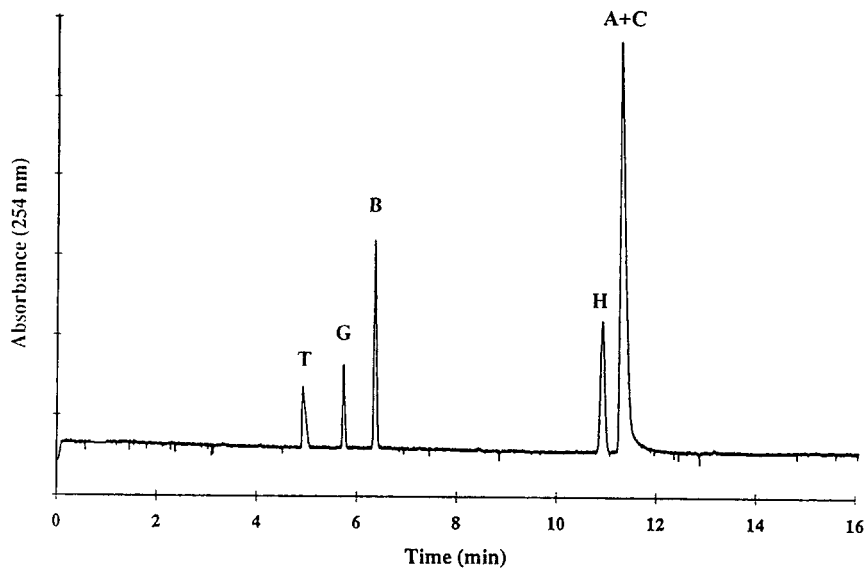


Fig. 1. Electropherogram of the anions in water at pH 4.4. For the symbols of the solutes see Table 1. Coated capillary: 75  $\mu\text{m}$  I.D., length: total 43 cm, to detector 35 cm. Voltage: -15 kV. Buffer: 50 mM acetate-Tris in water.

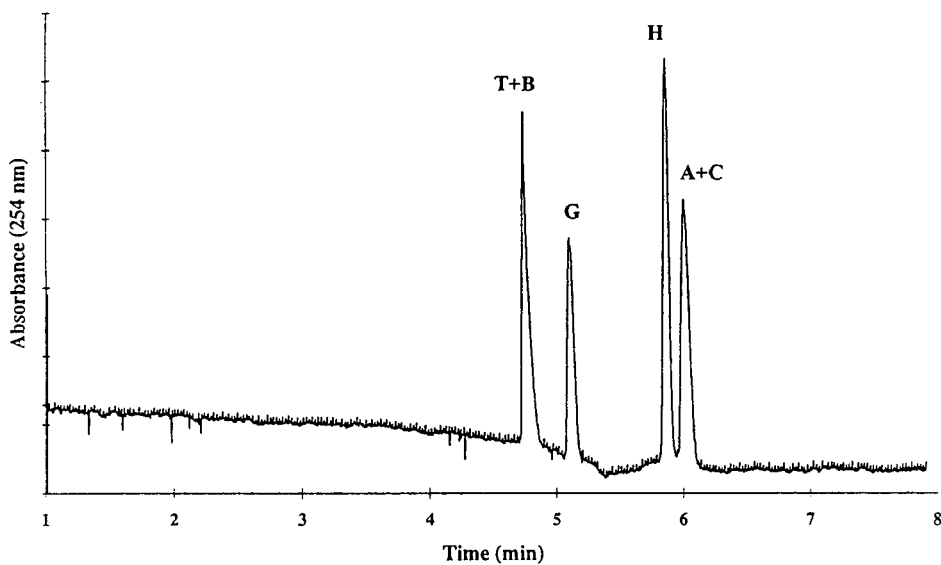


Fig. 2. Electropherogram of the anions in water at pH 8.0. Symbols, capillary and conditions as in Fig. 1. Buffer: 50 mM Tris-acetate in water.

Table 2  
List of effective mobilities in the different buffer systems

Acid	Effective mobility ( $10^{-9} \text{ m}^2 \text{ V}^{-1} \text{ s}^{-1}$ )				
	Water pH 4.4	Water pH 5.5	Water pH 6.2	Water pH 8.0	Methanol pH 8.5
<i>p</i> -Toluenesulfonic	34.0	32.0	32.0	35.3	25.0
N-Acryloylglycine	29.2	30.5	30.4	32.8	17.6
Benzoic	25.6	30.9	32.0	35.3	19.3
<i>p</i> -Hydroxycinnamic	15.3	23.9	25.3	28.5	13.9
N-Acryloyl- $\gamma$ -aminobutyric	14.8	23.5	25.3	27.9	14.9
Caffeic	14.8	22.6	23.7	27.9	12.9

by the concept of the medium effect,  $\log \gamma_i^m$  (or  $\ln \gamma_i^m$ ), given by

$$\log \gamma_i^m = \log \frac{(\mu_i^0)^s - (\mu_i^0)^w}{RT} \quad (1)$$

where the transfer activity coefficient or medium activity coefficient,  $\gamma_i^m$ , is defined as  $\gamma_i^m = \gamma_i^s / \gamma_i^w$  with  $\gamma_i^s$  and  $\gamma_i^w$  the activity coefficients of species *i* in the solvent and water, respectively. Further is  $\mu_i^0$  the chemical potential of component *i* in the standard state, indicated by S for the organic

solvent and by W for water, *R* is the gas constant and *T* the absolute temperature.

The medium effect is proportional to the reversible work required for the transfer of 1 mole of species *i* from infinite dilution in water, W, to infinite dilution in the organic solvent, S. If the particles of species *i* are better stabilized in organic solvent than in water, the medium effect has a negative value, and vice versa. The medium effect on the proton is a measure of the basicity of the solvents compared to water.

Discussing the transfer of a neutral acid (HA)

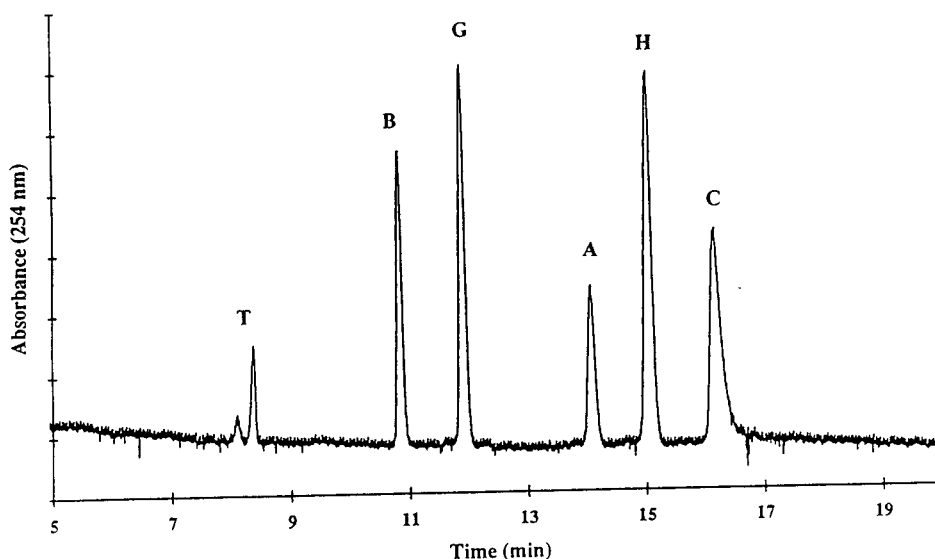


Fig. 3. Separation of the anions in methanolic buffer solution at apparent pH 8.5 in an uncoated capillary. Symbols and capillary dimensions as in Fig. 1. Voltage:  $-12 \text{ kV}$ . Buffer:  $100 \text{ mM}$  Tris-acetate in methanol.

species, as the solutes under consideration, from water, W, to solvent, S, we find that this acid undergoes the dissociation equilibrium  $\text{HA} = \text{H}^+ + \text{A}^-$  in both solvents. Thus, the reversible work done on the system in transferring 1 mole  $\text{H}^+$  and  $\text{A}^-$  from infinite dilution in water, W, to infinite dilution in the organic solvent, S, (and transferring 1 mole of HA from S to W) is given by the standard free energy of transfer,  $\Delta G_{\text{t}}^0$ . The change in the dissociation constant,  $K_{\text{a}}$ , is related to the standard free energy of transfer, and is given by

$$\Delta \text{p}K_{\text{a}} = \text{p}K_{\text{a}}^{\text{s}} - \text{p}K_{\text{a}}^{\text{w}} = \log \frac{\gamma_{\text{H}^+}^{\text{m}} \gamma_{\text{A}^-}^{\text{m}}}{\gamma_{\text{HA}}^{\text{m}}} \quad (2)$$

where  $\gamma_{\text{H}^+}^{\text{m}}$ ,  $\gamma_{\text{A}^-}^{\text{m}}$  and  $\gamma_{\text{HA}}^{\text{m}}$  are the transfer activity coefficients of the proton, the anion and the neutral molecule, respectively, the particles involved in the ionization equilibrium.

It is clear that the change in the  $\text{p}K_{\text{a}}$  values will be determined by the extent of stabilization or destabilization of the particles  $\text{H}^+$ ,  $\text{A}^-$  and HA in the organic solvent compared to water. It must be pointed out that the values for the transfer activity coefficients for the individual particles can be obtained by approximation methods only.

As a rough measure a mean value of zero (with a standard deviation of 2) is accepted in the literature for  $\log \gamma_{\text{H}^+}^{\text{m}}$  (cf. e.g. Ref. [5]), which means that the basicity of methanol is comparable to that of water, and the medium effect on the proton will not be decisive for the  $\text{p}K$  shift. This can also be supposed for HA, the neutral particle involved in the ionization equilibrium: for uncharged species the medium effect is of minor significance.

The most dramatic influence of methanol on the  $\text{p}K$  is based on the anion stabilization. As an anion solvent, methanol is inferior to water, which means that  $\log \gamma_{\text{A}^-}^{\text{m}}$  has positive and fairly large values. Because the medium effects on the proton and on the neutral moiety are of less significance, the medium effect on the anion dominates, resulting in higher  $\text{p}K$  values in methanol compared to water, according to Eq. 2. This is in fact what is observed for benzoic

acid, which has a  $\text{p}K_{\text{a}}$  of 4.2 in water and a  $\text{p}K_{\text{a}}$  of 9.28 in pure methanol; for mixed aqueous-methanolic solutions the  $\text{p}K_{\text{a}}$  values fall between these extremes: 6.42 for a binary mixture with 70 mol% methanol and 8.30 for a mixture with < 1 mol% methanol (cf. Ref. [3]).

From this discussion one can expect that the solutes considered in this paper (except the sulfonic acid) will exhibit a shift in their  $\text{p}K$  values from water (ranging between 3.6 to 4.6) to the methanolic buffer to roughly 4 to 5  $\text{p}K$  units higher, to about 8.5. This is the pH where the electropherogram shown in Fig. 3 was obtained. Thus it follows that the gain in selectivity can be attributed to the change in the  $\text{p}K$  values brought about by methanol, as discussed.

To provide a clearer insight into the effect of methanol on the selectivity, the change in mobility related to that of the sulfonic acid is shown in Fig. 4. The sulfonic acid is considered as the reference component because, due to its acidity, its  $\text{p}K$  will not be shifted into the pH region of the methanolic system.

First, it can be seen that in aqueous buffers hardly a pH can be predicted where the mobilities are so different that an electrophoretic separation is obtained, which supports the use of methanol.

Second, it can be seen that, in the case of

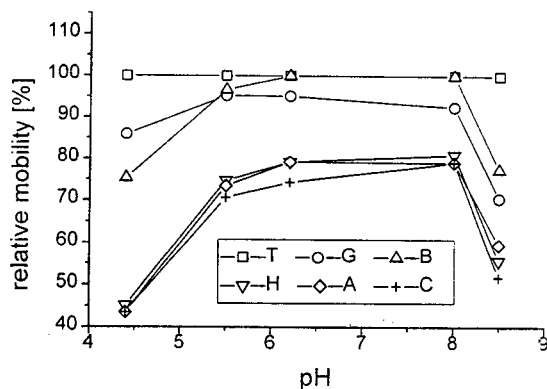


Fig. 4. Plot of the relative mobility of the anions,  $i$ , as a function of the (apparent) pH of the buffer. The mobilities  $u_i$  are related to that of *p*-toluenesulfonate ( $u_{\text{T}}$ ), according to  $100(u_i/u_{\text{T}})$ . Symbols of the solutes as in Table 1. Mobilities from Table 2.



those solutes with a similar structure (hydroxycinnamic and caffeic acid; N-acryloylglycine and N-acryloyl- $\gamma$ -aminobutyric acid), whether or not the solvent is water or methanol does not affect the sequence of mobility, which means that the actual mobilities of these solutes as well as their  $pK$  values are influenced by the two solvents in a rather parallel way. On the other hand, the electrophoretic properties of benzoic acid, which has a different chemical structure, with the carboxylic function directly linked to the aromatic ring, do differ in the two solvent systems. Benzoic acid exhibits the highest relative mobility in methanol, a situation which is comparable only to the high pH region in water. In none of the pH regions in water, however, is exactly the same migration sequence found as in methanol, which is caused by the rather specific shift of the  $pK$  values of the solutes in this solvent.

The results lead to the conclusion that methanol (and potentially other solvents) can be used to advantage in capillary electrophoresis, not only to increase the solubility of organic acids and bases (and to suppress the electroosmotic flow), but also to enhance separability by selectively changing the acid–base properties of these solutes. Unfortunately, these changes can at present be forecast only in terms of trends: actual values cannot be predicted exactly.

## References

- [1] C. Schwer and E. Kenndler, *Anal. Chem.*, 63 (1991) 1801.
- [2] W. Schützner and E. Kenndler, *Anal. Chem.*, 64 (1992) 1991.
- [3] E. Kenndler, in N.A. Guzman (Editor), *Capillary Electrophoresis Technology*, Marcel Dekker, New York, 1993.
- [4] R.G. Bates, in J.F. Coetzee and C.D. Ritchie (Editors), *Solvent–Solvent Interactions*, Marcel Dekker, New York, 1969.
- [5] E.J. King, in A.K. Covington and T. Dickinson (Editors), *Physical Chemistry of Organic Solvent Systems*, Plenum Press, London, 1973.
- [6] A.K. Covington and T. Dickinson (Editors), in *Physical Chemistry of Organic Solvent Systems*, Plenum Press, London, 1973.
- [7] I.M. Kolthoff and M.K. Chantooni, in I.M. Kolthoff and P.J. Elving (Editors), *Treatise on Analytical Chemistry, Part I, Theory and Practise, Vol. 2, Sect. D*, John Wiley, New York, 1979.
- [8] A.P. Popov and H. Caruso, in I.M. Kolthoff and P.J. Elving (Editors), *Treatise on Analytical Chemistry, Part I, Theory and Practise, Vol. 2, Sect. D*, John Wiley, New York, 1979.
- [9] E. Kenndler and P. Jenner, *J. Chromatogr.*, 390 (1987) 169.
- [10] E. Kenndler and P. Jenner, *J. Chromatogr.*, 390 (1987) 185.
- [11] E. Kenndler, C. Schwer and P. Jenner, *J. Chromatogr.*, 470 (1989) 57.
- [12] J.L. Beckers and F.M. Everaerts, *J. Chromatogr.*, 51 (1970) 339.
- [13] J.L. Beckers and F.M. Everaerts, *J. Chromatogr.*, 68 (1972) 207.
- [14] J.C. Reijenga, G.V.A. Aben, T.P.E.M. Verheggen and F.M. Everaerts, *J. Chromatogr.*, 260 (1983) 241.
- [15] H. Yoshida and Y. Hiram, *J. Chromatogr.*, 298 (1984) 243.
- [16] Y. Walbroehl and J.W. Jorgenson, *J. Chromatogr.*, 315 (1984) 135.
- [17] M. Koval, D. Kaniansky, M. Hutta and R. Lacko, *J. Chromatogr.*, 325 (1985) 151.
- [18] Y. Hiram and H. Yoshida, *J. Chromatogr.*, 322 (1985) 139.
- [19] S. Fujiwara and S. Honda, *Anal. Chem.*, 59 (1987) 487.
- [20] T. Hirokawa, T. Tsuyoshi and Y. Kiso, *J. Chromatogr.*, 408 (1987) 27.
- [21] S. Tanaka, T. Kaneta and H. Yoshida, *J. Chromatogr.*, 472 (1989) 303.
- [22] M. Idei, I. Mezö, Zs. Vadasz, A. Horvath, I. Teplan and Gy. Keri, *J. Liq. Chromatogr.*, 15 (1992) 3181.
- [23] M. Idei, I. Mezö, Zs. Vadasz, A. Horvath, I. Teplan and Gy. Keri, *J. Chromatogr.*, 648 (1993) 251.
- [24] M.P. Harrold, M.J. Wojtusik, J. Riviello and P. Henson, *J. Chromatogr.*, 640 (1993) 463.
- [25] M. Chiari, C. Micheletti, M. Nesi, M. Fazio and P.G. Righetti, *Electrophoresis*, 15 (1994) 177.
- [26] F. Kilar and S. Hjerten, *Electrophoresis*, 10 (1989) 23.





ELSEVIER

Journal of Chromatography A, 716 (1995) 311–317

JOURNAL OF  
CHROMATOGRAPHY A

# Determination of inorganic and small organic anions in pure boric acid using capillary zone electrophoresis

J. Boden, M. Darius, K. Bächmann\*

*Fachbereich Chemie, Technische Hochschule Darmstadt, D-64287 Darmstadt, Germany*

## Abstract

Inorganic and small organic anions were determined in pure boric acid using an on-line process for removal of the boric acid matrix from the capillary by adjusting the pH of the electrolyte and the electroosmotic flow. Employing this procedure, the matrix has no further influence on the separation and the analytes can be detected up to analyte-to-matrix ratios (ATMR) of  $1:5 \cdot 10^5$  to  $1:4 \cdot 10^5$  using hydrostatic injection. The limits of detection of the analytes were improved by on-line preconcentration procedures such as electrokinetic injection and sample stacking, resulting in an increased ATMR of  $1:1 \cdot 10^7$  to  $1:3 \cdot 10^7$  for sample stacking. These optimized conditions were applied to analyse two different batches of boric acid for impurities.

## 1. Introduction

The determination of inorganic anions in real samples containing a large excess of a matrix component is a fundamental analytical problem, which is becoming more and more important also for capillary zone electrophoretic (CZE) applications [1–3]. Recently, it has been shown that a matrix effect can be an advantage in comparison with a common CZE separation because a stacking process can occur, resulting in increased plate numbers for the analytes [3–6]. Thus, the matrix ion can act as the leading or the terminating species in an initial isotachophoretic state. The co-ion of the electrolyte has to be chosen in such a way that the mobilities of the analyte ions are between those of the electrolyte and the matrix ion.

Using this method, the inorganic anions can be

determined in the presence of a fluoride matrix up to an analyte-to-matrix ratio (ATMR) of  $1:6 \cdot 10^4$  [3]. Above this value, overlapping of the analyte peaks by the matrix peak occurs. With a non-ionic matrix, the matrix cannot co-migrate with the analyte ions and, further, it is not able to influence the isotachophoretic initial state.

Another difference between a non-ionic matrix and an ionic matrix is the possibility of using preconcentration methods for the analyte ions such as electrokinetic injection or sample stacking because the matrix does not contribute to the conductivity of the sample. Thus, the limit of detection (LOD) and the ATMR can be improved.

A disturbance of the CZE separation could happen only if the matrix component is moved by the electroosmotic flow (EOF) in the same direction as the analytes. Then, the different viscosity between the sample zone and the electrolyte, memory effects at the capillary wall and increased diffusion effects due to the high con-

\* Corresponding author.

centration gradient could influence the baseline and the migration times.

Therefore, with a non-ionic matrix the EOF should be adjusted in the opposite direction to the analyte ions. Hence the matrix will be removed from the capillary at the beginning of the separation and the analytes can be detected without matrix effects (see Fig. 1).

The dissociation of a number of matrices is strongly dependent on the pH of the solution. By choosing the pH of the electrolyte in such a way that the dissociation of the compound is decreased, the above-mentioned procedure is applicable to the determination of the ionic impurities in the substance. The purpose of this paper is to demonstrate the determination of inorganic and small organic anions in non-ionic matrices, e.g., in industrial chemical boric acids as matrix.

## 2. Experimental

The separations were carried out using a laboratory made CZE system and conventional untreated fused-silica capillaries (CS Chromatographie Service, Langerwehe, Germany). For detection the separation capillary passed through a Dionex (Sunnyvale, CA, USA) variable-wavelength UV detector and its outlets were placed in two 10-ml electrolyte vials. The high voltage from a 30 kV power supply (F.u.G. Electronic, Rosenheim, Germany) was applied with Pr–Ir electrodes dipping into the electrolyte. The positive electrode was placed in the outlet vessel.

Data were processed by an A/D board from ERC (Alteglöfshheim, Germany) using APEX

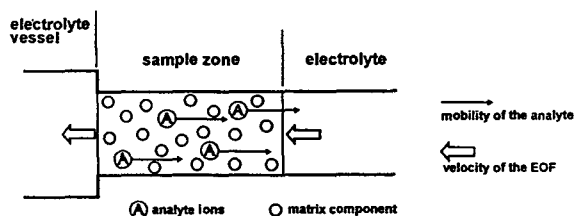


Fig. 1. Schematic illustration of the on-line matrix removal process.

chromatography software (Autochrom, Milford, MA, USA). The absorbance units (AU) of the detector were transformed by the A/D board into  $\mu\text{V}$ , and therefore the output of the data was in the voltage mode ( $19 \text{ V} = 1 \text{ AU}$ ).

### 2.1. Chemicals

All solutions, electrolytes and standards were prepared with ultra-pure water obtained from a Milli-Q system (Millipore, Eschborn, Germany). For the preparation of the electrolyte, sodium chromate and tetradecyltrimethylammonium bromide (TTAB) was used (Aldrich-Chemie, Steinheim, Germany). Boric acid was obtained from different companies in several purity grades. All other reagents were of analytical-reagent grade from Merck (Darmstadt, Germany).

## 3. Results and discussion

### 3.1. Optimization of electrolyte composition

In order to detect UV-inactive ions, the indirect detection mode [7–10] using a UV-active background electrolyte should be applied. To measure several inorganic and organic anions in the presence of boric acid, the pH of the electrolyte and the EOF additionally have to be optimized.

Depending on the pH of the electrolyte, boric acid exists as different dissociated species. As boric acid behaves as a weak acid in aqueous solutions ( $\text{p}K_a$  9.14, 12.74 and 13.80 [11]), at  $\text{pH} > 9$  it is strong dissociated and can cause the above-mentioned matrix effects. At  $\text{pH} < 9$  boric acid is not sufficiently dissociated and it can move only by the EOF. Therefore, the pH of the electrolyte should be  $< 9$ .

To shorten the analysis time for the determination of anions by reversing the EOF, a modifier (e.g., TTAB or CTAB) [12–14] is commonly applied as an additive to the electrolyte. Fig. 2a shows an electropherogram obtained using a chromate electrolyte at pH 8.1 with 0.2 mmol/l TTAB. It can be seen that the analyte peaks can

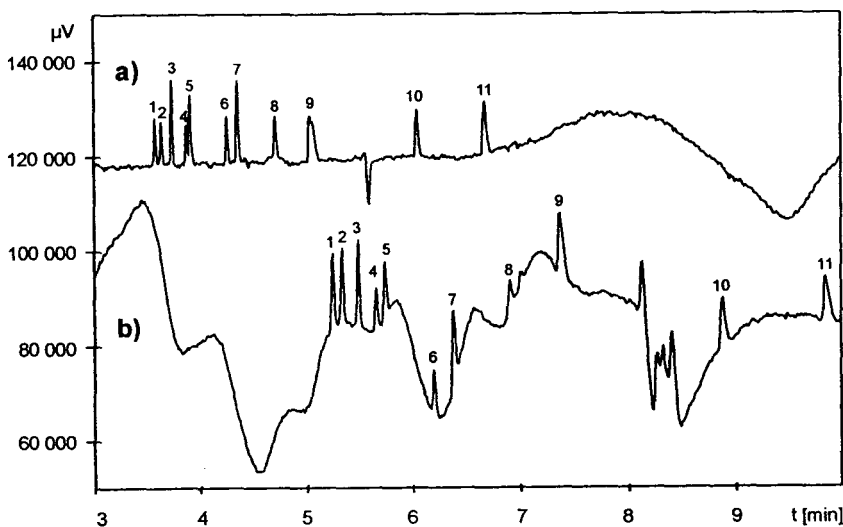


Fig. 2. Electropherograms of an anion mixture. (a) Anionic mixture without boric acid. (b) Anionic mixture with a 0.9 mol/l boric acid matrix. Electrolyte, 5 mmol/l sodium chromate–0.2 mmol/l TTAB (pH 8.1); samples: 1 = bromide; 2 = chloride; 3 = sulfate; 4 = nitrate; 5 = oxalate; 6 = chlorate; 7 = malonate; 8 = fluoride; 9 = phosphate; 10 = acetate; 11 = propionate; sample concentration, each 25  $\mu\text{mol/l}$ ; injection, hydrostatic (10 cm, 30 s); capillary, 70 cm to the detector, 85 cm total length, 75  $\mu\text{m}$  I.D.; detection, indirect UV, 254 nm; EOF, in the same direction as the analytes,  $v_{\text{EOF}} = -0.05$  cm/s.

be determined in short times and with a stable baseline. On the other hand, for a boric acid sample (0.9 mol/l) to which an anionic standard was added (see Fig. 2b), baseline interferences and longer migration times resulted using the same experimental conditions as in Fig. 2a. The reason for this effect is that for this modifier concentration the EOF and, therefore, also the matrix are moving in the same direction as the anions and so matrix effects can occur.

Therefore, it is necessary to adjust the EOF in the opposite direction to that of the analytes. Optimizing the electrolyte system by changing the concentration of the TTAB modifier, a reversal of the EOF takes place at a TTAB concentration of 0.07 mmol/l. Without the modifier the migration times of the analytes would be longer than 15 min. At a TTAB concentration of 0.01 mM the EOF is directed opposite to the anions but slowed down to obtain acceptable analysis times.

Fig. 3 shows two electropherograms of anions, (a) without and (b) with a matrix of boric acid, obtained using these optimized conditions. no difference concerning the baseline and migration

times can be seen between the two electropherograms because the matrix is removed from the capillary by the EOF and no matrix effect can occur.

It can be seen that the peak heights are comparable in both electropherograms, except for the chloride peak. This can be explained by chloride contamination of the boric acid used. A disadvantage of these experimental conditions is that acetate and propionate cannot be detected because of their slow mobility.

### 3.2. Determination of the blank value of boric acid using different injection techniques

Fig. 4 shows the electropherograms of 0.9 mol/l boric acid obtained using three different injection methods. Owing to the small injection volume and the low concentration of the sample, the LOD for the hydrostatic injection is relatively high. As can be seen in Fig. 4a, only chloride can be determined using hydrostatic injection. It is therefore not recommended to use this method for trace analysis.

In order to decrease the LOD, the sample had

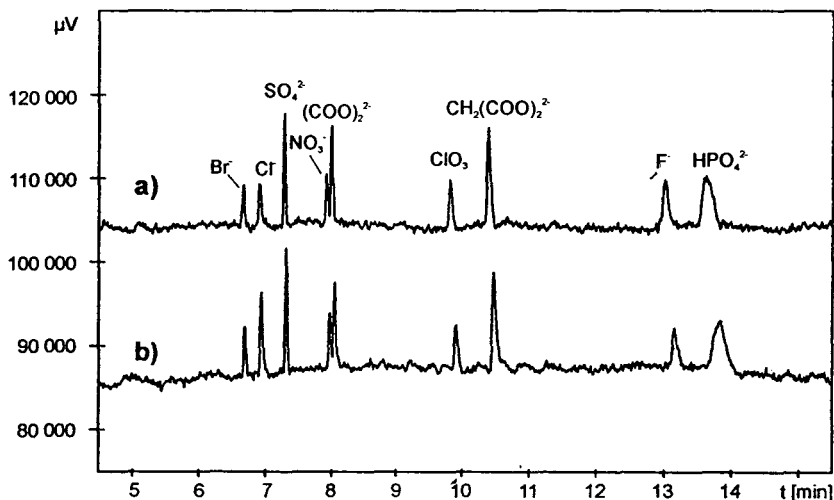


Fig. 3. Electropherograms of an anion mixture. (a) Anionic mixture without boric acid. (b) Anionic mixture with a 0.9 mol/l boric acid matrix. Electrolyte, 5 mmol/l sodium chromate–0.01 mmol/l TTAB (pH 8.1); EOF, in the opposite direction to the analytes,  $v_{\text{EOF}} = +0.12$  cm/s; all other conditions as in Fig. 2.

to be enriched by electrokinetic injection or by sample stacking [15,16]. Electrokinetic injection as a preconcentration method (see Fig. 4b) allows an improvement of the LOD of the fast analyte ions by a factor of 15. Thus, additionally to chloride also other analytes such as sulfate, nitrate, oxalate and hydrogenphosphate can be detected. Disadvantages of this method are the discrimination of ions having a low mobility, the dependence of the enrichment factor on the conductivity of the sample and the necessity for a correcting calculation using two internal standards [17] to quantify the results.

Another on-line preconcentration method by which the LOD can be improved is sample stacking. Sample stacking was performed by filling the capillary with the sample up to the detector, resulting in a sample volume of 2.6  $\mu\text{l}$ . After applying the high voltage, the analyte ions migrate rapidly toward the boundary between the sample and electrolyte. Simultaneously, the reverse-directed EOF removes the stacked cations and the water plug from the capillary. When the water plug leaves the capillary, a uniform field strength is reached and the current increases from zero to the common separation level. Then the CZE separation begins without

switching the polarity. The results of sample stacking are shown in Fig. 4c.

The main advantage is the very low LOD for all analyte ions. The amount of sample is increased by a factor of nearly 200 compared with hydrostatic injection, allowing an improvement of the LOD by a factor of 200 also, and also bromide can be determined. Further, there are no discriminating effects for slow analyte ions as observed in the electrokinetic injection method. A disadvantage of the stacking process with a boric acid sample is that the EOF takes 10.5 min to remove the boric acid from the capillary, whereas a water plug of a sample without matrix is removed after 5.3 min (not shown). Therefore, long analysis times and peak broadening occur, especially for the slow analytes fluoride and hydrogenphosphate in the presence of a boric acid matrix. The explanation of this effect is the high viscosity and the low pH (pH 3.5 of 0.9 M boric acid) of the boric acid solution. Both parameters decrease the EOF in the part of the capillary filled with the boric acid solution. In spite of these disadvantages, sample stacking is preferred because analyte discrimination does not take place and peak correction is not necessary.

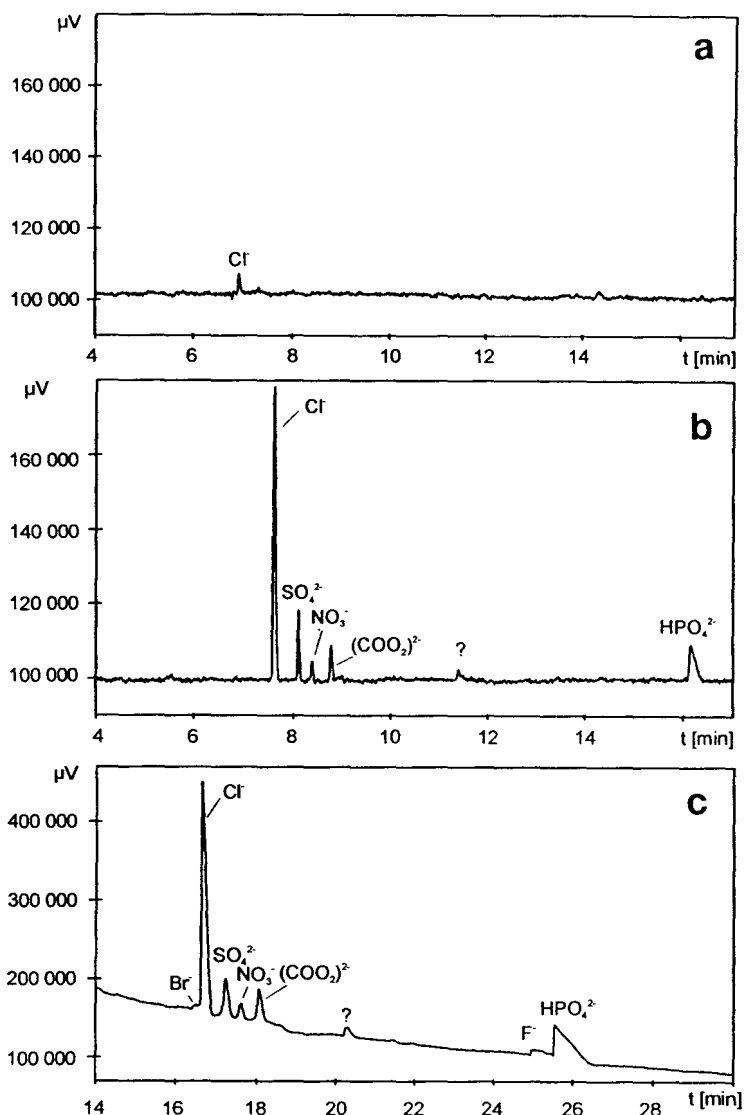


Fig. 4. Determination of the blank value of a commercially available boric acid of technical grade using different injection techniques. (a) Boric acid 2 using hydrostatic injection (10 cm, 30 s); (b) boric acid 2 using electrokinetic injection (3 kV, 10 s); (c) boric acid 2 using sample stacking (hydrodynamic injection up to the detector, sample volume  $2.6 \mu\text{l}$ , duration of the stacking process 10.5 min). Electrolyte, 5 mmol/l sodium chromate–0.01 mmol/l TTAB (pH 8.1); sample, 0.9 mol/l boric acid 1 without addition of anions; all other conditions as in Fig. 3.

In Table 1, the LOD and the ATMR for the different injection methods are summarized. The values with sample stacking are better than those for hydrostatic injection and electrokinetic injection. With sample stacking an LOD in the low nmol/l region is achieved.

To apply the developed CZE method, the

blank values of two boric acids from different companies were measured. For this purpose the boric acid was dissolved in pure water. According to its solubility, a maximum concentration of 0.9 mol/l was achieved. To determine the impurities, the standard addition method was carried out. In this way, systematic errors caused by

Table 1  
Comparison of different injection techniques for samples with boric acid matrix

Anion	Hydrostatic injection		Electrokinetic injection		Sample stacking	
	LOD <sup>a</sup> ( $\mu\text{mol/l}$ )	ATMR	LOD <sup>a</sup> ( $\mu\text{mol/l}$ )	ATMR	LOD <sup>a</sup> ( $\mu\text{mol/l}$ )	ATMR
Bromide	8	$1:1.1 \cdot 10^5$	0.3	$1:2.7 \cdot 10^6$	0.07	$1:1.2 \cdot 10^7$
Chloride	7	$1:1.3 \cdot 10^5$	0.5	$1:1.7 \cdot 10^6$	0.04	$1:2.1 \cdot 10^7$
Sulfate	5	$1:1.8 \cdot 10^5$	0.2	$1:3.8 \cdot 10^6$	0.02	$1:3.5 \cdot 10^7$
Nitrate	7	$1:1.3 \cdot 10^5$	0.3	$1:2.8 \cdot 10^6$	0.04	$1:2.2 \cdot 10^7$
Oxalate	5	$1:1.8 \cdot 10^5$	0.4	$1:2.1 \cdot 10^6$	0.03	$1:2.8 \cdot 10^7$
Chlorate	7	$1:1.3 \cdot 10^5$	0.4	$1:2.2 \cdot 10^6$	0.05	$1:1.5 \cdot 10^7$
Malonate	5	$1:1.8 \cdot 10^5$	0.4	$1:2.0 \cdot 10^6$	0.05	$1:1.7 \cdot 10^7$
Fluoride	10	$1:0.9 \cdot 10^5$	0.7	$1:1.2 \cdot 10^6$	0.89	$1:9.0 \cdot 10^5$

Experimental conditions as in Fig. 4c.

<sup>a</sup> The LOD was defined as three times the signal-to-noise ratio.

different migration times of samples with and without a matrix of boric acid can be prevented. The results are summarized in Table 2. It can be seen that the results achieved conform to the specified purities (boric acid 1 = analytical-reagent grade, boric acid 2 = technical grade).

#### 4. Conclusion

It has been shown that the combination of an electrophoretic separation with an on-line process for the removal of a non-ionic matrix is a very effective approach for improving the detectability of the anions. Using ion chromatography as separation method, an automated sample preparation step can be applied to prevent baseline disturbances due to the boric acid ma-

trix. In this case, removal of the matrix in addition to preconcentration of the analytes [18] takes place.

In the described CZE method a similar result occurs, because the matrix is removed by the reverse-directed EOF and, simultaneously, the analytes are concentrated by the stacking procedure. An advantage of the latter method is the on-line procedure without variation of the CZE device. Using the CZE method, the anionic impurities in two different boric acids were determined. For the anions in a 0.9 mol/l solution of boric acid an LOD of 5–10  $\mu\text{mol/l}$  is obtained with hydrostatic injection. On enriching the analytes by electrokinetic injection or sample stacking, the LOD is improved by a factor 15 or 200, respectively, in comparison with hydrostatic injection. It can be assumed that the described

Table 2  
Blank values ( $\mu\text{mol/l}$ ) for two different boric acids

Sample	Bromide ( $r^2 = 0.9885$ )	Chloride ( $r^2 = 0.9427$ )	Sulfate ( $r^2 = 0.9980$ )	Nitrate ( $r^2 = 0.9909$ )	Oxalate ( $r^2 = 0.9872$ )
Boric acid 1 (analytical-reagent grade)	1.1	4.2	0.9	1.5	0.4
Boric acid 2 (technical grade)	0.9	23.1	2.2	1.4	2.3

$r^2$  = Regression coefficient of the calibration line. For the electropherogram of boric acid 2, see Fig. 4c; for boric acid 1, no electropherogram shown.



method is applicable to all samples with neutral matrices and to matrices with low mobility. In the latter case, the matrix can influence the isotachophoretic state. Then, in addition to the pH of the electrolyte and the EOF, the mobility of the co-ion of the electrolyte also has to be considered.

## References

- [1] P. Jandik and W.R. Jones, *J. Chromatogr.*, 608 (1992) 385.
- [2] J. Romano, P. Jandik, W.R. Jones and P.E. Jackson, *J. Chromatogr.*, 546 (1991) 411.
- [3] J. Boden, K. Bächmann, L. Kotz, L. Fabry and S. Pahlke, *J. Chromatogr. A*, 696 (1995) 321.
- [4] P. Gebauer, W. Thormann and P. Bocek, *J. Chromatogr.*, 608 (1992) 47.
- [5] J.L. Beckers and F.M. Everaerts, *J. Chromatogr.*, 508 (1990) 3.
- [6] J.L. Beckers and F.M. Everaerts, *J. Chromatogr.*, 508 (1990) 19.
- [7] E.S. Yeung, *Acc. Chem. Res.*, 22 (1989) 125.
- [8] T. Wang and R.A. Hartwick, *J. Chromatogr.*, 607 (1992) 119.
- [9] W. Buchberger and P.R. Haddad, *J. Chromatogr.*, 608 (1992) 59.
- [10] W.R. Jones and P. Jandik, *Am. Lab.*, 22 (1990) 51.
- [11] *CRC Handbook of Chemistry and Physics*, CRC Press, Boca Raton, FL, 71st ed. 1990–91.
- [12] X. Huang, J.A. Luckey, M.J. Gordon and R.N. Zare, *Anal. Chem.*, 61 (1989) 766.
- [13] K.D. Altria and C.F. Simpson, *Chromatographia*, 24 (1987) 527.
- [14] T. Kaneta, S. Tanaka and H. Yoshida, *J. Chromatogr.*, 538 (1991) 385.
- [15] R.-L. Chien and D.S. Burgi, *Anal. Chem.*, 64 (1992) 1046.
- [16] R.-L. Chien and D.S. Burgi, *Anal. Chem.*, 64 (1992) 489A.
- [17] E.V. Dose and G.A. Guiochon, *Anal. Chem.*, 63 (1991) 1154–1158.
- [18] AN 56, Dionex, Sunnyvale, CA, 1988.





ELSEVIER

Journal of Chromatography A, 716 (1995) 319–322

JOURNAL OF  
CHROMATOGRAPHY A

# Optical resolution of amino acid derivatives by micellar electrokinetic chromatography with sodium N-tetradecanoyl-L-glutamate

Koji Otsuka<sup>a,\*</sup>, Hitomi Kawakami<sup>a</sup>, Wakako Tamaki<sup>a</sup>, Shigeru Terabe<sup>b</sup>

<sup>a</sup>Department of Industrial Chemistry, Osaka Prefectural College of Technology, Saiwai-cho, Neyagawa, Osaka 572, Japan

<sup>b</sup>Department of Material Science, Faculty of Science, Himeji Institute of Technology, Kamigori, Hyogo 678-12, Japan

## Abstract

Optical resolution by micellar electrokinetic chromatography with sodium N-tetradecanoyl-L-glutamate (STGlu) was investigated. Similar to the case when using sodium N-dodecanoyl-L-valinate (SDVal), sodium N-dodecanoyl-L-glutamate (SDGlu) and N-dodecanoyl-L-serine (DSer), addition of sodium dodecyl sulfate (SDS), urea and methanol to STGlu micellar solutions gave improved peak shapes and enhanced the enantioselectivity. With an STGlu–3-[(3-cholamidopropyl)dimethylammonio]-1-propanesulfonate–SDS–urea–methanol solution, five phenylthiohydantoin-DL-amino acids were separated and each enantiomeric pair was optically resolved. The resolution characteristic in the STGlu system, however, was not substantially different from those in SDVal, SDGlu and DSer systems.

## 1. Introduction

Micellar electrokinetic chromatography (MEKC) is capable of separating both neutral and charged compounds and has become a popular technique in capillary electrophoresis (CE) for separating small neutral compounds. In MEKC, an ionic micelle is used as a pseudo-stationary phase that migrates with a different velocity as an aqueous phase or the electro-osmotic velocity.

Optical resolution is one of important objectives in chromatography and also CE, especially in pharmaceutical and medical fields, and many reports on enantiomeric separations by CE have

already appeared [1,2], including by MEKC with chiral micelles and cyclodextrin-modified MEKC (CD-MEKC). The use of amino acid derivatives as chiral selectors in MEKC was first reported by Dobashi et al. [3,4]. We have reported the enantiomeric resolution of phenylthiohydantoin derivatives of racemic amino acids by MEKC using chiral micelles of amino acid derivatives, such as sodium N-dodecanoyl-L-valinate (SDVal) [5–7], sodium N-dodecanoyl-L-glutamate (SDGlu) [8] and N-dodecanoyl-L-serine (DSer) [9], and using digitonin [5,8], which is a neutral glycoside. Phenylthiohydantoin-amino acids (PTH-AAs) are produced from the Edman degradation of peptides and proteins and important materials for determining amino acid sequences. Also, each PTH-AA has a strong UV absorbance, hence we have been using them as model compounds.

\* Corresponding author. Present address: Department of Material Science, Faculty of Science, Himeji Institute of Technology, Kamigori, Hyogo 678-12, Japan.

In this study, another type of N-alkanoyl-L-amino acid, i.e., sodium N-tetradecanoyl-L-glutamate (STGlu), was used as a chiral surfactant. As additives to STGlu solutions, two surfactants, achiral and anionic sodium dodecyl sulfate (SDS) and chiral and neutral 3 - [(3 - cholamidopropyl)dimethylammonio] - 1 - propanesulfonate (CHAPS), were used. Urea and methanol or 2-propanol (IPA) were also added to micellar solutions. As with SDVal, SDGlu and DSer, some PTH-DL-AAs were optically resolved by using an STGlu-CHAPS-SDS-urea-methanol solution, and also with an STGlu-SDS-urea-methanol system. However, the enantioselectivity in the STGlu micellar system was not substantially different from those in the SDVal, SDGlu and DSer systems.

## 2. Experimental

STGlu, the structure of which was given in the previous paper [9], was obtained from Ajinomoto (Tokyo, Japan), SDS and methanol from Nacalai Tesque (Kyoto, Japan), urea and PTH-DL-AAs from Wako (Osaka, Japan) and CHAPS from Dojin (Osaka, Japan). Micellar solutions were prepared by dissolving the surfactants and urea in a 50 mM borate buffer (pH 11.0) followed by the addition of methanol to the micellar solutions. Sample solutions were made by dissolving enantiomers in methanol-water (1:1). Although the concentration of the sample was not determined precisely, it was around 1 mg ml<sup>-1</sup>. All the chemicals were of analytical-reagent grade and used as received.

Capillary electrophoresis was performed with a Beckman (Fullerton, CA, USA) P/ACE System 2000 controlled by an IBM (Tokyo, Japan) PS/V personal computer. As a separation capillary, an untreated fused-silica tube purchased from Polymicro Technologies (Phoenix, AZ, USA), 300 mm (effective length) × 52 μm I.D., was used. Separation was performed in the constant voltage mode and the temperature was maintained at 30°C.

## 3. Results and discussion

Since the solubility of STGlu in an aqueous solution is low, a basic buffer (pH 11.0) was used and the content of methanol was increased to 30% (v/v). As reported previously [6–9], addition of SDS, urea and methanol to the SDVal, SDGlu or DSer micellar solutions could give good efficiency and resolution in the enantiomeric resolution of PTH-DL-AAs. Similarly to those cases, we used STGlu-SDS mixed micellar systems (pH 11.0) containing urea and methanol to obtain good peak shapes and enhanced enantioselectivity. The addition of CHAPS to the above-mentioned solutions was also examined. It should be noted that these micellar solutions were sufficiently stable to achieve reproducible separations even containing urea in high-pH buffer. By using a 100 mM STGlu-25 mM CHAPS-100 mM SDS-1 M urea (pH 11.0) solution containing 30% (v/v) methanol, five PTH-DL-AAs were separated from each other and each enantiomeric pair was optically resolved, as shown in Fig. 1. Here, the order of the migration and the separation characteristic in the STGlu system were almost similar to those

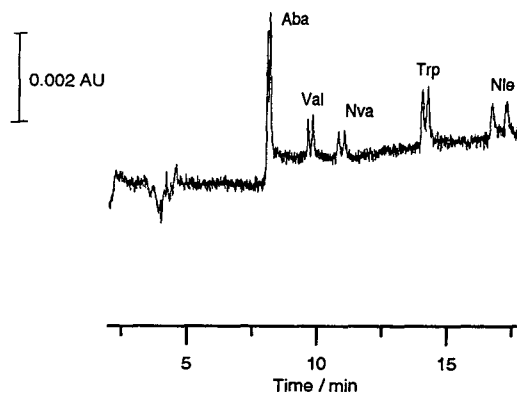


Fig. 1. Chiral separation of five PTH-DL-AAs by MEKC with STGlu-CHAPS. Corresponding AAs: Aba, Val, Nva, Trp and Nle as shown. Micellar solution, 100 mM STGlu-25 mM CHAPS-100 mM SDS-1 M urea (pH 11.0) containing 30% (v/v) methanol; separation capillary, 370 mm (effective length, 300 mm) × 52 μm I.D.; total applied voltage, 20 kV, electric field strength, 541 V cm<sup>-1</sup>; detection wavelength, 254 nm; temperature, 30°C.

obtained with SDVal, SDGlu, and DSer solutions [7–9].

By using IPA instead of methanol as an organic modifier, no enantiomeric resolution of any PTH-DL-AAAs was achieved. In general, IPA is not effective in enhancing the enantioselectivity and/or improving the resolution of PTH-DL-AAAs with N-alkanoyl-L-amino acids, except for the resolution of PTH-DL-Thr by using a DSer system [9], while the addition of methanol is essential to obtain good resolution: when an STGlu-CHAPS-urea system without methanol was used, the PTH-DL-AAAs were partially resolved.

By using an STGlu solution without CHAPS, or an STGlu-SDS-urea-methanol system, almost the same resolution of the five PTH-DL-AAAs as in Fig. 1 was obtained, as shown in Fig. 2. This implies that the addition of CHAPS does not affect the resolution characteristic of the STGlu system. On the other hand, by using a CHAPS-SDS-methanol solution or without STGlu, only PTH-DL-Met was optically resolved, as shown in Fig. 3. Although insufficient resolution was attained, the CHAPS-SDS mixed micelle system should be useful for enantiomeric resolution by MEKC.

In conclusion, the use of STGlu-SDS-urea-methanol solutions could provide good results

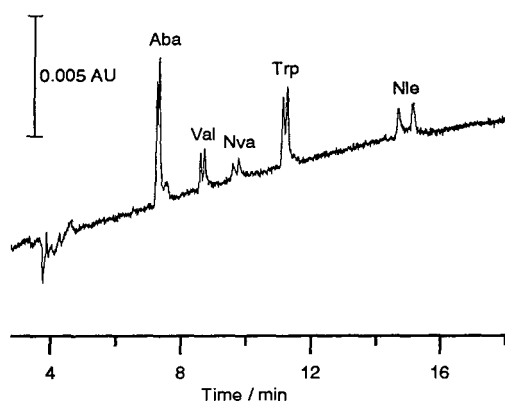


Fig. 2. Chiral separation of five PTH-DL-AAAs by MEKC with STGlu without CHAPS. Micellar solution, 100 mM STGlu-100 mM SDS-1 M urea (pH 11.0) containing 30% (v/v) methanol. Other conditions as in Fig. 1.

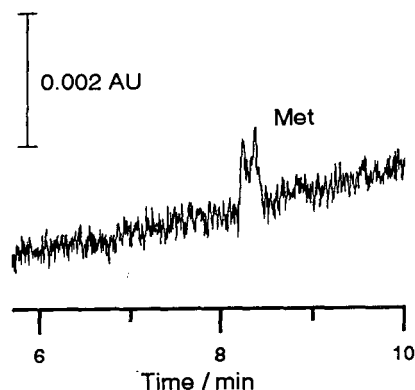


Fig. 3. Optical resolution of PTH-DL-Met by MEKC with CHAPS without STGlu. Micellar solution, 25 mM CHAPS-100 mM SDS-1 M urea (pH 11.0) containing 30% (v/v) methanol. Other conditions as in Fig. 2.

for the optical resolution of PTH-DL-AAAs, although the resolution characteristic was not substantially different from those with SDVal, STGlu, and DSer systems. Further investigations on chiral separations by MEKC with N-alkanoyl-L-amino acids and some other surfactants and additives are in progress.

## Acknowledgements

The authors are grateful to Dr. Akio Ishiwata of Ajinomoto for kindly providing various N-alkanoyl-L-amino acids. This work was supported in part by a Grant-in-Aid for Scientific Research (No. 06750838) from the Ministry of Education, Science and Culture, Japan.

## References

- [1] K. Otsuka and S. Terabe, in N.A. Guzman (Editor), *Capillary Electrophoresis Technology*, Marcel Dekker, New York, 1993, Ch. 20.
- [2] S. Terabe, K. Otsuka and H. Nishi, *J. Chromatogr. A*, 666 (1994) 295–319.
- [3] A. Dobashi, T. Ono, S. Hara and J. Yamaguchi, *Anal. Chem.*, 61 (1989) 1984–1986.
- [4] A. Dobashi, T. Ono, S. Hara and J. Yamaguchi, *J. Chromatogr.*, 480 (1989) 13–420.

- [5] K. Otsuka and S. Terabe, *J. Chromatogr.*, 515 (1990) 221–226.
- [6] K. Otsuka and S. Terabe, *Electrophoresis*, 11 (1990) 982–984.
- [7] K. Otsuka, J. Kawahara, K. Tatekawa and S. Terabe, 559 (1991) 209–214.
- [8] K. Otsuka, M. Kashihara, Y. Kawaguchi, R. Koike, T. Hisamitsu and S. Terabe, *J. Chromatogr. A*, 652 (1993) 253–257.
- [9] K. Otsuka, K. Karuhaka, M. Higashimori and S. Terabe, *J. Chromatogr. A*, 680 (1994) 317–320.



ELSEVIER

Journal of Chromatography A, 716 (1995) 323–329

JOURNAL OF  
CHROMATOGRAPHY A

# Capillary electrophoretic methods for a clear identification of selenoamino acids in complex matrices such as human milk

Bernhard Michalke

*GSF-Forschungszentrum für Umwelt und Gesundheit, 85758 Neuherberg (Oberschleissheim), Germany*

## Abstract

Selenoamino acids from size-exclusion chromatographic fractions of human milk were identified and determined by capillary electrophoresis (CE). For this purpose, different CE methods were developed to separate these selenoamino acids from other molecules with similar molecular masses. Methods were introduced for the clear identification of the analytes. These methods were designed to allow the identification of selenoamino acids in spite of the presence of many molecules with similar mobilities. Further, they overcome identification problems caused by shifts of migration times (due to different ionic compositions) compared with standard solutions.

## 1. Introduction

The high separation potential of capillary electrophoresis (CE) covers a broad field of applications and supplements other separation methods such as HPLC. The benefits make CE techniques of interest in speciation investigations. There, the organic binding partners of metals have to be identified, e.g., by capillary zone electrophoresis (CZE) [1].

Selenium is an essential trace element for humans. Sufficient selenium supplementation can protect against several heart diseases and has been discussed in prevention against cancer [2,3]. Newborns show very low serum selenium levels, which decrease during the first year of life [3]. The bioavailability of an element (here Se) is dependent on its binding form (species) [1]. Therefore, a clear identification and determination of such species in human milk is necessary. Fig. 1 shows the general structure of a selenoamino acid.

When analysing body fluids or size-exclusion

chromatographically (SEC) separated fractions, e.g., from human milk by CZE, even baseline-separated molecules usually show nearly identical migration times ( $t_m$ ). Further, molecules of interest often are present in low concentrations, probably migrating close to highly concentrated substances.

Migration times are altered by changes in ionic strength of buffers and samples [4–7]. Migration times of low-concentration molecules are influenced by closely migrating high-concentration compounds. Therefore, comparing standard  $t_m$  values with sample peak  $t_m$  values can lead to erroneous identifications [6–8].

The adjustment of ionic strength by mixing samples with a small aliquot of CE buffer is not sufficient when analysing samples with very high

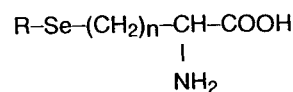


Fig. 1. General structure of a selenoamino acid. As an example, R = CH<sub>3</sub> and n = 2 for SM.

ionic strength. Large additions of buffer are not possible owing to sample dilution, which may bring low-concentration molecules below the determination limit. Consequently,  $t_m$  values in samples and standard solutions are different and a clear identification is no longer possible. Quantification may also be problematic owing to alterations in peak area for the same reasons.

Here, an easy and efficient method is described for identifying low-concentration amino acids in human milk despite  $t_m$  alterations from sample to sample. Different levels of security in identification are introduced. Determination of the molecules of interest can easily be done in parallel.

## 2. Experimental

### 2.1. Sampling

Sampling of human milk was carried out as described by Schramel et al. [9]. The tubing of the manual pump and the sampling vessels were cleaned with nitric acid and doubly-distilled water to avoid the contamination that can occur with commercially available pumps.

### 2.2. Sample preparation

Pooled human milk (second to seventh day after delivery) was defatted and milk proteins were precipitated by centrifugation (25 840 g, 30 min, 8°C), as described elsewhere [10]. The supernatant was injected into the LC system for SEC fractionation.

### 2.3. SEC fractionation and fraction treatment

The SEC fractionation was carried out on a metal-free Econo-System (Bio-Rad, Munich, Germany). The mobile phase was doubly distilled water at a flow-rate of 3 ml/min. The chromatographic column (500 × 50 mm I.D.) was metal-free, filled with Toyo Pearl TSK HW 40 as the stationary phase and temperature controlled at 20°C. A UV detector monitored the separation at 232 nm.

### Fraction treatment

Fractions were collected at 5-min intervals with a Model 100 fraction collector (Pharmacia). The fractions were frozen at -20°C and subsequently freeze-dried. The dry powder was resuspended with doubly-distilled water (500  $\mu$ l) and used for the Se determinations (350  $\mu$ l) and for different CE determinations (150  $\mu$ l).

### 2.4. Capillary electrophoresis

A Biofocus 3000 capillary electrophoresis system (Bio-Rad) was used for the CE experiments. The capillary and carousel temperature was 20°C. Two CZE methods (A and B) were developed for each of GSH, Se-CM, SC and SM (Table 1).

A standard addition of the analytes improved analyte identification and quantification. Fig. 2 shows the flow chart of consecutive investigations. An increasing security in identification of the investigated compounds is achieved by the combination of different methods (SEC, CZE methods A + B) for identification, obtaining increasing levels of security (ISL = identification security level).

### 2.5. Se determination

Se determinations were carried out by inductively coupled plasma mass spectrometry with an instrument from Perkin-Elmer (Überlingen, Germany) coupled with a graphite furnace using the standard addition method for quantification. Electrothermal vaporization was chosen to overcome the well known polyatomic interferences.

### 2.6. Chemicals

TSK-gel (ToyoPearl HW 40 S) was obtained from Toso Haas (Stuttgart, Germany). GSH, selenocystamine (Se-CM), selenocystin (SC) selenomethionine (SM) were purchased from Sigma (Munich, Germany). The capillaries and borate and phosphate buffer (pH 2.5) were bought from Bio-Rad and  $\text{H}_2\text{PO}_4^-$ - $\text{HPO}_4^{2-}$ , acetic acid and sodium acetate from Merck



Table 1  
Parameters of the different CZE methods

Analyte	Method	Capillary <sup>a</sup> (cm × μm I.D.)	Buffer	Polarity
GSH	A	24 × 25 (c)	Borate buffer, pH 8.5 (Bio-Rad 148-5023)	-/+
	B	24 × 25 (c)	H <sub>2</sub> PO <sub>4</sub> <sup>-</sup> -HPO <sub>4</sub> <sup>2-</sup> , 100 mM, pH 6.0	-/+
Se-CM	A	50 × 50	Borate buffer, pH 8.5 (Bio-Rad 148-5023)	+/-
	B	50 × 50	Na acetate, 100 mM, pH 5.5	+/-
SC	A	24 × 25 (c)	Phosphate buffer, 100 mM, pH 2.5 (Bio-Rad 148-5010)	+/-
	B	24 × 25 (c)	Acetic acid, 1%, pH 1.9	+/-
SM	A	24 × 25 (c)	Phosphate buffer, 100 mM, pH 2.5 (Bio-Rad 148-5010)	+/-
	B	24 × 25 (c)	Acetic acid, 1%, pH 1.9	+/-

Additional common parameters: injection by pressure,  $1.03 \cdot 10^5$  Pa s; voltage, 10 kV; temperature, 20°C (sample carousels and capillary); wavelength, 200 nm; purge between runs, (1) water, 60 s, and (2) buffer, 90 s.

<sup>a</sup> (c) = coated.

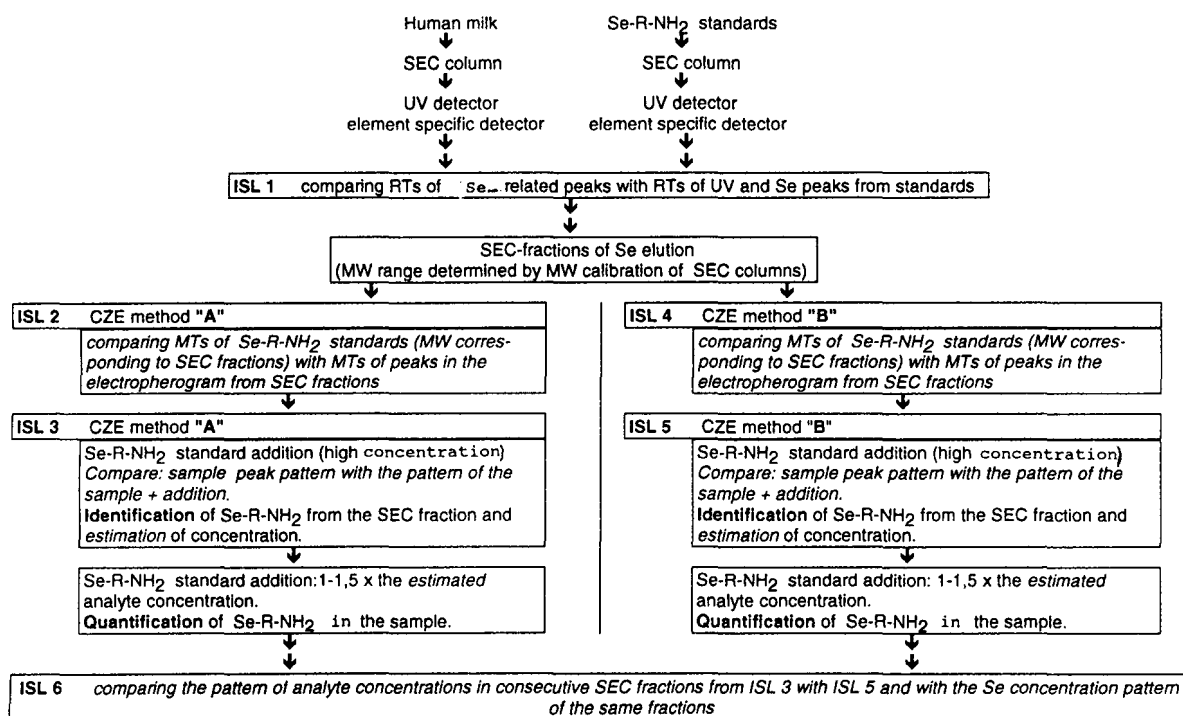


Fig. 2. Scheme of consecutive analytical steps for identification obtaining increasing levels of security. RT = Retention time; MT = migration time; MW = molecular mass.

(Darmstadt, Germany). The Se standards were purchased from Aldrich (Steinheim, Germany).

### 3. Results

The electropherogram of an individual SEC fraction showed good reproducibility for several replicates ( $n = 5$ ), but a  $t_m$  shift compared with standards was observed. This shift changed on analysing other fractions, owing to their different compositions. Therefore, the identification of an Se-R-NH<sub>2</sub> by comparing the standard CZE  $t_m$  with the peak CZE  $t_m$  in SEC fractions (ISL 2) was impossible.

Fig. 3 shows the analysis (methods A and B) of an SEC fraction containing GSH. A multitude of peaks migrated around the standard  $t_m$  and a slight  $t_m$  shift was obvious.

For Se-CM, SC and SM, no peaks were detected at the standard  $t_m$  values in the SEC fractions where the elution of these molecules was expected from  $M_r$  calibration of the SEC column (SM, Fig. 4d and e; Se-CM and SC, not shown). On the other hand, a peak with the SM standard CZE  $t_m$  was seen in SEC fractions of higher molecular mass (Fig. 4a and b).

The addition of analyte standards to the samples (ISL 3) showed marked  $t_m$  shifts in these samples. Now several sample peaks from different fractions could be correlated with analyte standards. These sample peaks "grew" with the standard additions, thus being identified by ISL 3 and ISL 5 procedures. Fig. 3b and c and 3e and f show the "growth" of the GSH peaks by methods A and B and Fig. 4e and f demonstrate the increasing peak height of SM.

The absence of the analytes in the resting SEC fractions was proved when a new peak appeared after a standard addition. As an example, Fig. 4b and c show the absence of SM in a SEC fraction where a sample peak simulates SM by an ISL 2 identification (Fig. 4a and b).

In some electropherograms, a hidden co-elution of another molecule was not totally excluded even by the ISL 3 procedure [e.g., Fig. 3b or for SC (not shown)]. Therefore, a second determination method was necessary for additional validation (ISL 4 and 5; e.g., Fig. 3d, e

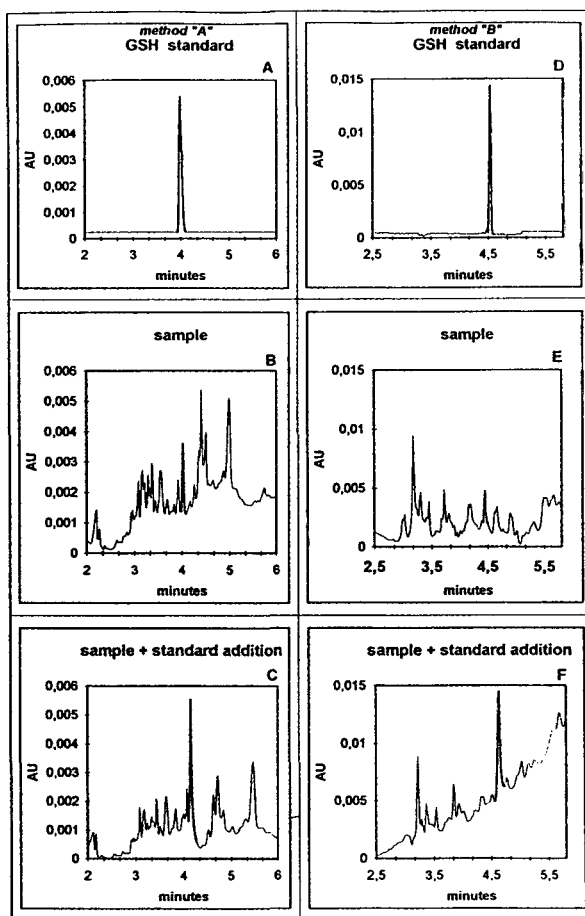


Fig. 3. Electropherograms of standards, samples and samples + standard addition for GSH by methods A and B. A clear identification by ISL 3 and ISL 5 procedures is shown.

and f). The presence and the identity of the molecules were proved by the ISL 5 procedure in those fractions where they had already been determined by the ISL 3 procedure. Co-elutions of other molecules were now excluded.

The amounts of the analytes in consecutive SEC fractions (ISL 6) showed close conformity of the values determined by methods A and B (ISL 3 and 5). The concentration patterns were further comparable to those of Se in consecutive SEC fractions (Fig. 5). The total amount of Se-R-NH<sub>2</sub> in human milk in these experiments is shown in Table 2.

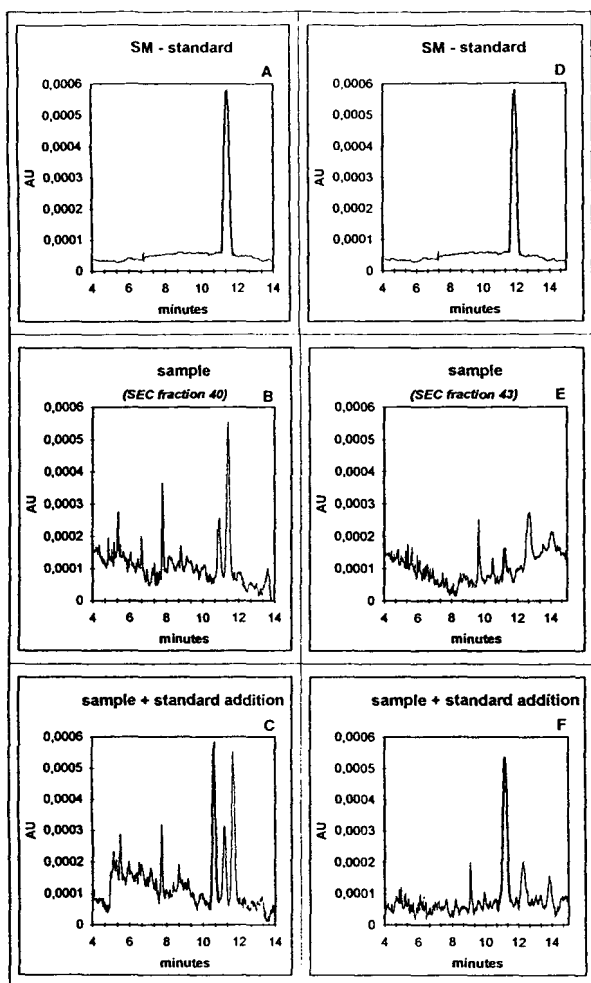


Fig. 4. (A) and (D) an SM standard is shown; (B) seemingly, SM is present in the sample according to ISL 2, but after addition of an SM standard (ISL 3) the lack of this analyte in the sample (SEC fraction 40) becomes obvious; (D) the SM standard; (E) seemingly, SM is not present in the sample according to ISL 2; (F) after addition of an SM standard (ISL 3), the presence of this analyte in the sample (SEC fraction 43) becomes obvious.

#### 4. Discussion

The analytes were well separated from other molecules. Replicate electropherograms of one individual fraction were strongly reproducible with respect to  $t_m$  and peak quantification.

The observed  $t_m$  shift from a standard to a

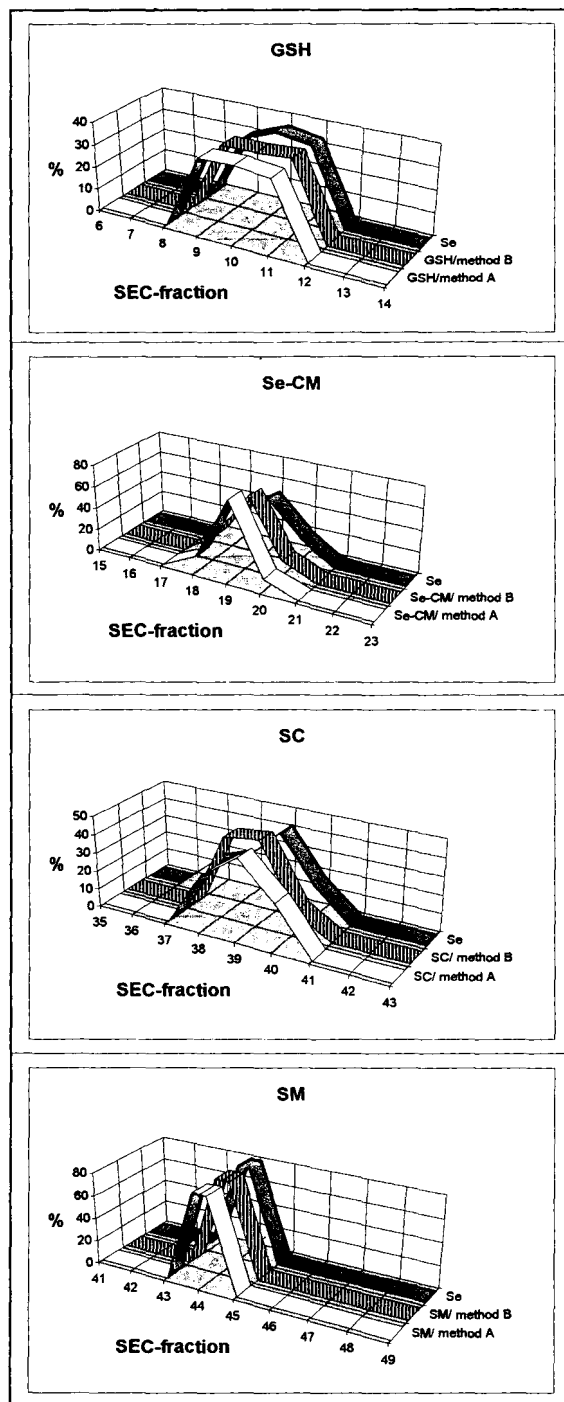


Fig. 5. Determination of Se and the four analytes in consecutive SEC fractions.

Table 2  
Concentrations of analytes in human milk determined by different CZE methods

Analyte	Concentration (mg/l)		Average
	CZE method A	CZE method B	
GSH	1.92 ± 0.20	1.95 ± 0.21	1.93 ± 0.19
Se-CM	1.99 ± 0.15	1.91 ± 0.20	1.95 ± 0.18
SC	3.96 ± 0.41	4.10 ± 0.25	4.02 ± 0.38
SM	1.08 ± 0.20	0.90 ± 0.20	1.03 ± 0.21

sample has been reported [5] and is explained by differences in ionic strength. The changes in  $t_m$  shifts from consecutive SEC fractions were a logical consequence of the different compositions of these fractions. Taking this as a basis, identification of an analyte by the ISL 2 procedure can easily lead to a wrong identification in such complex samples. The ISL 3 procedure overcame these problems. The analytes were identified clearly (Fig. 3b and c). The ISL 3 procedure is therefore necessary for quality assurance.

A further necessary tool for quality assurance was the application of a second determination method B. Doubtful identifications and possibly wrong quantifications (referring to possible co-elutions and closely migrating peaks) were now excluded by the ISL 5 procedure (Fig. 3e and f).

GSH was well separated from other molecules, but the multitude of closely migrating peaks called for the ISL 3 procedure. However, even after an ISL 3 identification, an accidental co-migration of another molecule was not totally excluded. Finally, the combination of ISL 3 and ISL 5 procedures provided absolute identification security. The amounts determined by the two methods were the same and the same concentration patterns in consecutive SEC fractions were observed (ISL 6), also indicating that there was no hidden peak.

A clear separation of Se-CM from other peaks [11] was provided. Identification and quantification were possible without interferences. Owing to the marked  $t_m$  shifts, the ISL 3 and ISL 5

procedures were essential for identification and quality assurance.

Neither SC nor SM was identified by the ISL 2 procedure owing to the  $t_m$  shifts (SM, Fig. 4d and e). Again, the ISL 3 and ISL 5 procedures helped to identify these molecules clearly in those SEC fractions where they should be expected. The necessity for the ISL 3 combined with the ISL 5 procedure for quality assurance is demonstrated impressively in Fig. 4a–c. There, SM seemed to appear at the standard  $t_m$ . Only the ISL 3 and ISL 5 procedures demonstrated clearly a marked  $t_m$  shift and the absence of the analyte in this SEC fraction.

For each analyte, the total amounts and the concentration patterns in consecutive SEC fractions were in accordance for both methods (Table 2). The selenium patterns agreed with the analyte patterns. Both findings strengthen further the identification security.

In the literature, the identification problems described here often seem to play a minor role. Shifts in  $t_m$  can often be observed (e.g., [12,13]), but usually no identification problems are referred to. This may be due to the investigation of model or standard solutions. However, when analysing complex, changing matrices, only standard additions with at least two methods (ISL 3 and ISL 5) guarantee sufficient identification and quality assurance.

This aspect can be found in other articles also. Deyl and Struzinsky [4] stated that there is a “large step from separations of a model solution to a real sample” and Gurley et al. [5] suggested a standard addition analogous to the ISL 3 procedure. However, even there, possible co-migration of other molecules (suspected by the authors themselves) could not be totally excluded.

A “normalization” as suggested by several groups [6–8] is not practicable for the samples analysed here. The  $t_m$  and peak areas were referred to an internal standard, which is not present in the original sample. However, the prediction of an analyte  $t_m$  in consecutive SEC fractions can hardly be done, because the  $t_m$  shifts vary from fraction to fraction.

The four analytes investigated here have been

partly described in the literature: GSH is well known in breast milk [14] and GSH with covalently bound Se has been described [15]. SC and SM have the same pathways as their sulfur analogues and close metabolic relationships between each of the analytes are known [15–17].

## 5. Conclusion

Selenium supplementation in human milk is provided by four Se ligands, which can be clearly identified and quantified by the ISL 3 and ISL 5 procedures. These identification procedures overcome the problems resulting from  $t_m$  shifts and from problems known from other identification techniques such as “normalization”. They are necessary for quality assurance and will be the basis for identifications of selenium binding partners in future Se speciation investigations.

## References

- [1] B. Michalke, *Fresenius' J. Anal. Chem.*, 350 (1994) 2.
- [2] P.D. Whanger, *J. Trace Elem. Electrolytes Health Dis.*, 6 (1992) 209.
- [3] T.W. Westermark, *Trace Elem. Anal. Chem. Med. Biol.*, 3 (1984) 49.
- [4] Z. Deyl and R. Struzinsky, *J. Chromatogr.*, 569 (1991) 63.
- [5] L.R. Gurley, J.S. Buchanan, J.E. London, D.M. Stavert and B.E. Lehnert, *J. Chromatogr.*, 559 (1991) 411.
- [6] G. Bondoux, P. Jandik and R.W. Jones, *J. Chromatogr.*, 602 (1992) 79.
- [7] R. Kuhn and S. Hofstetter-Kuhn, *Capillary Electrophoresis: Principles and practice*. Springer, Berlin, 1993.
- [8] B.F. Kenney, *J. Chromatogr.* 546 (1991) 423.
- [9] P. Schramel, G. Lill, S. Hasse and B.-J. Klose, *Biol. Trace Elem. Res.*, 16 (1988) 67.
- [10] B. Michalke, D.C. Münch and P. Schramel, *J. Trace Elem. Electrolytes Health Dis.*, 5 (1991) 251.
- [11] B. Michalke, *Fresenius' J. Anal. Chem.*, in press.
- [12] P.J. Oefner, A.E. Vorndran, E. Grill, C. Huber and G.K. Bonn, *Chromatographia*, 34 (1992) 308.
- [13] F.T.A. Chen, *J. Chromatogr.*, 559 (1991) 445.
- [14] K.T. Suzuki, H. Tamagawa, S. Hirano, E. Kobayashi, K. Takahashi and N. Shimojo, *Biol. Trace Elem. Res.*, 28 (1991) 109.
- [15] H.E. Ganther, *Trace Elem. Anal. Chem. Med. Biol.*, 3 (1984) 4.
- [16] K. Soda, *Phosphorus Sulfur Silicon*, 67 (1992) 461.
- [17] O.E. Kajander, R.J. Harvima, T.O. Elorant, H. Martikanainen, M. Kantola, S.O. Kärenlampi and K. Akerman, *Biol. Trace Elem. Res.*, 28 (1991) 57.





ELSEVIER

Journal of Chromatography A, 716 (1995) 331–334

JOURNAL OF  
CHROMATOGRAPHY A

# Study of the racemization of L-serine by cyclodextrin-modified micellar electrokinetic chromatography and laser-induced fluorescence detection

G. Nouadje<sup>a,b</sup>, M. Nertz<sup>a</sup>, F. Courderc<sup>c,\*</sup>

<sup>a</sup>ZETA Technology, Parc Technologique du Canal, 31520 Ramonville-Toulouse, France

<sup>b</sup>Laboratoire de Chimie Analytique et Bromatologie, Université des Sciences Pharmaceutiques, 31062 Toulouse Cedex, France

<sup>c</sup>Laboratoire de Biologie Moléculaire Eucaryote du CNRS, 118 Route de Narbonne, 31062 Toulouse Cedex, France

## Abstract

Cyclodextrin-modified micellar electrokinetic chromatography and laser-induced fluorescence detection were used for the determination of the racemization rate of L-serine in water at 100°C. A difference to ten times the half-lifetime was observed between the value in the literature and the present results.

## 1. Introduction

Capillary electrophoresis (CE) is now well known for allowing separations of enantiomers by using the cyclodextrin-modified micellar electrokinetic chromatography [1]. The resolution of D- and L-amino acids has been studied by this means [2].

Because very small sample volumes are injected in CE studies, laser-induced fluorescence (LIF) is one of the most successful methods used to achieve high sensitivity and selectivity [3,4]. Many interesting analytes are not natively fluorescent and most reports on LIF detection with CE involve the use of visible lasers and labelling of analytes with fluorescent functional groups, such as fluorescein isothiocyanate for amines, amino acids or proteins [5].

A century ago it was first observed that amino acids underwent racemization when heated in

strongly acidic and basic solutions. It soon became well established that the optically active amino acids isolated from biological materials could be converted into racemic mixtures by a variety of vigorous treatments. The earlier works on racemization in various systems was extensively reviewed in 1984 by Neuberger [6]. While racemization of amino acids at extreme pH and elevated temperatures has been known for a long time, it also takes place at neutral pH at rates which are comparable to those in dilute acids and bases [7].

Racemization was detected in fossils and the metabolically stable protein in living mammals [8], soils [9], trees [10] and wine [11] and was used in dating studies [12–14]. Kinetic data are not well established for a large number of amino acids [13,14].

Some years ago, Schwass and Finley [15] showed that serine is the most sensitive indicator of racemization among amino acids which can be measured, because of its particularly short

\* Corresponding author.

racemization half-lifetime (around 400 years estimated at 25°C [13]). Kinetic studies are difficult because of the very small amount of enantiomer produced, owing to the very long reaction time.

To obtain new data on the racemization of serine, we used the high performance of separation by cyclodextrin-modified micellar electrokinetic chromatography and the high sensitivity of detection by LIF. We measured the kinetics of the reaction of a solution of a  $10^{-8}$  M L-serine at 100°C in water. Differences from literature values were observed and are discussed.

## 2. Experimental

### 2.1. Apparatus and separation conditions

A modular injector and high-voltage power supply (SpectraPhoresis 100; TSP, Fremont, CA, USA) equipped with a modular CE–LIF detector (Zeta Technology, Toulouse-Ramonville, France) and a 488-nm wavelength laser (Type 54225A; ILT, Salt Lake City, UT, USA) were used. A 75 cm × 50 μm I.D. fused-silica capillary (Polymicro Technologies, Phoenix, AZ, USA) was used with an effective length of 42 cm.

All chemicals were purchased from Aldrich (St. Quentin Falavier, France).

The separation buffer consisted of 100 mM sodium dodecyl sulfate (SDS) (70% purity), 60 mM β-cyclodextrin and 100 mM boric acid (99.5% + purity) (pH 9.3, adjusted by addition of sodium hydroxide). The capillary was rinsed with 0.1 M NaOH for 3 min with water for 2 min and then with separation buffer for 3 min. Samples were injected by hydrodynamic injection for 2 s (15 nl). A separation potential of 28 kV was used. The electrophoretic current was typically 66 μA.

### 2.2. Data collection and analysis

Data collection, processing and analysis were performed using Boreal software (JMBS Developments, Grenoble, France). Data were collected at a sampling rate of 10 Hz. Peaks were identified by spiking samples with fluorescein

isothiocyanate (FITC)-labelled DL-serine. Average values for duplicate injections were calculated. The relative standard deviation ( $n = 5$ ) of the peak height for  $10^{-8}$  M DL-serine solution was 1.1%.

### 2.3. L-Serine kinetic study

Three solutions of 1.2 ml of  $10^{-4}$  M L-serine (99% purity) in water (pH 7.8) were heated concurrently under reflux at 100°C. Volumes of 100 μl were taken after 2, 4, 6, 8, 22, 24, 26 and 55 h and derivatized with FITC at 20°C prior to CE–LIF analysis.

### 2.4. Derivatization procedure

A  $2.1 \cdot 10^{-4}$  M solution of FITC isomer I (90% purity) in acetone was prepared by dissolving 2.5 mg of FITC in 3 ml of acetone. Then 2 mg of each amino acid were dissolved in 2 ml of 0.2 M carbonate buffer (pH 9.0). A 100-μl volume of serine solution ( $10^{-4}$  M) was allowed to react with 100 μl of FITC solution for 2 h in the dark. At the same time, 100 μl of a  $2.1 \cdot 10^{-4}$  M solution of FITC in acetone was mixed with 100 μl of 0.2 M carbonate buffer to obtain a blank and kept in darkness for 2 h. Then both the FITC solution and the amino acid plus FITC solution were diluted 10 000-fold in water prior to analysis. D- and L-serine have the same kinetic reaction of labelling. The total concentration of serine was constant with time.

## 3. Results and discussion

Racemization is a well established first-order reaction and the kinetic equation for this reaction is [13]

$$\ln(1 + D/L)_t - \ln(1 + D/L)_{t=0} = K_i t \quad (1)$$

where  $D/L$  is the L- to D-amino acid enantiomeric ratio at a particular time ( $t$ ) and  $K_i$  is the first-order rate constant for the interconversion of amino acid enantiomer. This equation may be



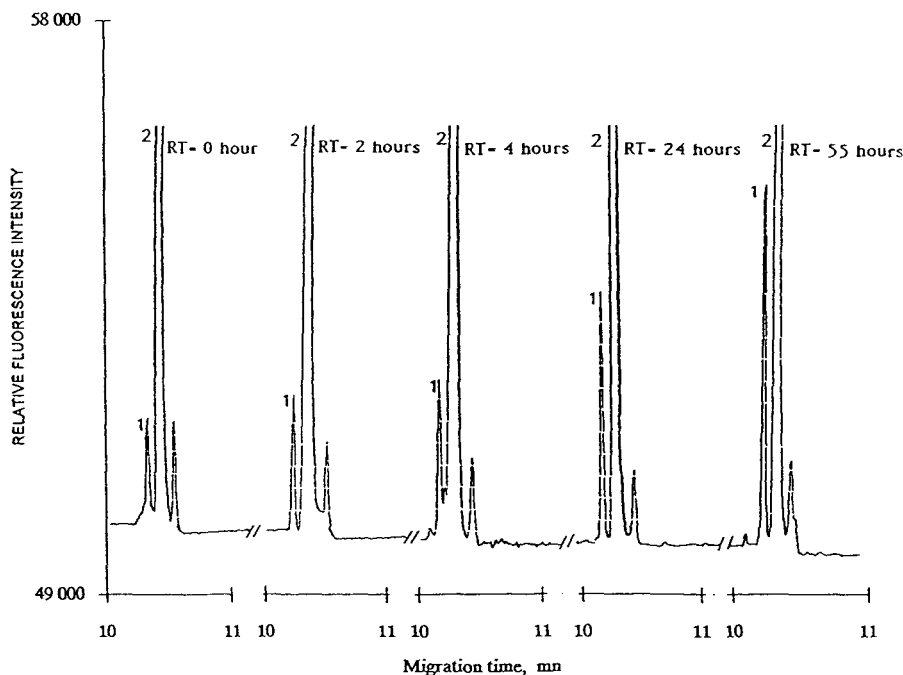


Fig. 1. Electropherogram showing  $10^{-8}$  M FITC-L-serine racemization in water at  $100^{\circ}\text{C}$  after 0, 2, 4, 24 and 55 h of reaction. Separation conditions: SDS, 100 mM;  $\beta$ -cyclodextrin, 60 mM; boric acid, 100 mM; pH, 9.2; fused-silica capillary,  $50\ \mu\text{m}$  I.D., 28 kV, 66  $\mu\text{A}$ . Peaks: 1 = D-serine; 2 = L-serine. RT = reaction time.

used when  $D/L < 0.15$ . In our case, for a reaction time of 55 h  $D/L = 0.074$ .

Fig. 1 shows five electropherograms of L-serine racemization after 0, 2, 4, 24 and 55 h of reaction. They show the growth of the peak of D-serine with time.

Mean values of the  $D/L$  ratio (R.S.D. < 4.49%) of the three reactions yielded a linear least-squares line fit:

$$\ln(1 + D/L) - \ln(1 + D/L)_{t=0} = 1.04 \cdot 10^{-3}t + 2.03 \cdot 10^{-3}$$

( $t$  in hours) with a correlation coefficient of 0.9965 (the intercept was nearly zero).

The rate constant allowed the calculation of the racemization half-lifetime as 40 days for L-serine at  $100^{\circ}\text{C}$  at pH 7.8. The literature value [16] is 4 days, calculated from measurements at  $122^{\circ}\text{C}$ , assuming that the ratio of the rates of racemization of serine and aspartic acid are the same at the same temperature.

The present value shows that racemization of serine during protein hydrolysis will be relatively slow and will not have an important influence on the  $D/L$  ratio.

The results show that amino acids racemization may be observed with CE-LIF, which could be used as a dating method to determine the age of amino acid-containing samples.

## References

- [1] S. Fanali and F. Kilár, *J. Capillary Electrophoresis*, 1 (1994) 72.
- [2] G. Nouadje and F. Couderc, *Spectra Anal.*, 184 (1995) 17.
- [3] J. Berguist, S.D. Gilman, A.G. Ewing and R. Ekman, *Anal. Chem.*, 66 (1944) 3512.
- [4] G. Nouadje, F. Couderc, Ph. Puig and L. Hernandez, *J. Capillary Electrophoresis*, 3 (1995) 117.
- [5] M. Hiroshi and K. Hiroshi, *Biophys. Biochem. Res. Commun.*, 31 (1968) 188.
- [6] A. Neuberger, *Adv. Protein Chem.*, 4 (1984) 298.

- [7] J.L. Bada, *J. Am. Chem. Soc.*, 94 (1972) 1371.
- [8] R.A. Schroeder and J.L. Bada, *Earth Sci. Rev.*, 12 (1976) 347.
- [9] C.U. Griffin and R.W.L. Kimber, *Aust. J. Soil Res.*, 26 (1988), 531.
- [10] I. Abe, K. Izumi, S. Kuramoto, S. Musha, *Bunseki Kagaku*, 31 (1982) 427.
- [11] H.J. Chaves das Neves, A.M.P. Vasconcelos and M.L. Costa, *Chirality and Biological Activity*, Alan R. Liss, New York, 1990, p. 137.
- [12] P.M. Helfman and J.L. Bada, *Nature*, 262 (1976) 279.
- [13] J.L. Bada, *Methods Enzymol.*, 106 (1984) 98.
- [14] J.L. Bada, in G.C. Barrett (Editor), *Chemistry and Biochemistry of Amino Acids*, Chapman and Hall, London, 1985, p. 399.
- [15] D.E. Schwass and J.W. Finley, *J. Agric. Food Chem.*, 32 (1984) 1377.
- [16] G.G. Smith and B.S. de Sol, *Science*, 207 (1980) 765.



ELSEVIER

Journal of Chromatography A, 716 (1995) 335–346

JOURNAL OF  
CHROMATOGRAPHY A

# Capillary electrophoretic determination of amino acids Improvement by cyclodextrin additives

Y.-H. Lee, T.-I. Lin\*

*Department of Chemistry, National Taiwan University, Roosevelt Road Section 4, Taipei 10764, Taiwan*

## Abstract

Previously, we have developed methods for the capillary electrophoretic determination (without derivatization) of twenty common amino acids with indirect absorbance detection [Y.-H. Lee and T.I. Lin, *J. Chromatogr. A*, 680 (1994) 287]. Here, we report a further improvement in the resolution, resulting from the use of various cyclodextrin (CD) additives. Capillary electrophoresis (CE) was performed at pH 11.0 with either *p*-aminosalicylic acid (PAS) or 4-(*N,N'*-dimethylamino)-benzoic acid (DMAB) as the background electrolyte (BGE). The effects on the CE separation brought about by various CD additives, e.g.  $\alpha$ - and  $\beta$ -cyclodextrins, methyl-, hydroxypropyl-, 2,6-dimethyl-, and 2,3,6-trimethyl- $\beta$ -cyclodextrins were investigated. These CD additives form inclusion complexes with the BGE and also with amino acids, altering the migration behavior of the analytes. For some amino acids which have previously proved difficult or impossible to separate, an improvement in the separation selectivity has been attained. Association constants of BGEs for cyclodextrins were determined on the basis of the CE mobility changes caused by the CD additive. The concentration of CD additive needed to achieve a suitable separation was calculated and optimized experimentally. Using 10 mM PAS or DMAB, in the presence of 20 mM  $\alpha$ -cyclodextrin at pH 11.0, eighteen amino acid peaks were baseline-resolved in under 35 min. Leu and Ile could also be separated in the presence of 15–20 mM  $\beta$ -CD under similar CE conditions. The performance of CE in separating amino acids in the presence of various CD additives is discussed.

## 1. Introduction

Amino acids are the building blocks of proteins; determination of the amino acid composition of proteins is often encountered in protein analysis. Amino acids are also present in a wide variety of biological tissues, body fluids, foods, and medicines. Therefore, determination and quantitation of amino acids is of considerable interest. The most efficient and convenient methods for simultaneous determination of amino acids developed in the past have been based on high-performance liquid chromatography

(HPLC). Since the majority of amino acids do not absorb light in the UV region, detection is often accomplished by introducing pre- or post-column derivatization of the analytes with fluorescent probes [1–3], the subsequent detection being by fluorescence or laser-induced fluorescence. The fluorescence method has the advantage of high detection sensitivity, reaching an attomolar mass detection limit [3]. However, the derivatization process can be very time-consuming and requires considerable additional work. The process also changes the native electrophoretic mobility of the analytes. Alteration of the electrophoretic mobility of the analyte always occurs because of the modification of physico-

\* Corresponding author.

chemical properties of the analyte by the reactive group of the derivatizing agents.

If capillary electrophoresis (CE) is used, detection of underivatized amino acids can also be accomplished by indirect methods similar to those employed in liquid chromatography. In capillary zone electrophoresis, indirect fluorescence detection has been developed for a variety of analytes, including amino acids [4,5]. To achieve the best detection limits, a laser light source is often required. Another very attractive alternative is the indirect absorbance detection method, since most commercial CE systems are equipped with UV–Vis absorbance detectors and a wide variety of background absorbers are available.

Indirect UV detection in CE has recently become popular, and has been applied to the detection of a wide variety of analytes, e.g. organic acids and bases, inorganic anions and metal cations (for reviews, see Refs. [6,7]). A few studies have been made on the CE of amino acids based on the indirect UV detection scheme [8–10]. In the indirect UV detection method, the choice of background electrolyte (BGE) is of critical importance because it dictates the resolution of the CE separation and the sensitivity. Benzoate, sorbate, salicylate, and quinine sulfate have been used as BGEs for the CE analysis of amino acids and related compounds. Other factors that also affect the CE resolution include pH and additives that modify the electroosmotic flow (EOF). Previously, we have investigated the potential use and suitability of various BGEs for the CE analysis of amino acids with indirect UV detection [11]. Of the nine BGEs studied, we found *p*-aminosalicylic acid (PAS) and 4-(*N,N'*-dimethylamino)benzoic acid (DMAB) to be most suitable as the carrier electrolytes and background absorbance providers as they have effective mobilities close to the mobilities of most amino acids at alkaline pH. pH also plays a role as it influences the separation behavior of amino acids in CE. Metal cations (e.g.  $Mg^{2+}$ ) and long-chain cationic surfactants (e.g. cetyltrimethyl ammonium bromide) are effective EOF modifiers (reducing or reversing EOF at high concentration); as buffer additives, they improve the CE resolution [11].

Although 17–19 peaks for twenty common amino acids could be effectively separated in 20–40 min using the method developed previously [11], there is still considerable room for improvement. For example, Phe, Val, and His, Met and Gln, and Ala, Thr, and Asn could not be baseline-resolved under any one single CE condition. An even more serious problem is that Leu and Ile could not be separated at all. Several studies have shown that adding cyclodextrins (CDs) can enhance the selectivity of CE because CDs can form inclusion complexes with a wide variety of guest organic molecules or ions (for review, see Ref. [12]). Selectivity is taken to be a function of whether the guest molecule fits into the CD hydrophobic cavity. Chiral separations of racemic mixtures of *D,L*-amino acids, peptides, carbohydrates, and various other chiral pharmaceuticals have been aided by the addition of different kinds of CDs and derivatives [13–18]. In the present study, we have investigated the effectiveness of various CDs and derivatives, e.g.  $\alpha$ - and  $\beta$ -cyclodextrins, methyl-, hydroxypropyl-, 2,6-dimethyl-, and 2,3,6-trimethyl- $\beta$ -cyclodextrins, in improving the CE separation of amino acids. Among the various CDs,  $\alpha$ -CD gives the best overall performance in terms of CE resolution for all amino acids except for Leu and Ile. On the other hand, complete baseline CE separation for the latter two amino acids could only be achieved by adding  $\beta$ -CD. The performance of CE in separating amino acids in the presence of various CD additives is discussed.

## 2. Experimental

### 2.1. Chemicals

BGEs, 20 common amino acids, DM- $\beta$ -CD [heptakis(2,6-di-O-methyl- $\beta$ -CD)] and TM- $\beta$ -CD [heptakis(2,3,6-tri-O-methyl- $\beta$ -CD)] were from Sigma. HP- $\alpha$ -CD (hydroxypropyl- $\alpha$ -CD, average molar substitution (MS) = 0.6), HP- $\beta$ -CD (hydroxypropyl- $\beta$ -CD, MS = 0.6), and methyl- $\beta$ -CD (average degree of substitution = 1.8) were from Aldrich (Milwaukee, WI, USA).  $\alpha$ -CD and  $\beta$ -CD were obtained from two manufacturers: Sigma (St. Louis, MO, USA) and

Janssen (Geel, Belgium); each brand gave very different CE results (see Results and Discussion). These chemicals were used as received without further purification. All other chemicals used were of analytical or reagent grade from several manufacturers. Doubly deionized water prepared from a Milli-Q system (Millipore, Bedford, MA, USA) or doubly deionized distilled water was used exclusively for all solutions. Infusion fluids containing amino acids (Aminol Infusion and Aminol-12X Injection) were supplied by Sintong Chem. (Tauyen, Taiwan).

#### *Samples, buffers and pH adjustment*

BGE solutions containing 10 mM of *p*-aminosalicylic (PAS) or 4-(*N,N'*-dimethylamino)benzoic (DMAB) acids, the standard solution of 20 amino acids and their mixture were prepared according to the procedure published previously [11]. The pH of the running BGE solution was adjusted by adding aliquots of 1 or 0.1 M NaOH to the desired pH, depending on the experiments, from 10 to 11.2 as specified in the figures. As noted previously, the solution had a rather high pH and if exposed to air, the pH could be lower by CO<sub>2</sub> dissolution. Thus, the vial must be capped tightly immediately after use. The original pH could be maintained for 3–4 days. The pH of the solution was checked periodically and readjusted if necessary. For the CD experiments, 20–30 mM solutions were made containing 10 mM BGE and then diluted to the desired concentration.

#### *2.2. Apparatus*

CE experiments were carried out in a fully automated Spectra Phoresis Model 1000 instrument (Thermo Separation Products, Fremont, CA, USA) as described previously [11]. The detector wavelength was fixed at 266 nm for PAS and at 288 nm for DMAB. In indirect detection, peaks in the electropherogram appeared originally as negative peaks but were inverted to positive peaks by using the vendor's software. The capillaries (bare fused-silica) from Polymicro Technologies (Phoenix, AZ, USA) were 75 μm I.D. (365 μm O.D.) × 70 cm (63 cm to the detector) for the determination of the mo-

bilities of BGEs and 75 μm I.D. (365 μm O.D.) × 90 cm (83 cm to the detector) for the separation of mixtures of amino acids. For the determination of the molar absorptivities for the various BGEs, the UV-Vis absorption spectra of BGEs (10<sup>-4</sup> M in 10 mM phosphate buffer, pH 11.0) were measured, using 0.5-cm quartz cuvettes (190–400 nm), by means of a double-beam scanning spectrophotometer (Hitachi U-2000, Tokyo, Japan). Electrospray ionization (ESI) mass spectrometric analysis of CD was performed in a Fisons Platform quadrupole mass spectrometer (Manchester, UK) and it was detected as [M + H]<sup>+</sup>. Experimental procedures for ESI-MS were similar to those previously published [19].

#### *2.3. Electrophoretic procedures*

Pretreatment of new capillaries and wash protocols for subsequent runs were carried out according to the established procedure [11]. The standard solution containing a mixture of 20 amino acids, each with a final concentration of 5 · 10<sup>-4</sup> M, was prepared from stock solutions of amino acids (10 mM, stored at 4°C) in deionized water. Sample injection was effected in the hydrodynamic (HD) mode for 1 s. The separation run was carried out at +20 kV constant voltage, at 25°C constant temperature, and with a current of ca. 10 μA. Other CE procedures for the determinations of amino acids were the same as described previously [11]. Peak identification for each analyte was carried out by spiking with the known standards and the peaks with increased height were identified. For the analysis of the infusion fluids containing amino acids, the real samples were suitably diluted, filtered, and injected direct into the capillary.

#### *2.4. Electrophoretic mobility determination*

Benzyl alcohol or dimethyl sulfoxide (DMSO) was added to samples as a neutral marker for the electrophoretic mobility determination. The mobilities of various BGEs under the specified CE conditions were determined in the buffer containing 20 mM sodium phosphate at pH 11.0. A mixture of all BGEs, 0.1 mM each in deionized

water at pH 11.0, was injected in HD mode for 1 s. The CE voltage applied was +15 kV. Detection was made by a rapid scanning of absorbance from 200 to 350 nm, which allowed a positive identification of the background provider. The electroosmotic mobility,  $\mu_{eo}$ , and the electrophoretic mobility of the BGE,  $\mu_e$ , were calculated as described previously [11].

### 2.5. Determination of the binding constant of CD with BGE

The binding constants for the various BGEs with CDs were determined by the CE method. The CE method is based on the changes in BGE electrophoretic mobility caused by the addition of CD, which formed a complex with the BGE. In the CE experiments, the analytes were prepared in 0.1 mM containing 0.05% DMSO as the EOF (neutral) marker. Various amounts of CD (0–20 mM) were added to the analyte solutions and the capillary electrophoreses were carried out in 20 mM phosphate buffer, pH 11.0, at 25°C. Samples were injected via the HD mode; the separation voltage was +20 kV. The BGE peak was detected by a rapid absorption spectral scan from 200–350 nm. The mobility was determined as described in Section 2.4.

Mathematical models describing the pH and concentration dependence of the electrophoretic mobilities during CE have been developed [20]. It has been demonstrated that  $K_2$  can be determined from the following equations [21]:

$$\mu_{\text{eff}} = \frac{\mu_B + \mu_{\text{BCD}}K_2[\text{CD}]_0}{1 + K_2[\text{CD}]_0 + ([\text{H}_3\text{O}^+]/K_a)(1 + K_1[\text{CD}]_0)} \quad (1)$$

where  $[\text{CD}]_0$  is the initial CD concentration added to the BGE solution,  $\mu_{\text{eff}}$ ,  $\mu_B$ , and  $\mu_{\text{BCD}}$  are the effective mobility of all BGE species, the mobilities of BGE in the absence of CD, and of the BGE-CD complex, respectively.  $K_1$  and  $K_2$  are the binding constants of CD with the unionized and ionized form of BGE, and  $K_a$  is the acid dissociation constant of BGE.

In the absence of CD, Eq. 1 is reduced to

$$\mu_{\text{eff}} = \frac{\mu_B}{1 + [\text{H}_3\text{O}^+]/K_a} \quad (2)$$

When  $\text{pH} \gg \text{p}K_a$ , Eq. 1 can be approximated by

$$\mu_{\text{eff}} = \frac{\mu_B + \mu_{\text{BCD}}K_2[\text{CD}]_0}{1 + K_2[\text{CD}]_0} \quad (3)$$

The binding constant  $K_2$  can be determined from Eq. 3 by the nonlinear least-squares curve fit technique. The equation was solved by adjusting the values of  $\mu_B$ ,  $\mu_{\text{BCD}}$ , and  $K_2$  (three-parameter curve fit) until the best fit of the calculated curve with the experimental data was obtained, using the Sigma Plot for Windows version 1.01 software (Jandel Scientific, Corte Madera, USA) on a 486 personal computer. The mobility  $\mu_B$  can also be determined experimentally, by using Eq. 2, from the mobility measurement of BGE in the absence of CD. We found that  $\mu_B$  determined by the curve fit technique was in good agreement with the value obtained experimentally.

## 3. Results and discussion

### 3.1. CE determination of the binding constant of CD with BGE

As described above, addition of CD to the BGE solution affects the mobility of BGE when a complex is formed by CD and the BGE. Figs. 1a and b show the effects of various CDs on the electrophoretic mobilities of PAS and DMAB, respectively. The mobility is expressed in negative values because of the negative charges carried by the BGE. Since CE was performed with positive voltage (at the injection side), the anions migrated opposite to the EOF; as the BGE formed a complex with CD, its mobility decreased (smaller negative value). Therefore, the complexed form of BGE actually migrated faster toward the cathode (the detector side) than the uncomplexed form. As the CD concentration is increased, the observed mobility of the BGE decreases as more BGE anions form

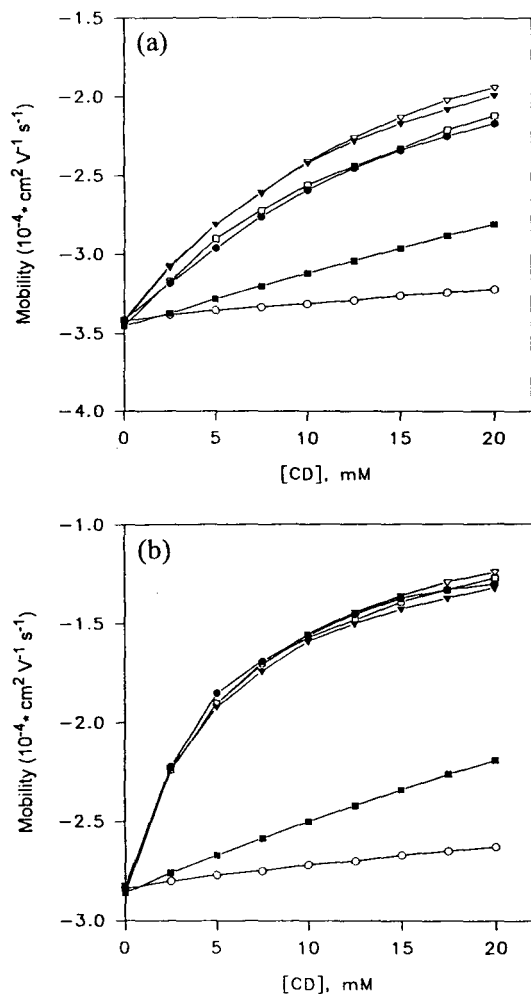


Fig. 1. Effects of concentration of various CDs on the electrophoretic mobilities of selected BGEs in (a) PAS and (b) DMAB.  $\circ$  =  $\alpha$ -CD;  $\bullet$  =  $\beta$ -CD;  $\nabla$  = HP- $\beta$ -CD;  $\blacktriangledown$  = methyl- $\beta$ -CD;  $\square$  = DM- $\beta$ -CD;  $\blacksquare$  = TM- $\beta$ -CD. Buffer: 20 mM phosphate at pH 11.0. Other conditions as in Experimental.

complexes with CD. The binding constants determined by the CE method for the various CDs with PAS and DMAB are listed in Table 1.

From the table and the two titration curves in Figs. 1a and b, it is obvious that  $\alpha$ -CD has the lowest affinity for both BGEs. Similarly, the affinity of TM- $\beta$ -CD is not as strong for either BGE as that of the other  $\beta$ -CDs. The affinities

Table 1

Determination of binding constants of PAS and DMAB with various CDs

Compound	Binding constant, $K_2$ ( $M^{-1}$ )	
	PAS	DMAB
$\alpha$ -CD	na <sup>a</sup>	na
$\beta$ -CD	$42 \pm 4$	$195 \pm 10$
DM- $\beta$ -CD	$52 \pm 2$	$178 \pm 5$
TM- $\beta$ -CD	na	na
Methyl- $\beta$ -CD	$61 \pm 3$	$174 \pm 8$
HP- $\beta$ -CD	$53 \pm 2$	$159 \pm 8$

<sup>a</sup> na: not applicable.

of DMAB for the other four types of  $\beta$ -CD are almost identical and are also the strongest. DMAB has a higher affinity than PAS, presumably because it possesses a hydrophobic dimethylamino group (whereas PAS has *p*-amino); therefore it is easier for DMAB to enter the hydrophobic cavity of the CD. The binding constant of TM- $\beta$ -CD is smaller, probably because of the steric hindrance caused by its bulky trimethyl group. Both BGEs have the same poor affinity for  $\alpha$ -CD because of the negative charge carried by the carboxyl group. In general,  $\alpha$ -CD forms a complex with a neutral molecule better than with a negatively charged molecule. The binding constants of  $\alpha$ -CD for the neutral and negatively charged molecules can sometimes differ by an order of magnitude or more [22].

### 3.2. Selection of the BGE and CE of the twenty common amino acids in the presence of $\alpha$ -CD

There are some drawbacks when using a CD that forms a strong complex with the BGE. Firstly, complex formation between the BGE and the CD could decrease the mobility of the BGE, reducing the EOF and thus increasing the CE run time. Secondly, when the BGE forms a strong complex with a CD, there are less CD molecules available for the analytes, lessening the role that CD plays in enhancing the selectivity of CE separation. Comparing the two BGEs,

PAS seems to work better with the CD additives. Our previous study showed that DMAB had a lower mobility than PAS [11], and that the EOF was smaller and the CE analysis time longer when DMAB was used as the BGE. Moreover, the binding constants of DMAB with most  $\beta$ -CDs are about three times as high as their PAS counterparts. The EOF in the PAS-CD solution is moderately reduced and the analytes have sufficient time to interact with CD. For these reasons, we chose PAS as the preferred BGE for the present method (see also Ref. [11] for other advantages). Fig. 2 compares the electropherograms of 20 common amino acids in 10 mM PAS (a) and 10 mM DMAB (b) at pH 11.0 in the presence of 20 mM  $\alpha$ -CD (Sigma).

Nineteen amino acid peaks are identified. The Arg peak merged with the system peak (the leading peak), thus is not shown. The order of amino acid migration is as follows: system peak (Arg), (1) K (Lys), (2) P (Pro), (3) L (Leu), I (Ile) (not resolved), (4) W (Trp), (5) F (Phe), (6) M (Met), (7) H (His), (8) V (Val), (9) Q (Gln), (10) T (Thr), (11) N (Asn), (12) A (Ala), (13) S (Ser), (14) G (Gly), (15) Y (Tyr), (16) C (Cys), (17) E (Glu), (18) D (Asp). Note that the order in which some amino acids migrate is different in the absence of CD (cf. Ref. [11]). Trp migrates faster than Leu and Ile, the order for Met and His is reversed, and Val migrates faster than Met. The changes in migration order suggest that  $\alpha$ -CD interacts more favorably with Leu, Ile, and Met, decreasing their mobilities.

Using PAS as the BGE, 18 amino acid peaks could be resolved in less than 35 min. Using DMAB, it would take about 50 min to resolve these peaks; however, the resolution would be better. Using PAS, only 16 peaks could be baseline-resolved. The Phe and Met peaks, and the Asn and Ala peaks could not be completely resolved. Using DMAB, on the other hand, the Asn and Ala peaks can be baseline-resolved. A drawback associated with using DMAB is that the last three tailing peaks are broader (peak width at half height is in the range of 0.23–0.76 min in PAS but 0.34–1.38 min in DMAB) and have poorer reproducibility.

### 3.3. Effect of impurities in the CD source

The impurities in the commercial sources of CD vary considerably. For example, mass spectrometric analysis (data not given) shows that a batch of  $\alpha$ -CD from Sigma (purity 99%) contains only a small amount of  $m/z$  506 impurity, whereas in a batch of  $\alpha$ -CD from Janssen (labeled purity >98%) several times as much of the same impurity is found. The relative intensity ratios of the  $m/z$  506 impurity peak to  $\alpha$ -CD ( $m/z$  974) peak were 0.30 and 1.58 for the Sigma and Janssen brands, respectively. The electropherogram of the twenty amino acids obtained with the  $\alpha$ -CD from Janssen (Fig. 3) looks very different from that of the Sigma  $\alpha$ -CD (Fig. 2a) under identical CE conditions (except for the concentration of CD). When CE was performed using the Janssen batch, which contains a higher impurity level, the EOF was lower and the analysis time longer. Note that for Fig. 3, a much lower  $\alpha$ -CD concentration (2 mM) was used; even so, it extended the analysis time to almost 55 min. The result suggests that the reduction in EOF and greater CE run time are due to the impurities in the Janssen brand altering the surface properties of the capillary. Note also that the migration order changed; most noticeably, for Trp, Met, and Thr. This is due in part to the difference in the CD concentration used in the two experiments. The impurity may be cyclic or acyclic dextrin which adsorbed to the capillary surface, thus reducing the EOF. It has been reported that several kinds of dextrin and dextran [23,24] could be used to enhance the CE separation of chiral compounds. The effect of impurities on the CE observed here seems to be similar to that caused by dextrin or dextran.

### 3.4. Effects of concentration of the various CDs on CE

The effects of concentration of various CDs on the electrophoretic mobilities of selected amino acids are shown in Figs. 4–6. HP- $\alpha$ -CD has a more pronounced effect on the mobilities of Met, aliphatic (Leu, Ile) and aromatic (Trp, Phe,



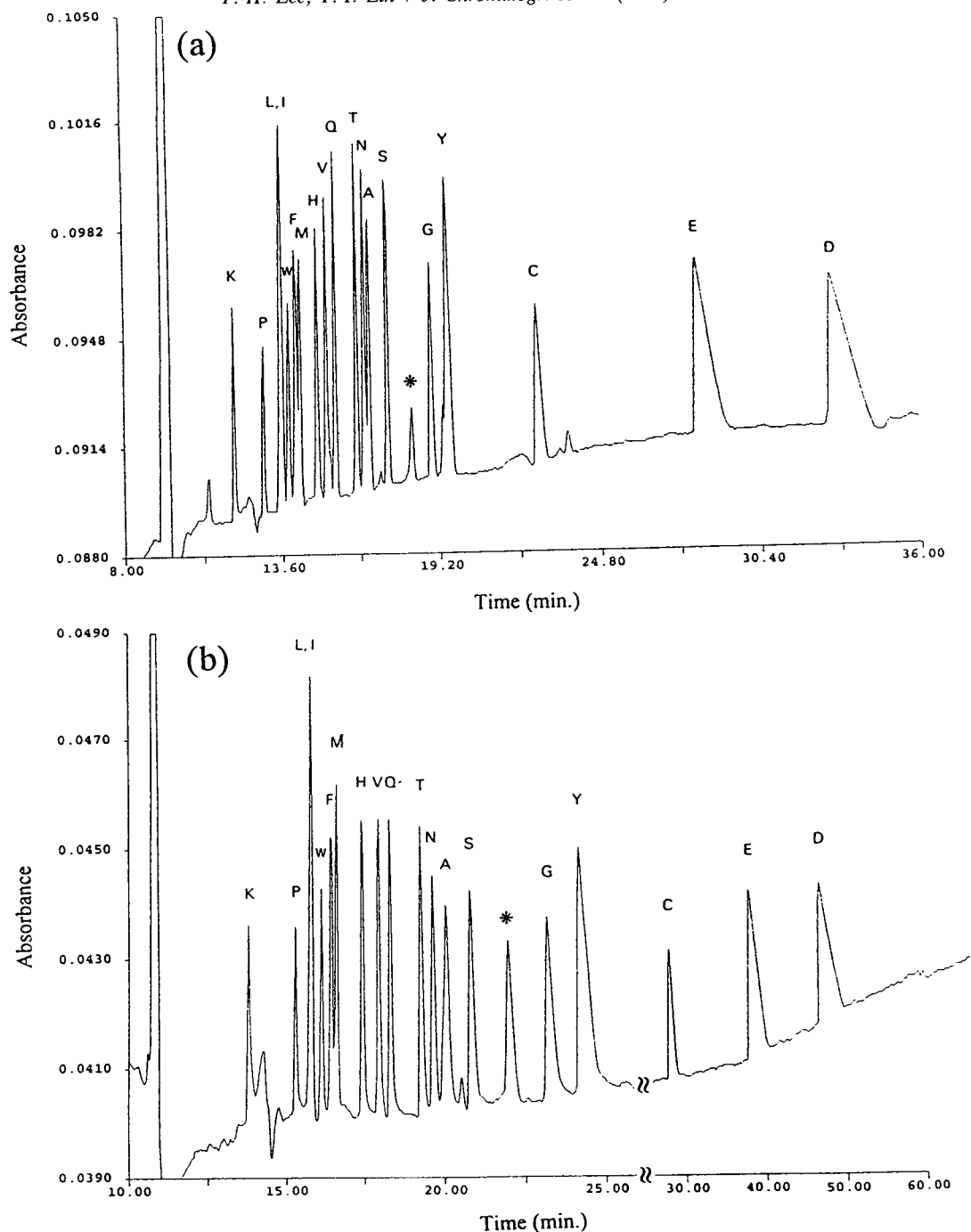


Fig. 2. Electropherograms of 20 common amino acids in 10 mM (a) PAS and (b) DMAB in the presence of 20 mM  $\alpha$ -CD (Sigma) at pH 11.0. Concentration of amino acids, 0.5 mM each. Peak identification: K = Lys, P = Pro, L = Leu, I = Ile (not resolved), W = Trp, F = Phe, M = Met, H = His, V = Val, Q = Gln, T = Thr, N = Asn, A = Ala, S = Ser, G = Gly, Y = Tyr, C = Cys, E = Glu, D = Asp. Arg is merged with the system peak (the first peak), \* is an unknown peak.

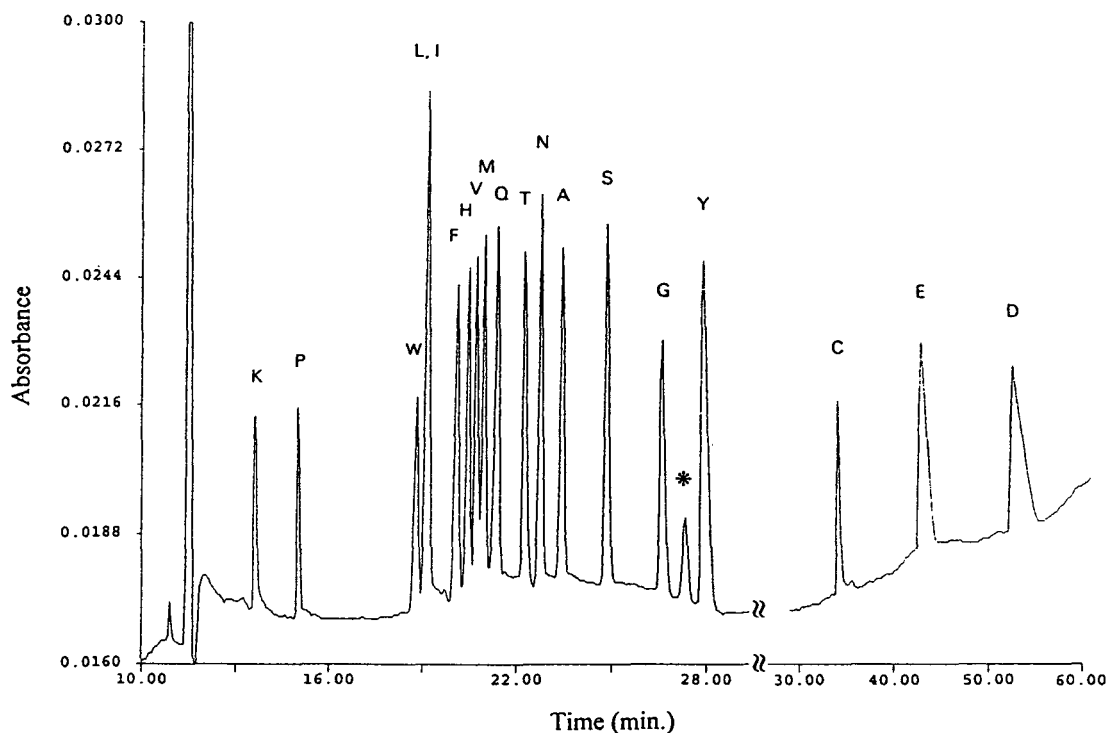


Fig. 3. Effects of impurities in 2 mM  $\alpha$ -CD (Janssen) on the electropherogram of 20 common amino acids. For other CE conditions see Fig. 2a.

Tyr) amino acids (Fig. 4b). The effect of  $\alpha$ -CD is similar (Fig. 4a) except for Trp. Since Trp has a larger indole ring, it may be unable to enter the small  $\alpha$ -CD cavity. The effects on Met and Leu/Ile are the most dramatic, changing their migration order. This is presumably because the long aliphatic chain enables these residues to exert a stronger interaction with  $\alpha$ -CD. However, Leu and Ile still could not be separated, presumably because the interactions of CD with these two amino acids are similar.  $\beta$ -CD and HP- $\beta$ -CD affect Tyr and Phe most significantly, changing their migration orders (Fig. 5). It is also noteworthy that with high  $\beta$ -CD concentrations, Leu and Ile could be separated. Comparing the effects of  $\alpha$ -CD and HP- $\alpha$ -CD on Tyr, the hydroxyl groups on either HP- $\alpha$ -CD or Tyr seem to be responsible for the stronger interaction. This suggestion is consistent with the similar result found for  $\beta$ -CD and HP- $\beta$ -CD. The effects of DM- $\beta$ -CD and methyl- $\beta$ -CD (Fig. 6) are

most noticeable on the aromatic amino acids but are less pronounced than those exerted by  $\beta$ -CD and HP- $\beta$ -CD. In particular, the interaction of DM- $\beta$ -CD with Tyr is less strong (Fig. 6). Presumably, the extra methyl and dimethyl groups cause some steric hindrance to the aromatic amino acids entering the DM- $\beta$ -CD cavity.

### 3.5. CE separation of Leu and Ile in the presence of various CDs

Separation of Leu and Ile was not successful using the method we developed previously [11]. Because of the structural similarity of Leu and Ile, their separation by CE is a most challenging problem. Among the various CDs that have been investigated, we found that while  $\alpha$ -CD was ineffective, several kinds of  $\beta$ -CD, including  $\beta$ -CD, HP- $\beta$ -CD, and DM- $\beta$ -CD, were promising. Fig. 7 depicts the effects of various CDs on the CE resolution ( $R_s$ ) between the Leu and Ile

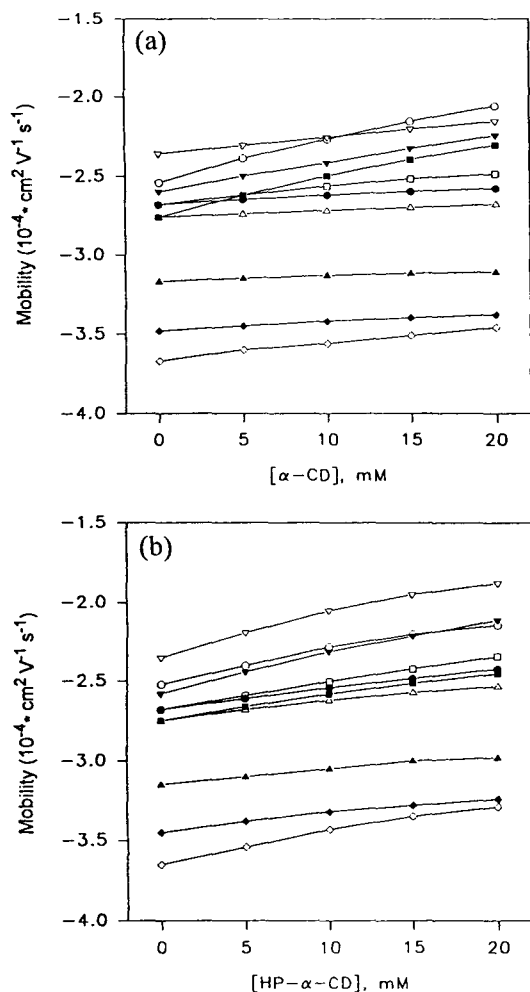


Fig. 4. Effects of concentration of (a)  $\alpha$ -CD and (b) HP- $\alpha$ -CD on the electrophoretic mobilities of selected amino acids.  $\circ$  = Leu/Ile;  $\bullet$  = Val;  $\nabla$  = Trp;  $\blacktriangledown$  = Phe;  $\square$  = His;  $\blacksquare$  = Met;  $\triangle$  = Gln;  $\blacktriangle$  = Ser;  $\diamond$  = Tyr;  $\blacklozenge$  = Gly. For other CE conditions see Fig. 2.

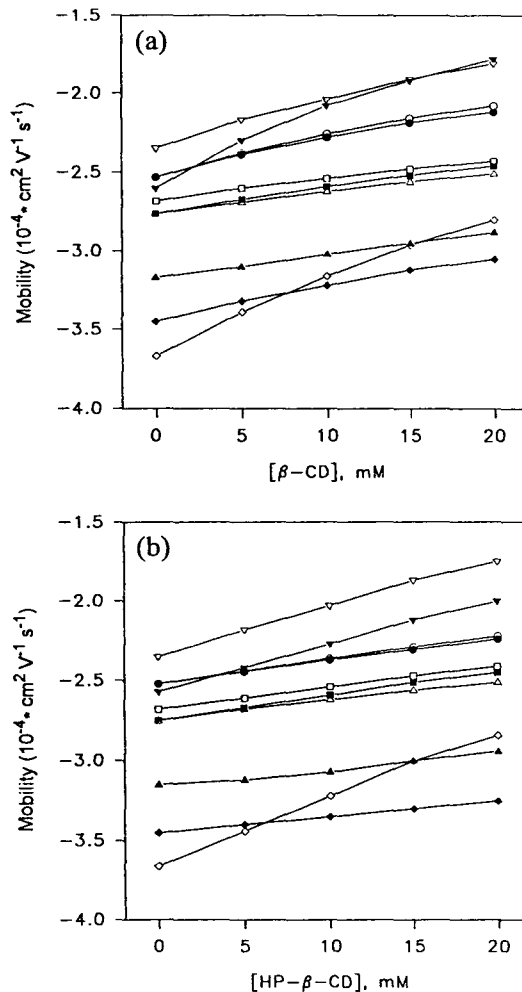


Fig. 5. Effects of concentration of (a)  $\beta$ -CD and (b) HP- $\beta$ -CD on the electrophoretic mobilities of selected amino acids.  $\circ$  = Leu;  $\bullet$  = Ile;  $\nabla$  = Trp;  $\blacktriangledown$  = Phe;  $\square$  = His;  $\blacksquare$  = Met;  $\triangle$  = Gln;  $\blacktriangle$  = Ser;  $\diamond$  = Tyr;  $\blacklozenge$  = Gly. For other CE conditions see Fig. 2.

peaks. Although both HP- $\beta$ -CD and DM- $\beta$ -CD do improve the separation of the two analytes to a certain extent, the improvement is less than ideal, even at the high concentration of 20 mM. On the other hand,  $\beta$ -CD could give a resolution better than one, even at a lower concentration of 15 mM. One note of caution, however, is that under the conditions where the best resolution of Leu and Ile could be obtained, the separation for several other amino acids became rather poor

(data not shown). Thus, so far there is still no method available that can separate all twenty amino acids in one single CE run. Further studies are needed in order to achieve this goal.

### 3.6. Analyses of real samples

To demonstrate the applicability of the present method to real samples, two infusion fluids containing several amino acids from a local

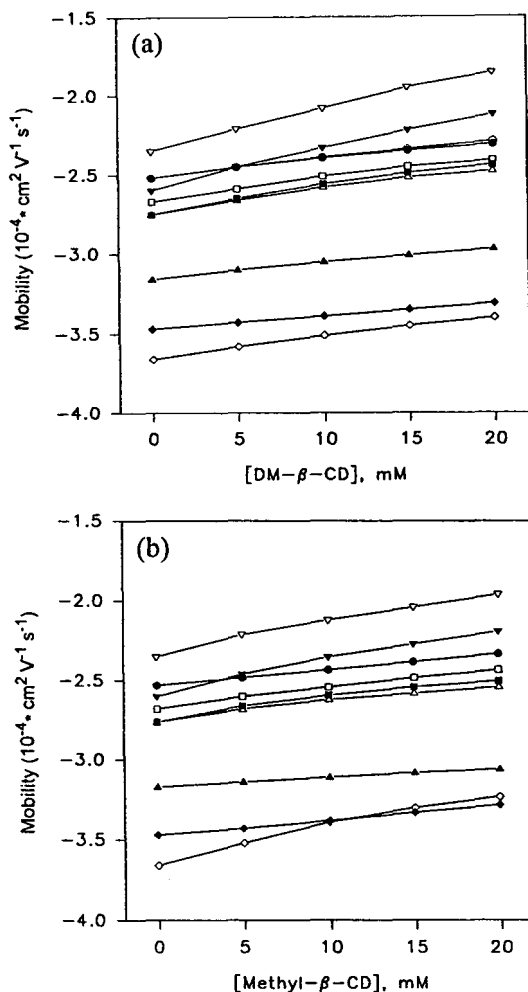


Fig. 6. Effects of concentration of (a) DM- $\beta$ -CD and (b) methyl- $\beta$ -CD on the electrophoretic mobilities of selected amino acids.  $\circ$  = Leu;  $\bullet$  = Ile;  $\nabla$  = Trp;  $\blacktriangledown$  = Phe;  $\square$  = His;  $\blacksquare$  = Met;  $\triangle$  = Gln;  $\blacktriangle$  = Ser;  $\diamond$  = Tyr;  $\blacklozenge$  = Gly. For other CE conditions see Fig. 2.

pharmaceutical company have been analyzed. Fig. 8 displays the electropherograms of the two infusion fluids. Thirteen and sixteen components were identified in the two samples, respectively, and the results agreed (qualitatively) with the ingredient labels. As noted previously, under the conditions best suited to the CE separation of most amino acids, Leu and Ile could not be separated. Thus, a separate analysis would be

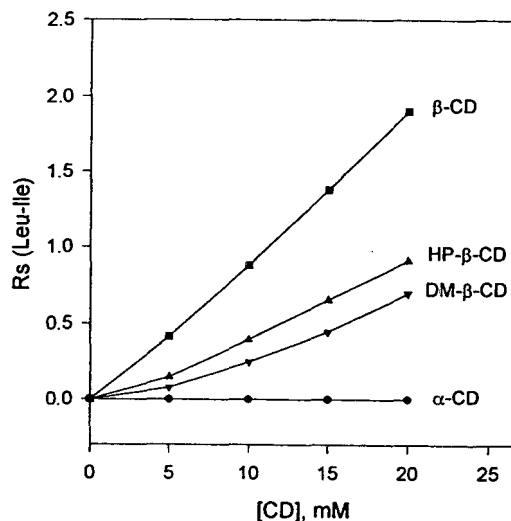


Fig. 7. Effects of concentration of various CDs on the resolution of Leu and Ile.

required for a complete determination of all twenty amino acids.

#### 4. Conclusion

CE methods for effective separation and detection of all twenty common amino acids with indirect UV absorbance detection have been developed using commercial CE instruments. By using 10 mM PAS (as the BGE), 20 mM  $\alpha$ -CD (to reduce EOF and enhance selectivity) at pH 11.0, all twenty amino acids except Leu and Ile were separated in less than 35 min. As an alternative, an even better resolution was obtained by replacing PAS with the same concentration of DMAB; however, a longer analysis time (55 min) was then required. Complete CE separation of Leu and Ile could only be achieved by replacing  $\alpha$ -CD with 15 or 20 mM  $\beta$ -CD, which gave inferior results for several other separations. Thus, at present, using the indirect absorbance detection method, two separate runs are still required for complete CE determination of all twenty amino acids.

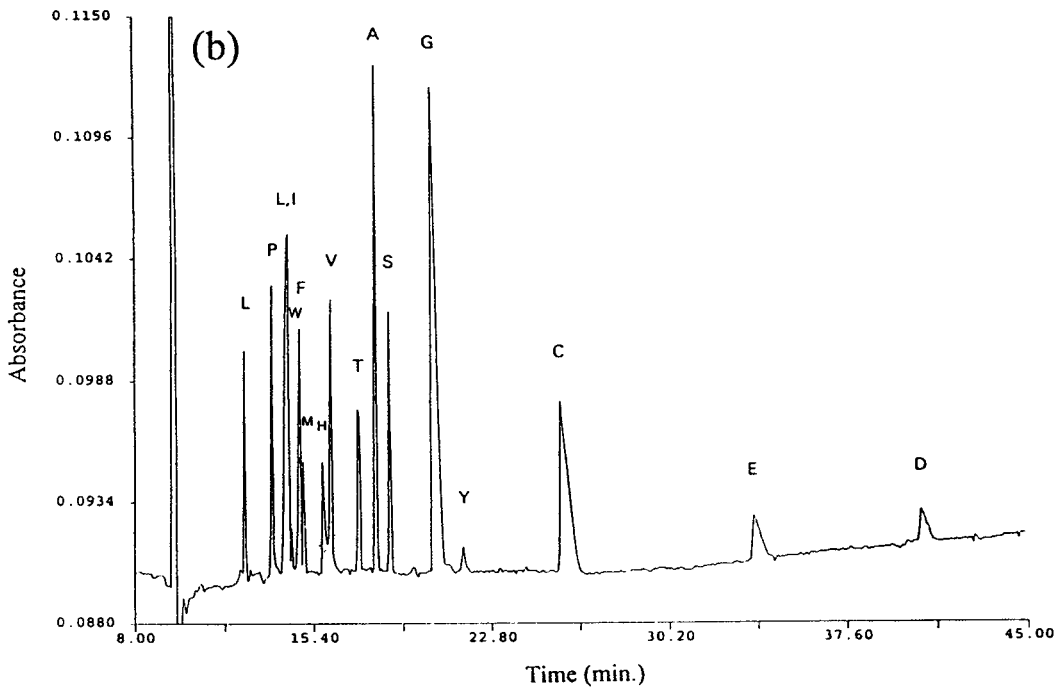
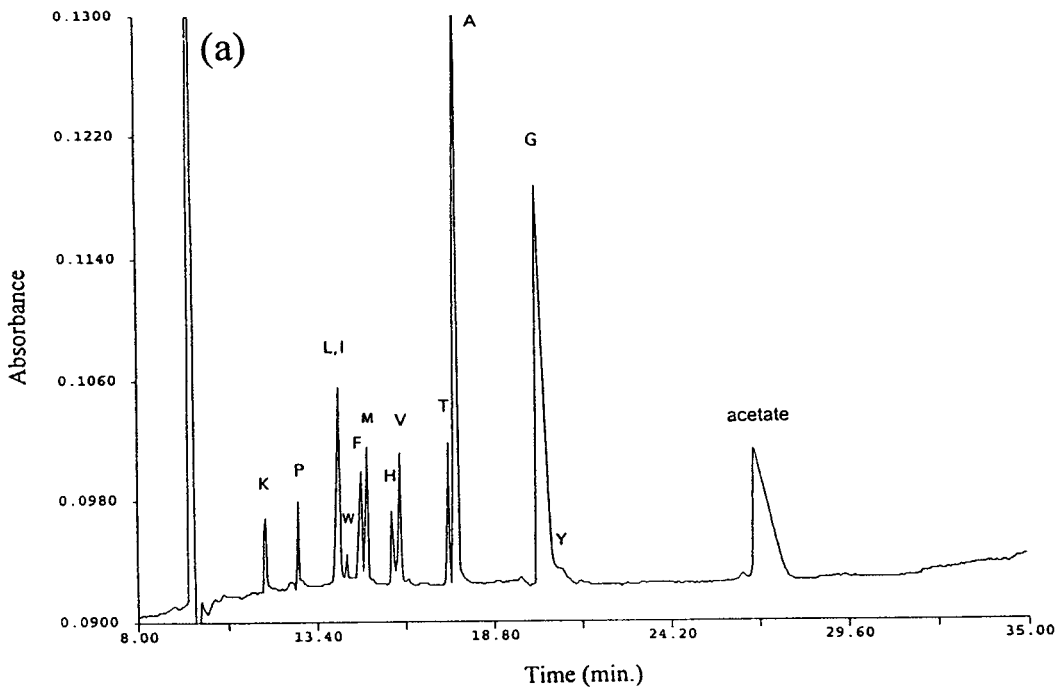


Fig. 8. Electropherograms of two infusion fluids containing amino acids. (a) Aminol Infusion and (b) Aminol-12X injection. (Both samples from Sintong Chem., Taiwan.) For CE conditions see Fig. 2.

## Acknowledgements

The authors wish to express their gratitude to T.-Y. Liu and G.-R. Her for the mass spectrometric analysis of cyclodextrin. This work was supported by a grant from the National Science Council, Taiwan.

## References

- [1] P. De Montigny, J.F. Stobaugh, R.S. Givens, R.G. Carlson, K. Srinivasachar, L.A. Sternson and T. Higuchi, *Anal. Chem.*, 59 (1987) 1096.
- [2] S.C. Beale, J.C. Savage, D. Wiesler, S.M. Wietstock and M. Novotny, *Anal. Chem.*, 60 (1988) 1765.
- [3] S.C. Beale, Y.-Z. Hsieh, D. Wiesler and M. Novotny, *J. Chromatogr.*, 499 (1990) 579.
- [4] W.G. Kuhr and E.S. Yeung, *Anal. Chem.*, 60 (1988) 1832.
- [5] E.S. Yeung and W.G. Kuhr, *Anal. Chem.*, 63 (1991) 275A.
- [6] W.G. Kuhr and C.A. Monnig, *Anal. Chem.*, 64 (1992) 389R.
- [7] C.A. Monnig and R.T. Kennedy, *Anal. Chem.*, 66 (1994) 280R.
- [8] F. Foret, S. Fanali, L. Ossicini and P. Bocek, *J. Chromatogr.*, 470 (1989) 299.
- [9] G.J.M. Bruin, A.C. van Asten, X.M. Xu and H. Poppe, *J. Chromatogr.*, 608 (1992) 97.
- [10] Y. Ma, R. Zhang and C.L. Cooper, *J. Chromatogr.*, 608 (1992) 93.
- [11] Y.-H. Lee, and T.-I. Lin, *J. Chromatogr. A*, 680 (1994) 287.
- [12] S.F.Y. Li, *Capillary Electrophoresis*, Elsevier, Amsterdam, 1992, Ch. 5.
- [13] R. Kuhn and S. Hoffstetter-Kuhn, *Chromatographia*, 34 (1992) 505.
- [14] I.E. Valko, H.A.H. Billiet, H.A.L. Corstjens and J. Frank, *LC·GC Int.*, 6 (1993) 420.
- [15] T.L. Bereuter, *LC·GC Int.*, 7 (1994) 78.
- [16] T.J. Ward, *Anal. Chem.*, 66 (1994) 632A.
- [17] M. Novotny, H. Soini and M. Stefansson, *Anal. Chem.*, 66 (1994) 646A.
- [18] S. Li and W.C. Purdy, *Chem. Rev.*, 92 (1992) 1457.
- [19] T.-Y. Liu, L.-L. Shiu, T.-Y. Luh and G.-R. Her, *Rapid Commun. Mass Spectrom.*, 9 (1995) 93.
- [20] Y.Y. Rawjee, D.U. Staerk and G. Vigh, *J. Chromatogr.*, 635 (1993) 291.
- [21] Y.Y. Rawjee and G. Vigh, *Anal. Chem.*, 66 (1994) 619.
- [22] K. Pptchumani and M. Vellayappan, *J. Incl. Phenom.*, 14 (1992) 157.
- [23] C. Quang and M.G. Khaledi, *J. High Resolut. Chromatogr.*, 17 (1994) 609.
- [24] P. Sun, G.E. Barker, G.J. Mariano and R.A. Hartwick, *Electrophoresis*, 15 (1994) 793.



ELSEVIER

Journal of Chromatography A, 716 (1995) 347–353

JOURNAL OF  
CHROMATOGRAPHY A

# Determination of thiols by capillary electrophoresis with electrochemical detection using a palladium field-decoupler and chemically modified electrodes

Xinjian Huang, W. Th. Kok\*

Laboratory for Analytical Chemistry, University of Amsterdam, Nieuwe Achtergracht 166, 1018 WV Amsterdam, Netherlands

## Abstract

Off-column electrochemical detection has been used for the determination of cysteine and related compounds after separation by capillary electrophoresis. For the decoupling of the high-voltage field, an improved palladium decoupler was developed with a dead volume of less than 10 nl. Micro-electrodes, bulk-modified with cobalt phthalocyanine, were used in a nanoliter-volume cell for detection of the thiol compounds. With a detection potential of +0.6 V vs. Ag/AgCl a high selectivity and sensitivity was obtained.

Baseline separation of cysteine, homocysteine and glutathione could be realized in 25 min, using a formate buffer with pH 2.7 as background electrolyte. Detection limits of  $0.5 \mu\text{mol l}^{-1}$  for homocysteine,  $1 \mu\text{mol l}^{-1}$  for cysteine and  $5 \mu\text{mol l}^{-1}$  for glutathione were obtained. The concentrations of free cysteine and total cysteine (after treatment with dithiothreitol) in urine samples could be measured.

## 1. Introduction

Capillary electrophoresis (CE) has been shown to be a powerful analytical tool with its high separation efficiency [1]. While new applications are still being explored and fundamental research is carried out with great interest in many laboratories, CE has already become an alternative or complementary analytical technique to high-performance liquid chromatography (HPLC) for routine analysis [2]. UV-absorption detection is by far the most commonly used detection technique, but it has a major inherent drawback: the dependence of the sensitivity on the light-path length, which is small in CE. This drawback does not exist in electrochemical de-

tection (ED). ED is based on the reaction of analytes on an electrode surface and only molecules in a thin diffusion layer contribute to the signal intensity. For compounds which can not be detected favourably by UV absorption, ED can be an alternative.

ED in capillary electrophoresis has received considerable attention from several research groups [3–16]. A prerequisite to perform ED in CE is to isolate the electrophoretic current generated by the high-voltage (HV) used for separation, from the electrochemical detection current. To achieve this, there are basically two approaches: the end-column mode [3–7] and the off-column mode [8–16]. End-column detection, where the detection electrode is positioned close to the capillary exit in the grounded end-vial, is restricted to very narrow capillaries ( $<25 \mu\text{m}$

\* Corresponding author.

I.D.) with a low electrophoretic current to minimize the interference of the high voltage on the detection current. Normal-sized capillaries (25–100  $\mu\text{m}$  I.D.) can only be used in off-column detection, provided that the influence of electrophoretic current is eliminated from the electrochemical detection signal. To achieve this, the separation capillary is connected to the detector through a field-decoupler made of porous material [8–11], an ion-exchange tube [12,13] or palladium metal [14–16]. This decoupler acts as the grounded end of the CE system. In this way, the electrophoretic current is separated from the electrochemical current.

Thiols play an important role in several biological processes. It is of clinical and pharmaceutical importance to determine these compounds in biological fluids and tissues [17]. The separation of thiols using HPLC has been reviewed [18]. Because of the absence of strong chromophores and fluorophores, pre- or post-column derivatization procedures are often used for sensitive and selective detection. Derivatization is not required in ED [19,20], but thiols are not easily detected with a normal carbon electrode, since their oxidation requires a high overpotential [21]. It has been shown that modification of the electrode with cobalt phthalocyanine (CoPC) as electrocatalyst reduces the required overpotential, so that thiols can be detected at a lower, more selective potential [22,23].

Recently, the separation of thiols by CE with UV [24–27] or fluorescence detection [28] has been described. O'Shea and Lunte [29,30] developed an off-column ED method for the determination of various thiol compounds in CE. They used a Nafion joint to decouple the electric field and amalgated gold [29] or CoPC-modified carbon-paste electrodes [30] for detection.

In previous work we have shown that conductive carbon cement (CCC) is a suitable matrix material for the preparation of chemically-modified electrodes to be used in flowing solutions [16,23,31], giving a higher electrode stability than carbon paste. With CoPC-modified CCC electrodes thiols could be reproducibly determined in urine samples after separation by liquid

chromatography [23]. Following up on the work of O'Shea and Lunte, in the study described in this paper CoPC-CCC microelectrodes were tested for the determination of underivatized cysteine compounds separated by CE. First, however, we report on an improvement of the palladium union we use to decouple the electric field. Since cysteine compounds are to be separated as positive ions, migrating in the same direction as the electroosmotic flow, the demands on the dead volume of a decoupler are very strict [14]. The dead volumes of two new types of the decoupler were determined by comparing the variances in off-column (UV) detection with that in on-column detection. The improved Pd-decoupler was used for off-column ED of reduced thiols using CoPC-modified CCC electrodes. The experimental conditions to separate cysteine, homocysteine and glutathione were studied. The determination of free and total cysteine in urine samples is shown.

## 2. Experimental

### 2.1. Apparatus

The field-decouplers were made from 6-mm diameter palladium rod. Fused-silica capillaries with an outer diameter of 375  $\mu\text{m}$  and different internal diameters were obtained from Polymicro Technologies (Phoenix, AZ, USA). For off-column amperometric detection, the experimental set-up was as described before [16]. A Prince programmable injector for capillary electrophoresis, including a 30-kV high-voltage supplier was obtained from Lauer Labs (Emmen, Netherlands). The 75  $\mu\text{m}$  I.D. separation capillary was 85 cm long. New capillary was etched with 1 M HCl for one hour before use unless stated otherwise. A 7-cm piece of poly ether ether keton (PEEK) tubing (Upchurch, Oak Harbor, WA, USA) with 63.5  $\mu\text{m}$  I.D. and 0.5 mm O.D. was used as the coupling capillary in ED. A piece of PEEK tube (I.D. 0.5 mm, O.D. 1/16") was used to construct CoPC-modified carbon working electrodes in the fashion described earlier for cuprous oxide modified microelectrodes



[16]. An Amor (Spark, Emmen, Netherlands) potentiostat/amplifier was used. The signals were registered with a HP 3394A integrator and a Kipp and Zonen strip-chart recorder. Samples were introduced hydrodynamically. The volume of sample loaded was calculated from the equation:

$$V_{inj} = \frac{\pi P_{inj} d_1^4 d_2^4 t}{128 \eta (d_1^4 L_2 + d_2^4 L_1)} \quad (1)$$

where  $P_{inj}$  is the injection pressure,  $t$  the injection time,  $\eta$  the viscosity, and  $L_1$ ,  $L_2$  and  $d_1$ ,  $d_2$  are the lengths and internal diameters of the separation and the coupling capillaries, respectively.

For UV absorbance detection, a Spectra 100 variable-wavelength UV detector (Spectra-Physics) was used, and a 2-mm detection window was made by burning off the coating of the capillary.

## 2.2. Chemicals and solutions

All chemicals were used as received. Conductive carbon cement (CCC) was supplied by Gerhard Neubauer (Münster, Germany). Cobalt phthalocyanine (CoPC) and *dl*-homocysteine (HCYS) were obtained from Aldrich (Milwaukee, WI, USA), MES hydrate from Aldrich (Steinheim, Germany). 1-Naphthol (NOH) was purchased from BDH, 1-cysteine (CYS), 1-naphthalenemethylamine ( $NMA^+$ ), 6-hydroxynaphthalenesulfonic acid ( $HNSA^-$ ) from Merck, and 2-naphthol-3,6-disulfonic acid ( $NDSA^{2-}$ ) from Fluka. Glutathione (reduced, GSH) and dithiothreitol (DTT) were obtained from Janssen Chimica. All other chemicals were analytical reagent grade. Concentrated stock solutions of NOH,  $NMA^+$ ,  $HNSA^-$  and  $NDSA^{2-}$  in water or methanol were kept at 4°C, and diluted to  $10^{-4}$  mol  $l^{-1}$  with buffer for injection. Stock solutions of thiols were prepared daily in buffer solutions and stored at 4°C and diluted to the desired concentrations before use. Both MES buffer and formate buffer contained 1 mM EDTA and 0.1 mM NaCl. Subboiled demineralized water was used to prepare solutions. Buffers were filtered

through a Millipore membrane filter (0.45- $\mu$ m pore size) and degassed with helium before used. Before each CE run, the inlet buffer vial was replaced with a vial filled with freshly degassed buffer, and the capillaries were washed with the buffer for 5 min.

## 2.3. Sample preparation

Fresh urine samples were diluted with the running buffer, filtered, and immediately subjected to injection. DTT-treated urine samples were prepared as follows. To 2 ml of urine sample, 1.8 ml of 0.1 M  $Na_2HPO_4$  (pH 8.0) and 0.2 ml of 0.1 M DTT were added and mixed. After 15 min the mixture was centrifuged and 2 ml of supernatant was mixed with 2 ml of formate buffer and subjected to injection.

## 3. Results and discussion

### 3.1. Evaluation of Pd decouplers

The decoupler used in previous studies suffered from a relatively large dead volume (ca. 15 nl). Two new types of palladium decouplers were developed (Fig. 1). Type A has the same configuration as the reported one [15] but with a narrower connecting channel (100  $\mu$ m). With

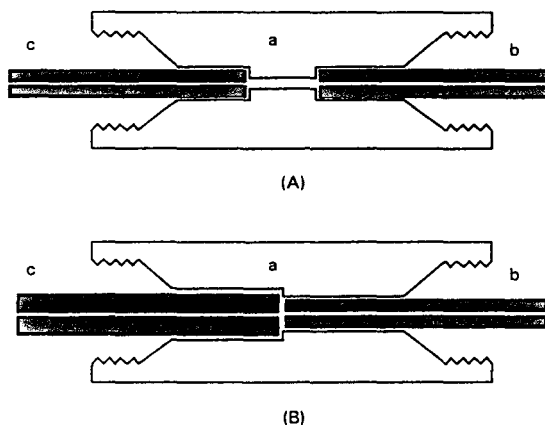


Fig. 1. Cross-section of the palladium decouplers type A and B. (a) Pd union; (b) separation capillary; (c) coupling capillary (not on scale).

type B the separation and coupling capillaries are positioned directly against each other, and electrical contact with the solution is made through the thin gap between them. These two decouplers were tested as described before [15]. The ability of the decouplers to dissipate the generated hydrogen was tested by measuring current–voltage relations. For both types of Pd decouplers, the electrophoretic current increased linearly with the applied voltage up to ca. 50  $\mu\text{A}$ . At higher voltages the linearity was lost but currents up to 150  $\mu\text{A}$  could be passed.

To determine the zone-broadening contribution of the decouplers, the zone widths of four differently charged naphthalene derivatives, obtained with on-column and off-column UV detection, were compared. With on-column detection a 85 cm  $\times$  75  $\mu\text{m}$  I.D. capillary with the detection window at 60 cm was used. For off-column detection, the separation capillary was 60 cm  $\times$  75  $\mu\text{m}$  I.D.. A 15 cm  $\times$  50  $\mu\text{m}$  I.D. coupling capillary was used with a detection window at 10 cm from the decoupler. A compensating pressure of 100 mbar was used to eliminate the

laminar backflow in the separation capillary. The results are given in Table 1. The difference between the calculated value of the zone variance and the experimental value obtained with off-column detection may be attributed to the contribution of the dead volume in the palladium decouplers. Typical dead volumes of 9 nl for type A decoupler and 7 nl for type B decoupler were found. The electroosmotic and electrophoretic mobilities from off-column detection match perfectly with those from on-column detection, which indicates that the calculation method [16] is reliable. In further experiments a decoupler of type B was used.

The influence of the applied high voltage on the noise level of off-column amperometric detection was investigated. As shown in Fig. 2A, a higher noise was obtained at higher voltages. It is not clear whether this is caused by an incomplete decoupling of the electrophoretic current or by the appearance of small hydrogen bubbles at high voltages. Interestingly, the noise on the electrophoretic current increases in a similar way with the applied voltage (Fig. 2B).

Table 1  
Comparison of on-column detection and off-column detection<sup>a</sup>

Parameter	Mode	Decoupler type	Compound			
			NMA <sup>+</sup>	NOH	HNSA <sup>-</sup>	NDSA <sup>2-</sup>
Elution time (s)	On-column		185	248	376	560
	Off-column	Type A	209	274	404	575
		Type B	208	272	402	590
Mobility ( $10^{-4} \text{ cm}^2 \text{ V}^{-1} \text{ s}^{-1}$ )	On-column		2.75	8.07 <sup>c</sup>	-2.72	-4.47
	Off-column <sup>b</sup>	Type A	2.86	8.02 <sup>c</sup>	-2.78	-4.53
		Type B	2.87	8.07 <sup>c</sup>	-2.80	-4.57
Zone variance $\sigma^2$ (s <sup>2</sup> )	On-column exp		0.41	0.76	1.37	5.06
	Off-column calc <sup>d</sup>		1.06	1.31 <sup>e</sup>	2.04	5.87
	Off-column exp	Type A	1.82	3.1	3.50	6.60
Type B		1.59	1.8	2.34	6.30	
$\Delta\sigma$ (nl)	Type A		9.3	14.3 <sup>e</sup>	7.2	9.1
	Type B		7.8	7.5 <sup>e</sup>	5.8	7.0

<sup>a</sup> For experimental details, see text.

<sup>b</sup> Calculated from the equations of Ref. [16].

<sup>c</sup> Electroosmosis.

<sup>d</sup> The calculated variance contributions of the coupling capillary were added to the results of on-column detection.

<sup>e</sup> Diffusion coefficient estimated [14].

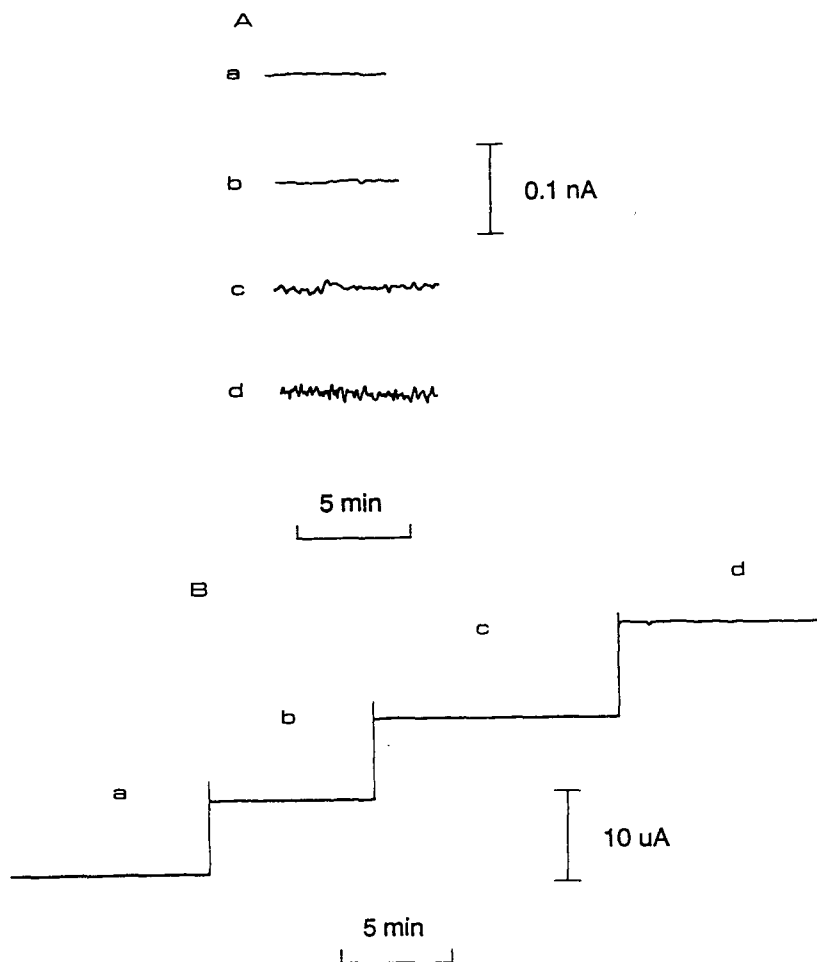


Fig. 2. (A) Influence of the applied voltage on the electrochemical detector baseline noise; (B) electrophoretic current trace at different applied voltages. (a) 0 kV; (b) 10 kV; (c) 20 kV; (d) 30 kV.

### 3.2. Detection and separation of thiols

In previous work CCC electrodes bulk-modified with CoPC have been used for detection of thiols in HPLC [23]. A miniaturized CoPC-CCC electrode, with an active surface of  $0.2 \text{ mm}^2$ , was constructed for ED in CE. Cyclic voltammetry was used to evaluate the response of the micro-electrodes to CYS. As illustrated in Fig. 3, CYS can be oxidized at anodic potentials higher than  $+0.4 \text{ V}$  with two anodic peaks. The mediated electrochemical process is identical to that observed with large-area ( $7 \text{ mm}^2$ ) electrodes. For

detection in CE, a potential of  $+0.6 \text{ V}$  vs. Ag/AgCl was chosen.

Although in the literature the separation of thiols using a MES buffer has been described [29,30], we have found no separation between CYS, HCYS and DTT with this buffer. In fact, at the pH of a MES buffer (pH 5.5–6.7), CYS and HCYS are close to their isoelectric point [32] and DTT is also neutral [33]. A baseline separation between the four model compounds was achieved using a formate buffer with pH 2.7, where the compounds are positively charged (see Fig. 4).

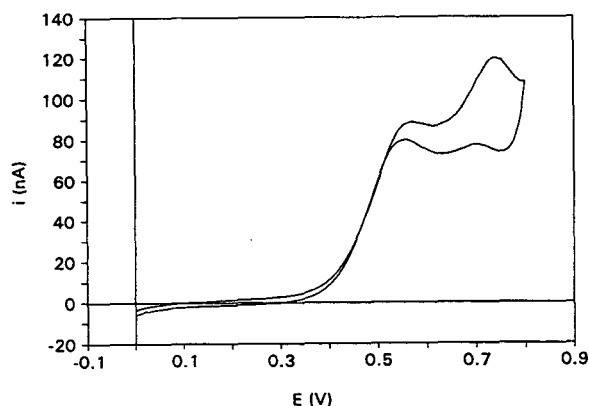


Fig. 3. Cyclic voltammogram of 1 mM cysteine in 5 mM formate buffer (pH 2.7) using a CoPC-modified micro-electrode. Scan rate:  $20 \text{ mV s}^{-1}$ .

At pH 2.7 an osmotic mobility of  $(1.4 \pm 0.1) \cdot 10^{-8} \text{ m}^2 \text{ V}^{-1} \text{ s}^{-1}$  was found using UV detection and phenol as neutral marker. It can be calculated [16] that with this osmotic mobility a compensating pressure of 3.5 mbar is required to

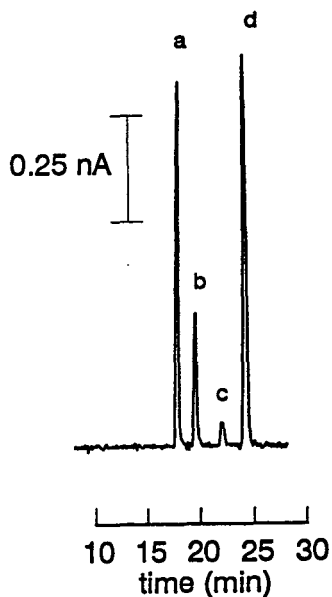


Fig. 4. Electropherogram of the separation of (a) homocysteine; (b) cysteine; (c) glutathione; (d) DTT. Concentrations:  $10 \mu\text{M}$  for each compound. Buffer: 5 mM formate + 1 mM EDTA + 0.1 mM NaCl (pH 2.7); injection volume: 20 nl; applied voltage: 30 kV;  $P_{\text{cmp}}$ : 5 mbar; CoPC-CCC electrode operated at +0.6 V.

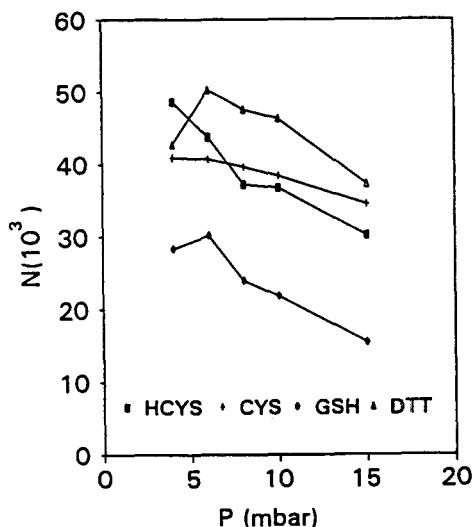


Fig. 5. Influence of the applied pressure on the observed plate numbers in formate buffer.

preserve the flat flow profile in the separation capillary. In Fig. 5 the influence of the applied compensation pressure on the observed plate numbers is shown. As has been pointed out before [14], the influence of  $P_{\text{cmp}}$  on the separation efficiency is not very profound for zones migrating in the same direction as the osmotic flow. Still, optimum values between 3 and 6 mbar were observed, with maximum plate numbers of approximately 50 000 for HCYS, CYS and DTT and 30 000 for GSH. Typical detection limits of  $0.5 \mu\text{M}$  for HCYS,  $1 \mu\text{M}$  for CYS and  $5 \mu\text{M}$  for GSH were found. Calibration plots from 10 to  $200 \mu\text{M}$  were linear ( $r = 0.9967$ ). Although appreciable differences in sensitivity between individual electrodes were found, the within-day reproducibility using the same electrode was within 8%.

An example of the application of the method for the determination of free and total (after treatment with DTT) CYS in urine is shown in Fig. 6. In this particular urine sample a free concentration of  $35 \mu\text{M}$  CYS was found, which is well within the normal range. The total concentration, after reduction of cystine and other cysteine-containing compounds [34,35], was found to be  $201 \mu\text{M}$  (Fig. 6B).

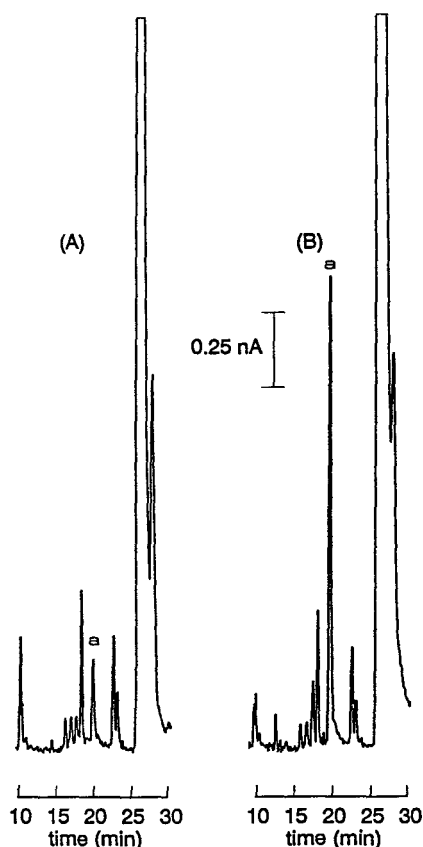


Fig. 6. Electropherograms of a urine sample (A) diluted with formate buffer and (B) treated with DTT. Total dilution factor 4. Peak (a): cysteine. Conditions as in Fig. 4.

## References

- [1] C.A. Monnig and R.T. Kennedy, *Anal. Chem.*, 66 (1994) 280R.
- [2] K.D. Altria, *J. Chromatogr.*, 646 (1993) 245.
- [3] X. Huang, R.N. Zare, S. Sloss and A.G. Ewing, *Anal. Chem.*, 63 (1991) 189.
- [4] S. Sloss and A.G. Ewing, *Anal. Chem.*, 65 (1993) 577.
- [5] L.A. Colón, R. Dadoo and R.N. Zare, *Anal. Chem.*, 65 (1993) 476.
- [6] W. Lu and R.M. Cassidy, *Anal. Chem.*, 65 (1993) 2878.
- [7] J. Ye and R.P. Baldwin, *Anal. Chem.*, 65 (1993) 3525.
- [8] R.A. Wallingford and A.G. Ewing, *Anal. Chem.*, 59 (1987) 1762.
- [9] Y.F. Yik, H.K. Lee, S.F.Y. Li and S.B. Khoo, *J. Chromatogr.*, 585 (1991) 139.
- [10] C.W. Whang and I.C. Chen, *Anal. Chem.*, 64 (1992) 2461.
- [11] I.C. Chen and C.W. Whang, *J. Chromatogr.*, 644 (1993) 208.
- [12] T.J. O'Shea, R.D. Greenhagen, S.M. Lunte, C.E. Lunte, M.R. Smyth, D.M. Radzik and N. Watanabe, *J. Chromatogr.*, 593 (1992) 305.
- [13] T.J. O'Shea, S.M. Lunte and W.R. LaCourse, *Anal. Chem.*, 65 (1993) 948.
- [14] W.Th. Kok, *Anal. Chem.*, 65 (1993) 1853.
- [15] W.Th. Kok and Y. Sahin, *Anal. Chem.*, 65 (1993) 2497.
- [16] X. Huang and W.Th. Kok, *J. Chromatogr. A*, 707 (1995) 335.
- [17] A. Russo, in D. Glick (Editor), *Methods of Biochemical Analysis*, Vol. 33, Wiley, New York, 1988, p. 165.
- [18] D. Perrett and S.R. Rudge, *J. Pharm. Biomed. Anal.*, 3 (1985) 3.
- [19] R. Saetre and D.L. Rabenstein, *Anal. Biochem.*, 90 (1978) 684.
- [20] X. Huang and W.Th. Kok, *J. Liq. Chromatogr.*, 14 (1991) 2207.
- [21] I. Mefford and R.N. Adams, *Life Sci.*, 23 (1978) 1167.
- [22] K.M. Korfhage, K. Ravichandran and R.P. Baldwin, *Anal. Chem.*, 56 (1984) 1514.
- [23] X. Huang and W.Th. Kok, *Anal. Chim. Acta*, 273 (1993) 245.
- [24] B. Lin Ling, W.R.G. Baeyens and C. Dewaele, *J. High. Res. Chromatogr.*, 14 (1991) 169.
- [25] J.S. Stamler and J. Loscalzo, *Anal. Chem.*, 64 (1992) 779.
- [26] M. Castagnola, D.D. Pierro, R. Scatena, B. Tavazzi, G. Nocca, D.V. Rossetti and B. Giardina, *Biomed. Chromatogr.*, 7 (1993) 220.
- [27] M. Cappiello, A.D. Corso, M. Camici and U. Mura, *J. Biochem. Biophys. Methods*, 26 (1993) 335.
- [28] E. Jellum, A.K. Thorsrud and E. Time, *J. Chromatogr.*, 559 (1991) 455.
- [29] T.J. O'Shea and S.M. Lunte, *Anal. Chem.*, 65 (1993) 247.
- [30] T.J. O'Shea and S.M. Lunte, *Anal. Chem.*, 66 (1994) 307.
- [31] X. Huang, J.J. Pot and W.Th. Kok, *Anal. Chim. Acta*, 300 (1995) 5.
- [32] IUPAC, *Ionization Constants of Organic Acids in Aqueous Solution*, Pergamon Press, Oxford, UK, 1979.
- [33] The Merck Index, 10th ed., M. Windholz (Editor), Merck and Co., Inc., NJ, USA, 1983.
- [34] M.P. Brigham, W.H. Stein and S. Moore, *J. Clin. Invest.*, 39 (1960) 1633.
- [35] U. Hannestad and B. Sörbo, *Clin. Chim. Acta*, 95 (1979) 189.





ELSEVIER

Journal of Chromatography A, 716 (1995) 355–362

JOURNAL OF  
CHROMATOGRAPHY A

## Inhibition of dipeptidyl peptidase IV (DP IV) by anti-DP IV antibodies and non-substrate X-X-Pro- oligopeptides ascertained by capillary electrophoresis

Torsten Hoffmann<sup>a</sup>, Dirk Reinhold<sup>a,\*</sup>, Thilo Kähne<sup>a</sup>, Jürgen Faust<sup>b</sup>,  
Klaus Neubert<sup>b</sup>, Rainer Frank<sup>c</sup>, Siegfried Ansorge<sup>a</sup>

<sup>a</sup>Center of Internal Medicine, Division of Experimental Internal Medicine, Otto-von-Guericke University Magdeburg, Leipziger Str. 44, D-39120 Magdeburg, Germany

<sup>b</sup>Department of Biochemistry/Biotechnology, Institute of Biochemistry, Martin-Luther University Halle-Wittenberg, Weinbergweg 16a, 06120 Halle, Germany

<sup>c</sup>Zentrum für Molekulare Biologie, University of Heidelberg, Heidelberg, Germany

### Abstract

Dipeptidyl peptidase IV (DP IV)-catalyzed hydrolysis of the NH<sub>2</sub>-X-Pro-containing N-terminal dodecapeptide of IL-2 was studied using free zone capillary electrophoresis as an alternative peptidase assay. In contrast to the conventional DP IV substrate glycyl-prolyl-*p*-nitroanilide (Gly-Pro-pNA), the hydrolysis of this peptide by DP IV was found to be significantly inhibited by anti-DP IV antibodies. Inhibition of DP IV was also observed with a number of non-substrate oligopeptides containing an N-terminal X-X-Pro- structure, including the HIV Tat protein. For Met-IL-2(1–6), we determined a competitive inhibition with an inhibition constant of ca. 100 μM.

### 1. Introduction

Dipeptidyl peptidase IV (DP IV, CD26, E.C. 3.4.14.5) is an exopeptidase localized on the surface of leukocytes. DP IV cleaves dipeptides with an X-Pro or X-Ala dipeptide sequence from the N-terminal part of peptides. Peptides containing proline or hydroxyproline in P1'-position will not be hydrolyzed by this enzyme [1].

Our data and that of other groups indicate that this membrane-bound exopeptidase is involved in the regulation of lymphocyte activation and immune response [2–15]. Most of these results were obtained from investigations with synthetic inhibitors, the microbial diprotins or anti-DP IV

antibodies. A number of peptides originating from the neuroendocrine system (e.g. substance P, β-casomorphin, neuropeptide Y, peptide YY, growth hormone releasing factor) were shown to be substrates of DP IV [16–21]. Callebaut et al. [22] reported that DP IV is involved in the HIV infection of T cells by functioning as a coreceptor molecule for the virus. It is postulated that HIV binds via the V3-loop of the gp120 molecule to DP IV. Furthermore, the HIV Tat protein is known to be an inhibitor of DP IV [23]. However, in the immune system, the physiological substrates or effectors of this enzyme are unknown, so far.

Recently, using capillary free zone electrophoresis, we showed that DP IV, alone or in combination with the aminopeptidase N, is ca-

\* Corresponding author.

pable of hydrolyzing oligopeptides analogous to the N-terminal structure of different cytokines (IL-1 $\beta$ , IL-2, IL-6, TNF- $\beta$ ). The hydrolysis rates of these oligopeptides were affected by their chain length and glycosylation [24,25]. However, intact cytokines were apparently no substrates of these exopeptidases.

Applying capillary electrophoresis, we searched for peptides and antibodies capable of influencing the DP IV-catalyzed oligopeptide hydrolysis. We studied the effects of one polyclonal and different monoclonal anti-DP IV antibodies on DP IV-catalyzed hydrolysis of IL-2(1–12), in comparison with the cleavage of the low-molecular-mass DP IV substrate Gly-Pro-pNA. Whereas Gly-Pro-pNA hydrolysis was not influenced by any of these antibodies, the hydrolysis of the oligopeptide was inhibited by two of the six investigated antibodies in a dose-dependent manner.

Moreover, we show that HIV gp120 as well as different synthetic peptides analogous to the V3-loop of gp120 have no inhibitory effects on DP IV-catalyzed hydrolysis of oligopeptides, whereas the HIV Tat protein and a number of non-substrate peptides with similar N-terminal X-X-Pro- sequences significantly inhibit the cleavage of oligopeptides as well as the degradation of Gly-Pro-pNA by DP IV in a competitive manner.

## 2. Experimental

### 2.1. Chemicals

Dipeptidyl peptidase IV (porcine kidney) was kindly provided by Dr. U. Demuth (Department of Biochemistry/Biotechnology, University Halle-Wittenberg).

The monoclonal anti-DP IV antibodies EF5/A3, PEG2/C3, EF6/B10, PEG2/G11, and EF6/F11 were produced in our laboratory using CD26<sup>+</sup> U937 cells for immunization. For production of the polyclonal goat-anti-DP IV antibody purified DP IV from pig kidney was used for immunization.

IL-2(1–12), Met-IL-2(1–6), and Met-IL-2(1–

12) were synthesized by solid-phase peptide synthesis with Fmoc technique using the peptide synthesizer 431A (Applied Biosystems). The HIV Tat protein was synthesized on polyoxyethylene–polystyrene graft resin in a continuous-flow instrument constructed and operated as described by Frank and Gausepohl [26]. Peptide chain assembly was performed using Fmoc chemistry [27] and in situ activation of amino acid building blocks by PyBOP [28]. The synthesized peptides were purified by reversed-phase HPLC and characterized by mass spectrometry.

Gp120 and its subpeptides HBX-2, NY/5, and V3-loop(313–320) were purchased from ABT (London, UK). Peptide YY(3–36), gastrin releasing factor(17–24), tuftsin, substance P(2–11), Met-Lys-Bradykinin and the tetrapeptides GGPA and AAPA as well as the Gly-Pro-pNA were obtained from Bachem (Heidelberg, Germany).

For enzymatic assays all compounds were diluted in a 0.01 M sodium phosphate buffer pH 7.4.

### 2.2. DP IV-catalyzed hydrolysis of oligopeptides

Influences of peptides or antibodies on DP IV-catalyzed oligopeptide hydrolysis were tested using IL-2(1–12) as substrate. A 2- $\mu$ l aliquot of peptide solution or buffer, respectively, was added to 0.5  $\mu$ l of DP IV (550 pkat/ml). The enzymatic reaction was started by addition of 2  $\mu$ l of a 1 mM substrate stock solution. Final concentration of substrate was 400  $\mu$ M. Samples were incubated for 30 min at 37°C. Thereafter the reaction was stopped by addition of 2  $\mu$ l of 0.03 M phosphoric acid containing 500  $\mu$ M histidine as an internal standard for capillary electrophoresis.

### 2.3. Capillary electrophoresis

Degradation of the IL-2(1–12) was measured by capillary free zone electrophoresis using the Biofocus 3000 system of Bio-Rad. Separations were performed under following conditions: capillary, 24 cm total length, 20 cm effective



length, 25  $\mu\text{m}$  I.D., 125  $\mu\text{m}$  O.D., coated (Bio-Rad, Munich, Germany); injection, pressure 1.03 MPa s; run, 14 kV constant voltage, positive to negative, 0.1 M sodium phosphate buffer pH 2.5 with linear polymer (Bio-Rad, Munich, Germany), current in the range of 20  $\mu\text{A}$ ; detection, UV 200 nm; capillary temperature, 15°C; carousel temperature, 10°C.

#### 2.4. Hydrolysis of Gly-Pro-pNA

DP IV-catalyzed hydrolysis of Gly-Pro-pNA was measured photometrically using the Cary 1 spectrophotometer (Varian, Darmstadt, Germany). DP IV-activity was determined by measurement of the rate of *p*-nitroaniline generation monitored at 392 nm.

#### 2.5. Determination of inhibition type and inhibitory constant

For the heptapeptide Met-IL-2(1–6), inhibition type and inhibitory constant ( $K_i$ ) were determined using Gly-Pro-pNA as substrate. We measured the rate of Gly-Pro-pNA cleavage at four substrate concentrations in the range of 20 to 200  $\mu\text{M}$  using inhibitor concentrations in the range of 5 to 400  $\mu\text{M}$ . Inhibition type and  $K_i$  were calculated with the help of a Dixon plot.

### 3. Results

DP IV-catalyzed peptide hydrolysis can be measured by the classical method using chromogenic substrates (e.g. Gly-Pro-pNA) or by studying the degradation of oligopeptides containing an N-terminal X-Pro- sequence. In comparison to the spectrophotometrical measurement of DP IV activity, capillary electrophoresis provides the opportunity of investigating potential physiological peptide substrates of different origin. In Fig. 1 the electrophoretical detection of IL-2(1–12) degradation by DP IV is shown (A and B). Effects of a non-inhibitory (C) and an inhibitory peptide (D) on this hydrolysis are also demonstrated.

#### 3.1. Inhibition of DP IV-catalyzed hydrolysis of oligopeptides by antibodies

The influence of the monoclonal anti-DP IV antibodies EF5/A3, PEG2/C3, EF6/B10, PEG2/G11, and EF6/F11 and a polyclonal goat-anti-DP IV antibody was studied by means of the DP IV-catalyzed hydrolysis of oligopeptides as well as the hydrolysis of the Gly-Pro-pNA. We found that hydrolysis of oligopeptides is inhibited by the polyclonal antibody and by the monoclonal PEG2/G11 in a dose-dependent manner (Fig. 2). In contrast to this, all investigated antibodies were not capable of inhibiting the hydrolysis of the low-molecular-mass substrate Gly-Pro-pNA. The observed increase of the Gly-Pro-pNA hydrolysis rate by antibodies seems to be nonspecific because addition of irrelevant mouse immunoglobulin or serum bovine albumin had similar effects (Fig. 2).

#### 3.2. Inhibition of DP IV activity by non-substrate peptides

Starting from the hypothesis of Callebaut et al. [22] that DP IV is a coreceptor of the HIV-virus, we looked for inhibitory effects of the gp120 and some V3-loop peptides on the DP IV-catalyzed oligopeptide hydrolysis. Under the conditions used, we could not find any significant effects of one of the tested gp120 peptides on this enzymatic activity (Table 1, Fig. 3). On the other hand, the DP IV-catalyzed oligopeptide hydrolysis was inhibited by the HIV Tat protein. This is in accordance with the results of Gutheil et al. [23] who found an inhibition of Ala-Pro-pNA hydrolysis by the Tat protein. Based on this result, we studied the effects of other peptides which have similar N-terminal structures, i.e. proline in the third position (Table 1). Tetrapeptides with the structures GGPA, AAPA, and TKPR were found to have no inhibitory effects. In contrast longer peptides were shown to exhibit significant inhibition (Table 1, Fig. 3). The highest inhibition was measured with the Tat protein. Hydrolysis of the inhibitory peptides themselves could be excluded by capillary electrophoresis. All peptides with an X-X-Pro se-

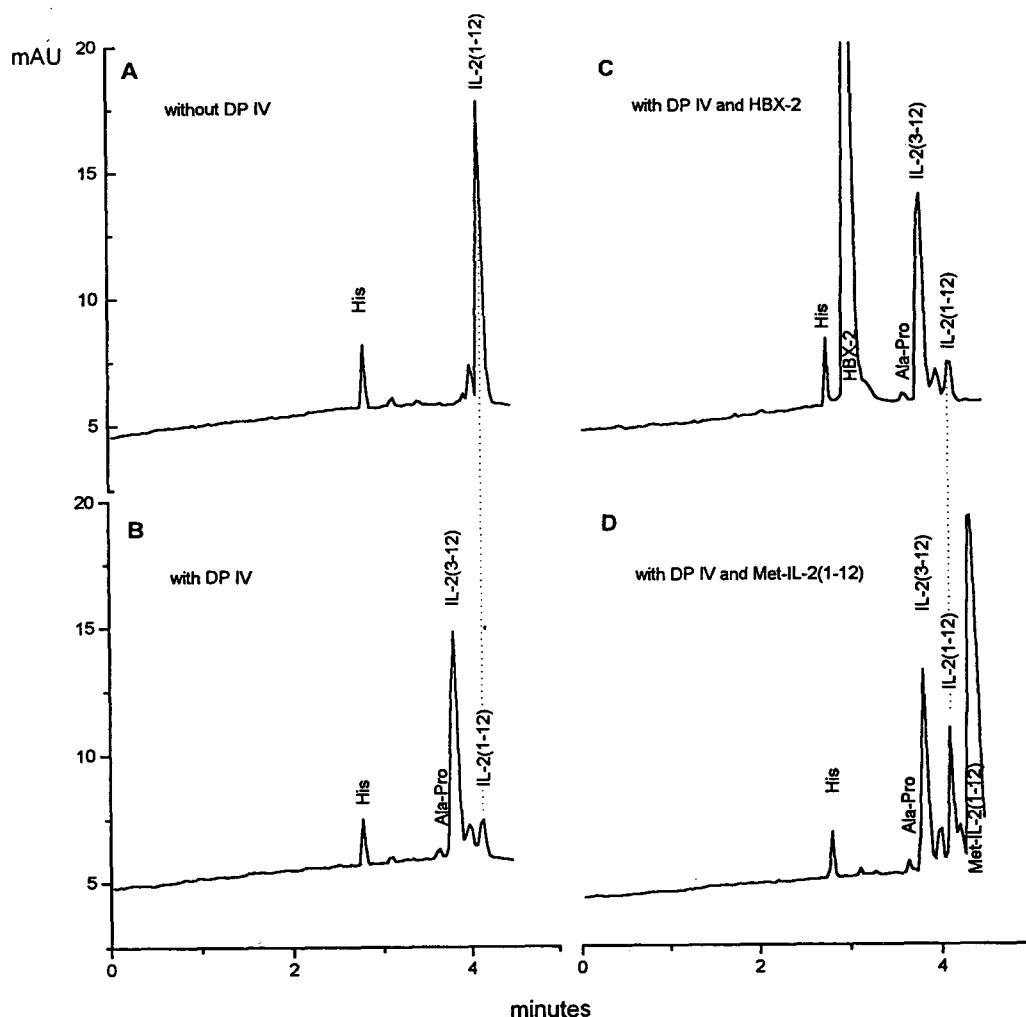


Fig. 1. Detection of DP IV-catalyzed hydrolysis of IL-2(1–12) by capillary electrophoresis. Electropherograms show IL-2(1–12) and its cleavage products after 30 min of incubation at 37°C without DP IV (A), with DP IV alone (B), with DP IV and the non-inhibitory peptide HBX-2 (C), and with DP IV and the inhibitory peptide Met-IL-2(1–12) (D). Concentrations of the substrate and the additional peptides were 400  $\mu$ M and of DP IV 60 pkat/ml. Histidine was used as an internal standard.

quence were resistant against treatment by DP IV for several hours. Thus, the inhibitory effect of the X-X-Pro- peptides cannot be explained by competitive cleavage of these peptides.

### 3.3. Determination of inhibitor type and inhibition constant

The kinetic characterization of the inhibition of DP IV by Met-IL-2(1–6) was studied in more detail using Gly-Pro-pNA as substrate. The point

of intersection in the second quadrant of the Dixon plot indicates that DP IV is inhibited competitively by this X-X-Pro- peptide. The  $x$ -value of the intersection represents the negative inhibition constant, which is ca. 100  $\mu$ M.

## 4. Discussion

DP IV is an exopeptidase localized on the surface of lymphocytes. This molecule plays an

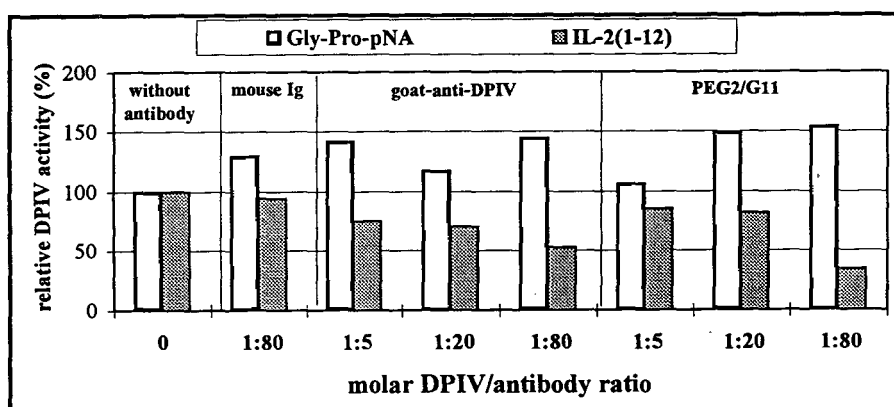


Fig. 2. Comparison between the effects of antibodies (goat-anti-DP IV, PEG2/G11) on DP IV-catalyzed hydrolysis of Gly-Pro-pNA and IL-2(1-12). Investigations were done with substrate concentrations of 400  $\mu$ M. In both enzyme assays the same DP IV/antibody ratios were used. The DP IV concentrations for oligopeptide hydrolysis were 0.44  $\mu$ g/ml and for Gly-Pro-pNA cleavage 0.013  $\mu$ g/ml ( $n = 3$ )

important role in the regulation of lymphocyte activation and immune response. Investigations with synthetic inhibitors showed that the enzymatic activity of DP IV is involved in these processes [2,4,7,9,29]. A number of antibodies (e.g. Ta1, 1F7) with different, in part contrary, effects on the activation of lymphocytes were designed [5,7,30–36]. None of the antibodies studied so far was found to have inhibitory

effects on the enzymatic activity of DP IV. Using capillary electrophoresis to measure DP IV-catalyzed oligopeptide hydrolysis, we found that two of the six antibodies investigated in this study are capable of inhibiting DP IV activity. The differences in the effects of antibodies on DP IV-catalyzed hydrolysis of oligopeptides could be explained by different epitope specificity. Interestingly, hydrolysis of the low-molecular-mass

Table 1  
Sequence and length of oligopeptides investigated for their inhibitory effects to DP IV-catalyzed oligopeptide hydrolysis

	Peptide	N-Terminal structure	Number of amino acids	Inhibition of DP IV activity <sup>a</sup>
HIV gp120 peptides	V3-loop(313–320)	RIQRGPR	7	–
	NY/5	CNTKKGIAIGPG...	20	–
	HBX2	CNTRKRIRIQRGPG...	22	–
	gp120	TEKLWVTVYYGV...	477	–
X-X-Pro-peptides	GGPA	GGPA	4	–
	AAPA	AAPA	4	–
	Tuftsia	TKPR	4	–
	Met-IL-2(1–6)	MAPTSSS	7	++
	Substance P(2–11)	PKPQQFFGLM	10	+
	Met-IL-2(1–12)	MAPTSSSTK...	13	++
	GRF(17–24)	MYPRGNHW...	14	++
	Peptide YY(3–36)	IKPEAPGEDA...	34	++
	Tat protein	MDPVDPNIEP...	86	+++
	Met-Lys-Bradykinin	MKRPPGFSPFR	11	–

<sup>a</sup> – = no inhibition; + = weak inhibition; ++ = medium inhibition; +++ = strong inhibition.

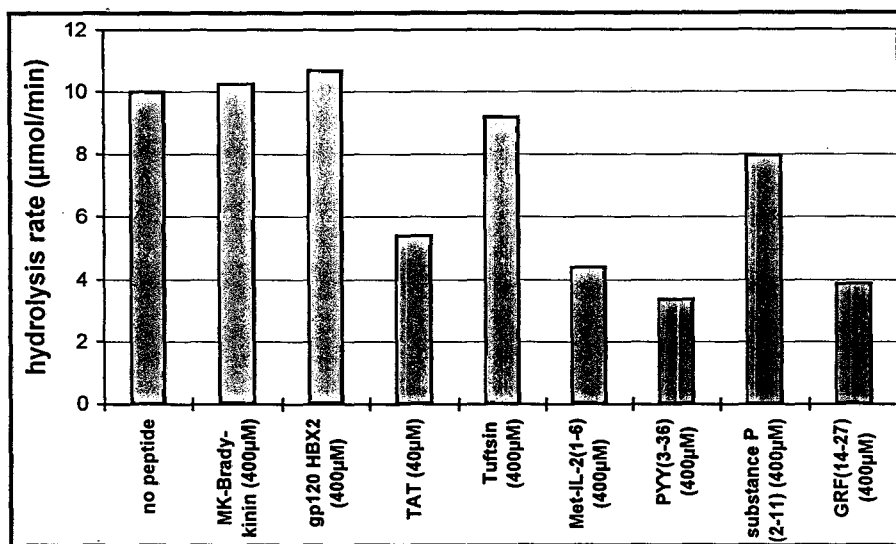


Fig. 3. Effects of different non-substrate peptides on DP IV-catalyzed hydrolysis of IL-2(1–12). DP IV-catalyzed hydrolysis of IL-2(1–12) was determined as described in the Experimental section. Met-Lys-Bradykinin was used as a negative control for peptide effects. All peptides with exception of the Tat protein were used in a concentration of 400  $\mu\text{M}$ . The concentration of the Tat protein was 40  $\mu\text{M}$  ( $n = 3$ )

Gly-Pro-pNA was not affected by one of these antibodies. This suggests that the inhibitory antibodies, goat-anti-DP IV and PEG2/G11, bind near the active site of the DP IV, resulting in a steric hindrance of the binding of longer peptides. An other explanation for the reduced accessibility of the active center could be a

conformational change of the DP IV molecule as a consequence of antibody binding. These results clearly demonstrate that the use of small DP IV substrates such as Gly-Pro-pNA is of limited value, and alternative approaches using oligopeptides as substrates and suitable detection techniques, e.g. capillary electrophoresis, are necessary for the study of the physiological role of DP IV and other peptidases.

Adenosine deaminase [37], HIV gp120 [22], and HIV Tat protein [23] are known as natural effectors of DP IV. Using the method described here, we could show that gp120 as well as some V3-loop peptides do not effect the DP IV activity *in vitro*. However, the Tat protein was found to show a strong inhibition of the DP IV-catalyzed hydrolysis of oligopeptides. Moreover a number of non-substrate peptides characterized by an N-terminal X-X-Pro- sequence, were also found to be capable of inhibiting DP IV activity. From the competitive type of inhibition, we can conclude that these peptides may represent a new type of DP IV inhibitor which is capable of binding to the active site of this enzyme but which cannot be cleaved. The extent of inhibition of these peptides obviously depends on their

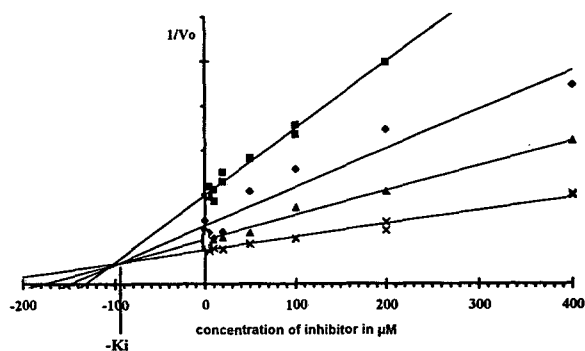


Fig. 4. Determination of inhibition type and inhibition constant of Met-IL-2(1–6) by a Dixon plot. Substrate concentrations (Gly-Pro-pNA) of 20, 50, 100, and 200  $\mu\text{M}$  were used. The DP IV activities were determined at eight concentrations of the inhibitor Met-IL-2(1–6) (up to 500  $\mu\text{M}$ ) at each substrate concentration. Measurements were done with a DP IV concentration of 13 ng/ml.

length. Smaller tetrapeptides do not show inhibitory effects, whereas the Tat protein, consisting of 86 amino acids, was the most potent inhibitor among the peptides tested. The effect of Tat is comparable with the inhibition of DP IV by diprotin A, a tripeptide with proline in the second position [38,39]. The DP IV inhibitors used so far are X-Pro dipeptide analogs where proline is replaced by the amino boronic acid of proline [29], by thiazolidide, or by pyrrolidide [9,40]. These are more potent inhibitors than the X-X-Pro- peptides investigated in this study. However, the X-X-Pro- peptides evoke our interest because a number of natural peptides contain this N-terminal structure. It is conceivable that the DP IV activity is regulated by such peptides in vivo. Also the in vivo effects of the HIV Tat protein could be based on a deregulation of DP IV-mediated growth processes. Other interesting candidates are neuropeptide Y and the peptide YY, because they are substrates of DP IV and cleavage products characterized by the N-terminal X-X-Pro- sequence might suppress the enzymatic activity of this enzyme.

### Acknowledgements

This study was supported by Deutsche Forschungsgemeinschaft, grant Re-1058/1-1, and Ministerium für Wissenschaft und Forschung des Landes Sachsen-Anhalt, grant 823 A 10313.

### Abbreviations

DP IV	Dipeptidylpeptidase IV
Gly-Pro-pNA	Glycyl-prolyl- <i>p</i> -nitroanilide
HBX-2	gp120 V3-loop peptide
HIV	Human immunodeficiency virus
IL	Interleukin
IL-2(1–12)	Synthetic N-terminal dodecapeptide of IL-2
IL-2(1–6)	Synthetic N-terminal hexapeptide of IL-2
$K_i$	Inhibition constant
NY/5	gp120 V3-loop peptide
PyBOP	Benzotriazol-1-yl-oxy-tris-

pyrrolidino-phosphonium-hexafluorophosphate

TNF- $\beta$   
U937

Tumor necrosis factor  $\beta$   
Human histiocyte cell line

### References

- [1] G. Küllertz, G. Fischer and A. Barth, Dipeptidyl-Peptidase IV–Biochemie, Physiologie und Pathobiochemie, Inst. f. Wirkstoffforschung, Berlin, 1986.
- [2] S. Ansorge, E. Schön and D. Kunz, Biomed. Biochim. Acta, 50 (1991) 799.
- [3] F. Bühling, D. Kunz, E. Schön, A.J. Ulmer, H.-D. Flad and S. Ansorge, Immunobiol., 183 (1991) 192. (Abstract)
- [4] T. Kubota, G.R. Flentke, W.W. Bachovchin and B.D. Stollar, Clin. Exp. Immunol., 89 (1992) 192.
- [5] T. Mattern, S. Ansorge, H.D. Flad and A.J. Ulmer, Immunobiol. 188 (1993) 36.
- [6] T. Mattern, W. Scholz, A.C. Feller, H.D. Flad and A.J. Ulmer, Scand. J. Immunol., 33 (1991) 737.
- [7] D. Reinhold, U. Bank, F. Buhling, K. Neubert, T. Mattern, A.J. Ulmer, H.D. Flad and S. Ansorge, Immunobiol., 188 (1993) 403.
- [8] W. Scholz, R. Mentlein, E. Heymann, A.C. Feller, A.J. Ulmer and H.-D. Flad, Cell. Immunol., 93 (1985) 199.
- [9] E. Schön, I. Born, H.U. Demuth, J. Faust, K. Neubert, T. Steinmetzer, A. Barth and S. Ansorge, Biol. Chem. Hoppe Seyler, 372 (1991) 305.
- [10] E. Schön and S. Ansorge, Biol. Chem. Hoppe Seyler, 371 (1990) 699.
- [11] E. Schön, H.U. Demuth, E. Eichmann, H.J. Horst, I.J. Korner, J. Kopp, T. Mattern, K. Neubert, F. Noll, A.J. Ulmer et al., Scand. J. Immunol., 29 (1989) 127.
- [12] E. Schön, E. Eichmann, S. Jahn, J. Kopp, H.D. Volk and S. Ansorge, Biol. Zent. bl., 107 (1988) 141.
- [13] E. Schön, S. Jahn, S.T. Kiessing, H.U. Demuth, K. Neubert, A. Barth, R. von Baehr and S. Ansorge, Eur. J. Immunol., 17 (1987) 1821.
- [14] E. Schön, E. Eichmann, R. Grunow, S. Jahn, S.T. Kiessing, H.D. Volk and S. Ansorge, Biomed. Biochim. Acta, 45 (1986) 1523.
- [15] E. Schön, H.-W. Mansfeld, H.U. Demuth, A. Barth and S. Ansorge, Biomed. Biochim. Acta, 44 (1985) K9.
- [16] J. Bongers, T. Lambros, M. Ahmad and E.P. Heimer, Biochim. Biophys. Acta, 147 (1992) 1122.
- [17] S. Ahmad, L. Wang and P.E. Ward, J. Pharmacol. Exp. Ther., 260 (1992) 1257.
- [18] L.H. Wang, S. Ahmad, I.F. Benter, A. Chow, S. Mizutani and P.E. Ward, Peptides, 12 (1991) 1357.
- [19] I. Nausch, R. Mentlein and E. Heymann, Biol. Chem. Hoppe Seyler, 371 (1990) 1113.
- [20] H. Stark, B. Lossner, H. Matthies, B. Hartrodt and I. Born, Biomed. Biochim. Acta, 47 (1988) 865.

- [21] J.R. McDermott, A.M. Gibson, J. Boublik and J.A. Biggins, *Biochem. Soc. Trans.*, 20 (1992) 351.
- [22] C. Callebaut, B. Krust, E. Jacotot and A.G. Hovanessian, *Science*, 262 (1993) 2045.
- [23] W.G. Gutheil, M. Subramanyam, G.R. Flentke, D.G. Sanford, E. Munoz, B.T. Huber and W.W. Bachovchin, *Proc. Natl. Acad. Sci. USA*, 91 (1994) 6594.
- [24] T. Hoffmann, K. Neubert and S. Ansorge, in M. Freund, H. Link, R.E. Schmidt and K. Welte (Editors), *Cytokines in Hemopoiesis, Oncology, and Immunology*, Vol. III, Springer-Verlag, Berlin Heidelberg, 1994, p. 317.
- [25] T. Hoffmann, J. Faust, K. Neubert and S. Ansorge, *FEBS Lett.*, 336 (1993) 61.
- [26] R. Frank and H. Gausepohl, in H. Tschesche (Editor), *Modern Methods in Protein Chemistry*, de Gruyter, Berlin, New York, 1988, p. 42.
- [27] L.A. Carpino and G.Y. Han, *J. Org. Chem.*, 37 (1972) 3404.
- [28] J. Coste, D. Le-Nguyen and B. Castro, *Tetrahedron Lett.*, 31 (1990) 205.
- [29] G.R. Flentke, E. Munoz, B.T. Huber, A.G. Plaut, C.A. Kettner and W.W. Bachovchin, *Proc. Natl. Acad. Sci. USA*, 88 (1991) 1556.
- [30] C. Morimoto, Y. Torimoto, G. Levinson, C.E. Rudd, M. Schrieber, N.H. Dang, N.L. Letvin and S.F. Schlossman, *J. Immunol.*, 143 (1989) 3430.
- [31] Y. Matsumoto, G.A. Bishop and G.W. McCaughan, *Hepatology*, 15 (1992) 1048.
- [32] Y. Torimoto, N.H. Dang, T. Tanaka, C. Prado, S.F. Schlossman and C. Morimoto, *Mol. Immunol.*, 29 (1992) 183.
- [33] J.L. Bednarczyk, S.M. Carroll, C. Marin and B.W. McIntyre, *J. Cell. Biochem.*, 46 (1991) 206.
- [34] S. Hartel Schenk, N. Loch, M. Zimmermann and W. Reutter, *Eur. J. Biochem.*, 196 (1991) 349.
- [35] M. Hegen, G. Niedobitek, C.E. Klein, H. Stein and B. Fleischer, *J. Immunol.*, 144 (1990) 2908.
- [36] A.J. Ulmer, T. Mattern, A.C. Feller, E. Heymann and H.D. Flad, *Scand. J. Immunol.*, 31 (1990) 429.
- [37] J. Kameoka, T. Tanaka, Y. Nojima, S.F. Schlossman and C. Morimoto, *Science*, 261 (1993) 466.
- [38] J. Rahfeld, M. Schierhorn, B. Hartrodt, K. Neubert and J. Heins, *Biochim. Biophys. Acta*, 1076 (1991) 314.
- [39] H. Umezawa, T. Aoyagi, K. Ogawa, H. Naganawa, M. Hamada and T. Takeuchi, *J. Antibiot.*, 37 (1984) 422.
- [40] H.U. Demuth, R. Baumgrass, C. Schaper, G. Fischer and A. Barth, *J. Enzym Inhib.*, 2 (1988) 129.



ELSEVIER

Journal of Chromatography A, 716 (1995) 363–369

JOURNAL OF  
CHROMATOGRAPHY A

# Studies of complexes between proteases, substrates and the protease inhibitor $\alpha_2$ -macroglobulin using capillary electrophoresis with laser-induced fluorescence detection

Oscar-Werner Reif, Ruth Freitag\*

*Institut für Technische Chemie, Universität Hannover, Callinstr. 3, 30167 Hannover, Germany*

## Abstract

Capillary zone electrophoresis (CZE) with laser-induced fluorescence (LIF) detection is shown to constitute a unique technique for the investigation of the interaction between proteases, protease inhibitors and substrates. Under optimized analysis conditions, the formation of a complex between FITC-labelled proteases such as trypsin, plasmin,  $\alpha$ -chymotrypsin and the (unlabelled) protease inhibitor  $\alpha_2$ -macroglobulin was studied. This is not possible with UV detection, since under such conditions the complex cannot be distinguished from the unreacted protease inhibitor. Low ratios of FITC bonded to the proteases further complex formation, while high ratios often prevent the reaction. Complex formation shows a strong dependence on the incubation conditions (pH, salt concentration, temperature, incubation time). Once formed, however, the complexes are stable under CZE conditions (e.g., a pH of the electrophoresis buffer of 10.5) for at least 30 min. Treatment with sodium dodecyl sulfate (5 min at 90°C or 30 min at 75°C) does not destroy the complexes, whereas treatment with mercaptoethanol (reduction of disulfide bonds) eliminates the peak from the electropherogram. Both findings argue for the formation of a covalent bond between the protease and the inhibitor during complex formation. Since the reaction of the proteases with  $\alpha_2$ -macroglobulin does not involve the binding site of the former, a residual proteolytic activity is still observed in the ensuing complex. The extent of the inhibition of the remaining trypsin activity in a trypsin –  $\alpha_2$ -macroglobulin complex was established to depend on the molecular mass of the second trypsin inhibitor.

## 1. Introduction

Capillary electrophoresis (CE) offers a wide range of methods for the determination of peptides and proteins. High-resolution separations can be performed based on subtle differences in the physical properties of these substances, e.g., the mass-to-charge ratio, the size and the hydrophobicity. Concomitantly, CE is emerging as a tool for the investigation of biological and biochemical interactions between peptides and pro-

teins or other specific components [1–7]. Among the advantages of using capillary electrophoresis in biological binding studies are the small sample volumes, the short separation times, the high selectivity and the possibility of on-line (column) detection. Especially when laser-induced fluorescence (LIF) detection is employed, highly specific investigations of minute amounts of sample become possible even in complex matrices [8,9]. Based on previous analysis of the interaction of FITC-labelled protein G and immunoglobulins [7], in this work the complex formation between protease and protease in-

\* Corresponding author.

hibitors was studied and compared with the results achieved with traditional techniques.

## 2. Experimental

### 2.1. Capillary electrophoresis

All separations were performed on a Beckman P/ACE 2100 capillary electrophoresis system with either LIF detection (argon ion laser, excitation wavelength 488 nm, emission wavelength 560 nm) or with UV detection. Post-run data were analysed using System Gold software (Beckman) and exported to Excel 5.0 (Microsoft) for publication purposes. Details of the electrophoretic conditions are given later in the text and in the figure captions. Capillaries were supplied by CS-Chromatographie Service (Langerwehe, Germany).

### 2.2. Chemicals

$\alpha$ -2-Macroglobulin and non-labelled proteases and inhibitors were used as supplied by the manufacturer. The labelled proteins were purified by liquid chromatography (size-exclusion and affinity chromatography) prior to the binding studies.

Protein labelling with FITC was done according to the supplier's instructions. For analysis, samples were dissolved in 50 or 100 mM phosphate buffer (pH 7.4) containing 50 mM NaCl. Typically, samples were incubated at 30°C for the indicated given period of time.

All chemicals were obtained from Sigma (Deisenhofen, Germany).

## 3. Results and discussion

$\alpha$ -2-Macroglobulin is one of the major protease inhibitors found in the blood. It accounts for ca. 10% of the total trypsin-inhibiting capacity and constitutes between 3% and 4% of the total protein content of plasma. With a relative molecular mass of 725 000,  $\alpha$ -2-macroglobulin is by far the largest of all known

protease inhibitors. The molecule consists of four identical subunits. Among the unique properties of the molecule is an unusual thioester bond in its structure. Rather than having one specific physiological function,  $\alpha$ -2-macroglobulin appears to be able to inhibit most known proteases. The inhibitor is consequently involved in modulating protease activity in a great variety of proteins and peptides in a manner unrelated to the protease-binding mechanism.

### 3.1. Complex formation between $\alpha$ -2-macroglobulin and FITC-labelled trypsin

When a mixture of  $\alpha$ -2-macroglobulin and FITC-labelled trypsin is subjected to CE analysis without prior incubation, two signals are detected by the UV detector (Fig. 1A), while the LIF detector shows only one signal, the FITC-trypsin peak (Fig. 1B). After 5 min of incubation of the  $\alpha$ -2-macroglobulin–FITC-trypsin mixture, a second peak appears in the electropherograms when LIF detection is used (Fig. 1C). Its height and area increase with increasing incubation time (Fig. 1D and E). This peak is the result of the formation of an affinity complex between the FITC-labelled protease and the protease inhibitor  $\alpha$ -2-macroglobulin. The control, i.e., an electrophoresis of FITC-labelled trypsin without  $\alpha$ -2-macroglobulin, shows no peak at this point (1.7 min) in the electropherogram, even after a 60-min incubation, thus confirming the signal to be the result of the formation of the affinity complex (Fig. 1F).

Irrespective of the incubation time, only two signals are found in the electropherograms recorded by the UV detector. As  $\alpha$ -2-macroglobulin is considerably larger than FITC-labelled trypsin, its mass-to-charge ratio tends to dominate the electrophoretic properties of the complexes. As a consequence, the migration time of the complexes will be similar to that of the unreacted  $\alpha$ -2-macroglobulin itself (see, e.g., Fig. 1A and E). Hence no differentiation between the complex and the unreacted  $\alpha$ -2-macroglobulin is possible by UV detection, whereas such a differentiation is easily achieved by LIF detection.

On the basis of concentration vs. peak height/



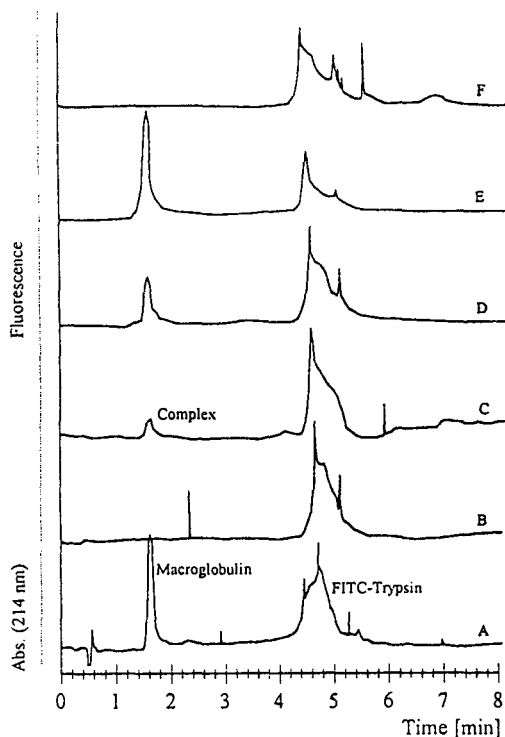


Fig. 1. Complex formation between  $\alpha_2$ -macroglobulin and FITC-labelled trypsin. Capillary, 27 cm  $\times$  50  $\mu$ m I.D.; buffer, 50 mM borate (pH 10.5); applied voltage, 12 kV; injection, 2 s; pressure, 50 mbar. (A)  $\alpha_2$ -Macroglobulin and FITC-labelled trypsin with UV detection (214 nm); (B) FITC-labelled trypsin and the  $\alpha_2$ -macroglobulin with LIF detection; (C) complex formation between FITC-labelled trypsin and  $\alpha_2$ -macroglobulin after an incubation time of 5 min with LIF detection; (D) complex formation between FITC-labelled trypsin and  $\alpha_2$ -macroglobulin after an incubation time of 30 min with LIF detection; (E) complex formation between FITC-labelled trypsin and  $\alpha_2$ -macroglobulin after an incubation time of 60 min with LIF detection; (F) FITC-labelled trypsin as a control after an incubation time of 60 min with LIF detection.

area calibration runs for the two fluorescence signals, it can be deduced that the ratio of  $\alpha_2$ -macroglobulin to trypsin in the affinity complex amounts to approximately two protease molecules per molecule of inhibitor. This corresponds to results achieved with conventional methods [10], while the finding that  $\alpha_2$ -macroglobulin is capable of binding up to six trypsin molecules [11] cannot be confirmed.

The investigation of the influence of the incu-

bation time showed that the reaction has reached equilibrium after ca. 60 min, since no further increase in the height and the area of the complex signal is observed for longer incubation times. An investigation of the influence of the pH of the incubation buffer and temperature on the complex formation showed that an increase in pH from 7 to 9 increases the rate of complex formation, and the optimum incubation temperature is ca. 30°C. As the mechanism of the protease inhibition by  $\alpha_2$ -macroglobulin is not yet fully understood and the experimental conditions suggested here have still to be further optimized, these results were not quantified and the binding constants were not calculated.

Once formed, the complexes appear to be unusually stable. Other than, e.g., the immunocomplexes investigated previously [7], the protease-inhibitor complex stability seems to be independent of the CE separation conditions. Even under the harsh conditions employed, i.e., using an electrophoresis buffer of pH 10.5 and prolonging the separation times by utilizing increasingly longer capillaries, did not influence the separation performance or reduce the total amount of the complexes detected in this case (Fig. 2A–C).

The high stability of the affinity complex is mainly the result of the unique protease-binding mechanism of  $\alpha_2$ -macroglobulin. A protease being inhibited by the  $\alpha_2$ -macroglobulin is "trapped" by one of the two "bait regions" which are found approximately in the middle of the subunit chain of the inhibitor. On proteolytic cleavage of a single bond in each subunit,  $\alpha_2$ -macroglobulin undergoes a conformational change to a more compact structure, leading to virtually irreversible binding of the respective protease. The active site of the protease, however, need not be involved in this reaction [12]. Although the exact nature of this mechanism is still under investigation, our results, i.e., the high stability of the complex over a prolonged period of time even at a high buffer pH, are in favour of the theory of entrapment of the protease by a conformational change of the inhibitor.

In addition to this reaction, another stabilizing

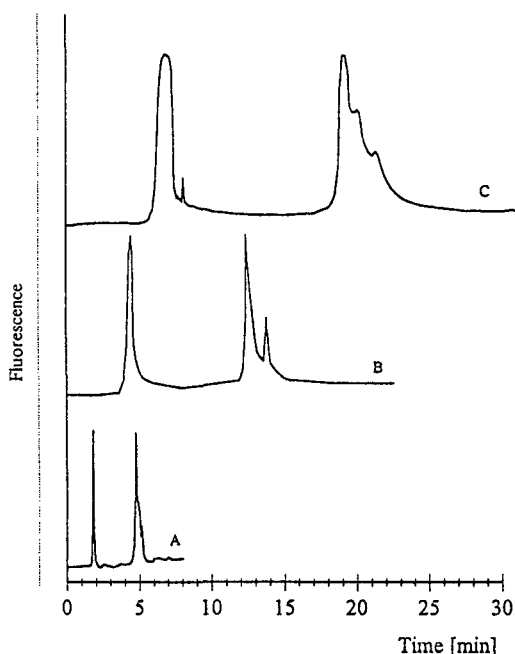


Fig. 2. Stability of the  $\alpha_2$ -macroglobulin-FITC-trypsin complex with regard to the separation time. (A) Capillary, 27 cm  $\times$  50  $\mu$ m I.D.; buffer, 50 mM borate (pH 10.5); applied voltage, 12 kV; injection, 2 s; pressure, 50 mbar; LIF detection. (B) Capillary, 47 cm  $\times$  50  $\mu$ m I.D.; buffer, 50 mM borate (pH 10.5); applied voltage, 12 kV; injection, 2 s; pressure, 50 mbar; LIF detection. (C) Capillary, 67 cm  $\times$  50  $\mu$ m I.D.; buffer, 50 mM borate (pH 10.5); applied voltage, 15 kV; injection, 2 s; pressure, 50 mbar; LIF detection.

mechanism has been recognized for protease- $\alpha_2$ -macroglobulin complexes [13]. On protease binding, the thioester bond, located roughly about two thirds of the distance from the  $\text{NH}_2$ -terminal end of the subunit chain, may break and the acyl group thus made available can form a covalent bond with any accessible primary amino group on the surface of the protease in question.

CE may once more serve to investigate the probability of this reaction. If an already formed complex (60-min incubation) is treated with sodium dodecyl sulfate (SDS) and heated for 5 min at 90°C (Fig. 3C) or for 30 min at 75°C (Fig.

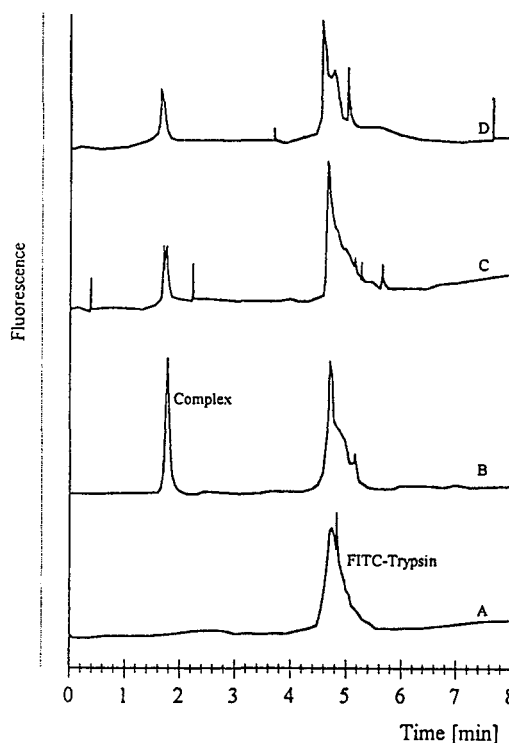


Fig. 3. Stability of the  $\alpha_2$ -macroglobulin-FITC-trypsin complex with regard to covalent linkage between the proteins. Capillary, 27 cm  $\times$  50  $\mu$ m I.D.; buffer, 50 mM borate (pH 10.5); applied voltage, 12 kV; injection, 2 s; pressure, 50 mbar; LIF detection. (A) FITC-labelled trypsin as a control after an incubation time of 60 min; (B) complex formation between FITC-labelled trypsin and  $\alpha_2$ -macroglobulin with LIF detection after an incubation time of 60 min; (C) complex stability between FITC-labelled trypsin and  $\alpha_2$ -macroglobulin with LIF detection after an incubation time of 60 min and heating for 5 min at 90°C in the presence of 50 mM SDS; (D) complex stability between FITC-labelled trypsin and  $\alpha_2$ -macroglobulin with LIF detection after an incubation time of 60 min and heating for 30 min at 75°C in the presence of 50 mM SDS.

3D), the affinity complex peak is still present in the electropherogram recorded afterwards, albeit at a lower concentration than without this treatment (Fig. 3B). This may be regarded an obvious indication for the stability of the complex. A further proof of this mechanism is given by the fact that the reduction of the disulfide bonds by mercaptoethanol in the presence of SDS eliminates the  $\alpha_2$ -macroglobulin-complex peak,

whereas the FITC-trypsin signal concomitantly increases.

### 3.2. Complex formation between $\alpha_2$ -macroglobulin and other FITC-labelled proteases

A drawback in the application of CE using LIF detection is the necessity to use a labelling agent such as FITC. A high ratio of molecules of the labelling substance per molecule of protease results in the lowest possible detection limit. Concomitantly, labelling may strongly influence the biochemical and biophysical behavior of a protein, including its affinity for the protease inhibitor.

The impact of FITC labelling was demonstrated by CE analysis using several proteases with different ratios of bound FITC per protease molecule under the above-defined reaction conditions.  $\alpha$ -Chymotrypsin with 4–7 molecules of FITC does not form complexes with  $\alpha_2$ -macroglobulin (Fig. 4A), whereas the same protease labelled with only 1–3 molecules of FITC per molecule shows a considerable affinity to the inhibitor (Fig. 4B). The same effect of FITC-labelling can be observed for the complex formation between plasmin and  $\alpha_2$ -macroglobulin (Fig. 4C and D). In this case labelling the plasmin with one or two molecules of FITC still allows complex formation, while three or more molecules of FITC prevent the reaction.

The observation that the effect of low FITC ratios on the affinity interaction is negligible, whereas a higher degree of FITC labelling causes considerable interference, may be interpreted in terms of steric hindrance in the “bait region” caused by the FITC. An effect of a putative blocking of the active site of the protease appears to be less likely, since the complex formation between protease and  $\alpha_2$ -macroglobulin would be influenced independently of the particular FITC-to-protease ratio in this case. Nevertheless, all results of binding studies performed by CE with LIF detection should be considered with respect to the possible influence of the FITC and thus be interpreted carefully.

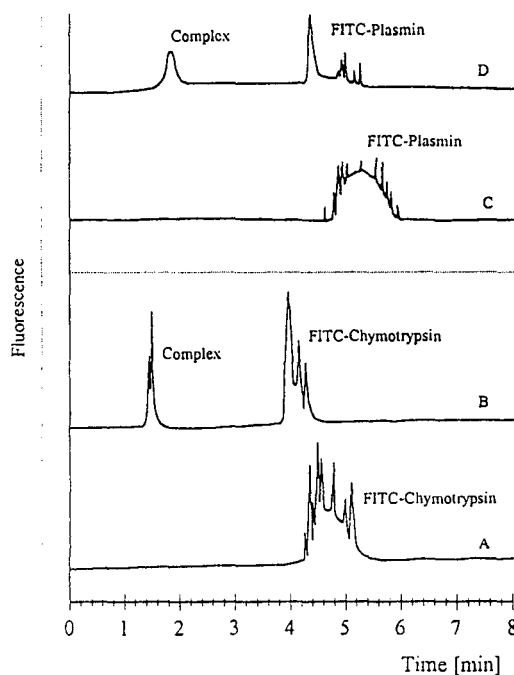


Fig. 4. Analysis of the  $\alpha_2$ -macroglobulin–FITC-plasmin and  $\alpha_2$ -macroglobulin–FITC- $\alpha$ -chymotrypsin complex formation with regard to the extent of FITC labelling. Capillary, 27 cm  $\times$  50  $\mu$ m I.D., buffer, 50 mM borate (pH 10.5); applied voltage, 12 kV; injection, 2 s; pressure, 50 mbar; LIF detection. (A) Complex formation between FITC-labelled  $\alpha$ -chymotrypsin (4–7 mol of FITC per mole of protein) and  $\alpha_2$ -macroglobulin with LIF detection after an incubation time of 30 min; (B) complex formation between FITC-labelled  $\alpha$ -chymotrypsin (1–3 mol of FITC per mole of protein) and  $\alpha_2$ -macroglobulin with LIF detection after an incubation time of 30 min; (C) complex formation between FITC-labelled plasmin (3–8 mol of FITC per mole of protein) and  $\alpha_2$ -macroglobulin with LIF detection after an incubation time of 30 min; (D) complex formation between FITC-labelled plasmin (1–2 mol of FITC per mole of protein) and  $\alpha_2$ -macroglobulin with LIF detection after an incubation time of 30 min.

### 3.3. Complex formation between $\alpha_2$ -macroglobulin-entrapped trypsin and a second trypsin inhibitor

As the entrapment of a protease by  $\alpha_2$ -macroglobulin does not necessarily involve the active site of the protease, an investigation of the residual protease activity (substrate or second

inhibitor) by CE is still possible. The protease aprotinin ( $M_r$  6500) is, e.g., capable of reacting with an already bound and inhibited trypsin in the  $\alpha_2$ -macroglobulin–protease complex. In Fig. 5A the separation of  $\alpha_2$ -macroglobulin and trypsin is shown; detection was effected by measuring the UV activity of the substance to ensure the registration of all proteins. Fig. 5B–D show analyses for FITC-labelled aprotinin (B) alone and in the presence of (C) unlabelled

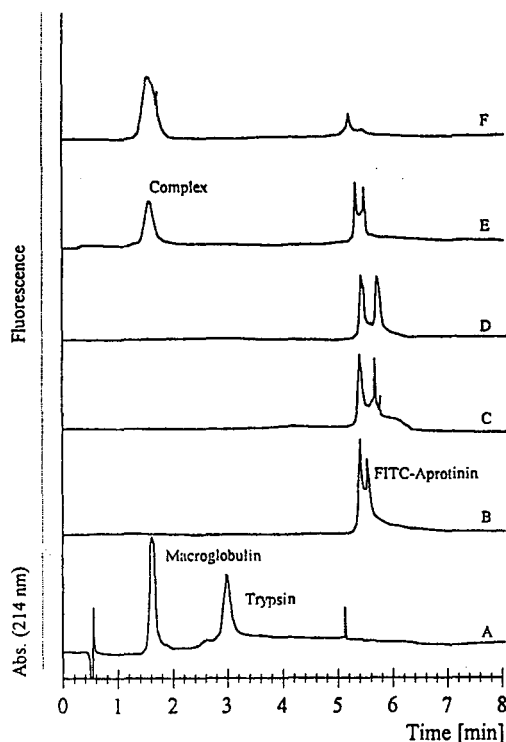


Fig. 5. Complex formation between a small FITC-labelled trypsin inhibitor (aprotinin) and the  $\alpha_2$ -macroglobulin–trypsin complex. Capillary, 27 cm  $\times$  50  $\mu$ m I.D.; buffer, 50 mM borate (pH 10.5); applied voltage, 12 kV; injection, 2 s; pressure, 50 mbar. (A)  $\alpha_2$ -Macroglobulin and trypsin with UV detection (214 nm); (B) FITC-labelled aprotinin with LIF detection; (C) FITC-labelled aprotinin and trypsin after an incubation time of 30 min with LIF detection; (D) FITC-labelled aprotinin and  $\alpha_2$ -macroglobulin after an incubation time of 30 min with LIF detection; (E) complex formation between FITC-labelled aprotinin and the  $\alpha_2$ -macroglobulin–trypsin complex after an incubation time of 30 min with LIF detection; (F) complex formation between FITC-labelled aprotinin and the  $\alpha_2$ -macroglobulin–trypsin complex after an incubation time of 60 min with LIF detection.

trypsin and (D)  $\alpha_2$ -macroglobulin. If the FITC-labelled aprotinin is incubated with the trypsin– $\alpha_2$ -macroglobulin complex, a “new” signal appears in the LIF electropherograms at approximately the migration time of the  $\alpha_2$ -macroglobulin in the UV electropherogram (E). The size of this signal increases with increasing incubation time (F). Apparently a three-component complex between trypsin,  $\alpha_2$ -macroglobulin and aprotinin has been formed, whose electromigration is once more strongly dominated by the properties of the  $\alpha_2$ -macroglobulin. This complex can be easily studied by capillary electrophoresis.

This effect is based on the unique inhibition reaction of  $\alpha_2$ -macroglobulin, i.e., the entrapment of the protease in the “bait region” without inhibition of its reactive site. The still active protease trapped in the “ $\alpha_2$ -macroglobulin bait” is capable of reacting with substrates (resulting in a reduced proteolytic activity of the protease [14]) or, as in the present case, with another protease inhibitor.

In view of the results concerning the influence of FITC on the complex formation, it is not surprising, that the size of the substrate and the second protease should be critical for the formation of the three-protein complex. Aprotinin with a relative molecular mass of 6500 is still capable of entering the “narrow bait region”, while the much larger soybean trypsin inhibitor ( $M_r$  21 700) is sterically hindered and therefore shows no reaction with the  $\alpha_2$ -macroglobulin–trypsin complex (Fig. 6A–D). The results of the effect of the size of the substrate or the second protease inhibitor on the reaction of the substances with the  $\alpha_2$ -macroglobulin–protease complex are again comparable to those achieved by conventional methods [15].

#### 4. Conclusion

Capillary electrophoresis has proved to be a versatile tool for binding studies of proteases and the protease inhibitors. While it need not replace the traditional techniques, it can provide additional information with a unique speed and easy handling. Nevertheless, further optimization has

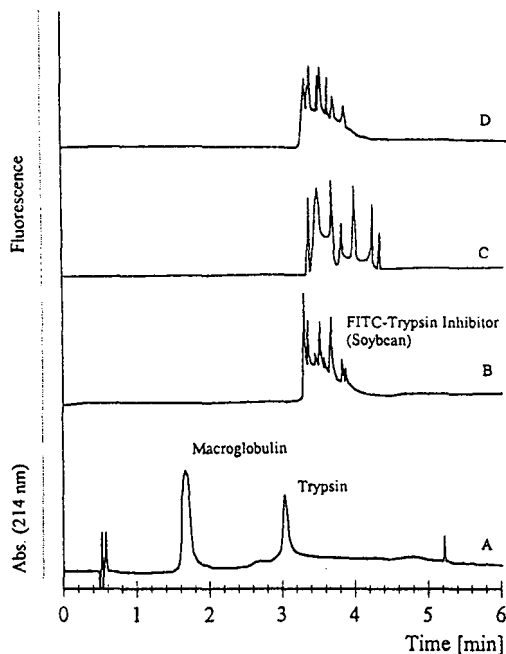


Fig. 6. Complex formation between a large FITC-labelled trypsin inhibitor (soybean) and the  $\alpha_2$ -macroglobulin–trypsin complex. Capillary, 27 cm  $\times$  50  $\mu$ m I.D.; buffer, 50 mM borate (pH 10.5), applied voltage, 12 kV; injection, 2 s; pressure, 50 mbar. (A) Separation of  $\alpha_2$ -macroglobulin and trypsin with UV detection (214 nm); (B) FITC-labelled trypsin inhibitor with LIF detection; (C) FITC-labelled trypsin inhibitor and trypsin after an incubation time of 30 min with LIF detection; (D) FITC-labelled trypsin inhibitor the  $\alpha_2$ -macroglobulin–trypsin complex after an incubation time of 30 min with LIF detection.

to be carried out with respect to the quantification problems of the binding assay in capillary electrophoresis.

## References

- [1] R.G. Nielsen, E.C. Rickard, P.F. Danta, D.A. Sharnkas and G.S. Sittampalam, *J. Chromatogr.*, 539 (1991) 177.
- [2] P.D. Grossman, J.C. Colburn, H.H. Lauer, R.G. Nielsen, R.M. Riggan, G.S. Sittampalam and E.C. Rickard, *Anal. Chem.*, 61 (1989) 1186.
- [3] S.M. Chen, J.E. Shively and T.D. Lee, *The Protein Society, Second Symposium, San Diego, CA, August 1988, Forward Press, Seattle, WA, Abstract No. 908.*
- [4] A.M. Arentoft, H. Frokar, S. Michaelsen, H. Sorensen and S. Sørensen, *J. Chromatogr. A*, 652 (1993) 189.
- [5] B.L. Karger, F. Foret, D. Schmalzing, K. Shimura and E. Szoko, presented at the 5th International Symposium on HPCE, Orlando, FL, January 1993.
- [6] N.M. Schultz and R.T. Kennedy, *Anal. Chem.*, 65 (1993) 3161.
- [7] O.-W. Reif, R. Lausch, T. Scheper and R. Freitag, *Anal. Chem.*, 66 (1994) 4027.
- [8] L. Hernandez, J. Eskalona, N. Joshi and N. Guzman, *J. Chromatogr.*, 559 (1991) 183.
- [9] S. Wu and N.J. Dovichi, *J. Chromatogr.*, 480 (1989) 141.
- [10] R.P. Swenson and J.B. Howard, *Proc. Natl. Acad. Sci. U.S.A.*, 76 (1979) 4213.
- [11] J.L. Ambrus (Editor), *J. Med.*, 16 (Nos. 1–3) (1985) 154.
- [12] L. Sottrup-Jensen, T.E. Petersen and S. Magnusson, *FEBS Lett.*, 128 (1981) 127.
- [13] G.S. Salvesen, C.A. Sayers and A.J. Barrett, *Biochem. J.*, 195 (1981) 453.
- [14] D. Wang, K. Wu, R.D. Feinman, *J. Biol. Chem.*, 256 (1981) 10934.
- [15] J.L. Ambrus (Editor), *J. Med.*, 16 (Nos. 1–3) (1985).





ELSEVIER

Journal of Chromatography A, 716 (1995) 371–379

JOURNAL OF  
CHROMATOGRAPHY A

## Evaluation of an optically active crown ether for the chiral separation of di- and tripeptides

Reinhard Kuhn<sup>a,\*</sup>, Daniel Riester<sup>a</sup>, Burkhard Fleckenstein<sup>b</sup>,  
Karl-Heinz Wiesmüller<sup>b</sup>

<sup>a</sup>*Institut für Angewandte Forschung, FH Reutlingen, Alteburgstrasse 150, 72762 Reutlingen, Germany*

<sup>b</sup>*Naturwissenschaftliches und Medizinisches Institut an der Universität Tübingen, Eberhardstrasse 29, 72762 Reutlingen, Germany*

### Abstract

The direct optical resolution of a number of di- and tripeptides was achieved by capillary zone electrophoresis using an enantioselective crown ether as buffer additive. The protonated primary amines form inclusion complexes with the crown ether. Chiral resolution is based on different stability constants of the diastereomeric complexes thereby changing the electrophoretic mobilities of the enantiomers. Enantioselectivity is strongly affected by the distance between the amine functionality and the chiral carbon atom. This effect was studied using di- and tripeptides especially synthesized for this purpose. In general, baseline resolution was obtained for those peptides with the amine group located as far as four bonds from the stereogenic center. Additionally, tripeptides possessing two chiral centers were separated to investigate the potential of the chiral selector for the analysis of complex analytes with related structures. Experimental factors such as crown ether concentration, buffer pH and temperature also show a strong influence on the resolution. These factors can be successfully employed for method optimization.

### 1. Introduction

Due to the growing significance of peptide-based drugs, liquid- and solid-phase syntheses of biologically active peptides have become an important challenge in the pharmaceutical industry. Today, analytical characterization of these peptides comprises not only determination of the proportion of by-products from synthesis but also the enantiomeric purity of the drug. In routine analysis chromatographic techniques are established for this purpose since chiral stationary phases became commercially available. The

resolution of dipeptides was described by Oi et al. [1] using gas chromatography. Lindner et al. [2] employed HPLC to separate peptides after derivatization and Pirkle and co-workers [3,4] resolved enantiomeric di- and tripeptides using Pirkle-type chiral stationary phases. Stationary phases based on optically active crown ethers were used by Cram and coworkers [5,6], Hilton and Armstrong [7] and Esquivel et al. [8]. Even though a huge number of stationary phases in liquid and gas chromatography are at hand, which virtually cover most separation problems, the results often show poor efficiency and method optimization may be time-consuming.

In 1985 Gassmann et al. [9] were the first to

\* Corresponding author.

describe the chiral resolution of enantiomers by capillary zone electrophoresis (CZE). The chiral selector was simply added to the buffer system. Enantio-separation was accomplished by the formation of diastereomeric complexes of the selector with the analytes leading to a change in electrophoretic mobilities. Subsequently, this basic principle has been extended by using other selectors. Today, enantio-separation in CZE is accomplished by utilizing ligand-exchange complexation [10], solubilization with optically active micelles [11,12], proteins [13] and host-guest complexation using cyclodextrins [14–17].

In previous papers we described the use of a chiral crown ether in CZE for the first time [18–21]. The focus of the present study is to evaluate the potential of 18-crown-6 tetracarbox-

ylic acid ( $18C_6H_4$ ) for the enantio-separation of di- and tripeptides in CZE. The effect of the location of the interactive amine functionality in relation to the chiral center is discussed.

## 2. Experimental

### 2.1. Instrumentation

Experiments were carried out using an HP  $^{3D}$ CE instrument (Hewlett-Packard, Waldbronn, Germany). Separations were performed in untreated open-tube fused-silica capillaries ( $58\text{ cm} \times 75\text{ }\mu\text{m}$  I.D.) applying a potential of 15 kV. If not otherwise stated the capillary temperature was maintained constant at  $25^\circ\text{C}$ . A  $10\text{ mM}$

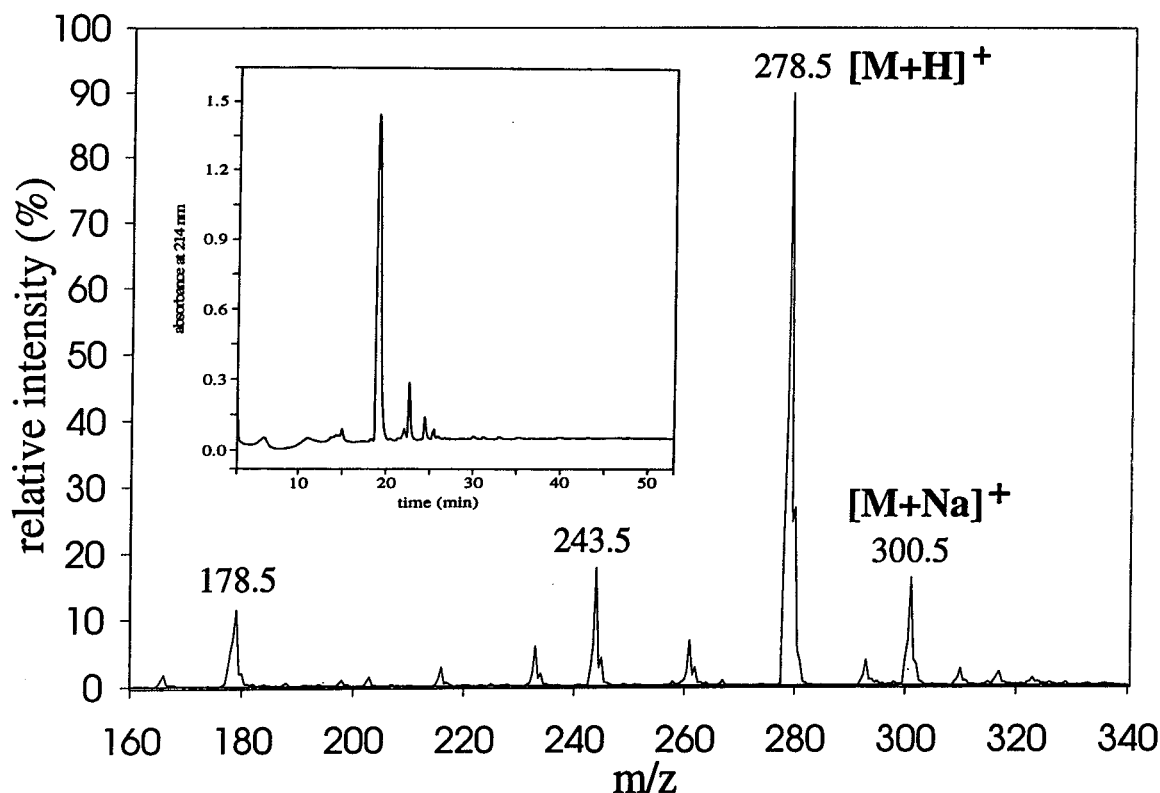


Fig. 1. HPLC profile and electrospray mass spectrum (main peak) of crude peptide D-Phe-Aca after cleavage from the resin. HPLC column: Nucleosil  $C_{18}$  ( $200 \times 2\text{ mm}$ ,  $5\text{ }\mu\text{m}$ , Grom Herrenberg, Germany); gradient 0–100% (within 45 min) acetonitrile-water (containing 0.1% trifluoroacetic acid). The flow-rate was  $0.3\text{ ml/min}$ . ES-MS: a triple quadrupole API III mass spectrometer equipped with a pneumatically assisted electrospray ion source (Sciex, Thornhill, Canada) was used for recording spectra in the positive mode. Solutions of  $1\text{ mg}$  peptides in  $1\text{ ml}$  *tert.*-butyl alcohol-water (4:1, v/v) were injected into the ion source at a flow-rate of  $5\text{ }\mu\text{l/min}$  using an autosampler [23].



Tris–citrate buffer (pH 2.5) with 10 mM 18C6H<sub>4</sub> in double-distilled water was used, unless stated otherwise. An appropriate amount of each sample (usually 0.05%, w/v) was dissolved in methanol–water (50:50, v/v) and injected by pressure for 2 s at 50 mbar and detected by UV absorbance at 210 nm. Whenever possible the elution order of the enantiomers was determined by spiking the mixture with the pure enantiomers.

## 2.2. Chemicals

All reagents were of analytical grade if not otherwise stated. Tris, citric acid, 18-crown-6 tetracarboxylic acid (18C6H<sub>4</sub>, purum grade) and sodium hydroxide were from Merck (Darmstadt, Germany). Gly–DL-Trp and Gly–DL-Phe were purchased from Sigma (St. Louis, MO, USA). Gly–DL-Leu–DL-Ala was from Serva (Heidelberg, Germany). Acetic acid, dimethylformamide (DMF), dichloromethane, diisopropylcarbodiimide (DIC), 1-hydroxybenzotriazole (HOBt), methanol and *tert*-butyl alcohol were from Fluka (Buchs, Switzerland). All other di- and tripeptides were synthesized by solid-phase peptide synthesis according to the following procedure. Their structures were confirmed by HPLC and mass spectrometry. No further purification of the synthesis products was performed.

## 2.3. Peptide synthesis

The peptides were synthesized on a robot system (Tecan, Switzerland) equipped with software for multiple peptide synthesis (MultiSyn Tech, Bochum, Germany). Fmoc-L-amino acid-2-chlorotrityl resin [22] (30 mg, 0.6 μmol/mg) was distributed in separate small filter tubes. Fmoc deprotection was effected with 0.2 ml 50% piperidine in DMF for 8 min and repeated once. Couplings were carried out using 10-fold excess of Fmoc-amino acids and HOBt–DIC (1:1, v/v) activation in DMF within 1 h. After coupling and deprotection the tubes were washed with DMF (0.3 ml) three and seven times, respectively.

Removal of the peptides from the resin was

achieved with acetic acid–dichloromethane–methanol (1:3:1, v/v, 2 ml) within 2 h. The filtrate was evaporated and the residue was dissolved in *tert*-butyl alcohol–water (4:1, v/v) and lyophilized. The identity and purity of the free peptides was determined by HPLC and electrospray mass spectrometry (Fig. 1).

## 3. Results and discussion

Crown ethers are macrocyclic polyether ring systems consisting of a number of oxygens joined by ethylene bridges. Crown ethers of the 18-crown-6 type contain a cavity which is able to form inclusion complexes (host–guest complexes) with potassium, ammonium and protonated primary amines. Although complexation of the primary amine is indispensable for chiral separation, it is insufficient for the discrimination of the enantiomers. This can be obtained by additional interactions of the four substituents of 18C6H<sub>4</sub> with the ligand (Fig. 2).

If 18C6H<sub>4</sub> is simply added to the buffer electrolyte, diastereomeric complexes of the crown ether with the enantiomers are formed which result in a change of their electrophoretic mobilities. In a previous study [19] we proposed two recognition mechanisms. First, the carboxylic acid pairs on both sides of the ring system behave like chiral obstacles dividing the space available for the substituents of the asymmetric center into two cavities. The position and size of these substituents affect the binding energies of the host–guest complexes. The second mechanism is directly related to the carboxylic acids which may show electrostatic interactions with polar substituents of the enantiomers.

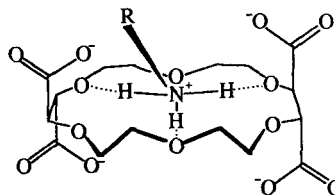


Fig. 2. Chemical structure of a host–guest complex of 18C6H<sub>4</sub> with a protonated primary amine.

Table 1  
Analytical data of the chiral resolution of dipeptides using 5 mM 18C6H<sub>4</sub>

Compound	Structure	$t_1$ (min)	$\alpha$	$R_s$
DL-Phe- $\beta$ -Ala		10.77	1.378	7.20
DL-Phe-Aca <sup>a</sup>		12.98	1.383	9.49
Gly-DL-Trp <sup>b</sup>		13.20	1.084	3.09
Gly-DL-Phe <sup>b</sup>		18.64	1.141	1.45
$\beta$ -Ala-DL-Phe		14.10	1.000	-
Aca <sup>a</sup> -DL-Phe		13.90	1.000	-

<sup>a</sup> Aca: 6-aminocaproic acid.

<sup>b</sup> Separation with 10 mM 18C6H<sub>4</sub> at 40°C.

$\alpha$  = separation factor,  $R_s$  = resolution.

In order to obtain enantiomeric separations with selectors of the “18-crown-6”-type a primary amine functionality is essential. Neither secondary nor tertiary nor other functional groups provide inclusion complexation required for chiral separation. As already demonstrated [20,21] the requisite interactions are dependent on charge and size. In addition, the distance of the interactive amine and the stereogenic center also influences the chiral recognition. In Table 1 the analytical data of 6 racemic dipeptides analyzed using 18C6H<sub>4</sub> are summarized. The dipeptides vary in their distances of the primary amine and the stereogenic center. While in DL-Phe-β-Ala and DL-Phe-Aca the chiral carbon is adjacent to the amine, four bonds separate the chiral carbon from the amine in the cases of Gly-DL-Trp and Gly-DL-Phe. Finally, β-Ala-DL-Phe and Aca-DL-Phe have their asymmetric center 5 and 8 bonds from the amine, respectively. The separation factor  $\alpha$  is calculated by

$$\alpha = \frac{t_2}{t_1} \quad (1)$$

where  $t_1$  is the migration time of the first eluting enantiomer and  $t_2$  the migration time of the antipode. The resolution is calculated by

$$R_s = \frac{2(t_2 - t_1)}{w_1 + w_2} \quad (2)$$

where  $w_1$  and  $w_2$  are the peak widths of both enantiomers. As one can readily see from Table 1 the separation factor and the resolution were the highest when the chiral center was adjacent to the amine function. Thus, both dipeptides DL-Phe-β-Ala and DL-Phe-Aca were excellently resolved using standard experimental conditions. The separation is shown in Fig. 3.

Hilton and Armstrong [7] investigated the “distance effect” on enantio-selectivity of dipeptides using a chiral crown ether in liquid chromatography. They found that dipeptides of the glycyl-amino acid type could not be baseline separated in HPLC. However, in capillary zone electrophoresis good separations were obtained for Gly-DL-Trp and Gly-DL-Phe (results not shown) with a resolution of 3.09 and 1.45, respectively. β-Ala-DL-Phe and Aca-DL-Phe

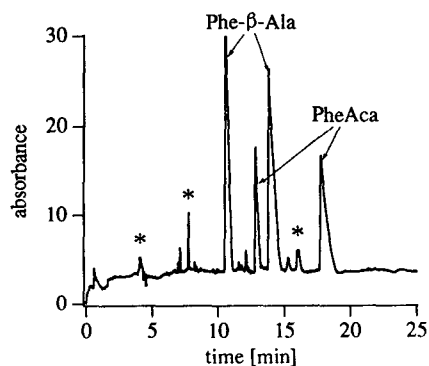


Fig. 3. Chiral separation of DL-Phe-β-Ala and DL-Phe-Aca by CZE using 5 mM 18C6H<sub>4</sub> as buffer additive. Peaks marked by an asterisk are impurities from synthesis.

could not be separated under these experimental conditions. It is obvious, that their stereogenic centers are located too far from the amine function and, consequently, from the crown ether substituents in the complex to show different interactions of the enantiomers.

In a second series of experiments chiral separation of tripeptides containing one or two asymmetric carbon atoms was studied. The analytical data are summarized in Table 2. Again, best separations were obtained if the stereogenic center is in close proximity to the protonated amine. For instance, DL-PheGlyGly and L-Ala-L-PheGly/D-Ala-D-PheGly showed resolutions of 4.92 and 6.55, respectively. The separation of the latter two enantiomers and one diastereomer is depicted in Fig. 4. While the diastereomer was separated from the enantiomers in an ordinary buffer system without any crown ether, chiral separation of the enantiomers succeeded in the same buffer containing 10 mM 18C6H<sub>4</sub>. Fairly good results were also obtained for Gly-DL-Leu-DL-Ala. However, in order to resolve the four optical isomers the buffer pH had to be adjusted to pH 3.0. This minor change had some dramatic effects on the separation: (i) the complex formation of the isomers with the crown ether are strongly enhanced causing anionic migration of the peptides, (ii) migration times were approx. twice as long as those obtained at pH 2.5. Interestingly the enantiomers of GlyGly-DL-Leu were also recognized by the crown ether even

Table 2  
Analytical data of the chiral resolution of tripeptides using 10 mM 18C6H<sub>4</sub>

Compound	Structure	$t_1$ (min)	$\alpha$	$R_s$
DL-PheGlyGly	$\begin{array}{ccccccc} & \text{H} & \text{O} & \text{H} & & \text{O} & \text{H} \\ &   &    &   & &    &   \\ \text{H}_2\text{N} & -\text{C}^* & -\text{C} & -\text{N} & -\text{CH}_2 & -\text{C} & -\text{N} & -\text{CH}_2 & -\text{COOH} \\ &   & & & & & & & \\ & \text{CH}_2 & & & & & & & \\ &   & & & & & & & \\ & \text{C}_6\text{H}_5 & & & & & & & \end{array}$	11.83	1.075	4.92
L-Ala-L-PheGly/ D-Ala-D-PheGly	$\begin{array}{ccccccc} & \text{H} & \text{O} & \text{H} & & \text{O} & \text{H} \\ &   &    &   & &    &   \\ \text{H}_2\text{N} & -\text{C}^* & -\text{C} & -\text{N} & -\text{C}^*\text{H} & -\text{C} & -\text{N} & -\text{CH}_2 & -\text{COOH} \\ &   & & &   & & & & \\ & \text{CH}_3 & & & \text{CH}_2 & & & & \\ & & & &   & & & & \\ & & & & \text{C}_6\text{H}_5 & & & & \end{array}$	12.43	1.158	6.55
Gly-DL-Leu-DL-Ala <sup>a</sup>	$\begin{array}{ccccccc} & \text{O} & \text{H} & & \text{O} & \text{H} & \text{CH}_3 \\ &    &   & &    &   &   \\ \text{H}_2\text{N} & -\text{CH}_2 & -\text{C} & -\text{N} & -\text{C}^*\text{H} & -\text{C} & -\text{N} & -\text{C}^*\text{H} & -\text{COOH} \\ & & & &   & & & & \\ & & & & \text{CH}_2 & & & & \\ & & & &   & & & & \\ & & & & \text{CH}(\text{CH}_3)_2 & & & & \end{array}$	35.34/ 37.88	1.014/ 1.079	1.56/ 2.94
Gly-L-Ala-L-Phe/ Gly-D-Ala-D-Phe	$\begin{array}{ccccccc} & \text{O} & \text{H} & & \text{O} & \text{H} \\ &    &   & &    &   \\ \text{H}_2\text{N} & -\text{CH}_2 & -\text{C} & -\text{N} & -\text{C}^*\text{H} & -\text{C} & -\text{N} & -\text{C}^*\text{H} & -\text{COOH} \\ & & & &   & &   & & \\ & & & & \text{CH}_3 & & \text{CH}_2 & & \\ & & & & & &   & & \\ & & & & & & \text{C}_6\text{H}_5 & & \end{array}$	17.69	1.054	1.01
GlyGly-DL-Leu	$\begin{array}{ccccccc} & \text{O} & \text{H} & & \text{O} & \text{H} \\ &    &   & &    &   \\ \text{H}_2\text{N} & -\text{CH}_2 & -\text{C} & -\text{N} & -\text{CH}_2 & -\text{C} & -\text{N} & -\text{C}^*\text{H} & -\text{COOH} \\ & & & & & & &   & \\ & & & & & & & \text{CH}_2 & \\ & & & & & & &   & \\ & & & & & & & \text{CH}(\text{CH}_3)_2 & \end{array}$	46.18	1.034	0.70

<sup>a</sup> Separation at pH 3.0 and 15 mM 18C6H<sub>4</sub>.  
 $\alpha$  = separation factor,  $R_s$  = resolution.

though resolution was poor under the experimental conditions.

### 3.1. Influence of the experimental conditions

Systematic investigations of the experimental factors revealed the method to be highly sensitive with respect to crown ether concentration, buffer pH and temperature.

The influence of the crown ether concentration

on the resolution of DL-Phe-Aca and DL-Phe- $\beta$ -Ala is shown in Fig. 5. According to the law of mass action an increase of the crown ether concentration enhances the complex formation and should improve the resolution. This holds for low crown ether concentrations. However, by increasing the concentration to approx. 5–10 mM the curves level off. Higher concentrations than 10 mM 18C6H<sub>4</sub> did not significantly improve the resolution but led to marked longer

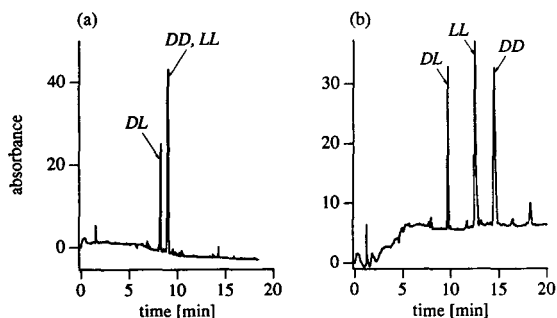


Fig. 4. Separation of the enantiomers L-Ala-L-PheGly and D-Ala-D-PheGly and the diastereomer D-Ala-L-PheGly in (a) 10 mM Tris-citrate (pH 2.5) and (b) 10 mM Tris-10 mM 18C6H<sub>4</sub>-citrate (pH 2.5).

migration times. Similar effects of crown ether concentration on the resolution were found in earlier investigations [17,18].

The pH of the buffer system is the most powerful and most sensitive factor for method optimization. The pH effects the dissociation of the crown ether's carboxylic acids and consequently the electrophoretic mobility of the selector. In addition, the association of a ligand to 18C6H<sub>4</sub> is known to depend on the dissociation degree of the crown ether because its carboxylate groups stabilize the complex stronger than the non-dissociated acids. The influence of the pH was investigated using Gly-DL-Leu-DL-Ala. Only a small pH range (pH 2.2–3.0) could be used for method optimization. Table 3 shows the

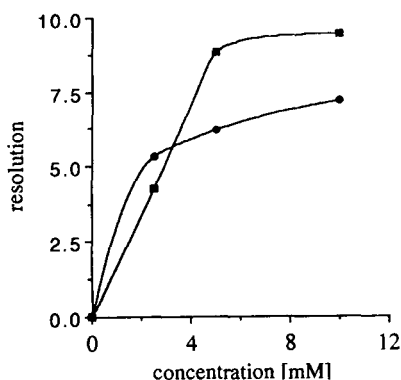


Fig. 5. Influence of the concentration of 18C6H<sub>4</sub> on the resolution of DL-Phe-β-Ala (●) and DL-Phe-Aca (■). Experimental conditions are given in the Experimental section.

Table 3

Influence of the buffer pH on the migration time of the first eluted isomer of Gly-DL-Leu-DL-Ala

pH	Migration time (min)	Remark
2.2	16.55	1 peak detected
2.5	16.13	3 peaks detected
3.0	35.34	complete separation
3.5, 4.0, 5.0, 6.0	>180	no peaks detected

Experimental conditions: temperature 20°C; pH 2.2 and 2.5: 15 mM Tris-15 mM 18C6H<sub>4</sub> adjusted to the given pH with citric acid; pH 3.0 to 6.0: 15 mM 18C6H<sub>4</sub> adjusted to the given pH with Tris; detection wavelength, 200 nm. Other conditions are given in the Experimental section

influence of the pH on the migration time of the first isomer. Obviously, pH values higher than 3.0 are not applicable because no peaks could be detected within 180 min. It can be assumed that the increasing net charge of the crown ether at higher pH values and the stronger complexation of the enantiomers were responsible for this results.

Finally, the temperature also has an influence on the separation. In general, increasing the temperature causes a decrease in the separation factor and resolution. This was demonstrated in a previous study with DL-tryptophan, DL-phenylalanine and (±)-naphthylethylamine [19]. However, the dipeptide Gly-DL-Phe showed an oppo-

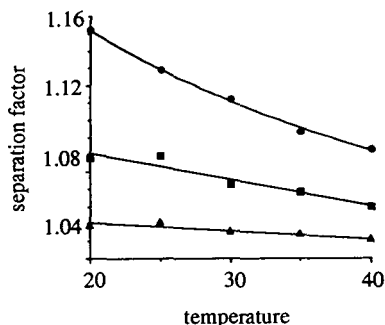


Fig. 6. Plot of the capillary temperature versus the separation factor for Gly-DL-Trp (●) and both enantiomeric pairs of Gly-DL-Leu-DL-Ala (■,▲). The buffer composition for the separation of the tripeptides was 15 mM 18C6H<sub>4</sub> adjusted to pH 3.0 with Tris. Detection wavelength was 200 nm. Other conditions are given in the Experimental section.

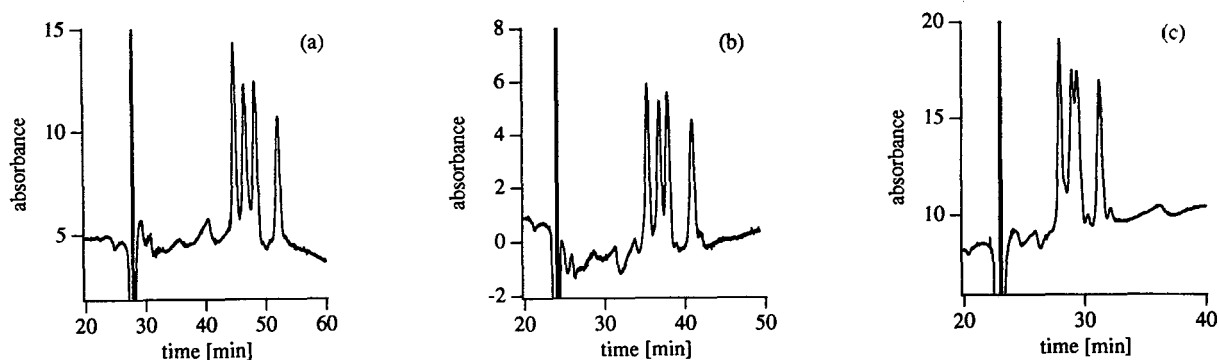


Fig. 7. Influence of the capillary temperature on the chiral separation of Gly-DL-Leu-DL-Ala: (a) 20°C, (b) 25°C, (c) 30°C. Other experimental conditions are described in Fig. 6.

site behavior in that investigation, which was explained by a different separation mechanism based on electrostatic interactions. In the present study we investigated the effects of the temperature on the separation factor of Gly-DL-Trp and Gly-DL-Leu-DL-Ala. The results are shown in Fig. 6. While the separation factor strongly decreases with increasing temperature in the case of Gly-DL-Trp, this effect is much less pronounced for both enantiomeric pairs of Gly-DL-Leu-DL-Ala. However, increasing the temperature decreased the resolution of all four components owing to the co-migration of two diastereomers (see Fig. 7a–c).

#### 4. Concluding remarks

The present paper proves the suitability of 18C6H<sub>4</sub> for enantio-separation of di- and tripeptides possessing one or two stereogenic centers. Most separation problems could be solved using a simple screening method. Nevertheless parameters such as crown ether concentration, buffer pH and temperature are effective for method optimization. However, even small changes of these parameters occasionally can have a dramatic effect on the separation power. Thus, careful adjustment of the experimental conditions is essential for obtaining reproducible results.

#### Acknowledgement

The authors thank Miss Beate Bachhuber for technical assistance.

#### References

- [1] N. Oi, M. Horiba, H. Kitahara and H. Shimada, *J. Chromatogr.*, 202 (1980) 302.
- [2] W. Lindner, J.N. Le Page, G. Davies, D.E. Seitz and B.L. Karger, *J. Chromatogr.*, 185 (1979) 323.
- [3] M.H. Hyun, I.-K. Balk and W.H. Pirkle, *J. Liq. Chromatogr.*, 11 (1988) 1249.
- [4] W.H. Pirkle, D.M. Alessi, M.H. Hyun and T. Pochapsky, *J. Chromatogr.*, 398 (1987) 203.
- [5] D.J. Cram, *Science*, 240 (1988) 760.
- [6] L.R. Sousa, D.H. Hoffman, L. Kaplan and D.J. Cram, *J. Am. Chem. Soc.*, 96 (1974) 7100.
- [7] M. Hilton and D.W. Armstrong, *J. Liq. Chromatogr.*, 14 (1991) 3673.
- [8] B. Esquivel, N. Nocholson, L. Peery and M. Fazio, *J. High Resolut. Chromatogr. Chromatogr. Commun.*, 14 (1991) 816.
- [9] E. Gassmann, J.E. Kuo and R.N. Zare, *Science*, 230 (1985) 813.
- [10] P. Gozel, E. Gassmann, H. Michelson and R.N. Zare, *Anal. Chem.*, 59 (1987) 44.
- [11] S. Terabe, M. Shibata and Y. Miyashita, *J. Chromatogr.*, 480 (1989) 403.
- [12] H. Nishi, T. Fukuyama, M. Matsuo and S. Terabe, *Anal. Chim. Acta*, 236 (1990) 281.
- [13] S. Busch, J.C. Kraak and H. Poppe, *J. Chromatogr.*, 635 (1993) 119.
- [14] S. Fanali, *J. Chromatogr.*, 545 (1991) 437.
- [15] S. Fanali, *J. Chromatogr.*, 474 (1989) 441.

- [16] S. Fanali and P. Bocek, *Electrophoresis*, 11 (1990) 757.
- [17] R. Kuhn and S. Hoffstetter-Kuhn, *Chromatographia*, 34 (1992) 505.
- [18] R. Kuhn, F. Stoecklin and F. Erni, *Chromatographia*, 33 (1992) 32.
- [19] R. Kuhn, F. Erni, T. Bereuter and J. Häusler, *Anal. Chem.*, 64 (1992) 2815.
- [20] R. Kuhn, C. Steinmetz, T. Bereuter, P. Haas and F. Erni, *J. Chromatogr. A*, 666 (1994) 367.
- [21] R. Kuhn, J. Wagner, Y. Walbroehl and T. Bereuter, *Electrophoresis*, 15 (1994) 828.
- [22] K. Barlos, D. Gatos, S. Kapolos, G. Papaphotion, W. Schäfer and Y. Wenquing, *Tetrahedron Lett.*, 30 (1989) 3947.
- [23] J.W. Metzger, C. Kempter, K.-H. Wiesmüller and G. Jung, *Anal. Biochem.*, 219 (1994) 261.







ELSEVIER

Journal of Chromatography A, 716 (1995) 381–388

JOURNAL OF  
CHROMATOGRAPHY A

# Determination of $\alpha$ -difluoromethylornithine in blood by microdialysis sampling and capillary electrophoresis with UV detection

Tao Hu<sup>a</sup>, Hong Zuo<sup>b</sup>, Christopher M. Riley<sup>a,1</sup>, John F. Stobaugh<sup>a</sup>,  
Susan M. Lunte<sup>a,\*</sup>

<sup>a</sup>Center for Bioanalytical Research, University of Kansas, 2095 Constant Avenue, Lawrence, KS 66047, USA

<sup>b</sup>Bioanalytical Systems Kansas, Lawrence, KS 66047, USA

## Abstract

A procedure is described for the analysis of  $\alpha$ -difluoromethylornithine (DFMO), an anti-cancer agent, in plasma microdialysis (MD) samples. DFMO has been shown to be effective alone or in combination with other agents in the treatment of several cancers. Precolumn derivatization of DFMO with naphthalene-2,3-dicarboxaldehyde-cyanide (NDA-CN) in pH 10.0 borate buffer results in the rapid formation of a stable mono-derivatized product (N-substituted 1-cyanobenz[*f*]isoindole, CBI), which is UV active. An analytical method has been developed to separate CBI-DFMO from NDA-CN derivatization products of 20 standard amino acids using capillary electrophoresis (CE). This method is then employed for the determination of DFMO in plasma microdialysis samples. Separation of DFMO from other components in the dialysate was achieved within 20 min. The response for DFMO in Ringer's solution was linear over the range of  $1.2 \cdot 10^{-6}$  to  $1.6 \cdot 10^{-4}$  M after derivatization. The detection limit of DFMO in the plasma dialysate is  $5 \mu\text{M}$  using UV detection at 254 nm. This method has been proven to have adequate sensitivity for quantitation of DFMO in i.v. microdialysate samples and has been successfully applied to monitoring the pharmacokinetics of DFMO by CE-UV.

## 1. Introduction

$\alpha$ -Difluoromethylornithine (DFMO) is an irreversible inhibitor of ornithine decarboxylase, which effectively blocks the biosynthesis of endogenous polyamines (putrescine, spermidine, and spermine) [1]. DFMO inhibits tumor cell growth in vitro and in vivo, and demonstrates chemopreventive activity in a variety of animal

tumors [2]. DFMO has been shown to be effective alone or in conjunction with other agents in the treatment of several cancers [3].

DFMO itself has no chromophore; therefore, derivatization is necessary for detection using conventional spectroscopic methods. To date, only a few published reports on the analysis of DFMO in biological fluids have appeared in the literature [4–6]. All of these employed precolumn derivatization with *o*-phthalaldehyde-thiol (OPA-thiol) [4,5] or dansyl chloride [6] and liquid chromatography (LC) with fluorescence or UV detection. The reported methods

\* Corresponding author.

<sup>1</sup> Present address: DuPont Merck Pharmaceutical Company, Wilmington, DE, USA.

provide adequate sensitivity for plasma analysis, but have certain disadvantages. Derivatization with dansyl chloride requires at least a 4-h reaction time [6]. The reaction with OPA–thiol is rapid, but the instability of the resulting fluorophore is well documented [7,8], making precise timing of the derivatization essential.

In this paper, NDA–CN is evaluated as a reagent for the determination of DFMO by capillary electrophoresis with UV detection (CE–UV). NDA reacts with primary amines in the presence of cyanide to form cyano[*f*]benzoisindole (CBI) derivatives, which are both spectroscopically and electrochemically active. Both the fluorescence efficiency and stability of the CBI derivatives are better than those of the OPA–thiol derivatives [9]. The determination of DFMO in plasma by LC using NDA–CN has been reported previously [10]. However, difficulties were encountered with this system due to the presence of naturally occurring amines in the sample matrix, which interfered with the separation. Adequate resolution of DFMO from amino acids could not be achieved using a single LC column [10] and, therefore, a multidimensional approach was employed. In addition, CBI–DFMO exhibited problematic chromatography, including peak tailing and splitting.

CE is a powerful analytical technique for the separation of charged substances. Very high separation efficiencies can be obtained using this approach. Amino acids have been determined previously by CE with UV, electrochemical, and fluorescence detection following derivatization with NDA–CN [11–15]. Microdialysis is an established technique for sampling drugs and endogenous compounds in tissues of awake, freely moving animals [16]. It has been used to study the metabolism and pharmacokinetics of a variety of drug substances in blood, liver, bile, and skin [17–21]. One of the advantages of microdialysis over other sampling methods is that dialysates are protein-free and can be directly injected into the analytical system with minimal sample preparation. In addition, since protein-bound molecules cannot pass through the membrane, only the biologically active “free” drug is measured. In this report, microdialysis sampling

was employed to investigate the pharmacokinetics of DFMO using CE–UV as the analysis system.

## 2. Experimental

### 2.1. Reagents

All amino acids were purchased from Sigma (St. Louis, MO, USA) and used as received. NDA was supplied by Bioanalytical Systems (West Lafayette, IN, USA). Sodium cyanide, sodium borate, and sodium phosphate (monobasic and dibasic) were obtained from Fisher Scientific (Fair Lawn, NJ, USA). DFMO monohydrate was kindly provided by Dr. Milan Slavik (V.A. Medical Research Service, Wichita, KS, USA).

### 2.2. Stock solutions

NDA was prepared in HPLC-grade acetonitrile, protected from light and stored at 5°C. All other solutions were prepared in Nanopure water (Sybron-Barnstead, Boston, MA, USA). Sodium borate was dissolved in Nanopure water and titrated to pH 10 with 2 *M* NaOH solution. Phosphate buffers (of different pH values) were prepared as reported in the Handbook of Biochemistry and Molecular Biology [22]. Amino acid mixtures were made by mixing together 1 ml of a 10 *mM* solution of each amino acid to yield a final concentration of 0.5 *mM*. All solutions were passed through a membrane filter (0.2  $\mu\text{m}$  pore size) before use.

### 2.3. Instrumentation

An ISCO Model 3850 capillary electrophoresis system was driven by a high-voltage d.c. (0–30 kV) power supply connected to a platinum electrode. The fused-silica capillary (50  $\mu\text{m}$  I.D., 360  $\mu\text{m}$  O.D.) was obtained from Polymicro Technologies (Phoenix, AZ, USA). A column length of 75 cm (50 cm to detector) was used. The detection wavelength was set at 254 nm. Sample introduction was accomplished by vac-

uum injection for 4 s, which corresponded to a 3.7 nl injection volume.

#### 2.4. Microdialysis system

Microdialysis sampling was performed using a CMA/100 microinjection pump from Bioanalytical Systems/CMA (West Lafayette, IN, USA) coupled to a microdialysis probe inserted into the jugular vein of the experimental animal. The laboratory-built flexible i.v. microdialysis probe has been described previously [19]. Perfusion was carried out with Ringer's solution (NaCl, 147 mM; KCl, 4 mM; CaCl<sub>2</sub>, 2.3 mM) at a flow-rate of 0.25  $\mu$ l/min. Microdialysis samples were collected by a CMA/142 fraction collector.

#### 2.5. Microdialysis probe calibration

In order to ascertain the in vivo concentration of DFMO giving rise to the concentration detected in the perfusion medium, it was necessary to determine the recovery of the dialysis probe. This was accomplished by placing the probe in a standard solution of 0.1 mM DFMO prepared in Ringer's solution. The flow-rate was 0.25  $\mu$ l/min, the same as that used for pharmacokinetic studies. Samples of the perfusate were collected and analyzed. Recovery was then expressed as the ratio of the concentration of DFMO in the perfusate to the concentration of standard. The average recovery for DFMO was  $49.6 \pm 3.1\%$  ( $n = 3$ ).

#### 2.6. In vivo pharmacokinetic experiments

Male Sprague–Dawley rats 4–6 months old (450–500 g) were anaesthetized with ketamine and xylazine (80 mg/kg and 4 mg/kg, respectively). The flexible microdialysis probe was implanted into the jugular vein and PE-50 tubing was cannulated into the femoral vein. Ringer's solution was perfused through the microdialysis probes at a flow-rate of 0.25  $\mu$ l/min, and dialysis samples were collected at 16-min intervals. Blanks were collected immediately following insertion of the microdialysis probe. The pharmacokinetic experiments were begun 24 h after

surgery. At that time, the animals were dosed with DFMO (70 mg/kg) in Ringer's solution via the cannula in the femoral vein. Following derivatization with NDA and NaCN using the procedure below, samples were analyzed by CE–UV until DFMO was no longer detected in the dialysate.

#### 2.7. Derivatization procedure

Derivatization conditions varied depending on the requirements of the reaction. In most cases, borate buffer (pH 10) was used as the reaction buffer. For these studies, a 1:1 molar ratio of NDA and NaCN was used. NDA was always added last to avoid the formation of possible side products. The final reaction solution contained a minimum of 20% acetonitrile to prevent precipitation of NDA. For the pharmacokinetic studies, 2  $\mu$ l of 50 mM borate buffer (pH 10) and 2  $\mu$ l of 15 mM NaCN solution were added to 4  $\mu$ l of microdialysate, followed by 2  $\mu$ l 15 mM NDA solution. The resulting solution was allowed to react for 10 min after the addition of NDA.

### 3. Results and discussion

#### 3.1. Derivatization reaction conditions

DFMO has both alpha and delta primary amino groups, which can potentially be derivatized. The alpha amino group is attached to the tertiary carbon and is more sterically crowded than the delta amino site. Therefore, for DFMO, the mono-derivatized product was expected to be dominant over the bis-derivatized product. Previously, experiments regarding the reaction of NDA–CN with primary amino groups have shown that the reaction rate is maximal when the pH of the reaction solution is equal to the  $pK_a$  of the primary amine [9]. Since the delta amine has a  $pK_a$  of 10.4 [10], a pH 10.0 borate buffer was used as the reaction buffer.

Fig. 1 shows the electropherograms of solutions containing (A) NDA and (B) DFMO reacted with NDA–CN in pH 10.0 borate buffer. NDA itself is UV active and can therefore serve

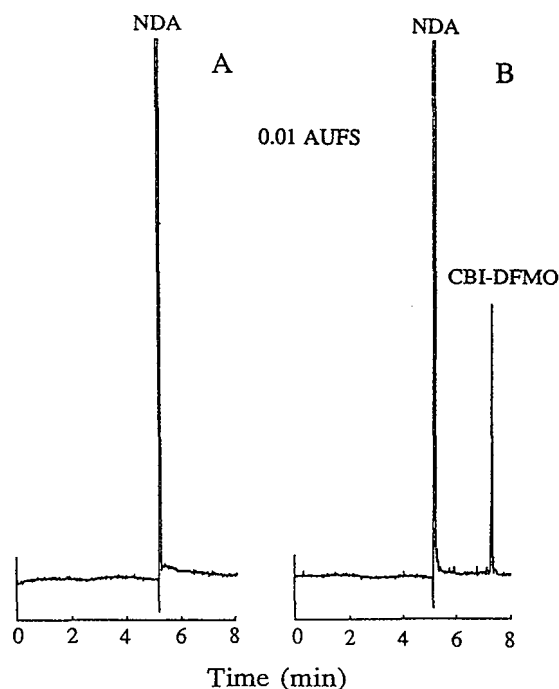


Fig. 1. Electropherograms of (A) 1.0 mM NDA and (B) 0.1 mM DFMO reacted with NDA–NaCN (1.0 mM each) for 10 min in pH 10 borate buffer. Separation conditions: 75 cm (50 cm to detector)  $\times$  50  $\mu$ m I.D. capillary in 20 mM sodium borate (pH 9.0); voltage, 20 kV (18  $\mu$ A).

as neutral marker in these studies (Fig. 1A). The derivatization of DFMO with NDA–CN gives rise to a new peak that corresponds to the mono-CBI–DFMO derivative (Fig. 1B). The reaction of DFMO with NDA–CN at pH 10.0 is very fast (ca. 3 min), and can be monitored by a change from colorless to bright yellow. While several different wavelengths (210, 254, and 420 nm) can be employed for the detection of the CBI derivative, 254 nm was found to provide the best sensitivity and was used for all subsequent studies.

In order to optimize the derivatization reaction, the effect of borate concentration and reaction time on product yield were evaluated. To maintain pseudo-first-order reaction in DFMO, excess NDA–NaCN should be used. However, side products may be formed at very high concentrations of NDA and NaCN. For these studies, a 1:1 molar ratio of NDA and CN

was used. Using a constant concentration of DFMO (0.05 mM), the mono-CBI-derivative peak increased with increasing concentrations of NDA and NaCN. The peak height achieved its maximum value (Fig. 2) after the concentration of NDA–CN reached ten times that of DFMO.

It has been reported that the concentration of borate has a catalytic effect on the derivatization reaction of NDA–CN with primary amines [9]. Therefore, the effect of borate concentration on reaction rate was also investigated over the range of 10–50 mM (final concentration). Fortunately, the concentration of borate was found not to have a substantial effect on the rate of this particular derivatization reaction. Using 10 mM borate buffer, the reaction of DFMO with NDA–CN was complete within 3 min and the derivative was stable for at least 5 h. Higher concentrations of borate buffer did not substantially increase the reaction rate. However, it was found that column efficiency decreased with increasing concentration of borate buffer, as shown in Fig. 3. This phenomenon has been

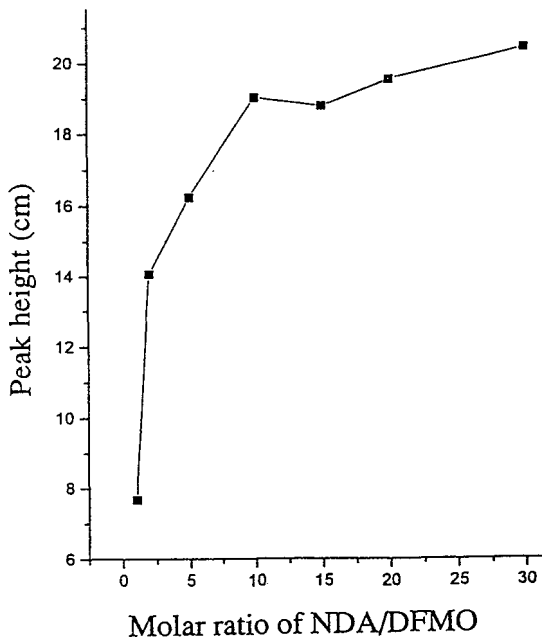


Fig. 2. Effect of molar ratio of NDA–DFMO on peak height of CBI–DFMO derivative. Concentration of DFMO, 0.05 mM; reaction time, 10 min.

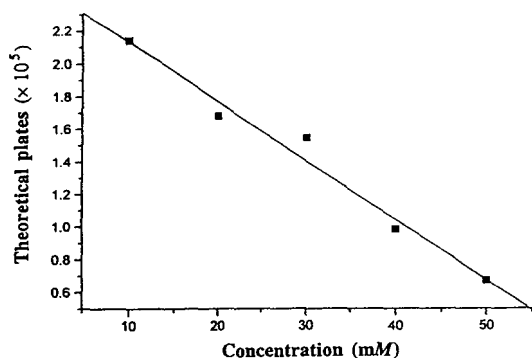


Fig. 3. Efficiency of CBI-DFMO peak as a function of borate buffer concentration in the derivatization reaction. Separation conditions: 75 cm (50 cm to detector)  $\times$  50  $\mu$ m I.D. capillary; 100 mM phosphate (pH 6.5); voltage, 15 kV (49  $\mu$ A).

described previously for the determination of CBI-amino acids by CE-UV [12]. Therefore, 10 mM pH 10.0 borate buffer was chosen to be reaction buffer throughout the studies.

### 3.2. Capillary electrophoresis method development

When performing i.v. microdialysis, there are a number of naturally occurring amino acids and small peptides that are present in the dialysate. Therefore, separation conditions that will isolate the CBI-DFMO from the rest of the amino acids must be developed. In order to accomplish this, we investigated the migration behavior of the 20 standard amino acids found in proteins relative to CBI-DFMO. CBI-amino acids with a neutral or negatively charged R-group are negatively charged above pH 3 and thus are easily resolved from CBI-DFMO. CBI-arginine possesses a positively charged R-group with a high  $pK_a$  and migrates early in the electropherogram. In the case of CBI-DFMO, the major interference was expected to be histidine since the  $pK_a$  of the free amino group (6.0) is close to that of DFMO (6.4).

In developing the separation of CBI-DFMO from the CBI-amino acids, several variables were investigated, including the pH and composition of the run buffer, the length of the capillary, and the applied voltage. Of these, pH and

composition of run buffer were found to have the greatest effects on the separation. At pH values above 9, both CBI-DFMO and the CBI-amino acid derivatives are anionic and the electroosmotic flow is very fast, resulting in poor resolution. Zwitterionic buffers were investigated at lower pH values, but no good separation was obtained over the range pH 7–9. Phosphate buffers in the range 8.5–5.5 were also investigated. With a pH 8.0 phosphate buffer, lysine was not resolved from CBI-DFMO and at pH 6 histidine comigrated with CBI-DFMO. However, all three compounds could be resolved between pH 6.5 and 7.5. A 50 mM phosphate (pH 6.7) buffer provided the best resolution of CBI-DFMO from all of the amino acids studied. Fig. 4 shows the separation of CBI-DFMO from the CBI-amino acid mixture. DFMO migrated between NDA and histidine.

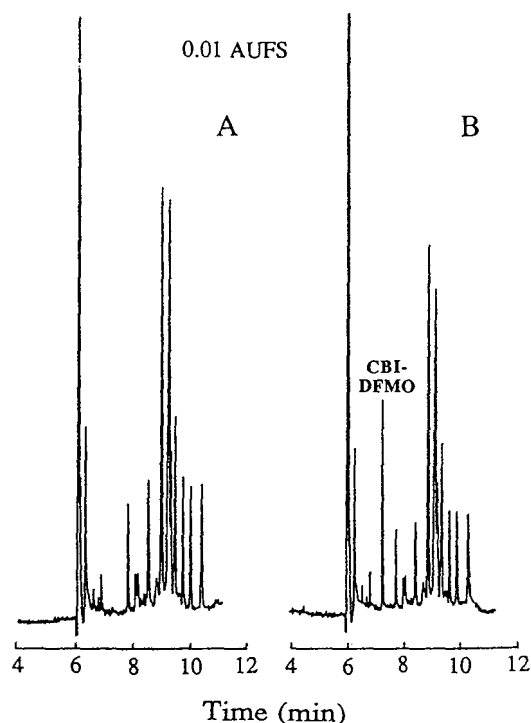


Fig. 4. Electropherograms of (A) 20 amino acids (0.02 mM each) and (B) DFMO (0.05 mM) and 20 amino acids (0.02 mM each) derivatized with NDA-CN. Separation conditions: 75 cm (50 cm to detector)  $\times$  50  $\mu$ m I.D. capillary; 50 mM phosphate (pH 6.7); voltage, 20 kV (33  $\mu$ A);  $\lambda$  = 254 nm.

A blank plasma microdialysis sample produced an electropherogram very similar to that of standard amino acids. However, a small unidentified peak appeared whose migration time was very close to that of CBI–DFMO (Fig. 5). Thus, the separation conditions required further optimization to resolve CBI–DFMO from the unknown peak. It was found that the use of higher concentrations of run buffer, lower applied voltages, and a longer capillary improved resolution. However, these conditions resulted in longer analysis times. In addition, the use of high concentrations of borate buffer resulted in high separation currents and increased Joule heating. Considering all of these factors, the best separation was obtained under the following conditions: 100 mM, pH 6.5, phosphate buffer, 75 cm (50 cm to detector)  $\times$  50  $\mu$ m capillary, 15 kV applied voltage. Fig. 5 shows the electropherograms of (A) a blank plasma microdialysis sample and (B) a sample spiked with DFMO. It can be seen that under these conditions, a baseline separation between DFMO and the unknown

small peak was obtained ( $R = 1.7$ ). In this case, the migration time for CBI–DFMO was about 11 min, and the overall analysis time was less than 20 min.

### 3.3. Calibration and detection limits

The system was calibrated over the concentration range expected in the microdialysis samples. The relationship between peak height and concentration of DFMO was linear over the range 3–400  $\mu$ M (original concentration of DFMO before derivatization) with a correlation coefficient of 0.9995. Since 4  $\mu$ l of DFMO was derivatized to give 10  $\mu$ l of final solution, the actual concentration range in the final solution after derivatization was between 1.2 and 160  $\mu$ M. In these studies, DFMO was dissolved in Ringer's solution in order to yield a matrix similar to that of microdialysis sample, and the NDA and NaCN concentrations used were at least ten times the concentration of DFMO.

The effect of NDA–CN concentration on the yield of CBI–DFMO in dialysates was also examined. Because the exact total concentration of amino acids in the microdialysis samples is unknown, it is important to add enough NDA to react with all of the amines in the sample. Therefore, the effect of NDA concentration on the yield of CBI–DFMO in a spiked microdialysis sample (10  $\mu$ M) was determined. It was found that using 15 mM NDA and NaCN ensured almost 100% yield of DFMO. Thus, the calibration curve of DFMO obtained in Ringer's solution under these conditions was used for the calculation of concentration values for pharmacokinetic studies.

The limit of detection (signal-to-noise ratio = 3) for CBI–DFMO in Ringer's solution was 3  $\mu$ M. It was slightly higher in microdialysate samples (5  $\mu$ M before derivatization, 2  $\mu$ M after derivatization). Using 3.7 nl as the injection volume, the corresponding mass detection limit was 7.4 fmol in the microdialysis sample. Based on a 50% recovery of DFMO with the flexible dialysis probe, the limit of detection for DFMO was approximately 10  $\mu$ M in vivo.

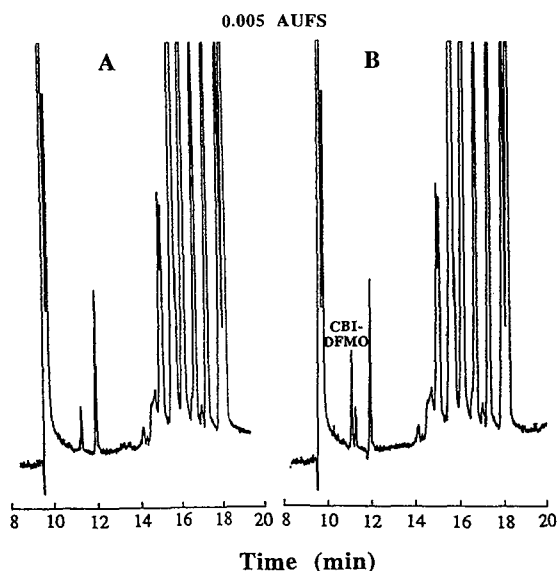


Fig. 5. Electropherograms of (A) blank plasma microdialysate sample and (B) plasma microdialysate spiked with 10 nM DFMO. Separation conditions: 75 cm (50 cm to detector)  $\times$  50  $\mu$ m I.D. capillary; 100 mM phosphate (pH 6.5); voltage, 15 kV (49  $\mu$ A).

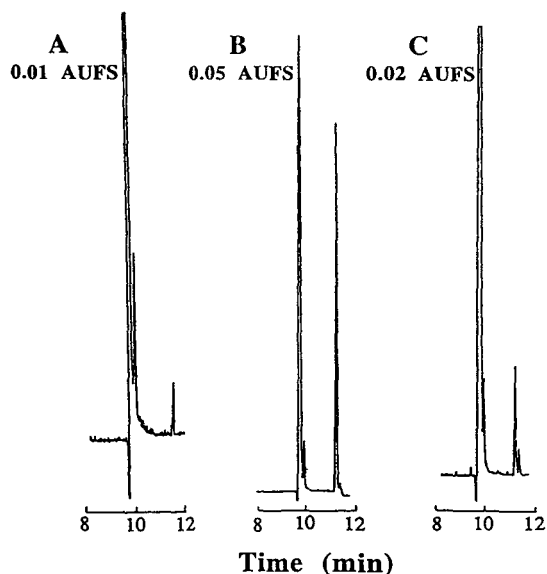


Fig. 6. Electropherograms obtained in the pharmacokinetic study. (A) Blank plasma dialysate, (B) 16 min after a 70 mg/kg i.v. dose of DFMO, (C) 64 min after same dose. Separation conditions: 75 cm (50 cm to detector)  $\times$  50  $\mu$ m I.D. capillary; 100 mM phosphate (pH 6.5); voltage, 15 kV (49  $\mu$ A).

### 3.4. Pharmacokinetics studies

Pharmacokinetic studies were performed on awake, freely moving rats. Typical electropherograms of blood dialysates by in vivo sampling are shown in Fig. 6. The blank sample was run at the high-sensitivity detector gain setting; no peak co-migrating with the CBI-DFMO derivative was present in the blank at this high gain (Fig. 6A). Fig. 6B shows an electropherogram of blood dialysate 16 min after an i.v. dose of 70 mg/kg DFMO. In the initial samples, the CBI-DFMO peak overwhelmed the interference peak. The concentration of DFMO in the microdialysate rapidly decreased, as shown in Fig. 6C.

Since microdialysis is a continuous sampling technique, each sample represents the average concentration of analyte in the blood during the sampling interval. A representative concentration versus time profile (plotted as a bar graph) of the microdialysis samples is shown in Fig. 7. The semi-log plot (log concentration DFMO versus time) gave a straight line (Fig. 7, inset),

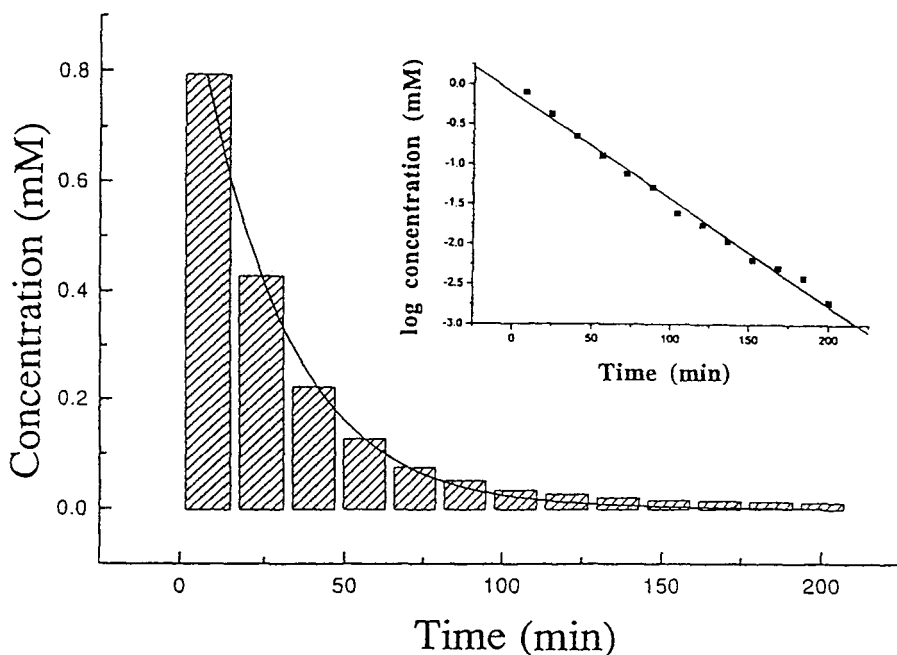


Fig. 7. Concentration versus time profile for a 70 mg/kg i.v. dose of DFMO in an awake, freely moving rat. Inset: plot of log concentration versus time.

indicating that the rapid i.v. dose of DFMO was distributed in the body according to a one-compartment model and eliminated by apparent first-order kinetics. The average half-life for an i.v. dose of DFMO ( $n = 4$ ) was  $21.0 \pm 4.8$  min.

#### 4. Conclusions

A capillary electrophoresis method for the analysis of CBI-DFMO derivatives in blood dialysates has been developed. The derivatization of DFMO using NDA and NaCN in pH 10 borate buffer produced the mono-CBI-DFMO derivative, which is UV active. For the CE separation, a phosphate run buffer (100 mM, pH 6.5) was found to provide the best separation of CBI-DFMO from the endogenous CBI-derivatized amino acids native to the dialysate samples. Peak height versus concentration was linear from 1.2 to 160  $\mu$ M with a correlation coefficient of 0.9995 (based on the final concentration after derivatization). The detection limit for DFMO in an i.v. dialysate was 5  $\mu$ M. The use of UV detection at 254 nm provided adequate sensitivity for the detection of the drug in blood microdialysates. The separation was faster and more efficient than those previously reported using LC with fluorescence detection. This method was used to monitor the pharmacokinetics of DFMO following an i.v. dose of 70 mg/kg of DFMO to awake, freely moving rats.

#### Acknowledgements

T.H. gratefully acknowledges the financial support of the National Cancer Institute through a NCI Training Grant at the University of Kansas. The authors thank Dr. M. Slavik for providing the DFMO sample and Nancy Harmony for help in the preparation of the manuscript.

#### References

- [1] A.E. Pegg and P.P. McCann, *Am. J. Physiol.*, 243 (1982) 212–221.
- [2] D. Kadmon, *J. Cell. Biochem.*, (1992) 122–127.
- [3] W.J. Moriconi and M. Slavik, *Kanser*, 16 (1986) 61–71.
- [4] J. Smithers, *Pharm. Res.*, 5 (1988) 684–686.
- [5] J. Grove, J.R. Fozard and P.S. Mamont, *J. Chromatogr.*, 223 (1981) 409–416.
- [6] J.L. Cohen, R.J. Ko, A.T. Ko, M.D. Shields and T.M. Gilman, *J. Pharm. Sci.*, 78 (1989) 114–116.
- [7] J.F. Stobaugh, A.J. Repta, L.A. Sternson and K.W. Garren, *Anal. Biochem.*, 135 (1983) 495–504.
- [8] J.F. Stobaugh, A.J. Repta and L.A. Sternson, *J. Pharm. Biomed. Anal.*, 4 (1986) 341–351.
- [9] S.M. Lunte and O. Wong, *LC·GC*, 7 (1989) 11–15.
- [10] M.F. Kilkenny, Ph.D. Dissertation, University of Kansas, 1990.
- [11] B. Nickerson and J.W. Jorgenson, *J. High Resolut. Chromatogr. Chromatogr. Commun.*, 11 (1988) 878–881.
- [12] P.L. Weber, T.J. O'Shea and S.M. Lunte, *J. Pharm. Biomed. Anal.*, 12 (1994) 319–324.
- [13] T.J. O'Shea, P.L. Weber, B.P. Bammel, C.E. Lunte, S.M. Lunte and M.R. Smyth, *J. Chromatogr.*, 608 (1992) 189–195.
- [14] R.T. Kennedy, M.D. Oates, B.R. Cooper, B. Nickerson and J.W. Jorgenson, *Science*, 246 (1989) 57–63.
- [15] T. Ueda, R. Mitchell, F. Kutamura, T. Metcalf, T. Kuwana and A. Nakamoto, *J. Chromatogr.*, 593 (1992) 265–274.
- [16] C.E. Lunte, D.O. Scott and P.T. Kissinger, *Anal. Chem.*, 63 (1991) 773A–780A.
- [17] D.O. Scott and C.E. Lunte, *Pharm. Res.*, 10 (1993) 335–342.
- [18] M. Telting-Diaz and C.E. Lunte, *Pharm. Res.*, 10 (1993) 44–48.
- [19] M. Telting-Diaz, D.O. Scott and C.E. Lunte, *Anal. Chem.*, 64 (1992) 806–810.
- [20] C.M. Riley, J.M. Ault, Jr. and C.E. Lunte, in C.M. Riley, W.J. Lough and I.W. Wainer (Editors), *Pharmaceutical and Biomedical Applications of Liquid Chromatography*, Pergamon, Oxford, 1994, p. 193.
- [21] J.M. Ault, C.M. Riley, N.M. Meltzer and C.E. Lunte, *Pharm. Res.*, 11 (1994) 1631–1639.
- [22] G.D. Fasman (Editor), *Practical Handbook of Biochemistry and Molecular Biology*, CRC Press, Boston, MA, p. 374.





ELSEVIER

Journal of Chromatography A, 716 (1995) 389–399

JOURNAL OF  
CHROMATOGRAPHY A

# Derivatization of dipeptides with 4-fluoro-7-nitro-2,1,3-benzoxadiazole for laser-induced fluorescence and separation by micellar electrokinetic chromatography

Ingegerd Beijersten, Douglas Westerlund\*

*Department of Analytical Pharmaceutical Chemistry, Uppsala University Biomedical Centre, P.O. Box 574, S-751 23 Uppsala, Sweden*

## Abstract

In capillary electrophoresis generally very small sample volumes are introduced, which often gives problems regarding determinations of low concentrations of the analytes. Frequently, therefore, they have to be transformed into products by suitable derivatization reagents. In this study 4-fluoro-7-nitro-2,1,3-benzoxadiazole (NBD-F) was used as a pre-capillary fluorogenic reagent for a series of dipeptides used as model compounds in order to study the characteristics of the derivatization procedure. Main emphasis was put on optimization of the reaction conditions using a chemometric approach involving a fractional factorial design for screening experiments and a central composite face-centred design for response surface modelling. The results showed that the reagent excess must be at least 70 times in order to get a linear response, the reaction mixture should consist of a phosphate buffer with low ionic strength (0.001) at pH 7 containing 15% of isopropanol. The presence of the micellar agent Brij 35 in the background electrolyte increased the fluorescence intensity of the analyte product at least 3 times, and the separation selectivity increased compared to using a neat buffer. Leu-Val, chosen as a model peptide for studies on quantitative determinations, could be determined at the level  $10^{-7}$  M (2 fmol injected) with a quantitative recovery and a relative standard deviation of 2.4%. The limit of detection was  $4 \cdot 10^{-9}$  M (70 amol injected).

## 1. Introduction

The determination of peptides present in complex matrices, like biological materials, in low concentrations requires generally derivatization procedures to be applied in combination with separation techniques like high-performance liquid chromatography (HPLC) or capillary electrophoresis (CE). Many different reagents have

been developed for the purpose, often being common for amino acids, peptides and proteins. The most used are probably *o*-phthalaldehyde (OPA) [1] and the related naphthalenedialdehyde [2]. For CE separations the derivatives are generally produced by off-line procedures [3–8], but post-capillary reactions have also been developed for OPA [9–12]. Post-capillary derivatization was advocated for the OPA reagent in studies on the analysis of some peptide-derived marine toxins due to degradation of the formed product [13]. Recently, OPA was utilized

\* Corresponding author.

in a pre-column reaction coupled on-line to CE separations on a microchip [14]. Fluorescein-isothiocyanate (FITC) was introduced as a marker for the detection of proteins a long time ago [15], and has in recent years also been applied for the laser-induced fluorescence detection (LIF) of very low amounts of amino acids [16–19] and peptides [20] in CE separations. A reagent, 3-(4-carboxybenzoyl)-2-quinolinecarboxaldehyde (CBQCA), designed to have spectral properties matching the output wavelength of the helium–cadmium laser (442 nm) and to give good migration behaviour of the products was presented by Novotny and co-workers [21]. The reagent was utilized in detection of small peptides [22] as well as larger ones [23] with cyclodextrin additives, and for the separation of amino acid homopolymers by capillary gel electrophoresis [24]. Other useful general fluorogenic reagents for peptide detection include fluorescamine [25,26] and 6-aminoquinolyl-N-hydroxy-succinimidyl carbamate [27]. In addition, reagents selective for arginine- [28,29] and tyrosine-containing [28] peptides have been presented.

For our studies an argon-ion laser with an output wavelength of 488 nm was available. Of the reagents discussed above only FITC and CBQCA have such spectral properties that they are potential candidates for use in combination with this laser. They were tested and compared with 4-fluoro-7-nitro-2,1,3-benzoxadiazole (NBD-F), and the latter was found to be the best reagent for the dipeptides used as model compounds in this study. NBD-F was introduced by Imai and Watanabe in 1981 [30] and univariate studies indicated that a reaction for 5 min at pH 7.5 and 70°C was optimal for secondary amino acids. The reagent has been applied extensively in HPLC for the analysis of amines and amino acids (for a review see Ref. [31]).

The optimization of the reaction conditions for tagging dipeptides with NBD-F was performed by a chemometric approach applying a fractional factorial design followed by response surface modelling. The separations were performed at high pH by micellar electrokinetic chromatography (MEKC) with the non-ionic surfactant Brij 35 as additive.

## 2. Experimental

### 2.1. Apparatus

The instrument used in the experiments was a Beckman P/ACE system 2050 with a laser Model 488 and data were collected and analyzed using a Micro Scan 2E ADI computer (Beckman Instrument, Palo Alto, CA, USA). The argon-ion laser gives excitation at 488 nm, and the emission wavelength was 523 nm. The capillaries were Beckman fused-silica with 75  $\mu\text{m}$  I.D., an effective length of 50 cm and a total length of 57 cm. The capillaries were thermostatted at 25°C. Before introduction of a new background electrolyte the capillaries were flushed with 0.1 M NaOH and water, then the capillaries were filled with new electrolyte and the system was allowed to equilibrate for about 10 min. The electrophoreses were carried out at a voltage between 9 and 15 kV. Samples were injected by pressure at 34 mbar (0.5 p.s.i.) for 5 s.

### 2.2. Chemicals

The background electrolyte consisted of boric acid p.A., phosphoric acid p.A. and sodium hydroxide p.A. from Merck (Darmstadt, Germany), diluted with deionized water. Methanol p.A. and isopropanol LiChrosolv were also from Merck. Ethanol (abs.) was from AB Kemetyl (Sweden).

The surfactant used was polyethylene glycol dodecyl ether (Brij 35) from FlukaBioChemie (Buchs, Switzerland).

The buffer solutions used in the reaction procedures were all prepared of chemicals from Merck and the quality was at least p.A.

The peptides were from Sigma (St. Louis, MO, USA), small amounts of CBQCA, FSE and NBD-F were gifts from Beckman; additional NBD-F was obtained from Molecular Probes (Eugene, OR, USA).

### 2.3. Reaction conditions

The reactions were initially performed according to guidelines from Beckman [32]: NBD-F in alcohol + the dipeptides in water + buffer pH 8

(2:2:1, v/v/v) were mixed, vortexed for 30 s, and the reaction was allowed to proceed for 20 min at 60°C. The concentration of alcohol in the mixture is then 40%. An aliquot of the reaction mixture was injected immediately after this period.

After the optimization studies the procedure was modified to give the highest yields: NBD-F (> 70 times in excess) in isopropanol + the dipeptides in water + phosphate buffer pH 7 were mixed and vortexed for 30 s, followed by a reaction time of 50 min at 56°C. The final concentration of NBD-F must be  $\geq 4 \cdot 10^{-4}$  M, and the volume of the reagent was chosen to give 15% of isopropanol in the final mixture. The ionic strength of the phosphate buffer was selected to give a ionic strength of 0.001 in the final mixture. Samples were then immediately injected for separation.

#### 2.4. Optimal background electrolyte

As a result of optimization studies the following composition of the background electrolyte was chosen: borate–phosphate (25/12.5 mM) buffer, pH 9 ( $I = 0.03$ ), containing 10 mM Brij 35. The use of a lower concentration of the micellar agent may in some cases be of advantage regarding selectivity.

#### 2.5. Chemometric evaluation

The program MODDE from Umetri (Umeå, Sweden) was used for design and evaluation of the chemometric studies.

### 3. Results and discussion

#### 3.1. Choice of reagent

In order to find a reagent suitable for use with the argon-ion laser available, with an output wavelength of 488 nm, four compounds were initially tested: FITC with an excitation wavelength maximum at 488 nm; CBQCA at 468 nm; 5-carboxyfluorescein succinimidyl ester (FSE), 491 nm; and NBD-F, 475 nm. Standard conditions recommended in the literature for an excess of the reagent [32] were used for the screening experiments, and Leu–Phe was selected as the model dipeptide. The results of this preliminary evaluation are given in Table 1.

With FITC the maximal fluorescence of the analyte was obtained after 4 h reaction, but many additional peaks originating from the reagent appeared in the electropherogram. It was concluded that a purification of the reagent or modified reaction conditions were necessary to develop FITC as a reagent useful for quantitative peptide assays. FITC has been frequently used as tag for amines, peptides and proteins giving derivatives with very intense fluorescence. However, according to our knowledge it has not been used for quantitative purposes; instead, a deficit of the reagent has been applied in the published reactions.

CBQCA was not tried extensively in the screening experiments, but the results indicated that the obtained derivative had a comparatively low fluorescence. One reason may be that the maximum excitation wavelength is about 20 nm away from the laser output. An advantage with

Table 1  
Preliminary evaluation of reagents

	FITC	CBQCA	FSE	NBD-F
Exc. wavelength (nm)	488	468	491	475
Reaction time (h)	4	1	1	0.3
Reaction temp.	RT <sup>a</sup>	RT	RT	60°C
Response	n.d. <sup>b</sup>	low	high	high
Reagent peaks	many	none	many	few
Reagent fluorescence	high	none	high	high

<sup>a</sup> Room temperature.

<sup>b</sup> Not determined.

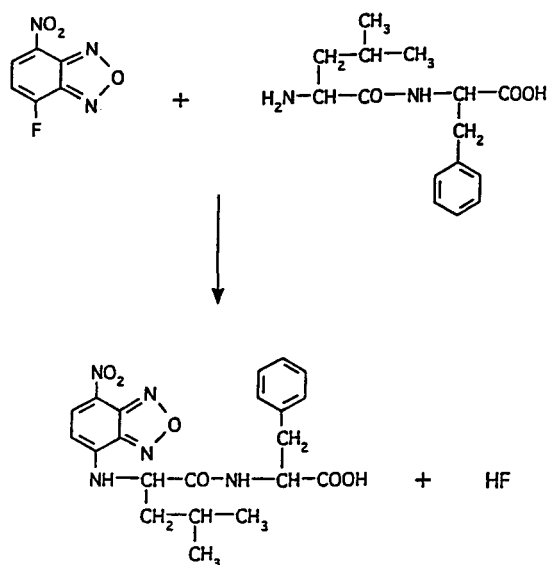


Fig. 1. Reaction of NBD-F with Leu-Phe.

CBQCA is a relatively fast reaction and that the reagent itself is non-fluorescent.

FSE with a maximum excitation wavelength close the laser light gave the highest response for the analyte product of all tested reagents, and the reaction time was relatively short (1 h). However, there were many additional potential interfering peaks in the electropherogram, indicating that an extensive clean up of the reagent

is necessary before it can be applied for quantitative purposes.

NBD-F, finally, gave a good response for the analyte peak after a short reaction time (less than 1 h) and the electropherogram was reasonably clean. In addition, its cheaper chloride analogue (NBD-Cl) was tried as a reagent. However, a disadvantage of that is a longer reaction time, increasing the risk for side reactions. Consequently, NBD-F was chosen as the most suitable reagent for further development. The reaction of this reagent with Leu-Phe is illustrated in Fig. 1. The product has an intact carboxyl function which will be charged at the slightly alkaline conditions used both in the reaction and during the capillary electroseparation presented below.

### 3.2. Preliminary screening of reaction conditions

#### Reagent excess

The reaction conditions used in the literature typically involve an excess of the reagent in slightly alkaline (pH 7–10) solutions containing an alcohol. Studies on the required excess of reagent were performed in solutions containing methanol, ethanol and isopropanol with borate-phosphate or bicarbonate buffers. The reaction time was 30 min and the temperature 56°C. A representative result is shown in Table 2, applying the reagent dissolved in isopropanol mixed

Table 2  
Dependence of reaction yield on reagent concentration and excess

Leu-Phe conc. (M)	Peak height (fluorescence) at NBD-F conc. (M)		
	$4.12 \cdot 10^{-5}$	$4.12 \cdot 10^{-4}$	$4.12 \cdot 10^{-3}$
$6 \cdot 10^{-8}$	–	0.7	–
$6 \cdot 10^{-7}$	0.36	7	–
$6 \cdot 10^{-6}$	–	71	114
$6 \cdot 10^{-6}$ (80% IPA)	–	30	–

Detection: LIF (488 nm). Capillary: Beckman fused-silica,  $570 \times 0.075$  mm I.D., effective length: 500 mm. Background electrolyte: 10 mM Brij 35 in borate-phosphate buffer, pH 9. Voltage: 10 kV. Injection: 34 mbar for 5 s. Reagent mixture: NBD-F in isopropanol-Leu-Phe in water- $\text{NaHCO}_3$  0.01 M (2:2:1) (40% isopropanol in the final mixture). Reaction time: 30 min. Reaction temperature: 56°C.

with 0.01 M NaHCO<sub>3</sub>; the analyte (Leu-Phe) was generally added dissolved in water in different concentrations. The background electrolyte used in the capillary electroseparations was a borate-phosphate buffer, pH 9, containing 10 mM of the micellar agent Brij 35. A linear response of analyte product peak heights was obtained in the concentration interval  $6 \cdot 10^{-8}$  to  $6 \cdot 10^{-6}$  M using an NBD-F concentration of  $4 \cdot 10^{-4}$  M. Increasing the reagent concentration ten times further gave an additional increase of the peak height. However, a too high reagent excess will increase the risk for the appearance of interfering peaks. On the other hand, decreasing the reagent concentration ten times gave a much lower response, even when keeping the reagent excess to ca. 70 times. Furthermore, when the analyte also was dissolved in the alcohol, giving a concentration of 80% in the reaction mixture, a considerably lower response was obtained. The result of the study indicates that the reagent must be added in a concentration  $\geq 4 \cdot 10^{-4}$  M at an excess of at least 70 times, and the concentration of the alcohol must be kept adequately low.

### Buffer

Studies performed at pH 8 using sodium bicarbonate, phosphate and phosphate-borate buffers indicated equivalency in response measured as peak heights in the electropherogram when either ethanol or isopropanol was the organic solvent. Bicarbonate gave higher response than phosphate-borate with methanol as the solvent; the levels were, however, much lower than when applying the other two solvents. The ionic strength of the buffer had a strong impact on the response; decreasing the buffer concentration ten times gave >3 times higher response for the model peptide (Leu-Phe). Phosphate buffer was selected for further studies, due to a better buffer capacity at pH  $\leq 8$  compared to bicarbonate.

### Reaction time and type of alcohol

As mentioned above, the presence of methanol in the reaction mixture gave a lower response than with ethanol or isopropanol, the difference

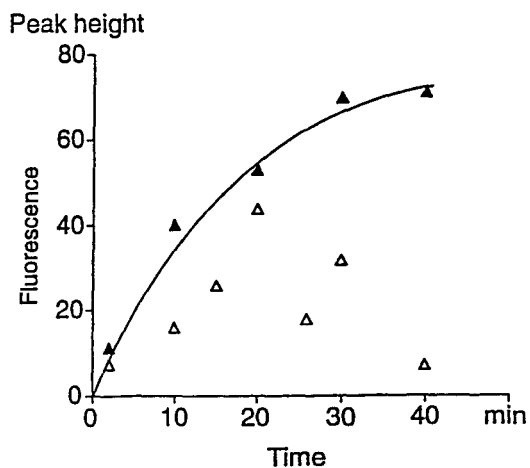


Fig. 2. Dependence of reaction yield on reaction time and type of alcohol ( $\Delta$  = ethanol;  $\blacktriangle$  = isopropanol). Reaction conditions: NBD-F ( $1 \cdot 10^{-3}$  M) in alcohol + Leu-Phe ( $1.5 \cdot 10^{-5}$  M) in water + sodium bicarbonate (0.01 M) pH 8 (2:2:1, v/v/v) were mixed, vortexed for 30 s, and the reaction was allowed to proceed for 20 min at 60°C. Background electrolyte: borate-phosphate (25/12.5 mM) buffer, pH 9 ( $I = 0.03$ ), containing 10 mM Brij 35.

was 2–3 times in peak height. A study on the reaction time was performed with ethanol and isopropanol, and the result is shown in Fig. 2. Reliable results were only obtained with isopropanol indicating that 30–40 min gave the maximal response. The data obtained using ethanol was severely scattered, and isopropanol was consequently chosen for further studies.

### 3.3. Conditions for capillary electrophoresis

A pH of 9–10 was chosen for the background electrolyte (BGE), mainly because the fluorescence intensity is maximal at high pH; in addition this will match the injected sample since the derivatization is performed at about the same pH, and it will also ensure complete ionization of the carboxylate group of the product, resulting in a high electrophoretic mobility. Scouting experiments showed that a borate-phosphate buffer at pH 9 gave much higher peak height, about 16 times, than a neat phosphate buffer at pH 10. It was also an advantage to use a low ionic strength of the buffer, i.e. applying the concentrations 25 and 12.5 mM of borate and phosphate gave a 1.4

times higher signal compared to twice the concentrations of the buffer components. It is well-known that fluorescence intensities may strongly depend on the environment, and the addition of the non-ionic micellar agent Brij 35 gave a further significant increase of the peak height, as illustrated in Fig. 3. The peak height of the analyte increased about 3 times when changing from neat buffer to a BGE containing 5 mM of Brij 35. Increasing the concentration of the

micellar agent further gave additionally higher signals. This indicates that the reaction product gives a more intense fluorescence at more non-polar conditions. A similar increase was observed for the main reagent peak, which probably is the corresponding phenolic compound ( $-F$  is substituted by  $-OH$ ), which at least partly is charged at the conditions used. The presence of the nitro group in *para*-position will increase the acidity of the phenol. The electroosmosis mi-

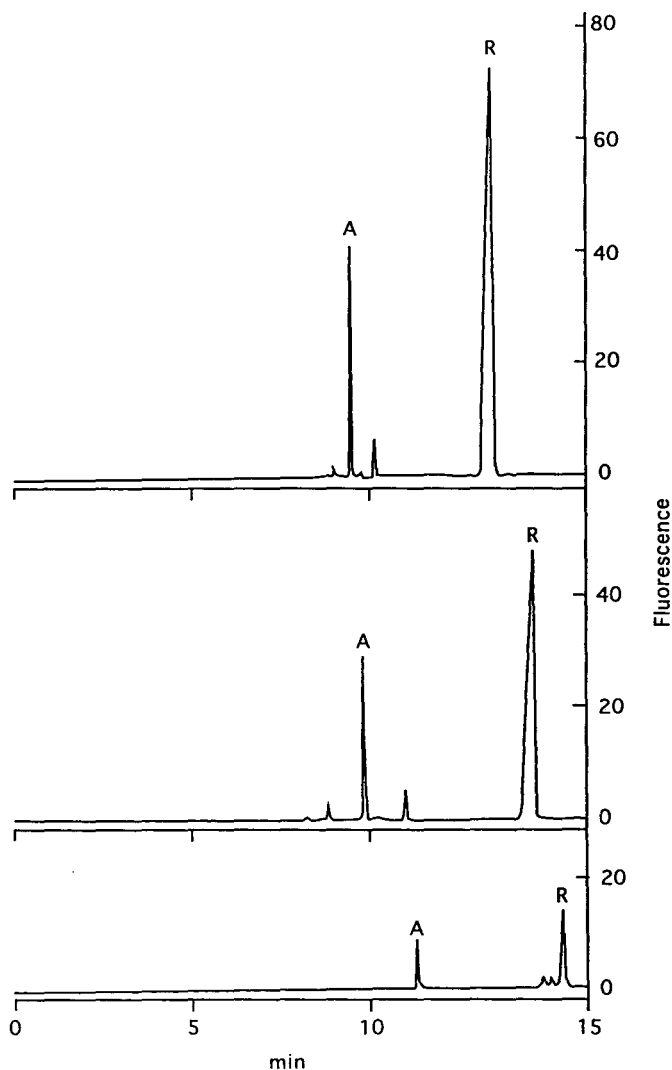


Fig. 3. Effects of Brij 35 in background electrolyte on fluorescence intensity. Background electrolyte: borate-phosphate buffer, pH 9 ( $I = 0.03$ ), with or without Brij 35. The concentration of Brij 35 is increased from the bottom to the top electropherogram: 0, 5 and 10 mM, respectively. Voltage: 10 kV.

grates at 8–8.5 min in the different systems, corresponding to an apparent mobility of  $(6-5.6) \cdot 10^{-4} \text{ cm}^2/\text{V}\cdot\text{s}$ ; the mobility decreasing somewhat with increasing micellar concentration. The micelles are non-ionic and migrate with the electroosmosis, and this means that the migration time of the analyte will decrease due to distribution to the micelles, since the analyte product is anionic and has an electrophoretic mobility towards the anode. The selectivity between the analyte and reagent products peaks increased in going from 0 to 5 mM Brij 35 (Table 3), and in addition some small impurity peaks became visible in the micellar system that were not observed in neat buffer. Some of those peaks may be hidden in the analyte peak when using plain buffer as the BGE. However, increasing the micellar concentration further, the selectivity decreases again, due to a too strong distribution of the components to the micellar phase. The efficiency is high in the systems (see Table 2) and increases with increasing micellar concentration from about 360 000 plates per m in the neat buffer system up to 540 000 with 10 mM Brij (the voltage was 10 kV).

### 3.4. Chemometric screening

Applying the experiences from the preliminary screening experiments described above, the most important variables were selected for a fractional factorial design experimental approach. It was decided to keep the reagent concentration con-

stant at an excess of 100 times using the concentration  $4 \cdot 10^{-4} \text{ M}$  in the derivatization of the model peptide Leu-Phe ( $4 \cdot 10^{-6} \text{ M}$ ). The variables studied were reaction time and temperature, ionic strength, pH and the concentration of isopropanol at the two levels given in Table 4. Sixteen experiments were performed according to the design also shown in the table. The peak areas were used as responses and they were plotted on a cumulative normal probability scale (*N*-plot), see Fig. 4. It was concluded that the three most important variables for the yield were the ionic strength, the pH and the amount of isopropanol, and the results indicated that lower values of all three factors than those chosen for this experimental series should be utilized. In addition there were some important interaction terms: temperature–ionic strength, temperature–pH and ionic strength–pH. Interestingly, the

Table 4  
Chemometric screening; fractional factorial design

Variable	Low level (-)	High level (+)
1. Time (min)	30	50
2. Temp. (°C)	56	76
3. Ionic strength	0.002	0.01
4. pH	8	9
5. Isopropanol (%)	20	40

Exp. no.	Variable				
	1	2	3	4	5
1	+	-	-	-	-
2	-	+	-	-	-
3	-	-	+	-	-
4	+	+	+	-	-
5	-	-	-	+	-
6	+	+	-	+	-
7	+	-	+	+	-
8	-	+	+	+	-
9	-	-	-	-	+
10	+	+	-	-	+
11	+	-	+	-	+
12	-	+	+	-	+
13	+	-	-	+	+
14	-	+	-	+	+
15	-	-	+	+	+
16	+	+	+	+	+

Table 3  
Efficiency and selectivity

Brij 35 conc. (mM)	Efficiency ( <i>N</i> /m)	$\alpha^a$ ( $t_{m,R}/t_{m,A}$ )
0	360 000	1.35
5	400 000	1.48
10	540 000	1.42

Detection: LIF. Capillary: Beckman fused-silica,  $570 \times 0.075$  mm I.D., effective length: 500 mm. Background electrolyte: borate-phosphate buffer, pH 9, with or without Brij 35. Voltage: 10 kV. Current: 25  $\mu\text{A}$ . Injection: 34 mbar for 5 s.

<sup>a</sup>  $t_{m,R}$  = migration time of reagent;  $t_{m,A}$  = migration time of analyte.

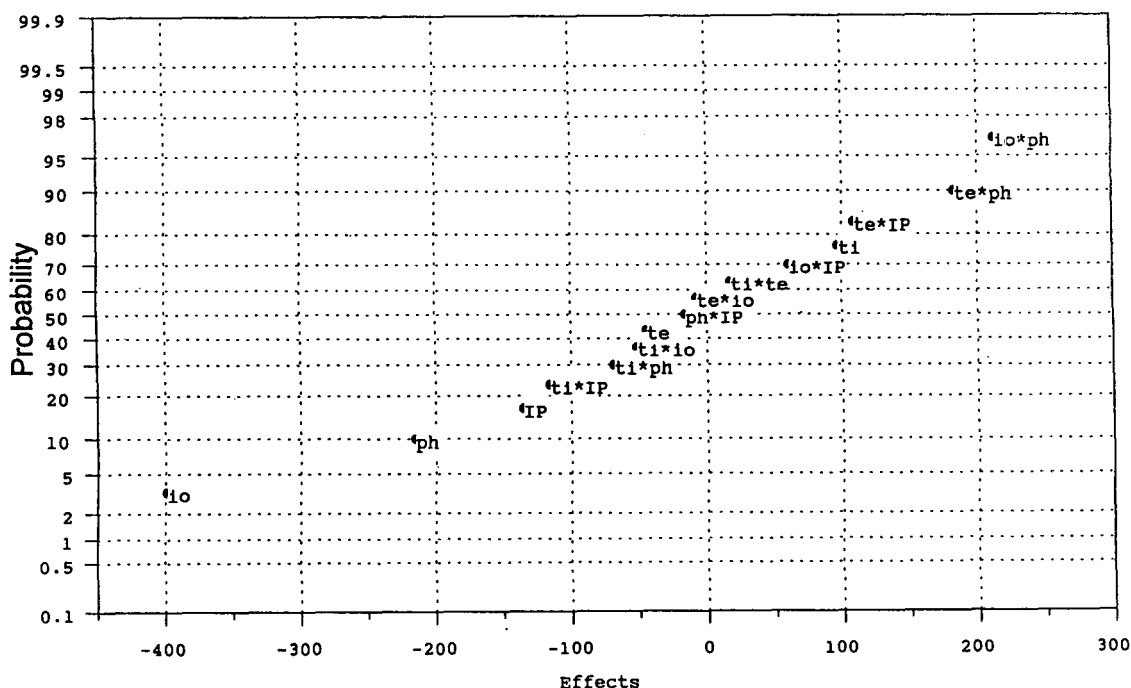


Fig. 4. *N*-plot of effects obtained after screening according to a fractional factorial design. Symbols: io = ionic strength; ph = pH; IP = isopropanol concentration; te = reaction temperature; ti = reaction time.

temperature itself had no significant effect on the response. There was also an indication that a longer reaction time had some impact on the outcome of the reaction. For further optimization of the reaction the three most important variables (ionic strength, pH and amount of isopropanol) were studied by response surface modelling, with the temperature and time kept constant at 56°C and 50 min, respectively.

### 3.5. Response surface modelling

A central composite face-centred (CCF) design was chosen for the response surface modelling (RSM) experiments. The ranges studied for the three variables were: ionic strength 0.001–0.002; pH 7.5–8; isopropanol 10–20%, and the experiments were run according to the worksheet given in Table 5. Four experiments (9, 10, 11 and 17) were unsuccessful according to the preliminary analysis by residuals plots and op-

timizations of the correlation between observed and predicted data, and were removed from the final analysis. The quadratic ionic-strength term gave a low significance according to an ANOVA analysis and was also eliminated. The multiple linear regression analysis gave an acceptable summary of fit with  $R^2 = 0.982$ ,  $R^2_{\text{adj}} = 0.953$  and  $Q^2 = 0.710$ , and a condition number of 4.683. The most important factors were the quadratic isopropanol term followed by the ionic strength and pH. The 3D contour plots (Fig. 5) show that there is an optimal isopropanol concentration (15%) and that the lowest values of the ionic strength and pH give the best response, indicating that even lower values would be optimal. However, it is not reasonable to use a lower ionic strength since this would give too low buffer capacity in the reaction, in which a strong acid (HF) is generated. The pH range chosen for the RSM studies was, however, too limited, and additional univariate experiments keeping the isopropanol amount to 15% and the ionic



Table 5  
Worksheet for response surface modelling with a CCF design

ExpNo	ExpName	RunOrder	InOut	Ionic	pH	IPA	Area
1	N1	11	in	0.001	7.5	10	3049
2	N2	15	in	0.002	7.5	10	2983
3	N3	15	in	0.001	8	10	2757
4	N4	3	in	0.002	8	10	2583
5	N5	10	in	0.001	7.5	20	3125
6	N6	7	in	0.002	7.5	20	2854
7	N7	17	in	0.001	8	20	3103
8	N8	12	in	0.002	8	20	2589
9	N9	2	out	0.001	7.75	15	2596
10	N10	4	out	0.002	7.75	15	2563
11	N11	8	out	0.0015	7.5	15	2878
12	N12	6	in	0.0015	8	15	3100
13	N13	14	in	0.0015	7.75	10	2653
14	N14	5	in	0.0015	7.75	20	2843
15	N15	13	in	0.0015	7.75	15	3075
16	N16	9	in	0.0015	7.75	15	3029
17	N17	1	out	0.0015	7.75	15	1057
18	N18	16	in	0.0015	7.75	15	3066

Parameters: ionic strength (Ionic), pH, isopropanol conc. (IPA).

strength at 0.001 showed that pH 7 was optimal (pH 6.5 gave lower response).

### 3.6. Separation and quantitation

An illustration of the separation capability of the MEKC system is given in Fig. 6, where ten

closely related dipeptides are separated after a simultaneous derivatization by the optimized reaction procedure. They are all migrating within a short time interval between 10 and 13 min, the reagent product peak does not interfere, since it migrates at 14.5 min.

A preliminary investigation of the potential of

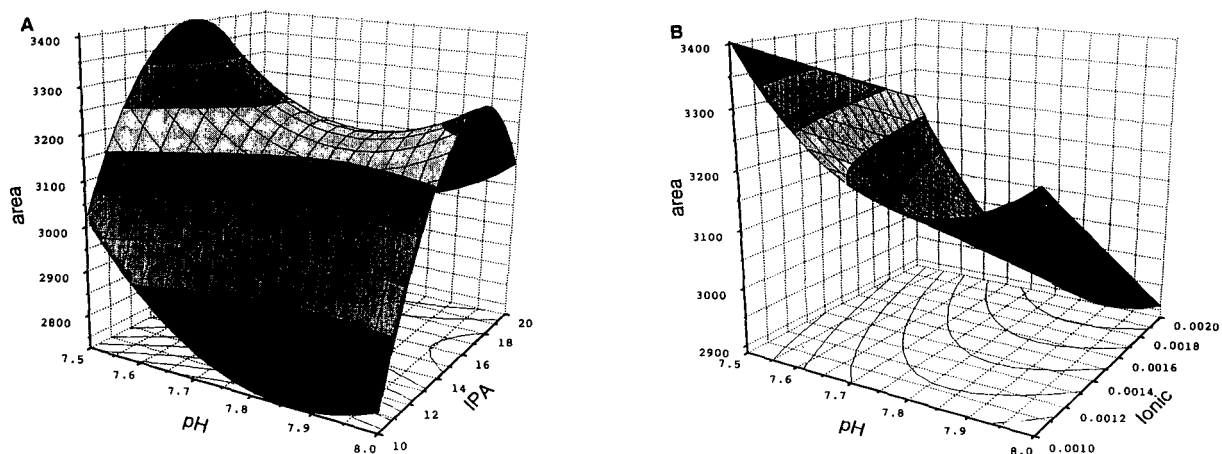


Fig. 5. Response surface modelling according to a central composite face-centred design: 3D contour plots. Experimental conditions: see Table 4. (A) Fixed parameter: ionic strength = 0.001. (B) Fixed parameter: isopropanol concentration = 15%.

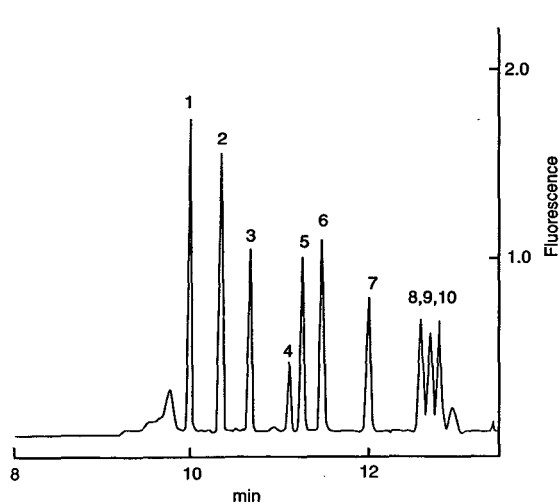


Fig. 6. MEKC separation of ten dipeptides. Reaction and capillary electrophoretic conditions according to the optimal procedures described in the Experimental section. Peptide concentrations:  $4 \cdot 10^{-7}$  M. Peptides: 1 = Phe-Phe; 2 = Leu-Phe; 3 = Phe-Leu; 4 = Phe-Val; 5 = Leu-Leu; 6 = Leu-Val; 7 = Leu-Ala; 8 = Phe-Ser; 9 = Leu-Ser; 10 = Leu-Met. The reagent peak migrates at 14.5 min. Voltage: 9 kV; current: 20  $\mu$ A.

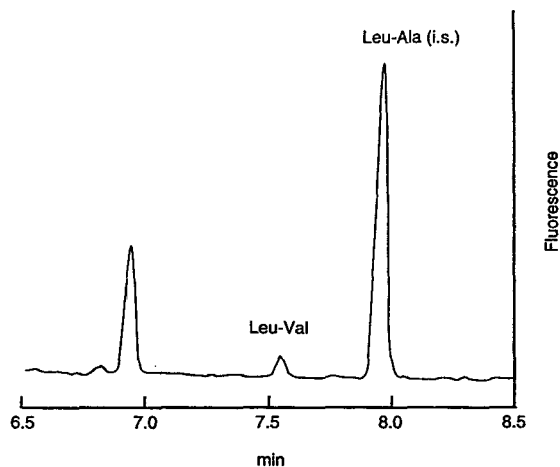


Fig. 7. Electropherogram from a quantitative analysis of Leu-Val. Reaction conditions: NBD-F ( $4 \cdot 10^{-4}$  M) in phosphate buffer, pH 7 ( $I=0.001$ ), and isopropanol (13%); temperature 56°C; and reaction time 50 min. Background electrolyte: borate-phosphate buffer, pH 9, with 11 mM Brij 35. Leu-Val concentration:  $5.2 \cdot 10^{-8}$  M (0.7 fmol injected). Leu-Ala concentration:  $1.1 \cdot 10^{-7}$  M.

the procedure for quantitative determinations was performed with Leu-Val as the analyte and utilizing Leu-Ala as the internal standard. A typical electropherogram is shown in Fig. 7, with 0.7 fmol of Leu-Val migrating before the internal standard at 7.5 min. Results from quantitative studies at two levels are given in Table 6, illustrating quantitative recoveries and good precisions at the levels  $10^{-7}$  M (2 fmol injected) and

$10^{-6}$  M (20 fmol), 2.4 and 3.8%, respectively; six samples at each concentration level were determined. Two separate standard curves had to be used to get good recoveries; in the broad concentration range 12 standards were used, while 8 standards comprised the curve in the lower concentration range. In each case they were constructed from two independent weighings of the analyte and internal standard. The limit of detection at a signal-to-noise ratio equal

Table 6  
Recovery and precision

Range of standard curve ( $10^7$ M)	$n^c$	Added concentration ( $10^7$ M)	Determined concentration ( $10^7$ M)	R.S.D. (%)	$n^d$
0.52–29.1 <sup>a</sup>	12	1.04	1.20	2.5	6
		10.1	10.1	3.8	6
0.54–2.33 <sup>b</sup>	8	1.01	1.02	2.4	6

Analyte: Leu-Val. Internal standard: Leu-Ala ( $3.4 \cdot 10^{-7}$  <sup>a</sup> respectively  $1.1 \cdot 10^{-7}$  <sup>b</sup> M). Linear regression: <sup>a</sup>  $y = 0.0061 + 0.122x$  ( $r = 0.9997$ ); <sup>b</sup>  $y = 0.0032 + 0.368x$  ( $r = 0.9993$ ).

<sup>c</sup> Number of standards; at six (<sup>a</sup>) and four (<sup>b</sup>) concentration levels from two independent weighings.

<sup>d</sup> Number of samples.

to 3 was determined to be  $4 \cdot 10^{-9}$  M (70 amol injected).

#### 4. Conclusions

The main parameters in optimizing the yield for the reaction between dipeptides and NBD-F were determined by chemometric studies applying a fractional factorial design for screening purposes and a central composite face-centred design for response surface modelling. It was found that the reagent excess should be >70 times, the ionic strength should be low ( $\leq 0.001$ ), optimal pH was 7 and the amount of 2-propanol should be ca. 15%. The derivatization products were anionic, and femto- to attomole amounts of a series of closely related dipeptides could be separated in a background electrolyte of pH 9 with Brij 35 as the micellar agent. The selectivity was improved in the micellar systems compared to applying a neat buffer as the background electrolyte. Furthermore, the use of high pH was necessary to get high fluorescence, and the intensity was further improved about four times in the presence of micelles. Using an argon-ion laser with an output wavelength of 488 nm, mass detection limits of about 70 amol were achieved, and the peptides could be quantified at the level  $10^{-7}$  M (ca. 2 fmol injected) with a relative standard deviation of 2.4%. In future studies the reagent will be applied for assays of larger peptides, like neuropeptides, and possibly also studied for its usefulness in peptide mapping of proteins.

#### References

- [1] M. Roth, *Anal. Chem.*, 43 (1971) 880.
- [2] R.G. Carlson, K. Srinivasachar, R.S. Givens and B.K. Matuszewski, *J. Org. Chem.*, 51 (1986) 3978.
- [3] M.C. Roach and M.D. Harmony, *Anal. Chem.*, 59 (1987) 411.
- [4] B.K. Matuszewski, R.S. Givens, K. Srinivasachar, R.G. Carlson and T. Higuchi, *Anal. Chem.*, 59 (1987) 1102.
- [5] B. Nickerson and J.W. Jorgenson, *J. High Resolut. Chromatogr.*, 11 (1988) 878.
- [6] B. Nickerson and J.W. Jorgenson, *J. High Resolut. Chromatogr.*, 11 (1988) 533.
- [7] K.C. Waldron, S. Wu, C.W. Earle, H.R. Harke and N.J. Dovichi, *Electrophoresis*, 11 (1990) 777.
- [8] T. Ueda, R. Kitamura, R. Mitchell, T. Metcalf, T. Kuwana and A. Nakamoto, *Anal. Chem.*, 63 (1991) 2979.
- [9] D.J. Rose, Jr. and J.W. Jorgenson, *J. Chromatogr.*, 447 (1988) 117.
- [10] S.L. Pentoney, Jr., X. Huang, E.S. Burgi and R.N. Zare, *Anal. Chem.*, 60 (1988) 2625.
- [11] B. Nickerson and J.W. Jorgenson, *J. Chromatogr.*, 480 (1989) 157.
- [12] M. Albin, R. Weinberger, E. Sapp and S. Moring, *Anal. Chem.*, 63 (1991) 417.
- [13] B.W. Wright, G.A. Ross and R.D. Smith, *J. Microcol. Sep.*, 1 (1989) 85.
- [14] S.C. Jacobson, R. Hergenröder, A.W. Moore, Jr. and J.M. Ramsey, *Anal. Chem.*, 66 (1994) 4127.
- [15] S. Udenfriend, *Fluorescence Assay in Biology and Medicine*, Academic Press, New York, 1962, p. 220.
- [16] Y.-F. Cheng and N.J. Dovichi, *Science*, 242 (1988) 562.
- [17] S. Wu and N.J. Dovichi, *J. Chromatogr.*, 480 (1989) 141.
- [18] T. Higashijima, T. Fuchigami, T. Imasaka and N. Ishibashi, *Anal. Chem.*, 64 (1992) 711.
- [19] J. Mattusch and K. Dittrich, *J. Chromatogr. A*, 680 (1994) 279.
- [20] J.Y. Zhao, K.C. Waldron, J. Miller, J.Z. Zhang, H. Harke and N.J. Dovichi, *J. Chromatogr.*, 608 (1992) 239.
- [21] J. Liu, Y.-Z. Hsieh, D. Wiesler and M.V. Novotny, *Anal. Chem.*, 63 (1991) 408.
- [22] J. Liu, K.A. Cobb and M.V. Novotny, *J. Chromatogr.*, 519 (1990) 189.
- [23] M. Novotny, K.A. Cobb and J. Liu, *Electrophoresis*, 11 (1990) 735.
- [24] V. Dolnik and M.V. Novotny, *Anal. Chem.*, 65 (1993) 563.
- [25] J.W. Jorgenson and K.D. Lukacs, *Anal. Chem.*, 218 (1981) 209.
- [26] J.W. Jorgenson and K.D. Lukacs, *J. High Resolut. Chromatogr. Chromatogr. Commun.*, 4 (1981) 230.
- [27] K.M. De Antonis, P.R. Brown, Y.-F. Cheng and S.A. Cohen, *J. Chromatogr. A*, 661 (1994) 279.
- [28] K.A. Cobb and M.V. Novotny, *Anal. Biochem.*, 200 (1992) 149.
- [29] K.A. Cobb and M.V. Novotny, *Anal. Chem.*, 64 (1992) 879.
- [30] K. Imai and Y. Watanabe, *Anal. Chim. Acta*, 130 (1981) 377.
- [31] K. Imai, S. Uzu and T. Toyooka, *J. Pharm. Biomed. Anal.*, 7 (1990) 1395.
- [32] Beckman Instruction 015-360808-A, 1992, LiFluor.





ELSEVIER

Journal of Chromatography A, 716 (1995) 401–412

JOURNAL OF  
CHROMATOGRAPHY A

# Capillary zone electrophoretic resolution of recombinant human bone morphogenetic protein 2 glycoforms

## An investigation into the separation mechanisms for an exquisite separation

Kalvin Yim\*, Joan Abrams, Amy Hsu

Genetics Institute, 1 Burt Road, Andover, MA 01810, USA

### Abstract

Recombinant human bone morphogenetic protein 2 (rhBMP-2) is a disulfide-linked homodimeric glycoprotein ( $M_r = 30\ 000$ ) which induces bone formation *in vivo* in several animal model systems. In this paper, we report the separation of a homogeneous rhBMP-2 sample into nine peaks by capillary zone electrophoresis (CZE), using a simple, pH 2.5, phosphate buffer containing no additives. The nine peaks have been identified to be glycoforms of rhBMP-2 [designated as (rhBMP-2)<sub>2</sub>-(GlcNAc)<sub>4</sub>(Man)<sub>Z</sub>, where Z varies from 10 to 18]. The difference between any adjacent pair of peaks is only one mannose residue ( $M_r = 162$ ). The ability of CZE to resolve rhBMP-2 glycoforms having the same charge and differing only 0.5% in molecular mass, without resorting to chemical complexation, is both unexpected and intriguing. Possible mechanisms explaining how the additional mannose can affect the mobility of rhBMP-2 glycoforms were explored. Zeta potentials of various glycoforms were calculated from their mobilities and interpreted in light of diffuse double layer parameters. Our results suggest that CZE employing a low-pH buffer, where proteins are highly charged, may be uniquely suitable for complex protein glycoform analysis.

### 1. Introduction

#### 1.1. Overview

Glycoproteins usually exist as heterogeneous populations of glycosylated variants (glycoforms) in which assemblies of different oligosaccharides are attached to each glycosylation site post-translationally. There is increasing evidence that the carbohydrate moieties of glycoproteins play major roles in their structures and functions [1–3]. Traditionally, glycans are studied only after

they are enzymatically released from the glycoproteins. High-performance capillary zone electrophoresis (CZE) is emerging as a technique for studying intact glycoproteins [4–12]. Glycoform analysis is particularly challenging because of the enormous diversity of oligosaccharide structures. For example, four different amino acids can only form 24 different tetrapeptides, whereas four different monosaccharides can form 36 000 tetrasaccharides.

There have been numerous reports on the separation of protein glycoforms using CZE [4–9]. However, the identities of the resolved peaks were generally not reported. As a result, it is

\* Corresponding author.



oligomannose 9 structure with the endoglycosidase H (Endo-H) and  $\alpha(1-2)$ mannosidase cleavage sites indicated, respectively.

### 1.3. Diffuse double layer model

Fig. 3 models a diffuse double layer around a charged colloidal particle, a protein molecule, for instance, in an electrolyte solution. In any electrolyte solution, there are counterions. Some counterions may be associated rather tightly (fixed diffuse layer), while others more loosely (mobile diffuse layer). The electrolyte forms an ion atmosphere around the particle, the ion atmosphere can effectively reduce the net charge on the protein because oppositely charged ions will tend to be attracted to the protein. The interface between the fixed portion of diffuse layer and the mobile portion of diffuse layer is called the surface of shear or the slip plane. It is

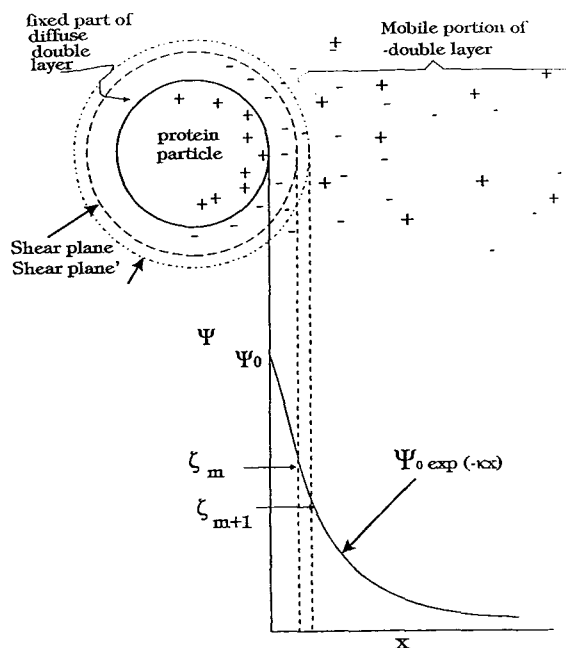


Fig. 3. A diagrammatic representation of a charged colloidal particle in an electrolyte solution, showing the relationship between the fixed and mobile parts of the diffuse double layer. Zeta potential  $\zeta_m$  is the potential at the shear plane. If the shear plane was pushed outward (shear plane'), the zeta potential will decrease to  $\zeta_{m+1}$ .

customary to regard the charges as a continuous distribution and to ignore individual charges. The variation of electrostatic potential with distance from a charged surface of arbitrary shape in a electrolyte solution is a classical electrostatic problem described by the Poisson–Boltzmann equation,

$$\nabla^2 \Phi = \kappa^2 \Phi \quad (1)$$

where  $\kappa$  is given by

$$\kappa = \left( \frac{8\pi N_0 e^2}{1000 \epsilon kT} \right)^{1/2} I^{1/2} \quad (2)$$

The ionic strength,  $I$ , is sum over all molar concentrations,  $C_i$ , and charges of species in the solution:

$$I = \frac{1}{2} \sum C_i Z_i^2 \quad (3)$$

The solution of Eq. 1 describing the potential at a distance  $x$  away from a uniformly charged sphere of radius  $a$  in an electrolyte solution has the form

$$\Psi = \Psi_0 \exp(-\kappa x) \quad (4)$$

where  $a \gg r$ ,  $\Psi$  is the potential at a distance  $x$  away from the surface of the particle,  $Z$  is the charge of the particle,  $e$  is the charge of an electron,  $\epsilon$  is the permittivity of the electrolyte and  $\Psi_0$  is the potential at the Stern layer. The equation indicates that the potential drops as an exponential function of distance  $x$  from the surface of the particle. The parameter  $\kappa^{-1}$  has the dimension of length and is sometimes called the double layer thickness. The  $\kappa$  parameter regulates how fast the potential of an ion falls off in solution. And  $\kappa^{-1}$  is the distance within the double layer through which the potential drops 37% ( $1/e$ ). It is evident from Eq. 3 that the higher the ionic strength, the more effectively the potential of an ion is screened. In a 0.1 M solution of phosphoric acid,  $\kappa^{-1}$  has a value of approximately 3 Å.

The mobility of a spherical molecule with radius  $a$  has been shown to be [20],

$$\mu = 2 \frac{\epsilon \zeta f_1(\kappa a)}{3\eta} \quad (5)$$

where  $f_1$  is the Henry function, which monotonically increases from 1.0 at  $\kappa a = 0$  to 1.5 at  $\kappa a = \infty$ , in which case the equation reduces to the Helmholtz–Smoluchoski equation (Eq. 6) for the electrolysis of large smooth particles [20].

$$\mu = \frac{\epsilon \xi}{\eta} \quad (6)$$

## 2. Experimental

### 2.1. Instrumentation

All capillary electrophoresis experiments were performed on the BioFocus-3000 capillary electrophoresis system from Bio-Rad Laboratories (Hercules, CA, USA). All the capillaries used were precoated capillaries furnished in the BioFocus cartridge assembly kit (50  $\mu\text{m}$  I.D.  $\times$  350  $\mu\text{m}$  O.D.  $\times$  50 cm) from Bio-Rad Laboratories. The capillaries were cut to desired lengths by the user (29 cm and 50 cm, respectively). The cartridge temperature was set at 20°C. Typically, injections were made electrophoretically at 6 to 12 kV for 4 to 8 s and running voltage was 5 to 12 kV. Detection was performed by UV absorbance at 200 nm. All rhBMP-2 samples were either buffer exchanged into or diluted with 10 mM phosphoric acid prior to CZE analysis. The running buffer was 100 mM phosphate buffer, pH 2.5.

Oligomannose analysis was done on a Dionex (Sunnyvale, CA, USA) high-pH anion-exchange chromatography with pulsed amperometric detection (HPAE–PAD) system consisting of a Bio LC gradient pump, a PAD2 detector and a PA-100 (250  $\times$  4 mm I.D.) column. Eluent A was 100 mM sodium hydroxide and eluent B was 100 mM sodium acetate in 100 mM sodium hydroxide. The gradient was 0% B to 100% B in 40 min. The flow-rate was 1.0 ml/min and detection was by PAD with a gold working electrode and triple-pulse amperometry.

Peptide mapping and fractionation were performed on a Hewlett-Packard (Palo Alto, CA, USA) 1090 HPLC with a Vydac (Sigma Chromatography, St. Louis, MO, USA) C<sub>18</sub> or C<sub>4</sub> column (25  $\times$  0.46 cm I.D.). The flow-rate was

1.0 ml/min. Solvent A was 4 mM heptafluorobutyric acid (HFBA), 6 mM trifluoroacetic acid (TFA) in water and solvent B is the same in 95% acetonitrile. The gradient was 11% B to 100% B in 75 min. Detection was at 200 nm.

Fast atom bombardment mass spectrometry was done on the HX110HF/HX110HF tandem mass spectrometer by JEOL (Peabody, MA, USA). Matrix-assisted laser desorption ionization-time of flight (MALDI-TOF) mass spectrometry was done on a Bruker (Billerica, MA, USA) REFLEX mass spectrometer equipped with a reflector.

### 2.2. Reagents and materials

rhBMP-2 was provided by the Genetics Institute (Andover, MA, USA). Endoproteinase Asp-N (Asp-N) was purchased from Boehringer Mannheim (Indianapolis, IN, USA). Endoglycosidase-H (Endo-H) was obtained from Genzyme (Cambridge, MA, USA). *Aspergillus saitoi*  $\alpha(1-2)$ -mannosidase [ $\alpha(1-2)$ -mannosidase] was purchased from Oxford GlycoSystems (Rosedale, NY, USA). Trifluoroacetic acid (TFA) and heptafluorobutyric acid (HFBA) and dithiothreitol (DTT) were purchased from Pierce (Rockford, IL, USA). Iodoacetic acid, sodium salt obtained from Aldrich (Milwaukee, WI, USA). Trizma Base, disodium EDTA, calcium chloride, guanidine HCl and glycerol from Sigma (St. Louis, MO, USA). HPLC grade acetonitrile was obtained from Burdick and Jackson (Muskegon, MI, USA).

### 2.3. Sample preparation

#### *Endo-H digestion*

rhBMP-2 and glycopeptide D5 samples were buffer exchanged into a pH 5.5, 10 mM sodium phosphate solution for endoglycosidase-H (Endo-H) digestion. A sample of rhBMP-2 (2.5 mg/ml) or D5 peptide was incubated with 40 mU/ml of Endo-H (specific activity = 40 U/mg) for 16 h at 37°C. The pH of the digested samples was adjusted to 2.5 using 0.1 M HCl before CZE analysis.



### $\alpha(1-2)$ Mannosidase digestion

rhBMP-2 was digested to rhBMP-2<sub>2</sub>(GlcNAc)<sub>4</sub>-(Man<sub>5</sub>,Man<sub>5</sub>) with  $\alpha(1-2)$ mannosidase at an enzyme/protein ratio of 50 mU/1 mg in 1 ml of sodium acetate, pH 5, at 37°C for 48 h.

### Reduction and carboxymethylation of rhBMP-2

A 10- $\mu$ l aliquot of 0.1 M dithiothreitol was added to 250  $\mu$ g rhBMP-2 in 480  $\mu$ l 0.5 M Tris buffer, 6 M guanidine, 5 mM EDTA, pH 8.5. The mixture was spun for 5 min on a bench centrifuge, layered with argon and was incubated at 37°C for 1.5 h. After the addition of 10  $\mu$ l 250 mM iodoacetic acid, the reaction mixture incubated under argon for 1 h in darkness. The sample was immediately desalted on RP-HPLC (C<sub>4</sub> column) and freeze dried.

### Glycan mapping

Oligomannoses were released from rhBMP-2 by Endo-H digestion. The deglycosylated protein was removed by centrifugation in a Amicon (Beverly, MA, USA) microcon-3 microconcentrator. Desalting was achieved through chromatography on a Bio-Gel P-2 column from Bio-Rad (Hercules, CA, USA) Oligomannoses were fractionated on a Dionex (Sunnyvale, CA, USA) CarboPac PA-100 column with pulsed amperometric detection. A gradient of sodium acetate from 0 to 100 mM over 40 min was used [21–22].

## 3. Results and discussion

### 3.1. Mobility calculations

A typical electropherogram of rhBMP-2 is shown in Fig. 4. The electropherogram shows nine peaks. The migration times of the nine peaks and their respective mobilities are summarized in Table 1. The average mobility ( $\mu_{ave}$ ) is  $1.32 \times 10^{-4} \text{ cm}^2 \text{ V}^{-1} \text{ s}^{-1}$  and the difference in mobility between adjacent peaks ( $\Delta\mu$ ) is  $0.100 \times 10^{-4} \text{ cm}^2 \text{ V}^{-1} \text{ s}^{-1}$ . The efficiency  $N$  of the separation is approximately 350 000 theoretical plates per 50 cm and the resolution ( $R_s$ ) is estimated to be 1.12.

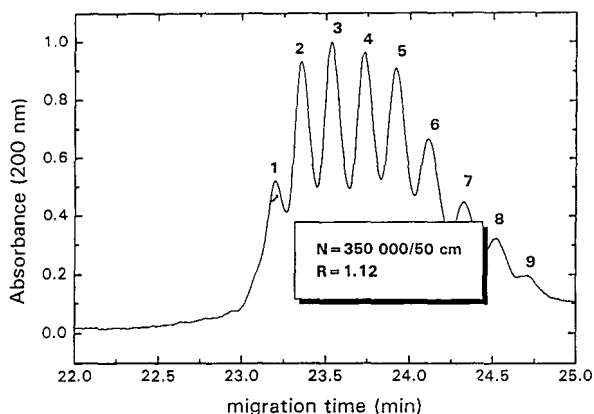


Fig. 4. CZE of rhBMP-2 in a 50 cm  $\times$  50  $\mu$ m I.D. Bio-Rad, coated capillary. Sample was electroinjected for 4–8 s at 6–12 kV in 0.1 M phosphoric buffer (pH 2.5). Detection is by absorbance at 200 nm. Capillary cartridge temperature was controlled at 20°C.

### 3.2. Peak identifications

Since the polypeptide portion of rhBMP-2 is homogeneous (data not shown), its microheterogeneity is believed to come from the carbohydrate portion of the molecule. As Asn<sup>56</sup>SerThr is the predicted glycosylation site, we began our investigation with the glycopeptide Asp<sup>53</sup>-Leu<sup>92</sup> (D5). The D5 glycopeptide was purified from the endoproteinase Asp-N digest of reduced and alkylated rhBMP-2 using RP-HPLC. Fig. 5 compares the D5 peptide before and after Endo-H digestion. The electropherograms showed that

Table 1  
Migration times and mobilities of rhBMP-2 glycoforms

Peak No.	Migration time (min)	Mobility ( $10^{-4} \text{ cm}^2 \text{ V}^{-1} \text{ s}^{-1}$ )
1	23.20	1.36
2	23.35	1.35
3	23.53	1.34
4	23.73	1.33
5	23.92	1.32
6	24.11	1.31
7	24.32	1.30
8	24.52	1.29
9	24.70	1.28

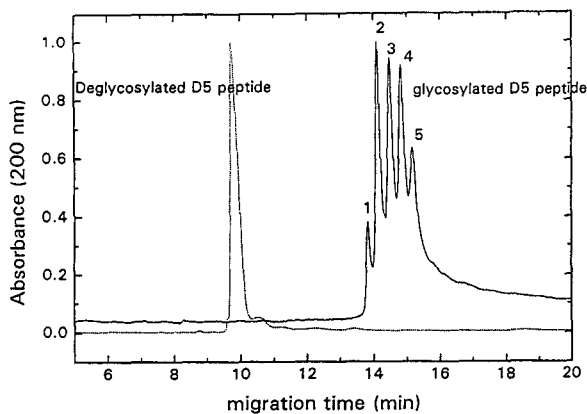


Fig. 5. Overlay of the CZE profiles of intact and deglycosylated D5 glycopeptide of rhBMP-2. A Bio-Rad, coated capillary was used. Sample was injected by electromigration for 4–8 s at 6–12 kV in 0.1 M phosphoric buffer (pH 2.5). Detection is by absorbance at 200 nm. Capillary cartridge temperature was controlled at 20°C.

D5 glycopeptide had five peaks before and one peak after Endo-H digestion. The collapse of the peaks by Endo-H digestion suggested that the microheterogeneity is due to a high-mannose-type carbohydrate. This postulate was confirmed by our FAB-mass spectrometric data. In order to enhance the sensitivity and accuracy of the mass spectrometric analysis, the D5 glycopeptide was further digested with endoproteinase Lys-C resulting a smaller glycopeptide Asp<sup>53</sup>-K<sup>73</sup>, which was recovered by RP-HPLC. Fig. 6 is the FAB-mass spectrum of the glycopeptide Asp<sup>53</sup>-K<sup>73</sup> [23]. The FAB-mass spectrum shows five distinct peaks. The masses correspond to the mass of the peptide (Asp<sup>53</sup>-Lys<sup>73</sup>) added to the masses of two N-acetylglucosamine (GlcNAc) residues and 5, 6, 7, 8 or 9 mannose residues [Asp<sup>53</sup>-K<sup>73</sup>-(GlcNAc)<sub>2</sub>Man<sub>X</sub>, where X = 5, 6, 7, 8 or 9]. That is, our MS data confirmed that the putative

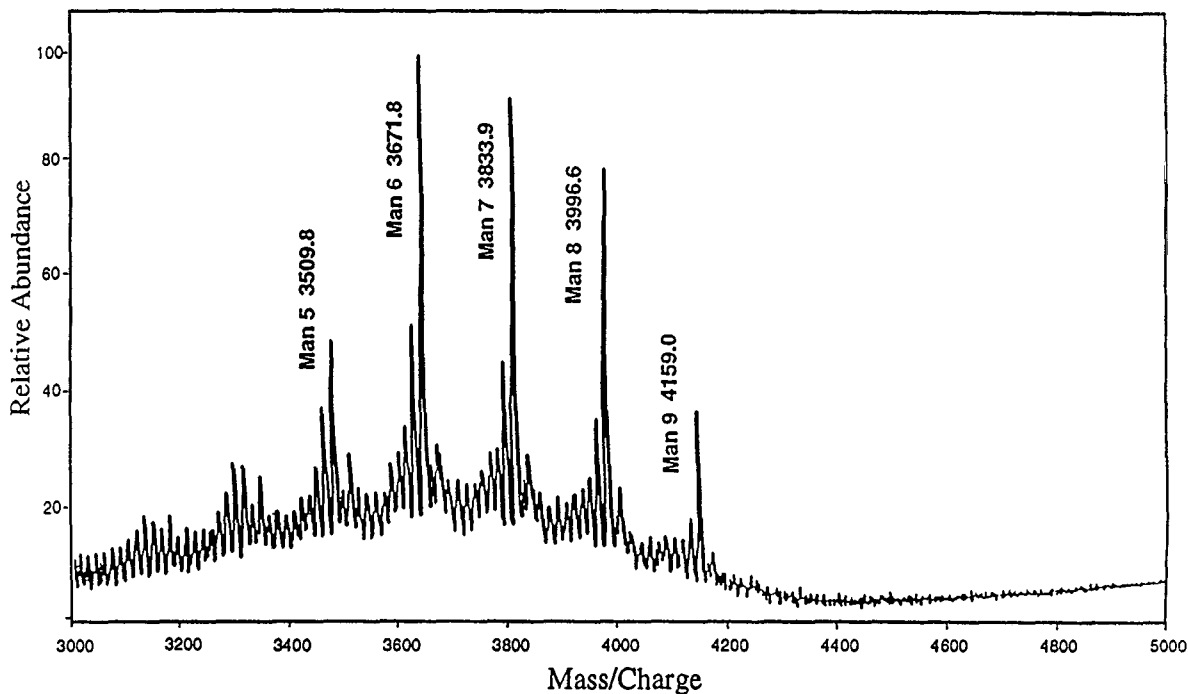


Fig. 6. Fast atom bombardment mass spectrum (FAB-MS) of the D5 glycopeptide of rhBMP-2 showing five glycoforms (D5-(GlcNAc)<sub>2</sub>Man<sub>X</sub>), where X varies from 5 to 9.

glycosylation site Asn<sup>56</sup> is indeed occupied by a high-mannose-type structure. The D5 electropherogram bears a striking resemblance with its FAB-mass spectrum, suggesting peak 1 to be D5-(GlcNAc)<sub>2</sub>Man<sub>5</sub>, peak 2 to be D5-(GlcNAc)<sub>2</sub>Man<sub>6</sub>, so forth. The migration pattern indicates that the D5 glycopeptide mobility decreases as mannose residues are added. The carbohydrate heterogeneity of rhBMP-2 can be further confirmed by using matrix-assisted laser desorption ionization-time of flight mass spectrometry (MALDI-TOF MS). Table 2 summarizes the mass spectrum of a reduced and alkylated rhBMP-2 sample [23]. The spectrum displayed five peaks. Strikingly, each peak in the mass spectrum corresponds to an individual glycosylation variant of the monomeric subunit. The 160 u difference between peaks is in excellent agreement with the mass of a single mannose residue ( $M_r = 162$ ). The observed masses for all the peaks are within 0.15% of the theoretical values. This confirmed that the rhBMP-2 monomer exists in five different glycoforms rhBMP-2-(GlcNAc)<sub>2</sub>Man<sub>X</sub>, where X = 5, 6, 7, 8 or 9.

We now turn to intact rhBMP-2. Fig. 7 compares intact rhBMP-2 before and after Endo-H digestion. The collapse of the nine rhBMP-2 peaks into one major peak (and two minor peaks) after Endo-H digestion again confirmed that its microheterogeneity is due to the high-mannose-type carbohydrate.

Since intact rhBMP-2 is a disulfide-linked homodimer of two identical monomers, simple combinatorial calculations, [ $n + c(n,r)$ , where  $n = 5$  and  $r = 2$ ] reveals that there are 15 glycoforms. The fifteen glycoforms can be represented by

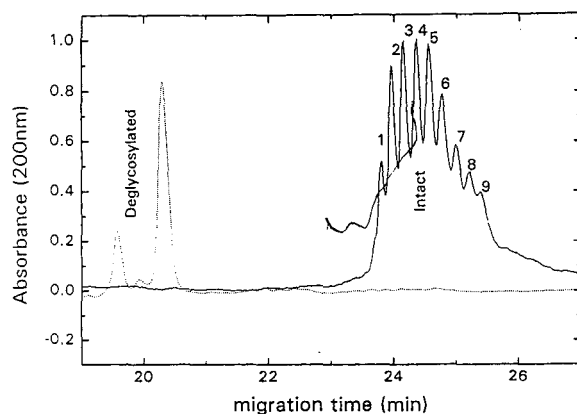


Fig. 7. Overlay of the CZE profiles of intact and deglycosylated rhBMP-2. A Bio-Rad, coated capillary was used. Sample was injected by electromigration for 4–8 s at 6–12 kV in 0.1 M phosphoric buffer (pH 2.5). Detection is by absorbance at 200 nm. Capillary cartridge temperature was controlled at 20°C.

the glycoform formula (rhBMP-2)<sub>2</sub>-(GlcNAc)<sub>4</sub>-(Man<sub>X</sub>,Man<sub>Y</sub>), where X and Y can vary from 5 to 9, respectively, and  $X \leq Y$ .

However, only nine peaks have been separated. A simple hypothesis can be proposed. If the hypothesis is confirmed, it will also shed light on the mechanism of separation. The hypothesis is: Even though there are fifteen rhBMP-2 glycoforms, there are only nine groups with distinct masses. Namely, the groups rhBMP-2<sub>2</sub>-(GlcNAc)<sub>4</sub>(Man<sub>Z</sub>) where Z varies from 10 to 18. Accordingly, if the CZE mechanism separates with reference to the number of mannoses a given rhBMP-2 molecule possesses, then it could only resolve nine peaks. For example, the following three glycoforms: (rhBMP-2)<sub>2</sub>-(GlcNAc)<sub>4</sub>-(Man<sub>5</sub>,Man<sub>9</sub>), (rhBMP-2)<sub>2</sub>-(GlcNAc)<sub>4</sub>(Man<sub>6</sub>,Man<sub>8</sub>), (rhBMP-2)<sub>2</sub>-(GlcNAc)<sub>4</sub>(Man<sub>7</sub>,Man<sub>7</sub>),

Table 2  
MALDI-TOF MS results of reduced and alkylated rhBMP-2

Peak No.	Glycoform	Theoretical $M_r$	Observed $M_r$
1	BMP-2 (GlcNAc) <sub>2</sub> Man <sub>5</sub>	14 529	14 520
2	BMP-2 (GlcNAc) <sub>2</sub> Man <sub>6</sub>	14 690	14 680
3	BMP-2 (GlcNAc) <sub>2</sub> Man <sub>7</sub>	14 852	14 840
4	BMP-2 (GlcNAc) <sub>2</sub> Man <sub>8</sub>	15 014	15 010
5	BMP-2 (GlcNAc) <sub>2</sub> Man <sub>9</sub>	15 176	15 160

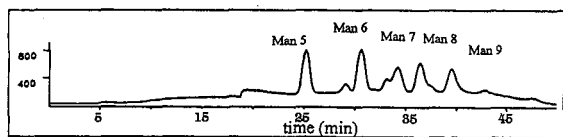


Fig. 8. High-pH anion-exchange chromatography with pulsed amperometric detection (HPAE-PAD) analysis of the N-linked oligomannose oligosaccharides released from rhBMP-2 by Endo-H digestion.

Table 3

The theoretical glycoform distribution calculated from the N-linked oligomannose analysis results

Species	Area	Fraction
M5	7.6	0.23
M6	7.5	0.23
M7	6.6	0.20
M8	6.4	0.19
M9	4.9	0.15

Species	Isoforms	Fraction
M10	55	0.05
M11	56,65	0.10
M12	57,75,66	0.14
M13	58,85,67,76	0.18
M14	59,95,68,86,77	0.20
M15	69,96,78,87	0.15
M16	79,97,88	0.10
M17	89,98	0.06
M18	99	0.02

all have 14 mannose residues each; consequently, they all have the same mobility and migrate as one peak.

### 3.3. Peak assignments

A theoretical glycoform distribution (the relative proportion of glycoforms) can be calculated from a rhBMP-2 glycan map. A glycan map is the high-pH anion-exchange chromatography with pulsed amperometric detection (HPAE-PAD) chromatogram of the oligosaccharides released from a glycoprotein by glycosidase digestion. A typical rhBMP-2 glycan map is shown in Fig. 8. The theoretical distribution of the rhBMP-2 glycoforms is calculated as shown in Table 3. An electropherogram of rhBMP-2 is compared to theoretical glycoform distributions I and II, as shown in Figs. 9a and 9b, respectively. In Fig. 9a, the glycoform distribution I is shown with number of mannose residues arranged in descending order. In Fig. 9b, the theoretical distribution II is shown with number of mannose residues arranged in ascending order. The similarity between the CZE profile and theoretical distribution II suggests that the peak assignments in Fig. 9b are correct. In other words, the migration time increases (or the mobility decreases) as the number of mannoses is increased.

However, an independent verification is still

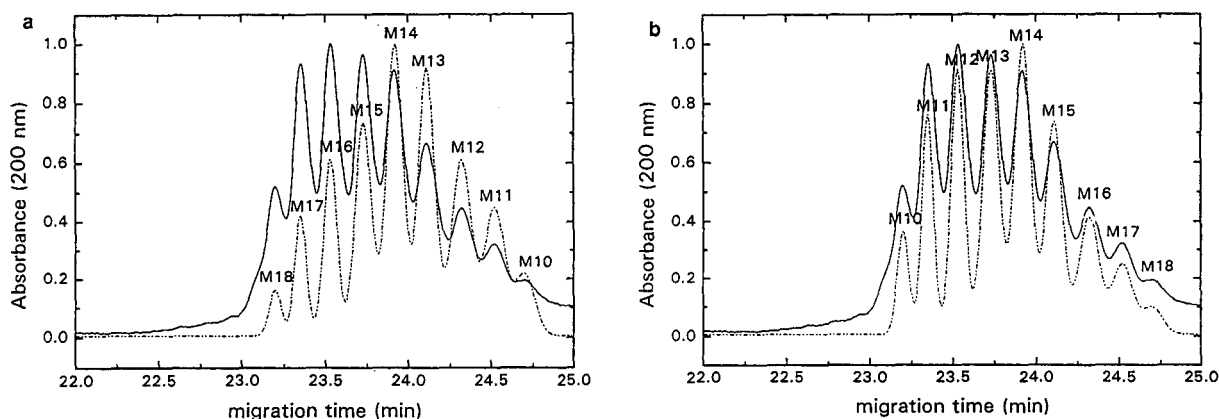


Fig. 9. (a) Comparison of the CZE profile of rhBMP-2 with the theoretical glycoform distribution I calculated from the oligosaccharides analysis results. (b) Comparison of the CZE profile of rhBMP-2 with the theoretical glycoform distribution II calculated from the oligosaccharides analysis results.

required. A direct proof can be realized if an enzyme which can convert all rhBMP-2 glycoforms to  $(\text{rhBMP-2})_2\text{-(GlcNAc)}_4(\text{Man}_5, \text{Man}_5)$  can be found. Fortunately, such an enzyme does exist and it is  $\alpha(1\text{--}2)$ mannosidase. As shown in Fig. 10, when rhBMP-2 is digested with  $\alpha(1\text{--}2)$ mannosidase, the cluster of nine peaks does collapse into a single peak coincident with the  $(\text{rhBMP-2})_2\text{-(GlcNAc)}_4(\text{Man}_5, \text{Man}_5)$ , thus confirming the peak assignments.

#### 3.4. Mobility depends on the number of mannoses

When the mobilities and migration times of the rhBMP-2 glycoforms are plotted against the numbers of mannose residues, two straight lines with  $R^2 > 0.999$  result. Two observations can be made from these results. Firstly, the mobility of a given glycoform decreases when its number of mannose residues increases. Secondly, the slope  $\delta\mu/\delta n|_n$  is constant and is equal to  $0.1 \cdot 10^{-4} \text{ cm}^2 \text{ V}^{-1} \text{ s}^{-1}$ .

Since rhBMP-2 is homogeneous in charge and oligomannoses are neutral, the rhBMP-2 glycoforms are not expected to be resolved by CZE as there are no charge differences. But, interesting-

ly enough, nine peaks were indeed resolved and it is important to examine possible mechanisms of separation. In other words, how does an incremental mannose residue affect the mobility of rhBMP-2?

#### 3.5. Plausible mechanisms

Since mobility of a particle is defined as

$$\mu = \frac{q}{f} \quad (7)$$

where  $\mu$  is the mobility of a particle,  $q$  is its surface charge and  $f$  its frictional coefficient. A neutral mannose molecule can reduce the mobility of rhBMP-2 by increasing its frictional coefficient or decreasing its effective charge.

#### Effect of mass of a mannose on rhBMP-2 mobility

rhBMP-2 belongs to the transforming growth factor  $\beta$  (TGF- $\beta$ ) family of growth factors and is believed to have a rod shape like TGF- $\beta$ . If we assume rhBMP-2 to have a rod shape, then its frictional coefficient should be proportional to its molecular mass ( $M_r$ ) raised to the power 0.8 [24]. After substituting  $M^{0.8}$  for  $f$ , differentiating Eq. 4 and noting that charge  $q$  is constant, we obtain

$$\frac{d\mu}{\mu} = -0.8 \frac{dm}{m} \quad (8)$$

This equation states that the fractional change in mobility is equal to eight tenths the fractional change in molecular mass. Given that the mass of a mannose is 162 and that the mass of rhBMP-2 $_2\text{-(GlcNAc)}_4\text{Man}_{14}$  is 29 680, the fractional mass change ( $dm/m$ ) is  $162/29\,680$  or 0.54%. Thus, the calculated fractional change in mobility ( $\Delta\mu_r/\mu$ ) is  $(-0.8 \times 0.54\%)$  or  $-0.43\%$ . Since the experimentally determined fractional change in mobility ( $\Delta\mu_r/\mu$ ) is  $(-0.100 \cdot 10^{-4} \text{ cm}^2 \text{ V}^{-1} \text{ s}^{-1}) / (1.32 \cdot 10^{-4} \text{ cm}^2 \text{ V}^{-1} \text{ s}^{-1}) = -0.75\%$ , the incremental mass change of a mannose can account for  $(0.43/0.75) = 57\%$  of the observed

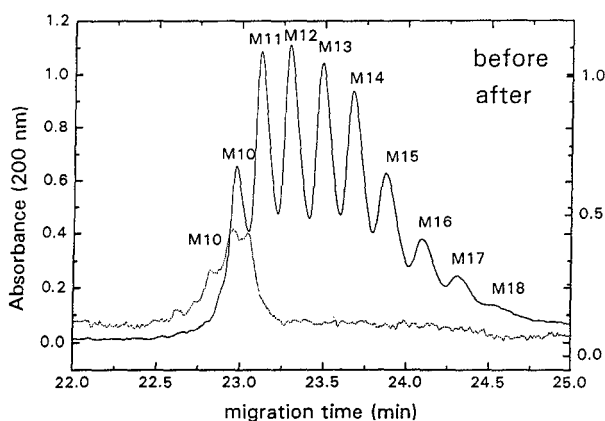


Fig. 10. Overlay of the CZE profiles of intact and  $\alpha(1\text{--}2)$ -mannosidase digested rhBMP-2. rhBMP-2 was digested to rhBMP-2 oligomannose 10 with  $\alpha(1\text{--}2)$ mannosidase at an enzyme-protein ratio of 50 mU/mg in 1 ml of sodium acetate, pH 5, at 37°C for 48 h.

mobility change ( $\Delta\mu$ ) on rhBMP-2 through its effect on the frictional coefficient  $f$ .

#### Effect of one charge on rhBMP-2 mobility

Fig. 11 is the electropherogram of a mixture two rhBMP-2 charge variants. The two charge variants arise because the N-terminal of rhBMP-2 is a glutamine (Gln form) which can cyclize to form a pyroglutamic acid (pyroglu form). The Gln terminus is positively charged under acidic conditions while the pyroglu terminus is not; so there is a two-charge difference between the two forms (rhBMP-2 being a dimer). The mobility differences between the corresponding pair of glycoforms should be attributable to their charge differences alone. In other words, since the charge difference between the (Gln-rhBMP-2)<sub>2</sub>-(GlcNAc)<sub>4</sub>Man<sub>10</sub> and (pyroglu-rhBMP-2)<sub>2</sub>-(GlcNAc)<sub>4</sub>Man<sub>10</sub> forms is two charges, the 'effective charge difference' between adjacent glycoforms can be estimated to be 0.51 charges. In other words, adding a mannose to rhBMP-2 has the same effect on its mobility as reducing its total charge by 0.51.

By using a simple particle model, we can already gain insight on how a mannose residue can affect the mobility of rhBMP-2 through a

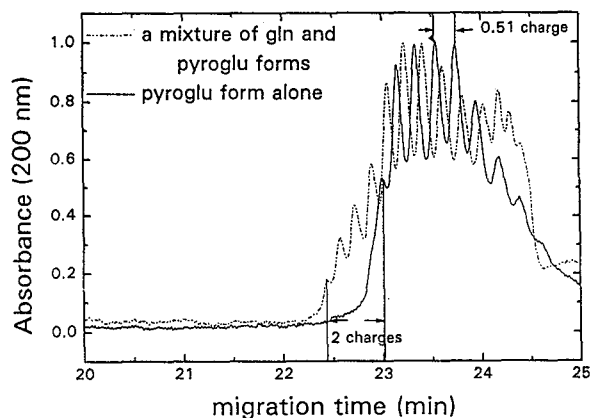


Fig. 11. Overlay of the CZE profiles of a mixture of the pyroglu and gln forms of rhBMP-2 and that of the pyroglu form of rhBMP-2.

charge shielding effect, hydrodynamic drag ( $f$ ) effect, or a combination of the two.

It is difficult to ascribe a meaning to the charges on a colloid particle; it is more useful to consider the electrostatic potential on its surface. From the mobilities of the rhBMP-2 glycoforms, their respective zeta potentials can be calculated. Substituting  $\eta = 0.010$  P and  $\epsilon = 80.4$  for water at 20°C into Eq. 6, the zeta potential,  $\zeta$ , of (rhBMP-2)<sub>2</sub>-(GlcNAc)<sub>4</sub>(Man<sub>5</sub>Man<sub>5</sub>) is 38 mV and  $\Delta\zeta$  is  $-0.29$  mV per mannose residue. One interpretation is that, as shown diagrammatically in Fig. 3, the zeta potential  $\zeta$  of a particle is the potential at its 'surface of shear' or 'slip plane'. The location of the 'slip plane' or 'surface of shear' is not known independently, but it seems reasonable that it is not far away from the Stern plane. In fact, it is often assumed that they coincide, and that  $\psi_0 \approx \zeta$ . It is likely that the slip plane is just slightly further out into the outer edge of the Stern layer. The potential  $\zeta$  depends on all those things that fix the structure of the diffuse double layer, including the presence of neutral species. The addition of the mannose units to rhBMP-2 has the effect of extending the shear plane outward, reducing the zeta potential by 0.29 mV. Whether the incremental mannose residue extends the shear plane further into the double layer, thus reducing the zeta potential, or the incremental mannose residue increases the frictional coefficient of the particle and at the same time shields and reduces the 'effective charge' on the protein particle cannot be discerned. Both the charge and hydrodynamic factors seem to be involved.

It is illuminating to examine Fig. 12, which is the X-ray crystal structure of TGF- $\beta$ 2 [25,26] drawn on the same scale with an oligomannose 9 structure, to obtain an appreciation of their spatial arrangement. The reader can almost mentally form a bond between Asn<sup>56</sup> and the N-acetylglucosamine of the oligomannose 9 structure. The most salient feature of the structure is that the oligomannose 9 structure is large relative to the protein, considering its molecular mass. One consequence of this large size is that the oligomannose may conceivably wrap around

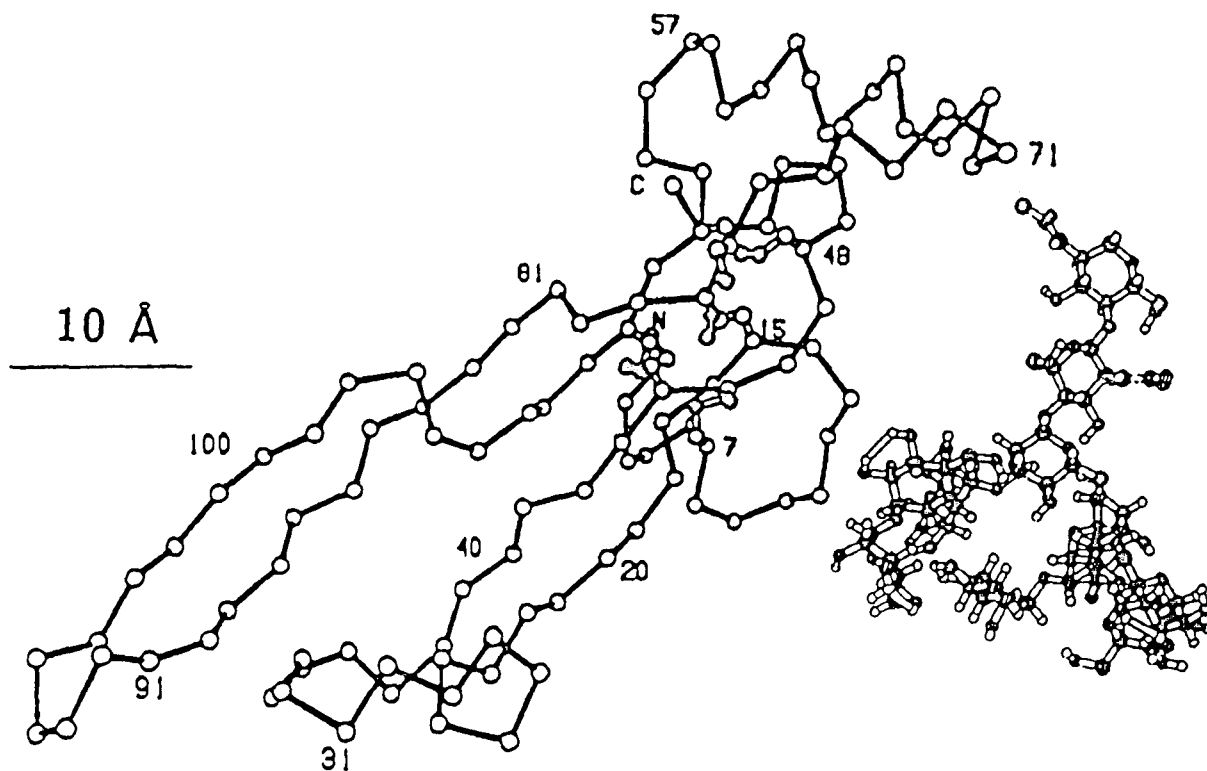


Fig. 12. X-ray crystal structures of TGF-β2 and an oligomannose 9 (GlcNAc<sub>2</sub>Man<sub>9</sub>).

the N-terminal region (where numerous positive charges are located) and as a result reduces the 'effective charge' on the protein particle.

#### 4. Conclusion

We have shown that recombinant human bone morphogenetic protein 2 (rhBMP-2) has fifteen glycoforms. Their structures can be described by the formula (rhBMP-2)<sub>2</sub>-(GlcNAc)<sub>4</sub>(Man<sub>X</sub>, Man<sub>Y</sub>), where  $X \leq Y$  and  $X$  and  $Y$  can vary from 5 to 9, respectively. We have separated the fifteen glycoforms into nine peaks. The identities of the nine peaks are (rhBMP-2)<sub>2</sub>-(GlcNAc)<sub>4</sub>(Man<sub>X</sub>, Man<sub>Y</sub>) where  $X + Y = 10, 11, \dots, 18$ . In other words, we were able to separate two proteins ( $M_r \approx 30\,000$ ) that differ by only one

mannose residue. We were not able to separate the rhBMP-2 glycoforms that have the same number of mannose residues (stereoisomers). Since mannose is a neutral molecule and the protein is homogeneous, all the rhBMP-2 glycoforms have the same charge and were not expected to be separated without resorting to chemical complexation. We explored several separation mechanisms and concluded that the size of the mannose residue is the key to the separation mechanism. The mannose residue is large compared to the size of a protein. Consequently, it either provides enough drag or shields enough charges on the molecule to reduce its mobility to be resolved. Since the slope of the mobility versus number of mannose plot ( $\delta\mu/\delta n|_n$ ) is so constant, we believe the drag effect rather than charge shielding to be primarily responsible for the decrease in mobility. The

novelty of our separation is that no complexation is invoked and all the glycoforms carry the same charge. Based on our results, we can infer that CZE using a simple low-pH buffer can resolve not only glycoforms with uncharged (neutral) glycans but also glycoforms with charged glycans (sialylated species for example) [4]. Therefore, CZE under low-pH conditions, when the proteins are fully positively charged, is a technique uniquely suitable for complex glycoform analysis without resorting to complexation reactions.

### Acknowledgements

The authors would like to thank Leah Abraham, Yangkil Kim and Bi Xu for technical assistance; Dr. John Steckert, Dr. David Williams, Dr. Michael Yet, and Dr. Brian Tripp for valuable discussions; and the Structural Biochemistry group at the Genetics Institute for the mass spectral data and the sequence diagram for rhBMP-2. The authors would specially like to thank Dr. Richard Kenley and Dr. Godfrey Amphlett for their support.

### References

- [1] A. Variki, *Glycobiology*, 3 (1993) 97.
- [2] S. Dube, J.W. Fischer and J.S. Powell, *J. Biol. Chem.*, 263 (1988) 17516.
- [3] M. Takeuchi and A. Kobata, *Glycobiology*, 1 (1991) 337.
- [4] K.W. Yim, *J. Chromatogr.*, 559 (1991) 401.
- [5] A.D. Tran, S. Park, P.J. Lisi, O.T. Huynh, R.R. Ryall and P.A. Lane, *J. Chromatogr.*, 480 (1989) 351.
- [6] F. Kilar and S. Hjerten, *Electrophoresis*, 10 (1989) 23.
- [7] S.L. Wu, G. Teshima, J. Cacia and W.S. Hancock, *J. Chromatogr.*, 516 (1990) 115.
- [8] J.P. Landers, *Anal. Biochem.*, 205 (1992) 115.
- [9] R.P. Oda, B.J. Madden, T.C. Spelsberg and J.P. Landers, *J. Chromatogr. A*, 680 (1994) 85.
- [10] P.M. Rudd, H.C. Joao, E. Coghill, P. Fiten, M.R. Saunders, G. Opendakker and R.A. Dwek, *Biochemistry*, 33 (1994) 17.
- [11] P.M. Rudd, I.G. Scagg, E. Coghill and R.A. Dwek, *Glycoconjugate J.*, 9 (1992) 86.
- [12] H.C. Joao, I.G. Scagg and R.A. Dwek, *FEBS Lett.*, 307 (1992) 343.
- [13] E.A. Wang, V. Rosen, P. Cordes, R.M. Hewick, M.J. Kriz, D.P. Luxenberg, B.C. Sibley and J.M. Wozney, *Proc. Natl. Acad. Sci. USA*, 85 (1988) 9484.
- [14] J.M. Wozney, V. Rosen, A.J. Celeste, L.M. Mitscock, M.J. Whitters, R.W. Kriz, R.M. Hewick and E.A. Wang, *Science*, 242 (1988) 1528.
- [15] A.J. Celeste, J.A. Iannazzi, R.C. Taylor, V. Rosen, E.A. Wang and J.M. Wozney, *Proc. Natl. Acad. Sci. USA*, 87 (1990) 9843.
- [16] J.M. Wozney, *Prog. Growth Factor Res.*, 1 (1989) 267.
- [17] E.A. Wang, V. Rosen, J.S. D'Alesandro, M. Bauduy and J.M. Wozney, *Proc. Natl. Acad. Sci. USA*, 87 (1990) 2220.
- [18] A.W. Yasko, J.M. Lane, J.M. Wozney, V. Rosen and E.A. Wang, *J. Bone Joint Surg.*, 74 (1992) 659.
- [19] D.M. Touiymi, H.S. Kotler, D.P. Luxenberg and E.A. Wang, *Arch. Otolaryngol. Neck Surg.*, 117 (1991) 1101.
- [20] P.C. Hiemenz, *Principles of Colloid and Surface Chemistry*, Marcel Dekker, New York, 1991.
- [21] M.R. Hardy and R.R. Townsend, *Proc. Natl. Acad. Sci. USA*, 85 (1988) 3289.
- [22] Y.C. Lee, *Anal. Biochem.*, 189 (1990) 151.
- [23] M.D. Bond, M.A. Jankowski, S.A. Martin and H.A. Scoble, *Sixth International Symposium of the Protein Society*, San Diego, CA, 1992, abstract.
- [24] C.R. Cantor and P.R. Schimmel, *Biophysical Chemistry*, Freeman, New York, 1980.
- [25] S. Daopin, K.A. Piez, Y. Ogawa and D. Davies, *Science*, 257 (1992) 369.
- [26] S. Daopin, M. Li and D.R. Davies, *Proteins: Structure, Function and Genetics*, 17 (1993) 176.



## PUBLICATION SCHEDULE FOR THE 1996 SUBSCRIPTION

### Journal of Chromatography A

MONTH	Oct. 1995	Nov. 1995	Dec. 1995 <sup>a</sup>	
Journal of Chromatography A	715/1	715/2 716/1 + 2 717/1 + 2	718/1 718/2	The publication schedule for further issues will be published later.
Bibliography Section				

<sup>a</sup> Vol. 701 (Cumulative Indexes Vols. 652–700) expected in December.

### INFORMATION FOR AUTHORS

(Detailed *Instructions to Authors* were published in *J. Chromatogr. A*, Vol. 657, pp. 463–469. A free reprint can be obtained by application to the publisher, Elsevier Science B.V., P.O. Box 330, 1000 AH Amsterdam, Netherlands.)

**Types of Contributions.** The following types of papers are published: Regular research papers (full-length papers), Review articles, Short Communications, Discussions and Letters to the Editor. Short Communications are usually descriptions of short investigations, or they can report minor technical improvements of previously published procedures; they reflect the same quality of research as full-length papers, but should preferably not exceed five printed pages. Discussions (one or two pages) should explain, amplify, correct or otherwise comment substantively upon an article recently published in the journal. Letters to the Editor (max. two printed pages) bring up ideas, comments, opinions, experiences, advice, disagreements, insights, etc. For Review articles, see inside front cover under Submission of Papers.

**Submission.** Every paper must be accompanied by a letter from the senior author, stating that he/she is submitting the paper for publication in the *Journal of Chromatography A*.

**Manuscripts.** Manuscripts should be typed in **double spacing** on consecutively numbered pages of uniform size. The manuscript should be preceded by a sheet of manuscript paper carrying the title of the paper and the name and full postal address of the person to whom the proofs are to be sent. As a rule, papers should be divided into sections, headed by a caption (e.g., Abstract, Introduction, Experimental, Results, Discussion, etc.). All illustrations, photographs, tables, etc., should be on separate sheets. Manuscripts should be accompanied by a 5.25- or 3.5-in. disk. Your disk and (**exactly matching**) printed version (printout, hardcopy) should be submitted together to the accepting editor or Editorial Office **according to their request**. Please specify the type of computer and word-processing package used (do not convert your textfile to plain ASCII). Ensure that the letter "l" and digit "1" (also letter "O" and digit "0") have been used properly, and format your article (tabs, indents, etc.) consistently. Characters not available on your word processor (Greek letters, mathematical symbols, etc.) should not be left open but indicated by a unique code (e.g. gralpha, @, #, etc., for the Greek letter  $\alpha$ ). Such codes should be used consistently throughout the entire text. Please make a list of such codes and provide a key. Do not allow your word processor to introduce word splits and do not use a "justified" layout. Please adhere strictly to the general instructions on style/arrangement and, in particular, the reference style of the journal. Further information may be obtained from the Publisher.

**Abstract.** All articles should have an abstract of 50–100 words which clearly and briefly indicates what is new, different and significant. No references should be given.

**Introduction.** Every paper must have a concise introduction mentioning what has been done before on the topic described, and stating clearly what is new in the paper now submitted.

**Experimental conditions** should preferably be given on a *separate* sheet, headed "Conditions". These conditions will, if appropriate, be printed in a block, directly following the heading "Experimental".

**Illustrations.** The figures should be submitted in a form suitable for reproduction, drawn in Indian ink on drawing or tracing paper. Each illustration should have a caption, all the *captions* being typed (with double spacing) together on a *separate sheet*. If structures are given in the text, the original drawings should be provided. Coloured illustrations are reproduced at the author's expense. The written permission of the author and publisher must be obtained for the use of any figure already published. Its source must be indicated in the legend.

**References.** References should be numbered in the order in which they are cited in the text, and listed in numerical sequence on a separate sheet at the end of the article. Please check a recent issue for the layout of the reference list. Abbreviations for the titles of journals should follow the system used by *Chemical Abstracts*. Articles not yet published should be given as "in press" (journal should be specified), "submitted for publication" (journal should be specified), "in preparation" or "personal communication".

Vols. 1–651 of the *Journal of Chromatography*; *Journal of Chromatography, Biomedical Applications* and *Journal of Chromatography, Symposium Volumes* should be cited as *J. Chromatogr.* From Vol. 652 on, *Journal of Chromatography A* should be cited as *J. Chromatogr. A* and *Journal of Chromatography B: Biomedical Applications* as *J. Chromatogr. B*.

**Dispatch.** Before sending the manuscript to the Editor please check that the envelope contains four copies of the paper complete with references, captions and figures. One of the sets of figures must be the originals suitable for direct reproduction. Please also ensure that permission to publish has been obtained from your institute.

**Proofs.** One set of proofs will be sent to the author to be carefully checked for printer's errors. Corrections must be restricted to instances in which the proof is at variance with the manuscript.

**Reprints.** Fifty reprints will be supplied free of charge. Additional reprints can be ordered by the authors. An order form containing price quotations will be sent to the authors together with the proofs of their article.

**Advertisements.** The Editors of the journal accept no responsibility for the contents of the advertisements. Advertisement rates are available on request. Advertising orders and enquiries may be sent to: Elsevier Science, Advertising Department, The Boulevard, Langford Lane, Kidlington, Oxford, OX5 1GB, UK; Tel: (+44) (0) 1865 843565; Fax (+44) (0) 1865 843952. USA and Canada: Weston Media Associates, Dan Lipner, P.O. Box 1110, Greens Farms, CT 06436-1110, USA; Tel (203) 261 2500; Fax (203) 261 0101. Japan: Elsevier Science Japan, Ms Noriko Kodama, 20-12 Yushima, 3 chome, Bunkyo-Ku, Tokyo 113, Japan; Tel (+81) 3 3836 0810; Fax (+81) 3 3839 4344.

# Chiral HPLC Column

## Application Guide for Chiral HPLC Column Selection

### **SECOND EDITION!**

**FREE OF CHARGE**

**Application Guide**  
for chiral column selection  
CROWNPAK-CHIRALCEL+CHIRALPAK  
Chiral HPLC column for Optical Resolution

Second Edition

 DAICEL CHEMICAL INDUSTRIES, LTD.

The 112-page green book contains chromatographic resolutions of over 350 chiral separations, cross-indexed by chemical compound class, structure, and the type of chiral column respectively. This book also lists chromatographic data together with analytical conditions and structural information. A quick reference guide for column selection from a wide range of DAICEL chiral HPLC columns is included.

*To request this book, please let us know by fax or mail.*

 **DAICEL CHEMICAL INDUSTRIES, LTD.**

#### AMERICA

##### CHIRAL TECHNOLOGIES, INC.

730 Springdale Drive, P.O. Box 564  
Exton, PA 19341  
Phone: 800-624-4725  
Facsimile: 610-594-2325

#### EUROPE

##### DAICEL (EUROPA) GmbH

Oststr. 22  
D-40211 Düsseldorf, Germany  
Phone: +49-211-369848  
Facsimile: +49-211-364429

#### ASIA/OCEANIA

##### DAICEL CHEMICAL INDUSTRIES, LTD.

CHIRAL CHEMICALS NDD  
8-1, Kasumigaseki 3-chome,  
Chiyoda-ku, Tokyo 100, JAPAN  
Phone: +81-3-3507-3151  
Facsimile: +81-3-3507-3193